UNIVERSITÀ
degli STUDI
di CATANIA

DEPARTMENT OF BIOMEDICAL AND BIOTECHNOLOGICAL SCIENCES
PH.D. SCHOOL IN NEUROSCIENCE
CYCLE XXXVIII

Anna Monai

DISTINCT PREFRONTAL SOMATOSTATIN NEURON SUBPOPULATIONS DIFFERENTIALLY MODULATE EMOTION DISCRIMINATION IN MICE

Tutor: Prof. Gian Marco Leggio
Co-Tutor: Prof. Francesco Papaleo

Coordinators: Prof. Filippo Drago
Prof. Claudio Bucolo

Academic Year 2024-2025

Abstract

Our social lives rely heavily on being able to recognise, process, and respond to the emotions of others. These socio-emotional skills are crucial for our well-being and for adapting to life within groups, and their impairment is a key feature of several neuropsychiatric disorders, including schizophrenia. The medial prefrontal cortex (mPFC) and its sub-regions, such as the anterior cingulate cortex (ACC) and prelimbic cortex (PrL), have been strongly linked to emotion perception and recognition in both humans and rodents. However, the underlying circuit-level mechanisms remain poorly understood.

In the first part of this thesis, we explored the role of somatostatin-expressing (SOM) interneurons in emotion discrimination, employing a validated behavioural paradigm in mice, the Emotion Discrimination Task (EDT). This test involves an observer mouse interacting with two demonstrators in distinct emotional states, allowing us to investigate how animals discriminate between conspecifics based on emotional cues. By combining this approach with optogenetic manipulations in a genetically modified strain of mice (Som-Cre), we identified a previously uncharacterized long-range inhibitory projection from the mPFC to the retrosplenial cortex (RSC). Viral tracing demonstrated that SOM neurons in the mPFC target RSC pyramidal neurons, which in turn project back to the mPFC. Manipulating this pathway in a bidirectional way altered emotion discrimination, and restoring its function rescued deficits in mouse models of psychiatric vulnerability. This highlights the critical role of long-range inhibitory communication in supporting socio-emotional recognition.

In addition to circuit mechanisms, we examined the influence of self-experience and individual factors on emotion recognition. Observer mice that had undergone similar experiences as stressed demonstrators responded in a divergent manner depending on sex and social hierarchy: female mice varied depending on their estrus cycle, while dominant males displayed distinct behavioural patterns compared to subordinates. At the cellular level, corticotropin-releasing factor (CRF) neurons in the mPFC mediated the impact of prior stress experience. Silencing these neurons abolished the modulatory effect of self-experience on recognition, suggesting that CRF-expressing cells encode the integration of internal states with social perception.

We next examined the contributions of SOM neurons within the ACC and PrL. Our findings showed that optogenetic activation of SOM neurons in either region disrupted discrimination, whereas inhibition selectively impaired discrimination in the PrL, but not in the ACC. Circuit-mapping studies revealed that ACC SOM neurons project to multiple downstream targets, implicating them in a distributed network spanning cognitive and limbic systems. These results indicate that SOM interneurons in both regions influence socio-emotional behavior, albeit with region-specific roles.

Focusing on the ACC, we further analyzed the dynamics of SOM interneurons alongside pyramidal neurons during emotion discrimination. Both cell types were found to contribute to inter-brain synchrony, with synchronization and desynchronization patterns emerging depending on emotional context. These findings indicate that social behavior is shaped not only by local computations but also by inter-brain coupling, positioning inhibitory and excitatory neurons as key elements of adaptive social cognition.

Together, these findings advance our understanding of how inhibitory neurons shape emotion recognition across multiple levels of organisation. SOM interneurons in the PrL and ACC serve distinct functions, ranging from local discrimination to inter-brain coordination. At the same time, long-range projections to the RSC reveal new inhibitory pathways critical for cortico-cortical communication. Moreover, the modulatory effects of prior experience, sex, and hierarchy underscore the importance of contextual and individual factors in socio-emotional processing.

By integrating behavioural assays, optogenetics, viral tracing, and circuit analyses, this work provides a multi-scale account of how inhibitory and excitatory dynamics in the prefrontal cortex regulate emotion recognition. These insights refine our mechanistic understanding of social cognition and point toward specific circuit-level targets for intervention in psychiatric disorders characterised by deficits in emotion recognition.

Index

Chapter 1

General Introduction

The Prefrontal Cortex

The prefrontal cortex occupies roughly the anterior half of the frontal lobe in non-human primates and about two-thirds in humans. The primary motor cortex (M1) or area 4 of Brodmann, marks the posterior extent of the frontal lobe, and the premotor cortex (also known as area 6) is interposed between the primary motor and prefrontal cortices. The medial prefrontal cortex is located in front of the medial parts of the premotor cortex –the supplementary motor area (SMA), or MII – and the cingulate motor areas, and extends from the anterior part of the corpus callosum in the anterior cingulate to the medial part of the frontal pole (Fig. 1, (Barbas, 2010))

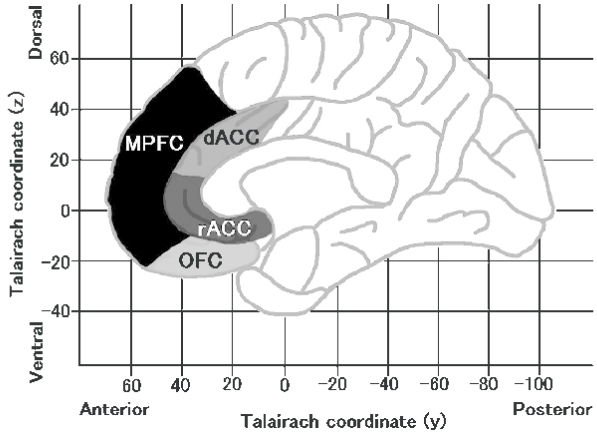

Fig. 1 Schematic illustration of medial frontal regions in humans. Sagittal plane. Medial Prefrontal Cortex (mPFC), Orbitofrontal Cortex (OFC), Dorsal Anterior Cingulate Cortex (dACC), rostral-ventral anterior cingulate cortex (rACC). (Nakao, 2010)

In mice, the mPFC lies in front of the thalamus, slightly over the striatum, in a more dorsal area in respect to its human counterpart, and can be subdivided into the anterior cingulate cortex (ACC), the prelimbic (PrL) and the infralimbic cortex (IL) (Fig. 2, Bloem et al. (2014)).

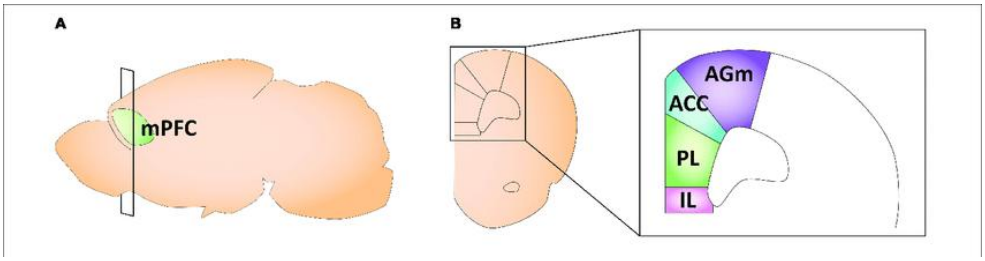

Fig. 2 Schematic of the adult mouse medial prefrontal cortex. (A) Illustration in the sagittal plane depicting the adult mouse medial prefrontal cortex. mPFC, medial prefrontal cortex. (B) Illustration of the coronal view of the medial prefrontal cortex at the plane of section depicted in (A). mAG, medial agranular cortex; ACC, anterior cingulate cortex; PL, prelimbic cortex; IL, infralimbic cortex. Ramachandran, S et al. (2020) (Ramachandran et al., 2020)

Most prefrontal areas have six layers, including a granular layer IV. However, the width and density of neurons in layer IV vary widely among prefrontal regions. The most posterior parts of the medial cortex have fewer than six layers, either due to the absence of the layer or because it is poorly developed. In the anterior cingulate areas, the deeper layers (V and VI) predominate in cell density compared to the upper layers (II–III)(Barbas, 2010).

In the mPFC, projection neurons are found throughout layers 2 to 6 and often form reciprocal circuits with other cortical regions, such as the thalamus, basolateral amygdala, or the claustrum ((Harris & Shepherd, 2015); (Collins et al., 2018)). These projecting neurons include various cell types based on their targets: brainstem and spinal cord (pyramidal tracts, PT), cortico-thalamic (CT), or intra-telencephalic (IT), which also communicate through local collateral excitation (Fig. 3). Additionally, different GABAergic interneuron subtypes are distributed across layers, mediating local collateral or layer-specific inhibition. While PV+ and VIP+ interneurons are the most common, a significant portion consists of SOM+ cells, which may contribute to differences in local neural computations (Kim et al., 2017).

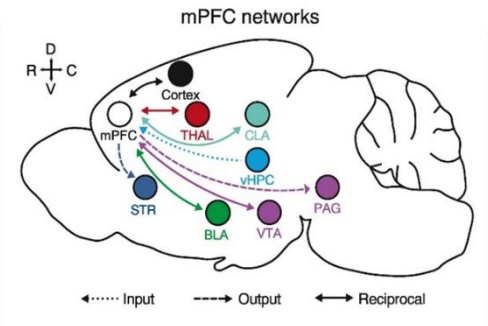

Fig. 3. General organization of the rodent medial prefrontal cortex (mPFC). (A) Key brain regions that communicate with the mPFC, by providing input, receiving output, or making reciprocal connections. Abbreviations: BLA, basolateral amygdala; CLA, claustrum; PAG, periaqueductal gray; STR, striatum; THAL, thalamus; vHPC, ventral hippocampus; VTA, ventral tegmental area. Anastasiades (Anastasiades et al., 2021)

Several studies have identified the mPFC as a fundamental component in adaptive decision-making. It has been demonstrated that the entire mPFC receives a broad range of sensory and limbic inputs which can activate contextually appropriate representations of goals or task rules ((Miller, 2000);(Miller & Cohen, 2001)). It has been associated with a role in decisions making by anticipating emotional outcomes and enacting them as bodily states ((Bechara A, 2005); (Fellows, 2007)) and it is involved in several cognitive and behavioral processes: memory consolidation, both of recent and remote events ((Takashima et al., 2006);(Corcoran & Quirk, 2007)), emotion regulation ((Diorio et al., 1993); (Maier et al., 2006)) and discrimination (Scheggia et al., 2020), reward-guided learning (Rushworth et al., 2011), just to name a few.

Emotion discrimination in social settings depends on recognizing subtle affective signals and interpreting their valence and significance. In rodent studies, the mPFC is crucial for distinguishing conspecifics based on emotional states, as demonstrated by behavioural tests like the EDT (Scheggia et al., 2020). Through the use of optogenetic to target a specific subset on inhibitory cells, the SOM+ neurons, it was discovered their role in processing and understanding social-emotional cues.

In humans, functional imaging research has similarly highlighted the role of the mPFC in tasks involving mental state attribution, emotional empathy, and moral decision-making ((Amodio & Frith, 2006); (Etkin et al., 2011)). These roles are closely connected to “emotional simulation", where the observer internally recreates another person’s emotional state. It has been suggested that the mPFC supports these simulations by combining visceral signals (such as those from the insula and anterior cingulate cortex) with socially relevant contextual cues (Roy et al., 2012).

The mPFC is also believed to play a key role in generating anticipatory emotional responses by linking past experiences with expected outcomes; in this way, it supports emotion-driven decision-making (Bechara et al., 2000). This predictive function is crucial in emotionally complex social settings where accurately interpreting emotional signals can influence whether a person approaches, avoids, or adjusts their actions. Impairments in mPFC function have been linked to difficulties in social interactions and emotion recognition in various psychiatric disorders, such as schizophrenia, depression, and autism spectrum disorder ((Davidson et al., 2002); (Frith & Frith, 2007)). Also lesions to this area in humans lead to difficulties in emotion

and regulation ((Bechara et al., 1994); (Anderson et al., 2006)). Patients present flattened affect, impulsivity, incapability of risk evaluation, and emotional outbursts ((Barrash et al., 2000); (Berlin et al., 2004)). Another effect is the inability to recognize emotions in others ((Dal Monte et al., 2013); (Hiser & Koenigs, 2018)). The most common and well-known case of lesion of the PFC is the study case of Phineas Cage that presented a near-complete lesion of the mPFC in 1848 following a work accident. Despite motor and cognitive deficits, Phineas Cage also presented a novel and more aggressive behavior.

Rats with lesions to the right mPFC show decreased stress reactivity, while left-sided damage does not affect the stress response (Sullivan & Gratton, 1999). Some studies have reported pronounced cardiovascular activation in mPFC lesion patients ((Critchley et al., 2003); (Hilz et al., 2006)). Furthermore, neuroimaging studies have suggested that the mPFC exerts inhibitory control over autonomic and endocrine output (Wang et al., 2005). Damage to this region, then, could result in a disinhibition of psychological and physiological responses to stress. Brains with lesions in the intra-limbic (IL) sub-region seemed to conserve the ability of recent memory consolidation but lost the ability to recall remote events (Corcoran & Quirk, 2007). The function of the mPFC cannot be generalized to lesion studies due to the differential role played by excitatory output neurons as well as the different types of GABAergic interneurons.

In conclusion, the mPFC is a crucial structure for emotion discrimination through its role in contextual integration, predictive processing, and modulation of affectively guided behavior. Its bidirectional communication with limbic regions such as the amygdala and anterior cingulate cortex supports a dynamic network that underlies the nuanced interpretation of social-emotional cues necessary for adaptive interaction.

1.1 The Anterior Cingular Cortex

1.1.1 Location and Anatomy

The ACC is situated adjacent to the corpus callosum and connects to both the “emotional” limbic system and the “cognitive” prefrontal cortex (Stevens et al., 2011). In humans, the ACC

is formed by Brodmann's areas (BA) 24, 25, 32, and 33, and can be divided into three other sub-regions:

1. The perigenual anterior cingulate cortex (**pACC**) is mainly responsible for processing emotions and regulating the endocrine and autonomic responses to emotions.
2. The dorsal anterior cingulate cortex (**dACC**), also known as the mid-cingulate cortex. It is responsible for cognitive processing, specifically reward-based decision-making (Vogt, 2016).
3. The cingulate motor areas (**CMA**), positioned inside the cingulate sulcus and next to the primary and supplementary motor cortices. They are higher-order motor areas that process information from internal and external states (e.g., emotional state signals from the limbic system) and translate them into motor commands executed by the primary and supplementary motor cortices and spinal cord ((Strick et al., 1998); (Jumah & Dossani, 2025))

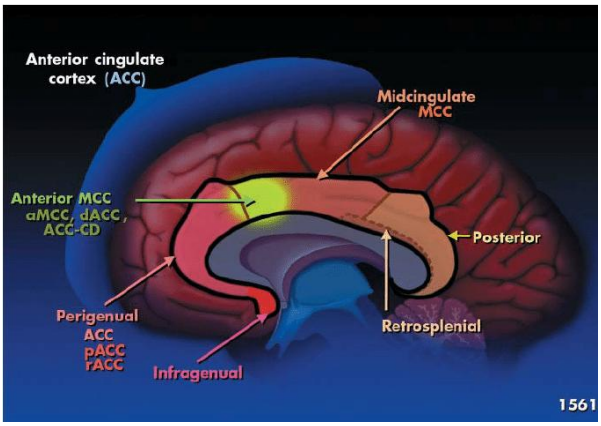

Fig. 6 Structure of the cingulate cortex. The anterior region of the mid cingulate cortex (MCC, shown in green) is a sub region called the anterior mid cingulate cortex of the ACC (aMCC); it has a variety of other names, including the caudal ACC, the dorsal ACC (dACC), or the cognitive division of the ACC (ACC-CD). pACC, anterior perigenual ACC; rACC, rostral ACC. (Drossman, 2005).

1.1.2 Functions

The ACC is thought to be involved in a range of social and cognitive behaviors, from emotional processing to decision-making ((Stevens et al., 2011); (Apps et al., 2016);(Keum et al., 2018)). Additionally, because the ACC comprises different regions, each plays a distinct role depending on the task. For example, the ACC gyrus—located next to and dorsal to the genu of the corpus callosum in humans—has a crucial function in evaluating others' behaviors and estimating their

motivation levels (Apps et al., 2016). Meta-analyses of fMRI studies show that the MCC and the subgenual ACC (sACC) – positioned ventrally to the pACC – display decreased activity during fear conditioning in individuals with PTSD. This reduced activation in sACC may suggest impaired emotion regulation and fear extinction, while abnormalities in the aMCC might be linked to a diminished experience of negative emotions. Patients with schizophrenia, who often exhibit flattened affect, demonstrate less activation in the aMCC during executive tasks (Stevens et al., 2011).

For many years, the primary role of the ACC was believed to be error detection, based on its activation during the Stroop task —a test that measures any delay in reaction time between congruent and incongruent stimuli (Posner, 1998). It is typically performed using a mismatch between the color name (e.g., blue, green, or red) and the color of the font in which it is printed (e.g., the word red printed in a blue font). The participant is asked to name the font color; the greater the mismatch, the longer the delay may be (Scarpina & Tagini, 2017). Another method to test the involvement of the ACC in error detection was through error-related negativity (ERN), a type of electrical activity in the brain measured using electroencephalography (EEG) (Bush et al., 2000). In the same paper, it was also demonstrated that the ACC, specifically the dorsal part, is involved in emotional regulation and motivation (Bush et al., 2000).

Furthermore, it plays a role in pain perception and the emotional component of pain, both physical and social: the ACC is indeed activated during experiences of social exclusion, supporting the theory that the brain processes social pain similarly to physical pain (Eisenberger & Lieberman, 2004). This overlap aligns with the ACC's integrative function, connecting cognitive and emotional inputs to help guide adaptive behavior.

The ACC's connections with the mPFC, amygdala, and insula link it to social awareness and empathy and lesions in this area can impair social behavior ((Keum et al., 2018)). Neuroimaging studies highlight its activation during tasks that involve perspective-taking and emotional understanding (Schneider et al., 2020). The ACC is thought to mediate the emotional aspect of empathy, allowing individuals to connect with and respond to others' feelings. Dysfunction in this region has been associated with neuropsychiatric disorders such as depression, schizophrenia, and autism spectrum disorder, often involving deficits in social cognition and emotional processing ((Etkin et al., 2011); (Antonelli F., 2025)).

In summary, the ACC is a vital center for cognitive control, emotional assessment, and social interaction. Its numerous functions are supported by its connectivity with both cortical and subcortical structures, enabling it to integrate and prioritize information relevant to adaptive behavioural responses.

1.1.3 Connectivity

As previously mentioned, the ACC is a central hub in a network of brain regions that integrate cognitive and emotional information. Its peculiar position serves as a medial ground between limbic and prefrontal structures. The functional heterogeneity of the ACC is supported by its extensive connectivity, which varies across its dorsal, rostral, and subgenual subdivisions ((Bush et al., 2000);(Devinsky et al., 1995)).

The ACC has a well-studied connection with the medial prefrontal cortex (mPFC), forming part of the default mode network (DMN) (Buckner et al., 2008). Past studies revealed that the mPFC and ACC activate together during tasks related to self-reflection, emotion regulation, and social judgment ((Andrews-Hanna et al., 2010);(Etkin et al., 2011)). Among species, the rostral ACC shows strong connectivity with the ventromedial PFC, aiding in evaluative and emotional decision-making (Ongur & Price, 2000). Diffusion tensor imaging (DTI) scans have also identified white matter pathways linking the ACC with both dorsal and ventral medial prefrontal cortex (mPFC) areas, providing an anatomical foundation for their functional relationship (Beckmann et al., 2009).

Another important pathway involves the ACC and anterior insula, which participate in detecting, evaluating, and responding to significant stimuli from the environment and within the body. It is thought to coordinate the shift between the default mode network and the central executive network ((Menon & Uddin, 2010); (Medford & Critchley, 2010)). The ACC and insula share bidirectional anatomical and functional connections and are active during tasks involving emotional arousal and empathy ((Craig, 2009);(Singer et al., 2004)). The insula processes information from visceral and somatosensory sources, transmitting it to the ACC, which may then initiate appropriate autonomic or behavioural responses. It is also involved in emotion regulation, empathy, and pain processing. For example, both regions are activated during tasks involving observation of others in pain, highlighting their role in the affective component of

empathy (Singer et al., 2004). Additionally, functional disruptions within this circuit have been observed in various psychiatric conditions such as major depressive disorder, generalized anxiety, and autism spectrum disorder, often correlating with deficits in emotion regulation and social functioning (Hamilton et al., 2011).

The ACC also interacts with subcortical regions such as the amygdala, nucleus accumbens, hypothalamus, and periaqueductal grey (PAG). Notably, the ventral ACC forms part of a limbic circuit with the amygdala, orbitofrontal cortex, and nucleus accumbens (Rolls, 2019). It has functional connections with the striatum, which support the ACC's role in reward-based decision-making and motivation. These circuits are crucial in reinforcement learning, as the ACC processes outcome feedback and prediction errors to influence future actions (Rushworth & Behrens, 2008). Disruption of these ACC–striatal pathways has been linked to addiction and mood disorders, highlighting the significance of ACC connectivity for adaptive functioning ((Zhang et al., 2017); (Li et al., 2024)).

1.1.4 Pathology

Typically, lesions or abnormalities in the ACC are linked to cognitive deficits or neurodegenerative disorders such as autism, depression, or schizophrenia ((Schmaal et al., 2017); (Fornito et al., 2009)). Damage to the ACC tissue or its connectivity can impair memory, error detection, emotional stability, or attention ((Janer & Pardo, 1991); (Bush et al., 2000)). Furthermore, fMRI studies have demonstrated that participants with ADHD show reduced activation of the dorsal cingulate region during the Stroop task, an attentional and cognitive interference task that engages such area. Additionally, various studies have associated the ACC with the onset of OCD, PTSD, and anxiety disorders ((Biria et al., 2023); (Young et al., 2018); (Zeidan et al., 2014)).

Autism Spectrum Disorder

Patients with autism spectrum disorder (ASD) can be characterised by impairments in social interaction, verbal and non-verbal communication, and repetitive or stereotyped behaviors. A method used to diagnose them is voxel-based morphometry (VBM), which provides clinicians

with a probabilistic measure of local grey matter (GM) and white matter concentration. A 2011 study, which employed the activation likelihood estimation (ALE), a quantitative voxel-based meta-analysis method that can be used to estimate consistent activations across different imaging studies, demonstrated reduced GM volume in the right anterior cingulate cortex (Cauda et al., 2011). Another 2011 study conducted in children with an ASD diagnosis showed reduced theta activity in the ACC when performing the GO/No-Go task (Chan et al., 2011).

Schizophrenia

Schizophrenia is the most well-known pathology associated with abnormalities in the ACC.

This region is vital in cognitive and emotional processing, both of which are severely affected in schizophrenic patients (Andreasen et al., 1998). Over the years, various studies have demonstrated how abnormalities in ACC volume (Fujiwara et al., 2007), decreased activity (Taylor et al., 2012), and abnormal connectivity with other brain regions (Grimaldi et al., 2025) are associated with this pathology. Furthermore, differences in the cellular and synaptic architecture of the region in patients compared to healthy individuals have also been observed, such as reductions of pyramidal neurons in layers II-VI at varying percentages (Todtenkopf et al., 2005), a decrease in dendrites of pyramidal cells in layers III and V (Moyer et al., 2016), and a reduction in the density of non-pyramidal cells in layer II ((Benes et al., 1986); (Benes et al., 1998)).

There is a basic understanding that alterations in cortical inhibitory γ-aminobutyric acid (GABA) neurons could be linked to the pathology of schizophrenia (Gonzalez-Burgos et al., 2010), and it has already been demonstrated that in the mPFC and other frontal regions there is a significant deficit of SOM messenger RNA (mRNA) (Dienel et al., 2025). There is yet to be demonstrated a similar disruption of SOM neurons in the ACC of schizophrenic patients.

1.2 The Social Brain and Emotion Recognition

The ability to recognise conspecifics and interpret their emotional and mental states—often conveyed through facial expressions, vocalisations, and body language—is a fundamental aspect of social behavior and survival across species (Li & Jeong, 2020). This socio-cognitive skill

allows animals to engage in affiliative interactions, avoid threats, establish hierarchies, and coordinate group behavior, all of which are essential for reproductive success and long-term survival.

Underlying these abilities is a distributed network of brain regions often referred to as the "social brain" ((Brothers, 2002); (Frith & Frith, 2007)). In humans, this network comprises structures such as the medial and lateral prefrontal cortices (PFC), the inferior frontal gyrus, the superior temporal sulcus (STS), the amygdala, and the anterior insula, among others ((Frith & Frith, 2007);(Adolphs, 2009)). These areas work together to process social signals, interpret intentions, and modulate emotional responses appropriately within context.

The mPFC, in particular, exerts the “top-down” executive modulatory control over socio-cognitive functions, and it is recognized as a fundamental hub for social cognition ((Adolphs, 2009) ; (Amodio & Frith, 2006); (Friedman & Robbins, 2022); (Kietzman & Gourley, 2023)).

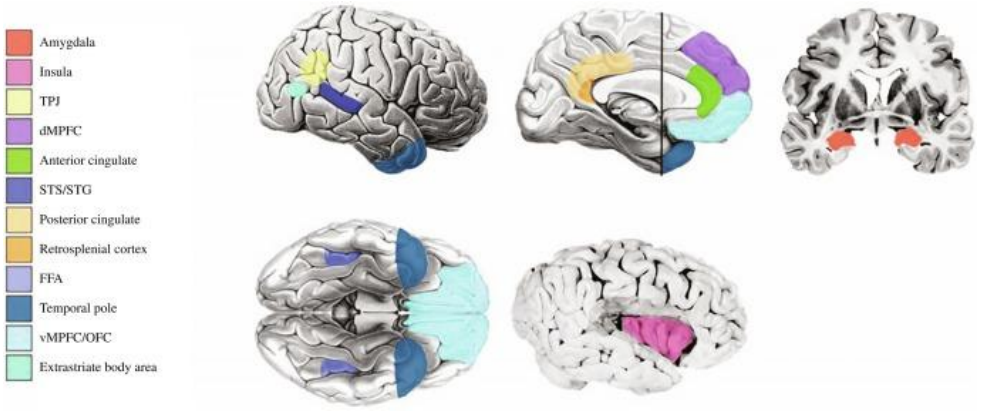

Fig. 2 Figure adapted from (Kennedy & Adolphs, 2012), Neuron—graphical representation of the “Social Brain” illustrating all the brain structures engaged in socio-cognitive functions.

Disruptions in its functions—due to neurodevelopmental, neurodegenerative, or psychiatric disorders—are often linked to deficits in social cognition and emotion recognition, emphasising its essential role in supporting adaptive social behavior ((Frith, 2008); (Adolphs, 2009)). Therefore, the mPFC acts as a vital interface between emotion, cognition, and social behavior, serving as a core neural substrate for emotion discrimination mechanisms.

1.2.1. The Social Brain through Species

Rodents do not exhibit the full range of cortical specialisation seen in primates; several functional and anatomical homologies have been recognized. In mice, for instance, the prefrontal cortex (PFC) is involved in complex functions such as sensory integration, attention, and decision-making—similar to those of the human PFC ((Le Merre et al., 2018); (Kim et al., 2016); (Miller, 2000); (Rossi et al., 2009)), and emotion discrimination (Scheggia et al., 2020).

Similarly, the cingulate cortex in rodents exhibits both functional similarities and anatomical differences compared to its human counterpart. In both species, the cingulate is involved in functions such as memory (Lenartowicz & McIntosh, 2005), reward evaluation and motivation (Elston & Bilkey, 2017), and pain perception (Johansen & Fields, 2004). In rodents, this region is typically divided into Cg1 and Cg2, which are located dorsally and differ in connectivity and function. Conversely, the primate cingulate cortex is more commonly divided into the anterior (ACC) and mid-cingulate cortex (MCC), based on cytoarchitectural features.

A key challenge occurs when attempting to map rodent cingulate areas onto the human ACC/MCC framework. The border between Cg1 and Cg2 in rodents runs perpendicular to the ACC/MCC division seen in primates, making direct comparisons difficult (van Heukelum et al., 2020). Despite this, many studies still equate rodent Cg1 and Cg2 with the MCC for consistency in comparative research. However, this oversimplification risks overlooking important differences in function and connectivity.

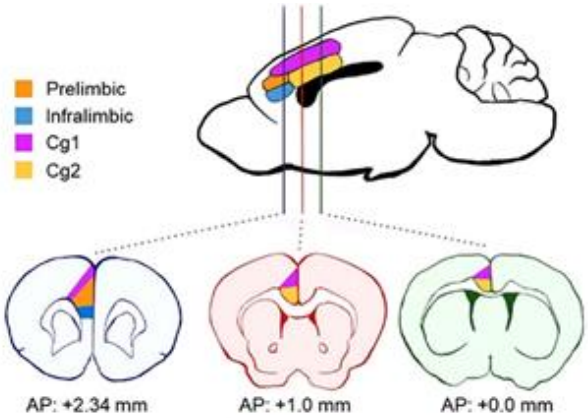

Fig. 3 Schematics of anatomical divisions in the prefrontal cortex. Areas according to Paxinos' Mouse Brain Atlas (Franklin and Paxinos, 2001). The cingulate cortex is divided horizontally into two distinct regions across the coronal plane (Cg1 and Cg2). (Francis-Oliveira et al., 2022)

Understanding these interspecies homologies and divergences is crucial for the translational validity of animal models in neuroscience, particularly in the investigation of social cognition and neuropsychiatric disorders. While mice offer powerful genetic and circuit-level tools, such as optogenetics and in vivo imaging, their simplified cortical structure necessitates careful interpretation when compared to the human brain. Nonetheless, conserved functions in structures, like the mPFC and the ACC, provide a compelling basis for exploring the neural foundations of social behavior in health and disease.

1.3 Emotion Recognition Deficits Across Neuropsychiatric Disorders

Impairments in emotion discrimination are observed across various neurological conditions. In autism spectrum disorder or schizophrenia, social cognitive deficits are central features, while in conditions like Parkinson's or Alzheimer's disease, they are more subtle and more complicated to recognise (Henry et al., 2016).

Research has shown that people with Parkinson's disease often struggle with facial recognition and understanding emotions, particularly in identifying emotional categories ((Borg et al., 2012); (Heller et al., 2018);(Jacobs et al., 1995);(Mattavelli et al., 2021)). They tend to find it more challenging to recognise negative emotions, such as anger, disgust, and fear, than positive ones, such as happiness and surprise ((Gray & Tickle-Degnen, 2010);(Kan et al., 2002); (Lawrence et al., 2007)).

Dysfunction in social cognition is common in neurodegenerative diseases like Alzheimer's disease (AD). Early in Alzheimer's, when mild episodic memory issues are present, deficits in emotion processing are often subtle and complex to detect clinically. As the disease advances and memory problems worsen, deficits in other cognitive areas become more evident. Typically, individuals with AD show reduced emotion processing skills, including trouble recognizing and differentiating emotions, as demonstrated by tests such as the Ekman Face's test ((Henry et al., 2016);(Kumfor et al., 2014);(Miller et al., 2012)).

Post-traumatic stress disorder (PTSD) patients often experience difficulties with cognitive functions and emotional regulation. They frequently show impairments in processing emotional information, characterised by abnormal emotional responses and expressions ((Ehring & Quack, 2010); (Frewen et al., 2017); (Miles et al., 2016)). They also find it more challenging to interpret

emotions from facial expressions compared to healthy individuals accurately ((Bardeen et al., 2013); (Castro-Vale et al., 2020)). Furthermore, PTSD patients tend to have trouble recognizing negative emotions, such as fear and sadness (Poljac et al., 2011). Neuroimaging studies have linked these cognitive deficits to significant reductions in brain volume, particularly in regions such as the hippocampus ((Bremner et al., 1997); (Gilbertson et al., 2002); (Villarreal et al., 2002)), amygdala (Morey et al., 2012), the mPFC (Rauch et al., 2003), and the ACC ((Kitayama et al., 2006); (Woodward et al., 2006)). However, it remains unclear whether these structural changes are a pre-existing vulnerability or develop as a consequence of trauma.

Difficulties in recognizing and expressing facial emotions are key features in conditions with cognitive impairments, such as schizophrenia (SCZ) and Autism spectrum disorders (ASD). In schizophrenia, many studies strongly suggest that patients find it hard to accurately identify emotions in others through facial cues ((Gur et al., 2002); (Kohler et al., 2010); (Mandal et al., 1998)). Specifically, individuals with SCZ exhibit altered abilities to understand and infer others' mental states, indicating an impaired theory of mind (ToM) ((Fett et al., 2011); (Green et al., 2008); (Pickup & Frith, 2001)), which may explain many of the positive and negative symptoms associated with SCZ. Neuroimaging studies of emotional processing have linked recognition deficits in SCZ patients to abnormal neural activity in regions such as the prefrontal cortex, amygdala, and visual areas ((Dyck et al., 2014); (Garcia-Leon et al., 2021); (Spilka et al., 2015); (Takahashi et al., 2004)). People with ASD, a lifelong neurodevelopmental disorder, often have challenges in socio-cognitive tasks such as recognizing, distinguishing, and remembering facial expressions (Lai et al., 2014). They tend to perceive faces atypically ((Adolphs et al., 2001); (Davies et al., 1994)), have impaired emotional processing (Corbett et al., 2009), and experience differences in mental states (Senju, 2012). However, research on emotion recognition in ASD remains inconsistent. Some studies indicate that individuals with ASD struggle with identifying emotions accurately. In contrast, others demonstrate that they perform similarly to healthy controls, often employing compensatory strategies such as verbal mediation or feature-based learning (Harms et al., 2010). This variability arises from factors such as differences in participant demographics, task designs, and measurement approaches, underscoring the complexity of understanding emotion recognition.

In summary, accurately interpreting others' emotions is crucial for effective communication in social settings. This ability is crucial for everyday interactions and building relationships with others ((Dunbar, 2009); (Fett et al., 2011)). Deficits in socio-cognitive skills can negatively impact the quality of life (Penn et al., 1997), leading to social isolation, loneliness, and poorer overall well-being ((Green et al., 2008); (Penn et al., 1997)). These social difficulties often manifest as challenges in understanding others' mental states and recognizing that these may differ from one's own, which disrupts social perception. Such disruptions hinder accurate interpretation of facial expressions, body language, and voice cues, resulting in inappropriate behavioural responses (Henry et al., 2016). Over the past twenty years, neuroscience has extensively explored the neurobiological mechanisms behind emotion recognition. However, effective treatments for these social deficits remain scarce, mainly because our understanding of their biological foundations is still limited.

This is why it is crucial to investigate emotion recognition further, including at the cellular and circuit levels, to provide new insights for a more accurate and targeted therapeutic approach in the future.

1.4 Emotion Recognition in Mice: a Breakthrough Behavioural Test

As previously noted, studying the brain circuits involved in emotion recognition is crucial for understanding the neuronal and non-neuronal mechanisms underlying these functions. Given the importance of socio-cognitive skills in daily social interactions, the limited knowledge about the brain circuits that enable us to perceive others' emotions represents a major gap in our understanding. Therefore, exploring the neurobiological processes underlying emotion recognition is vital for a comprehensive understanding of social brain functioning in both healthy and pathological states.

The Emotion Discrimination Task (EDT) used in this research was created by Papaleo's team ((Ferretti et al., 2019; V. Ferretti & F. Papaleo, 2019); (Scheggia et al., 2020)) and is inspired by human emotion recognition tests (ERT) that evaluate the ability to identify basic emotional expressions. These human tests usually involve presenting both positive and negative emotional stimuli ((Ekman, 1992); (Kohler et al., 2003); (Cecilione et al., 2017)). In response, we designed

a two-choice discrimination task that focused on the observable behaviors of the observer mice, incorporating methods to elicit both positive and negative emotional states in the demonstrator mice.

Our study aimed to determine whether a testing mouse, referred to as the "observer," could distinguish unfamiliar peers by sensing a positive emotional state. We presented the observer mice with two "demonstrators" that differed in their emotional condition. One remained neutral, while the other was given 1 hour of free access to water after 23 hours of water deprivation (see Figures 4A and 4B). Water was used as a reward to avoid olfactory cues that might distinguish the demonstrators. We hypothesized that relief from stressful water deprivation would evoke a positive emotional state called "relief." Our findings demonstrated that 1 hour of ad libitum water access resulted in a conditional place preference in mice that experienced 23 hours of water deprivation, but not in mice with ad libitum water access (see Figures 4E and 4F). Furthermore, relief mice exhibited lower corticosterone levels after water was provided (see Figure 4G). Both male and female observers showed increased social exploration towards the relief demonstrator compared to the neutral one, particularly within the first two minutes of the task (Figures 4C and 4D). There were no significant changes in rearing or grooming behaviors directed at the demonstrators throughout the session (Figures 4H and 4I). Additionally, observers showed typical reductions in locomotor activity (Figure 4J) without exhibiting freezing, escape attempts, or other stress-related behaviors during the test session. Overall, these findings suggest that mice can recognise and respond socially to unfamiliar conspecifics in a positively valence emotional state.

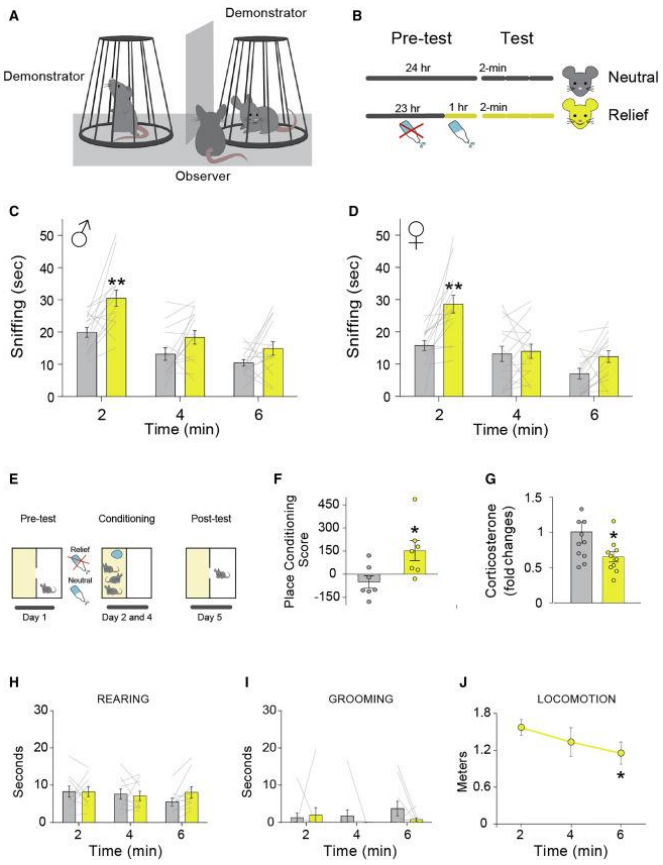

Fig.4 Mouse Emotion Discrimination for Relief.

From (Ferretti et al., 2019) Current Biology

Schematic drawing of the test setting. (B) Timeline of pre-test and test procedures to evoke in one of the two demonstrators a "relief" state during the testing phase. (C and D) Time (in seconds) spent sniffing demonstrators in neutral (gray bars) or water-induced relief (yellow bars) states displayed by (C) male and (D) female observer mice during the 6 min of the test, divided into three consecutive 2-min epochs (first 2-min RM ANOVA for males $F_{1,14} = 15.07$, $p = 0.001$ and females $F_{1,14} = 14.60$, $p = 0.001$; no significant differences for the 2- to 4-min and 4- to 6-min epochs). $**p < 0.005$ versus the exploration of the neutral demonstrator. n = 15 observers per group. (E) Place conditioning procedure used to assess whether the relief manipulation was associated with a negative-, neutral-, or positive-valence affective state. (F) Place conditioning scores (in seconds) displayed by mice conditioned during a neutral (gray bar) or relief (yellow bar) state. For each mouse, a place conditioning score was calculated as the post- minus the pre-conditioning time spent in the conditioning-paired compartment of the apparatus. A positive score indicates place preference, a negative score a place aversion, and 0 no place conditioning (t test: $df = 12$; $p = 0.02$). $*p < 0.05$ versus the neutral control group. n = 7 per group. (G) Blood corticosterone levels displayed by demonstrator mice immediately after a period of 24-h water deprivation (gray bar) or after a period of 1 h ad libitum access to water following 23-h water deprivation (yellow bar; t test: df: 19; $p = 0.05$). $*p = 0.05$ versus water deprived mice. n = 11 per group. (H and I) Time (in seconds) spent in (H) rearing and (I) grooming in proximity of demonstrators in neutral (gray bars) or relief (yellow bars) state displayed by observer mice during the test (RM ANOVAs showed no significant differences). (J) Locomotor activity displayed by the same observer mice during the test (RM ANOVA $F_{2, 18} = 4.35$; $p = 0.04$). $*p < 0.05$ versus minute 0–2. n = 10 observers. Error bars represent standard error of the mean.

We also developed a different protocol for negative affective states (Scheggia et al., 2020). In this procedure, we used the same EDT setup. However, the observers were presented with a demonstrator that had undergone mild stress, involving 15 minutes of acute restraint before the emotion discrimination task, alongside a neutral one (see Fig.5A). We observed increased exploration directed toward the stressed demonstrator (Fig.5B) and more time spent in the corresponding zone of the apparatus (see Fig.5C). Furthermore, mice initially entered the zone associated with the stressed demonstrator (see Fig.5D) and spent longer durations in this zone during the first 2 minutes of the test (Fig.5E). The total number of visits did not significantly differ between the stressed and neutral demonstrators (see Fig.5F). Data from EDTs performed on naive animals, as well as on mice implanted with electrodes and tested under 'light off' conditions, were combined and presented as percent exploration of the stress demonstrator (see Fig.5G). Affective state discrimination was a consistently observable behavior, with only 12% of mice failing to discriminate between a stressed and a neutral affective state (stress, 13 out of 93; see Fig.5H). The exploration scores for the stressed and relieved demonstrators followed a normal distribution (D'Agostino and Pearson normality test, stressed: n=93, K2=1.54, P=0.46). These results indicate that affective state discrimination is a stable trait in mice. No differences were observed between male and female mice in their ability to discriminate between sex-matched stressed demonstrators (see Fig.5I).

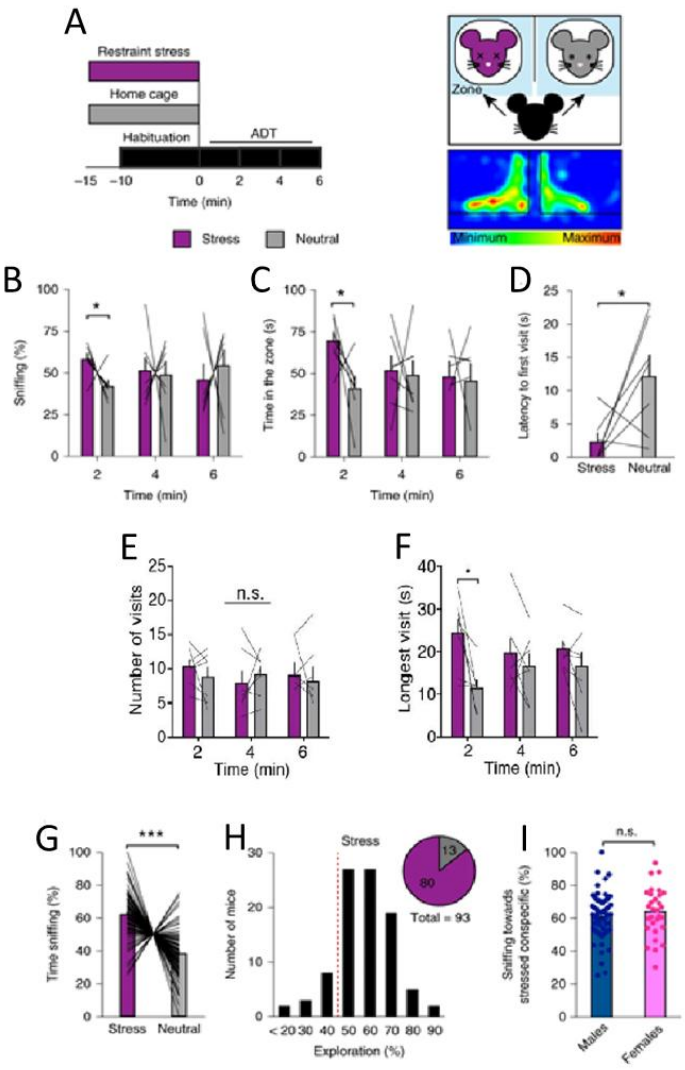

Fig.5 Mouse Emotion Discrimination for Stress.

Adapted from (Scheggia et al., 2020) Nature Neuroscience

(A) Timeline of pre-test and test procedures to evoke in one of the two demonstrators a ''stress'' manipulation during the testing phase. In the stress protocol, one demonstrator (stress, purple) was subjected to the restraint stress test for 15 min immediately before the beginning of the ADT. The other demonstrator (neutral, gray) waited undisturbed in the home cage. (B) Increased sniffing of the stressed demonstrator (two-tailed multiple t-test, Bonferroni correction, 2 min: t = 3.22, d.f. = 12, P = 0.021) (C) and time spent in the zone with the stressed compared with the neutral demonstrator (two-tailed multiple t-test, Bonferroni correction, 2 min: t = 3.23, d.f. = 12, P = 0.021). (D) The latency to the first visit was significantly lower for the stressed demonstrator than for the neutral demonstrator (two-tailed paired t-test: t = 2.43, d.f. = 6, P = 0.050). (E), Average number of visits to each zone did not differ (two-tailed multiple t-test, Bonferroni correction, t=0.81, df=12, p>0.999). (F) Observers made longer visits in the zone related to the stressed demonstrators (two-tailed multiple t-test, Bonferroni correction, 2 min: t=3.46, df=12, p=0.017). (G) More exploration of the stressed than of the neutral demonstrator in several replications of the ADT (two-

*tailed paired t-test: t = 8.22, d.f. = 92, P < 0.0001). (H) (I) Exploration of the stressed demonstrator was higher than chance in a large number of mice (80 of 93, one-sample t-test against chance, defined as 50%: t = 8.22, d.f. = 92, P < 0.0001) (H) and did not change depending on gender (63 male, 30 female; two-tailed unpaired t-test: t = 0.92, d.f. = 91, P = 0.357). Bar and line graphs show mean ± s.e.m. *P < 0.05. **P < 0.005. ***P < 0.0005. n.s., not significant.*

Overall, these results showed that mice can similarly discriminate others based on both positive and negative affective states.

1.5 GABA-ergic system

It is well known that GABA is the primary inhibitory neurotransmitter in the mammalian brain, accounting for approximately 30% of cortical neurons in rats (Bloom & Iversen, 1971) and 25% in primates (Jones, 1993). During prenatal stages, GABA plays a crucial role in neurodevelopment, as it is excitatory. In contrast, in the adult stage, GABA acquires its inhibitory function in the nervous system. GABA can modulate the functioning of other organs and systems, including the endocrine and immune systems. Dysfunctions of GABA are responsible for various pathologies, both neurological and non-neurological, including schizophrenia, depression, and immunological disorders (Vargas, 2018).

1.5.1 GABA neurotransmission

Three enzymes are involved in GABA synthesis: glutamate decarboxylase (GAD), GABA transaminase (GABA-T), and succinate semi-aldehyde dehydrogenase (SSADH). The process, known as the GABAergic shunt, begins with glutamate, which is derived from glucose. The first enzyme in the process is GAD, which produces GABA by catalyzing the decarboxylation of glutamate. This enzyme is cytoplasmic and has two subtypes: GAD65 and GAD67. It can be found in both interneurons and non-neuronal tissues.

After being synthesized, GABA is stored in vesicles that move to the presynaptic terminals and are released when a nervous stimulus depolarizes the synaptic terminal.

The released GABA reaches the postsynaptic neuron, where it binds to specific receptors. The GABA that does not interact with the postsynaptic receptors is taken up for metabolism, either

by the presynaptic neuron or by glial cells. Reuptake is performed by a GABA cytoplasmic membrane transporter (GAT), of which four subtypes have been identified (GAT 1-4). Inside the cell, GABA is degraded to succinic semi-aldehyde through the enzymes GABA-T and SSADH, and then to succinate. The GABA-T enzyme is present throughout the nervous system in neurons, glial cells, and ependymal cells ((Bak et al., 2006); (Bowery et al., 1979)) (Fig. 7).

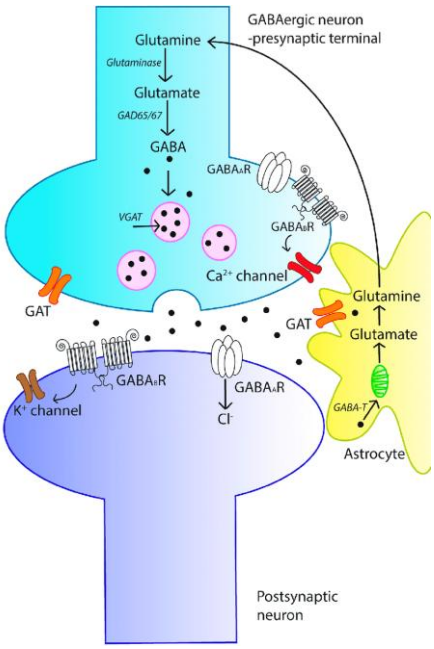

Fig. 7 Scheme of GABA Neurotransmission. GABA is synthesized in the presynaptic terminal from glutamate by glutamic acid decarboxylase (GAD). GABA is then recruited into synaptic vesicles via the action of vesicular GABA transporter (vGAT). Following membrane depolarization, GABA is released into the synapse and can bind to either ionotropic GABAA receptors (GABAAR) or metabotropic GABAB receptors (GABABR) on the postsynaptic membrane, resulting in inhibition of the postsynaptic neuron. Released GABA is cleared from the synapse by membrane-bound GABA transporters (GATs), localized to neurons and astrocytes. In astrocytes, GABA is recycled into synaptic vesicles or taken up by mitochondria, where it is metabolized by GABA transaminase (GABA-T) to glutamine for neuronal uptake. (Govindpani et al., 2017)

1.5.2 GABA receptors

There are three receptors for GABA: two fast-acting receptors, GABA-A and GABA-C, and one with slow action, GABA-B ((Dionisio et al., 2011); (Bowery et al., 1985)).

The GABA-A receptor is a pentameric chloride ionotropic channel receptor composed of five different subunits, each with various isoforms, resulting in a total of 19 subunits: alpha (α1-6), beta (β1-3), gamma (γ1-3), and delta (δ), epsilon (ε), theta (θ), pi (π), and rho (isoforms ρ1-3). Most receptors contain two alpha subunits, two beta subunits, and one gamma subunit. The specific combination of subunits influences the efficacy of the GABA agonist site and the affinity for other allosteric sites. Each subunit features four transmembrane hydrophobic domains embedded in the cell membrane: M1, M2, M3 and M4 (Bowery et al., 1985). Activated GABA-A receptors allow chlorine ions to enter, causing hyperpolarization of the cell membrane

and reducing nerve impulse conduction. This results in postsynaptic inhibitory potentials (IPSPs).

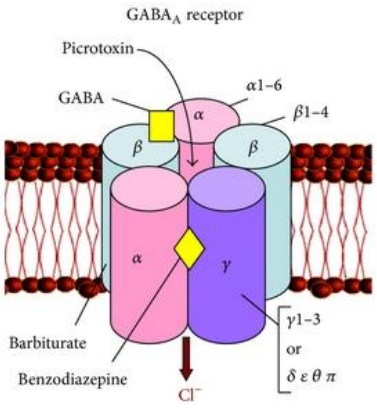

Fig. 8 GABA A receptor (Popova, 2014)

The GABA B receptor is a heterodimer linked to a G protein, placing it within the family of metabotropic receptors. This receptor is a membrane protein that features seven transmembrane hydrophobic domains. Generally, the GABA-B receptor is anchored in the plasma membrane of both presynaptic and postsynaptic terminals, where it modulates calcium and potassium channels by interacting with protein G and adenylyl cyclase. Pre-synaptically, when the GABA-B receptor interacts with an agonist, calcium influx decreases, resulting in lower calcium levels and a reduced release of excitatory neurotransmitters, such as glutamate, thereby decreasing the excitatory glutamatergic effect. Conversely, activation of the postsynaptic GABA-B receptor by a GABAergic agonist increases potassium efflux into the extracellular medium, producing a slow inhibitory potential that hyperpolarizes the membrane and generates IPSPs ((Chronwall et al., 2001); (Kaupmann et al., 1998); (Bormann, 2000)).

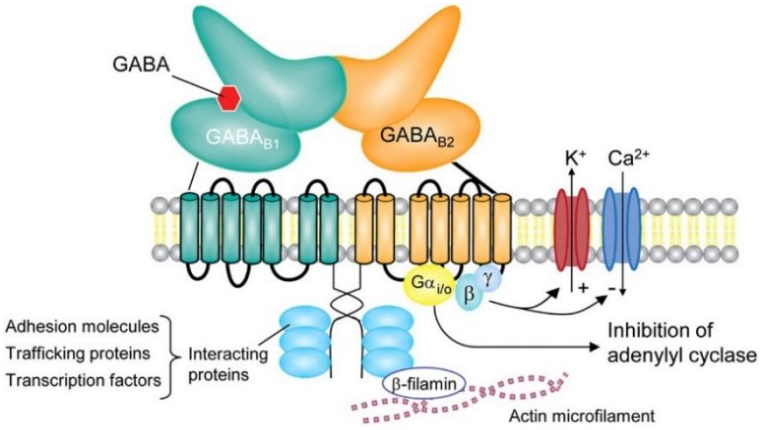

Fig. 9 GABA B receptor (Benarroch, 2012)

The GABA-C receptor is an ionotropic receptor that was isolated in the vertebrate retina. GABA-C receptors are characterised as GABA receptors that do not respond to the GABA analogues bicuculline or baclofen. They are receptors that regulate chloride channels, generating IPSPs (Bowery & Brown, 1997).

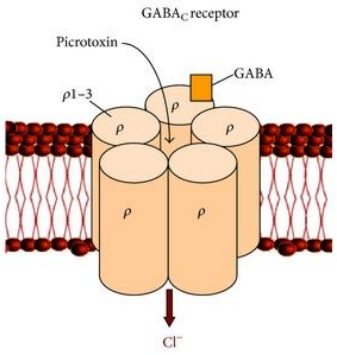

Fig. 10 GABA C receptor (Popova, 2014)

1.5.3 GABA-ergic interneurons

Cortical networks rely on highly interconnected and dynamic microcircuits composed of two types of neurons: glutamatergic excitatory neurons (also known as principal cells, PCs) and GABAergic interneurons (INs). The activity of these latter ones is crucial for information processing in the cortex (Tremblay et al., 2016).

From an anatomical perspective, cortical GABAergic interneurons are morphologically diverse, whether considering their somas, dendrites, axons, or their specific connection points with pyramidal cells or other interneurons ((Kawaguchi & Kubota, 1997); (Kubota, 2014); (Markram et al., 2004); (Somogyi et al., 1998)).

The IN's importance has been recognized since they were first described, and data suggest that they play significant roles in several cortical functions, including dynamic range modulation of cortical circuits, plasticity, and the maintenance of the excitatory-inhibitory balance. Indeed, most problems with inhibitory INs have been associated with the development of several types of epilepsy (Goldberg & Coulter, 2013), schizophrenia, anxiety disorders, and autism ((Lewis, 2014); (Marin, 2024)).

Because of their great diversity and small proportion within the overall neuronal population, they have been challenging to study. Recent research employing new molecular genetic methods

of labelling has helped improve understanding of INs' circuits and their role in cortical functions in animals ((Kepecs & Fishell, 2014); (Roux & Buzsaki, 2015)).

1.5.3.1 GABAergic interneurons in the mPFC

As previously discussed, GABAergic interneurons (INs) in the medial prefrontal cortex (mPFC) are a highly heterogeneous population, comprising distinct subtypes that, despite their shared release of γ-aminobutyric acid (GABA), exhibit profound differences in their molecular markers, connectivity patterns, synaptic dynamics, and intrinsic membrane properties. These differences enable highly specific spatio-temporal regulation of pyramidal neuron activity and local circuit function (Tremblay et al., 2016). One method of distinguishing these interneuron subpopulations involves characterizing their responses to neuromodulators such as acetylcholine (ACh), serotonin (5-HT), norepinephrine, and dopamine—each of which plays a crucial role in modulating prefrontal network states and behavioral flexibility ((Kawaguchi & Shindou, 1998); (Munoz & Rudy, 2014)).

In the mPFC, all major classes of cortical GABAergic interneurons—particularly those expressing parvalbumin (PV), somatostatin (SOM), and cholecystokinin (CCK)—are present, although their laminar distribution and relative densities differ from other neocortical areas. Notably, SOM+ and CCK+ interneurons appear to be more prevalent than PV+ cells in the infralimbic (IL) and prelimbic (PrL) cortices, especially in the superficial layers ((Whissell et al., 2015); (Liu et al., 2020)). This shift in cell-type composition suggests a region-specific rebalancing of inhibitory control mechanisms, which may contribute to the mPFC's unique roles in emotional regulation and executive function.

Traditionally, interneurons have been broadly classified as inhibitory cells that target pyramidal neurons (Fino & Yuste, 2011). Nonetheless, recent findings in the mPFC reveal a more detailed pattern of target selectivity. For instance, PV+ and SOM+ interneurons preferentially inhibit layer 2 cortico-amygdala (CA) projecting neurons over nearby cortico-cortical (CC) or cortico-striatal (CS) pyramidal cells ((McGarry & Carter, 2016); (Lu et al., 2017)). This targeted inhibition also extends to deeper cortical layers, where these interneurons favor pyramidal tract

(PT) neurons in layer 5 rather than intratelencephalic (IT) neurons (Lu et al., 2017). Such projection-specific inhibitory patterns highlight the precision of GABAergic microcircuits in the mPFC and their essential role in controlling information flow across different output pathways.

Summary Table 1

Subtype	Molecular Marker(s)	Laminar Distribution	Preferred Targets	Functional Role
Parvalbumin+ (PV)	Parvalbumin	Broad (especially L2–L5)	Cortico-amygdala > cortico-cortical / cortico-striatal (L2); PT > IT (L5)	Fast, perisomatic inhibition; precise control of spike timing; network synchronization
Somatostatin+ (SOM)	Somatostatin	Enriched in superficial layers (L2–L3)	Similar to PV: CA > CC/CS (L2); PT > IT (L5)	Dendritic inhibition; modulates synaptic integration and plasticity
Cholecystokinin+ (CCK)	CCK, often CB1R+	Superficial layers (L2–L3), variable	Less defined projection specificity	Slower inhibition; modulated by endocannabinoids; emotional regulation
VIP+ (Vasoactive Intestinal Peptide)	VIP	Primarily L1–L3	Inhibits other INs (especially SOM+), disinhibits pyramidal neurons	Gating of inhibition, contributes to top-down modulation

1.5.3.2 GABAergic interneurons in the ACC

Although limited studies have been conducted on the inhibitory interneurons of the ACC, typical neocortical distribution patterns can serve as a rough guide: PV interneurons make up about 40% of the GABAergic population, SOM cells around 30%, and VIP and 5-HT_3aR-presenting neurons approximately the remaining 30% ((Rudy et al., 2011); (Almasi et al., 2019); (Girgenti et al., 2019)).

In the ACC specifically, dual tracing studies in mice reveal differential afferent connectivity: PV interneurons in the ACC preferentially receive monosynaptic excitatory input from the lateral

posterior thalamic nucleus, whereas projections from the ventral hippocampus more strongly target SOM interneurons (Qi et al., 2025). Functionally, these subtypes serve divergent roles: PV cells, which often display fast-spiking basket and chandelier morphologies, deliver perisomatic inhibition with high temporal precision, which is essential for controlling spike timing and gamma-band synchrony. SOM interneurons—often Martinotti cells with axonal projections to layer I—provide dendritic inhibition and integrate inputs more gradually, modulating excitatory drive over a longer timescale (Cardin, 2018).

Furthermore, interneuron-to-interneuron connectivity creates a reciprocal inhibitory circuit: SOM cells inhibit PV interneurons, and PV cells reciprocally inhibit SOM cells. VIP interneurons predominantly inhibit SOM neurons—thus disinhibiting pyramidal neurons and PV cells—and also connect reciprocally with PV cells (Cardin, 2018).

Summary Table 2

Interneuron Subtype	Approximate % of GABAergic Neurons	Inputs & Connectivity Summary
PV (Parvalbumin)	~40%	Input from lateral posterior thalamus; fast perisomatic inhibition; receives inhibition from SOM and VIP; strongly interconnects with other PVs
SOM (Somatostatin)	~30%	Input from ventral hippocampus; dendritic inhibition; reciprocal connections with PV; inhibited by VIP
VIP / 5-HT$_3$aR+	~30% (VIP subset ~10–15%)	Inhibit SOM (leading to disinhibition); also target PV; less extensively characterised in ACC.

1.5.3.3 Somatostatin interneurons

One specific type of cortical GABAergic interneuron (IN) expressing somatostatin has recently attracted significant interest in the neuroscience community due to its unusual properties. While most GABAergic interneurons target the soma or proximal dendrites of pyramidal cells, SOM interneurons appear to target the distal dendrites ((Dennison-Cavanagh et al., 1993); (de Lima & Morrison, 1989); (Kawaguchi & Kubota, 1996); (Kawaguchi & Kubota, 1997); (Wang et al.,

2004)). This is reflected in pyramidal neurons by a variation in the dynamics of excitatory inputs. Although most INs have strongly or moderately depressing excitatory synapses, excitatory inputs onto SOM INs are highly facilitating ((Beierlein et al., 2003); (Kapfer et al., 2007); (Pouille & Scanziani, 2004); (Silberberg & Markram, 2007); (Thomson, 2003); (Xu et al., 2013)). The short-term plasticity of excitatory synapses onto GABAergic interneurons was assessed by focusing on the postsynaptic cells: the same excitatory axon appeared to have depressing synapses on a PV cell and facilitating synapses onto SOM INs ((Buchanan et al., 2012); (Reyes et al., 1998); (Scanziani et al., 1998)).

As a result of these facilitative dynamics and other membrane properties that allow excitatory postsynaptic current (EPSP) summation, excitatory inputs to these cells produce supra-linear responses. The facilitation onto SOM INs enables a single high-frequency burst from one presynaptic cell to recruit SOM INs and generate feedback inhibition ((Kapfer et al., 2007); (Silberberg & Markram, 2007)). Another feature is a muscarinic-mediated depolarization. If the depolarization is sufficiently strong, it can produce prolonged spiking ((Beierlein et al., 2000); (Fanselow et al., 2008); (Kawaguchi, 1997); (Xu et al., 2013)).

Based on morphology, SOM INs can be divided into two main subgroups: Martinotti and non-Martinotti cells. Martinotti cells are SOM interneurons with an axonal plexus in layer 1, where they target the tuft dendrites of pyramidal cells, including making synapses on spines (Fig. 11; (Chiu et al., 2013); (Kawaguchi & Kubota, 1996); (Wang et al., 2004)). Martinotti cells are also found in layers 2/3 and 5/6. Besides arborizing in L1, a significant portion of their axonal arbor extends into the layer where their soma resides.

Non-Martinotti cells are, instead, SOM INs that lack this substantial axonal plexus. Since they form synapses onto different subcellular compartments or cell types, SOM INs have a different influence on cellular and network computations than Martinotti cells.

SOM INs seem to diffuse in the supragranular layers, and Martinotti cells comprise a substantial portion of those in the infragranular layers. The axon of most SSM INs in L4 of S1 mostly remains within this layer, with some projecting to L2/3 ((Ma et al., 2006); (Xu et al., 2013)).

In addition to these types, a few SOM cells in deep layers express nNOS (neuronal nitric oxide synthase) and are believed to have long-range projecting axons (Tamamaki & Tomioka, 2010).

Currently, it is not well established how other reported differences among SOM INs fit into this morphological classification. SOM INs also show molecular heterogeneity. About 15–30% of the SOM INs in the mouse neocortex express CR, along with several other molecules, which define additional subpopulations.

The relationship between molecular expression and morphological or electrophysiological diversity remains unclear. However, recent transcriptional analysis of single cells suggests that SOM INs consist of genetically distinct subtypes (Tasic et al., 2016), and some molecules expressed by these subpopulations are evidently important physiologically.

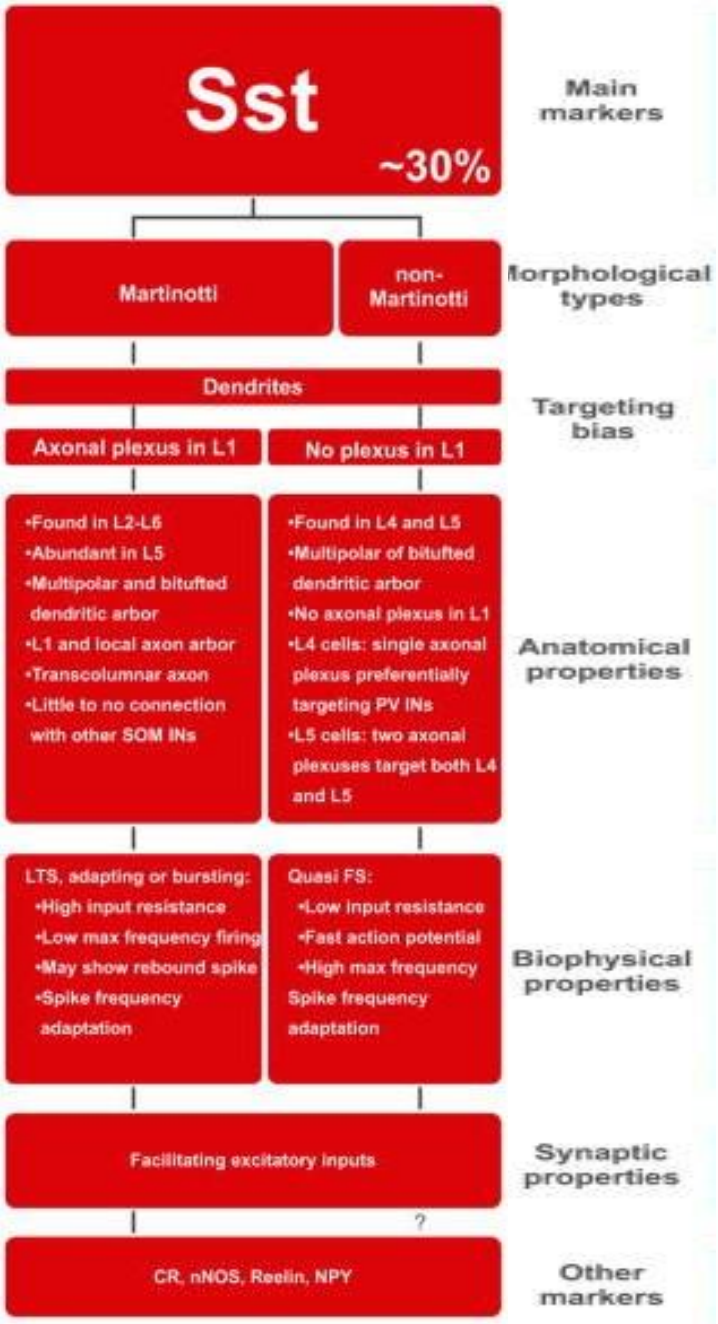

Fig. 11 Diversity, Classification, and Properties of Neocortical SOM GABAergic Ins. Depicted morphological features, cellular and subcellular targeting biases, expression of other markers, anatomical, electrophysiological, and synaptic properties (Tremblay et al., 2016)

Bibliography

1. Adolphs, R. (2001). The neurobiology of social cognition. *Curr Opin Neurobiol*, *11*(2), 231–239. https://doi.org/10.1016/s0959-4388(00)00202-6
2. Adolphs, R. (2009). The social brain: neural basis of social knowledge. *Annu Rev Psychol*, *60*, 693–716. https://doi.org/10.1146/annurev.psych.60.110707.163514
3. Adolphs, R., Sears, L., & Piven, J. (2001). Abnormal processing of social information from faces in autism. *J Cogn Neurosci*, *13*(2), 232–240. https://doi.org/10.1162/089892901564289
4. Almasi, Z., David, C., Witte, M., & Staiger, J. F. (2019). Distribution Patterns of Three Molecularly Defined Classes of GABAergic Neurons Across Columnar Compartments in Mouse Barrel Cortex. *Front Neuroanat*, *13*, 45. https://doi.org/10.3389/fnana.2019.00045
5. Amodio, D. M., & Frith, C. D. (2006). Meeting of minds: the medial frontal cortex and social cognition. *Nat Rev Neurosci*, *7*(4), 268–277. https://doi.org/10.1038/nrn1884
6. Anastasiades, P. G., Collins, D. P., & Carter, A. G. (2021). Mediodorsal and Ventromedial Thalamus Engage Distinct L1 Circuits in the Prefrontal Cortex. *Neuron*, *109*(2), 314–330 e314. https://doi.org/10.1016/j.neuron.2020.10.031
7. Anderson, S. W., Barrash, J., Bechara, A., & Tranel, D. (2006). Impairments of emotion and real-world complex behavior following childhood- or adult-onset damage to ventromedial prefrontal cortex. *J Int Neuropsychol Soc*, *12*(2), 224–235. https://doi.org/10.1017/S1355617706060346
8. Andreasen, N. C., Paradiso, S., & O'Leary, D. S. (1998). "Cognitive dysmetria" as an integrative theory of schizophrenia: a dysfunction in cortical-subcortical-cerebellar circuitry? *Schizophr Bull*, *24*(2), 203–218. https://doi.org/10.1093/oxfordjournals.schbul.a033321
9. Andrews-Hanna, J. R., Reidler, J. S., Sepulcre, J., Poulin, R., & Buckner, R. L. (2010). Functional-anatomic fractionation of the brain's default network. *Neuron*, *65*(4), 550–562. https://doi.org/10.1016/j.neuron.2010.02.005
10. Antonelli F., Monai A., Bernardi F., Koul A., Engel N.M., Carta I., Managò F., Benedetti A., Borruto A.M., Spattini L., Maltese F., Yi C., Dumas G., Panzeri S., Novembre G., Papaleo F. . (2025). *Inter-Brain Dynamics Modulate Emotion Discrimination*.
11. Apps, M. A., Rushworth, M. F., & Chang, S. W. (2016). The Anterior Cingulate Gyrus and Social Cognition: Tracking the Motivation of Others. *Neuron*, *90*(4), 692–707. https://doi.org/10.1016/j.neuron.2016.04.018
12. Arioli, M., Cattaneo, Z., Ricciardi, E., & Canessa, N. (2021). Overlapping and specific neural correlates for empathizing, affective mentalizing, and cognitive mentalizing: A coordinate-based meta-analytic study. *Hum Brain Mapp*, *42*(14), 4777–4804. https://doi.org/10.1002/hbm.25570
13. Bak, L. K., Schousboe, A., & Waagepetersen, H. S. (2006). The glutamate/GABA-glutamine cycle: aspects of transport, neurotransmitter homeostasis and ammonia transfer. *J Neurochem*, *98*(3), 641–653. https://doi.org/10.1111/j.1471-4159.2006.03913.x

14. Barbas, H. (2010). *Prefrontal Cortex: Structure and Anatomy*.
15. Bardeen, J. R., Kumpula, M. J., & Orcutt, H. K. (2013). Emotion regulation difficulties as a prospective predictor of posttraumatic stress symptoms following a mass shooting. *J Anxiety Disord*, *27*(2), 188–196. https://doi.org/10.1016/j.janxdis.2013.01.003
16. Barrash, J., Tranel, D., & Anderson, S. W. (2000). Acquired personality disturbances associated with bilateral damage to the ventromedial prefrontal region. *Dev Neuropsychol*, *18*(3), 355–381. https://doi.org/10.1207/S1532694205Barrash
17. Bechara A, D. A. (2005). The somatic marker hypothesis: A neural theory of economic decision *Games and Economic Behavior*, *52*, 336–372. https://doi.org/https://doi.org/10.1016/j.geb.2004.06.010
18. Bechara, A., Damasio, A. R., Damasio, H., & Anderson, S. W. (1994). Insensitivity to future consequences following damage to human prefrontal cortex. *Cognition*, *50*(1-3), 7–15. https://doi.org/10.1016/0010-0277(94)90018-3
19. Bechara, A., Damasio, H., & Damasio, A. R. (2000). Emotion, decision making and the orbitofrontal cortex. *Cereb Cortex*, *10*(3), 295–307. https://doi.org/10.1093/cercor/10.3.295
20. Beckmann, M., Johansen-Berg, H., & Rushworth, M. F. (2009). Connectivity-based parcellation of human cingulate cortex and its relation to functional specialization. *J Neurosci*, *29*(4), 1175–1190. https://doi.org/10.1523/JNEUROSCI.3328-08.2009
21. Beierlein, M., Gibson, J. R., & Connors, B. W. (2000). A network of electrically coupled interneurons drives synchronized inhibition in neocortex. *Nat Neurosci*, *3*(9), 904–910. https://doi.org/10.1038/78809
22. Beierlein, M., Gibson, J. R., & Connors, B. W. (2003). Two dynamically distinct inhibitory networks in layer 4 of the neocortex. *J Neurophysiol*, *90*(5), 2987–3000. https://doi.org/10.1152/jn.00283.2003
23. Benarroch, E. E. (2012). GABAB receptors: structure, functions, and clinical implications. *Neurology*, *78*(8), 578–584. https://doi.org/10.1212/WNL.0b013e318247cd03
24. Benes, F. M., Davidson, J., & Bird, E. D. (1986). Quantitative cytoarchitectural studies of the cerebral cortex of schizophrenics. *Arch Gen Psychiatry*, *43*(1), 31–35. https://doi.org/10.1001/archpsyc.1986.01800010033004
25. Benes, F. M., Kwok, E. W., Vincent, S. L., & Todtenkopf, M. S. (1998). A reduction of nonpyramidal cells in sector CA2 of schizophrenics and manic depressives. *Biol Psychiatry*, *44*(2), 88–97. https://doi.org/10.1016/s0006-3223(98)00138-3
26. Berlin, H. A., Rolls, E. T., & Kischka, U. (2004). Impulsivity, time perception, emotion and reinforcement sensitivity in patients with orbitofrontal cortex lesions. *Brain*, *127*(Pt 5), 1108–1126. https://doi.org/10.1093/brain/awh135
27. Bertero, A., Feyen, P. L. C., Zurita, H., & Apicella, A. J. (2019). A Non-Canonical Cortico-Amygdala Inhibitory Loop. *J Neurosci*, *39*(43), 8424–8438. https://doi.org/10.1523/JNEUROSCI.1515-19.2019
28. Biria, M., Banca, P., Healy, M. P., Keser, E., Sawiak, S. J., Rodgers, C. T., Rua, C., de Souza, A., Marzuki, A. A., Sule, A., Ersche, K. D., & Robbins, T. W. (2023). Cortical glutamate and GABA are

related to compulsive behaviour in individuals with obsessive compulsive disorder and healthy controls. *Nat Commun*, *14*(1), 3324. https://doi.org/10.1038/s41467-023-38695-z

29. Bloem, B., Schoppink, L., Rotaru, D. C., Faiz, A., Hendriks, P., Mansvelder, H. D., van de Berg, W. D., & Wouterlood, F. G. (2014). Topographic mapping between basal forebrain cholinergic neurons and the medial prefrontal cortex in mice. *J Neurosci*, *34*(49), 16234–16246. https://doi.org/10.1523/JNEUROSCI.3011-14.2014
30. Bloom, F. E., & Iversen, L. L. (1971). Localizing 3H-GABA in nerve terminals of rat cerebral cortex by electron microscopic autoradiography. *Nature*, *229*(5287), 628–630. https://doi.org/10.1038/229628a0
31. Borg, C., Bedoin, N., Bogey, S., Michael, G. A., Poujois, A., Laurent, B., & Thomas-Anterion, C. (2012). Implicit and explicit emotional processing in Parkinson's disease. *J Clin Exp Neuropsychol*, *34*(3), 289–296. https://doi.org/10.1080/13803395.2011.639296
32. Bormann, J. (2000). The 'ABC' of GABA receptors. *Trends Pharmacol Sci*, *21*(1), 16–19. https://doi.org/10.1016/s0165-6147(99)01413-3
33. Bowery, N. G., & Brown, D. A. (1997). The cloning of GABA(B) receptors. *Nature*, *386*(6622), 223–224. https://doi.org/10.1038/386223a0
34. Bowery, N. G., Brown, D. A., White, R. D., & Yamini, G. (1979). [3H]gamma-Aminobutyric acid uptake into neuroglial cells of rat superior cervical sympathetic ganglia. *J Physiol*, *293*, 51–74. https://doi.org/10.1113/jphysiol.1979.sp012878
35. Bowery, N. G., Hill, D. R., & Hudson, A. L. (1985). [3H](-)Baclofen: an improved ligand for GABAB sites. *Neuropharmacology*, *24*(3), 207–210. https://doi.org/10.1016/0028-3908(85)90075-9
36. Bremner, J. D., Randall, P., Vermetten, E., Staib, L., Bronen, R. A., Mazure, C., Capelli, S., McCarthy, G., Innis, R. B., & Charney, D. S. (1997). Magnetic resonance imaging-based measurement of hippocampal volume in posttraumatic stress disorder related to childhood physical and sexual abuse--a preliminary report. *Biol Psychiatry*, *41*(1), 23–32. https://doi.org/10.1016/s0006-3223(96)00162-x
37. Brothers, L. (2002). *The Social Brain: A Project for Integrating Primate Behavior and Neurophysiology in a New Domain*. https://doi.org/10.7551/mitpress/3077.003.0029
38. Buchanan, K. A., Blackman, A. V., Moreau, A. W., Elgar, D., Costa, R. P., Lalanne, T., Tudor Jones, A. A., Oyrer, J., & Sjostrom, P. J. (2012). Target-specific expression of presynaptic NMDA receptors in neocortical microcircuits. *Neuron*, *75*(3), 451–466. https://doi.org/10.1016/j.neuron.2012.06.017
39. Buckner, R. L., Andrews-Hanna, J. R., & Schacter, D. L. (2008). The brain's default network: anatomy, function, and relevance to disease. *Ann N Y Acad Sci*, *1124*, 1–38. https://doi.org/10.1196/annals.1440.011
40. Bush, G., Luu, P., & Posner, M. I. (2000). Cognitive and emotional influences in anterior cingulate cortex. *Trends Cogn Sci*, *4*(6), 215–222. https://doi.org/10.1016/s1364-6613(00)01483-2
41. Cardin, J. A. (2018). Inhibitory Interneurons Regulate Temporal Precision and Correlations in Cortical Circuits. *Trends Neurosci*, *41*(10), 689–700. https://doi.org/10.1016/j.tins.2018.07.015

42. Castro-Vale, I., Severo, M., & Carvalho, D. (2020). Lifetime PTSD is associated with impaired emotion recognition in veterans and their offspring. *Psychiatry Res*, *284*, 112666. https://doi.org/10.1016/j.psychres.2019.112666
43. Cauda, F., Geda, E., Sacco, K., D'Agata, F., Duca, S., Geminiani, G., & Keller, R. (2011). Grey matter abnormality in autism spectrum disorder: an activation likelihood estimation meta-analysis study. *J Neurol Neurosurg Psychiatry*, *82*(12), 1304–1313. https://doi.org/10.1136/jnnp.2010.239111
44. Cecilione, J. L., Rappaport, L. M., Verhulst, B., Carney, D. M., Blair, R. J. R., Brotman, M. A., Leibenluft, E., Pine, D. S., Roberson-Nay, R., & Hettema, J. M. (2017). Test-retest reliability of the facial expression labeling task. *Psychol Assess*, *29*(12), 1537–1542. https://doi.org/10.1037/pas0000439
45. Chan, A. S., Cheung, M. C., Sze, S. L., Leung, W. W., & Shi, D. (2011). An herbal nasal drop enhanced frontal and anterior cingulate cortex activity. *Evid Based Complement Alternat Med*, *2011*, 543648. https://doi.org/10.1093/ecam/nep198
46. Chiu, C. Q., Lur, G., Morse, T. M., Carnevale, N. T., Ellis-Davies, G. C., & Higley, M. J. (2013). Compartmentalization of GABAergic inhibition by dendritic spines. *Science*, *340*(6133), 759–762. https://doi.org/10.1126/science.1234274
47. Chronwall, B. M., Davis, T. D., Severidt, M. W., Wolfe, S. E., McCarson, K. E., Beatty, D. M., Low, M. J., Morris, S. J., & Enna, S. J. (2001). Constitutive expression of functional GABA(B) receptors in mIL-tsA58 cells requires both GABA(B(1)) and GABA(B(2)) genes. *J Neurochem*, *77*(5), 1237–1247. https://doi.org/10.1046/j.1471-4159.2001.00323.x
48. Collins, D. P., Anastasiades, P. G., Marlin, J. J., & Carter, A. G. (2018). Reciprocal Circuits Linking the Prefrontal Cortex with Dorsal and Ventral Thalamic Nuclei. *Neuron*, *98*(2), 366–379 e364. https://doi.org/10.1016/j.neuron.2018.03.024
49. Corbett, B. A., Carmean, V., Ravizza, S., Wendelken, C., Henry, M. L., Carter, C., & Rivera, S. M. (2009). A functional and structural study of emotion and face processing in children with autism. *Psychiatry Res*, *173*(3), 196–205. https://doi.org/10.1016/j.pscychresns.2008.08.005
50. Corcoran, K. A., & Quirk, G. J. (2007). Activity in prelimbic cortex is necessary for the expression of learned, but not innate, fears. *J Neurosci*, *27*(4), 840–844. https://doi.org/10.1523/JNEUROSCI.5327-06.2007
51. Craig, A. D. (2009). How do you feel--now? The anterior insula and human awareness. *Nat Rev Neurosci*, *10*(1), 59–70. https://doi.org/10.1038/nrn2555
52. Critchley, H. D., Mathias, C. J., Josephs, O., O'Doherty, J., Zanini, S., Dewar, B. K., Cipolotti, L., Shallice, T., & Dolan, R. J. (2003). Human cingulate cortex and autonomic control: converging neuroimaging and clinical evidence. *Brain*, *126*(Pt 10), 2139–2152. https://doi.org/10.1093/brain/awg216
53. Dal Monte, O., Krueger, F., Solomon, J. M., Schintu, S., Knutson, K. M., Strenziok, M., Pardini, M., Leopold, A., Raymont, V., & Grafman, J. (2013). A voxel-based lesion study on facial emotion recognition after penetrating brain injury. *Soc Cogn Affect Neurosci*, *8*(6), 632–639. https://doi.org/10.1093/scan/nss041

54. Dautan, D., Monai, A., Maltese, F., Chang, X., Molent, C., Mauro, D., Galbusera, A., Vecchia, D., Antonelli, F., Benedetti, A., Drago, F., Leggio, G. M., Pagani, M., Fellin, T., Gozzi, A., Schumann, G., Manago, F., & Papaleo, F. (2024). Cortico-cortical transfer of socially derived information gates emotion recognition. *Nat Neurosci*, *27*(7), 1318–1332. https://doi.org/10.1038/s41593-024-01647-x
55. Davidson, R. J., Pizzagalli, D., Nitschke, J. B., & Putnam, K. (2002). Depression: perspectives from affective neuroscience. *Annu Rev Psychol*, *53*, 545–574. https://doi.org/10.1146/annurev.psych.53.100901.135148
56. Davies, S., Bishop, D., Manstead, A. S., & Tantam, D. (1994). Face perception in children with autism and Asperger's syndrome. *J Child Psychol Psychiatry*, *35*(6), 1033–1057. https://doi.org/10.1111/j.1469-7610.1994.tb01808.x
57. de Lima, A. D., & Morrison, J. H. (1989). Ultrastructural analysis of somatostatin-immunoreactive neurons and synapses in the temporal and occipital cortex of the macaque monkey. *J Comp Neurol*, *283*(2), 212–227. https://doi.org/10.1002/cne.902830205
58. de Waal, F. B. (2008). Putting the altruism back into altruism: the evolution of empathy. *Annu Rev Psychol*, *59*, 279–300. https://doi.org/10.1146/annurev.psych.59.103006.093625
59. Dennison-Cavanagh, M. E., Papadopoulos, G., & Parnavelas, J. G. (1993). The emergence of the cortical GABAergic neuron: with particular reference to some peptidergic subpopulations. *J Neurocytol*, *22*(9), 805–814. https://doi.org/10.1007/BF01181325
60. Devinsky, O., Morrell, M. J., & Vogt, B. A. (1995). Contributions of anterior cingulate cortex to behaviour. *Brain*, *118 (Pt 1)*, 279–306. https://doi.org/10.1093/brain/118.1.279
61. Dienel, S. J., Wade, K. L., Fish, K. N., & Lewis, D. A. (2025). Alterations in Prefrontal Cortical Somatostatin Neurons in Schizophrenia: Evidence for Weaker Inhibition of Pyramidal Neuron Dendrites. *Biol Psychiatry*, *98*(2), 156–166. https://doi.org/10.1016/j.biopsych.2025.01.010
62. Dionisio, L., Jose De Rosa, M., Bouzat, C., & Esandi Mdel, C. (2011). An intrinsic GABAergic system in human lymphocytes. *Neuropharmacology*, *60*(2-3), 513–519. https://doi.org/10.1016/j.neuropharm.2010.11.007
63. Diorio, D., Viau, V., & Meaney, M. J. (1993). The role of the medial prefrontal cortex (cingulate gyrus) in the regulation of hypothalamic-pituitary-adrenal responses to stress. *J Neurosci*, *13*(9), 3839–3847. https://doi.org/10.1523/JNEUROSCI.13-09-03839.1993
64. Drossman, D. A. (2005). Brain imaging and its implications for studying centrally targeted treatments in irritable bowel syndrome: a primer for gastroenterologists. *Gut*, *54*(5), 569–573. https://doi.org/10.1136/gut.2004.058446
65. Dunbar, R. I. (2009). The social brain hypothesis and its implications for social evolution. *Ann Hum Biol*, *36*(5), 562–572. https://doi.org/10.1080/03014460902960289
66. Dyck, M., Loughead, J., Gur, R. C., Schneider, F., & Mathiak, K. (2014). Hyperactivation balances sensory processing deficits during mood induction in schizophrenia. *Soc Cogn Affect Neurosci*, *9*(2), 167–175. https://doi.org/10.1093/scan/nss120

67. Ehring, T., & Quack, D. (2010). Emotion regulation difficulties in trauma survivors: the role of trauma type and PTSD symptom severity. *Behav Ther*, *41*(4), 587–598. https://doi.org/10.1016/j.beth.2010.04.004
68. Eisenberger, N. I., & Lieberman, M. D. (2004). Why rejection hurts: a common neural alarm system for physical and social pain. *Trends Cogn Sci*, *8*(7), 294–300. https://doi.org/10.1016/j.tics.2004.05.010
69. Ekman, P. (1992). **An argument for basic emotions**. *Cognition and Emotion 6*(3-4), 169–200.
70. Elston, T. W., & Bilkey, D. K. (2017). Anterior Cingulate Cortex Modulation of the Ventral Tegmental Area in an Effort Task. *Cell Rep*, *19*(11), 2220–2230. https://doi.org/10.1016/j.celrep.2017.05.062
71. Etkin, A., Egner, T., & Kalisch, R. (2011). Emotional processing in anterior cingulate and medial prefrontal cortex. *Trends Cogn Sci*, *15*(2), 85–93. https://doi.org/10.1016/j.tics.2010.11.004
72. Fanselow, E. E., Richardson, K. A., & Connors, B. W. (2008). Selective, state-dependent activation of somatostatin-expressing inhibitory interneurons in mouse neocortex. *J Neurophysiol*, *100*(5), 2640–2652. https://doi.org/10.1152/jn.90691.2008
73. Fellows, L. K. (2007). Advances in understanding ventromedial prefrontal function: the accountant joins the executive. *Neurology*, *68*(13), 991–995. https://doi.org/10.1212/01.wnl.0000257835.46290.57
74. Ferretti, V., Maltese, F., Contarini, G., Nigro, M., Bonavia, A., Huang, H., Gigliucci, V., Morelli, G., Scheggia, D., Manago, F., Castellani, G., Lefevre, A., Cancedda, L., Chini, B., Grinevich, V., & Papaleo, F. (2019). Oxytocin Signaling in the Central Amygdala Modulates Emotion Discrimination in Mice. *Curr Biol*, *29*(12), 1938–1953 e1936. https://doi.org/10.1016/j.cub.2019.04.070
75. Ferretti, V., & Papaleo, F. (2019). Understanding others: Emotion recognition in humans and other animals. *Genes Brain Behav*, *18*(1), e12544. https://doi.org/10.1111/gbb.12544
76. Fett, A. K., Viechtbauer, W., Dominguez, M. D., Penn, D. L., van Os, J., & Krabbendam, L. (2011). The relationship between neurocognition and social cognition with functional outcomes in schizophrenia: a meta-analysis. *Neurosci Biobehav Rev*, *35*(3), 573–588. https://doi.org/10.1016/j.neubiorev.2010.07.001
77. Fino, E., & Yuste, R. (2011). Dense inhibitory connectivity in neocortex. *Neuron*, *69*(6), 1188–1203. https://doi.org/10.1016/j.neuron.2011.02.025
78. Fornito, A., Yucel, M., Dean, B., Wood, S. J., & Pantelis, C. (2009). Anatomical abnormalities of the anterior cingulate cortex in schizophrenia: bridging the gap between neuroimaging and neuropathology. *Schizophr Bull*, *35*(5), 973–993. https://doi.org/10.1093/schbul/sbn025
79. Francis-Oliveira, J., Leitzel, O., & Niwa, M. (2022). Are the Anterior and Mid-Cingulate Cortices Distinct in Rodents? *Front Neuroanat*, *16*, 914359. https://doi.org/10.3389/fnana.2022.914359
80. Frewen, P., Thornley, E., Rabellino, D., & Lanius, R. (2017). Neuroimaging the traumatized self: fMRI reveals altered response in cortical midline structures and occipital cortex during visual and verbal self- and other-referential processing in women with PTSD. *Eur J Psychotraumatol*, *8*(1), 1314164. https://doi.org/10.1080/20008198.2017.1314164
81. Friedman, N. P., & Robbins, T. W. (2022). The role of prefrontal cortex in cognitive control and executive function. *Neuropsychopharmacology*, *47*(1), 72–89. https://doi.org/10.1038/s41386-021-01132-0

82. Frith, C. D. (2008). Social cognition. *Philos Trans R Soc Lond B Biol Sci*, *363*(1499), 2033–2039. https://doi.org/10.1098/rstb.2008.0005
83. Frith, C. D., & Frith, U. (2007). Social cognition in humans. *Curr Biol*, *17*(16), R724–732. https://doi.org/10.1016/j.cub.2007.05.068
84. Fujiwara, H., Hirao, K., Namiki, C., Yamada, M., Shimizu, M., Fukuyama, H., Hayashi, T., & Murai, T. (2007). Anterior cingulate pathology and social cognition in schizophrenia: a study of gray matter, white matter and sulcal morphometry. *Neuroimage*, *36*(4), 1236–1245. https://doi.org/10.1016/j.neuroimage.2007.03.068
85. Garcia-Leon, M. A., Fuentes-Claramonte, P., Valiente-Gomez, A., Natividad, C., Salgado-Pineda, P., Gomar, J. J., Guerrero-Pedraza, A., Portillo, F., Ortiz-Gil, J., Alonso-Lana, S., Maristany, T., Radua, J., Salvador, R., Sarro, S., & Pomarol-Clotet, E. (2021). Altered brain responses to specific negative emotions in schizophrenia. *Neuroimage Clin*, *32*, 102894. https://doi.org/10.1016/j.nicl.2021.102894
86. Gilbertson, M. W., Shenton, M. E., Ciszewski, A., Kasai, K., Lasko, N. B., Orr, S. P., & Pitman, R. K. (2002). Smaller hippocampal volume predicts pathologic vulnerability to psychological trauma. *Nat Neurosci*, *5*(11), 1242–1247. https://doi.org/10.1038/nn958
87. Girgenti, M. J., Wohleb, E. S., Mehta, S., Ghosal, S., Fogaca, M. V., & Duman, R. S. (2019). Prefrontal cortex interneurons display dynamic sex-specific stress-induced transcriptomes. *Transl Psychiatry*, *9*(1), 292. https://doi.org/10.1038/s41398-019-0642-z
88. Goldberg, E. M., & Coulter, D. A. (2013). Mechanisms of epileptogenesis: a convergence on neural circuit dysfunction. *Nat Rev Neurosci*, *14*(5), 337–349. https://doi.org/10.1038/nrn3482
89. Gonzalez-Burgos, G., Hashimoto, T., & Lewis, D. A. (2010). Alterations of cortical GABA neurons and network oscillations in schizophrenia. *Curr Psychiatry Rep*, *12*(4), 335–344. https://doi.org/10.1007/s11920-010-0124-8
90. Govindpani, K., Calvo-Flores Guzman, B., Vinnakota, C., Waldvogel, H. J., Faull, R. L., & Kwakowsky, A. (2017). Towards a Better Understanding of GABAergic Remodeling in Alzheimer's Disease. *Int J Mol Sci*, *18*(8). https://doi.org/10.3390/ijms18081813
91. Gray, H. M., & Tickle-Degnen, L. (2010). A meta-analysis of performance on emotion recognition tasks in Parkinson's disease. *Neuropsychology*, *24*(2), 176–191. https://doi.org/10.1037/a0018104
92. Green, M. F., Penn, D. L., Bentall, R., Carpenter, W. T., Gaebel, W., Gur, R. C., Kring, A. M., Park, S., Silverstein, S. M., & Heinssen, R. (2008). Social cognition in schizophrenia: an NIMH workshop on definitions, assessment, and research opportunities. *Schizophr Bull*, *34*(6), 1211–1220. https://doi.org/10.1093/schbul/sbm145
93. Grimaldi, D. A., Patane, A., Cattarinussi, G., & Sambataro, F. (2025). Functional connectivity of the striatum in psychosis: Meta-analysis of functional magnetic resonance imaging studies and replication on an independent sample. *Neurosci Biobehav Rev*, *174*, 106179. https://doi.org/10.1016/j.neubiorev.2025.106179

94. Gur, R. C., Sara, R., Hagendoorn, M., Marom, O., Hughett, P., Macy, L., Turner, T., Bajcsy, R., Posner, A., & Gur, R. E. (2002). A method for obtaining 3-dimensional facial expressions and its standardization for use in neurocognitive studies. *J Neurosci Methods*, *115*(2), 137–143. https://doi.org/10.1016/s0165-0270(02)00006-7
95. Hamilton, J. P., Glover, G. H., Hsu, J. J., Johnson, R. F., & Gotlib, I. H. (2011). Modulation of subgenual anterior cingulate cortex activity with real-time neurofeedback. *Hum Brain Mapp*, *32*(1), 22–31. https://doi.org/10.1002/hbm.20997
96. Harms, M. B., Martin, A., & Wallace, G. L. (2010). Facial emotion recognition in autism spectrum disorders: a review of behavioral and neuroimaging studies. *Neuropsychol Rev*, *20*(3), 290–322. https://doi.org/10.1007/s11065-010-9138-6
97. Harris, K. D., & Shepherd, G. M. (2015). The neocortical circuit: themes and variations. *Nat Neurosci*, *18*(2), 170–181. https://doi.org/10.1038/nn.3917
98. Heeger, D. J., & Ress, D. (2002). What does fMRI tell us about neuronal activity? *Nat Rev Neurosci*, *3*(2), 142–151. https://doi.org/10.1038/nrn730
99. Heller, J., Mirzazade, S., Romanzetti, S., Habel, U., Derntl, B., Freitag, N. M., Schulz, J. B., Dogan, I., & Reetz, K. (2018). Impact of gender and genetics on emotion processing in Parkinson's disease - A multimodal study. *Neuroimage Clin*, *18*, 305–314. https://doi.org/10.1016/j.nicl.2018.01.034
100. Henry, J. D., von Hippel, W., Molenberghs, P., Lee, T., & Sachdev, P. S. (2016). Clinical assessment of social cognitive function in neurological disorders. *Nat Rev Neurol*, *12*(1), 28–39. https://doi.org/10.1038/nrneurol.2015.229
101. Hilz, M. J., Devinsky, O., Szczepanska, H., Borod, J. C., Marthol, H., & Tutaj, M. (2006). Right ventromedial prefrontal lesions result in paradoxical cardiovascular activation with emotional stimuli. *Brain*, *129*(Pt 12), 3343–3355. https://doi.org/10.1093/brain/awl299
102. Hiser, J., & Koenigs, M. (2018). The Multifaceted Role of the Ventromedial Prefrontal Cortex in Emotion, Decision Making, Social Cognition, and Psychopathology. *Biol Psychiatry*, *83*(8), 638–647. https://doi.org/10.1016/j.biopsych.2017.10.030
103. Huang, S., Wu, S. J., Sansone, G., Ibrahim, L. A., & Fishell, G. (2024). Layer 1 neocortex: Gating and integrating multidimensional signals. *Neuron*, *112*(2), 184–200. https://doi.org/10.1016/j.neuron.2023.09.041
104. Ibrahim, H. M., Kulikova, A., Ly, H., Rush, A. J., & Sherwood Brown, E. (2022). Anterior cingulate cortex in individuals with depressive symptoms: A structural MRI study. *Psychiatry Res Neuroimaging*, *319*, 111420. https://doi.org/10.1016/j.pscychresns.2021.111420
105. Jacobs, D. H., Shuren, J., Bowers, D., & Heilman, K. M. (1995). Emotional facial imagery, perception, and expression in Parkinson's disease. *Neurology*, *45*(9), 1696–1702. https://doi.org/10.1212/wnl.45.9.1696
106. Janer, K. W., & Pardo, J. V. (1991). Deficits in selective attention following bilateral anterior cingulotomy. *J Cogn Neurosci*, *3*(3), 231–241. https://doi.org/10.1162/jocn.1991.3.3.231

107. Johansen, J. P., & Fields, H. L. (2004). Glutamatergic activation of anterior cingulate cortex produces an aversive teaching signal. *Nat Neurosci*, *7*(4), 398–403. https://doi.org/10.1038/nn1207
108. Jones, E. G. (1993). GABAergic neurons and their role in cortical plasticity in primates. *Cereb Cortex*, *3*(5), 361–372. https://doi.org/10.1093/cercor/3.5.361-a
109. Jumah, F. R., & Dossani, R. H. (2025). Neuroanatomy, Cingulate Cortex. In *StatPearls*.
110. Kan, Y., Kawamura, M., Hasegawa, Y., Mochizuki, S., & Nakamura, K. (2002). Recognition of emotion from facial, prosodic and written verbal stimuli in Parkinson's disease. *Cortex*, *38*(4), 623–630. https://doi.org/10.1016/s0010-9452(08)70026-1
111. Kapfer, C., Glickfeld, L. L., Atallah, B. V., & Scanziani, M. (2007). Supralinear increase of recurrent inhibition during sparse activity in the somatosensory cortex. *Nat Neurosci*, *10*(6), 743–753. https://doi.org/10.1038/nn1909
112. Katona, L., Lapray, D., Viney, T. J., Oulhaj, A., Borhegyi, Z., Micklem, B. R., Klausberger, T., & Somogyi, P. (2016). Sleep and Movement Differentiates Actions of Two Types of Somatostatin-Expressing GABAergic Interneuron in Rat Hippocampus. *Neuron*, *91*(5), 1183. https://doi.org/10.1016/j.neuron.2016.08.023
113. Kaupmann, K., Malitschek, B., Schuler, V., Heid, J., Froestl, W., Beck, P., Mosbacher, J., Bischoff, S., Kulik, A., Shigemoto, R., Karschin, A., & Bettler, B. (1998). GABA(B)-receptor subtypes assemble into functional heteromeric complexes. *Nature*, *396*(6712), 683–687. https://doi.org/10.1038/25360
114. Kawaguchi, Y. (1997). Neostriatal cell subtypes and their functional roles. *Neurosci Res*, *27*(1), 1–8. https://doi.org/10.1016/s0168-0102(96)01134-0
115. Kawaguchi, Y., & Kubota, Y. (1996). Physiological and morphological identification of somatostatin- or vasoactive intestinal polypeptide-containing cells among GABAergic cell subtypes in rat frontal cortex. *J Neurosci*, *16*(8), 2701–2715. https://doi.org/10.1523/JNEUROSCI.16-08-02701.1996
116. Kawaguchi, Y., & Kubota, Y. (1997). GABAergic cell subtypes and their synaptic connections in rat frontal cortex. *Cereb Cortex*, *7*(6), 476–486. https://doi.org/10.1093/cercor/7.6.476
117. Kawaguchi, Y., & Shindou, T. (1998). Noradrenergic excitation and inhibition of GABAergic cell types in rat frontal cortex. *J Neurosci*, *18*(17), 6963–6976. https://doi.org/10.1523/JNEUROSCI.18-17-06963.1998
118. Kennedy, D. P., & Adolphs, R. (2012). The social brain in psychiatric and neurological disorders. *Trends Cogn Sci*, *16*(11), 559–572. https://doi.org/10.1016/j.tics.2012.09.006
119. Kepecs, A., & Fishell, G. (2014). Interneuron cell types are fit to function. *Nature*, *505*(7483), 318–326. https://doi.org/10.1038/nature12983
120. Keum, S., Kim, A., Shin, J. J., Kim, J. H., Park, J., & Shin, H. S. (2018). A Missense Variant at the Nrxn3 Locus Enhances Empathy Fear in the Mouse. *Neuron*, *98*(3), 588–601 e585. https://doi.org/10.1016/j.neuron.2018.03.041
121. Khundakar, A. A., Morris, C. M., Oakley, A. E., & Thomas, A. J. (2011). Cellular pathology within the anterior cingulate cortex of patients with late-life depression: a morphometric study. *Psychiatry Res*, *194*(2), 184–189. https://doi.org/10.1016/j.pscychresns.2011.04.008

122. Kietzman, H. W., & Gourley, S. L. (2023). How social information impacts action in rodents and humans: the role of the prefrontal cortex and its connections. *Neurosci Biobehav Rev*, *147*, 105075. https://doi.org/10.1016/j.neubiorev.2023.105075
123. Kim, H., Ahrlund-Richter, S., Wang, X., Deisseroth, K., & Carlen, M. (2016). Prefrontal Parvalbumin Neurons in Control of Attention. *Cell*, *164*(1-2), 208–218. https://doi.org/10.1016/j.cell.2015.11.038
124. Kim, Y., Yang, G. R., Pradhan, K., Venkataraju, K. U., Bota, M., Garcia Del Molino, L. C., Fitzgerald, G., Ram, K., He, M., Levine, J. M., Mitra, P., Huang, Z. J., Wang, X. J., & Osten, P. (2017). Brain-wide Maps Reveal Stereotyped Cell-Type-Based Cortical Architecture and Subcortical Sexual Dimorphism. *Cell*, *171*(2), 456–469 e422. https://doi.org/10.1016/j.cell.2017.09.020
125. Kitayama, N., Quinn, S., & Bremner, J. D. (2006). Smaller volume of anterior cingulate cortex in abuse-related posttraumatic stress disorder. *J Affect Disord*, *90*(2-3), 171–174. https://doi.org/10.1016/j.jad.2005.11.006
126. Kohler, C. G., Turner, T. H., Bilker, W. B., Brensinger, C. M., Siegel, S. J., Kanes, S. J., Gur, R. E., & Gur, R. C. (2003). Facial emotion recognition in schizophrenia: intensity effects and error pattern. *Am J Psychiatry*, *160*(10), 1768–1774. https://doi.org/10.1176/appi.ajp.160.10.1768
127. Kohler, C. G., Walker, J. B., Martin, E. A., Healey, K. M., & Moberg, P. J. (2010). Facial emotion perception in schizophrenia: a meta-analytic review. *Schizophr Bull*, *36*(5), 1009–1019. https://doi.org/10.1093/schbul/sbn192
128. Kubota, Y. (2014). Untangling GABAergic wiring in the cortical microcircuit. *Curr Opin Neurobiol*, *26*, 7–14. https://doi.org/10.1016/j.conb.2013.10.003
129. Kumfor, F., Sapey-Triomphe, L. A., Leyton, C. E., Burrell, J. R., Hodges, J. R., & Piguet, O. (2014). Degradation of emotion processing ability in corticobasal syndrome and Alzheimer's disease. *Brain*, *137*(Pt 11), 3061–3072. https://doi.org/10.1093/brain/awu246
130. Lai, M. C., Lombardo, M. V., & Baron-Cohen, S. (2014). Autism. *Lancet*, *383*(9920), 896–910. https://doi.org/10.1016/S0140-6736(13)61539-1
131. Lawrence, A. D., Goerendt, I. K., & Brooks, D. J. (2007). Impaired recognition of facial expressions of anger in Parkinson's disease patients acutely withdrawn from dopamine replacement therapy. *Neuropsychologia*, *45*(1), 65–74. https://doi.org/10.1016/j.neuropsychologia.2006.04.016
132. Le Merre, P., Esmaeili, V., Charriere, E., Galan, K., Salin, P. A., Petersen, C. C. H., & Crochet, S. (2018). Reward-Based Learning Drives Rapid Sensory Signals in Medial Prefrontal Cortex and Dorsal Hippocampus Necessary for Goal-Directed Behavior. *Neuron*, *97*(1), 83–91 e85. https://doi.org/10.1016/j.neuron.2017.11.031
133. Lenartowicz, A., & McIntosh, A. R. (2005). The role of anterior cingulate cortex in working memory is shaped by functional connectivity. *J Cogn Neurosci*, *17*(7), 1026–1042. https://doi.org/10.1162/0898929054475127
134. Lewis, D. A. (2014). Inhibitory neurons in human cortical circuits: substrate for cognitive dysfunction in schizophrenia. *Curr Opin Neurobiol*, *26*, 22–26. https://doi.org/10.1016/j.conb.2013.11.003

135. Li, P., & Jeong, H. (2020). The social brain of language: grounding second language learning in social interaction. *NPJ Sci Learn*, *5*, 8. https://doi.org/10.1038/s41539-020-0068-7
136. Li, Y. D., Luo, Y. J., Su, W. K., Ge, J., Crowther, A., Chen, Z. K., Wang, L., Lazarus, M., Liu, Z. L., Qu, W. M., & Huang, Z. L. (2024). Anterior cingulate cortex projections to the dorsal medial striatum underlie insomnia associated with chronic pain. *Neuron*, *112*(8), 1328–1341 e1324. https://doi.org/10.1016/j.neuron.2024.01.014
137. Liu, X., Dimidschstein, J., Fishell, G., & Carter, A. G. (2020). Hippocampal inputs engage CCK+ interneurons to mediate endocannabinoid-modulated feed-forward inhibition in the prefrontal cortex. *Elife*, *9*. https://doi.org/10.7554/eLife.55267
138. Lu, R., Sun, W., Liang, Y., Kerlin, A., Bierfeld, J., Seelig, J. D., Wilson, D. E., Scholl, B., Mohar, B., Tanimoto, M., Koyama, M., Fitzpatrick, D., Orger, M. B., & Ji, N. (2017). Video-rate volumetric functional imaging of the brain at synaptic resolution. *Nat Neurosci*, *20*(4), 620–628. https://doi.org/10.1038/nn.4516
139. Ma, Y., Hu, H., Berrebi, A. S., Mathers, P. H., & Agmon, A. (2006). Distinct subtypes of somatostatin-containing neocortical interneurons revealed in transgenic mice. *J Neurosci*, *26*(19), 5069–5082. https://doi.org/10.1523/JNEUROSCI.0661-06.2006
140. Maier, S. F., Amat, J., Baratta, M. V., Paul, E., & Watkins, L. R. (2006). Behavioral control, the medial prefrontal cortex, and resilience. *Dialogues Clin Neurosci*, *8*(4), 397–406. https://doi.org/10.31887/DCNS.2006.8.4/smaier
141. Maltese, F., Pacinelli, G., Monai, A., Bernardi, F., Capaz, A. M., Niello, M., Walle, R., de Leon, N., Manago, F., Leroy, F., & Papaleo, F. (2025). Self-experience of a negative event alters responses to others in similar states through prefrontal cortex CRF mechanisms. *Nat Neurosci*, *28*(1), 122–136. https://doi.org/10.1038/s41593-024-01816-y
142. Mandal, M. K., Pandey, R., & Prasad, A. B. (1998). Facial expressions of emotions and schizophrenia: a review. *Schizophr Bull*, *24*(3), 399–412. https://doi.org/10.1093/oxfordjournals.schbul.a033335
143. Marin, O. (2024). Parvalbumin interneuron deficits in schizophrenia. *Eur Neuropsychopharmacol*, *82*, 44–52. https://doi.org/10.1016/j.euroneuro.2024.02.010
144. Markram, H., Toledo-Rodriguez, M., Wang, Y., Gupta, A., Silberberg, G., & Wu, C. (2004). Interneurons of the neocortical inhibitory system. *Nat Rev Neurosci*, *5*(10), 793–807. https://doi.org/10.1038/nrn1519
145. Mattavelli, G., Barvas, E., Longo, C., Zappini, F., Ottaviani, D., Malaguti, M. C., Pellegrini, M., & Papagno, C. (2021). Facial expressions recognition and discrimination in Parkinson's disease. *J Neuropsychol*, *15*(1), 46–68. https://doi.org/10.1111/jnp.12209
146. McGarry, L. M., & Carter, A. G. (2016). Inhibitory Gating of Basolateral Amygdala Inputs to the Prefrontal Cortex. *J Neurosci*, *36*(36), 9391–9406. https://doi.org/10.1523/JNEUROSCI.0874-16.2016
147. Medford, N., & Critchley, H. D. (2010). Conjoint activity of anterior insular and anterior cingulate cortex: awareness and response. *Brain Struct Funct*, *214*(5-6), 535–549. https://doi.org/10.1007/s00429-010-0265-x

148. Menon, V., & Uddin, L. Q. (2010). Saliency, switching, attention and control: a network model of insula function. *Brain Struct Funct*, *214*(5-6), 655–667. https://doi.org/10.1007/s00429-010-0262-0
149. Mercer, S. W., & Reynolds, W. J. . (2002). *Empathy and quality of care* (Vol. 52 Suppl(Suppl)).
150. Meyza, K. Z., Bartal, I. B., Monfils, M. H., Panksepp, J. B., & Knapska, E. (2017). The roots of empathy: Through the lens of rodent models. *Neurosci Biobehav Rev*, *76*(Pt B), 216–234. https://doi.org/10.1016/j.neubiorev.2016.10.028
151. Miles, S. R., Menefee, D. S., Wanner, J., Teten Tharp, A., & Kent, T. A. (2016). The Relationship Between Emotion Dysregulation and Impulsive Aggression in Veterans With Posttraumatic Stress Disorder Symptoms. *J Interpers Violence*, *31*(10), 1795–1816. https://doi.org/10.1177/0886260515570746
152. Miller, E. K. (2000). The prefrontal cortex and cognitive control. *Nat Rev Neurosci*, *1*(1), 59–65. https://doi.org/10.1038/35036228
153. Miller, E. K., & Cohen, J. D. (2001). An integrative theory of prefrontal cortex function. *Annu Rev Neurosci*, *24*, 167–202. https://doi.org/10.1146/annurev.neuro.24.1.167
154. Miller, L. A., Hsieh, S., Lah, S., Savage, S., Hodges, J. R., & Piguet, O. (2012). One size does not fit all: face emotion processing impairments in semantic dementia, behavioural-variant frontotemporal dementia and Alzheimer's disease are mediated by distinct cognitive deficits. *Behav Neurol*, *25*(1), 53–60. https://doi.org/10.3233/BEN-2012-0349
155. Morey, R. A., Gold, A. L., LaBar, K. S., Beall, S. K., Brown, V. M., Haswell, C. C., Nasser, J. D., Wagner, H. R., McCarthy, G., & Mid-Atlantic, M. W. (2012). Amygdala volume changes in posttraumatic stress disorder in a large case-controlled veterans group. *Arch Gen Psychiatry*, *69*(11), 1169–1178. https://doi.org/10.1001/archgenpsychiatry.2012.50
156. Moyer, C. E., Erickson, S. L., Fish, K. N., Thiels, E., Penzes, P., & Sweet, R. A. (2016). Developmental Trajectories of Auditory Cortex Synaptic Structures and Gap-Prepulse Inhibition of Acoustic Startle Between Early Adolescence and Young Adulthood in Mice. *Cereb Cortex*, *26*(5), 2115–2126. https://doi.org/10.1093/cercor/bhv040
157. Munoz, W., & Rudy, B. (2014). Spatiotemporal specificity in cholinergic control of neocortical function. *Curr Opin Neurobiol*, *26*, 149–160. https://doi.org/10.1016/j.conb.2014.02.015
158. Nakao, T. O., Hideki & Northoff, Georg. (2010). Decision making and the medial prefrontal cortex function in social context. *Japanese Journal of Physiological Psychology and Psychophysiology*, *28*, 45–55.
159. Ongur, D., & Price, J. L. (2000). The organization of networks within the orbital and medial prefrontal cortex of rats, monkeys and humans. *Cereb Cortex*, *10*(3), 206–219. https://doi.org/10.1093/cercor/10.3.206
160. Paxinos, G., & Franklin, K. B. J. . (2001). *The mouse brain in stereotaxic coordinates (2nd ed.)*.
161. Penn, D. L., Corrigan, P. W., Bentall, R. P., Racenstein, J. M., & Newman, L. (1997). Social cognition in schizophrenia. *Psychol Bull*, *121*(1), 114–132. https://doi.org/10.1037/0033-2909.121.1.114

162. Pickup, G. J., & Frith, C. D. (2001). Theory of mind impairments in schizophrenia: symptomatology, severity and specificity. *Psychol Med*, *31*(2), 207–220. https://doi.org/10.1017/s0033291701003385
163. Poljac, E., Montagne, B., & de Haan, E. H. (2011). Reduced recognition of fear and sadness in post-traumatic stress disorder. *Cortex*, *47*(8), 974–980. https://doi.org/10.1016/j.cortex.2010.10.002
164. Popova, E. (2014). Ionotropic GABA Receptors and Distal Retinal ON and OFF Responses. *Scientifica (Cairo)*, *2014*, 149187. https://doi.org/10.1155/2014/149187
165. Posner, M. I., & DiGirolamo, G. J. (1998). Executive attention: conflict, target detection, and cognitive control. *The Attentive Brain*.
166. Post, S. G., Ng, L. E., Fischel, J. E., Bennett, M., Bily, L., Chandran, L., Joyce, J., Locicero, B., McGovern, K., McKeefrey, R. L., Rodriguez, J. V., & Roess, M. W. (2014). Routine, empathic and compassionate patient care: definitions, development, obstacles, education and beneficiaries. *J Eval Clin Pract*, *20*(6), 872–880. https://doi.org/10.1111/jep.12243
167. Pouille, F., & Scanziani, M. (2004). Routing of spike series by dynamic circuits in the hippocampus. *Nature*, *429*(6993), 717–723. https://doi.org/10.1038/nature02615
168. Qi, C., Sima, W., Mao, H., Hu, E., Ge, J., Deng, M., Chen, A., Ye, W., Xue, Q., Wang, W., Chen, Q., & Wu, S. (2025). Anterior cingulate cortex parvalbumin and somatostatin interneurons shape social behavior in male mice. *Nat Commun*, *16*(1), 4156. https://doi.org/10.1038/s41467-025-59473-z
169. Radua, J., & Mataix-Cols, D. (2009). Voxel-wise meta-analysis of grey matter changes in obsessive-compulsive disorder. *Br J Psychiatry*, *195*(5), 393–402. https://doi.org/10.1192/bjp.bp.108.055046
170. Ramachandran, S., Krogh, N., Jorgensen, T. E., Johansen, S. D., Nielsen, H., & Babiak, I. (2020). The shift from early to late types of ribosomes in zebrafish development involves changes at a subset of rRNA 2'-O-Me sites. *RNA*, *26*(12), 1919–1934. https://doi.org/10.1261/rna.076760.120
171. Rauch, S. L., Shin, L. M., Segal, E., Pitman, R. K., Carson, M. A., McMullin, K., Whalen, P. J., & Makris, N. (2003). Selectively reduced regional cortical volumes in post-traumatic stress disorder. *Neuroreport*, *14*(7), 913–916. https://doi.org/10.1097/01.wnr.0000071767.24455.10
172. Reyes, A., Lujan, R., Rozov, A., Burnashev, N., Somogyi, P., & Sakmann, B. (1998). Target-cell-specific facilitation and depression in neocortical circuits. *Nat Neurosci*, *1*(4), 279–285. https://doi.org/10.1038/1092
173. Rolls, E. T. (2019). The cingulate cortex and limbic systems for emotion, action, and memory. *Brain Struct Funct*, *224*(9), 3001–3018. https://doi.org/10.1007/s00429-019-01945-2
174. Roozendaal, B., McEwen, B. S., & Chattarji, S. (2009). Stress, memory and the amygdala. *Nat Rev Neurosci*, *10*(6), 423–433. https://doi.org/10.1038/nrn2651
175. Rossi, A. F., Pessoa, L., Desimone, R., & Ungerleider, L. G. (2009). The prefrontal cortex and the executive control of attention. *Exp Brain Res*, *192*(3), 489–497. https://doi.org/10.1007/s00221-008-1642-z
176. Roux, L., & Buzsaki, G. (2015). Tasks for inhibitory interneurons in intact brain circuits. *Neuropharmacology*, *88*, 10–23. https://doi.org/10.1016/j.neuropharm.2014.09.011

177. Roy, M., Shohamy, D., & Wager, T. D. (2012). Ventromedial prefrontal-subcortical systems and the generation of affective meaning. *Trends Cogn Sci*, *16*(3), 147–156. https://doi.org/10.1016/j.tics.2012.01.005

178. Rudy, B., Fishell, G., Lee, S., & Hjerling-Leffler, J. (2011). Three groups of interneurons account for nearly 100% of neocortical GABAergic neurons. *Dev Neurobiol*, *71*(1), 45–61. https://doi.org/10.1002/dneu.20853

179. Rushworth, M. F., & Behrens, T. E. (2008). Choice, uncertainty and value in prefrontal and cingulate cortex. *Nat Neurosci*, *11*(4), 389–397. https://doi.org/10.1038/nn2066

180. Rushworth, M. F., Noonan, M. P., Boorman, E. D., Walton, M. E., & Behrens, T. E. (2011). Frontal cortex and reward-guided learning and decision-making. *Neuron*, *70*(6), 1054–1069. https://doi.org/10.1016/j.neuron.2011.05.014

181. Scanziani, M., Gahwiler, B. H., & Charpak, S. (1998). Target cell-specific modulation of transmitter release at terminals from a single axon. *Proc Natl Acad Sci U S A*, *95*(20), 12004–12009. https://doi.org/10.1073/pnas.95.20.12004

182. Scarpina, F., & Tagini, S. (2017). The Stroop Color and Word Test. *Front Psychol*, *8*, 557. https://doi.org/10.3389/fpsyg.2017.00557

183. Scheggia, D., Manago, F., Maltese, F., Bruni, S., Nigro, M., Dautan, D., Latuske, P., Contarini, G., Gomez-Gonzalo, M., Requie, L. M., Ferretti, V., Castellani, G., Mauro, D., Bonavia, A., Carmignoto, G., Yizhar, O., & Papaleo, F. (2020). Somatostatin interneurons in the prefrontal cortex control affective state discrimination in mice. *Nat Neurosci*, *23*(1), 47–60. https://doi.org/10.1038/s41593-019-0551-8

184. Schmaal, L., Hibar, D. P., Samann, P. G., Hall, G. B., Baune, B. T., Jahanshad, N., Cheung, J. W., van Erp, T. G. M., Bos, D., Ikram, M. A., Vernooij, M. W., Niessen, W. J., Tiemeier, H., Hofman, A., Wittfeld, K., Grabe, H. J., Janowitz, D., Bulow, R., Selonke, M.,…Veltman, D. J. (2017). Cortical abnormalities in adults and adolescents with major depression based on brain scans from 20 cohorts worldwide in the ENIGMA Major Depressive Disorder Working Group. *Mol Psychiatry*, *22*(6), 900–909. https://doi.org/10.1038/mp.2016.60

185. Schneider, K. N., Sciarillo, X. A., Nudelman, J. L., Cheer, J. F., & Roesch, M. R. (2020). Anterior Cingulate Cortex Signals Attention in a Social Paradigm that Manipulates Reward and Shock. *Curr Biol*, *30*(19), 3724–3735 e3722. https://doi.org/10.1016/j.cub.2020.07.039

186. Senju, A. (2012). Spontaneous theory of mind and its absence in autism spectrum disorders. *Neuroscientist*, *18*(2), 108–113. https://doi.org/10.1177/1073858410397208

187. Silberberg, G., & Markram, H. (2007). Disynaptic inhibition between neocortical pyramidal cells mediated by Martinotti cells. *Neuron*, *53*(5), 735–746. https://doi.org/10.1016/j.neuron.2007.02.012

188. Silveira, S., Shah, R., Nooner, K. B., Nagel, B. J., Tapert, S. F., de Bellis, M. D., & Mishra, J. (2020). Impact of Childhood Trauma on Executive Function in Adolescence-Mediating Functional Brain Networks and Prediction of High-Risk Drinking. *Biol Psychiatry Cogn Neurosci Neuroimaging*, *5*(5), 499–509. https://doi.org/10.1016/j.bpsc.2020.01.011

189. Singer, T., Seymour, B., O'Doherty, J., Kaube, H., Dolan, R. J., & Frith, C. D. (2004). Empathy for pain involves the affective but not sensory components of pain. *Science*, *303*(5661), 1157–1162. https://doi.org/10.1126/science.1093535
190. Smith, M. L., Asada, N., & Malenka, R. C. (2021). Anterior cingulate inputs to nucleus accumbens control the social transfer of pain and analgesia. *Science*, *371*(6525), 153–159. https://doi.org/10.1126/science.abe3040
191. Somogyi, P., Tamas, G., Lujan, R., & Buhl, E. H. (1998). Salient features of synaptic organisation in the cerebral cortex. *Brain Res Brain Res Rev*, *26*(2-3), 113–135. https://doi.org/10.1016/s0165-0173(97)00061-1
192. Spilka, M. J., Arnold, A. E., & Goghari, V. M. (2015). Functional activation abnormalities during facial emotion perception in schizophrenia patients and nonpsychotic relatives. *Schizophr Res*, *168*(1-2), 330–337. https://doi.org/10.1016/j.schres.2015.07.012
193. Stevens, F. L., Hurley, R. A., & Taber, K. H. (2011). Anterior cingulate cortex: unique role in cognition and emotion. *J Neuropsychiatry Clin Neurosci*, *23*(2), 121–125. https://doi.org/10.1176/jnp.23.2.jnp121
194. Stevenson, A. (2010). *Oxford Dictionary of English (3rd ed.)*.
195. Strick, P. L., Dum, R. P., & Picard, N. (1998). Motor areas on the medial wall of the hemisphere. *Novartis Found Symp*, *218*, 64–75; discussion 75–80, 104–108. https://doi.org/10.1002/9780470515563.ch5
196. Sullivan, R. M., & Gratton, A. (1999). Lateralized effects of medial prefrontal cortex lesions on neuroendocrine and autonomic stress responses in rats. *J Neurosci*, *19*(7), 2834–2840. https://doi.org/10.1523/JNEUROSCI.19-07-02834.1999
197. Takahashi, H., Koeda, M., Oda, K., Matsuda, T., Matsushima, E., Matsuura, M., Asai, K., & Okubo, Y. (2004). An fMRI study of differential neural response to affective pictures in schizophrenia. *Neuroimage*, *22*(3), 1247–1254. https://doi.org/10.1016/j.neuroimage.2004.03.028
198. Takashima, A., Petersson, K. M., Rutters, F., Tendolkar, I., Jensen, O., Zwarts, M. J., McNaughton, B. L., & Fernandez, G. (2006). Declarative memory consolidation in humans: a prospective functional magnetic resonance imaging study. *Proc Natl Acad Sci U S A*, *103*(3), 756–761. https://doi.org/10.1073/pnas.0507774103
199. Tamamaki, N., & Tomioka, R. (2010). Long-Range GABAergic Connections Distributed throughout the Neocortex and their Possible Function. *Front Neurosci*, *4*, 202. https://doi.org/10.3389/fnins.2010.00202
200. Tasic, B., Menon, V., Nguyen, T. N., Kim, T. K., Jarsky, T., Yao, Z., Levi, B., Gray, L. T., Sorensen, S. A., Dolbeare, T., Bertagnolli, D., Goldy, J., Shapovalova, N., Parry, S., Lee, C., Smith, K., Bernard, A., Madisen, L., Sunkin, S. M.,…Zeng, H. (2016). Adult mouse cortical cell taxonomy revealed by single cell transcriptomics. *Nat Neurosci*, *19*(2), 335–346. https://doi.org/10.1038/nn.4216
201. Taylor, S. F., Kang, J., Brege, I. S., Tso, I. F., Hosanagar, A., & Johnson, T. D. (2012). Meta-analysis of functional neuroimaging studies of emotion perception and experience in schizophrenia. *Biol Psychiatry*, *71*(2), 136–145. https://doi.org/10.1016/j.biopsych.2011.09.007

202. Thomson, A. M. (2003). Presynaptic frequency- and pattern-dependent filtering. *J Comput Neurosci*, *15*(2), 159–202. https://doi.org/10.1023/a:1025812808362
203. Todtenkopf, M. S., Vincent, S. L., & Benes, F. M. (2005). A cross-study meta-analysis and three-dimensional comparison of cell counting in the anterior cingulate cortex of schizophrenic and bipolar brain. *Schizophr Res*, *73*(1), 79–89. https://doi.org/10.1016/j.schres.2004.08.018
204. Tomioka, R., Okamoto, K., Furuta, T., Fujiyama, F., Iwasato, T., Yanagawa, Y., Obata, K., Kaneko, T., & Tamamaki, N. (2005). Demonstration of long-range GABAergic connections distributed throughout the mouse neocortex. *Eur J Neurosci*, *21*(6), 1587–1600. https://doi.org/10.1111/j.1460-9568.2005.03989.x
205. Tremblay, R., Lee, S., & Rudy, B. (2016). GABAergic Interneurons in the Neocortex: From Cellular Properties to Circuits. *Neuron*, *91*(2), 260–292. https://doi.org/10.1016/j.neuron.2016.06.033
206. Urban-Ciecko, J., & Barth, A. L. (2016). Somatostatin-expressing neurons in cortical networks. *Nat Rev Neurosci*, *17*(7), 401–409. https://doi.org/10.1038/nrn.2016.53
207. Utashiro, N., MacLaren, D. A. A., Liu, Y. C., Yaqubi, K., Wojak, B., & Monyer, H. (2024). Long-range inhibition from prelimbic to cingulate areas of the medial prefrontal cortex enhances network activity and response execution. *Nat Commun*, *15*(1), 5772. https://doi.org/10.1038/s41467-024-50055-z
208. van Heukelum, S., Mars, R. B., Guthrie, M., Buitelaar, J. K., Beckmann, C. F., Tiesinga, P. H. E., Vogt, B. A., Glennon, J. C., & Havenith, M. N. (2020). Where is Cingulate Cortex? A Cross-Species View. *Trends Neurosci*, *43*(5), 285–299. https://doi.org/10.1016/j.tins.2020.03.007
209. Vargas, R. A. (2018). The GABAergic System: An overview of physiology, physiopathology and therapeutics. *International Journal of Clinical Pharmacology & Pharmacotherapy*, *3*. https://doi.org/https://doi.org/10.15344/2456-3501/2018/142
210. Villarreal, G., Hamilton, D. A., Petropoulos, H., Driscoll, I., Rowland, L. M., Griego, J. A., Kodituwakku, P. W., Hart, B. L., Escalona, R., & Brooks, W. M. (2002). Reduced hippocampal volume and total white matter volume in posttraumatic stress disorder. *Biol Psychiatry*, *52*(2), 119–125. https://doi.org/10.1016/s0006-3223(02)01359-8
211. Vogt, B. A. (2016). Midcingulate cortex: Structure, connections, homologies, functions and diseases. *J Chem Neuroanat*, *74*, 28–46. https://doi.org/10.1016/j.jchemneu.2016.01.010
212. Wang, J., Rao, H., Wetmore, G. S., Furlan, P. M., Korczykowski, M., Dinges, D. F., & Detre, J. A. (2005). Perfusion functional MRI reveals cerebral blood flow pattern under psychological stress. *Proc Natl Acad Sci U S A*, *102*(49), 17804–17809. https://doi.org/10.1073/pnas.0503082102
213. Wang, Y., Toledo-Rodriguez, M., Gupta, A., Wu, C., Silberberg, G., Luo, J., & Markram, H. (2004). Anatomical, physiological and molecular properties of Martinotti cells in the somatosensory cortex of the juvenile rat. *J Physiol*, *561*(Pt 1), 65–90. https://doi.org/10.1113/jphysiol.2004.073353
214. Whissell, P. D., Cajanding, J. D., Fogel, N., & Kim, J. C. (2015). Comparative density of CCK- and PV-GABA cells within the cortex and hippocampus. *Front Neuroanat*, *9*, 124. https://doi.org/10.3389/fnana.2015.00124

215. Woodward, S. H., Kaloupek, D. G., Streeter, C. C., Martinez, C., Schaer, M., & Eliez, S. (2006). Decreased anterior cingulate volume in combat-related PTSD. *Biol Psychiatry*, *59*(7), 582–587. https://doi.org/10.1016/j.biopsych.2005.07.033

216. Wu, S. J., Sevier, E., Dwivedi, D., Saldi, G. A., Hairston, A., Yu, S., Abbott, L., Choi, D. H., Sherer, M., Qiu, Y., Shinde, A., Lenahan, M., Rizzo, D., Xu, Q., Barrera, I., Kumar, V., Marrero, G., Pronneke, A., Huang, S.,…Fishell, G. (2023). Cortical somatostatin interneuron subtypes form cell-type-specific circuits. *Neuron*, *111*(17), 2675–2692 e2679. https://doi.org/10.1016/j.neuron.2023.05.032

217. Xu, H., Jeong, H. Y., Tremblay, R., & Rudy, B. (2013). Neocortical somatostatin-expressing GABAergic interneurons disinhibit the thalamorecipient layer 4. *Neuron*, *77*(1), 155–167. https://doi.org/10.1016/j.neuron.2012.11.004

218. Young, D. A., Chao, L., Neylan, T. C., O'Donovan, A., Metzler, T. J., & Inslicht, S. S. (2018). Association among anterior cingulate cortex volume, psychophysiological response, and PTSD diagnosis in a Veteran sample. *Neurobiol Learn Mem*, *155*, 189–196. https://doi.org/10.1016/j.nlm.2018.08.006

219. Zeidan, F., Martucci, K. T., Kraft, R. A., McHaffie, J. G., & Coghill, R. C. (2014). Neural correlates of mindfulness meditation-related anxiety relief. *Soc Cogn Affect Neurosci*, *9*(6), 751–759. https://doi.org/10.1093/scan/nst041

220. Zhang, Z., Fan, Q., Zhu, Y., Tan, L., Chen, Y., Gao, R., Zhang, H., Li, Y., & Xiao, Z. (2017). Intrinsic functional connectivity alteration of dorsal and rostral anterior cingulate cortex in obsessive-compulsive disorder: A resting fMRI study. *Neurosci Lett*, *654*, 86–92. https://doi.org/10.1016/j.neulet.2017.06.026

2. Scope and Outlines of the Thesis

The main aim of my thesis was to explore the role of prefrontal and anterior cingulate cortex circuits in emotion discrimination. My contribution on this topic include 4 connected and consecutive projects addressing: the implication of SOM long range projections (Chapter 2); the impact of emotional self-experience (Chapter 3); the distinct contribution of SOM in the prelimbic or anterior cingulate cortex (Chapter 4); and the multibrain connections between PFC SOM neurons (Chapter 5).

Chapter 2 consists of a research where we identified a conserved brain circuit involved in emotion recognition, where long-range inhibitory and excitatory connections between the mPFC and the retrosplenial cortex (RSC). In mice, SOM GABAergic neurons project from the mPFC to the RSC, with an excitatory feedback loop from the RSC back to the mPFC. Using optogenetics, calcium imaging in mice, and functional imaging in humans, we confirmed the role of this circuit in socio-cognitive processing. Importantly, dysfunction in this pathway was found in mouse models of psychiatric disorders, and targeted intervention restored emotion recognition abilities. This reveals a key cortico-cortical circuit underlying emotional understanding.

Chapter 3, we demonstrated that mice respond differently to others in stress—either showing preference or avoidance—only if they have personally experienced the same stress. These responses vary by sex: females' behavior depends on their estrus cycle, while males' behavior depends on their dominance status. The corticotropin-releasing factor (CRF) in the mPFC plays a key role: silencing it reduces this stress-related social behavior. Through imaging and optogenetic experiments, we revealed that CRF neurons in the mPFC become more active in response to others' stress only after experiencing personal stress, and this activity drives the behavioural shift. The findings reveal a neural mechanism that links personal emotional experiences to social responses toward others in distress.

Chapter 4 presents the findings from the past three years on ACC and PrL SOM neurons, highlighting how optogenetic inhibition during the Emotion Discrimination Task (EDT) causes varying effects depending on the brain area, while activation disrupts this task across regions. In collaboration with the Normal Veterinary Anatomy Service of the Department of Veterinary

Medical Sciences of the University of Bologna, initial tracing data are also presented, showing projection sites and quantification of SOM neurons based on whether their cell bodies reside in the mPFC or the ACC.

In **Chapter 5,** I present a study where we investigated how interbrain neural synchrony (INS) among three mice—one observer and two demonstrators—affects emotional discrimination. By recording activity in the ACC and using optogenetic manipulation, we found that INS, particularly involving SOM neurons in the observer's ACC, plays a causal role in guiding social decisions based on emotional states.

Chapter 2

Article

https://doi.org/10.1038/s41593-024-01647-x

Cortico-cortical transfer of socially derived information gates emotion recognition

Daniel Dautan[1,7+], **Anna Monai[1+]**, Federica Maltese[1,8#], Xiao Chang[2#], Cinzia Molent[1], Daniele Mauro[1], Alberto Galbusera[3], Dania Vecchia[4], Federica Antonelli[1], Arianna Benedetti[1], Filippo Drago[5], Gian Marco Leggio[5], Marco Pagani[3], Tommaso Fellin[4], Alessandro Gozzi[3], Gunter Schumann[2,6], Francesca Managò[1], Francesco Papaleo[1*].

[1]*Genetics of Cognition Laboratory, Neuroscience area, Istituto Italiano di Tecnologia, via Morego, 30, 16163 Genova, Italy.*

[2]*Centre for Population Neuroscience and Stratified Medicine (PONS), Institute for Science and Technology of Brain-inspired Intelligence (ISTBI), Fudan University, Shanghai, P.R. China.*

[3]*Functional Neuroimaging Laboratory, Center for Neuroscience and Cognitive systems, Istituto Italiano di Tecnologia, Rovereto.*

[4]*Optical Approaches to Brain Function Laboratory, Istituto Italiano di Tecnologia, 16163 Genova, Italy.*

[5]*Department of Biomedical and Biotechnological Sciences, University of Catania, Catania, Italy.*

[6]*Centre for Population Neuroscience and Stratified Medicine (PONS), Charite Mental Health, Dept. of Psychiatry and Psychotherapy, CCM, Charite Universitätsmedizin Berlin, Germany.*

[7]*Current address: Bioclinicum, Karolinska Institute, Stockholm, Sweden.*

+first author and #second author contributed equally.

*Corresponding author: francesco.papaleo@iit.it

Abstract

Emotion recognition and the resulting responses are important for survival and social functioning. However, how socially derived information is processed for reliable emotion recognition is incompletely understood. Here, we reveal an evolutionarily conserved long-range inhibitory/excitatory brain network mediating these socio-cognitive processes. Anatomical tracing in mice revealed the existence of a subpopulation of somatostatin (SOM) GABAergic neurons projecting from the medial prefrontal cortex (mPFC) to the retrosplenial cortex (RSC). Through optogenetic manipulations and Ca2+ imaging fiber photometry in mice and functional imaging in humans, we demonstrate the specific participation of these long-range SOM projections from the mPFC to the RSC, and an excitatory feedback loop from the RSC to the mPFC, in emotion recognition. Notably, we show that mPFC-to-RSC SOM projections are dysfunctional in mouse models relevant to psychiatric vulnerability and can be targeted to rescue emotion recognition deficits in these mice. Our findings demonstrate a cortico-cortical circuit underlying emotion recognition.

Main

Recognition and reaction to others' emotions is a fundamental and evolutionarily conserved ability shaping animals' life and survival[1,2]. Altered emotion recognition might prevent assisting a conspecific or escape an imminent threat[3]. Deficits in these socio-cognitive abilities are commonly observed in psychiatric and neurodevelopmental disorders, including schizophrenia and autism, having a profound functional impact on patients' lives[4,5].

Large-scale brain networks are involved in socio-cognitive abilities[6,7]. Intriguingly, components of the mammalian social brain also participate in the organization of the so-called default mode network (DMN)[8]. This evolutionarily conserved network plays a key role in healthy brain activity[9], and is vulnerable to disruption in psychiatric and neurodevelopmental disorders[9,10]. Core hubs of the DMN, such as the mPFC, and the posterior cingulate cortex (PCC), which in humans contains the evolutionarily ancient RSC, show strong anatomical interconnections[11,12]. Connectivity changes between these two brain regions might be present during emotion recognition in healthy and diseased states[13,14,15,16]. However, the circuit mechanisms through which these cortico-cortical networks mediate emotion recognition are unknown.

SOM neurons regulate cortical neuronal activity[17,18]. We uncovered a pivotal role for mPFC SOM neurons in emotion recognition[17]. This was achieved using a paradigm that allows the investigation of the ability of mice to perceive, process and react to positive and negative affective states in conspecifics[17,19]. This paradigm approximates features of human emotion recognition tasks, and addresses previously unexplored social cognitive functions in mice, distinct from sociability, social memory and social reward. Briefly, using olfactory and visual cues, an 'observer' mouse differentially interacts with a conspecific ('demonstrator') in an emotionally altered state compared to another in a neutral state[17,19]. Here, we hypothesized that mPFC SOM neurons participate in the larger-scale mPFC–RSC network, an evolutionary precursor of the human PFC–PCC axis[9,20], to better determine the processing and reaction to others' emotions.

Results

SOM neurons in the mPFC project to the RSC

Most SOM neurons target the dendrites of local pyramidal neurons[18,21], but might show long-range projections across the brain[22,23]. To define the nature of the mPFC–RSC pathway, we used retrograde tracing with the injection of the subunit B of the cholera toxin (Ctb-647) in the RSC of SOM-TdTomato mice (Fig. 1a–f). We confirmed the presence of RSC input from the mPFC (Fig. 1b). We confirmed the specificity of the SOM-TdTomato line with high co-labeling between SOM staining and TdTomato in the mPFC (Extended Data Fig. 1a) but scarce overlapping with other GABAergic markers (Extended Data Fig. 1b–e). Notably, we found that ~10% of TdTomato^{+} neurons were also coexpressing Ctb, with a homogeneous distribution along the mPFC anteroposterior axis (Fig. 1d–f and Extended Data Fig. 1f–i). This suggests that ~10% of mPFC SOM neurons project to the RSC.

To validate the existence of these long-range SOM-projecting neurons from the mPFC to the RSC, we injected an adeno-associated virus carrying Cre-dependent YFP (AAV-DIO-YFP) into the mPFC of SOM-cre mice (Fig. 1g). Whole-brain mapping revealed clear output to the RSC, but also to the anterior cingulate cortex (ACC), lateral septum, ventral forebrain, nucleus accumbens, medial thalamic nuclei and amygdala (Fig. 1g). Axonal reconstruction of YFP-positive terminals in the RSC revealed the highest distribution in the superficial (L1), followed by deeper layer 6, and with no-to-little distribution in the middle layers (Fig. 1h). Conditional retrograde tracing by injection of AAVrg-DIO-TdTomato in the RSC in SOM-cre mice (Fig. 1i) combined with a whole-brain mapping, revealed the presence of TdTomato+ neurons exclusively in the mPFC and the ACC with no signal in the rest of the brain (Fig. 1j). Reconstruction of TdTomato+ neurons (that is, mPFC SOM neurons projecting to the RSC) revealed two different shapes: a minority (15/47) displayed a longitudinal dendritic branch that spread in the superficial layers, while the majority showed multipolar and proximal dendritic distribution (Fig. 1k). This suggests that mPFC SOM neurons projecting to the RSC are also involved in mPFC microcircuit connectivity. Overall, this evidence highlights the existence in the mPFC of a subpopulation of inhibitory SOM neurons projecting to the RSC.

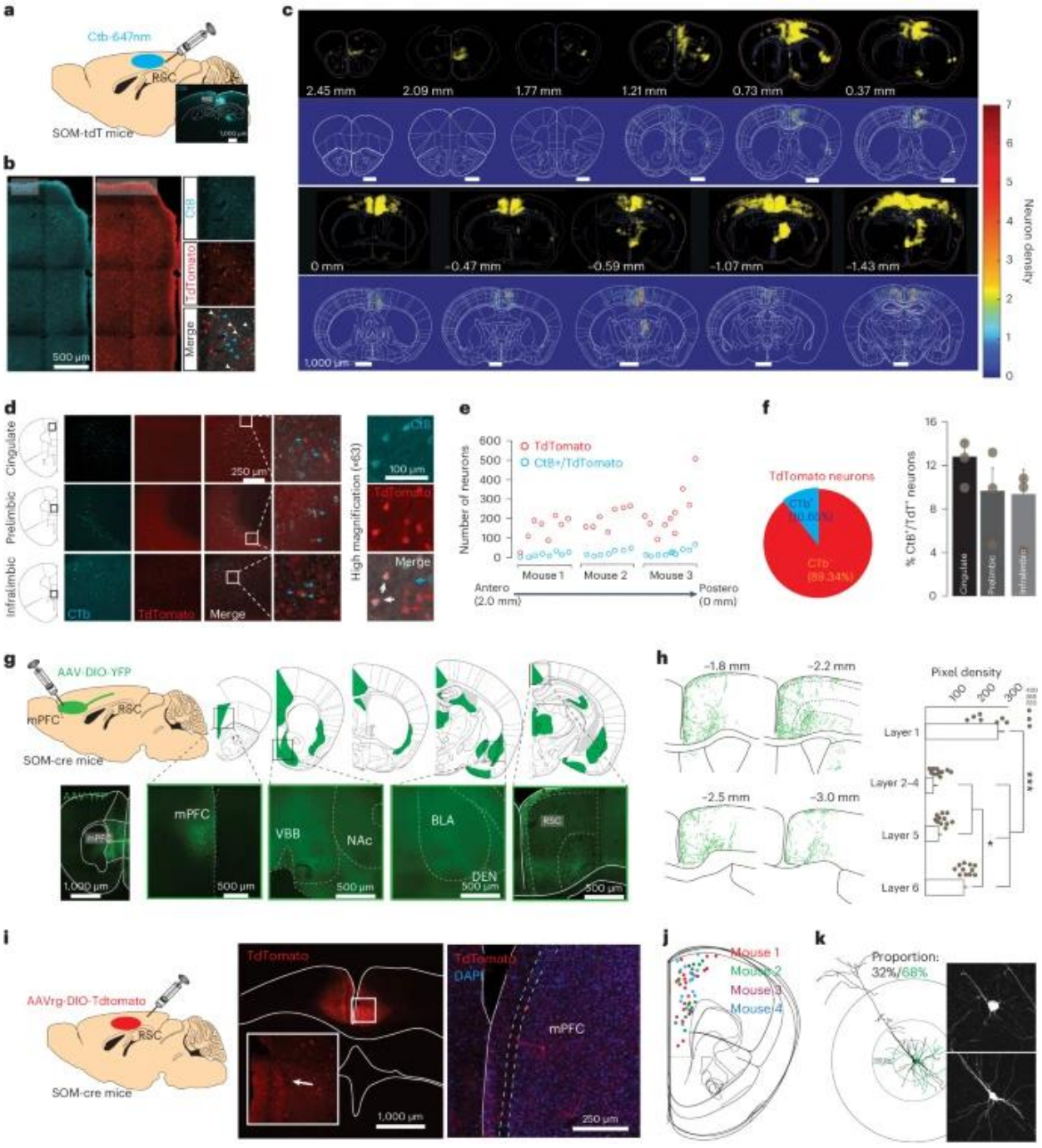

Fig. 1: A subpopulation of SOM-positive cells within the mPFC shows long-range projections to the RSC.

a, Retrograde tracing of RSC inputs in SOM-TdTomato mice ($n = 3$ male mice) using Ctb-647 tracers. **b**, Low-magnification images of the presence of Ctb^+ and $TdTomato^+$ neurons in the mPFC; the high magnification (right) highlights the presence of $TdTomato^+/Ctb^-$ (red arrow), $TdTomato^-/Ctb^+$ (blue arrows) and overlapping $TdTomato^+/Ctb^+$ (white arrow) within the mPFC. **c**, Single Ctb^+ neurons (yellow circles, upper) and Ctb^+ density (bottom) in the whole-brain mapping (blue squares are background). Neuronal density is expressed as the number of

Ctb^+ cells per 100 µm^2. **d**, Cell counting from the mPFC (cingulate, prelimbic and infralimbic subregions), of $TdTomato^+$ (red), Ctb^+ (blue) and overlapped neurons ($TdTomato^+/Ctb^+$, white arrow, repeated in three mice). **e**, Cell counting for each mouse along the anteroposterior axes. Each dot represents the counting of TdTomato (red) and $Ctb^+/TdTomato^+$ (blue) for a single 50-µm-thick brain slice containing the mPFC. **f**, Around 10% of $TdTomato^+$ neurons were also Ctb^+ (across entire PFC, left) with a uniform distribution between the cingulate, prelimbic and infralimbic subdivisions of the mPFC (right, $n = 3$ mice). Dots refer to the average value for each mouse. **g**, Whole-brain mapping of SOM projections from the mPFC ($n = 5$ mice, 2 males, 3 females). All brain regions receiving substantial axonal inputs from the SOM mPFC neurons are highlighted in green, with denser innervation of YFP-positive terminals in the vertical band of Broca (VBB), the nucleus accumbens (NAc), the basolateral amygdala (BLA) and the RSC. **h**, Reconstruction of YFP-positive terminals within the RSC (one-way analysis of variance (ANOVA), $***P < 0.0001$, $*P < 0.05$ versus layer 1 or 6). **i**, Conditional adenoviral retrograde tracing in the RSC of SOM-cre mice ($n = 4$ female mice) showed TdTomato-positive neurons within the mPFC. **j**, Placements of the soma of SOM-positive cells within the mPFC that project to the RSC following the strategy illustrated in **i**. **k**, Anatomical reconstruction of mPFC SOM^+ projecting neurons. Proportion of neurons with long (black) or short (green) dendritic arborization calculated from 94 SOM reconstructed neurons (two-sided *t*-test $P < 0.05$ short > long arborization). Individual data points and the mean ± s.e.m. are shown. Complete statistics are available in Supplementary Table 1 and https://doi.org/10.48557/FEXUTZ.

mPFC SOM projections to the RSC control emotion recognition

We then tested whether inhibiting or exciting mPFC SOM projections to the RSC could modulate emotion recognition (Fig. 2a–c and Extended Data Fig. 2), using an optogenetic approach used to manipulate the entire mPFC SOM population[17].

We bilaterally injected in the mPFC of SOM-cre mice either an AAV-DIO-NphR or a ChR2 (Fig. 2a) and placed a red or blue light-emitting-diode (LED) above the RSC to inhibit or excite, respectively, the mPFC-to-RSC SOM projections. As expected[17], without optogenetic manipulation, observer mice discriminated both the stress and relief demonstrators (Fig. 2b–e). In contrast to inhibition of whole mPFC SOM neurons[17], inhibiting mPFC-to-RSC SOM projections enhanced stress and relief recognition (Fig. 2b–e). No sex-dependent differences were evident (Extended Data Fig. 3). No effects in other behavioral measures were evident (Extended Data Fig. 4), apart from a decreased time in the transition empty zone and reduced entries in the demonstrators' zone (Extended Data Fig. 4), which combined with the increased exploration toward the emotionally altered mice (Fig. 2) strengthens the fact that this

manipulation prolongs the willingness of mice to socially interact. Conversely, photostimulation of mPFC-to-RSC SOM projections abolished both stress and relief recognition (Fig. 2b–e). No sex-dependent differences were evident (Extended Data Fig. 3). No effects in other behavioral measures were evident apart from an increased number of entries in both zones (Extended Data Fig. 4). We confirmed in vivo that optogenetic stimulation of mPFC SOM neurons increased GCaMP activity in both SOM mPFC soma and RSC terminals (Extended Data Fig. 2a,b), while stimulation of SOM RSC terminals did not affect the GCaMP signal of the SOM mPFC soma (Extended Data Fig. 2c), suggesting no antidromic activation. Moreover, we found that photoinhibition of mPFC-to-RSC SOM terminals during emotion recognition increased ex vivo cFos activity within the RSC (Extended Data Fig. 2d,e). Conversely, in vivo photoactivation of mPFC-to-RSC SOM terminals sharply decreased RSC activity (Extended Data Fig. 2f,g). These findings confirmed that mPFC-to-RSC SOM terminals were inhibitory projections.

Notably, both activation and inhibition of the SOM terminals in the RSC had no effect on the preference to spend more time with a mouse compared to an object (Extended Data Fig. 2h), in the ability to discriminate a familiar versus a novel mouse (Extended Data Fig. 2i) and in locomotor activity (Extended Data Fig. 2j). Similarly, no effects of activation and inhibition lights were evident on emotion recognition in YFP-injected SOM-cre mice (Extended Data Fig. 2k,l). Overall, these results indicate that inhibitory mPFC-to-RSC SOM projections are involved in emotion recognition, but not in sociability or social novelty.

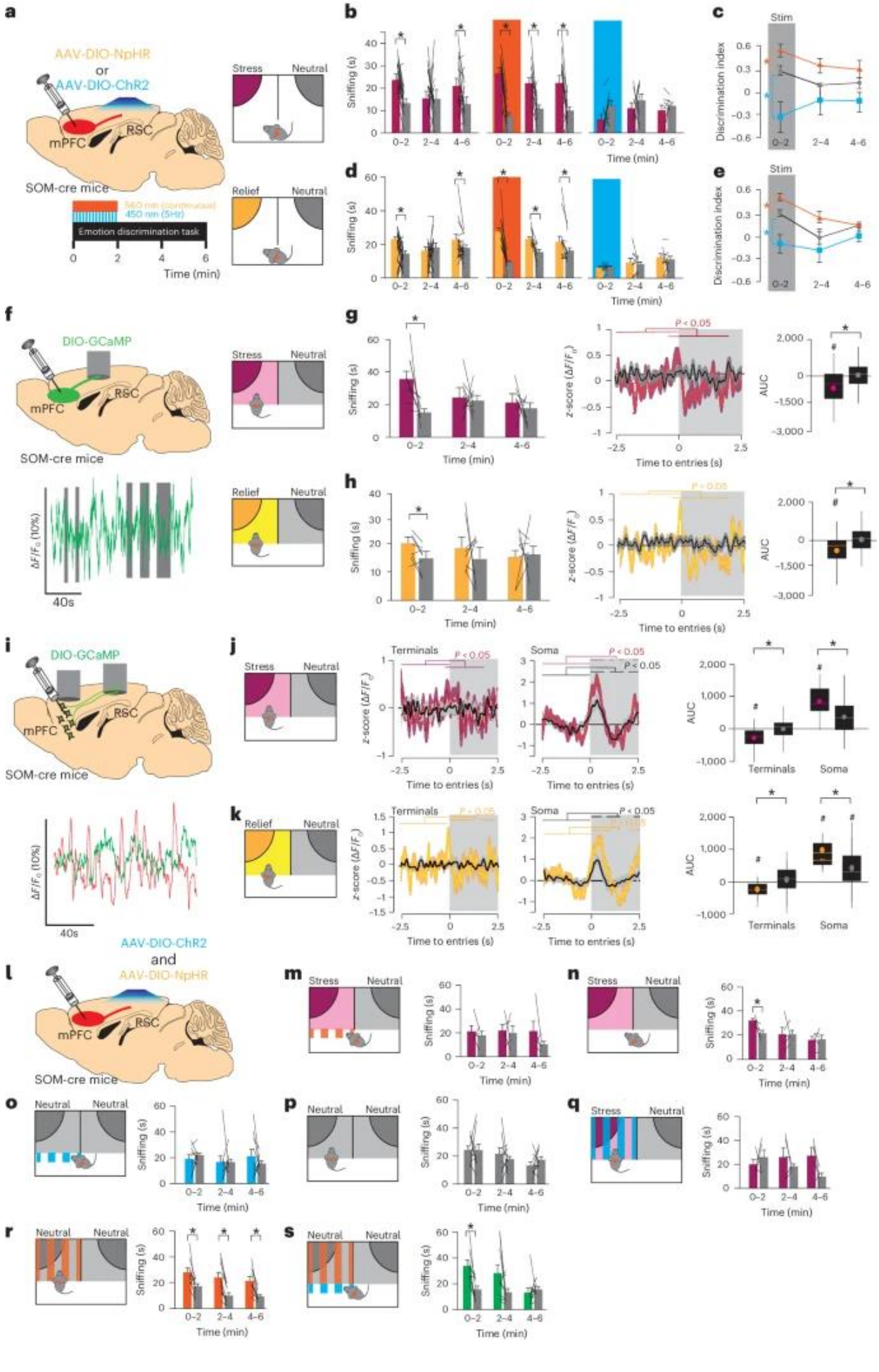
a
AAV-DIO-NpHR
or
AAV-DIO-ChR2
mPFC
RSC
SOM-cre mice
560 nm (continuous)
450 nm (5Hz)
Émotion discrimination task
Time (min)
Stress
Neutral
Relief
b
Sniffing (s)
Time (min)
c
Stim
Discrimination index
d
e
f
DIO-GCaMP
ΔF/F0 (10%)
40s
g
z-score (ΔF/F0)
Time to entries (s)
AUC
P < 0.05
h
i
j
Terminals
Soma
k
AAV-DIO-ChR2
and
AAV-DIO-NpHR
l
m
n
o
p
q
r
s

Fig. 2: mPFC-to-RSC SOM terminals are involved in emotion recognition.

a, SOM-cre mice were bilaterally injected in the mPFC with either AAV-DIO-NphR (orange, $n = 14$ mice, 6 males, 8 females) or AAV-DIO-ChR2 (blue, $n = 9$ mice, 5 males, 4 females), and after at least 4 weeks a 560-nm continuous light or 450-nm 5-Hz light was delivered in the RSC during the first 2 min of the emotion recognition tasks. **b**–**d**, Time (in seconds) spent sniffing demonstrators in neutral (gray), restrain-induced stress (purple) or water-induced relief (yellow) affective states displayed by the same observer mice without light stimulation (first column graphs), with photoinhibition (second column graphs, orange background bars) or photostimulation (third column graphs, blue background bars) performed for 2 min from the beginning of the test (**b**, repeated-measures (RM) ANOVA; post hoc Bonferroni $^{*}P < 0.05$ stress versus neutral; **d**, RM-ANOVA; post hoc Bonferroni $^{*}P < 0.05$ relief versus neutral). **c**–**e**, Comparison of the no-light (gray circles), photoinhibition (orange triangle) and photostimulation (blue squares) conditions by calculating a discrimination index ([time spent with emotionally altered demonstrator − time spent with neutral demonstrator] / [total time spent with both demonstrators]) (**c**, two-way RM-ANOVA stress paradigm; post hoc Bonferroni on optostimulation effect: $^{*}P = 0.0008$ ChR2 versus no light, $^{*}P = 0.007$ NphR versus no light, $P < 0.0001$ NphR versus ChR2; **e**, two-way RM-ANOVA relief paradigm; post hoc Bonferroni on optostimulation effect: $^{*}P = 0.02$ ChR2 versus no light, $^{*}P = 0.05$ NphR versus no light, $P = 0.0001$ ChR2 versus NphR). **f**, Injection of AAV-DIO-GCaMP6f in the mPFC of SOM-cre mice (5 females, 4 males) and implantation of an optic fiber in the RSC, to record calcium oscillations of mPFC-to-RSC SOM neuron terminals using fiber photometry. Bottom graph, example of calcium signal at the terminal level. **g**,**h**, (left, bar graphs) Sniffing behavior (in seconds) of implanted observer mice toward stressed (**g**, RM-ANOVA; post hoc Bonferroni $^{*}P = 0.02$ stress versus neutral) or relieved (**h**, RM-ANOVA; post hoc Bonferroni $^{*}P < 0.005$ relief versus neutral) demonstrators. **g**,**h**, (middle, line graphs) GCaMP signal in the RSC during discrimination for stress (**g**, $n = 77$ entries to stress mouse zone, $n = 61$ entries to neutral mouse) or relief (**h**, $n = 78$ entries to relief, $n = 72$ entries to neutral mouse) increased shortly 250 ms before entries to emotionally altered mice followed by a decrease of the signal (Bonferroni-corrected two-sided *t*-test, horizontal lines indicate the time range that differed from baseline $P < 0.05$; stress, purple; relief, yellow; neutral, gray). **g**,**h**, (right, bar graphs) AUC during entries in the stress (purple), relief (yellow) and neutral (gray) demonstrators' zones (two-tailed paired *t*-test: $^{\#}P < 0.0001$ versus baseline; $^{*}P < 0.0001$ versus neutral). **i,** SOM-cre mice were injected with AAV-DIO-GCaMP6f in the mPFC and implanted with an optic fiber above the mPFC and another above the superficial layers of the RSC for simultaneous recording of GCaMP oscillation of SOM neurons in the mPFC (red trace) and their terminals in the RSC (green trace, $n = 5$ female mice). **j**,**k**, (left line graphs) Calcium signal in the RSC (terminals) when in the stress (purple), relief (yellow), and neutral (gray) demonstrator mouse zones ($n = 104$ entries to stress, $n = 32$ entries to neutral; $n = 157$ entries to relief, $n = 52$ entries to neutral; Bonferroni-corrected two-sided *t*-test, horizontal lines indicate the time range that differed from baseline $P < 0.05$). **j**,**k**, (middle graphs lines) Fiber photometry recordings of calcium signal at the mPFC level (soma) following entries to the stress (purple), relief (yellow) and neutral (gray) demonstrators (Bonferroni-corrected, two-sided *t*-test, horizontal lines indicate the time range that differed from baseline $P < 0.05$). **j**,**k**, (right bar graphs) The AUC during entries in the demonstrators' zones (two-tailed paired *t*-test: $^{\#}P < 0.05$ versus baseline; $^{*}P < 0.05$ versus neutral). **l**, SOM-cre mice ($n = 5$–10) were bilaterally injected in the

mPFC with both AAV-DIO-ChR2 (blue) and AAV-DIO-NphR (orange) and implanted with a bilateral optic fiber in the RSC, for specific optogenetics manipulation of SOM terminals. **m**, Photoinhibition before the entries to the stress mouse zone (200 ms, for the 6-min test, RM-ANOVA). **n**, Without light stimulation (RM-ANOVA; post hoc Bonferroni $*P < 0.05$ stress versus neutral). **o**, Activation of the mPFC-to-RSC SOM terminals (5 Hz, 200 ms) before the entry to a zone of one of two neutral demonstrators randomly selected (for the 6-min test). **p**, No light stimulation (0–2 min, 2–4 min, 4–6 min). **q**, Stimulation (5 Hz, with a 5-ms pulse) of the mPFC-to-RSC SOM terminals, but only when in the stress demonstrator zone, impaired emotion recognition. **r**, Inhibition (continuous light) of SOM terminals in the RSC during entry to a random zone of one of two neutral mice (RM-ANOVA; post hoc Bonferroni $*P < 0.05$ stimulated versus non-stimulated zone). **s**, Mimicking the same pattern of activation of mPFC-to-RSC SOM terminals found by fiber photometry by stimulation before the entry zone (200 ms, 5 Hz, entire 6 min) followed by inhibition within the zone (continuous, entire 6 min) of only one of two neutral demonstrators (RM-ANOVA; post hoc Bonferroni $*P < 0.005$ stimulated versus non-stimulated zone). Experiments were replicated in different groups of mice tested in different moments, from different cages, and of different sex (Extended Data Fig. 8). Bar and line graphs show the mean ± s.e.m. AUC values are represented as box-and-whisker plots, presenting the upper and lower quartiles, mean and median. Complete statistics are available in Supplementary Table 1 and https://doi.org/10.48557/FEXUTZ.

Activity of mPFC-to-RSC SOM terminals in emotion recognition

To clarify how mPFC-to-RSC SOM projections physiologically respond to emotion recognition, we performed fiber photometry imaging of mPFC SOM terminals in the RSC expressing a genetically encoded GCaMP6f calcium indicator (Fig. 2f).

Photometry recording did not affect emotion recognition for a stress (Fig. 2g) or a relief (Fig. 2h) mouse. Calcium activity of SOM terminals was aligned to the entries into the stress, relief or neutral demonstrators' zones. An entry duration threshold of 2.5 s was selected as 95% of demonstrators' sniffing occurred when entries lasted at least 2.5 s (Extended Data Fig. 2m), also avoiding overlapping of signal analyses. Calcium variations from 2.5 s before to 2.5 s after entries in a demonstrator zone were analyzed every 250 ms, and as a variation of the area under the curve (AUC), compared to the 2.5-s pre-entry period. We found a decrease of the terminals' signal during entries to the stress (Fig. 2g) or the relief (Fig. 2h) mouse zone, but not when entering the neutral mouse zone. This decrease was always preceded by an increase of the signal 150–200 ms before entry (Fig. 2g,h). This effect was equally evident in male and female mice (Extended Data Fig. 3). No calcium signal changes were observed during the recognition

between an object and an unfamiliar mouse (Extended Data Fig. 5a) or between a familiar and an unfamiliar mouse (Extended Data Fig. 5b), ruling out also any motor artifacts. Furthermore, mice injected with a control virus (AAV-DIO-YFP) did not display changes of the signal during stress or relief recognitions (Extended Data Fig. 5c,d).

We next asked how the signal of SOM RSC terminals would correlate with the signal at the soma level of all mPFC SOM neurons (Fig. 2i). By dual-photometry recordings, we confirmed a similar pattern of activation at the terminals with increased signal immediately before entrance in the zone of an emotionally altered mouse followed by reduced activity within the altered mouse zones (Fig. 2j,k; terminals). In contrast, in the mPFC, an increase in the overall signal was observed during interactions with either a neutral or an emotionally altered mouse, but the response to emotionally altered demonstrators was higher (Fig. 2j,k, soma). This latter evidence is in line with what we observed with in vivo electrophysiology and miniscope techniques17. Moreover, we found no correlation between the mPFC and the RSC overall signals within each mouse, as aligning calcium events in the mPFC to the RSC terminals' bulk activity revealed increased RSC signal in 45.2% of the mPFC events, while showing decreased signal in 45% of mPFC events (Extended Data Fig. 5e,f).

Altogether, these findings indicate that compared to the entire SOM population in the mPFC, mPFC-to-RSC SOM terminals are functionally distinct and exhibit a specific pattern of activation when interacting with emotionally altered mice.

Emotion recognition needs precise SOM mPFC-to-RSC activation

We next tested if the observed pattern of activation of mPFC-to-RSC SOM terminals drives emotion recognition using a validated within-subject dual-opsin stimulation that shows no cross-talk between wavelengths24.

We first tested whether the short activation (200 ms) before entries to the zone of an emotionally altered mouse (Fig. 2g–k) was determinant. Photoinhibition (200 ms) delivered when mice were in the area adjacent to the entry zone of the emotionally altered mouse impaired discrimination over the neutral demonstrator (Fig. 2m). The same mice with no optogenetic manipulation had intact emotion recognition (Fig. 2n). We then asked whether stimulation of SOM mPFC-to-RSC

terminals, only when approaching a demonstrator zone could induce discrimination between two conspecifics in an equal neutral state. Activation before the entries did not affect social preference (Fig. 2o), similarly to no-stimulation conditions (Fig. 2p). No sex-dependent effects were evident (Extended Data Fig. 3). These data suggest that an increased activation of mPFC SOM terminals in the RSC before approaching an emotionally altered mouse is important, but not sufficient to induce social discrimination.

We next addressed the implication of the apparent inhibition observed for SOM mPFC-to-RSC terminals while interacting with emotionally altered mice (Fig. 2g–k). Blocking this inhibition by photostimulation of SOM mPFC-to-RSC terminals only when the observer was in the zone of an emotionally altered mouse abolished emotion recognition (Fig. 2q). Conversely, simulating this inhibition by photoinhibition of SOM mPFC-to-RSC terminals when the observer was in the zone of only one of two neutral demonstrators induced a social preference (Fig. 2r). These data indicate that the inhibition of SOM mPFC-to-RSC terminals during the interaction with an emotionally altered mouse is an important component of emotion recognition.

We tried to optogenetically mimic the entire physiological pattern of activation of the SOM mPFC-to-RSC terminals. Combining a short activation before the entries followed by inhibition when in the zone of one of two neutral mice induced a preference that lasted only the first 2 min of the test (Fig. 2s), better mimicking the normal emotion recognition behavior (Fig. 2b,d,g,h,n). Activating or inhibiting SOM mPFC-to-RSC terminals with the same patterns but in absence of stimulus mice, did not induce any side preference or change in the number of entries (Extended Data Fig. 5g–l). These data indicate that the observed pattern of activity of the SOM mPFC-to-RSC terminals is determinant for emotion recognition.

mPFC SOM projections modulate emotion recognition in RSC recognition

SOM cells regulate cortical neuronal activity18,21. However, ex vivo whole-cell patch-clamp recording revealed that while optogenetic activation of ChR2-expressing mPFC SOM cells induce inhibitory postsynaptic currents in mPFC pyramidal neurons (Extended Data Fig. 6a–c), optogenetic activation of mPFC SOM terminals never induced reliable postsynaptic currents in

RSC pyramidal neurons (Extended Data Fig. 6d,e). This could be due to cutting the few long-range projections in ex vivo slices as observed for other pathways25.

Thus, we simultaneously recorded calcium activity of RSC pyramidal neurons while optogenetically inhibiting mPFC SOM terminals in vivo (Fig. 3a). In the home cage single-house condition, repeated inhibition of SOM terminals (Fig. 3b) did not change the average activity of deeper-layer RSC pyramidal neurons (Fig. 3c). However, enhanced increase or decrease in calcium signal in pyramidal neurons was evident following inhibition of the SOM terminals (Fig. 3d), but not in the absence of opsin (Extended Data Fig. 2n), suggesting some modulatory effects. To test whether a more reliable effect could be evident in the context of social stimuli, we used the same optogenetic/fiber photometry conditions during emotion recognition (Fig. 3e–i). We found that without optogenetic inhibition, the overall activity of RSC pyramidal neurons increased during entries to both stress and neutral zones, with a higher magnitude in the stress mouse zone (Fig. 3e). This same pattern of RSC pyramidal activity was confirmed in another cohort of mice without opsin expression in the mPFC, for both stress and relief conditions (Extended Data Fig. 7a,b). If the zone of the emotionally altered mouse was paired with optogenetic inhibition of SOM terminals (Fig. 3f), the increase in RSC pyramidal activity associated with the stress mouse was of higher magnitude and lasted longer (Fig. 3e–h). Without stimulus mice, these changes were less evident (Fig. 3g,h). mPFC SOM terminals can then differentially regulate RSC pyramidal cell activity depending on the context.

To further quantify and directly compare such effects, we calculated the signal-to-noise ratio (SNR) as the ratio of signal amplitude to the noise variance26. The SNR was higher during entries to the stress mouse zone when paired with optogenetic inhibition of mPFC SOM terminals compared to the stress without optoinhibition, to neutral mouse zone, and to an empty zone with the same optoinhibition (Fig. 3i). Thus, optoinhibition of SOM terminals increases the variation of the signal in deeper-layer RSC pyramidal neurons when in the presence of emotionally salient social stimuli.

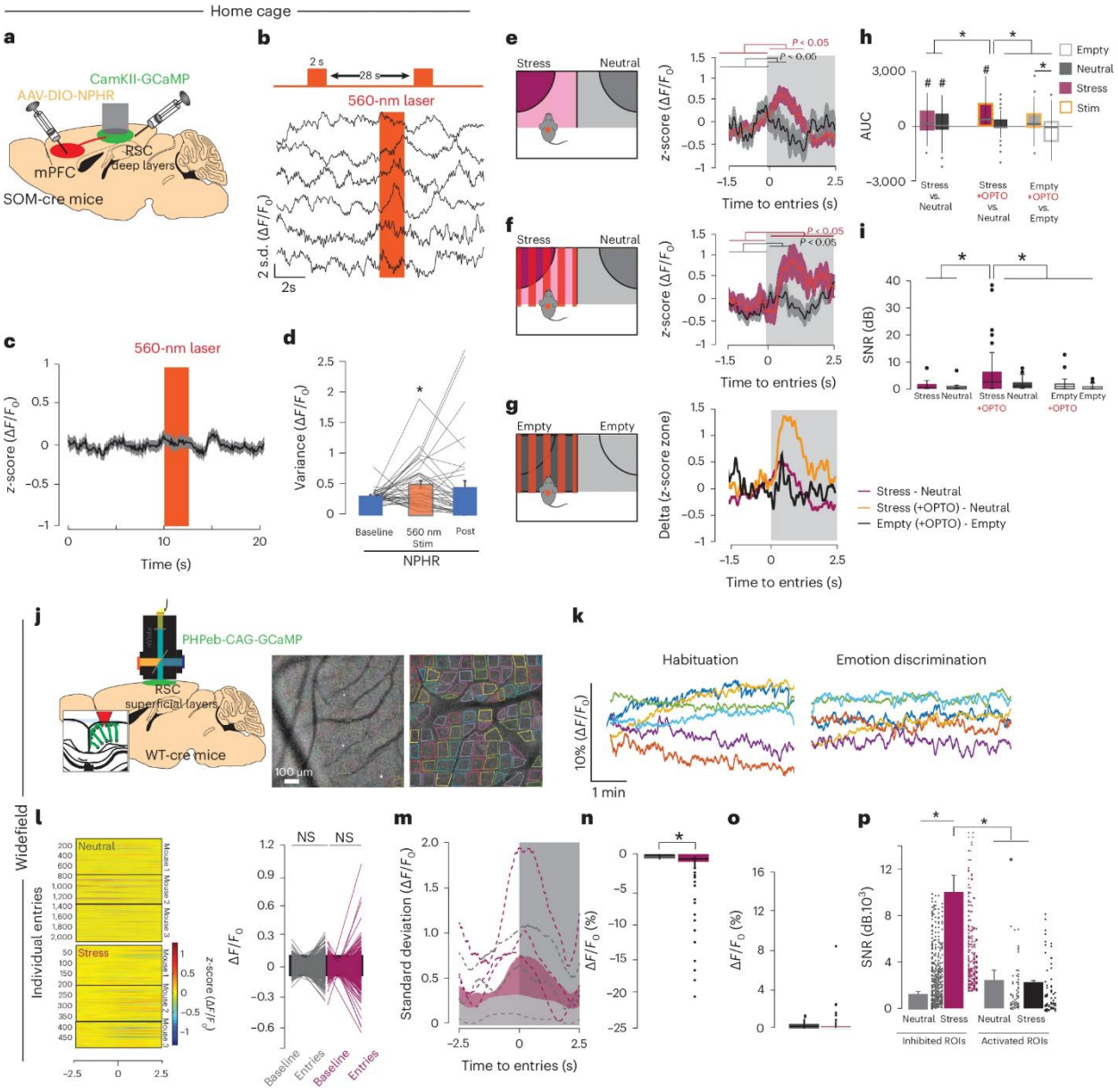

Fig. 3: mPFC-to-RSC SOM terminals amplify RSC differential activation responses between encounter of a neutral versus emotionally altered mouse.

a, SOM-cre mice ($n = 5$ male mice) were injected with AAV-DIO-NphR in the mPFC and AAV-CaMKII-GCaMP6 in the RSC to allow recording of RSC pyramidal neurons using fiber photometry while optogenetically inhibiting mPFC SOM terminals. **b**–**d**, Mice were first tested in their home cage (single housed). **b**, Examples of single trials following 560-nm light delivery for 2 s every 28 s for 15 min. **c**, *z*-score normalization of all trials with photoinhibition showing no modulation of the overall average RSC pyramidal cell activity. **d**, Comparison of the variability of the photometry signal before (10 s, baseline), during (2 s, 560 nm, stim) or after (8 s, post) stimulation (*$P = 0.007$ versus baseline and post). **e**, GCaMP fiber photometry recordings of RSC pyramidal neurons during exploration of stress (purple) or neutral (gray) demonstrators ($n = 5$ mice, $n = 47$ entries neutral; $n = 145$ entries

stress). **f**, Fiber photometry recordings of RSC pyramidal neurons with photoinhibition of mPFC SOM terminals, when the observer mouse was in the stress mouse zone (same five mice, $n = 23$ entries neutral, $n = 45$ entries stress). **g**, Fiber photometry recordings of RSC pyramidal neurons with the same photoinhibition of **f**, but when the observer was in one random side of the apparatus with no mice (empty zone) ($n = 7$ male mice, entire 6 min, $n = 27$ entries unpaired side, $n = 45$ entries light-paired side). The *z*-score difference (delta) was obtained for each experiment by subtracting the pyramidal neuron signal when in the neutral mouse zone (or empty with no light delivery) minus that when in the stress mouse zone (or empty with optogenetics stimulation). **h**, AUC of the zone entries for all conditions tested ($^{\#}P < 0.05$ versus own baseline; post hoc Bonferroni $^{*}P < 0.05$). **i**, Evaluation of the SNR in decibels (dB; one-way ANOVA; post hoc Bonferroni $^{*}P < 0.0001$ stress + opto versus all other). **j**, Widefield imaging of overall activity of superficial layers of the RSC throughout the cranial window using an nVoke miniscope. Right, example of the design of the ROIs ($n = 3$ male mice, 96.7 average ROIs per mouse, $n = 330$ total ROIs). Blood vessels were excluded from ROIs. **k**, Example traces from the same mouse of GCaMP $\Delta F/F_0$ of different ROIs (color coded) during the habituation and emotion recognition test phases. **l**, Raster plot for each entry for each ROI (left) and average GCaMP signal (right) during baseline (−2.5 s to 0 s) and entries (0 s to 2.5 s) showing the variation of the GCaMP $\Delta F/F_0$. **m**, Standard deviation for each mouse (line, $n = 3$ mouse) and group (shade) during entries to the stress (purple) or neutral (gray) demonstrator. **n**, Entries associated with a decrease of the signal when in the stress or neutral mouse zone ($^{*}P = 0.049$ stress versus neutral; ROIs: 364 for stress, 102 for neutral). **o**, Entries associated with an increase of the signal when in the stress or neutral mouse zone (ROIs: 270 for stress, 98 for neutral). **p**, SNR for the ROIs that are presenting a reduction of the $\Delta F/F_0$ or an increase following entry to neutral or stress demonstrators (two-way ANOVA; post hoc Bonferroni $^{*}P < 0.005$ versus stress-inhibited ROIs). Bar plots are represented as the mean ± s.e.m. Box-and-whisker plots show the upper and lower quartiles, mean and median. NS, not significant. Complete statistics are available in Supplementary Table 1 and https://doi.org/10.48557/FEXUTZ.

Emotion recognition increases RSC activity

Superficial layers of the RSC receive more projections from mPFC SOM terminals (Fig. 1h), and are receiving more inputs and better integrate sensory stimuli in behaving mice21. To test if mPFC-to-RSC SOM terminals might modulate overall activity of RSC superficial layers depending on the integration of socially derived information, we combined cranial window widefield imaging (focal plan 100–200 µm deep) in freely moving mice, together with whole-brain expression of GCaMP7f (Fig. 3j and Extended Data Fig. 2f,g)27. This images the overall activity of RSC superficial layers, including extrinsic inputs, interneurons and local dendritic signals. Regions of interest (ROIs), excluding all blood vessels and representing an average signal of ~100 × 100 µm, were analyzed during habituation and emotion recognition (Fig. 3k).

Overall, no differences in the change of fluorescence relative to background fluorescence (ΔF/F0) for all ROIs were evident when entering either neutral or emotionally altered mouse zones (Fig. 3l). However, an increase of the standard deviation was present when entering emotionally altered mouse zones compared to the neutral (Fig. 3l,m). Next, we divided zone entries associated with a decrease (Fig. 3n) or an increase of the RSC signal (Fig. 3o) and compared the response amplitude if located in the neutral or the stress side. In entries associated with an inhibition, the decrease of the GCaMP signal was of higher magnitude when in the stress zone compared to the neutral zone (Fig. 3n). No differences were evident for entries associated with an increase of the ΔF/F0 (Fig. 3o). Furthermore, the SNR was highest when in the stress zone, but only for ROIs showing an inhibition (Fig. 3p), in line with the photometry data in deeper layers (Fig. 3i). Overall, these findings confirm and expand to RSC superficial layers the evidence that increased inhibition of the RSC is associated with increased signal over general variance of the noise (including both extrinsic and local signal), only when mice interact with an emotionally altered conspecific.

RSC pyramidal neurons generally encode social information

The different responses of RSC pyramidal neurons between a neutral and an emotionally altered mouse appear to be relevant for emotion recognition (Fig. 3). We then tested whether inhibiting or exciting RSC pyramidal cells could modulate emotion recognition (Fig. 4a–e), using the same approach used for mPFC-to-RSC SOM projections (Fig. 2a–e). Photoinhibition of RSC pyramidal neurons reverted preference for stress (Fig. 4b,c) and relief (Fig. 4d,e). Photostimulation of RSC pyramidal neurons abolished recognition for stress (Fig. 4b,c) and relief (Fig. 4d,e). However, time-locked photoinhibition of RSC pyramidal cells only when in the zone of emotionally altered mice did not alter emotion recognition (Fig. 4f–i). This suggests that the overall population of RSC pyramidal cells might not specifically code for recognition of altered emotions.

We also found that photostimulation, but not photoinhibition, of RSC pyramidal neurons reduced total exploration independently from the emotional state of the demonstrators (Extended

Data Fig. 7c–e). Moreover, photostimulation, but not photoinhibition, of RSC pyramidal neurons also impaired preferences for a mouse over an object, as well as the preference for an unfamiliar compared to a familiar mouse (Extended Data Fig. 7f–i). This further suggests that the overall population of RSC pyramidal neurons might code for social information, but not specifically for emotions. In agreement, RSC pyramidal cells increased their activity also during exploration of a mouse, but not of an object (Fig. 4j), and during interaction with an unfamiliar mouse, but not with a familiar mouse (Fig. 4k).

The RSC is commonly associated with the storage of spatial information28. To assess if our findings might be influenced by nonsocial spatial navigation, we photostimulated only one side of the apparatus, but without social stimuli. No changes in side preference, distance traveled and the number of entries to the stimulated or non-stimulated zones were evident (Extended Data Fig. 7j–m). In contrast, if RSC pyramidal neurons were photostimulated only in one of two neutral mouse zones, an increase of entries was evident in the zone paired with the activation (Extended Data Fig. 7n–q). These data strengthen the conclusion that RSC pyramidal neurons generally encode for social information.

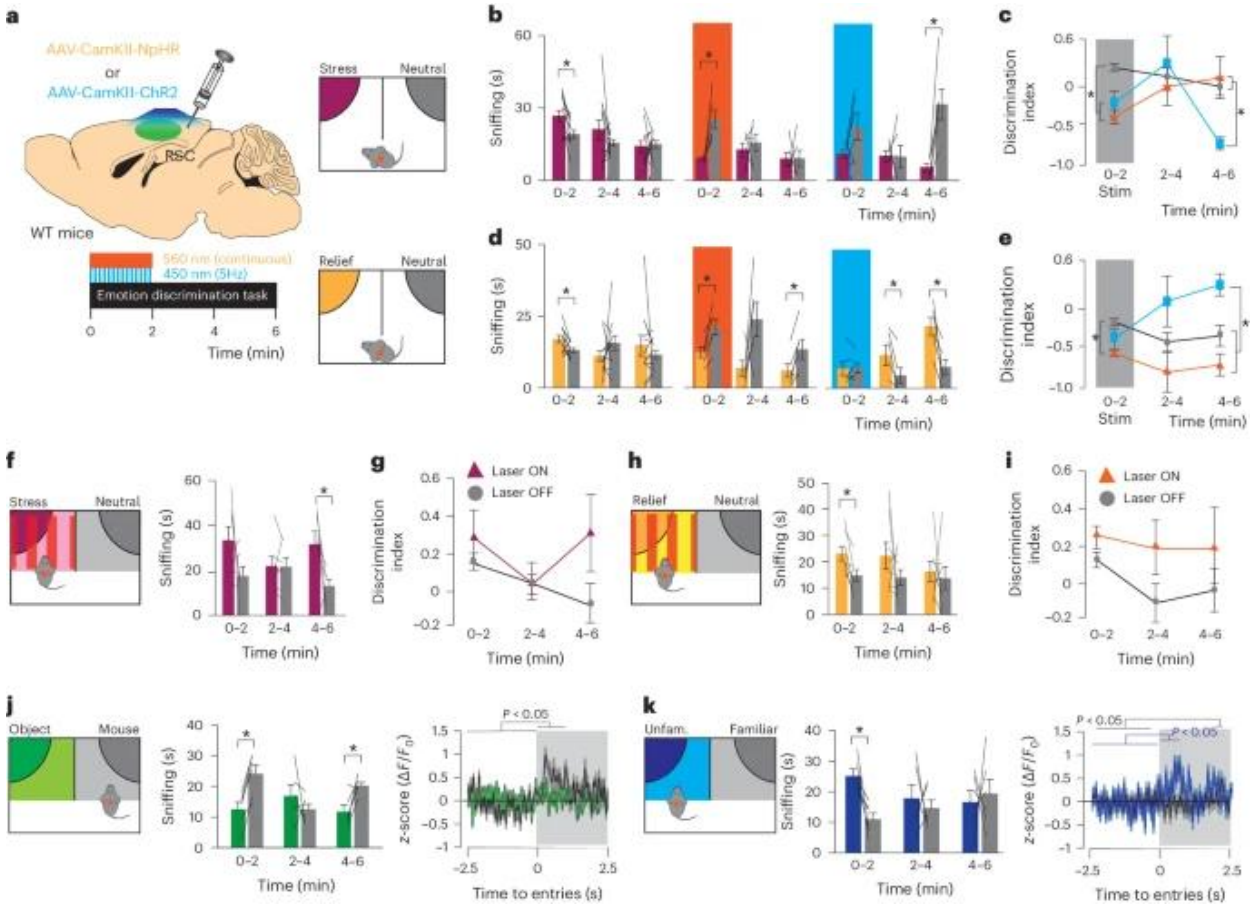

Fig. 4: RSC pyramidal neurons generally encode social information.

a, WT mice ($n = 12$ females) were bilaterally injected in the RSC with either AAV-CamKII-NphR (orange, $n = 6$ females) or AAV-CamKII-ChR2 (blue, $n = 6$ females), and after at least 4 weeks a 560-nm continuous light or a 450-nm 5 Hz light was delivered during the first 2 min of the stress and relief emotion recognition task for inhibition or activation, respectively, of RSC pyramidal neurons. **b**,**d**, Time (in seconds) spent sniffing demonstrators in neutral (gray bars), stress (purple bars) or relief (yellow bars) affective states displayed by the same observer mice without light stimulation (graphs in first column), with photoinhibition (graphs in second column, orange background) or photostimulation (graphs in third column, blue background). (RM-ANOVAs; post hoc Bonferroni $^*P < 0.05$ emotionally altered versus neutral). **c**,**e**, Discrimination index of the no-light (gray circles), photoinhibition (orange triangle) and photostimulation (blue squares) conditions during the emotion recognition test (**c**,**e**, two-way RM-ANOVA; post hoc Bonferroni $^*P < 0.005$ versus no light at 0–2 min, $^*P < 0.05$ versus ChR2 at 4–6 min). **f**–**i**, In these same mice, photoinhibition of RSC pyramidal cells only when in the stress (**f** and **g**) or relief (**h** and **i**) demonstrator zone (RM-ANOVAs; post hoc Bonferroni $^*P < 0.05$ versus stress). **j**, Behavior (RM-ANOVAs; post hoc Bonferroni $^*P < 0.05$ object versus mouse) and fiber photometry recording of RSC pyramidal neurons of observer mice ($n = 6$ males) during discrimination between a mouse and an object

($n = 35$ entries to object, $n = 65$ entries to neutral). **k**, Behavior (RM-ANOVAs; post hoc Bonferroni $*P = 0.02$ familiar versus unfamiliar) and fiber photometry recording of RSC pyramidal neurons from the same mice during recognition between a familiar (gray) and an unfamiliar (blue) mouse ($n = 66$ entries to unfamiliar, $n = 70$ entries to familiar). All bar plots are represented as the mean ± s.e.m. Complete statistics are available in Supplementary Table 2 and https://doi.org/10.48557/FEXUTZ.

RSC-to-mPFC pyramidal neurons modulate emotion recognition

Reciprocal projections between the mPFC and the RSC are reported29, as we confirmed by whole-brain mapping of RSC pyramidal projections (Extended Data Fig. 8). Thus, we tested whether checking only RSC pyramidal projections to the mPFC could have a more restricted involvement in emotion recognition.

Mice were injected in the RSC with AAV-CamKII-GCaMP6f and the overall signal of mPFC-terminals was recorded during different social tasks by fiber photometry (Fig. 5a–d). RSC pyramidal terminals in the mPFC showed increased activity when in the zone of an emotionally altered mouse, whether in the stress or relief zone, compared to when in the neutral demonstrator zone (Fig. 5a,b). In contrast, no change of activation was evident when discriminating an object versus a mouse (Fig. 5c), or a familiar versus an unfamiliar mouse (Fig. 5d). Thus, in contrast to the overall population of RSC pyramidal neurons (Fig. 4), those projecting to the mPFC might have a more selective involvement in emotion recognition.

We then tested whether photoinhibition of only RSC pyramidal terminals in the mPFC when mice were in the zone of the emotionally altered mouse would impair emotion recognition. With no optogenetic manipulation, the usual emotion recognition was evident (Fig. 5e,f). However, and in contrast to photoinhibition of all RSC pyramidal neurons (Fig. 4f–i), emotionally altered mouse-locked photoinhibition of RSC-to-mPFC pyramidal terminals abolished emotion recognition for stress and relief (Fig. 5e,f). This photoinhibition did not induce side preference/aversion if no mice were present (Fig. 5g). Finally, mimicking fiber photometry data (Fig. 5a,b), we found that photoactivation of RSC-to-mPFC pyramidal terminals induces a social preference for an otherwise neutral mouse when paired with the light-induced activation

(Fig. 5h). Overall, these findings highlight a reciprocal and more prominent involvement of the mPFC–RSC–mPFC inhibitory–excitatory circuit in emotion recognition (Fig. 5i).

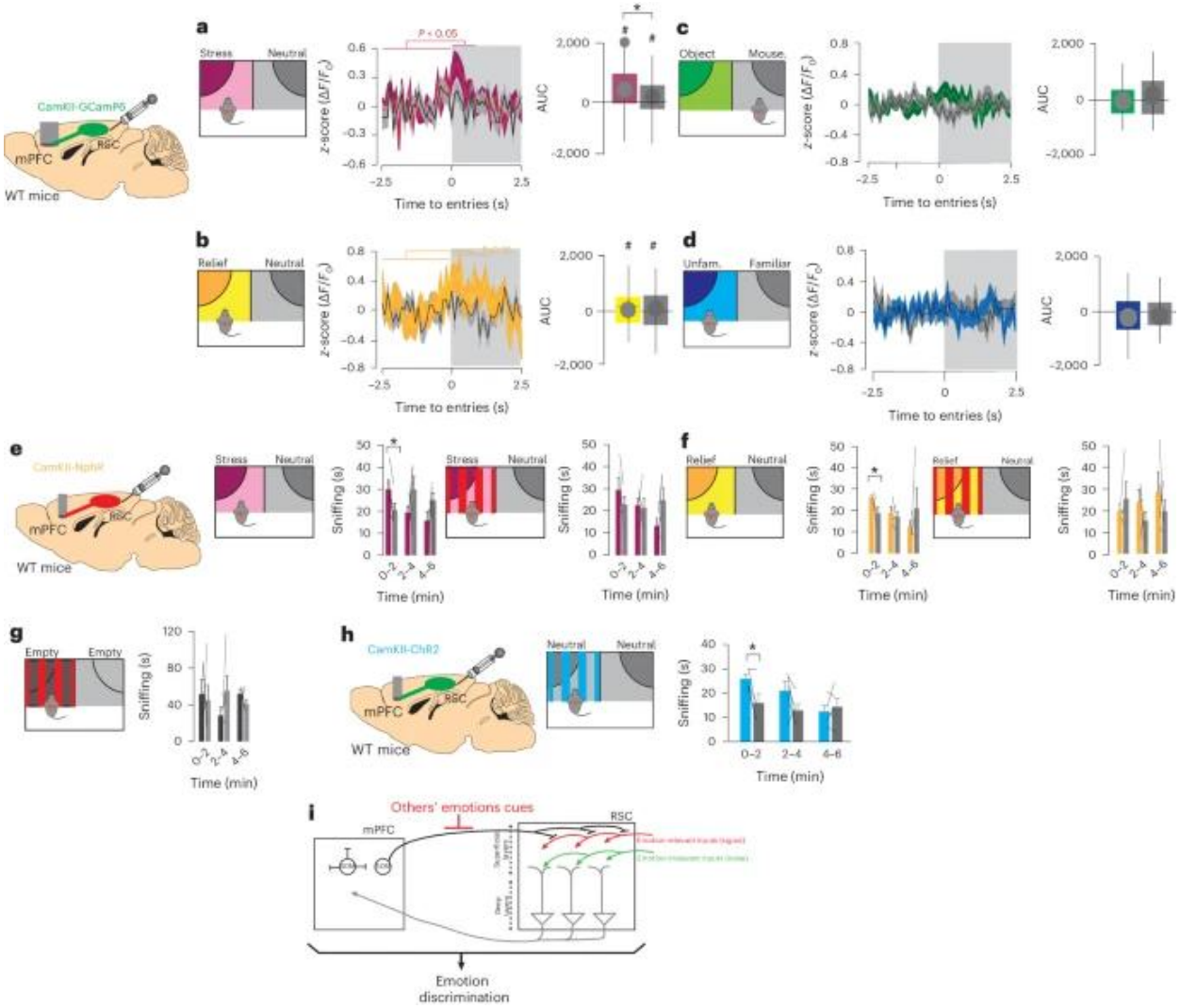

Fig. 5: RSC pyramidal neurons projecting to the mPFC regulate emotion recognition.

a,**b**, Fiber photometry recording ($n = 6$ male mice) of the RSC pyramidal terminals in the mPFC during emotion recognition for stress (purple) and neutral (gray) ($^{\#}P < 0.05$ versus baseline, $*P < 0.0001$ stress versus neutral; $n = 75$ entries to stress, $n = 54$ entries to neutral) (**a**) and relief (yellow) and neutral (gray) ($^{\#}P < 0.0001$ versus baseline; $n = 77$ entries to relief, $n = 72$ to neutral) (**b**). **c**, GCaMP signal in these same mice during discrimination between an object and a mouse ($n = 34$ entries to neutral, $n = 26$ entries to object) and (**d**) between an unfamiliar and a familiar mouse. **e**, WT mice ($n = 5$ males) were bilaterally injected in the RSC with AAV-CaMKII-NphR (orange), and implanted with a bilateral optic fiber in the mPFC, to allow specific optogenetics manipulation of

RSC-to-mPFC pyramidal terminals. **e**,**f**, Emotion recognition performance without light stimulation (first graph) or with photoinhibition (560-nm continuous light) of RSC-to-mPFC pyramidal terminals only when in the stress (**e**) or relief (**f**) demonstrator zone (RM-ANOVA; post hoc Bonferroni $*P \leq 0.05$ versus neutral). **g**, Inhibition of RSC-to-mPFC pyramidal terminals during entry to a random zone of one of two empty zones. **h**, Bilateral stimulation of the RSC pyramidal terminals in the mPFC of observer mice ($n = 5$ males) when in one of two neutral mouse zones for the entire 6 min (RM-ANOVA; post hoc Bonferroni $*P < 0.05$ versus neutral + light). **i**, Schematic of the revealed mPFC–RSC inhibitory–excitatory circuitry during emotion recognition. Bar and line graphs show the mean ± s.e.m. AUC values are represented as box-and-whisker plots presenting the upper and lower quartiles, mean and median. Complete statistics are available in Supplementary Table 2 and https://doi.org/10.48557/FEXUTZ.

mPFC–RSC inversely correlate in humans' emotion recognition

To start exploring if this mouse mPFC–RSC circuit could be relevant for human emotion recognition, we analyzed whole-brain functional connectivity (FC) from 1,263 healthy participants when observing an altered emotion (angry or happy), a participant with no altered emotions (neutral) or an object (control; Fig. 6a,b). Sixty-one components with peak activations in gray matter were manually selected and categorized into seven functional domains (Fig. 6c and Extended Data Table 1)30·31. Time-varying FC was correlated with the occurrence of task stimuli (angry, happy, neutral and control) to reflect coupling between FC changes and task stimuli (Fig. 6b,d). The whole-brain FC of the five DMN components revealed a distinct correlation in emotional stimuli (angry or happy) compared to neutral and object stimuli (Fig. 6e). The anatomical location of the mPFC/ACC and the RSC identified by their peak activation coordinates, revealed a negative coupling for angry and happy faces. In contrast, a positive coupling was evident for neutral faces and control stimuli (Fig. 6f). Correlations were different across types of task stimuli, and between each pair of task stimuli, except for angry and happy face conditions. Overall, these data indicate that also in humans there is an inversely correlated engagement of the mPFC/ACC–RSC connectivity during emotion recognition.

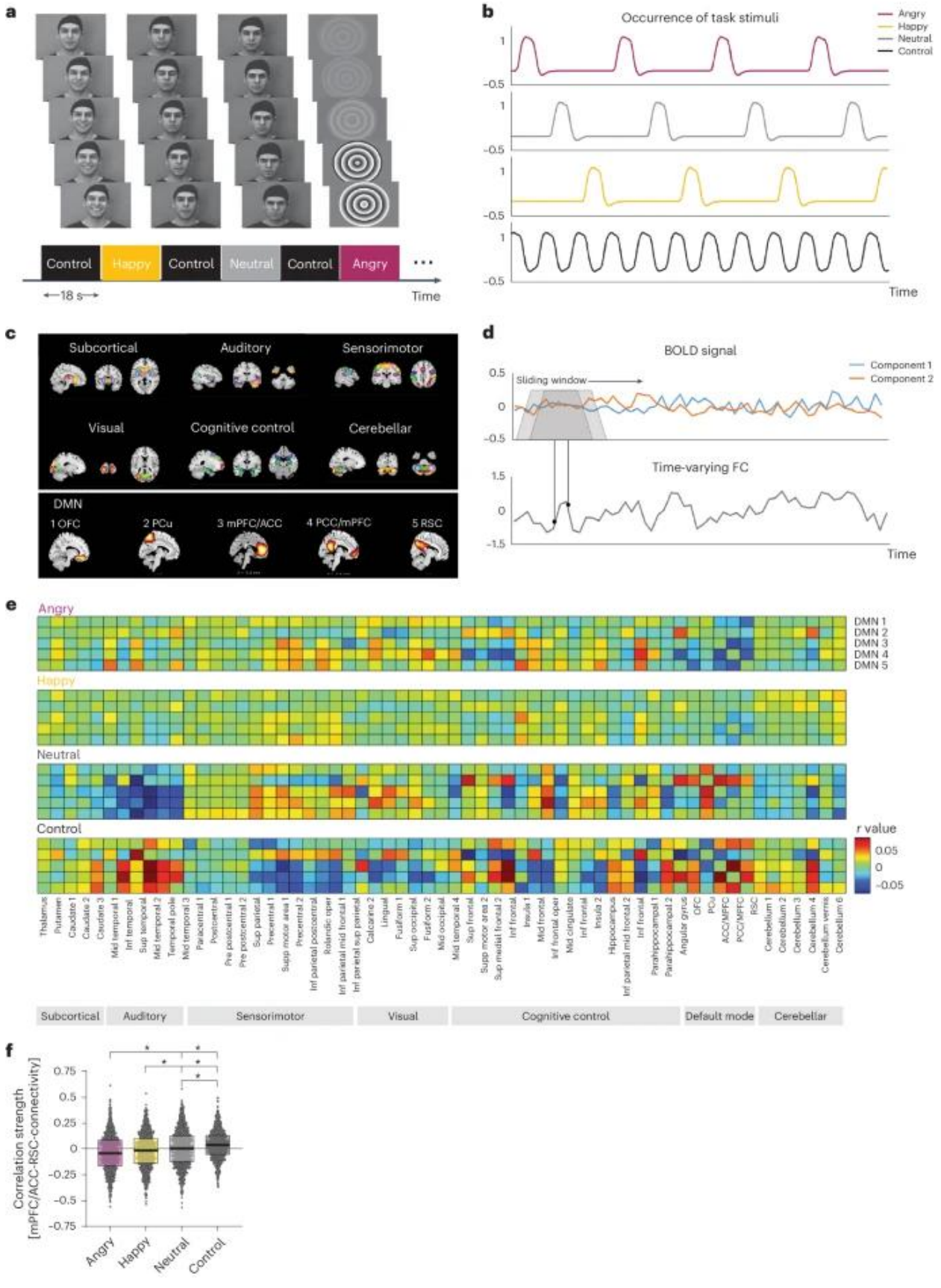
a
Control
Happy
Control
Neutral
Control
Angry
18 s
Time
b
Occurrence of task stimuli
Angry
Happy
Neutral
Control
Time
c
Subcortical
Auditory
Sensorimotor
Visual
Cognitive control
Cerebellar
DMN
1 OFC
2 PCu
3 mPFC/ACC
4 PCC/mPFC
5 RSC
d
BOLD signal
Component 1
Component 2
Sliding window
Time-varying FC
Time
e
Angry
Happy
Neutral
Control
DMN 1
DMN 2
DMN 3
DMN 4
DMN 5
r value
0.05
0
-0.05
Thalamus
Putamen
Caudate 1
Caudate 2
Caudate 3
Mid temporal 1
Inf temporal
Sup temporal
Mid temporal 2
Temporal pole
Mid temporal 3
Paracentral 1
Postcentral
Pre postcentral 1
Pre postcentral 2
Sup parietal
Precentral 1
Supp motor area 1
Precentral 2
Inf parietal postcentral
Rolandic oper
Inf parietal mid frontal 1
Inf parietal sup parietal
Calcarine 2
Lingual
FusiForm 1
Sup occipital
FusiForm 2
Mid occipital
Mid temporal 4
Sup frontal
Supp motor area 2
Sup medial frontal 2
Inf frontal
Insula 1
Mid frontal
Inf frontal oper
Mid cingulate
Inf frontal
Insula 2
Hippocampus
Inf parietal mid frontal 2
Inf frontal
Parahippocampal 1
Parahippocampal 2
Angular gyrus
OFC
PCu
ACC/MPFC
PCC/MPFC
RSC
Cerebellum 1
Cerebellum 2
Cerebellum 3
Cerebellum 4
Cerebellum vermis
Cerebellum 6
Subcortical
Auditory
Sensorimotor
Visual
Cognitive control
Default mode
Cerebellar
f
Correlation strength
[mPFC/ACC-RSC-connectivity]
Angry
Happy
Neutral
Control

Fig. 6: FC of the DMN components during emotion recognition in humans.

a, During a block design of human emotional faces task, 1,263 participants were instructed to view a video clip of either face (angry, happy, neutral) or non-face (control) stimuli. Every block lasted 18 s. Each type of face stimuli was repeated four times and intermixed with the control stimuli. **b**, onset of angry (violet), happy (yellow), neutral (gray) and control (black) stimuli convolved with canonical hemodynamic response function (HRF) within the entire session. **c**, The spatial distribution of the 61 brain components extracted from the group independent component analysis (ICA) on task fMRI data. The components were categorized into seven domains based on their anatomical locations and functional properties: subcortical, auditory, sensorimotor, visual, cognitive control, cerebellar and DMN. For each domain, each color represents a single component. Five components of the DMN are individually plotted on the bottom row. **d**, Time-varying FC between two components was calculated using their BOLD signals within a time window. Then, the time window was moved forward by one repetition time (TR) to get the next FC and repeated until the end of a scanning session. **e**, Correlations between task stimuli and whole-brain time-varying FC of the five DMN components. **f**, Anatomical location of mPFC/ACC and RSC was identified by their peak activation coordinates (mPFC/ACC: $x = -0.5$, $y = 41.5$, $z = 4.5$; RSC: $x = -5.5$, $y = -70.5$, $z = 34.5$). Time-varying FC between the mPFC/ACC (DMN 3) and the RSC (DMN 5) differed across task stimuli ($^*P < 0.05$). Mean associations between FC and stimuli occurrence were negative for angry faces (violet) and happy faces (yellow), not significant for neutral faces (gray) and positive for control stimuli (black). Correlation was significantly different across types of task stimuli, except for the comparison of angry and happy faces. OFC, orbitofrontal cortex; PCu, precuneus. Bar plots are represented as the mean ± s.e.m. Complete statistics are available in Supplementary Table 2 and https://doi.org/10.48557/FEXUTZ.

mPFC-to-RSC SOM projections rescue emotion recognition deficits

Alterations of the mPFC and RSC DMN hubs have been reported in a number of psychiatric disorders characterized by emotion recognition[10,32], such as schizophrenia.

In Arc knockout mice, a model relevant to schizophrenia[33], we found reduced resting-state functional magnetic resonance imaging (rsfMRI) connectivity between the mPFC and the RSC (Fig. 7a–c) when the seed was located either in the RSC (Fig. 7a) or in the mPFC (Fig. 7b). The effect was absent when selecting the somatosensory cortex as seed (Extended Data Fig. 9a,b). Considering functional magnetic resonance imaging (fMRI) human data (Fig. 6), and our data in mice (Figs. 1–5), these rsfMRI mouse data suggest that reduced coupling between these regions could be indicative of altered emotion recognition in Arc knockout mice. In agreement, while

$Arc^{+/+}$ mice showed the usual pattern of discrimination, we found a loss of stress (Fig. 7d) and relief (Fig. 7e) recognition, in a sex-independent way (Extended Data Fig. 3), with partial (+/−) or complete (−/−) ablation of Arc. To show that these impairments were related to the coupling between the mPFC and the RSC, we crossbred SOM-cre with $Arc^{+/-}$ mice (SOM-cre-$Arc^{+/-}$) and simultaneously recorded the overall SOM activity in the mPFC and their terminals in the RSC (Fig. 7f). Within the mPFC, $Arc^{+/-}$ mice showed an equally increased signal when in the stress or neutral zones (Fig. 7g) in contrast with what we observed in wild-type (WT) animals (Fig. 2i–k). Moreover, at the level of the SOM terminals in the RSC, $Arc^{+/-}$ mice did not show any modulation of their signal linked to the emotionally altered mouse (Fig. 7h) again in contrast to WT animals (Fig. 2i–k). This indicates that ARC deficiency impairs both the mPFC–RSC SOM activity and emotion recognition.

To causally link ARC-dependent alterations in mPFC–RSC SOM projection activity with their deficits in emotion recognition, we optogenetically mimicked SOM terminals' physiological inhibition linked to emotion recognition (Fig. 2) in SOM-cre-$Arc^{+/-}$ mice (Fig. 7i,j). SOM terminals' photoinhibition paired to the emotionally altered mouse reestablished emotion recognition in $Arc^{+/-}$ mice (Fig. 7i). We replicated in these same mice the emotion recognition deficits in the light-off condition (Extended Data Fig. 9c). This same inhibition protocol did not affect side preference in SOM-cre-$Arc^{+/-}$ mice in absence of social stimuli (Fig. 7j). These data provide evidence of the potential translation relevance of the mPFC–RSC SOM circuit in emotion recognition disabilities.

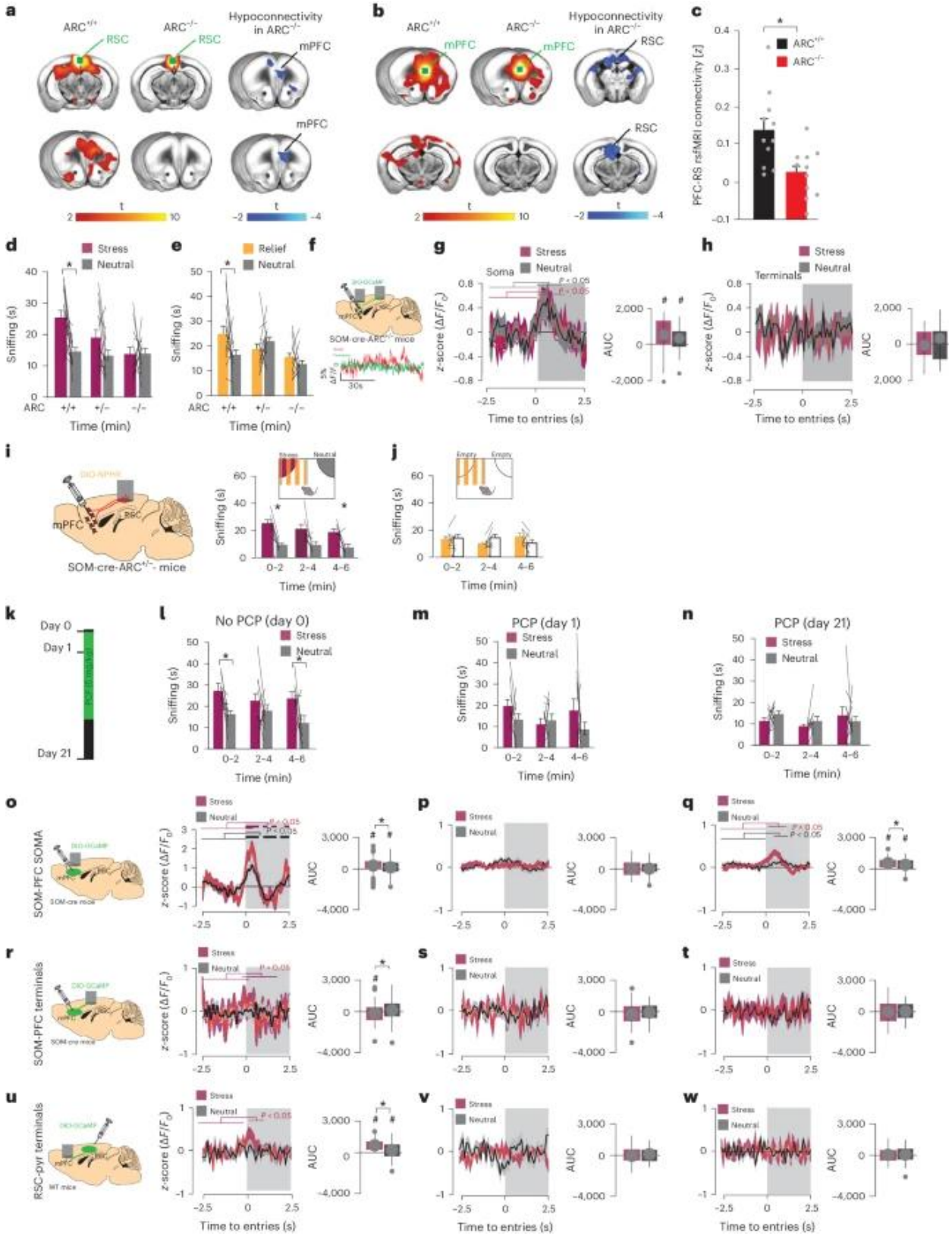
a
ARC+/+
RSC
ARC−/−
RSC
Hypoconnectivity in ARC−/−
mPFC
mPFC
t
2
10
t
−2
−4
b
ARC+/+
mPFC
ARC−/−
mPFC
Hypoconnectivity in ARC−/−
RSC
RSC
t
2
10
t
−2
−4
c
PFC-RS rsfMRI connectivity [z]
ARC+/+
ARC−/−
d
Stress
Neutral
Sniffing (s)
ARC +/+ +/− −/−
Time (min)
e
Relief
Neutral
Sniffing (s)
ARC +/+ +/− −/−
Time (min)
f
SOM-cre-ARC−/− mice
30s
g
Stress
Soma
Neutral
z-score (ΔF/F0)
AUC
Time to entries (s)
h
Stress
Terminals
Neutral
z-score (ΔF/F0)
AUC
Time to entries (s)
i
mPFC
RSC
SOM-cre-ARC+/− mice
Sniffing (s)
Time (min)
j
Sniffing (s)
Time (min)
k
Day 0
Day 1
Day 21
l
No PCP (day 0)
Stress
Neutral
Sniffing (s)
Time (min)
m
PCP (day 1)
Stress
Neutral
Sniffing (s)
Time (min)
n
PCP (day 21)
Stress
Neutral
Sniffing (s)
Time (min)
o
SOM-PFC SOMA
z-score (ΔF/F0)
AUC
p
AUC
q
AUC
r
SOM-PFC terminals
z-score (ΔF/F0)
AUC
s
AUC
t
AUC
u
RSC-pyr terminals
z-score (ΔF/F0)
AUC
Time to entries (s)
v
AUC
Time to entries (s)
w
AUC
Time to entries (s)

Fig. 7: Emotion recognition deficits in genetic and pharmacological schizophrenia-relevant mouse models are associated with functional alterations of the mPFC–RSC inhibitory–excitatory circuit.

a,**b**, Seed-based connectivity mapping of the RSC (**a**) and the mPFC (**b**) in control $Arc^{+/+}$ mice ($n = 11$) and $Arc^{-/-}$ ($n = 11$) mutants. Red-yellow represents brain regions showing rsfMRI FC with the RSC and the mPFC in control $Arc^{+/+}$ and mutant $Arc^{-/-}$ mice. Brain regions showing notable reduced rsfMRI connectivity with the RSC and the mPFC in $Arc^{-/-}$ mutants with respect to $Arc^{+/+}$ littermates are depicted in blue-light blue (right). **c**, rsfMRI connectivity between the mPFC and the RSC in $Arc^{-/-}$ mice quantified in reference volumes of interest. **d**,**e**, Emotion recognition for stress (**d**) and relief (**e**) showed by $Arc^{+/+}$ ($n = 15$, 10 males, 5 females), $Arc^{+/-}$ ($n = 13$, 9 males, 4 females) and $Arc^{-/-}$ littermates ($n = 15$, 9 males, 6 females; two-way RM-ANOVA; post hoc Bonferroni $^{*}P < 0.05$ versus neutral). **f**, Fiber photometry recording of SOM neurons in the mPFC (soma) and their terminals in the RSC (terminals) of SOM-$Arc^{+/-}$ mice ($n = 6$ females) during emotion recognition. **g**, Similar increase of GCaMP signal shown at the level of the mPFC in both stress (purple) and neutral (gray) entries ($^{\#}P < 0.05$ versus baseline, $n = 29$ stress entries, $n = 33$ neutral entries). **h**, GCaMP signal at the level of mPFC SOM terminals in the RSC during entries to the stress (purple) and neutral (gray) demonstrators. **i**,**j**, SOM-$Arc^{+/-}$ mice ($n = 10$, 5 males 5 females) with inhibition of mPFC SOM terminals in the RSC during emotion recognition for stress (**i**) (only in the zone of the stress demonstrator for the entire 6 min) (RM-ANOVA; post hoc Bonferroni $^{*}P < 0.05$ stress versus neutral), or without social stimuli (**j**). **k**, Timeline of emotion recognition at baseline (day 0), following acute (day 1), or 7-day washout after 14 days of PCP (5 mg per kg body weight, $n = 11$ mice, 6 females, 5 males) treatment (day 21). **l**–**n**, Emotion recognition performance at baseline (day 0), acute (day 1), or after 7-day washout after 14 days of PCP (day 21) (RM-ANOVA; post hoc Bonferroni $^{*}P < 0.05$ stress versus neutral). **o**–**q**, Fiber photometry recording of SOM neurons in the mPFC ($n = 5$ mice) during emotion recognition for stress (purple) and neutral (gray) following no PCP (day 0, **o**; same animals as Fig. 2j), acute PCP (day 1, **p**) or chronic and washout PCP (day 21, **q**). **o**, $^{\#}P < 0.05$ versus baseline; $^{*}P = 0.05$ stress versus neutral. $n = 156$ entries to stress, $n = 143$ entries to neutral. **p**, $n = 45$ entries to stress, $n = 81$ entries to neutral. **q**, $^{\#}P < 0.005$ versus baseline; $^{*}P = 0.04$ stress versus neutral. $n = 63$ entries to stress, $n = 30$ entries to neutral. **r**–**t**, Fiber photometry recording of the mPFC-to-RSC SOM terminals following no PCP (day 0, **r**; same animals as Fig. 2j), acute PCP (day 1, **s**) or chronic and washout PCP (day 21, **t**). **r**, $^{\#}P = 0.008$ versus baseline; $^{*}P = 0.002$ stress versus neutral. These are the same mice from Fig. 2h; $n = 156$ entries to stress, $n = 143$ entries to neutral. **s**, $n = 45$ entries to stress, $n = 81$ entries to neutral. **t**, $n = 63$ entries to stress, $n = 30$ entries to neutral. **u**–**w**, Fiber photometry recording of the RSC pyramidal terminals in the mPFC following no PCP (day 0, **u**; same animals as Fig. 4h), acute PCP (day 1, **v**) or chronic and washout PCP (day 21, **w**). **u**, $^{\#}P < 0.05$ versus baseline; $^{*}P < 0.0001$ stress versus neutral. $n = 75$ entries to stress, $n = 54$ entries to neutral. **v**, $n = 84$ entries to stress, $n = 35$ entries to neutral. **w**, $n = 74$ entries to stress, $n = 64$ entries to neutral. Bar and line graphs show the mean ± s.e.m. AUC values are represented as box-and-whisker plots showing the upper and lower quartiles, mean and median. Complete statistics are available in Supplementary Table 2 and https://doi.org/10.48557/FEXUTZ.

PCP impairs mPFC–RSC loop activity in emotion recognition

We finally tested whether alterations in the mPFC–RSC SOM circuit could be found in another nongenetic model relevant to schizophrenia. Phencyclidine (PCP) is used as a pharmacological model of schizophrenia[34], inducing cognitive dysfunction related to mPFC[35], and altering neuronal activity in the RSC[36].

Drug-naive mice showed the usual emotion recognition (Fig. 7k,l), which was impaired following both acute (Fig. 7k,m) and chronic PCP (Fig. 7k,n), in both males and females (Extended Data Fig. 3). We then assessed if these emotion recognition deficits could be associated with dysfunctions of the mPFC–RSC inhibitory–excitatory circuit. We recorded the overall activity of SOM neurons in the mPFC (Fig. 7o–q), their terminals in the RSC (Fig. 7r–t) and the RSC pyramidal terminals in the mPFC (Fig. 7u–w). Drug-naive mice showed the usual pattern of activation linked to emotion recognition for mPFC SOM neurons (Figs. 2j and 7o), SOM terminals to the RSC (Figs. 2j and 7r) and RSC pyramidal terminals into mPFC (Figs. 4g and 7u). Acute PCP abolished the difference of the GCaMP signal at the level of the SOM mPFC neurons (Fig. 7p), SOM terminals (Fig. 7s) and RSC pyramidal terminals in the mPFC (Fig. 7v). With chronic PCP, SOM neurons in the mPFC presented a reduced response to stress and neutral states (Fig. 7q), while emotion recognition-related activity of mPFC SOM terminals in the RSC (Fig. 7t) and of RSC pyramidal neurons in the mPFC (Fig. 7w) was abolished. This indicates that also in the schizophrenia-relevant PCP mouse model there are emotion recognition deficits associated with alterations of the activity of the mPFC–RSC circuit.

Discussion

We discovered a mPFC–RSC inhibitory–excitatory circuit driving emotion recognition, by combining recently developed socio-cognitive paradigms with fiber photometry recordings and optogenetic manipulations. Detection of emotions in others was associated with reduced activity of mPFC-to-RSC SOM projections, and with activation of RSC-to-mPFC pyramidal neuron projections (Fig. 5i). This corresponded to an inverse fMRI mPFC–RSC coupling in human emotion recognition. Precisely paced optogenetic interventions showed that these patterns of activity were causally linked to emotion recognition. Reestablishing emotion-related suppression of the mPFC SOM inhibitory drive to the RSC rescued emotion recognition deficits. These experiments identified cellular, circuital, physiological and pathological properties of a cortico-cortical inhibitory–excitatory circuit underling emotion recognition.

SOM long-range projections from the mPFC to the RSC process socially derived information for reliable emotion recognition. This is in line with evidence reporting a more specific role for cortical SOM inhibitory neurons in socio-cognitive abilities[17,37] with less involvement in basic sociability, social memory and social dominance[17,38]. We extend the existence of inhibitory long-range projections, as those reported from the hippocampus to RSC and entorhinal cortex[39,40], from the mPFC to the nucleus accumbens[41], from the auditory cortex to the lateral amygdala[23], and from the motor cortex to the dorsal striatum[42]. Notably, our results detailed a functional hitherto uncharacterized inhibitory pathway to the RSC originating from a subpopulation of mPFC SOM neurons. Retrograde and anterograde tracing revealed that about 10% of the entire SOM population within the mPFC can target the RSC, a proportion similar to that of other cortical structures[42]. Our experiments suggest that SOM terminals inhibit the firing probability of RSC pyramidal cells depending on the presence of socio-emotional stimuli from conspecifics. In particular, inhibition of mPFC-to-RSC SOM terminals paired to an emotionally altered mouse increases the delta of activation of RSC pyramidal neurons between neutral and emotionally altered mice, and increases the SNR within the RSC. Thus, SOM terminals are a key factor in determining the relative RSC activation between exploration of an emotionally altered mouse and another in a neutral state. Furthermore, a stronger inhibition of mPFC-to-RSC SOM terminals is associated with disinhibition of RSC pyramidal neurons, and the increased

activity of RSC pyramidal neurons projecting to the mPFC is key for emotion recognition. Notably, we found that overall pyramidal cells in the RSC generally encode social valence, while those projecting to the mPFC are more specific for emotion recognition. Importantly, the inverse inhibitory/excitatory link between the mPFC and the RSC (included in human PCC43) fits with the inverse correlation we found in humans during emotion recognition. Detection of emotions in others activates mPFC SOM neurons increasing local inhibition (current data and ref. 17), while it decreases the activity of SOM projections to the RSC disinhibiting the RSC (Fig. 5i). This can correspond at the general activity level (fMRI) with increased coupling between the mPFC and the RSC, but in an anticorrelated way (as we found in humans). Thus, our findings provide a circuital mechanism by which a major evolutionarily conserved cortico-cortical network integrates the flow of emotionally relevant information mediating emotion recognition.

We demonstrated a distinct functional role in emotion recognition played by mPFC-to-RSC SOM terminals, compared to the entire population of mPFC SOM neurons. While the general activity of SOM neurons in the mPFC increases during interaction with emotionally altered mice, mPFC-to-RSC SOM projections show a reduction. This extends evidence on the heterogeneity of cortical SOM cells in terms of their activity during emotion recognition17, anatomy44 and physiology18,45. Photoinhibition of the entire mPFC SOM population abolished emotion recognition17, while photoinhibition of mPFC SOM terminals at the level of the RSC strengthened it. In agreement, we could induce a preference for an emotionally neutral mouse if paired with photoinhibition of mPFC-to-RSC SOM projections, revealing that reduction of the activity observed during photometry is important for emotion recognition. Notably, if photoinhibition of SOM terminals into the RSC occurs in the absence of social stimuli, no place preference is observed. Conversely, activation of mPFC-to-RSC SOM projections abolished emotion recognition. Neocortical SOM neurons provide a specific role in channeling network activity or in controlling information flow18,21,46; thus, it is not surprising that their modulatory role at the level of the mPFC or the RSC can have distinct functional consequences. However, the exact mechanisms at the cellular level that distinguish the entire SOM population from those projecting to RSC will require further studies.

We provide initial evidence of the clinical relevance of mPFC-to-RSC SOM projections in emotion recognition deficits observed in psychiatric disorders such as schizophrenia. In particular, functional alterations of the mPFC–RSC inhibitory–excitatory circuit were associated with emotion recognition deficits in both genetic[33] and pharmacological[34,35] models relevant to schizophrenia. In agreement, patients with schizophrenia show altered connectivity between these two equivalent cortico-cortical hubs, in basal conditions and during emotion perception and processing[7,16,32]. Furthermore, our data are in line with and strengthen evidence of a schizophrenia-specific alteration of SOM neurons in the PFC[47]. Intriguingly, our data indicate that there is a balanced coupling of the inhibitory–excitatory mPFC–RSC circuit to maintain emotion recognition at an 'optimal' level. Indeed, both stimulation and inhibition of mPFC-to-RSC SOM projections altered, in an opposite way, emotion recognition. Deficits to recognize, understand and adequately respond to the emotional states of others ('social blindness') is common in patients with autism and schizophrenia, negatively affecting their daily life[5,7,48]. Conversely, hyper sociability and higher sensitivity to others' emotions could also be detrimental, increasing the risk of social exclusion and vulnerability to abuse[49,50]. We show that reestablishing the functional activity of mPFC-to-RSC SOM projections can rescue emotion recognition deficits. Thus, we hypothesize that this specific cortico-cortical circuit might be an important target to improve socio-cognitive dysfunctions.

In summary, we uncovered a pivotal role for mPFC SOM neurons projecting to the RSC in emotion recognition. This provides a deeper mechanistic understanding of evolutionarily conserved socio-cognitive processes. Our findings hold both fundamental and clinical relevance, refining the idea of cortical excitatory–inhibitory balance as a core feature of recognition and reaction to others' emotions.

Methods

Mice

All procedures were approved by the Italian Ministry of Health (permit nos. 107/2015-PR, 749/2017-PR, 191/2020-PR and 639/2020-PR) and the local Animal Use Committee of the Istituto Italiano di Tecnologia, and were conducted in accordance with the Guide for the Care and Use of Laboratory Animals of the National Institutes of Health and the European Community Council Directives. Routine veterinary care and animal maintenance were provided by dedicated and trained personnel. Male and female mice on a C57BL/6J background and aged 3–6 months old were used. Mice were weaned at postnatal day 28, separated by sex and housed at 2–4 animals per cage. Animals were housed in a climate-controlled facility (temperature 22 °C ± 2 °C, humidity 45–65%), with ad libitum access to food and water throughout, and with a 12-h light–dark cycle (19:00/7:00 schedule). Experiments were run during the light phase (within 10:00–17:00). All mice were handled on alternate days during the week preceding the first behavioral testing.

SOM-cre-recombinase mice17 (SOM-cre; The Jackson Laboratory, 013044), WT (C57BL/6J Charles River; The Jackson Laboratory, 000664, or bred in house), TdTomato reporter mice (TdTomato; The Jackson Laboratory, 007909) and Arc knockout colonies33 used were bred in our animal facility. Mouse genotypes were determined by PCR of ear snip tissue. Except for anatomical tracing experiments using AAVrg-DIO-TdTomato, all mice used were heterozygous. Distinct cohorts of naive mice were used for each experiment, and all experiments were repeated at least three times. Experiments with >5 mice were replicated in different groups of mice, tested in different moments, from different cages and of different sex.

Immunohistochemistry

All animals used for behavioral experiments or tracing were deeply anesthetized following all experiments with an overdose of urethane (>2 g per kg body weight) and then transcardially perfused with ice-cold 0.05 M PBS pH 7.4, followed by 4% wt/vol paraformaldehyde in phosphate buffer (0.1 M, pH 7.4). Brains were removed and stored in PBS until sectioning. Following 48 h of cryoprotection in 30% sucrose solution (in PBS), the brain was frozen and

sliced along the coronal axis using a microtome (HM45, Thermo Fisher) at 50 µm. Sections were collected in 24-well plates, and one randomly selected well was used for histological analyses. For immunohistochemistry, all sections were first incubated in a blocking solution consisting of 10% normal donkey serum (NDS) in PBS containing 1% Triton X-100 for a minimum of 1 h. For immunostaining of SOM, sections were then incubated in a 50% ethanol solution for 30 min before being processed for primary staining. Following 3–5 washes in PBS solution, all sections were processed for primary staining, and primary antibodies were selected based on the purpose of the immunohistochemistry. The primary solution consisted of the primary antibody diluted in 1% NDS, 0.03% Triton X-100 in PBS. Primary incubation occurred at 4 °C for 24–48 h. Following primary incubation, slices were washed 3–5 times and prepared for the secondary incubation that consists of a solution containing the secondary antibody diluted in 1% NDS, 0.03% Triton X-100 in PBS. Secondary incubation occurred at room temperature (RT) for 4–6 h. Primary antibodies used were: Against GFP (made in rabbit, 1:1,000 dilution; Invitrogen, A11122), against GFP (made in chicken, 1:1,000 dilution; Abcam, AB290), against TdTomato (made in rabbit, 1:1,000 dilution; Thermo Fisher, 150128) and against SOM (made in rabbit, 1:250 dilution; Abcam, 108456). Secondary antibodies were: Alexa Fluor 488 (anti-rabbit, 1:1,000 dilution; A11034, ABclonal), Alexa Fluor 488 (anti-chicken, 1:1,000 dilution; A11039, ABclonal) and anti-568 (anti-rabbit, 1:1,000 dilution; A11036, ABclonal). Fluorescence images were obtained with a confocal microscope (Leica, CTR6500) using the following filter: 504 nm for Alexa Fluor 488, 560 nm for Alexa Fluor 568, and 650 nm for Ctb. Images were collected at ×20 in air or ×10, ×20 and ×63 in oil. Retrograde and anterograde tracing was done using the software Neurolucida (MBF Bioscience), and all fluorescence images were treated using the software ImageJ and Adobe Illustrator CS6. All primary and secondary antibodies have been previously validated.

Neuronal density analyses

A selected section every 300 µm of the whole brain was processed and scanned, and the Cartesian coordinates of each Ctb-positive neuron were extracted using the software Neurolucida (MBF Bioscience). The contour of the brain was drawn using the same software. Sections at the same level of multiple mice were then aligned, and their Cartesian coordinates were transferred to MATLAB. Using a custom script, the sections were divided into a

40 × 40 µm grid, and the number of Ctb-positive neurons was estimated to the total and provided a neuronal density map.

Output whole-brain mapping

A minimum of three mice (SOM-cre or WT, adult mice) for each group (mPFC, cingulat gyrus (CG) and RSC) were processed. One randomly selected brain was then scanned using high-resolution images and representative images of the location of YFP-positive signal was done. For each group, the whole-brain mapping was then compared to all remaining mice and adjusted for the structure that was undervalued.

Viral injections

Mice were naive and prepared for stereotaxic surgeries at 2–3 months old. All mice were anesthetized with a mix of isoflurane (2%) in oxygen (O_2, 1%) before being mounted on a stereotaxic frame (Kopf Instruments). Brain coordinates were defined based on the Allen Mouse Brain Atlas as follows (AP/ML/DV, in mm from Bregma and the dura): mPFC (1.7 mm, 0.3 mm, 2.1 mm; 2.4 mm), CG (1.0 mm/0.3 mm/0.8 mm), RSC (−1 mm, −1.7 mm, −2.1 mm; −2.9 mm/0.1 mm/0.8 mm). Mediolateral coordinates for RSC injections were adjusted per mouse based on the position of the blood sinus to allow injection in superficial layers. Injected volume was adjusted based on the serotype and the experiments. For output mapping of the mPFC and the CG, the injected volumes were 25 nl and 50 nl, respectively. For the photometry experiment of the mPFC and the RSC, the injected volumes were 250 nl and 150–200 nl, respectively. For Ctb tracing of the RSC, a volume of four times 10 nl was used. For AAVrg tracing of the RSC, a volume of four times 50 nl was used. For optogenetic experiments of the mPFC, and the RSC, the injected volumes were 200 nl and 400 nl, respectively.

Virus and tracers were infused through a borosilicate micropipette connected to a 10 µl Hamilton syringe filled with mineral oil. The injection rate was set to last between 5 min and 10 min and the pipette was maintained in position for at least 5 min to allow proper diffusion. After viral injection, mice were given between 2 and 3 weeks to recover. After Ctb injection, mice were euthanized 10 days after injections. Viruses used for all experiments were as follows: Optogenetic activation: AAV-DIO-ChR2-YFP (20298-AAV5, Addgene), AAV-DIO-Chrimson-

TdTomato (62723-AAV5, Addgene), AAV-CaMKII-ChR2-YFP (26969-AAV1, Addgene). Optogenetic inhibition: AAV-DIO-NphR3.0-YFP (26966-AAV5, Addgene), AAV-CaMKIIa-eNphR 3.0-eYFP (26971-AAV1, Addgene). Calcium imaging: AAV-DIO-GCaMP6f (100833–AAV1, Addgene), AAV-CaMKII-GCaMP6f (1000834-AAV1), PHPeB-hSyn-GCaMP7F (104488-PHPeB, Addgene). Viral tracing: AAVrg-Flex-TdTomato (28306-AAV2), AAV-DIO-YFP (27056-AAV5, Addgene), AAV-CaMKII-YFP (CS0934-AAV1, Penn Vector Core). Nonviral tracer was as follows: Ctb (B-647; Thermo Fisher, 34778). Following diffusion of the virus, mice used for optogenetic experiments underwent second surgeries where a dual fiber-optic cannula (200 µm, 0.37 NA, Doric lenses) or a micro-LED in blue (LB G6SP, OSRAM) or red (GD GTLPS1, OSRAM), and for dual-optogenetic experiments (ChR2/NphR) a bilateral fiber (Doriclenses), was combined to a fused patch cord connected to both a red (560 nm) and a blue (450 nm) LED and were implanted above the mPFC or the RSC. Optic fibers were lowered 500 µm to 300 µm above the viral injection site. Two to three anchor screws (PlasticOne) were used to stabilize the implant and were finalized using epoxy (C&B Metabond) and dental cement (Paladur Kulzer). For LED optogenetic experiments (stimulation cortex), the LEDs were positioned on a thinned skull to reduce heat effects. Following diffusion of the virus, mice used for photometry experiments underwent a second surgery where a 200 µm (for recording in the soma, MM fiber, FP200URT Thorlabs, 0.5NA, flat cut, custom made) or 400 µm (for recording at the level of the terminals; FP400URT, Thorlabs, 0.48NA, flat cut, custom made) fiber-optic cannula was lowered 200 µm above the viral injection site. For an experiment consisting of single-site recording, a second dummy fiber was placed in the dental cement and used to limit movement artifact and rotation. Two to three anchor screws (PlasticOne) were used to stabilize the implant and were finalized using epoxy (C&B Metabond) and dental cement (Paladur Kulzer).

Mouse behavior

Apparatus

The emotion recognition task apparatus was printed in three dimensions onto a square apparatus (34 × 25 × 23 cm) containing a two-quarter circle (10 cm ray) on two opposite sides. Each quarter circle is formed with metal rods (0.8 cm) that allow sufficient space for social contact between the observer (freely moving in the apparatus) and the stimuli (freely moving in the

quarter circle). A three-dimensional-printed separator (15 × 23 cm) was inserted between the quarter circles to block the reciprocal view of the demonstrators' animals. For scoring, a virtual square (11 × 11 cm, see scheme in Figs. 2a,f,j–s, 3e,i,g, 4a,f–k and 5a–h) was placed between each quarter circle and the separator to define a zone associated with each demonstrator. Following each experiment, the apparatus was thoroughly cleaned with 50% ethanol, wiped and allowed to air-dry. Between testing with females or males, an additional cleaning using 70% ethanol was done, and a minimum of 24 h air-drying was allowed. During habituation and testing, the cages were placed inside a dimly lit (6 ± 1 lux) soundproof cubicle (Med Associates).

Testing

Procedures were performed as previously described17,19. To allow optogenetic modulation or photometry recording, an 8-cm hole was made in the cubicle above the cage. A high-resolution monochrome camera (Imaging source, DMK 22AUC03) was placed above the cage to record the mouse's behavior during testing. Videos were collected at high contrast and high resolution using the behavioral tracking system (Anymaze 6.0, Stoelting). Live tracking of the mice was done using tracking software and allowed, based on the experiment, to deliver 5V transistor–transistor logic (TTL) signal through an Anymaze interface (Ami1) to the lasers, an Arduino Uno interface, or the photometry acquisition hardware. Habituation to the testing cage occurred on 3 consecutive days before the first experiment, and each session lasted for 10 min.

Observer mice

All observer mice were the same age and sex of the demonstrator mice. Before the experiments, observer mice were gently moved into the testing apparatus for 10 min. For optogenetic experiments or photometry experiments, observer mice were connected to the patch cord or the electric cord (for LED stimulation) during this period. The 6-min experiment began after placing the demonstrators and/or objects on their compartment. The order of insertion of the two demonstrators was randomly assigned.

Demonstrator mice

Demonstrator mice were matched by age and sex to the observers, were habituated, without the observer, inside the same cage in the quarter circle 10 min for 3 consecutive days. Neutral,

stress, relief, unfamiliar and familiar demonstrators were counterbalanced in the two sides of the testing apparatus. On the day of the test, all demonstrators were brought into the experimental room at least 1 h before the experiment began. All demonstrators were group housed.

Neutral: these mice were habituated to the experimental setting as described above. All demonstrators were naive to the test and used for a maximum of two to three times, with at least 1 week between each experiment. No differences were observed in the performance of the observer mice depending on the previous experience of the demonstrator.

Stress: these mice were habituated to the experimental setting as described above. Then, they were subjected to restraint in a 50 ml Falcon tube (with a small hole at the end to let the mouse breathe) for 15 min before the beginning of the test, and then were moved immediately to their respective side of the arena.

Relief: these mice were habituated to the experimental setting as described above. They were water deprived 23 h before the experiment. Ad libitum access to water was given 1 h before the test, and mice were transferred to their respective side of the arena for testing. Food was always ad libitum.

Familiar: these mice were manipulated as neutral demonstrators but exposed to the observers for 6 min before testing.

Object

A black 3 × 3 × 7 cm object was used. These objects were validated to not induce any particular aversion/preference in mice[17,33].

Behavioral scoring

Acquired videos were used offline by an experimenter blind to the manipulation of both observers and demonstrators for scoring of social contact (sniffing). Data on the time spent in each zone, the number of entries in each zone and or the distance traveled were collected using tracking software (Anymaze). Manual behavioral scorings were performed with videos using custom-made keyboard-scoring software.

Optogenetic manipulations

During behavioral testing, the cannula for the optogenetic experiment was connected to a 2 × 1 rotary joint by a dual-site patch cord (Doric lenses, DFP_200_0.37_1.0m_GS0.7_2xFC) with the other extremity connected to a blue (465-nm laser, CNI Laser or 450-nm LED, Doric Lenses), a red (560-nm LED, Doric Lenses) or a yellow (594-nm LED Cobolt, Vretenvagen, Sweden) light source. Laser and LED stimulations were adjusted to a maximum of 3 mW per fiber, under the control of the behavioral tracking software and interface (Anymaze, Ami1). In specific conditions (that is, time or position of the animals), the Anymaze interface generates a TTL output that was transmitted to the laser used for optogenetic stimulation. For LED stimulation, the behavioral tracking software (Anymaze) was configured to send a TTL signal to an ARDUINO board connected to a low-friction rotary slip (AiCheaX PTZ). Micro-LED output intensity was adjusted by using resistances positioned in series (maximum power 3 mW). Laser and LED stimulations were controlled at 5 Hz or 30 Hz, with a pulse width of 5 ms and a maximum power of 3 mW. Laser inhibitions were controlled as continuous for 2 min or the duration of the animal was tracked inside a specific area. For the 594-nm laser (experiments in Fig. 5), an ARDUINO was used with a ramp-down protocol to gradually lower the laser's power from 100% to 0% over the course of 1 s after the observer mouse exited the selected demonstrator/empty zone. The laser beam was modulated through an acousto-optic modulator (Gooch & Housego).

Photometry experiment

For single sites or dual sites, experiment protocols were similar. Optic-fiber implants connected to metal or zirconia ferrules were cleaned and connected to a low-autofluorescence patch cord (2.5 m long, 0.5 NA, Doric Lenses). For single sites, a second dummy patch cord was attached and connected to the dummy ferrule to prevent artifacts. For dual sites, a second equivalent patch cord was used and fixed to the first one. During the experiment, GCaMP was excited using a 450-nm LED. For the control signal, 560-nm LED stimulation was used. Both beams were pulsed at an anti-synchronized frequency and merged into a specific dichroic and filter minicube (Doric Lenses). Excitation beams were merged onto the patch cord connected to the animal and emitted fluorescence was collected, filtered and divided into the same dichroic mirror. GCaMP emission (500–540 nm) and TdTomato (580–680 nm) were filtered and focused

on a femtowatt photoreceptor (Newport, DC mode). Control signal was collected on the red wavelength to remove artifact and movement control. For simultaneous optogenetic activation or inhibition and photometry recording, non-filter pulses at 560 nm were delivered throughout the same minicube. Excitation wavelengths were calibrated at ~30 µW. Due to the lower SNR collected at the level of the terminals, a higher excitation power was used, but never exceeding 50 µW. Control mice injected with the control YFP virus were recorded similarly and analyzed in the same way as GCaMP-expressing mice. The digital output of the photoreceiver was thus converted into analog output and transferred in a photometry interface (RZ5P, Tucker-Davis instrument), processed using Synapse software and deconvolved to their specific excitation frequency directly onto the software, and deconvolved signal were then converted for analyses on MATLAB. The signal was collected at 1,017 Hz (6th order). Entries and exits to specific demonstrator mouse zones were converted into TTL output using the tracking software (Anymaze) and sent to the photometry interface (RZ5P) using BNC connector together with the video stream of the mice during experiments. A custom-made MATLAB script was used to extract entries that occurred at least 2.5 s from each other to avoid overlapping of entries and that lasted for at least 2.5 s. Across all animals, the number of entries to specific zones that lasted more than 2.5 s were similar (Results) in specific conditions (that is, stress, neutral, relief, object, familiar and unfamiliar). We first checked whether the trends of calcium variation in specific entries were similar for each animal in the same group. Next, to compensate for the signal variability, we pooled all entries in a specific group, independently of the animals. Following the pooling, all the data were considered as paired when comparing within the same 5-s windows, or unpaired when comparing between conditions. Following extraction of entries in a specific zone of the apparatus, a 5-s window centered on the moment of the entries (baseline 2.5 s) was extracted for the entire 6 min of the experiment, detrended using a linear order (order 1) and *z*-scored to the 5-s window (F_0) to obtain the $\Delta F/F_0$. The signal was then downsampled to 10 Hz. To avoid a nonreal signal, no further transformation was done on the signal. Similarly, the control signal was analyzed in the same way, but no correction of the two signals was done. Movement artifacts were rare and manually removed using TdTomato controls. The position of the emotionally altered demonstrators, order of the experiment and day of the experiments were randomized to avoid position preference. Photometry data were analyzed in two different ways:

1. *z*-score of the $\Delta F/F_0$ during the baseline (2.5 s, 10 bins of 250 ms) were used as a reference to compare the $\Delta F/F_0$ of each 250-ms bin of the entire recording (2.5 s baseline and 2.5 s post-entries) using a paired two-sided *t*-test corrected for multiple-comparison (Bonferroni) analyses of each 250 ms of the 5-s period compared to the baseline (2.5 s before entry) average value. These analyses allow us to detect variation that might occur at any moment in the 5-s windows. If across all entries a bin was found to be significantly different to the baseline signal ($P < 0.05$), a horizontal line was placed above the 250-ms bin and color coded in relation to the entries (stress, relief, neutral, object, familiar, unfamiliar and empty).
2. A second analysis was done on the AUC). For each entry, the AUC of the baseline was compared to the AUC following the entries (2.5 s each) using a paired *t*-test. Next, to compare the signal changes during entries to emotionally altered or neutral demonstrators, the delta-AUC was obtained by the differences between the $AUC_{baseline}$ and $AUC_{stress\ or\ relief\ or\ neutral}$ ($AUC_{stress\ or\ relief\ or\ neutral} - AUC_{baseline}$). Then, this delta value for the emotionally altered demonstrator was compared to that of the neutral entries (with unpaired *t*-test). The delta value was needed to compare the response amplitude between different entries (in emotionally altered mice versus neutral), normalizing to their own baseline GCaMP signal. The AUC for each trial was extracted using the MATLAB trapZ function for the baseline (2.5 s), as well as the 2.5 s following entries to a demonstrator mouse zone that lasted more than 2.5 s.

Analyses of the SNR ratio

In fiber photometry experiments, the SNR was determined by the variability of the response amplitude to entries to a specific area of the emotion recognition test apparatus at a time *n* compared to the same variability across the entire experiment using the formula:

$$SNR = \frac{(\text{signal amplitude}_n)^2}{\text{noise variance}}$$

Where the noise variance was defined as the variance of the response amplitude to the entire population using the formula:

$$\text{Noise variance} = \sum_{k=1}^{n} \binom{n}{k} \frac{(x_n - \bar{x})^2}{n-1}$$

Where n is the number of trials, x is the signal amplitude and $\bar{x}$ is the average of the signal amplitude in all trials as previously described[49]. The SNR was expressed in decibels and corresponded to the variability of the response across the trial, where a higher SNR corresponds to a low noise variance and a lower variability across trials.

Widefield experiment

Four weeks before implantation of the cranial windows, WT mice received a retro-orbital injection of PHPeb-CAG-GCaMP7f (titer 10^{12}; volume 100 µl). On the day of the surgery, mice were anesthetized and the skull exposed as previously described above. A 3 × 3 mm craniotomy was perfromed by carefully drilling above the RSC preserving the dura. A 3 × 3 mm custom-made cranial window (no. 1.5 coverslip) was then placed in contact with the brain and maintained in position with anchor screws and dental cement. Windows were then protected using silicone (QuickSil). One week following implantation of the cranial window, a baseplate (Inscopix) was positioned above the cranial window to align the miniscope (nVoke2.0, Inscopix) focal plane with the surface of the brain, which allows imaging of 100–200 µm of the brain surface. The baseplate was then maintained in position using dental cement. On the day of the recording, a small drop of distilled water was then used to allow better contact between the cranial window and the relay lens of the miniscope (nVoke2.0, Inscopix). The miniscope was then maintained using magnets and a safety screw. Behavior recording and calcium imaging were synchronized using TTL inputs from the Anymaze interface. For each mouse, a focus was defined and conserved across all experiments, excitation power was set at 2 mW, gain was set at 4, and the recording frequency was 30 Hz. Both habituation and emotion recognition task periods were recorded. All recordings were analyzed in the same way. The raw signal was preprocessed, spatially filtered and motion corrected using basic functions of the data analysis software (Inscopix). Following motion correction, ROIs were manually drawn using the identify polygon cell selection tool, covering the entire field of view and avoiding all visible blood vessels. Signals for all ROIs and all TTL inputs were then converted for analyses using

MATLAB. For all mice, for each ROI in each frame, the signal (F) was first normalized from the average signal of the entire field of view to obtain the $\Delta F/F$, before being normalized using individual 5-s moving windows (150 frames). For each entry to the stress, relief or neutral mouse, a 5-s window centered on the entry time was then detrended (linear, order 1) to correct photobleaching and extracted. The standard deviation and the GCaMP signal of all ROIs × entries were then compared. A $\Delta F/F_0$ threshold of 0.1 was then used for selecting an increasing or decreasing signal based on the change of the signal between baselines (2.5 s) and entries (2.5 s).

cFos staining

All animals were first tested in the emotion recognition for stress (stress versus neutral) combined with photoinhibition (continuous when entering the stress) or without stimulation (control). At the end of the tasks, the animals were transferred back to their home cage for 30 min. Following this period, the animals were quickly anesthetized and transcardially perfused before their brains were collected and processed for immunohistochemistry. Brains were transferred in 30% sucrose (0.1 M PB) for cryoprotection before being sliced coronally using a microtome. Slices containing the mPFC and the RSC were collected for confirmation of the injection site and early gene (cFos) expression. Free-floating sections were rinsed in 1× PBS containing a quenching agent (0.3% Triton X-100) and a blocking solution (10% NDS) for 2–4 h. Following rinses, all the sections were then incubated in a primary solution containing cFos polyclonal antibody (sc-52, made in rabbit, 1:2,000 dilution, Santa Cruz Biotechnology) overnight at 4 °C as similarly reported[51]. Sections were then rinsed thoroughly and incubated in the secondary antibody solution containing Alexa Fluor 488 anti-rabbit for 4–6 h. After washing, sections were mounted on glass slides using Vectashield Mounting Medium and scanned using a fluorescence microscope. Cell counting was done online by an experimenter blind to the experiment design and reported as the number of cFos-positive cells in the RSC.

Mouse rsfMRI

rsfMRI time series were acquired in $Arc^{+/+}$ ($n = 11$) and $Arc^{-/-}$ ($n = 11$) mice as detailed in previous studies[52,53]. Briefly, animals were anesthetized with isoflurane (5% induction), intubated and artificially ventilated (2% maintenance). After surgery, isoflurane was

discontinued and replaced with halothane (0.7%). Recordings started 45 min after isoflurane cessation. Functional scans were acquired with a 7T MRI scanner (Bruker Biospin) using a 72-mm birdcage transmit coil and a four-channel solenoid coil for signal reception. For each animal, in vivo anatomical images were acquired with a fast spin echo sequence (TR, 5,500 ms; echo time (TE), 60 ms; matrix, 192 × 192; field of view, 2 × 2 cm; 24 coronal slices; slice thickness, 500 μm). Co-centered single-shot BOLD rsfMRI time series were acquired using an echo planar imaging (EPI) sequence with the following parameters: TR/TE, 1,200/15 ms; flip angle (FA), 30°; matrix, 100 × 100; field of view, 2 × 2 cm; 24 coronal slices; slice thickness, 500 μm for 500 volumes.

FC analysis

Before mapping rsfMRI connectivity, raw data were preprocessed and denoised as previously described[54]. First, the initial 50 volumes were removed to allow for T1 equilibration effects. Time series were then despiked, motion corrected and registered to a common reference template. Motion traces of head realignment parameters and mean ventricular signal were then used as nuisance covariates and regressed out from each time course. Before FC mapping, all time series underwent bandpass filtering (0.01–0.1 Hz) and spatial smoothing (FWHM = 0.6 mm). Target regions of long-range connectivity alterations in $Arc^{-/-}$ mice were mapped using seed-based analysis. Specifically, seeds of 3 × 3 × 1 voxels were placed in the mPFC and the RSC of $Arc^{+/+}$ and $Arc^{-/-}$ mice to probe impaired FC between these regions and the rest of the brain. Unilateral seeds were also placed in the left and right somatosensory cortex. The location of the seeds used for mapping is indicated with green lettering in Figs. 6a,b and 7a. FC was measured with Pearson's correlation, and *r*-scores were transformed to *z*-scores using Fisher's *r*-to-*z* transform before group-level statistics. Voxel-wise intergroup differences for seed-based mapping were assessed using a two-tailed Student's *t*-test ($|t| > 2$, $P < 0.05$) and a family-wise error rate-corrected cluster threshold of $P = 0.01$ was applied. To quantify rsfMRI alterations, we also carried out FC measures in cubic ROIs (3 × 3 × 1 voxels). The statistical significance of these region-wise intergroup effects was quantified using a two-tailed Student's *t*-test ($|t| > 2$, $P < 0.05$).

PCP administration

We used the same treatment protocol as previously described35, which is used as a prominent pharmacological model of schizophrenia that produces cognitive executive dysfunction related to the mPFC34,35. At least 7 days after the last experiment, mice that underwent the PCP treatment received an intraperitoneal injection (5 mg per kg body weight) 30 min before recording (acute testing) of the photometry signal and the emotion recognition tasks for stress. All mice then received daily administration of the same dose for another 13 days. After a 7-day washout period, mice were tested for photometry signal and the emotional recognition for stress.

Slice preparation

Acute cortical coronal slices were prepared from the neocortex of animals (2–6 months old) similarly to before55. Mice were anesthetized with urethane (16.5%, 1.65 g per kg of body weight), the brain was quickly dissected and placed in an ice-cold cutting solution containing: 130 mM potassium gluconate, 15 mM KCl, 0.2 mM ethylene glycol tetraacetic acid (EGTA), 20 mM HEPES and 25 mM glucose, with pH adjusted to 7.4 with NaOH and oxygenated with O_2 100%. Coronal slices (slice thickness, 250–300 µm) were cut with a vibratome (VT1000S, Leica Microsystems) and then were immersed for 1 min in solution at RT containing: 225 mM D-mannitol, 25 mM glucose, 2.5 mM KCl, 1.25 mM NaH_2PO_4, 26 mM $NaHCO_3$, 0.8 mM $CaCl_2$, 8 mM $MgCl_2$, pH 7.4 with 95% O_2/5% CO_2. Slices were then incubated for 30 min at 35 °C in standard ACSF containing: 125 mM NaCl, 2.5 mM KCl, 25 mM $NaHCO_3$, 1.25 mM NaH_2PO_4, 2 mM $MgCl_2$, 1 mM $CaCl_2$, 25 mM glucose, pH 7.4 with 95% O_2/5%CO_2 and then maintained at RT until use.

Ex vivo electrophysiology

Slices were transferred to a submerged recording chamber (RC26, Warner Instruments) and continuously perfused with fresh bathing solution composed of: 125 mM NaCl, 2.5 mM KCl, 1.25 mM NaH_2PO_4, 25 mM $NaHCO_3$, 2 mM $MgCl_2$, 2 mM $CaCl_2$, 25 mM glucose, pH 7.4 with 95%O_2/5% CO_2. The solution was maintained at 30 °C by an inline solution heater and temperature controller (TC-344B, Warner Instruments). The electrical signals were recorded through a Multiclamp 700B patch-clamp amplifier, digitized using a Digidata 1440 interface and analyzed with pClamp 10.2 software (Molecular Devices). Current-clamp recordings were

sampled at 50 kHz and filtered at 10 kHz. Voltage-clamp recordings were sampled at 10 kHz and filtered at 2 kHz. Pipettes (tip resistance 4 MΩ) were filled with a potassium-based internal solution containing: 140 mM potassium gluconate,1 mM $MgCl_2$, 8 mM NaCl, 2 mM Na_2ATP, 0.5 mM Na_3GTP, 10 mM HEPES, 10 mM Tris-phosphocreatine to pH 7.2 with KOH. For some recordings a cesium-based intracellular solution was used: 145 mM cesium-methansulfonate, 8 mM NaCl, 2 mM Na_2ATP, 0.5 mM Na_3GTP, 0.3 mM EGTA, 10 mM HEPES, 10 mM Tris-phosphocreatine and 5 mM Qx-314 bromide (Sigma-Aldrich) to pH 7.25 with CsOH. Series resistance (range 6–20 MΩ) was not compensated, and data were not corrected for the liquid junction potential. Cells with average resting potential more depolarized than −63 mV were excluded from the analysis. In all the recordings obtained with the potassium-based intracellular solution, neurons were held at −70 mV and −50 mV in current-clamp and voltage-clamp modes, respectively. To record inhibitory postsynaptic currents, antagonists of glutamate receptors were added to the bathing solution: 10 µm NBQX and 50 µm D-AP5 (Tocris). Neurons recorded using the cesium-based intracellular solution were held at +10 mV, corresponding to the reversal potential of excitatory postsynaptic currents. Optogenetics stimulation was performed using a continuous wave, solid-state laser source ($\lambda = 488$ nm; Cobolt) and was delivered via an optical fiber (fiber diameter: 200 µm, AMS Technologies). Blue light was presented at an intensity of 3.5–22 mW; the power intensity was measured at the fiber tip. Light pulses (2–10 ms long) were delivered every 5–10 s for 5–15 consecutive trials.

Statistics

Results are expressed as the mean ± s.e.m. throughout the paper. Each observer's behavior toward the two different demonstrator mice was analyzed using a within-groups RM-ANOVA. The discrimination index with optogenetics stimulation was analyzed by two-way ANOVAs with optostimulation (no light, ChR2, NphR) as between-subjects factors, and time intervals (0–2 min, 2–4 min and 4–6 min) as RM within-subjects factors. *Arc* mutant mice behavior was analyzed by two-way ANOVAs with genotype (+/+, +/−, −/−) as the between-subjects factor, and sniffing toward the two different demonstrators as the RM within-subject factor. Bonferroni's post hoc test with multiple-comparison corrections was used for making comparisons within groups when the overall ANOVA showed statistically significant differences. All tests were two sided. Specific details on statistics are included in the statistics

files in the repository at https://doi.org/10.48557/FEXUTZ. For photometry experiments, a paired two-sided *t*-test corrected for multiple-comparison analyses was done between the average of the baseline and each 250-ms bin. This allowed us to detect variations in the GCaMP signal that are repeated across entries at specific time points following entries as well as detection of events that might occur before the entries. In a subsequent analysis, the AUC of the baseline period (2.5 s) and the entry period (2.5 s) were compared using a two-tailed paired or unpaired *t*-test. For optogenetic experiments, sniffing time, distance traveled, number of entries in each zone and time in each zone was then compared across different conditions to the control (no stimulation) experiments. The accepted value for significance was $P \leq 0.05$. Statistical analyses were done using Statistica (Tibco). The number of mice is reported in the legends and corresponds to similar numbers used in previous publications. Experiments reported in the paper were replicated at least two to four times for a different group, cage, sex or generation (see specifics in the figure legends). No statistical measures were taken to predetermine the sample size of the experiments. The number of animals per group was similar to previous studies[17,19,35,51]. For each animal, only entries to the stimulus area that lasted more than 2.5 s were used for analyses. Mouse exclusion criteria were defined before the beginning of the experiments and include genotyping errors, viral injection and fiber misplacement, and uncompleted experiments due to loss of implants. For all experiments, the side of the allocated stimulus mice, the day of training the order of the testing, the sex of the experimental group and the drug testing were randomized. Statistical tests were adjusted based on comparison. For two groups, a two-sided paired or unpaired *t*-test was used; for RM and for more than three groups, ANOVAs were used. Data distribution was assumed to be normal, but this was not formally tested. For all behavioral experiments, the position of the stimulus (stress, relief and neutral), the protocol of optogenetic stimulation or the order of the animals were always randomized. For behavioral scoring, the observer was blinded to the experiment's conditions.

Humans

The dataset is part of a population-based neuroimaging genetics study: the IMAGEN cohort[56]. For this study, we analyzed neuroimaging data from 1,417 participants at 19 years old. After the quality-control procedure, 1,263 participants (aged 19.08 ± 0.76 years old, 52.7% female) were included in the analysis. Participants were recruited from eight research centers in the United

Kingdom, Germany, France and Ireland, and each center enrolled 101 to 200 participants. Ethics approval was obtained at each site by a local research ethics committee. Written consent was obtained from each participant.

Emotional faces task fMRI paradigm

The task paradigm was adapted from ref. 57 to assess social-emotional processing in humans. Participants were instructed to watch an 18-s block of either face (angry, happy, neutral) or non-face (control) stimuli. Each block of face stimuli comprises black and white video clips (2–5 s) of one type of face in movement (three males and three females). The control stimuli block consists of black and white concentric circles expanding or contracting at various speeds, roughly matching the contrast and motion of the face clips. Each type of face stimuli was repeated four times and intermixed with 12 blocks of the control stimuli. The total scanning session of the task lasted about 7 min.

MRI acquisition and preprocessing

Neuroimaging data were collected on 3T scanners at eight study centers with different manufacturers (Siemens: four sites, Philips: two sites, General Electric: one site, and Bruker: one site). Scanning parameters were harmonized across sites before the study. The visual stimulus was presented using the standardized hardware (Nordic Neurolabs). For each participant, we collected a high-resolution T1-weighted MRI (T1) scan using the Magnetization Prepared Rapid Acquisition Gradient Echo (MPRAGE) sequence, and functional images with the gradient-echo, EPI sequence. Scanning parameters of T1-weighted images were: TR, 2,300 ms; TE, 2.8 ms; FA = 8°; isotropic voxel size, 1.1 mm; 256 × 256 × 160 matrix; sagittal slice plane. Acquisition parameters of functional images are: TR = 2,200 ms, TE = 30 ms, FA = 75°; 64 × 64 × 40 matrix; voxel size, 3.4 × 3.4 × 2.4 mm; slice gap, 1 mm. Task-based fMRI scans were preprocessed using Statistical Parametric Mapping (SPM12; http://www.fil.ion.ucl.ac.uk/spm/). Preprocessing steps included: non-brain tissue removal, slice-timing correction, head movement realignment using a rigid body transformation, and images were nonlinearly warped on the MNI space using a customized EPI template. Normalized images were smoothed using a 5-mm FWHM Gaussian kernel and resliced to 3-mm isotropic voxels. The first five volumes were discarded to allow for scanner equilibrium. To

ensure the quality of data for further analysis, we excluded: (1) participants with incomplete demographic information or task onset files simultaneously recorded during scanning; (2) participants with excessive head movement (mean framewise displacement > 0.2 mm); (3) participants with unsuccessful normalization (using the criterion of a correlation between the individual mask and group mask < 0.85)[58]. To obtain a functional parcellation of the cortex, we applied group ICA on preprocessed functional images[59]. Time-varying FC was calculated using the sliding-window approach[60,61,62]. In total, we analyzed neuroimaging data from 1,263 participants.

Group ICA and postprocessing

The ICA is a commonly used method to decompose resting-state and task-based fMRI data into a set of spatially independent components[59]. Group ICA was applied on preprocessed functional images using the GIFT software[59]. We derived 100 components, and selected those with peak activations in gray matter, exhibiting low spatial overlap with known artifacts, and corresponding time courses dominated by low-frequency fluctuations[30]. In total, 61 brain components were identified and categorized into 7 domains based on their known anatomical and functional properties: subcortical, auditory, sensorimotor, visual, cognitive control domain, default mode domain and cerebellar domain. Time courses of the selected components underwent postprocessing to: (1) remove linear, quadratic and cubic trends; (2) regress six head motion parameters estimated during realignment; (3) de-spike detected outliers; (4) low-pass filter with a cutoff frequency of 0.18 Hz. The low-pass filter was chosen to remove physiological sources (heartbeat, respiration) and motor response in tasks that were higher than 0.18 Hz[63].

Time-varying FC

Time-varying FC between each pair of brain components was calculated using the sliding-window approach[60,61]. Specifically, time-varying FC was estimated between components in a segment of the scanning period (time window). The tapered time window was created by convolving a rectangle (window size = 8 TR or 17.6 s) with a Gaussian kernel (sigma = 3 TR) to obtain a time-specific connectivity strength. Then, the time window was moved forward by 1 TR to get the next connectivity strength and repeated until the end of a scanning session. This resulted in 184 windowed FC values for every participant during the emotional faces task

scanning. As studies suggested that task-induced brain activation will inflate estimation of connectivity by imposing co-occurring changes in BOLD signal due to task stimulation[64,65]., we regressed task-evoked activation by including task design matrix as covariates when calculating FC. The task design matrix was calculated by convolving the timing of task stimuli with a canonical HRF.

Correlation between FC and task stimuli

We examined whether whole-brain FC of the default mode components, encompassing the mPFC and the RSC, covaries with the presence of task stimuli. Coupling between FC strength and occurrence of task stimuli (convolved with HRF) was calculated using Pearson's correlation and compared across stimulus types using one-way ANOVA and post hoc two-sample *t*-tests, correcting for six multiple comparisons ($P < 0.005/6$).

Data availability

All scripts used in the paper were based on the provided scripts from the Tucker-Davis Technology database and were adjusted for our needs. The individual data and statistical analyses are shared on the open repository at https://doi.org/10.48557/FEXUTZ. All raw images, photometry recordings or videos are shared on reasonable request to the corresponding author due to their large sizes. Human data are available on the IMAGEN database via https://imagen-project.org/the-imagen-dataset/.

Extended Data

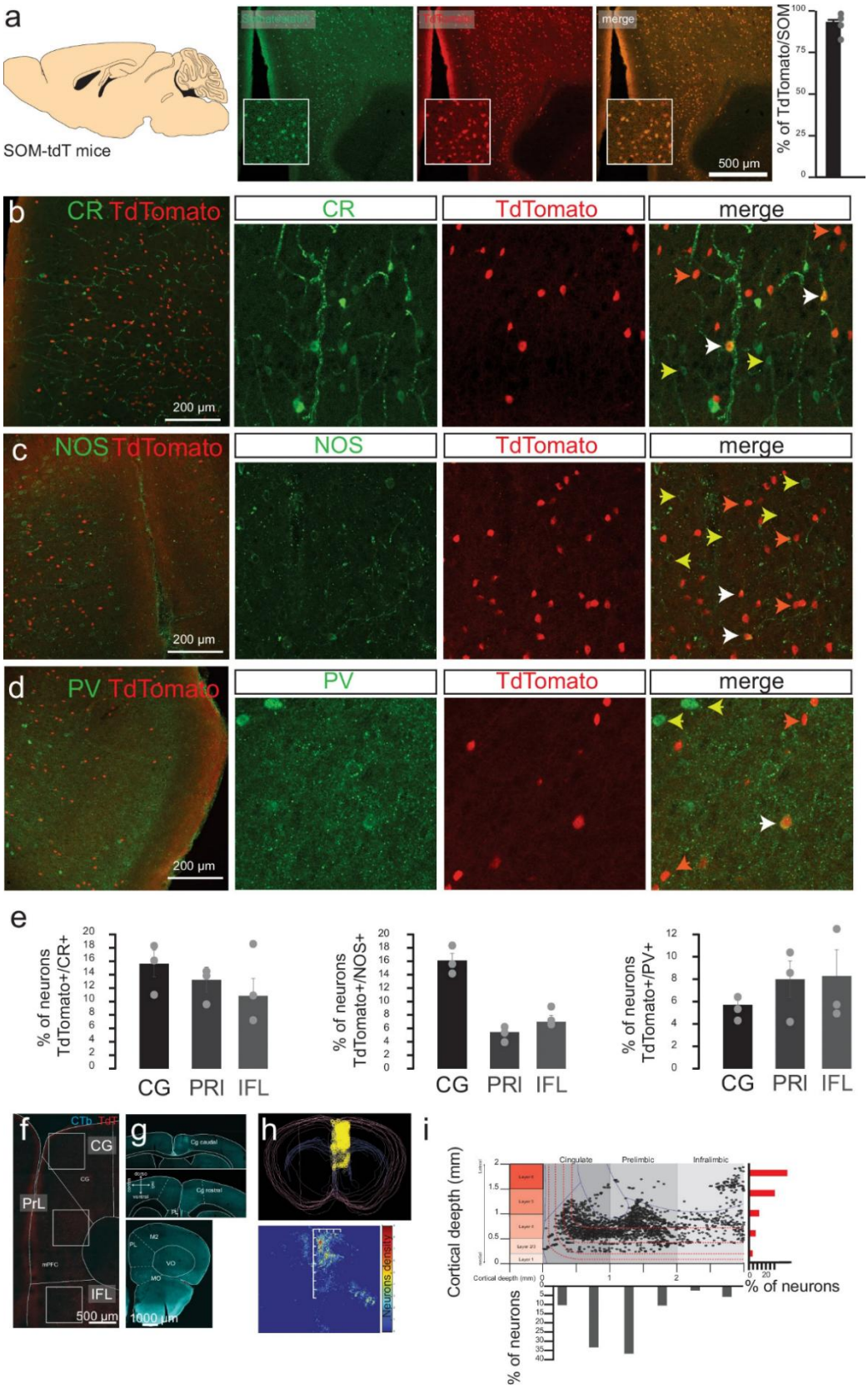

Extended Data Fig. 1 Refer to Fig. 1.

In mice expressing TdTomato in all somatostatin neurons (SOM-tdT) quantification of immunolabelled somatostatin cell of the mPFC (a) revealed a high-colocalization (n = 3 mice, 91.31 + /-2.02% overlapping). The same immunostaining for (b) Calretinin (CR), (c) Nitric oxide synthase (NOS), or (d) Parvalbumin (PV) revealed (e) an overall low colocalization with TdTomato positive cells (CR:13.24 + /-1.29, PV: 7.32 + /-0.94, NOS: 9.50 + /-1.73%). (f-g) Following injection of Ctb-560 in the RSC of SOM-TdT mice, we observed CtB expressing cells across the entire cortex, including the different subregions of the mPFC (the cingulate, prelimbic and infralimbic cortex, repeated in 3 animals). (h-i) The overlapping of all sections containing the mPFC and the mapping of CtB-Positive neurons revealed a distribution along the different layers and the dorsoventral axis. Data are represented as means + /-SEM. Cg, cingulate cortex; PrL, Prelimbic cortex, iFl, infralimbic cortex. Bar plots are represented as mean ± SEM. * is used for $P < 0.05$.

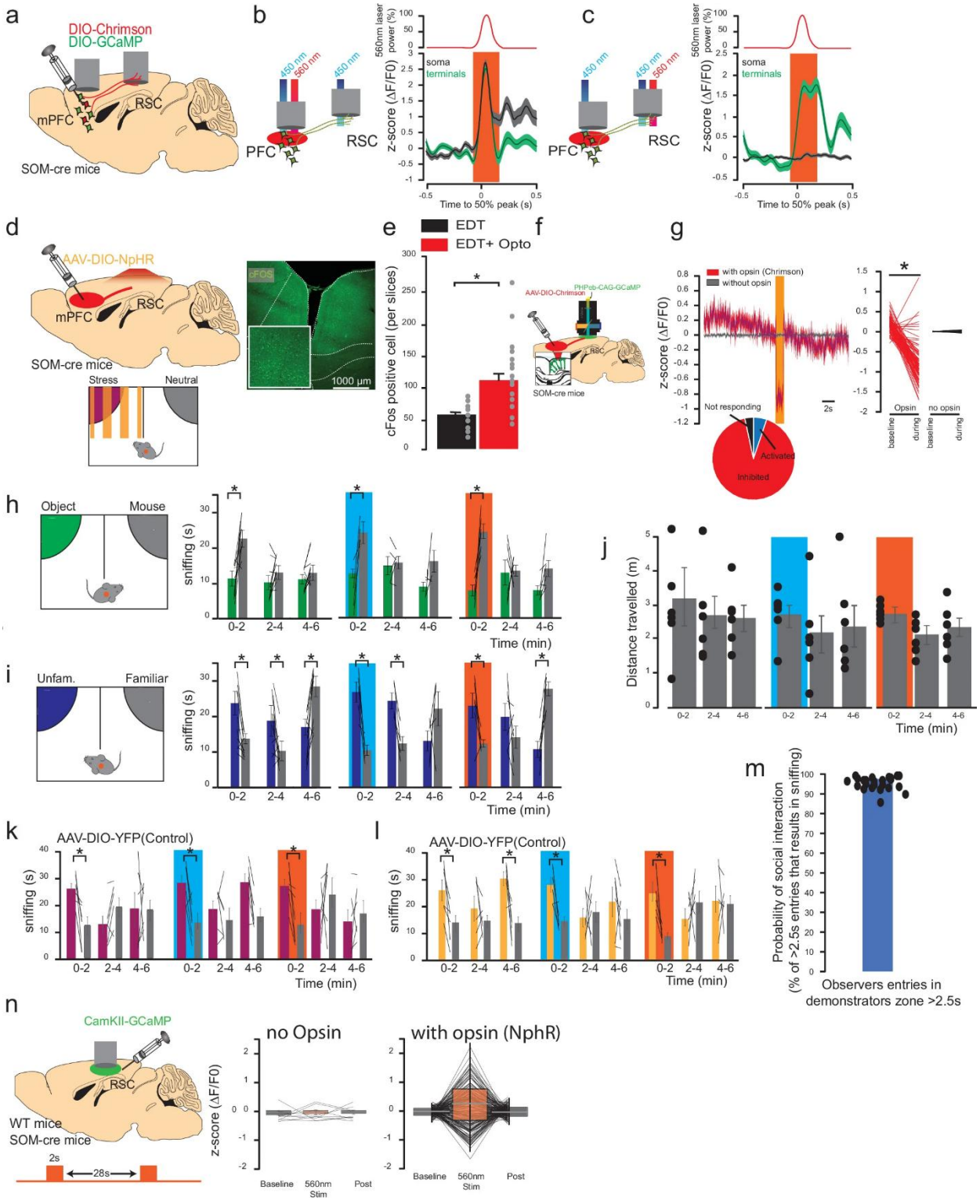

Extended Data Fig. 2 Refer to Figs. 2–3.

(a) In SOM-cre mice AAV-DIO-Chrimson and AAV-DIO-GCaMP were injected in the mPFC to record and activate SOM neurons in the mPFC and their terminals in the RSC. (b) Activation of the soma induces an increase

of the signal in both the mPFC and the RSC while (c) stimulation of the terminals results in an increased GCAmP signal only in the terminals but not in the soma. (d) SOM-cre mice receiving inhibition (red, AAV-DIO-NphR) or control (black, AAV-DIO-TdTomato) of the mPFC-to-RSC terminals when in the stress demonstrator zone, and sacrificed 30 min following the task for cFOS immunohistochemistry. (e) Ex vivo quantification of cFOS positive neurons in the RSC (n = 6 mice, 8 to 13 sections per mice within the PFC, *P < 0.0001). (f) SOM-cre mice (n = 4 males) were injected with AAV-DIO-Chrimson in the mPFC, receiving retroorbital administration of PHPeb-CAG-GCamP and implanted with a widefield miniscope above the RSC, while control mice (WT n = 2) received only the retroorbital administration of PHPeb-CAG-GCamP and implanted with a widefield miniscope above the RSC. (g) GCaMP-activity in the RSC during activation (5 Hz, 2 seconds long) of mPFC-to-RSC SOM terminals (red, n = 386 stimulations, *P < 0.0001 2 sec light period versus 5 sec baseline). Control mice were treated in the same way but not having injected the chrimson opsin (gray line, n = 100 stimulation). Left panel represent the average GCamP-Signal during the baseline (5 s) and the stimulation (2 s) across all stimulation trials. The cake graph shows that in opsin injected animals, 91.5% of the stimulation pulses delivered induced a reduction in the signal (353/386 stim) while a minor part was associated with an increase (20/386, 5.2%) or no significant changes (13/386, 3.4%). (h) SOM-cre mice injected in the mPFC with AAV-DIO-ChR2 (n = 8 mice) or AAV-DIO-NphR (n = 14), and tested for discrimination between an object and a mouse without light, with optostimulation (blue background), or photoinhibition (orange background), (*P < 0.05 mouse versus object). Light stimulation was delivered only during the first 2 minutes of the test. (i) Discrimination between a familiar and an unfamiliar mouse (n = 11) without light, with optostimulation (blue background) or photoinhibition (orange background), (*P < 0.05 familiar versus unfamiliar). Light stimulation was delivered during the first 2 minutes of the test. (j) Distance travelled during the emotion recognition with photoactivation (blue background) or photoinhibition (orange background, n = 6). (k-l) SOM-cre mice injected with AAV-DIO-YFP (Control, n = 6) and implanted with a LED on the RSC to deliver blue (blue background) or red light (orange background) during the first 2 minutes of the emotion recognition task. (*P < 0.05 neutral versus emotionally altered). (m) In all tested mice, most social contacts (95.95 + /-0.71%) between the observer and a demonstrator mouse occurred with entries of ≥2.5 s from crossing the stimulus mouse zone (n = 24 mice). (n) Calcium signal in WT mice (n = 9) injected with AAV-CamKII-GCamP in the RSC or SOM cre mice (same as Fig.3d) injected with AAV-DIO-Chrimson in the mPFC, before, during and after the delivery of red light (560 nm). Bar plots are represented as mean ± SEM. Whisker-plot presenting upper and lower quartile, mean and median. Complete statistics in Supplementary Table 3.

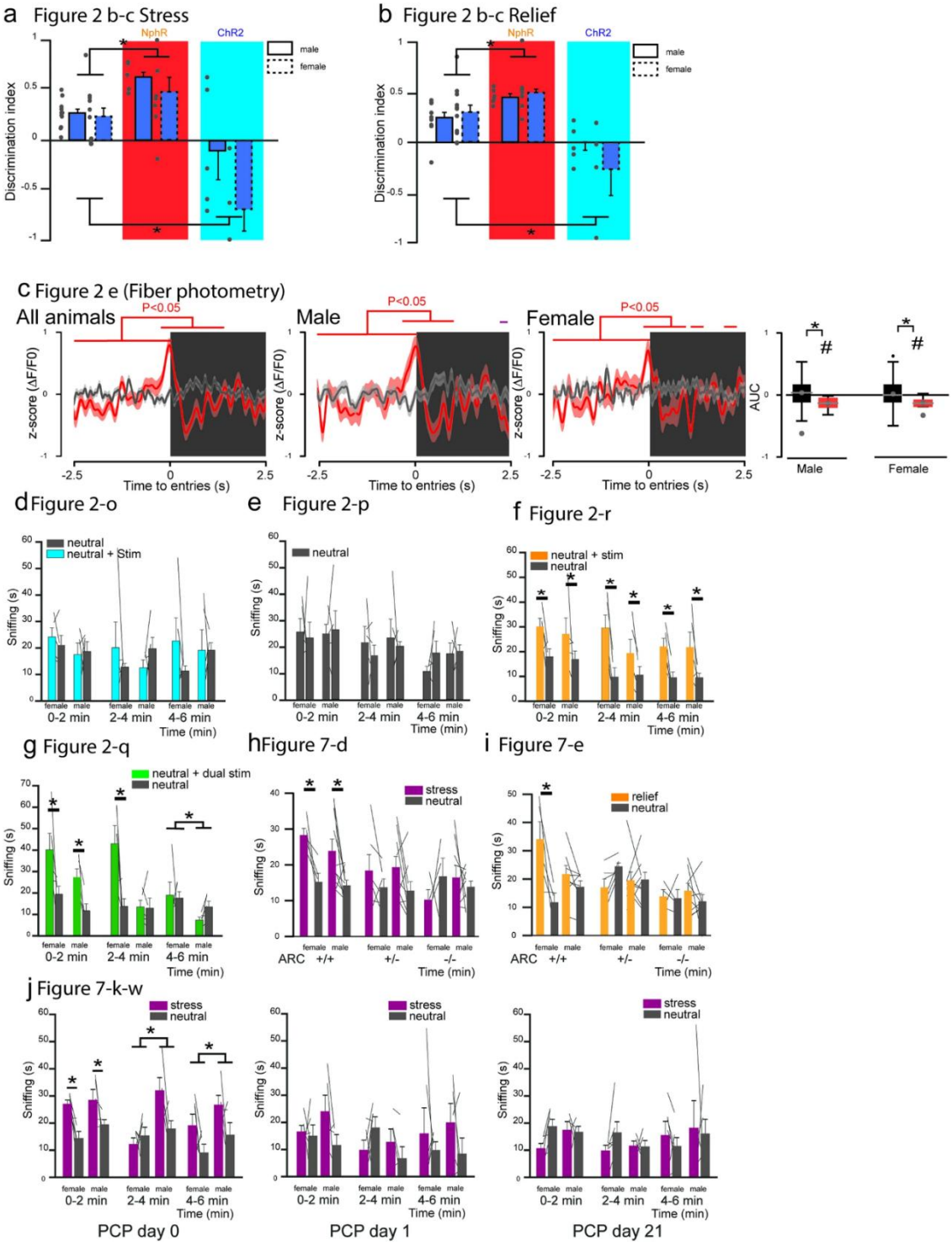

Extended Data Fig. 3 Refer to Figs. 2 and 7.

Optogenetic inhibition (NphR) and stimulation (ChR2) of mPFC-to-RSC SOM terminals during (a) stress emotion recognition in male (n = 5 for ChR2 and 6 for NphR) and female (n = 4 for ChR2 and 8 for NphR) observers, or (b) during relief emotion recognition in male (n = 5 for ChR2 and 6 for NphR) and female (n = 4 for ChR2 and 8 for

NphR) observers (*P < 0.05 versus no light). (c) Fiber photometry signal of mPFC-to-RSC SOM terminals during emotion recognition when entering the neutral mouse zone (grey lines) or the zone of emotionally altered demonstrators (red lines) in all animals, or divided by males and females (n = 23; #P < 0.0001 versus baseline; *P < 0.005 versus neutral). Whisker-plot are presenting upper and lower quartile, mean and median. (d) Optogenetic ChR2 stimulation of the mPFC-to-RSC SOM terminals of male (n = 5) and female (n = 5) observers in neutral versus neutral recognition with entries to a randomly selected neutral mouse zone paired with 5 Hz stimulation (Stim). (e) Control group with no stimulation of the mPFC-to-RSC SOM terminals of male (n = 5) and female (n = 5) observers in neutral versus neutral recognition. (f) Observer mice tested with two neutral demonstrators. Entrance in one of these demonstrators (randomly chosen) triggered optogenetic inhibition (NphR) of the mPFC-to-RSC SOM terminals (continuous light). (*P < 0.05 neutral + stim versus neutral). (g) Dual stimulation of the mPFC-to-RSC SOM terminals in neutral versus neutral condition with entries to a randomly selected demonstrator paired with a short activation (200 ms, 5 Hz) follow by inhibition (continuous). (*P < 0.05 neutral + dual stim versus neutral). (h) Stress emotion recognition in ARC mice (+/+, + /- and -/-) in males (+/+ n = 10, +/- n = 9, -/- n = 9) and females (+/+ n = 5, +/- n = 6, -/- n = 4). (*P < 0.05 ARC + /+ neutral versus ARC + /+ stress). (i) Relief emotion recognition in ARC mice (+/+, + /- and -/-) in males and female (*P = 0.01 ARC + /+ neutral versus ARC+ /+ relief). (j) Emotion recognition with no PCP (PCP day 0), following acute PCP (PCP day 1) and 14 days PCP + 7 days washout (PCP day 21) in males (n = 5) and females (n = 6). Bar plots are represented as mean ± SEM. Whisker-plot presenting upper and lower quartile, mean and median. * is used for P < 0.05. Complete statistics in Supplementary Table 3.

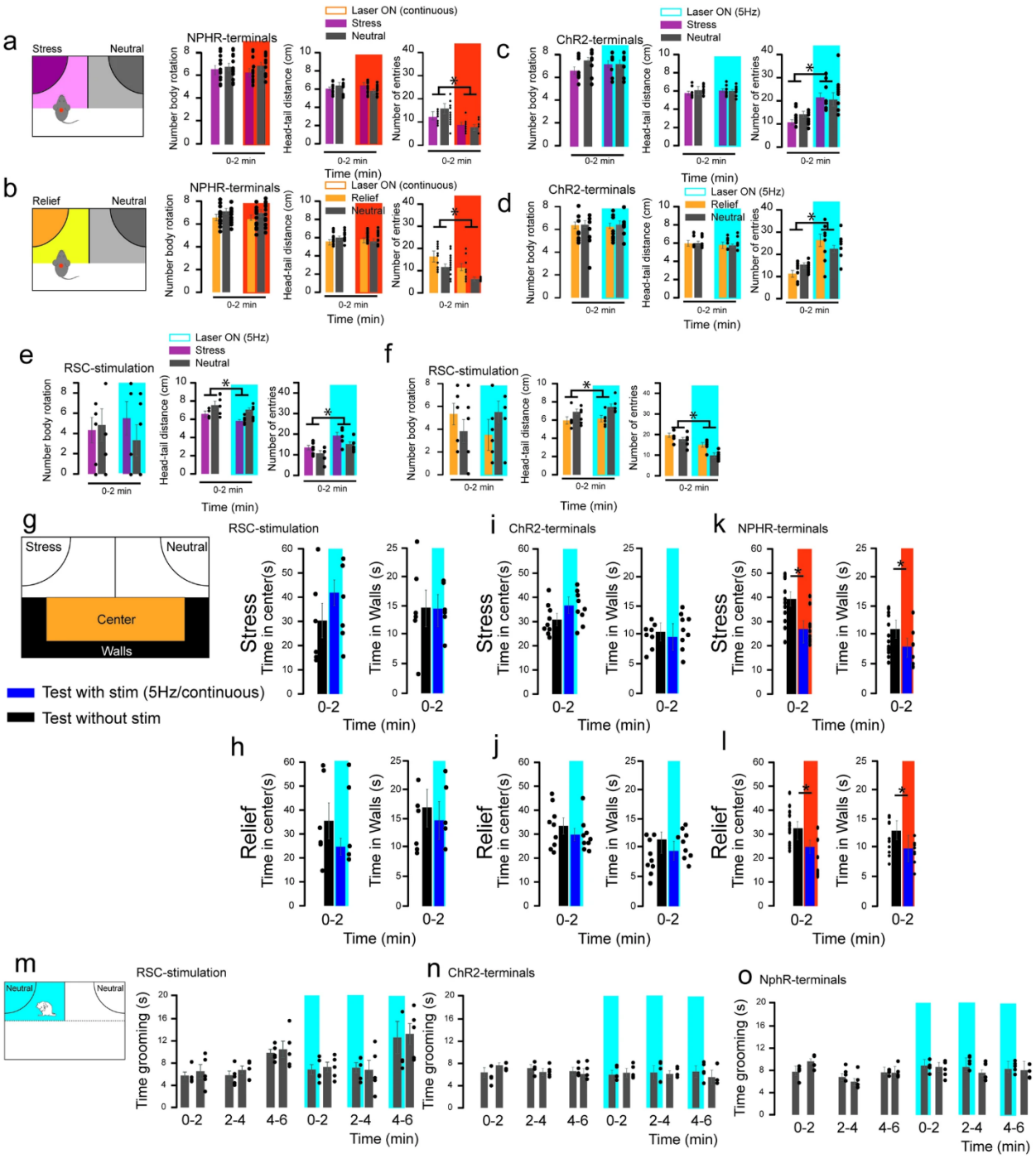

Extended Data Fig. 4 Refer to Figs. 2 and 4.

(a-b) Number of body rotation, head-tail distance, and number of entries without light and following optogenetic inhibition of mPFC-to-RSC SOM terminals (NphR-terminals) during recognition for (a) stress or (b) relief (*P < 0.0001 no light versus light). (c-d) Number of body rotation, head-tail distance, and number of entries without light and following optogenetic stimulation of mPFC-to-RSC SOM terminals (ChR2-terminals) during recognition for (c) stress or (d) relief (*P < 0.001 no light versus light). (e-f) Number of body rotation, head-tail distance, and

number of entries without light and following optogenetic stimulation of RSC-pyramidal neurons during recognition for (e) stress or (f) relief (*P < 0.05 no light versus light). The increase in the number of entries in both the emotionally altered is associated with a reduction of social-interaction (Fig. 2) and less sniffing (see Fig. 4b-c). (g-h) Time spent in the no demonstrator mice zone subdivided by central area or close to the walls without light or following optogenetic stimulation of RSC-pyramidal neurons in (g) stress or (h) relief emotion recognition (Figures show only 0-2 min for clarity). (i-j) Time spent in the no demonstrator mice zone subdivided by central area or close to the walls without light or following optogenetic stimulation of mPFC-to-RSC SOM terminals in (i) stress or (j) relief emotion recognition. (k-l) Time spent in the no demonstrator mice zone subdivided by central area or close to the walls without light or following optogenetic inhibition of mPFC-to-RSC SOM terminals in (k) stress or (l) relief emotion recognition. Together with increased entrance (Extended Data Fig. 9c-d), these data suggest that opto inhibition of mPFC-to-RSC SOM terminals increase mouse willingness to interact with other mice, consistent with its increased emotion recognition effect (Fig. 2), unrelated to anxiety-like behaviors (effects both in center and walls time). (m) Grooming time in no stimulated side versus the side with optogenetic stimulation of RSC pyramidal neurons in a neutral versus neutral condition. (n) Grooming time in no stimulated side versus the side with optogenetic stimulation of mPFC-to-RSC SOM terminals in a neutral versus neutral condition. (o) Grooming time in no stimulated side versus the side with optogenetic inhibition of mPFC-to-RSC SOM terminals in a neutral versus neutral condition. Bar plots are represented as mean ± SEM. * is used for P < 0.05. Complete statistics in Supplementary Table 4.

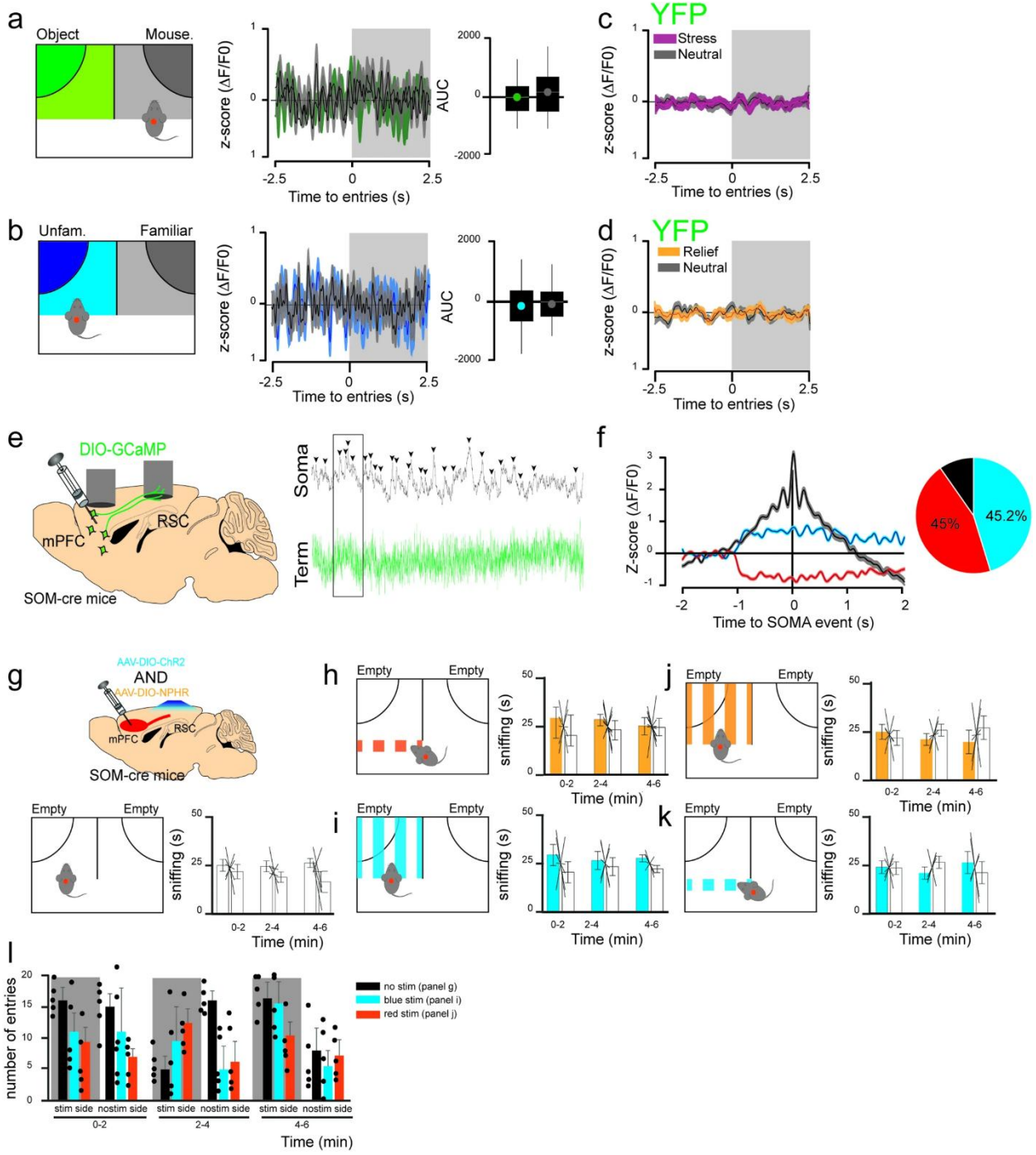

Extended Data Fig. 5 Refer to Figs. 2–3–4.

Photometry recording of mPFC-to-RSC SOM terminals during recognition (a) between an object and a novel mouse (n = 4; object: green; mouse: grey. n = 25 entries to object, n = 34 entries to neutral) or (b) between a familiar and unfamiliar mouse (n = 29 entries to unfamiliar, n = 18 entries to familiar). (c-d) Photometry recording in SOM-cre mice (n = 6) injected with AAV-DIO-YFP in the mPFC and recorded in RSC during recognition (c) for stress (; stress: purple; neutral: grey; n = 199 entries to stress, n = 97 entries to neutral) or (d) relief (n = 198 entries to relief,

n = 194 entries to neutral). (e) SOM-Cre mice (n = 4) were injected with AAV-DIO-GCAmP in the mPFC, and implanted with optic fibers both in the mPFC and RSC to record calcium activity of SOM cells at the level of the soma (Soma) or their terminals in the RSC (Term), allowing a direct correlation of both signals. (f) Calcium events in the Soma were selected as the threshold for the peristimulus analyses, showing that GCamP-signal increased in the mPFC (grey line), while presenting two patterns in the RSC, either an increase in 45% of the events (blue line) or a decrease (red line). (g) Som-cre mice were injected in the mPFC with AAV-DIO-ChR2 and AAV-DIO-NphR (n = 5 mice) and bilateral optic fiber was put on top of the RSC to test if activation or inhibition of mPFC-to-RSC SOM terminals could induce side preference in the absence of stimulus mice (empty) which are normally neutral in their side bias. (h) Short (250 ms) inhibition of the terminals (entire 6 minutes, n = 5 mice) prior to entry to a randomly selected side. (i) Activation of the terminals (n = 5 mice) only when in a randomly selected side zone. (j) Inhibition of the terminals (n = 5 mice) when in a randomly selected side zone. (k) Activation of the terminals (entire 6 minutes, n = 5 mice) prior to entry to a randomly selected side. (l) Number of entries in each zone during no stimulation (black bars), activation (blue bars) or inhibition (red bars) (n = 5 mice). For experiment empty-empty all mice were tested in all stimulation conditions. Whisker-plot are presenting upper and lower quartile, mean and median. Bar plots are represented as mean ± SEM. * is used for $P < 0.05$. Complete statistics in Supplementary Table 4.

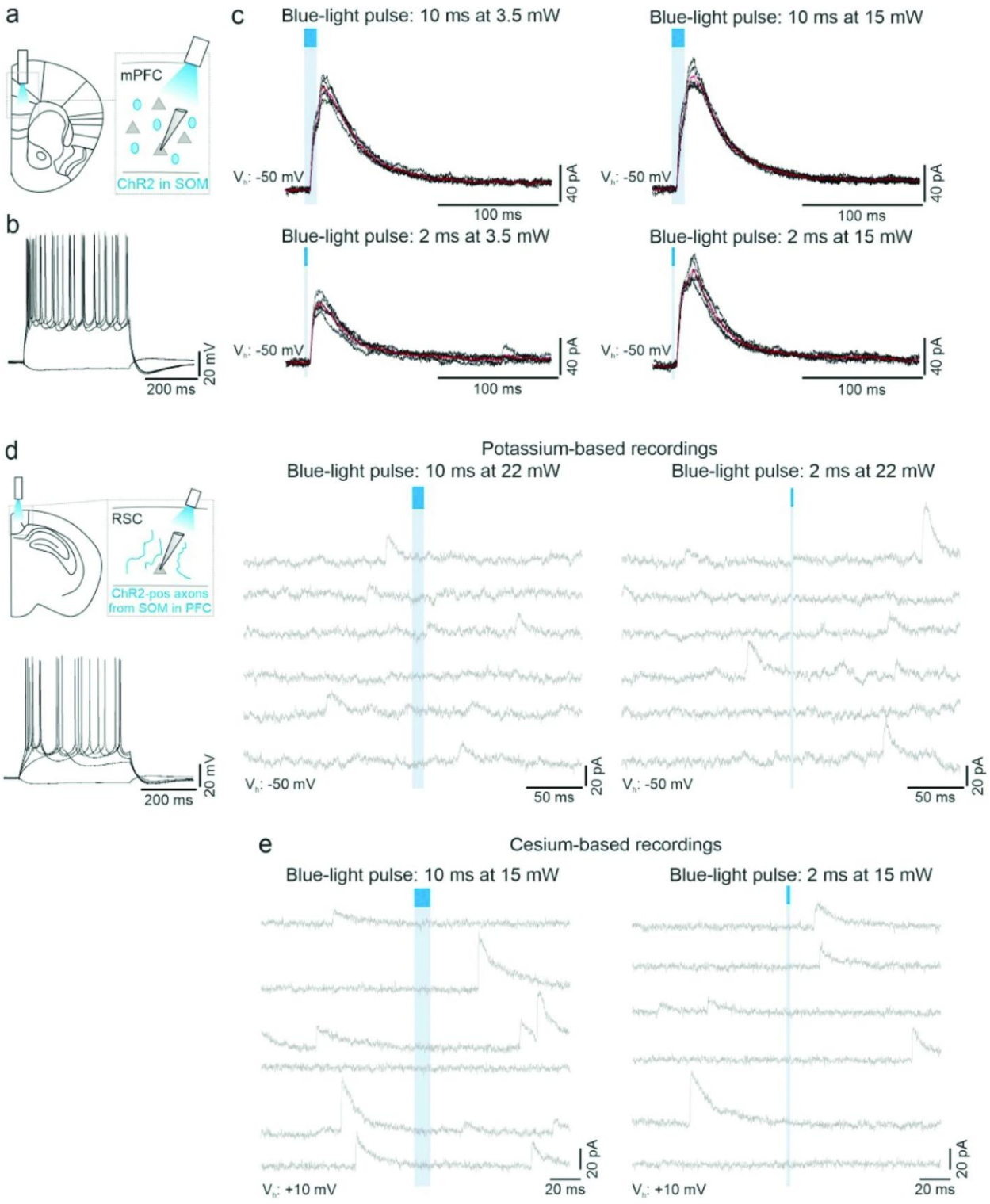

Extended Data Fig. 6 Refer to Fig. 3.

(a) Schematic of the experiment in cortical slices containing mPFC. The blue oval indicates ChR2-positive SOM neurons. The gray triangle indicates ChR2-negative excitatory cells. (b) Representative current-clamp patch-clamp

recording of a ChR2-negative excitatory cell showing the membrane potential responses to current injections (-50, +250, +300, +350 pA). (c) Left: five representative current traces (black) and their average (red) recorded at – 50 mV in voltage-clamp configuration from a ChR2-negative excitatory neuron during photoactivation of ChR2-positive SOM cells in PFC. Currents are recorded in the presence of antagonists of glutamatergic ionotropic receptors (see methods for details). Laser power: 3.5 mW. Light pulse duration: 10 ms (top) and 2 ms (bottom). Right: same as in left using 15 mW of laser power. Note that current amplitude evoked with 10 ms long of blue light at 3.5 mW (top left) and 15 mW (top right) was similar. (d) Top left: schematic of the experiment in cortical slices containing RSC. The gray triangle indicates a ChR2-negative excitatory cell. The blue lines indicate ChR2-positive axonal projections from SOM interneurons in mPFC. Bottom left: representative current-clamp patch-clamp recording of a ChR2-negative excitatory cell showing the membrane potential responses to current injections (-50, +100, +150, +200, +250 pA). Right: representative current traces recorded at – 50 mV in voltage-clamp configuration from a RSC excitatory cell during 10 ms or 2 ms of blue light stimulation at 22 mW. No currents were recorded from this as well from other 9 excitatory cells in RSC during photoactivation of ChR2-positive axons originating from SOM neurons located in mPFC. (e) Representative current traces recorded at +10 mV in voltage-clamp configuration from a RSC excitatory cell during 10 ms or 2 ms of blue light stimulation at 15 mW. Bar plots are represented as mean ± SEM. * is used for $P < 0.05$. Complete statistics in Supplementary Table 4.

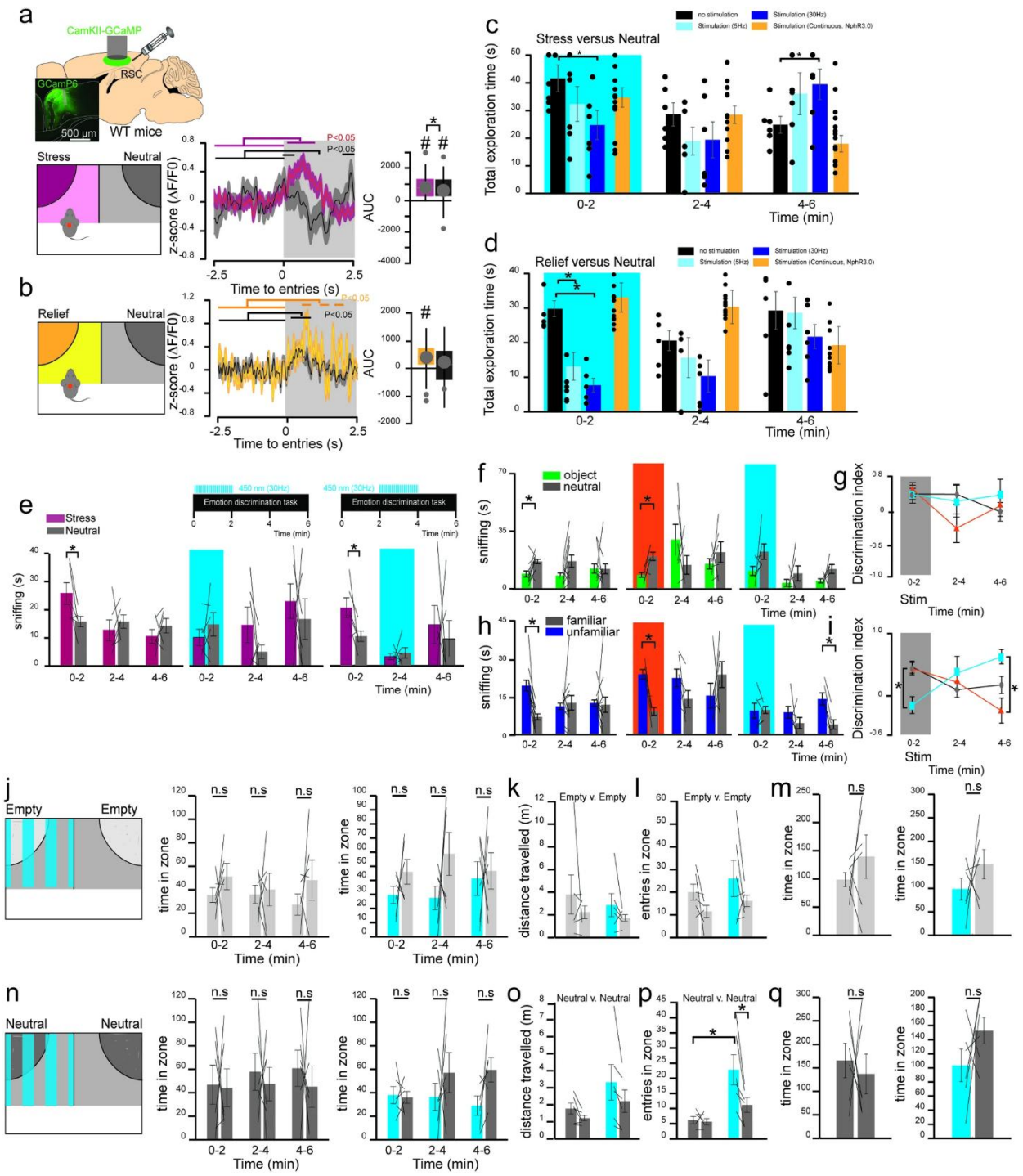

Extended Data Fig. 7 Refer to Fig. 4.

(a-b) Wild type mice (n = 6 males) were injected with AAV-CamKII-GCamP6 in the RSC to allow the recording of GCamP signal from RSC pyramidal cells during recognition (a) for stress (stress: purple; neutral: grey; #P < 0.001 versus baseline; *P = 0.03 neutral versus stress; n = 77 entries to stress, n = 57 entries to neutral) and (b) relief (relief: yellow; neutral: grey; #P = 0.02 relief versus baseline; n = 122 entries to relief, n = 120 entries to neutral).

Isosbetic signal was collected on the red wavelength to remove artifact and movement control. (c-d) Wild-type mice (n = 6 males) injected bilaterally in the RSC with AAV-CamKII-ChR2 with light on or off for the first 2 minutes of the (c) stress and (d) relief emotion recognition test (*P < 0.05 versus no stimulation). (e) Same stimulation protocol, but this time in the second two minutes interval of the task (*P < 0.05 stress light off versus all other groups). (f-i) WT mice (n = 12 females) were bilaterally injected in the RSC with either AAV-CamKII-NphR (orange, n = 6 females) or AAV-CamKII-ChR2 (blue, n = 6 females), and after at least 4 weeks a 560 nm continuous light or 450 nm 5 Hz light was delivered during the first two minutes of the object/mouse and familiar/unfamiliar recognition task for inhibition or activation, respectively, of RSC pyramidal neurons. Time (in seconds) spent sniffing a mouse/familiar (gray bars), or an unfamiliar (violet bars) or object (green bars) displayed by the same observer mice without light stimulation (first column), with photoinhibition (second column, orange background) or photostimulation (third column, blue background) performed for 2 minutes from the beginning of the test (f, *P < 0.05 object versus mouse) (h, *P < 0.01 familiar versus unfamiliar). (g,i) A direct comparison of the no light (gray circles), photoinhibition (orange triangle), and photostimulation (blue squares) conditions by the discrimination index (*P < 0.05 versus ChR2). (j-m) These same mice were then tested with optogenetic stimulation in an empty versus empty discrimination (n = 6 mice) (P > 0.05 stimulated side versus no stimulated side). Empty-side paired stimulation had similarly no effects in (k) the total distance traveled (P = 0.59), (l) the number of zones entries (P = 0.59), and (m) the time spent in the zone (P = 0.99). (n-q) When these same mice were tested in these same conditions but in the presence of two neutral mice (one being paired to 5 Hz stimulation), we found no significant effect (n) on the time spent in the zone (P = 0.11), (o) the distance traveled (P = 0.09), and (q) the time in each zone (P = 0.08), but a significant effect of the stimulation in (p) the number of entries (P = 0.01 stimulated versus no stimulated side). The same animals were tested in both empty versus empty and Neutral versus Neutral. Bar plots are represented as mean ± SEM. Complete statistics in Supplementary Table 5.

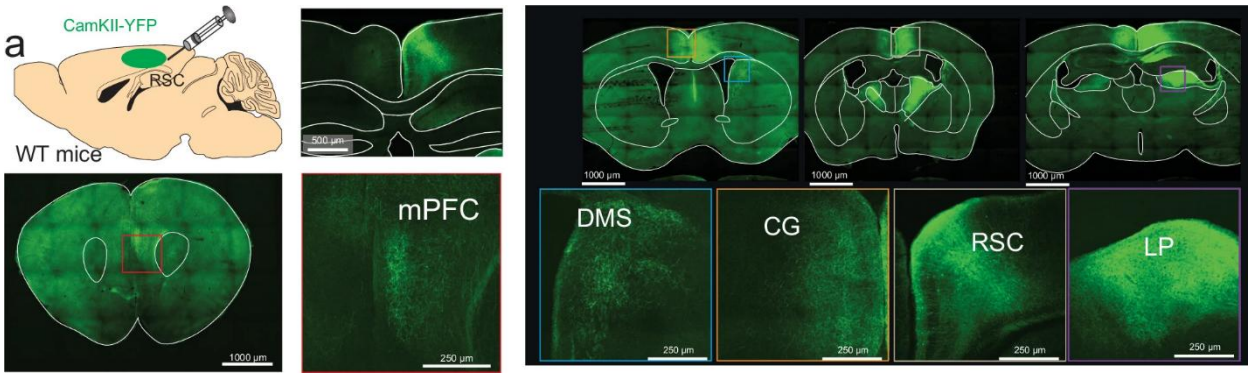

Extended Data Fig. 8 Refer to Fig. 4.

(a) Following injection in the RSC of AAV-CamKII-YFP in wild-type mice (n = 3), we found YFP-positive signal in different brain regions including the medial prefrontal cortex (mPFC), the dorsomedial striatum (DMS), the cingulate (CG), the contralateral retrosplenial cortex (RSC), and the lateroposterior thalamic nuclei (LP).

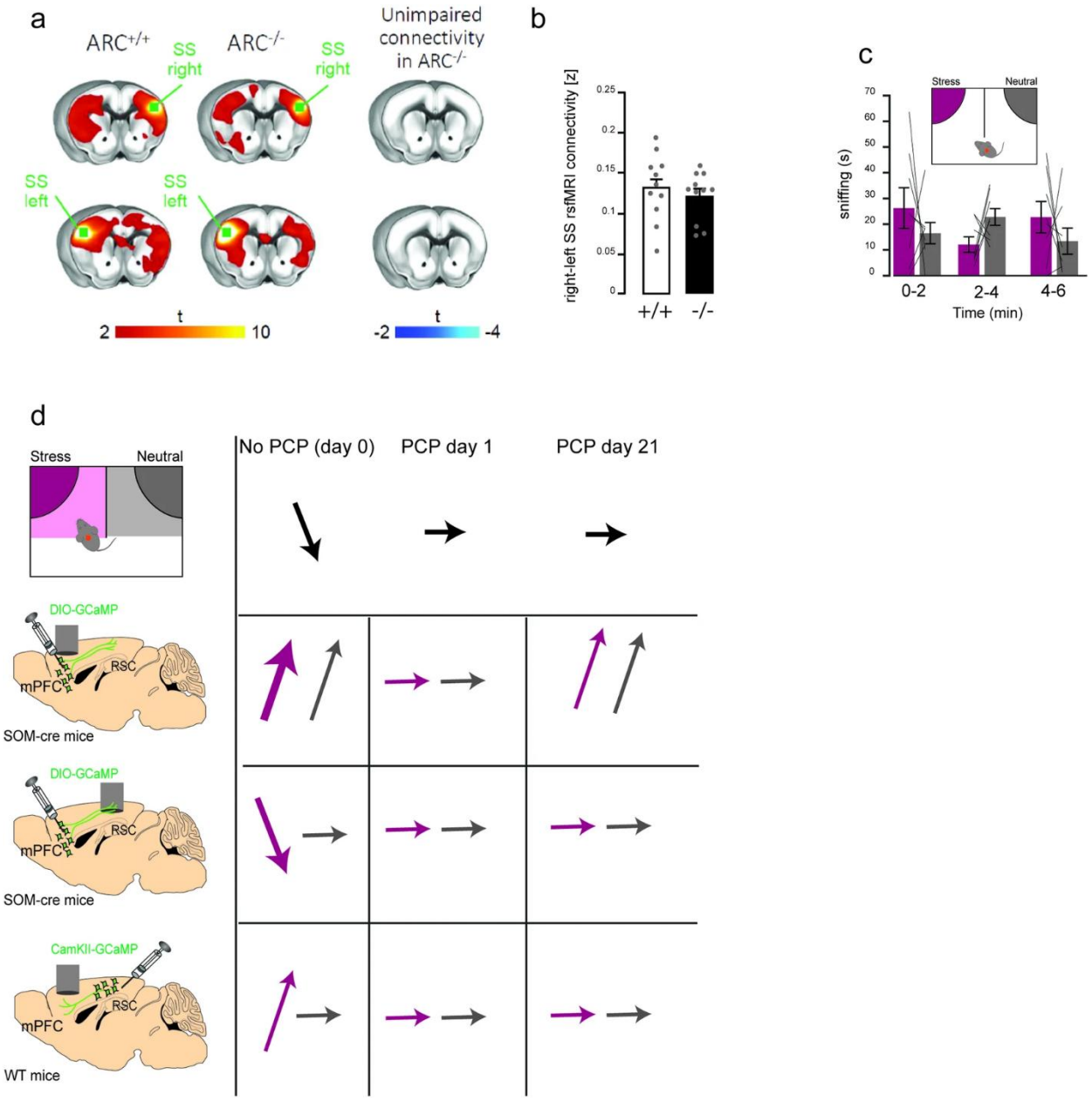

Extended Data Fig. 9 Refer to Fig. 6.

(a) Seed-based connectivity mapping of the right (upper row) and left (bottom row) somatosensory cortex (SS) in ARC + /+ and ARC-/- littermates. Red-yellow represents brain regions showing significant rsfMRI functional connectivity with the right and left SS cortex in control ARC+ /+ (left) and ARC -/- mice (middle). Seed regions are depicted in green. No changes of functional connectivity of the right and left SS were identified in ARC-/- mutants compared to ARC+ /+ mice (right). (b) Unimpaired rsfMRI connectivity between right and left SS cortex was also quantified in reference volumes of interest ($t = 0.70$, $P = 0.49$) ($n = 11$ ARC+/+, $n = 11$ ARC-/-, unpaired

two-tailed T-test). (c) SOM- ARC+ /- mice (n = 8) injected with AAV-DIO-NphR in the mPFC and implanted with a LED above the RSC present no emotion recognition in absence of light stimulation (paired two-tailed T-test; 0-2 min: P = 0.40 neutral versus stress; 2-4 min: P = 0.11 neutral versus stress; 4-6 min: P = 0.38 neutral versus stress). Bar plots are represented as mean ± SEM. * is used for P < 0.05. (d) Graphical resume of the photometry results obtained in the PCP-treated animals (n = 11 mice) during no drug condition (No PCP), acute (PCP day1) and chronic (PCP day 21) treatments. All same animals were tested in no PCP, PCP day 1 and PCP day 21. Arrow represents the variation of GCamP signal during entries to the stress (purple) or the neutral (grey) demonstrators. The thickness of the arrow is used for the relative strength of the signal variation.

Component	Domain	Region	MNI_X	MNI_Y	MNI_Z
39	Subcortical	Thalamus	-9.5	-24.5	16.5
46	Subcortical	Putamen	-24.5	5.5	-1.5
73	Subcortical	Caudate 1	14.5	23.5	13.5
84	Subcortical	Caudate 2	12.5	-3.5	16.5
92	Subcortical	Caudate 3	8.5	17.5	1.5
67	Auditory	Mid Temporal 1	62.5	-24.5	3.5
74	Auditory	Inf Temporal	-47.5	5.5	-32.5
80	Auditory	Sup Temporal	56.5	-49.5	13.5
96	Auditory	Mid Temporal 2	50.5	1.5	-23.5
97	Auditory	Temporal Pole	39.5	7.5	-37.5
99	Auditory	Mid Temporal 3	-48.5	-46.5	6.5
3	Sensorimotor	Paracentral 1	0.5	-24.5	69.5
4	Sensorimotor	Postcentral	-54.5	-9.5	31.5
10	Sensorimotor	Pre Postcentral 1	-39.5	-24.5	60.5
15	Sensorimotor	Pre Postcentral 2	41.5	-22.5	58.5
19	Sensorimotor	Paracentral 2	-2.5	-25.5	58.5
24	Sensorimotor	Sup Parietal	-21.5	-51.5	69.5
32	Sensorimotor	Precentral 1	-20.5	-10.5	67.5
63	Sensorimotor	Supp Motor Area 1	-0.5	7.5	49.5
68	Sensorimotor	Precentral 2	42.5	-3.5	48.5
72	Sensorimotor	Inf Parietal Postcentral	59.5	-19.5	40.5
76	Sensorimotor	Rolandic Oper	45.5	-31.5	21.5
77	Sensorimotor	Inf Parietal Mid Frontal 1	-56.5	-31.5	42.5
98	Sensorimotor	Inf Parietal Sup Parietal	27.5	-67.5	49.5
16	Visual	Calcarine 1	-21.5	-96.5	-4.5
30	Visual	Calcarine 2	2.5	-84.5	0.5
33	Visual	Lingual	12.5	-64.5	7.5
38	Visual	Fusiform 1	29.5	-42.5	-11.5
47	Visual	Sup Occipital	-17.5	-91.5	24.5
49	Visual	Fusiform 2	26.5	-70.5	-10.5
86	Visual	Mid Occipital	-30.5	-73.5	7.5
89	Visual	Mid Temporal 4	48.5	-69.5	-2.5
28	Cognitive Control	Sup Frontal	-27.5	61.5	-1.5
34	Cognitive Control	Supp Motor Area 2	2.5	17.5	58.5
35	Cognitive Control	Sup Medial Frontal 1	-15.5	34.5	40.5
43	Cognitive Control	Sup Medial Frontal 2	-0.5	55.5	31.5
54	Cognitive Control	Inf Frontal	-54.5	17.5	6.5
56	Cognitive Control	Insula 1	-42.5	4.5	-11.5
58	Cognitive Control	Mid Frontal	-32.5	55.5	24.5
61	Cognitive Control	Inf Frontal Oper	-45.5	19.5	27.5
64	Cognitive Control	Mid Cingulate	-0.5	-27.5	28.5
70	Cognitive Control	Inf Frontal	39.5	44.5	0.5
71	Cognitive Control	Insula 2	35.5	25.5	3.5
83	Cognitive Control	Hippocampus	-24.5	-25.5	-10.5
85	Cognitive Control	Inf Parietal Mid Frontal 2	47.5	-58.5	51.5
87	Cognitive Control	Inf Frontal	54.5	13.5	12.5
90	Cognitive Control	Parahippocampal 1	-24.5	-9.5	-28.5
94	Cognitive Control	Parahippocampal 2	35.5	14.5	-22.5
95	Cognitive Control	Angular Gyrus	-47.5	-61.5	48.5
31	Default mode	Orbital Frontal	-11.5	40.5	-16.5
37	Default mode	Precuneus	-5.5	-63.5	61.5
42	Default mode	Med Prefrontal Ant Cing	-0.5	41.5	4.5
75	Default mode	Pos Cing Med Prefrontal	-0.5	-57.5	21.5
88	Default mode	Retrosplenial	-5.5	-70.5	34.5
2	Cerebellum	Cerebellum 1	-12.5	-60.5	-46.5
6	Cerebellum	Cerebellum 2	-32.5	-58.5	-41.5
11	Cerebellum	Cerebellum 3	8.5	-60.5	-34.5
12	Cerebellum	Cerebellum 4	35.5	-60.5	-43.5
22	Cerebellum	Cerebellum 5	-20.5	-85.5	-35.5
25	Cerebellum	Cerebellum Vermis	3.5	-60.5	-19.5
62	Cerebellum	Cerebellum 6	12.5	-69.5	-29.5

Extended Data Table 1 Refer to Fig 6

Bibliography

1. Ferretti, V. & Papaleo, F. Understanding others: emotion recognition in humans and other animals. Genes Brain Behav. 18, e12544 (2019).

2. Panksepp, J. & Panksepp, J. B. Toward a cross-species understanding of empathy. Trends Neurosci. 36, 489–496 (2013).

3. Keysers, C., Knapska, E., Moita, M. A. & Gazzola, V. Emotional contagion and prosocial behavior in rodents. Trends Cogn. Sci. 26, 688–706 (2022).

4. Weinreb, S., Li, F. & Kurtz, M. M. A meta-analysis of social cognitive deficits in schizophrenia: does world region matter? Schizophrenia Res. 243, 206–213 (2022).

5. Yeung, M. K. A systematic review and meta-analysis of facial emotion recognition in autism spectrum disorder: the specificity of deficits and the role of task characteristics. Neurosci. Biobehav. Rev. 133, 104518 (2022).

6. Behrens, T. E., Hunt, L. T. & Rushworth, M. F. The computation of social behavior. Science 324, 1160–1164 (2009).

7. Green, M. F., Horan, W. P. & Lee, J. Social cognition in schizophrenia. Nat. Rev. Neurosci. 16, 620–631 (2015).

8. Mars, R. B. et al. On the relationship between the “default mode network” and the “social brain. Front. Hum. Neurosci. 6, 189 (2012).

9. Whitesell, J. D. et al. Regional, layer, and cell-type-specific connectivity of the mouse default mode network. Neuron 109, 545–559 (2021).

10. Broyd, S. J. et al. Default-mode brain dysfunction in mental disorders: a systematic review. Neurosci. Biobehav. Rev. 33, 279–296 (2009).

11. Li, P. et al. Structural and functional brain network of human retrosplenial cortex. Neurosci. Lett. 674, 24–29 (2018).

12. Greicius, M. D., Supekar, K., Menon, V. & Dougherty, R. F. Resting- state functional connectivity reflects structural connectivity in the default mode network. Cereb. Cortex 19, 72–78 (2009).

13. Wager, T. D. et al. A Bayesian model of category-specific emotional brain responses. PLoS Comput. Biol. 11, e1004066 (2015).

14. Li, W., Mai, X. & Liu, C. The default mode network and social understanding of others: what do brain connectivity studies tell us. Front. Hum. Neurosci. 8, 74 (2014).

15. Pessoa, L. Emotion and the interactive brain: insights from comparative neuroanatomy and complex systems. Emot. Rev. 10, 204–216 (2018).

16. Hiser, J. & Koenigs, M. The multifaceted role of the ventromedial prefrontal cortex in emotion, decision making, social cognition, and psychopathology. Biol. Psychiatry 83, 638–647 (2018).

17. Scheggia, D. et al. Somatostatin interneurons in the prefrontal cortex control affective state discrimination in mice. Nat. Neurosci. 23, 47–60 (2020).

18. Urban-Ciecko, J. & Barth, A. L. Somatostatin-expressing neurons in cortical networks. Nat. Rev. Neurosci. 17, 401–409 (2016).

19. Ferretti, V. et al. Oxytocin signaling in the central amygdala modulates emotion discrimination in mice. Curr. Biol. 29, 1938–1953 (2019).

20. Gozzi, A. & Schwarz, A. J. Large-scale functional connectivity networks in the rodent brain. NeuroImage 127, 496–509 (2016).

21. Huang, S., Wu, S. J., Sansone, G., Ibrahim, L. A. & Fishell, G. Layer 1 neocortex: gating and integrating multidimensional signals. Neuron 112, 184–200 (2024).

22. Katona, L. et al. Sleep and movement differentiates actions of two types of somatostatin-expressing GABAergic interneuron in rat hippocampus. Neuron 91, 1183 (2016).

23. Bertero, A., Feyen, P. L. C., Zurita, H. & Apicella, A. J. A non-canonical cortico-amygdala inhibitory loop. J. Neurosci. 39, 8424–8438 (2019).

24. Assous, M., Dautan, D., Tepper, J. M. & Mena-Segovia, J. Pedunculopontine glutamatergic neurons provide a novel source of feedforward inhibition in the striatum by selectively targeting interneurons. J. Neurosci. 39, 4727–4737 (2019).

25. Dautan, D. et al. Segregated cholinergic transmission modulates dopamine neurons integrated in distinct functional circuits. Nat. Neurosci. 19, 1025–1033 (2016).

26. Vander Weele, C. M. et al. Dopamine enhances signal-to-noise ratio in cortical-brainstem encoding of aversive stimuli. Nature 563, 397–401 (2018).

27. Chan, K. Y. et al. Engineered AAVs for efficient noninvasive gene delivery to the central and peripheral nervous systems. Nat. Neurosci. 20, 1172–1179 (2017).

28. Czajkowski, R. et al. Encoding and storage of spatial information in the retrosplenial cortex. Proc. Natl Acad. Sci. USA 111, 8661–8666 (2014).

29. Ahrlund-Richter, S. et al. A whole-brain atlas of monosynaptic input targeting four different cell types in the medial prefrontal cortex of the mouse. Nat. Neurosci. 22, 657–668 (2019).

30. Allen, E. A. et al. Tracking whole-brain connectivity dynamics in the resting state. Cereb. Cortex 24, 663–676 (2014).

31. Tu, Y. et al. Distinct thalamocortical network dynamics are associated with the pathophysiology of chronic low back pain. Nat. Commun. 11, 3948 (2020).

32. Bluhm, R. L. et al. Retrosplenial cortex connectivity in schizophrenia. Psychiatry Res. 174, 17–23 (2009).

33. Manago, F. et al. Genetic disruption of Arc/Arg3.1 in mice causes alterations in dopamine and neurobehavioral phenotypes related to schizophrenia. Cell Rep. 16, 2116–2128 (2016).

34. Jentsch, J. D. & Roth, R. H. The neuropsychopharmacology of phencyclidine: from NMDA receptor hypofunction to the dopamine hypothesis of schizophrenia. Neuropsychopharmacol. 20, 201–225 (1999).

35. Scheggia, D., Bebensee, A., Weinberger, D. R. & Papaleo, F. The ultimate intra-/extra-dimensional attentional set-shifting task for mice. Biol. Psychiatry 75, 660–670 (2014).

36. Vesuna, S. et al. Deep posteromedial cortical rhythm in dissociation. Nature 586, 87–94 (2020).

37. Keum, S. et al. A missense variant at the Nrxn3 locus enhances empathy fear in the mouse. Neuron 98, 588–601 (2018).

38. Zhang, C. et al. Dynamics of a disinhibitory prefrontal microcircuit in controlling social competition. Neuron 110, 516–531 (2022).

39. Melzer, S. et al. Long-range-projecting GABAergic neurons modulate inhibition in hippocampus and entorhinal cortex. Science 335, 1506–1510 (2012).

40. Yamawaki, N. et al. Long-range inhibitory intersection of a retrosplenial thalamocortical circuit by apical tuft-targeting CA1 neurons. Nat. Neurosci. 22, 618–626 (2019).

41. Lee, A. T., Vogt, D., Rubenstein, J. L. & Sohal, V. S. A class of GABAergic neurons in the prefrontal cortex sends long-range projections to the nucleus accumbens and elicits acute avoidance behavior. J. Neurosci. 34, 11519–11525 (2014).

42. Melzer, S. et al. Distinct corticostriatal GABAergic neurons modulate striatal output neurons and motor activity. Cell Rep. 19, 1045–1055 (2017).

43. Vogt, B. A., Vogt, L. & Laureys, S. Cytology and functionally correlated circuits of human posterior cingulate areas. NeuroImage 29, 452–466 (2006).

44. Munoz, W., Tremblay, R., Levenstein, D. & Rudy, B. Layer-specific modulation of neocortical dendritic inhibition during active wakefulness. Science 355, 954–959 (2017).

45. Kawaguchi, Y. & Kubota, Y. GABAergic cell subtypes and their synaptic connections in rat frontal cortex. Cereb. Cortex 7, 476–486 (1997).

46. Brockway, D. F. et al. Somatostatin peptide signaling dampens cortical circuits and promotes exploratory behavior. Cell Rep. 42, 112976 (2023).

47. Dienel, S. J. et al. Diagnostic specificity and association with cognition of molecular alterations in prefrontal somatostatin neurons in schizophrenia. JAMA Psychiatry 80, 1235–1245 (2023).

48. Biedermann, F., Frajo-Apor, B. & Hofer, A. Theory of mind and its relevance in schizophrenia. Curr. Opin. Psychiatry 25, 71–75 (2012).

49. Fisher, M. H., Moskowitz, A. L. & Hodapp, R. M. Differences in social vulnerability among individuals with autism spectrum disorder, Williams syndrome, and Down syndrome. Res Autism Spectr. Disord. 7, 931–937 (2013).

50. Toth, M. The other side of the coin: hyper sociability. Genes Brain Behav. 18, e12512 (2019).

51. Scheggia, D. et al. Reciprocal cortico-amygdala connections regulate prosocial and selfish choices in mice. Nat. Neurosci. 25, 1505–1518 (2022).

52. Rocchi, F. et al. Increased fMRI connectivity upon chemogenetic inhibition of the mouse prefrontal cortex. Nat. Commun. 13, 1056 (2022).

53. Bertero, A. et al. Autism-associated 16p11.2 microdeletion impairs prefrontal functional connectivity in mouse and human. Brain 141, 2055–2065 (2018).

54. Pagani, M. et al. mTOR-related synaptic pathology causes autism spectrum disorder-associated functional hyperconnectivity. Nat. Commun. 12, 6084 (2021).

55. Vecchia, D. et al. Temporal sharpening of sensory responses by layer V in the mouse primary somatosensory cortex. Curr. Biol. 30, 1589–1599 (2020).

56. Schumann, G. et al. The IMAGEN study: reinforcement-related behaviour in normal brain function and psychopathology. Mol. Psychiatry 15, 1128–1139 (2010).

57. Grosbras, M. H. & Paus, T. Brain networks involved in viewing angry hands or faces. Cereb. Cortex 16, 1087–1096 (2006).

58. Fu, Z. et al. Transient increased thalamic-sensory connectivity and decreased whole-brain dynamism in autism. NeuroImage 190, 191–204 (2019).

59. Calhoun, V. D., Adali, T., Pearlson, G. D. & Pekar, J. J. A method for making group inferences from functional MRI data using inde- pendent component analysis. Hum. Brain Mapp. 14, 140–151 (2001).

60. Preti, M. G., Bolton, T. A. & Van De Ville, D. The dynamic functional connectome: state-of-the-art and perspectives. NeuroImage 160, 41–54 (2017).

61. Xie, H. et al. Efficacy of different dynamic functional connectivity methods to capture cognitively relevant information. NeuroImage 188, 502–514 (2019).

62. Gonzalez-Castillo, J. & Bandettini, P. A. Task-based dynamic functional connectivity: recent findings and open questions. NeuroImage 180, 526–533 (2018).

63. Xie, H. et al. Time-varying whole-brain functional network connectivity coupled to task engagement. Netw. Neurosci. 3, 49–66 (2019).

64. Cole, M. W. et al. Task activations produce spurious but systematic inflation of task functional connectivity estimates. NeuroImage 189, 1–18 (2019).

65. Fair, D. A. et al. A method for using blocked and event-related fMRI data to study “resting state” functional connectivity. NeuroImage 35, 396–405 (2007).

Chapter 3

Article https://doi.org/10.1038/s41593-024-01816-y

Self-experience of a negative event alters responses to others in similar states through prefrontal cortex CRF mechanisms

Federica Maltese[1,4], Giada Pacinelli[1], **Anna Monai**[1], Fabrizio Bernardi[1], Ana Marta Capaz[1], Marco Niello[1], Roman Walle[1], Noelia de Leon[2], Francesca Managò[1], Felix Leroy[2] & Francesco Papaleo[1,3]

[1]*Genetics of Cognition Laboratory, Neuroscience Area, Istituto Italiano di Tecnologia, Genoa, Italy.*

[2]*Instituto de Neurociencias, Consejo Superior de Investigaciones Cientıficas, Universidad Miguel Hernandez de Elche, San Juan de Alicante, Alicante, Spain.*

[3]*IRCCS Ospedale Policlinico San Martino, Genoa, Italy. 4Present address: Institute of Neuroscience, National Research Council, Vedano al Lambro, Italy.*

e-mail: francesco.papaleo@iit.it

Abstract

Our own experience of emotional events influences how we approach and react to others' emotions. Here we observe that mice exhibit divergent interindividual responses to others in stress (that is, preference or avoidance) only if they have previously experienced the same aversive event. These responses are estrus dependent in females and dominance dependent in males. Notably, silencing the expression of the corticotropin-releasing factor (CRF) within the medial prefrontal cortex (mPFC) attenuates the impact of stress self-experience on the reaction to others' stress. In vivo microendoscopic calcium imaging revealed that mPFC CRF neurons are activated more toward others' stress only following the same negative self-experience. Optogenetic manipulations confirmed that higher activation of mPFC CRF neurons is responsible for the switch from preference to avoidance of others in stress, but only following stress self-experience. These results provide a neurobiological substrate underlying how an individual's emotional experience influences their approach toward others in a negative emotional state.

Main

Fundamental to socio-cognitive processes is the ability to detect, interpret and properly react to altered emotions in others. This ability is required for all social interactions in all social species, greatly influencing everyday life[1]. Notably, the reaction to altered emotional states in others can show inter-individual differences depending on previous negative emotional experiences (hereafter 'negative self-experience')[2,3]. Observing another person in a particular emotional state can trigger memories of a similar emotion that took place in the past[2,3,4]. Negative self-experience could then induce self-oriented feelings of distress, which may negatively affect emotion recognition by decreasing our attention toward others in stress[3]. Conversely, negative self-experience could prompt prosocial behaviors[2], increasing accuracy in emotion recognition and responding with care to the distress of others[4]. This could explain why different studies report divergent conclusions: a positive correlation[5], a negative correlation[3] or even no correlation[6] between affective empathy and emotion recognition accuracy. However, the neurobiology underlying the divergent impact of negative self-experience in the reaction to others' stress is poorly understood.

Emotion recognition tasks are used to measure the basic ability to perceive and react to others' affective states in humans and other mammals including nonhuman primates and rodents[1,7,8,9,10]. Indeed, rodents can recognize altered emotions in conspecifics and show complex reactions including emotional contagion, social buffering, helping and consolatory behaviors and prosocial or selfish choices[7,11,12,13,14,15,16]. However, whether rodents' reactions to others' emotions can be influenced by self-experience and the underlying mechanisms are unknown.

Coping with stressful components of social interactions is an important aspect of an individual propensity to respond to others' emotions[17]. A master regulator of stress-coping responses is the corticotropin-releasing factor (CRF)[18,19]. The CRF system is implicated in emotional and cognitive components of stress responses[18,20] and in different aspects of social behaviors such as social memory, social defeat, pair bonding, aggressive responses and sexual behavior[21,22,23,24,25]. Moreover, human studies revealed that the CRF system modulates the

effect of stress on empathic behaviors[26]. CRF neurons are found also in the medial prefrontal cortex (mPFC)[18,27], which is a major regulator of emotion recognition and other sociocognitive abilities[9,10,28]. Moreover, the mPFC structure and function can be affected by stress[29] and the mPFC has a critical role in the regulation of response to stress by promoting adaptation and survival[30]. Despite this, whether the CRF system within the mPFC modulates responses to others' emotions and the impact of negative self-experience are unexplored.

Here, we investigated whether sharing the same stressful experience could affect mice's ability to respond to altered affective states in conspecifics. We found that self-experience of a stressful event leads to interindividual and sex hormone-dependent differences in the approach toward others only if exposed to the same negative state. Using a viral approach to silence CRF mRNA within the mPFC, we found that mPFC CRF is involved in stress self-experience modulation of stress emotion recognition. Moreover, in vivo microendoscopic calcium imaging revealed that mPFC CRF neurons show opposite patterns of activation toward stress or neutral demonstrators depending on the past experience of the observer. Notably, optogenetic manipulations found that a relatively reduced activity of mPFC CRF neurons could induce social preference while their activation induced social avoidance, but only in mice with self-experience of stress. Our results demonstrate that sharing the same stressful experience influences social approach to others in stress and that the CRF in the mPFC modulates these social responses.

Results

Restraint experience alters responses to same stress in others

We first tested whether sharing the same stressful experience could impact mice's ability to recognize and approach conspecifics on the basis of their emotional state.

In the emotion discrimination task (EDT)[8,9,10], an observer mouse is placed in front of two conspecifics (demonstrators) in different emotional states. To induce an altered affective state with negative valence, one unfamiliar demonstrator ('stress') underwent a mild stress protocol, consisting of 15 min of acute restraint immediately before the EDT (Fig. 1a,e). The second demonstrator was a naive unfamiliar mouse directly taken from the homecage ('neutral'; Fig. 1a,e). As previously reported[9,10], naive observers displayed increased sniffing toward restraint stress conspecifics compared to neutral demonstrators (Fig. 1b). No sex-dependent differences were observed (Fig. 1c and Extended Data Fig. 1a–e). In the restraint stress self-experience group, observers experienced the same stressful challenge as the stress demonstrators 24 h before the EDT (Fig. 1e). The day of the test, demonstrator mice were manipulated as described above. Self-experience of restraint stress abolished overall observers' discrimination behavior (Fig. 1f). This was equally evident in male and female mice (Fig. 1g and Extended Data Fig. 1f–j).

We next explored individual differences in social approach toward a restraint stress mouse. In naive observers, the exploration scores toward restraint stress demonstrators fit a normal distribution (D'Agostino and Pearson normality test, $K^2 = 4.027$, $P = 0.14$), with 77% of mice showing a preference toward stress demonstrators (56 of 73; Fig. 1d). A similar normal distribution was found in observers that experienced restraint stress (D'Agostino and Pearson normality test, $K^2 = 1.28$, $P = 0.53$). Thus, both populations had a unimodal distribution. However, the restraint stress self-experience reduced the proportion of observers showing an increased sniffing toward restraint stress demonstrators to 55% (51 of 93), while the other 45% (42 of 93; Fig. 1h) displayed a reduced approach toward restraint stress compared to neutral demonstrators. Moreover, in contrast to naive observers, only in restraint stress self-experience conditions there were mice that exclusively preferred (100% exploration) or completely avoided

(0% exploration) restraint stress demonstrators (Fig. 1h). In agreement, in the restraint stress self-experience condition, there was a higher variability in the distribution of sniffing toward both the restraint stress and the neutral demonstrators, which was different from naive observers (Fig. 1i). In particular, the sniffing toward demonstrators revealed that, compared to naive observers, a reduction in the social exploration toward the restraint stress but not the neutral demonstrator was found in restraint self-experienced observers (Fig. 1j,k). This also indicates no general effect on sociability when emotions are not involved. This was also confirmed by the analysis of the discrimination index toward neutral and stress demonstrators between naive and restraint self-experienced observers (Fig. 1l). Altogether, these data show that negative self-experience increased the variability of responses toward a stress mouse, with some observers even showing avoidance.

We then assessed stress levels in observer mice to check whether any correlation between observers' stress and social preference was present. The amount of self-grooming in restraint stress self-experienced observers was higher compared to naive ones (Fig. 1m). However, this increased grooming in restraint stress self-experienced mice was not correlated with their discrimination index (Fig. 1n). This indicates that self-grooming is not directly linked to preference or avoidance toward restraint stress demonstrators. In both conditions, restraint stress demonstrators displayed the same increased grooming compared to neutral ones (Extended Data Fig. 1k), with no correlation with observers' discrimination behavior (Extended Data Fig. 1l,n). Similarly, no correlation was found in grooming behavior between observers and restraint stress demonstrators (Extended Data Fig. 1m,o). Restraint self-experienced observers also showed increased corticosterone plasma levels after exposure to stress demonstrators (Fig. 1o), further proving the different affective state induced by self-experience. However, no correlation was found between corticosterone levels and stress discrimination in restraint stress self-experienced observer mice (Fig. 1p). These measurements indicate that stress self-experience alters the affective state of the observer when facing a conspecific that underwent the same stress. However, these physiological quantifications are not predictive of the exploratory reaction toward the stress demonstrator.

Overall, these results show that past experience of a stressful event individually alters mice's reaction to conspecifics undergoing the same stressful affective state.

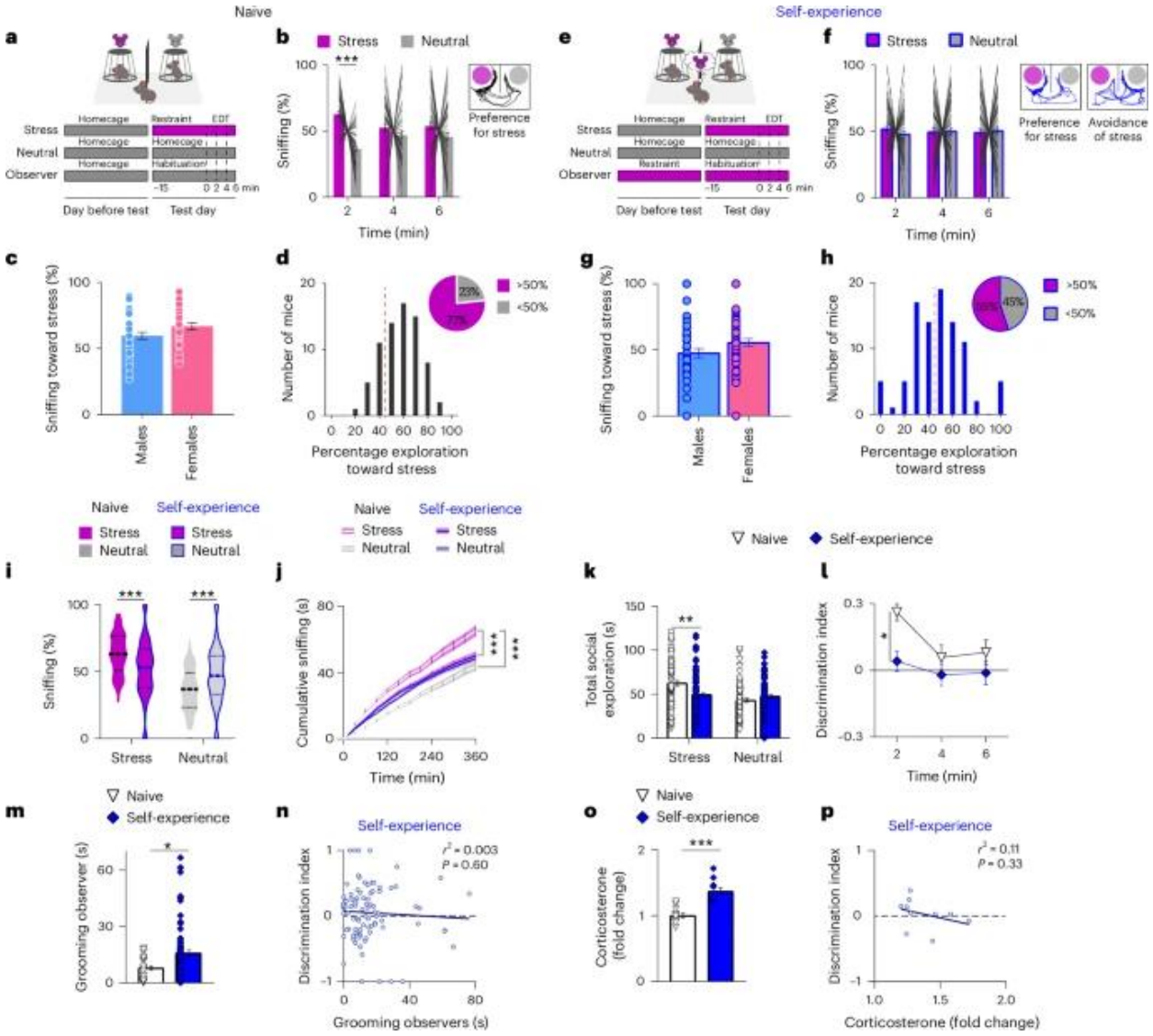

Fig. 1: Restraint stress self-experience changes individual responses to others' stress.

a,e, Experimental design of the EDT with one restraint stress (purple) versus one neutral (gray) demonstrator in naive (a) and restraint stress self-experience (e) conditions. b,f, Percentage of time spent sniffing demonstrators in restraint stress (purple bars) or neutral (gray bars) state during the 6-min test, divided into 3 consecutive 2-min epochs, displayed by naive (b) and restraint stress self-experienced (f) observer mice (two-tailed multiple t-test,

Bonferroni correction; n = 73 naive and 93 self-experienced observers). Inset: representative tracking traces. c,g, No sex differences during the first 2 min of the test in both naive (c) and restraint stress self-experience (g) conditions (two-tailed unpaired t-test; n = 38 naive males and 35 naive females; n = 38 self-experienced males and 55 self-experienced females). d,h, Observers' distribution based on exploration toward restraint stress demonstrator for naive (d) and restraint stress self-experience (h) conditions (one-sample t-test against chance, defined as 50%; naive: 56 of 73 higher than 50%, $P < 0.0001$; restraint stress self-experience: 51 of 93 higher than 50%, $P = 0.37$). i, Violin plot of the percentage of exploration toward restraint stress (purple) or neutral (gray) demonstrator (two-way RM ANOVA, Bonferroni correction; n = 73 naive and 93 restraint stress self-experienced observers). j, Cumulative time spent sniffing one neutral and one restraint stress demonstrator in naive and stress self-experience conditions (three-way RM ANOVA, Bonferroni correction; n = 73 naive and 93 restraint self-experienced observers). k–m, Total amount of social exploration (k), discrimination index (l) and amount of time spent grooming (m) displayed by naive (white) and restraint stress self-experienced (blue) observers toward restraint stress and neutral demonstrators (k–l, two-way RM-AMOVA, Bonferroni correction; n = 73 naive and 93 restraint self-experienced observers; m, two-tailed unpaired t-test; n = 25 naive and 89 restraint stress self-experienced observers). n, No correlation was found between discrimination index (y axis) and grooming (x axis) within the restraint stress self-experience group (two-tailed Pearson correlation; n = 89 mice). o, Corticosterone levels in naive (white) and restraint stress self-experienced (blue) observers after the EDT (two-tailed unpaired t-test; n = 10 mice). p, No correlation between discrimination index (y axis) and corticosterone (x axis) within the restraint stress self-experience group (two-tailed Pearson correlation; n = 10 mice). Bar and line graphs show the mean ± s.e.m. *$P < 0.05$, **$P < 0.005$ and ***$P < 0.0005$.

Footshock experience alters responses to same stress in others

Empathic responses toward conspecifics in distress can only be triggered by the same stressful experience[3,31]. To confirm this, we evaluated the impact of another kind of stressful event on our model of negative self-experience modulation of emotion recognition.

This time, observer mice were tested with one neutral and one footshocked (instead of restrained) demonstrator, which was exposed to footshock immediately before the task (Fig. 2a and Extended Data Fig. 2a). Naive observers showed a significant preference for the footshock mouse compared to the neutral one (Fig. 2b and Extended Data Fig. 2b). In the footshock self-experience condition, observers went through the same footshock stress the day before the test (Fig. 2c and Extended Data Fig. 2c). In contrast to naive observers, footshock self-experienced mice avoided footshocked demonstrators compared to neutral ones (Fig. 2d and Extended Data Fig. 2d). This was confirmed by a drastic reduction in negative self-experienced compared to naive observers only for their exploration of footshock demonstrators (Fig. 2e,f).

Sniffing and social exploration toward neutral demonstrators were not affected (Fig. 2e,f), indicating no general effect on sociability. This was further evident by an inversion of the discrimination index induced by footshock self-experience (Fig. 2g). Footshock self-experienced observers did more freezing but not grooming than naive observers (Fig. 2h and Extended Data Fig. 2e,f). However, freezing behavior did not correlate with discrimination index (Fig. 2i).

These data demonstrate that different kinds of stress self-experience similarly change the responses to the same stress observed in others.

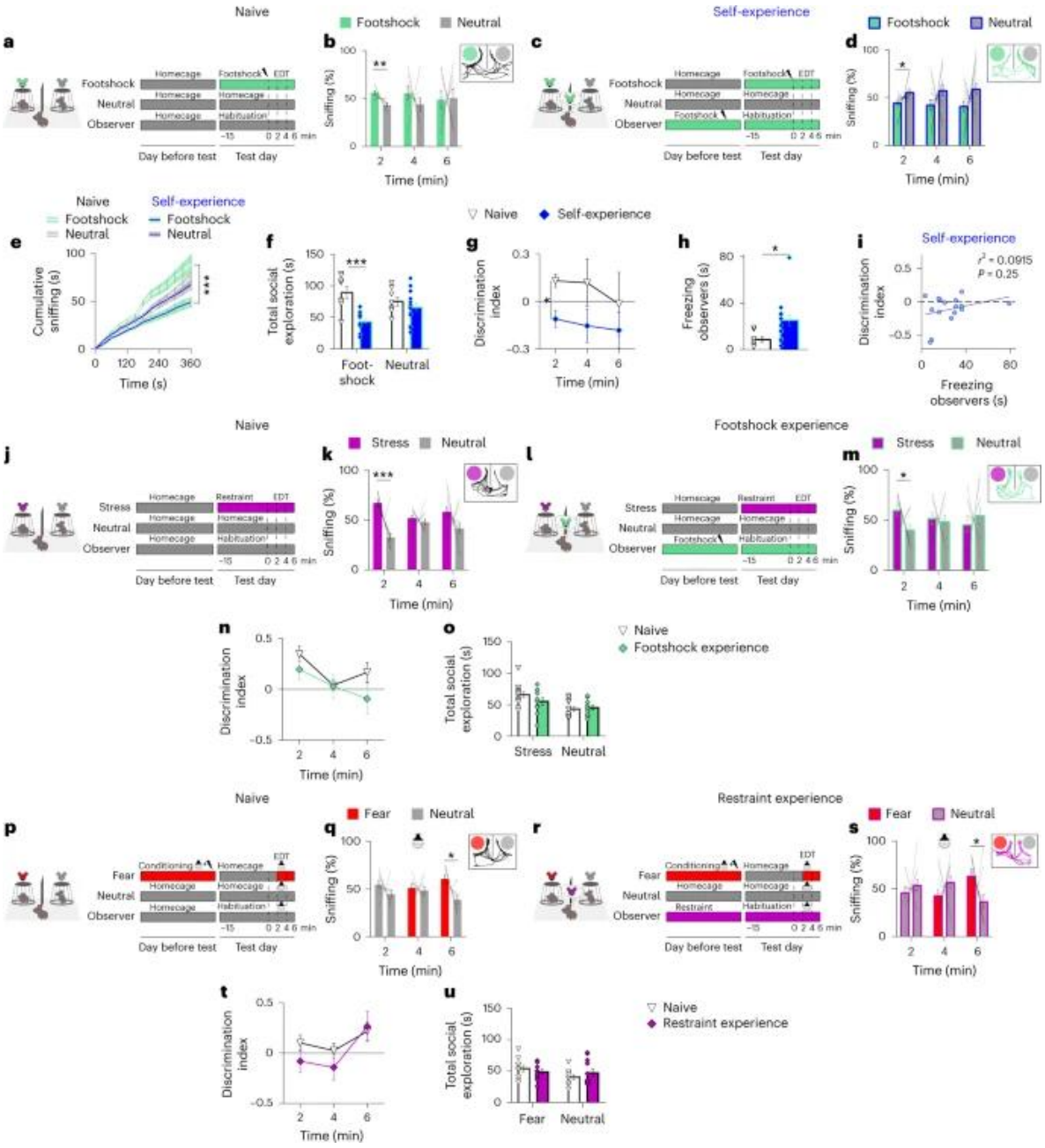

Fig. 2: Emotion recognition is altered only by matching observer and demonstrator with the same negative emotional experience.

a,c, Experimental design of the EDT with one footshock (green) and one neutral (gray) demonstrator in naive (a) and footshock self-experienced (c) observers. b,d, Percentage of time spent sniffing demonstrators in footshock (green bars) or neutral (gray bars) state during the 6-min test, divided into 3 consecutive 2-min epochs, displayed by naive (b) and footshock self-experienced (d) observer mice (two-tailed multiple t-test, Bonferroni correction; n = 8 naive and 16 footshock self-experienced observers). Inset: representative tracking traces. e, Cumulative time spent

sniffing one footshock and one neutral demonstrator in naive and footshock self-experienced observers (three-way RM ANOVA, Bonferroni correction; n = 8 naive and 16 footshock self-experienced observers). f, Total amount of social exploration in naive (white) and footshock self-experienced (blue) observers toward footshock and neutral demonstrators (two-way RM ANOVA, Bonferroni correction; n = 8 naive and 16 footshock self-experienced observers). g, Discrimination index shown by naive (white) and footshock self-experienced (blue) observers (two-way RM ANOVA, Bonferroni correction; n = 8 naive and 16 footshock self-experienced observers). h, Amount of time spent freezing across the 6-min test (two-tailed unpaired t-test; n = 8 naive and 16 footshock self-experienced observers). i, No correlation between discrimination index (y axis) and freezing (x axis) of footshock self-experienced observers (two-tailed Pearson correlation; n = 16 mice). j,l, Experimental design of the EDT with one restraint stress (purple) and one neutral (gray) demonstrator in naive (j) and footshock self-experienced (l) observers. k,m, Percentage of time spent sniffing demonstrators in restraint stress (purple bars) or neutral (gray bars) state during the 6-min test, divided into 3 consecutive 2-min epochs, displayed by naive (k) and footshock self-experienced (m) observer mice (two-tailed multiple t-test, Bonferroni correction; n = 14 naive and 11 footshock self-experienced observers). Inset: representative tracking traces. n, Discrimination index in naive (white) and footshock self-experienced (green) observers (two-way RM ANOVA; n = 14 naive and 11 footshock self-experienced observers). o, Amount of social exploration toward restraint stress and neutral demonstrators (two-way RM ANOVA; n = 14 naive and 11 footshock self-experienced observers). p,r, Experimental design of the EDT with one fear (red) and one neutral (gray) demonstrator in naive (p) and restraint self-experienced (r) observers. q,s, Percentage of time spent sniffing demonstrators in fear (red bars) or neutral (gray bars) state during the 6-min test, divided into 3 consecutive 2-min epochs, displayed by naive (q) and restraint self-experienced (s) observers (two-tailed multiple t-test, Bonferroni correction; n = 10 naive and 12 restraint self-experienced observers). Inset: representative tracking traces. t, Discrimination index in naive (white) and restraint stress self-experienced (purple) observers (two-way RM ANOVA; n = 10 naive and 12 restraint self-experienced observers). u, Total amount of social exploration toward fear and neutral demonstrators (two-way RM ANOVA; n = 10 naive and 12 restraint self-experienced observers). Bar and line graphs show the mean ± s.e.m. *P < 0.05, **P < 0.005 and ***P < 0.005.

Mismatched experiences do not affect emotion recognition

We then tested whether emotion recognition could be influenced by subjecting the observer to a stressor distinct from that experienced by the emotionally altered demonstrator. We tested naive (Fig. 2j and Extended Data Fig. 2g) and footshock self-experienced (Fig. 2l and Extended Data Fig. 2i) observer mice with one neutral and one restraint stress demonstrator. Footshocked observers displayed increased sniffing toward restraint stress conspecifics compared to neutral demonstrators (Fig. 2m and Extended Data Fig. 2j), as the naive condition (Fig. 2k and Extended Data Fig. 2h). No differences in the discrimination index and the total social exploration toward restraint stress and neutral demonstrators were evident between naive and footshock self-

experienced observers (Fig. 2n,o). Notably, the amount of self-grooming, which was increased in restraint self-experienced observers (Fig. 1m), did not differ between footshock self-experienced and naive observers (Extended Data Fig. 2k). Moreover, footshock self-experienced mice did not show any correlation between self-grooming and discrimination index (Extended Data Fig. 2l). These findings demonstrate that a different stressful experience between the observer and the demonstrator did not alter observers' social approach during emotion recognition.

We then checked whether the restraint manipulation used in our stress self-experience mouse model (Fig. 1) could have a generalized impact on mice's emotion recognition. Naive (Fig. 2p and Extended Data Fig. 2m) and restraint self-experienced (Fig. 2r and Extended Data Fig. 2o) observers were tested with one neutral and one fear demonstrator as previously described8 (Fig. 2p,r). Restraint self-experience did not alter by itself the observers' ability to discriminate between a neutral and a fear mouse. Indeed, the observers showed increased sniffing toward fear demonstrators compared to neutral ones (Fig. 2s and Extended Data Fig. 2p), as the naive condition (Fig. 2q and Extended Data Fig. 2n). This was confirmed by no difference in the discrimination indices (Fig. 2t). Moreover, in contrast to same-stress self-experience (Fig. 1k,m), the amount of total exploration (Fig. 2u) and self-grooming (Extended Data Fig. 2q) between restraint self-experienced and naive observers were unchanged. No correlation was found between self-grooming and discrimination index of restraint self-experienced observers (Extended Data Fig. 2r). Thus, the restraint manipulation per se did not alter emotion recognition.

These results demonstrate that emotion recognition is altered only when observer mice share the same negative experience with emotionally altered demonstrators.

Hierarchy influences how self-experience affect emotion recognition in males

Testosterone levels can affect emotion recognition abilities in humans32. Moreover, social dominance, which reflects testosterone levels33, has a modulatory effect on social fear transmission in male rodents34. Thus, we hypothesized that social dominance could influence emotion recognition and self-experience of stress.

We used the well-validated tube test to assess social hierarchy in mice[15,35], splitting observers into dominants (rank 1) and subordinates (ranks 2 and 3). Hierarchy status did not modulate emotion recognition abilities in females, whether in naive (Supplementary Fig. 1a–e) or in negative self-experience (Supplementary Fig. 1f–m) conditions, or in naive males (Fig. 3a–c and Extended Data Fig. 3a,b). In contrast, in negative self-experienced male observers, dominant mice avoided stress demonstrators compared to neutral ones (Fig. 3d,e and Extended Data Fig. 3d,e, left), whereas subordinate males did not show any overall preference (Fig. 3f and Extended Data Fig. 3e, right). The cumulative sniffing clearly showed that the time interacting with neutral demonstrators did not change with self-experience, whereas the preference for the stress mouse was abolished in both dominant and subordinate mice (Fig. 1g,h). However, the discrimination index revealed that negative self-experience affected more dominant mice compared to the subordinates, completely reverting their discrimination behavior (Fig. 3i,j). Compared to naive observers, both dominant and subordinate negative self-experienced mice showed a significant decrease in their total social exploration toward stress but not neutral demonstrators (Extended Data Fig. 3g), indicating a hierarchy-independent impact of negative self-experience on social engagement. Grooming behavior did not differ between negative self-experienced dominant and subordinate mice (Extended Data Fig. 3h) nor did corticosterone levels (Extended Data Fig. 3i). Lastly, comparing the different ranks within the subordinate group (ranks 2 and 3), we did not find any difference in their behavioral outcome (Extended Data Fig. 3l,m). However, considering the social status of all observers and demonstrators, it was revealed that, when belonging to the same rank, the avoidance behavior was more evident (Supplementary Fig. 2a–f). Furthermore, this avoidance behavior was more evident when stress demonstrators were subordinates while neutral ones were dominants (Supplementary Fig. 2g–j). Indeed, we found an opposite interaction between hierarchical status and demonstrators' emotional state (Supplementary Fig. 2k).

Overall, dominant male mice were more susceptible to negative self-experience modulation of stress emotion recognition, reverting their preference for a stress mouse to an avoidance. However, the relative hierarchical status between observers and demonstrators, combined with the emotional state of the latter, could also influence the appearance of this avoiding behavior in self-experienced mice.

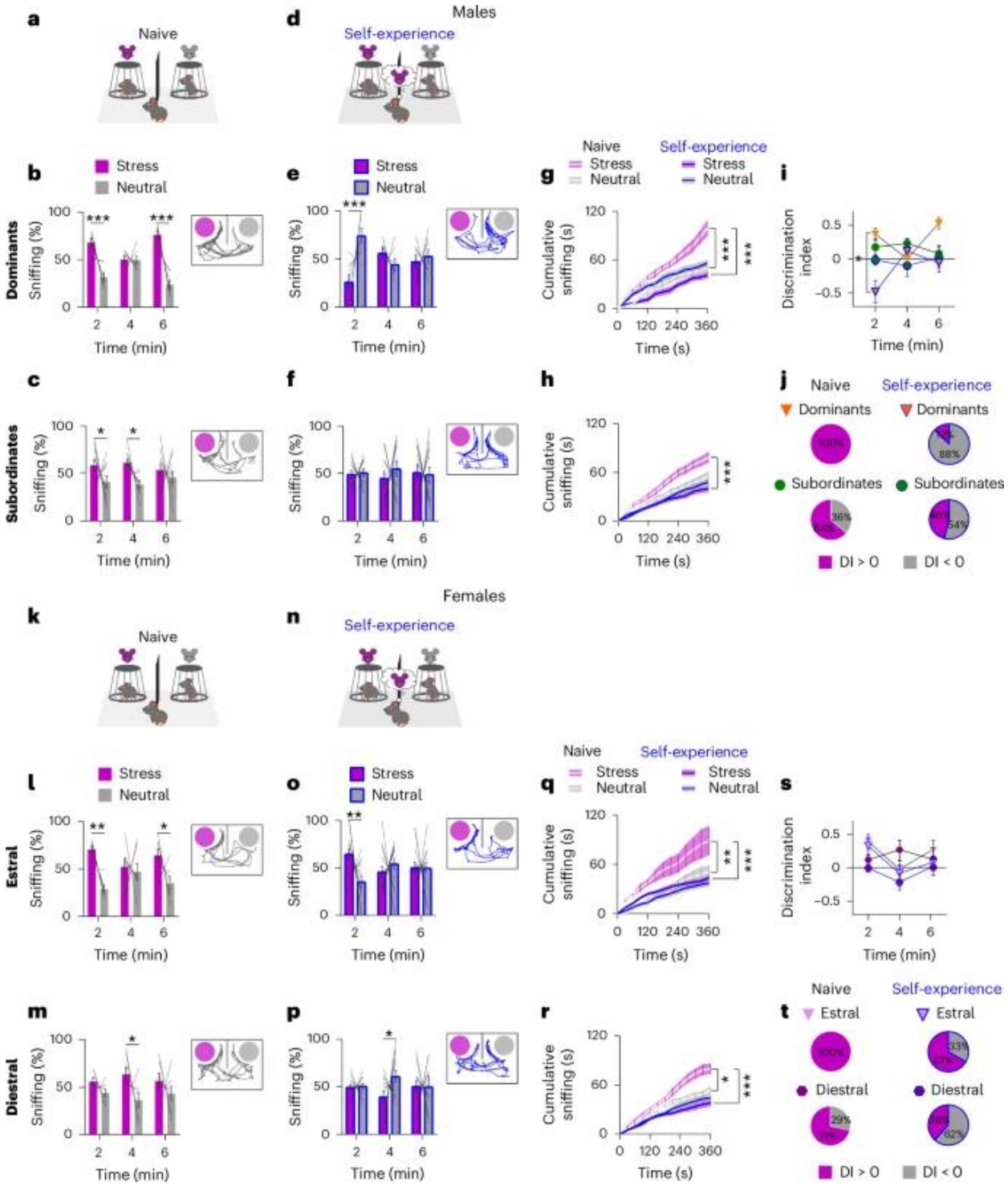

Fig. 3: Sex-dependent differences in self-experience modulation of emotion recognition.

a,**d**, Experimental design of the EDT with one restraint stress (purple) versus one neutral (gray) demonstrator in naive (**a**) and negative self-experience (**d**) conditions. **b**,**c**, Percentage of time spent sniffing demonstrators in stress

(purple bars) or neutral (gray bars) state during the 6-min test, divided into 3 consecutive 2-min epochs, displayed by dominant (**b**) and subordinate (**c**) naive males (two-tailed multiple *t*-test, Bonferroni correction; $n = 7$ dominant and 11 subordinate observers). Inset: representative tracking traces. **e**,**f**, Percentage of time spent sniffing demonstrators in stress (purple bars) or neutral (gray bars) state during the 6-min test, divided into 3 consecutive 2-min epochs, displayed by negative self-experienced dominant (**e**) and self-experienced subordinate (**f**) males (two-tailed multiple *t*-test, Bonferroni correction; $n = 8$ dominant and 13 subordinate observers). Inset: representative tracking traces. **g**,**h**, Cumulative time spent sniffing one stress and one neutral demonstrator in naive and self-experienced dominant (**g**) or subordinate (**h**) observers (three-way RM ANOVA, Bonferroni correction; $n = 7$ naive and 8 self-experienced dominant males; $n = 11$ naive and 13 self-experienced subordinate males). **i**, Discrimination index in dominant (orange) and subordinate (dark green) mice for both naive and self-experience conditions (three-way RM ANOVA, Bonferroni correction; $n = 7$ naive dominants and 11 naive subordinates; $n = 8$ self-experienced dominants and 13 self-experienced subordinates). **j**, Percentage of dominant or subordinate mice in naive and self-experience conditions with a preference toward stress (purple, discrimination index > 0) or neutral (gray, discrimination index < 0) demonstrators ($n = 7$ naive dominants, $n = 11$ naive subordinates, $n = 8$ self-experienced dominants and $n = 13$ self-experienced subordinates). **k**,**n**, Experimental design of the EDT with one restraint stress (purple) versus one neutral (gray) demonstrator in naive (**k**) and negative self-experience (**n**) conditions. **l**,**m**, Percentage of time spent sniffing demonstrators in stress (purple bars) or neutral (gray bars) state during the 6-min test, divided into 3 consecutive 2-min epochs, displayed by estral (**l**) and diestral (**m**) naive females (two-tailed multiple *t*-test, Bonferroni correction; $n = 7$ estral and 7 diestral female observers). Inset: representative tracking traces. **o**,**p**, Percentage of time spent sniffing demonstrators in stress (purple bars) or neutral (gray bars) state during the 6-min test, divided into 3 consecutive 2-min epochs, displayed by negative self-experienced estral (**o**) and diestral (**p**) females (two-tailed multiple *t*-test, Bonferroni correction; $n = 15$ estral and 13 diestral observers). Inset: representative tracking traces. **q**,**r**, Cumulative time spent sniffing one stress and one neutral demonstrator in naive and self-experienced estral (**q**) or diestral (**r**) observers (three-way RM ANOVA, Bonferroni correction; $n = 7$ naive and 15 self-experienced estral females; $n = 7$ naive and 13 self-experienced diestral females). **s**, Discrimination index in estral (light purple) and diestral (purple) mice for both naive and self-experienced conditions (three-way RM ANOVA; $n = 7$ naive estral, $n = 7$ naive diestral, $n = 15$ self-experienced estral and $n = 13$ self-experienced diestral). **t**, Percentage of estral or diestral mice in naive and negative self-experience conditions with a preference toward stress (purple, discrimination index > 0) or neutral (gray, discrimination index < 0) demonstrators ($n = 7$ naive estral, $n = 7$ naive diestral, $n = 15$ self-experienced estral and $n = 13$ self-experienced diestral). Bar and line graphs show the mean ± s.e.m. *$P < 0.05$, **$P < 0.005$ and ***$P < 0.0005$.

Estrus prevents self-experience impact on emotion recognition

We next tested the same hypothesis about sexual hormones on female mice. Evidence suggests the influence of menstrual cycle on emotion recognition and empathy in women[36]. Moreover, in female rodents, emotional contagion can be susceptible to the estrus cycle[37].

We tested whether female mice in different phases of the estrus cycle had diverse emotion recognition with and without negative self-experience. In mice, the estrus cycle averages 4–5 days and is generally divided into four phases: proestrus, estrus, metestrus and diestrus[38]. We monitored the estrus cycle every day using the vaginal cytological evaluation method[39], such that mice were tested during a specific phase of the cycle. As previously described[37], mice were tested in the estrus or diestrus phases, which are the longest within the cycle and have opposite hormonal configuration[39]. In naive females, we observed increased sniffing toward stress demonstrators compared to neutral mice for both estral and diestral mice (Fig. 3k–m and Extended Data Fig. 3c). In negative self-experience conditions, estral and diestral females showed different behavioral outcomes. Negative self-experienced estral females showed increased sniffing toward stress demonstrators (Fig. 3n,o and Extended Data Fig. 3f, left), while negative self-experienced diestral females avoided stress demonstrators (Fig. 3p and Extended Data Fig. 3f, right). However, in both estral and diestral observers, the sniffing toward stress but not neutral demonstrators was reduced compared to naive mice (Fig. 3q,r). This was confirmed by a reduction in the social exploration toward stress demonstrators only in self-experienced estral and diestral observers (Extended Data Fig. 3j). Despite no major differences being evident between estral and diestral self-experienced mice in the discrimination index (Fig. 3s), we found that 67% of estral females showed a preference toward stress mice (discrimination index > 0) in contrast to only 38% of diestral observers (Fig. 3t). Negative self-experience did not change the amount of self-grooming (Extended Data Fig. 3k). Lastly, no differences in stress emotion recognition were evident by dividing observers depending on the cycle phase in which they were when the stress experience occurred (Extended Data Fig. 3n,o), indicating that estrus cycle modulation of negative self-experience does not occur during experience of stress.

Overall, these data show that the estral phase prevents the impact of negative self-experience on the response toward others' stress.

mPFC CRF mediates self-experience effect on emotion recognition

The negative self-experience model presented in this study focuses on the experience of stress and the reaction to others' stress. Thus, we investigated a possible involvement of the CRF system, which is an important modulator of emotional and cognitive responses to stress[19,20].

The mPFC is known to be involved in sociocognitive processes[40], particularly in emotion recognition[9]. Notably, mPFC CRF expression is sex and androgen dependent[41] and circulating ovarian steroids modulate cognitive actions of mPFC CRF[42,43].

We first silenced mPFC CRF expression using a viral approach based on short hairpin RNA (shRNA) specific for CRF[24] (AAV2/9 CMV-DIO-(mCherry-U6)-shRNA$^{anti\text{-}Crf}$), bilaterally injecting the mPFC of CRF-Cre male mice. The specific control (scrambled) virus was used (AAV2/9 CMV-DIO-(mCherry-U6)-shRNA^{scrambled}) (Fig. 4a). Notably, CRF-Cre mice showed the same behavioral outcome observed in C57BL/6J mice for both naive and negative self-experience conditions (Supplementary Fig. 3).

In naive conditions, silencing of mPFC CRF did not change emotion recognition, with both *scrambled* and *anti-CRF* shRNA-injected observers showing an equal preference toward stress demonstrators (Fig. 4b–d and Extended Data Fig. 4a–c). In contrast, the *anti-Crf* shRNA re-established in negative self-experienced observers a preference for stress demonstrators, which was confirmed to be lost in the *scrambled* shRNA group (Fig. 4e–g and Extended Data Fig. 4d–f). In agreement, the sniffing toward stress demonstrators was different between naive and self-experienced observers only within the *scrambled* (Fig. 4h) but not *anti-CRF* shRNA groups (Fig. 4i). All groups except for *scrambled* shRNA negative self-experienced observers had a discrimination index higher than chance level (Fig. 4j). In negative self-experienced mice, the *anti-Crf* shRNA also re-established the amount of social exploration toward stress demonstrators, which was reduced in the negative self-experienced *scrambled* shRNA group (Fig. 4k). In naive observers, silencing mPFC CRF did not alter the amount of social exploration toward both neutral and stress mice (Fig. 4k), indicating that this manipulation does not affect sociability in general. Lastly, we found that *anti-CRF* shRNA equally re-established preference toward stress compared to neutral demonstrators in both dominant and subordinate negative self-experienced observers (Fig. 4l–n and Extended Data Fig. 4g,h).

Overall, these results demonstrate an involvement of mPFC CRF in negative self-experience modulation of stress emotion recognition.

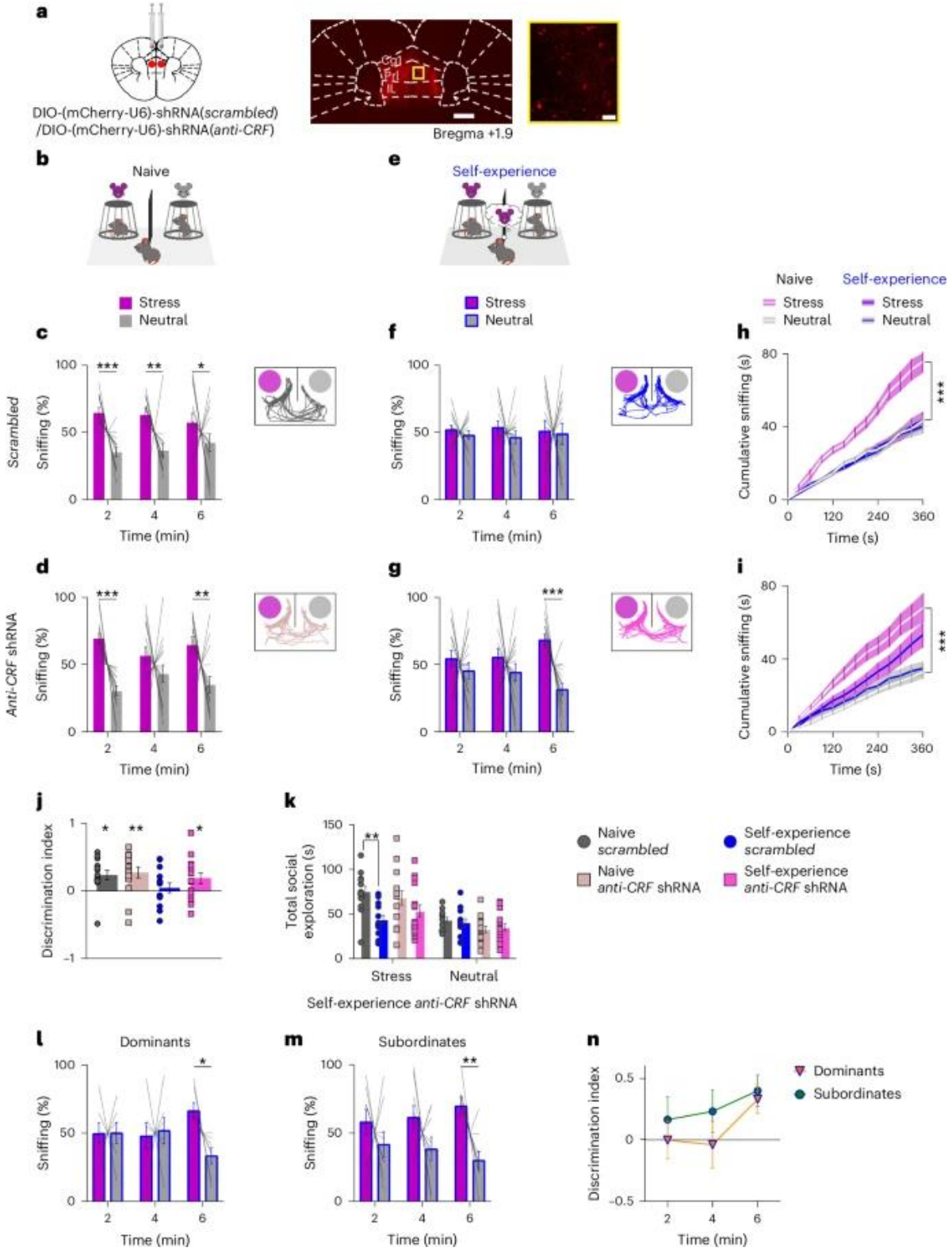
a
DIO-(mCherry-U6)-shRNA(scrambled)
/DIO-(mCherry-U6)-shRNA(anti-CRF)
Bregma +1.9
b
Naive
e
Self-experience
Stress
Neutral
c
f
h
Scrambled
Sniffing (%)
Time (min)
Cumulative sniffing (s)
Time (s)
d
g
i
Anti-CRF shRNA
j
Discrimination index
k
Total social exploration (s)
Stress
Neutral
Naive scrambled
Naive anti-CRF shRNA
Self-experience scrambled
Self-experience anti-CRF shRNA
Self-experience anti-CRF shRNA
l
Dominants
m
Subordinates
n
Dominants
Subordinates

Fig. 4: Silencing CRF in the mPFC attenuated self-experience impact on stress emotion recognition.

a, Left, CRF-Cre mice were injected in the mPFC with CMV-DIO-(mCherry-U6)-shRNA(anti-Crf) or CMV-DIO-(mCherry-U6)-shRNA(scrambled). Right, representative image of coronal mPFC section (scale bar, 500 μm) and zoom-in view of infected zone (scale bar, 50 μm). b,e, Experimental design of the EDT with one restraint stress (purple) versus one neutral (gray) demonstrator in naive (b) and negative self-experience (e) conditions. c,d, Percentage of time spent sniffing demonstrators in stress (purple bars) or neutral (gray bars) state during the 6-min test, divided into 3 consecutive 2-min epochs, displayed by naive scrambled (c) and anti-CRF (d) shRNA observers (two-tailed multiple t-test, Bonferroni correction; n = 14 scrambled and 15 anti-CRF shRNA observers). Inset: representative tracking plots. f,g, Percentage of time spent sniffing demonstrators in stress (purple bars) or neutral (gray bars) state during the 6-min test, divided into 3 consecutive 2-min epochs, displayed by negative self-experienced scrambled (f) and anti-CRF (g) shRNA observers (two-tailed multiple t-test, Bonferroni correction; n = 14 scrambled and 16 anti-CRF shRNA observers). Inset: representative tracking plots. h,i, Cumulative time spent sniffing one neutral and one stress demonstrator in naive and self-experienced scrambled (h) or anti-CRF (i) shRNA observers (three-way RM ANOVA, Bonferroni correction; n = 14 scrambled shRNA naive and 14 self-experienced scrambled shRNA observers; n = 15 anti-CRF shRNA naive and 16 anti-CRF shRNA self-experienced observers). j, Discrimination index of scrambled shRNA naive (gray), scrambled shRNA negative self-experienced (blue), anti-CRF shRNA naive (light pink) and anti-CRF shRNA negative self-experienced (pink) observers (one-way ANOVA against chance, defined as 0, Bonferroni post hoc; n = 14 naive and 14 negative self-experienced scrambled shRNA observers; n = 15 naive and 16 negative self-experienced anti-CRF shRNA observers). k, In self-experienced observers, anti-CRF shRNA re-established the social exploration time toward stress demonstrators (three-way RM ANOVA, Bonferroni correction; n = 14 naive and 14 self-experienced scrambled shRNA observers; n = 15 naive and 16 self-experienced anti-CRF shRNA observers). l,m, Percentage of time spent sniffing demonstrators in stress (purple bars) or neutral (gray bars) state during the 6-min test, divided into 3 consecutive 2-min epochs, displayed by anti-CRF shRNA negative self-experienced dominants (l) and subordinates (m) (two-tailed multiple t-test, Bonferroni correction; n = 7 dominant and 9 subordinate observers). n, The anti-CRF shRNA self-experienced dominants and subordinates did not differ on the basis of discrimination index during the 6-min test, divided into 3 consecutive 2-min epochs (two-way RM ANOVA; n = 7 dominants and 9 subordinates). Bar and line graphs show the mean ± s.e.m. *P < 0.05, **P < 0.005 and ***P < 0.0005.

Self-experience shifts mPFC CRF activity toward others' stress

We then investigated the physiological involvement of mPFC CRF cells in negative self-experience modulation of stress emotion recognition. An adeno-associated virus (AAV) carrying a Cre-dependent GCaMP6f (AAV1.Syn.Flex.GCaMP6f.eYFP) was injected into the mPFC of CRF-Cre mice, which were subsequently implanted with a gradient-index (GRIN) lens terminating dorsally to this area for in vivo microendoscope imaging (Fig. 5a and Extended Data

Fig. 5a,b). Mice were tested in naive or negative self-experience conditions (Fig. 5b,c, Extended Data Fig. 5c–f, and Supplementary Videos 1 and 2). We calculated the peristimulus time histogram (PSTH), using the entering time into the stress or the neutral zone to synchronize calcium events to behavioral outcome. Negative self-experience reverted mPFC CRF neuronal activation compared to naive condition. Specifically, naive observers showed an increased calcium signal in mPFC CRF cells when in the zone of the neutral demonstrator, whereas negative self-experienced mice had higher activation of mPFC CRF cells when in the stress zone (Fig. 5d). The area under the curve (AUC) (Fig. 5e) and the frequency of calcium events (Fig. 5f), but not the amplitude (Fig. 5g), were higher in negative self-experienced compared to naive observers when in the stress zone. These effects were not simply because of a general reaction of mPFC CRF neurons to stress as, during restraint, mPFC CRF cells showed fewer peaks (Extended Data Fig. 5k,l) with the same amplitude (Extended Data Fig. 5m) compared to baseline. In contrast, mPFC somatostatin (SOM) neurons, which are implicated in emotion recognition in naive conditions[9], showed the same pattern of activation with stress compared to a neutral demonstrator in both naive[9,10] and negative self-experience conditions (Supplementary Fig. 4c–i). Notably, both SOM and CRF cells in the mPFC are inhibitory γ-aminobutyric acid (GABA)ergic cells[27,44] but belonging to two different populations with no overlap (Supplementary Fig. 4a,b). Thus, negative self-experience induced a specific higher activation of mPFC CRF cells toward the stress-matched demonstrator.

We then performed single-cell analyses considering active and inactive neurons for each entrance in the neutral or stress zone. In naive observers, mPFC CRF neurons were more activated and in a higher number in the neutral zone compared to the stress one (Fig. 5h,i). Moreover, more entrances in the stress zone were associated with the inactivation of CRF neurons in naive observers (Extended Data Fig. 5g,h). Conversely, in negative self-experienced observers, more entrances in the stress zone were associated with higher mPFC CRF neuronal activation compared to the neutral zone (Fig. 5j,k). Moreover, we found an increased number of entrances in the neutral zone associated with the inactivation of these neurons (Extended Data Fig. 5i,j). The percentage of entrances events that were associated with CRF neuronal activation was higher for the stress zone in negative self-experience compared to naive conditions, while no difference was found for the neutral zone (Fig. 5l). Lastly, considering the percentage of

activation in each interaction zone (neutral and stress), we found an increased modulation of mPFC CRF neurons following negative self-experience (Fig. 5m). Notably, self-experienced dominant mice had higher activation of mPFC CRF neurons in the stress zone compared to subordinate mice (Fig. 5n).

Our results indicate that negative self-experience reverts the relative pattern of mPFC CRF neuronal activity between neutral and stress demonstrators.

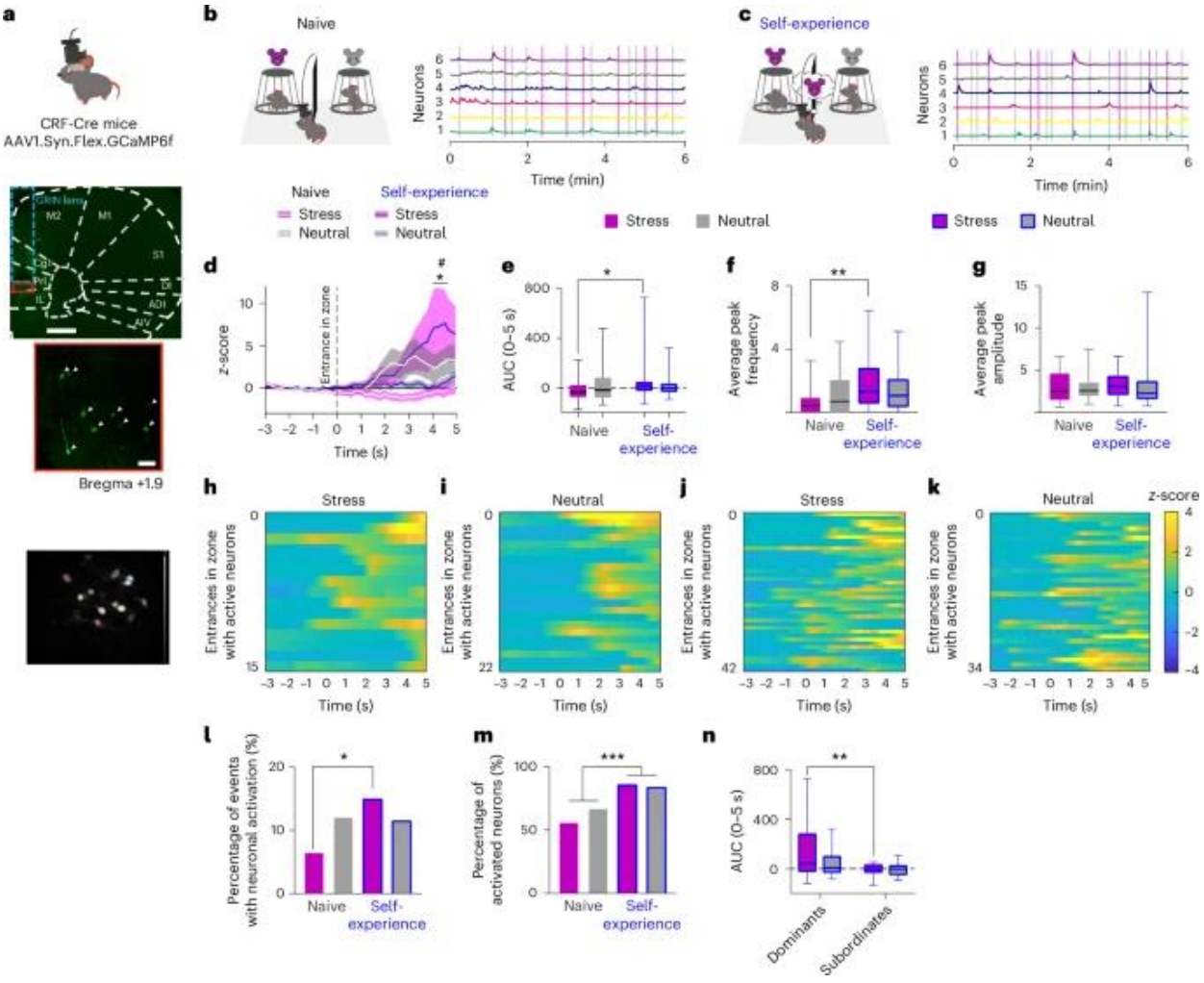

Fig. 5: Negative self-experience reverts mPFC CRF neuronal activity toward others in stress.

a, Top, CRF-Cre mice were injected into the mPFC with Syn.Flex.GCaMP6f.eYFP and implanted with a GRIN lens (n = 5 mice). Middle, representative image of coronal mPFC section (scale bar, 500 µm) and zoom-in view of recorded area (scale bar, 50 µm). Bottom, representative picture of CRF neurons visualized with the miniscope.

Findings were replicated in two independent experiments with similar results (naive: n = 27 neurons in 4 mice; self-experience: n = 37 neurons in 5 mice). b,c, Left, experimental design of the EDT with one restraint stress (purple) and one neutral (gray) demonstrator in naive (b) and self-experience (c) conditions. Right, representative calcium traces aligned with behavioral outputs (purple, entrance in stress zone; gray, entrance in neutral zone). d, PSTH before and after entrance in the zone with stress (purple) or neutral (gray) demonstrators in naive and self-experience condition (three-way RM ANOVA, Bonferroni correction; *P < 0.05 stress demonstrator in naive versus self-experience condition and #P < 0.5 stress demonstrator in self-experience condition versus baseline; n = 29 entrances in the neutral and 34 in the stress zone for naive observers; n = 42 entrances in the neutral and 41 entrances in the stress zone for self-experienced observers). e, AUC of mPFC CRF neuronal activity from naive (no outline) and self-experienced (blue outline) observers after entrance in the zone with stress (purple) or neutral (gray) (two-way ANOVA, Bonferroni correction; n = 34 entrances in stress and 28 entrances in neutral zone for naive observers; n = 37 entrances in stress and 41 entrances in neutral zone for self-experienced observers). f, CRF neuronal activity of naive and negative self-experienced observers differs in the average peak frequency when in the stress (purple) but not in the neutral (gray) zone (two-way ANOVA, Bonferroni correction; n = 27 neurons for naive and 37 for self-experience). g, CRF neuronal activity of naive and negative self-experienced observers did not differ in the average peak amplitude when in the stress (purple) or the neutral (gray) zone (two-way ANOVA; n = 15 peaks for stress zone and 18 for neutral zone in naive observers; n = 32 peaks for stress and 31 for neutral zone in self-experience). h–k, Heat maps of entrances in stress (h,j) or neutral (i,k) zone associated with neuronal activation in naive (h,i) and self-experience (j,k) conditions. l, Percentage of entrances in stress (purple) or neutral (gray) zone associated with neuronal activation in the naive and negative self-experience conditions (chi-square; n = 15 entrances for stress and 22 entrances for neutral zone in naive observers; n = 42 entrances for stress and 34 entrances for neutral zone in self-experience). m, Percentage of active neurons when observers were in the stress (purple) or neutral (gray) zone in the naive and negative self-experience conditions (chi-square; n = 27 neurons for naive and n = 37 neurons for self-experience). n, AUC of mPFC CRF neuronal activity for dominant and subordinate self-experienced observers following entrance in the zone with stress (purple) or neutral (gray) demonstrators (two-way ANOVA, Bonferroni correction; n = 16 entrances for stress and 16 entrances for neutral zone in dominant mice; n = 21 entrances for stress and 25 entrances for neutral zone in subordinate mice). Box plots in e–g and n show the median (center), 25th and 75th percentiles (box), and most extreme data points (whiskers). Bar and line graphs show the mean ± s.e.m. *P < 0.05, **P < 0.005 and ***P < 0.0005.

Inhibiting mPFC CRF cells induces social preference in naive mice

In naive conditions, we found that CRF neurons in the mPFC were more active toward a neutral compared to a stress demonstrator (Fig. 5d). To test whether this pattern of activation might be responsible for the increased sniffing toward stress mice in the naive condition, we bilaterally injected an AAV carrying a Cre-dependent halorhodopsin (AAV-EF1a-DIO-eNpHR3.0- eYFP) into the mPFC of CRF-Cre mice, which were subsequently implanted with optic fibers

terminating dorsally to this area (Fig. 6a and Supplementary Fig. 6a). Delivery of continuous green light (532 nm) resulted in efficient silencing of mPFC CRF neurons (Supplementary Fig. 5).

Inhibition of mPFC CRF cells, only when interacting with the neutral mouse (Fig. 6b and Extended Data Fig. 6a), induced a preference toward the neutral demonstrator (Fig. 6c,d and Extended Data Fig. 6b). This was confirmed by increased sniffing of the neutral mouse in light on compared to light off conditions (Fig. 6e) and by the discrimination index, which was reverted in light on compared to light off conditions (Fig. 6f). This manipulation did not affect the behavior of mice injected with an enhanced yellow fluorescent protein (eYFP) control virus (Supplementary Fig. 6g–k) and did not alter the total duration of social exploration (Extended Data Fig. 6c). Thus, blocking the increased activity of mPFC CRF neurons when interacting with the neutral mouse shifted the observer's preference from the stress to the neutral demonstrator.

Notably, we demonstrated that such social preference is driven by the relative inhibition of mPFC CRF neurons, as naive mice showed increased sniffing toward one of two neutral demonstrators only if one is coupled with the inhibition of mPFC CRF neurons (Extended Data Fig. 6d–h). These effects were evident only when inhibiting mPFC CRF neurons in the presence of social stimuli, as no effects were found in mice injected with eYFP (Supplementary Fig. 6b–f) or when exposed to inanimate objects (Extended Data Fig. 6n,p).

These data demonstrate that, in naive conditions, a relative reduction in mPFC CRF cells activity induces social preference toward stress mice.

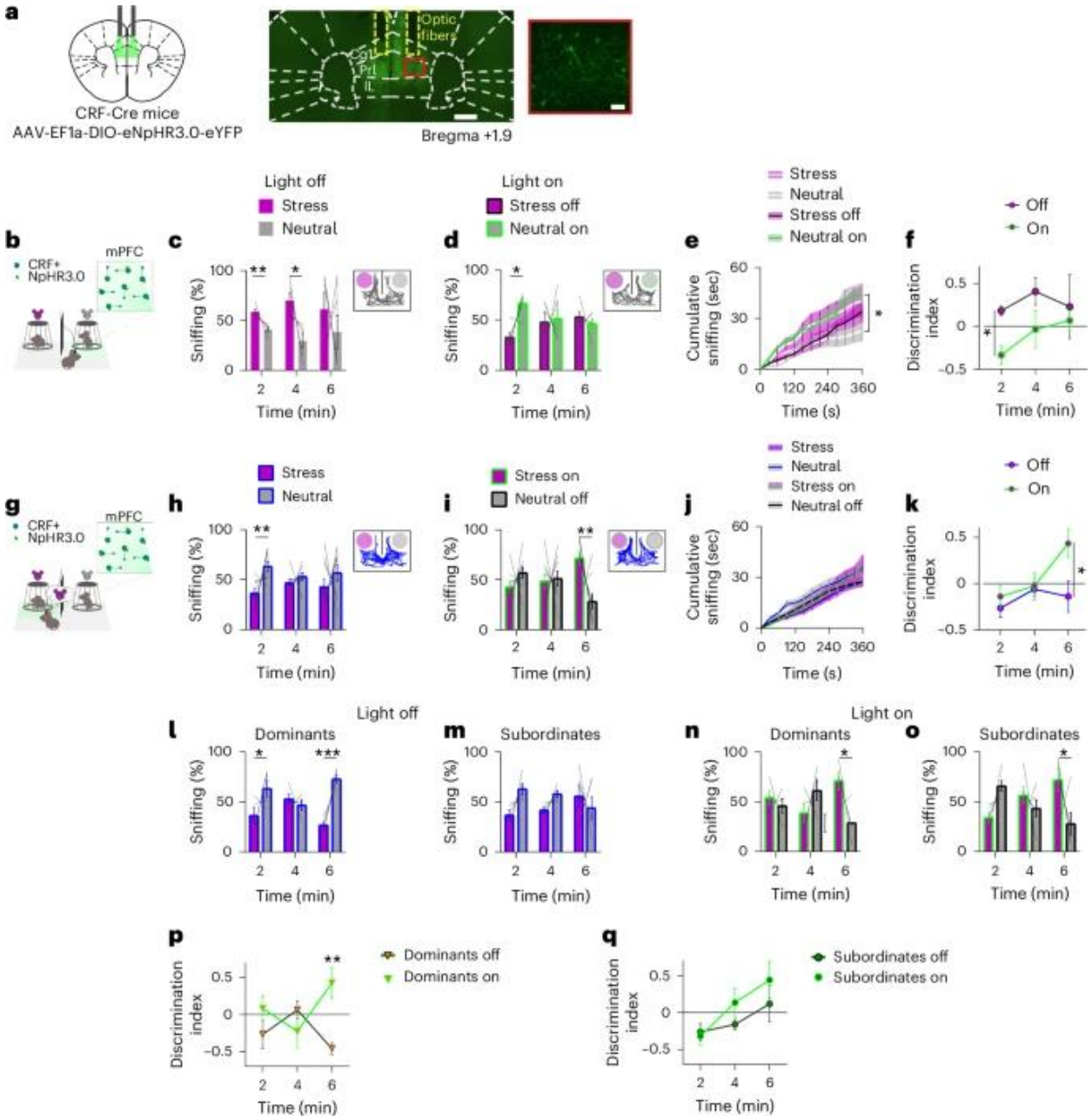

Fig. 6: Inhibition of mPFC CRF neurons induces social preference in naive condition and abolishes self-experience impact on stress emotion recognition.

a, Left, CRF-Cre mice were injected in the mPFC with EF1a-DIO-eNpHR3.0-eYFP and implanted bilaterally with optic fibers. Right, representative image of coronal mPFC section (scale bar, 500 µm) and zoomed-in view of infected area (scale bar, 50 µm). Findings were replicated in two independent experiments with similar results. b, Experimental design of the EDT with one restrain stress (purple) and one neutral (gray) demonstrator in naive conditions. Photoinhibition (λ = 532 nm) was paired to the exploration of neutral mice. c,d, Percentage of time spent

sniffing demonstrators in stress (purple bars) or neutral (gray bars) state during the 6-min test, divided into 3 consecutive 2-min epochs, displayed by naive observers tested in light off (c) and light on (d) conditions (two-tailed multiple t-test, Bonferroni correction; n = 5 observers for light off and 5 for light on). Inset: representative tracking plot. e, Cumulative sniffing toward stress and neutral demonstrators with light off and light on conditions (three-way RM ANOVA, Bonferroni correction; n = 5 observers per condition). f, Discrimination index during the 6-min test, divided into 3 consecutive 2-min epochs, displayed by naive observers tested in EDT stress versus neutral in light off and light on conditions (two-way RM ANOVA, Bonferroni correction; n = 5 observers per condition). g, Experimental design of the EDT with one restraint stress (purple) versus one neutral (gray) demonstrator in self-experience condition. Photoinhibition (λ = 532 nm) was paired to the exploration of stress demonstrator. h,i, Percentage of time spent sniffing demonstrators in stress (purple bars) or neutral (gray bars) state during the 6-min test, divided into 3 consecutive 2-min epochs, displayed by self-experienced observers tested in light off (h) and light on (i) conditions (two-tailed multiple t-test, Bonferroni correction; n = 9 observers). Inset: representative tracking plots. j, Cumulative time spent sniffing stress and neutral demonstrators in light off and light on conditions (three-way RM ANOVA, Bonferroni correction; n = 9 observers per condition). k, Discrimination index during the 6-min test, divided into 3 consecutive 2-min epochs, displayed by self-experienced observers tested in EDT stress versus neutral in light off and light on conditions (two-way RM ANOVA, Bonferroni correction; n = 9 observers per condition). l,m, Percentage of time spent sniffing demonstrators in stress (purple bars) or neutral (gray bars) state during the 6-min test, divided into 3 consecutive 2-min epochs, displayed by self-experienced dominant (l) and subordinate (m) mice tested in light off condition (two-tailed multiple t-test, Bonferroni correction; n = 4 dominant and 5 subordinate observers). n,o, Percentage of time spent sniffing demonstrators in stress (purple bars) or neutral (gray bars) state during the 6-min test, divided into 3 consecutive 2-min epochs, displayed by self-experienced dominant (n) and subordinate (o) mice tested in light on condition (two-tailed multiple t-test, Bonferroni correction; n = 4 dominant and 5 subordinate observers). p,q, Discrimination index during the 6-min test, divided into 3 consecutive 2-min epochs, displayed by dominant (p) or subordinate (q) self-experienced observers tested in EDT stress versus neutral in light off and light on conditions (two-way RM ANOVA, Bonferroni correction; n = 4 dominant and 5 subordinate observers). Bar and line graphs show the mean ± s.e.m. *P < 0.05, **P < 0.005 and ***P < 0.0005.

Inhibiting mPFC CRF cells abolishes self-experience impact on emotion recognition

In contrast to naive conditions, mice with negative self-experience showed increased activity of mPFC CRF neurons during the interaction with stress demonstrators (Fig. 5d). Thus, we assessed whether disrupting this activation could prevent the behavioral outcome induced by negative self-experience. Accordingly, 24 h after the self-experience of restraint stress, observer mice were tested with one neutral and one stress demonstrator and a continuous green light (532 nm) was delivered every time observers entered the zone of the stress mouse (Fig. 6g and Extended Data Fig. 6i). In light off condition, negative self-experienced observers showed

avoidance toward the stress demonstrators (Fig. 6h and Extended Data Fig. 6j, left). Stress mouse-paired silencing of mPFC CRF cells activity re-established increased sniffing toward this demonstrator (Fig. 6i and Extended Data Fig. 6j, right). This was not evident considering the cumulative sniffing (Fig. 6j), but was confirmed by an inversion of the discrimination index between light off and light on conditions (Fig. 6k). No light-dependent effects were evident in mice injected with eYFP (Supplementary Fig. 6l–p) and in the total amount of social exploration (Extended Data Fig. 6k).

Considering our findings in the dominance modulation of negative self-experience processes (Fig. 3), we divided these negative self-experienced mice into dominants and subordinates. Inhibiting mPFC CRF neurons when interacting with the stress demonstrator seemed to re-establish the preference for the stress mouse in both dominant and subordinate negative self-experienced mice (Fig. 6l–o and Extended Data Fig. 6l,m). However, analysis of the discrimination index revealed a significant difference between light off and light on conditions only in dominants (Fig. 6p) but not in subordinates (Fig. 6q). This was not related to a change in hierarchy status, as silencing mPFC CRF neurons during the tube test led to a change in rank in only two of 11 mice (Extended Data Fig. 6q–s), indicating a more marginal role of these neurons in social hierarchy.

These results show that inhibiting the activity of mPFC CRF neurons suppresses the avoidance for stress demonstrators in negative self-experienced observers in a dominance-dependent manner.

Activating mPFC CRF cells does not induce avoidance in naive mice

Next, we asked whether mimicking the self-experience increase in activity of mPFC CRF cells (Fig. 5d) in naive observers would lead to the same social avoidance. We bilaterally injected an AAV carrying a Cre-dependent channelrhodopsin-2 (AAV-EF1a-DIO-ChR2-eYFP) into the mPFC of CRF-Cre mice, which were subsequently implanted with optic fibers terminating dorsally to this area (Fig. 7a and Supplementary Fig. 7a).

Naive observer mice were exposed to a neutral and a stress demonstrator and mPFC CRF neurons were activated every time they entered the zone of the stress demonstrator (Fig. 7b and Extended Data Fig. 7a), using the same laser stimulation protocol applied in our previous study9 (pulses of 473-nm light; 5 ms, 30 Hz). This manipulation did not abolish the preference toward stress demonstrators (Fig. 7c,d and Extended Data Fig. 7b). Indeed, increased sniffing toward stress mice was equally evident in light on and light off conditions (Fig. 7e,f). No alterations in general social exploration (Extended Data Fig. 7c) and in eYFP-injected mice (Supplementary Fig. 7g–k) were evident. Furthermore, coupling the activation of mPFC CRF neurons with one of two neutral demonstrators did not induce any avoidance (Extended Data Fig. 7d–g). This optomanipulation also had no effects in eYFP control mice (Supplementary Fig. 7b–f), did not alter general social exploration (Extended Data Fig. 7h) and did not induce a preference or avoidance toward an inanimate object (Extended Data Fig. 7n–p).

These results demonstrate that, without negative self-experience, the increased mPFC CRF cell activity does not induce social avoidance.

Activating mPFC CRF cells induce avoidance in self-experienced dominant mice

We finally tested whether these same optostimulations would have an effect in stress self-experienced observers.

We mimicked the self-experience increased activity of mPFC CRF cells toward a stress mouse (Fig. 5d) in an otherwise neutral mouse (Fig. 7g and Extended Data Fig. 7i). Overall, no difference between sniffing the two neutral mice was detected (Fig. 7h–k and Extended Data Fig. 7j). However, splitting observers according to their social rank showed an avoidance toward neutral demonstrators paired with mPFC CRF photostimulation in dominant but not subordinate negative self-experienced observers (Fig. 7l–q and Extended Data Fig. 7l–m). This manipulation did not affect the behavior of mice injected with eYFP (Supplementary Fig. 7l–p), did not alter the total amount of social exploration (Extended Data Fig. 7k), did not induce any preference toward inanimate objects (Extended Data Fig. 7q–s) and did not change the hierarchy status of mice (Extended Data Fig. 7t–v).

These results confirmed that the increased activity pattern of mPFC CRF neurons needs negative self-experience to induce avoidance toward a demonstrator mouse, specifically in dominant mice.

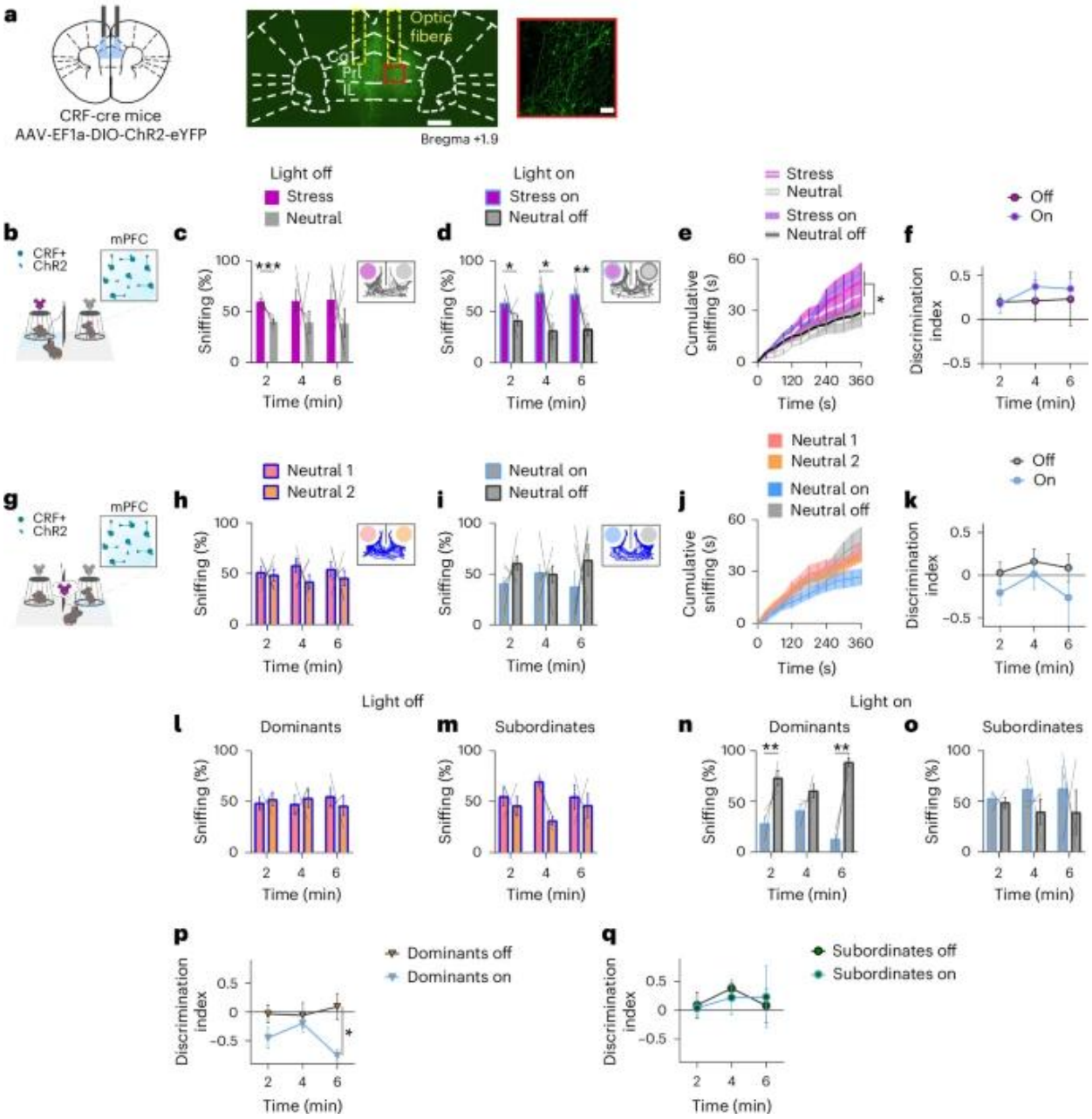

Fig. 7: Increased activity of mPFC CRF neurons induces social avoidance only in self-experienced dominant observers.

a, Left, CRF-Cre mice were injected in the mPFC with EF1a-DIO-ChR2-eYFP and implanted bilaterally with optic fibers. Right, representative image of coronal mPFC section (scale bar, 500 μm) and zoomed-in view of infected area (scale bar, 50 μm). Findings were replicated in two independent experiments with similar results. b, Experimental design of the EDT with one stress (purple) and one neutral (gray) demonstrator in naive condition. Photostimulation (λ = 473 nm) was paired to the exploration of stress demonstrators. c,d, Percentage of time spent sniffing demonstrators in stress (purple bars) or neutral (gray bars) state during the 6-min test, divided into 3 consecutive 2-min epochs, displayed by naive observers tested in light off (c) and light on (d) conditions (two-tailed multiple t-test, Bonferroni correction; n = 6 light off and 7 light on observers). Inset: representative tracking plot. e, Cumulative time spent sniffing stress and neutral demonstrators in light off and light on conditions (three-way RM ANOVA, Bonferroni correction; n = 7 observers per condition). f, Discrimination index during the 6-min test, divided into 3 consecutive 2-min epochs, displayed by naive observers tested in EDT neutral versus stress in light off and light on conditions (two-way RM ANOVA; n = 7 observers per condition). g, Experimental design of the EDT with two neutral demonstrators and a negative self-experienced observer. Photostimulation (λ = 473 nm) was paired to the exploration of one of the two demonstrators. h,i, Percentage of time spent sniffing two neutral demonstrators during the 6-min test, divided into 3 consecutive 2-min epochs, displayed by self-experienced observers tested in light off (h) and light on (i) conditions (two-tailed multiple t-test, Bonferroni correction; n = 6 light off and 6 light on observers). Inset: representative tracking plot. j, Cumulative time spent sniffing two neutral demonstrators in light off and light on conditions (three-way RM ANOVA; n = 6 observers per condition). k, Discrimination index during the 6-min test, divided into 3 consecutive 2-min epochs, displayed by self-experienced observers tested in EDT neutral versus neutral in light off and light on conditions (two-way RM ANOVA; n = 6 observers per condition). l,m, Percentage of time spent sniffing two neutral demonstrators during the 6-min test, divided into 3 consecutive 2-min epochs, displayed by self-experienced dominant (l) and subordinate (m) mice tested in light off condition (two-tailed multiple t-test, Bonferroni correction; n = 3 observers per condition). n,o, Percentage of time spent sniffing two neutral demonstrators during the 6-min test, divided into 3 consecutive 2-min epochs, displayed by self-experienced dominant (n) and subordinate (o) mice tested in light on condition (two-tailed multiple t-test, Bonferroni correction; n = 3 observers per condition). p,q, Discrimination index during the 6-min test, divided into 3 consecutive 2-min epochs, displayed by dominant (p) or subordinate (q) self-experienced observers tested in EDT neutral versus neutral in light off and light on conditions (two-way RM ANOVA, Bonferroni correction; n = 3 observers per condition). Bar and line graphs show the mean ± s.e.m. *P < 0.05, **P < 0.005 and ***P < 0.0005.

Discussion

Here, we demonstrate that self-experience of a stressful event modulates the response to others undergoing the same stress. The extent of this effect varies with the estrus cycle in females and social hierarchy in males. Moreover, we demonstrated that the influence of self-experience on stress emotion recognition is modulated by CRF activity in the mPFC.

Self-experienced stress elicited divergent interindividual responses in mice, ranging from preference to avoidance toward conspecifics experiencing the same stressor. Similarly, humans observing others in specific emotional states may recall similar feelings based on past experiences, leading to interindividual divergent reactions. These can range from empathic concern that increases attention toward others[2,4] to personal distress that prompts avoidance[3]. We speculate that mice spending more time with stressed conspecifics might be more engaged in others' distress, which would be in line with evidence of prosocial behaviors in rodents[11,12,15]. In contrast, mice avoiding the stress demonstrator may perceive others' stress as aversive, analogous to how humans associate personal distress with distancing from others' suffering[45]. Notably, 'similarity in experience' is a crucial factor influencing these socioemotional reactions in humans[3]. In agreement, we demonstrated that self-experience in mice changes responses only toward same-stress demonstrators (that is, restraint or footshock). This suggests that observers with self-experience may perceive in others the specific stress they went through. This could be plausible considering that restraint and footshock trigger different behavioral responses (grooming and freezing, respectively) and that the emotion recognition paradigm depends on visual and olfactory cues[8,9]. Other studies also highlighted the importance of previous negative self-experience, reporting a facilitatory effect on vicarious freezing in the observer subject[31,46,47]. However, these studies did not investigate how prior experience could influence observers' responses toward others' emotions. Instead, one study revealed that male rats that usually avoid shocked demonstrators preferred to approach them if they had been previously shocked[48], which is opposite to what we found (that is, a shift from approach to avoidance). However, different factors might contribute to this discrepancy: hierarchy relationship between interacting subjects, mouse versus rat differences and/or the stress intensity (footshock: 0.5 mA for 2 s in this study versus 1 mA for 5 s in their study). Overall, our data

provide new insights into the role of negative self-experience in socioemotional reactions to others.

Self-experience affects reactions to others in stress in a sex-dependent way, influenced by hormonal status. Self-experience in dominant, but not subordinate, males reverted the approach of mice into avoidance. As dominant male mice show higher anxiety and increased susceptibility to chronic social defeat than subordinates[49], the hypothesis of increased self-distress triggered by self-experience could be supported. This was not correlated to peripheral corticosterone, as we and others did not find hierarchy-dependent changes[50]. However, our findings are in line with evidence of the influence of testosterone and social status on sociocognitive performance[15,34,51]. Importantly, we showed that the relative social rank between observers and demonstrators, combined with their emotional state, increases the complexity of self-experience modulation of emotion recognition. This could explain some variability among experiments in which we saw either a strong avoidance or no overall preference for stress demonstrators (with some preferring and some avoiding). In contrast, no effect of hierarchy was evident in female mice, possibly because of their lower testosterone levels. Instead, in agreement with human studies[36], we found a correlation between the menstrual cycle and emotion recognition. Intriguingly, female mice in estrus were not affected by self-experience. Estrus corresponds to sexual receptivity, which might be associated with reduced sensitivity to self-distress. In agreement, a rat model of observational fear learning showed no social transfer of fear in estral females[37]. In summary, our self-experience behavioral model addressed several complex aspects of emotion recognition, revealing ethologically relevant sex-dependent individual responses.

The mPFC is involved in social cognition, including processing and retrieval of emotional memory[9,10,15,52,53,54,55]. Human studies also reported that the mPFC regulates the emotional impact of a past event, influencing individuals' goals[56]. Our results expand this mPFC role to how aversive past experiences affect reactions to others' emotions. We demonstrated that mPFC CRF neurons are specifically involved in this self-experience modulation of emotion recognition. This extends the role of mPFC CRF neurons to empathy-related behaviors, whereas this role was previously observed for opioid reward[57], cognitive dysfunction[58], social

familiarity[24] and behavioral responses to stress[27]. In particular, we demonstrated that the photoactivation of mPFC CRF neurons induces social avoidance only following self-experience, but not in its absence. This aligns with evidence showing that mPFC CRF neurons did not influence social interaction in the nonstress condition[27]. Furthermore, silencing mPFC CRF cells diminished the effect of self-experience while not affecting emotion recognition in the naive condition. In agreement, single-cell calcium imaging revealed increased mPFC CRF activity toward a stress demonstrator only following self-experience. In contrast, mPFC CRF neurons were less active during restraint stress compared to baseline. These findings imply that mPFC CRF neurons may store stress memories and are later recruited to appropriately cope with others in similar stress conditions.

An intriguing and still open question is whether mPFC CRF neurons might integrate stress-related and social valence information coming from other brain regions. As mainly GABAergic neurons[27], mPFC CRF cells can successfully orchestrate socioemotional responses integrating self-experience with information about others' emotions by inhibiting other neuronal populations. We found that different subpopulations of GABAergic inhibitory neurons within the mPFC have different implications in emotion recognition. Parvalbumin (PV) neurons modulate basic sociability[59] but not emotion recognition[9]. Conversely, SOM neurons modulate emotion recognition but not basic sociability[9,10]. CRF neurons, instead, are selectively involved in emotion recognition when self-experience of stress occurs. This suggests that neuropeptide modulation or circuit-specific GABA inhibition may better influence specific aspects of sociability and emotion recognition. Future studies should investigate how mPFC PV, SOM and CRF neurons modulate different aspects of social behavior through the release of their specific neuropeptide and/or local GABA microcircuitry.

In summary, our data offer new insights into how negative self-experience influences responses to the same emotions in others, revealing ethologically relevant sex-dependent interindividual differences. Our results highlight mPFC CRF neurons as potential targets for modulating self-experience responses to others' emotions.

Methods

Mice

All procedures were approved by the Italian Ministry of Health (107/2015-PR and 749/2017-PR) and local animal use committee and were conducted in accordance with the Guide for the Care and Use of Laboratory Animals of the National Institutes of Health and the European Community Council Directives. Routine veterinary care and animal maintenance were provided by dedicated and trained personnel. Male and female C57BL/6J animals aged 3–6 months old were used. Founders of the CRF-Cre line (B6(Cg)-*Crh*$^{tm1(cre)Zjh}$/J; 012704) and SOM-Cre line (Som$^{tm2.1(cre)Zjh}$/J mice; 013044) were purchased from the Jackson Laboratory and then bred and expanded in our animal facility for successive testing. CRF-Cre mice crossed with the *Ai9* TdTomato Cre-reporter mice (Jackson Laboratories, 007909) were used to visualize CRF^{+} neurons in immunohistochemistry experiments. All transgenic mice were on the C57BL6/J background. Mouse genotypes were identified by PCR analysis of ear DNA. Distinct cohorts of naive mice were used for each experiment. Animals were housed two to four per cage in a climate-controlled facility (22 ± 2 °C), with ad libitum access to food and water throughout and a 12 h light–dark cycle (7:00 p.m.–7:00 a.m. schedule). Experiments were run during the light phase (within 10:00 a.m.–5:00 p.m.). All mice were handled on alternate days during the week preceding the first behavioral testing.

Behavioral paradigms

EDT

Experiments were performed inside a three-dimensionally (3D) printed apparatus (35.5 × 23.5 × 19 cm) containing two quarter-circles (4 cm radius) on two opposite sides as previously described[8,9,10]. Each quarter-circle was formed by metal rods (8 mm), which allowed social contact between the observer (freely moving in the apparatus) and the demonstrators (confined within the quarter-circle). A 3D-printed separator (11 × 19 cm) was inserted between the two quarter-circles to block the reciprocal view of the demonstrators. Both observers and demonstrators went through habituation to the testing setting for 10 min on three consecutive days before the first experiment. During both habituation and behavioral testing, the cages were placed inside a dimly lit (10 ± 1 lux) soundproof cubicle (Med Associates). Between

each habituation and testing session, the apparatus was thoroughly cleaned with 50% ethanol, wiped and allowed to air-dry. All demonstrators were group-housed accordingly to the type of manipulation they went through (neutral, stress, footshock or fear). Demonstrators were tested naive and used a maximum of two or three times, always with at least 1 week between each consecutive test. No differences were observed in the performance of the observer mice depending on the previous experience of the demonstrators.

Observers

On the day of testing, 1 h before the test, observer mice were placed, inside their homecage, in a room adjacent to the testing room. Then, 15 min before the start of the test, observer mice were moved in the testing room and gently put into the EDT apparatus, inside the dimly lit testing cubicles. For calcium imaging or optogenetics experiments, observer mice were connected to a miniscope or an optic fiber. Then, one neutral and one emotionally altered demonstrator (stress, shock or fear) were placed within the quarter-circles and the 6-min test was started.

Naive

Observers did not undergo any manipulation.

Self-experience of restraint

Observer mice were subjected to a stress consisting of the restraint test[60] for 30 min, 24 h before the experiment.

Self-experience of footshock

Observer mice were subjected to six footshocks (0.5 mA, 2-s duration, 90-s intershock interval) delivered through a grid floor (Ugo Basile), 24 h before the experiment.

Demonstrators

On the day of testing, 1 h before the test, all demonstrator mice cages were brought in the testing room (except fear demonstrators).

Neutral demonstrators

Neutral mice did not receive any manipulation.

Stress demonstrators

On the testing day, stress mice were subjected to a mild stress consisting of 15 min of restraint before the beginning of the EDT.

Footshock demonstrators

On the testing day, footshocked mice were subjected to three shocks (0.5 mA, 2-s duration, 90-s intershock interval) delivered through the grid floor (Ugo Basile) immediately before the beginning of the EDT.

Fear demonstrators

The day before the test, fear mice were subjected to fear conditioning as previously described[8]. Briefly, the conditioned stimulus was a tone (4 kHz, 80-dB sound pressure level, 30 s) and the unconditioned stimulus was three shocks (0.7 mA, 2-s duration, 90-s intershock interval) delivered through the grid floor (Ugo Basile) that terminated simultaneously with the tone (2 s). The day of the test, these mice were brought in a room adjacent to the testing room for 1 h before the test; they were consequently brought inside the experimental room one by one, before placing them within the quarter-circle of the EDT apparatus.

For both observers and demonstrators, mice that belong to the same condition (that is, naive, stress and footshock self-experienced observers and neutral, stress, footshock and fear demonstrators) were housed together and subjected to the same manipulation at the same time.

Behavioral recording

Digital cameras (Imaging Source, DMK 22AUC03 monochrome) were placed facing the long side and the top of the cage to record the test from different angles using a behavioral tracking system (ANY-maze 6.0, Stoelting). These videos were used offline by experimenters blind to the manipulations for a posteriori scoring of sniffing, grooming and freezing.

Tube test

After EDT, the social hierarchy of male and female mice was assessed as previously described[15,35]. Briefly, this test consisted of two phases: training and testing. The training phase lasted two consecutive days during which mice were trained to walk through a Plexiglas tube (30 cm in length; 3 cm in diameter for males and 2.5 cm in diameter for females) five times from each side. In the testing phase, cagemate mice were tested in a pairwise fashion (one trial per pair) until they reached stability for four consecutive days.

Estrus cycle assessment

Estrus cycle assessment was carried out daily in observer females using the cytological vaginal evaluation method as previously described[39]. Briefly, vaginal cells samples were taken between 10:00 a.m. and 12:00 p.m. and stained with 1% Toloudine blue. Stained smears were then analyzed under a light microscope. Observers were tested during the estrus phase, characterized by the presence of numerous unnucleated cornified cells in the vaginal smear, or during the diestrus phase, characterized by a smear enriched of leukocytes and with sparse nucleated cells.

Corticosterone assay

The corticosterone concentration was analyzed from plasma. Thirty minutes after the behavioral test, each mouse was killed by decapitation. The blood was quickly collected in tubes coated with 0.5 M EDTA and centrifuged at 664 rcf for 10 min; the supernatant obtained was immediately processed. The corticosterone concentration was detected by a commercially available Detect X corticosterone ELISA kit (Arbor Assays, K014-H1) following the manufacturer's protocol and plates were read into a Victor 3V (Perkin Elmer) multiplate reader. The level of corticosterone was expressed as fold changes compared to the control group average.

Viral injections and optic lens implants

Viral vectors

AAV5-EF1a-DIO-eNpHR3.0-eYFP.WPRE.hGH (Addgene, 20949; qTiter: 1.95×10^{13} genome copies (GC) per ml, injected volume per hemisphere: 250 nl), AAV5-EF1a-DIO-hChR2(H134R)-eYFP.WPRE.hGH (Addgene, 20298P; ddTiter: 2.76×10^{13} GC per ml; injected volume per hemisphere: 250 nl), AAV5-EF1a-DIO-eYFP.WPRE.hGH (Addgene, 27056; qTiter

5.82×10^{12} GC per ml; injected volume per hemisphere: 250 nl) and AAV1.Syn.Flex.GCaMP6f.eYFP (Addgene, 100833; 100 µl at titer $\geq 7 \times 10^{12}$ GC per ml of virus venom; injected volume for each DV site: 300 nl for miniscope and 200 nl for fiber photometry) were purchased from the University of Pennsylvania Viral Vector Core. rAAV-CMV-DIO-(mCherry-U6)-shRNA(CRF)-WPREs (injected volume per hemisphere: 250 nl) was gifted by F. Levroy[24].

Surgical procedures

C57BL/6J, CRF-Cre or SOM-cre mice were naive and 2–3 months old at the time of surgery. Mice were anesthetized with a mix of isoflurane (2%) and oxygen (1.5%) by inhalation and mounted into a stereotaxic frame (Kopf Instruments) linked to a digital micromanipulator. Brain coordinates of viral injection in the mPFC were taken from the skull surface: anterior–posterior, +1.9 mm; medial–lateral: ±0.25 mm; dorsal–ventral: −2.4 mm (for miniscope experiment: −2.9, −2.6 and −2.3 mm). Virus was infused through a glass micropipette connected to a 10-µl Hamilton syringe. After infusion, the pipette was kept in place for 10 min and then slowly withdrawn. Mice were tested 4 weeks after virus injection to let the viral transgenes adequately express.

Optic fibers implantation for optogenetics and fiber photometry

Mice underwent stereotaxic surgery for fiber-optic implantation 2 weeks after viral injection. The skull was exposed and the previous holes were used to target the mPFC. Optic fibers (dual fiber-optic cannulae for optogenetics: 200-µm core, 0.37 numerical aperture (NA), 2-mm length, 0.7-mm fiber distance, Doric Lenses; multimode fiber-optic cannula for fiber photometry: 200-µm core, 0.39 NA, ~ 3.5-mm length, RWD) were lowered at 400 µm (for optogenetics) or 150 µm (for fiber photometry) dorsal to the virus injection site and were secured to the skull with MetaBond. After optic fiber implantation, mice were allowed to recover for 7–10 days depending on their general health.

Lens implantation for microendoscopic calcium imaging

Two weeks after viral injection, mice underwent stereotaxic surgery for implantation of a 0.5-mm-outer-diameter GRIN lens (ProView Integrated lenses, Inscopix). Before lowering the

GRIN lens, a pretrack was performed using a blunted needle (25 gauge) to reduce tissue damage and minimize brain pressure. GRIN lens insertion was monitored and positioned at the focal point presenting the highest Ca^{2+} signal and was maintained in position using a thin layer of Kwik-Sil (World Precision Instruments), a blunted skull screw and adhesive dental cement (Sun Medical Super-Bond C&B Kit, Dental Leader).

In vivo optogenetics

Fiber-optic cannulae were connected to patch cords (Doric Lenses), which were in turn connected to green-light (532 nm) or blue-light (473 nm) lasers (CNI Laser) using a 1 × 2 intensity division fiber-optic rotary joint (Doric Lenses). Mice were habituated to the patch cable for at least three consecutive days before behavioral testing. Manipulation protocols were performed as previously described9. Specifically, laser power was adjusted such that the light exiting the fiber-optic cable was approximately 4.5 mW. For photoinhibition experiments, continuous green light was used, whereas, for photostimulation experiments, 30-Hz 5-ms pulses of blue light were used. For each photoinhibition and photostimulation manipulation, a control group of mice injected with an eYFP control virus was tested to check whether light delivery (532 nm or 473 nm) could affect the behavior. Mice were tested on consecutive weeks, with treatments (light off and light on) randomly assigned and counterbalanced.

EDT

To control optical inhibition or stimulation with a closed-loop system, a tracking system (ANY-maze 6.0, Stoelting) performed online detection of the location of the observer mouse. When the mouse entered an area that included the demonstrator to be paired with optogenetic manipulations (the neutral or the stress demonstrator; one of the two naive neutral demonstrators), the software triggered the laser.

Object 'discrimination' test

This test was used to control the social specificity of optogenetic manipulations. The same testing cage and behavioral procedures of the EDT were used. Specifically, two identical plastic objects were placed within the quarter-circles of the EDT box for 6 min (different pairs of identical objects were used across mice). As described above, when the observer entered an area

that included the object to be paired with optogenetic manipulations, the software triggered the laser.

Tube test

A 30-cm tube with a 12-mm slit was used. After three consecutive days of rank stability (from day −3 to day −1), mice underwent the optogenetic manipulation on the fourth day (day 0). On this day, tube test ranks were first measured without light. Then, photoinhibition (532 nm) or photostimulation (473 nm) started right before mice entered the tube. For each cage, each combination was performed twice such that the optogenetic manipulation could occur for one mouse at a time. For each couple, mice had to win or lose at least two of three times for each side of the tube. Only when test mice won or lost from both sides of the tube we conclude that the optogenetic manipulation caused a successful rank change. After day 0, mice were tested for other three consecutive days to check whether the rank change induced by the optogenetic manipulation was preserved.

In vivo microendoscopic calcium imaging

Calcium signal acquisition

The nVista miniature microscope (nVista 3.0, Inscopix) with an integrated blue light-emitting diode (LED; 475 nm, average power: 1 mW mm^{-2}) was used to image GCaMP6f-expressing CRF neurons during EDT. Mice were habituated to the miniature microscope for at least three consecutive days before behavioral testing. Using the Acquisition Software (version 1.2.0, Inscopix), laser power, imaging gain and focal distance were selected for each animal and conserved across all experiments. The ANY-maze tracking program (Stoelting) was used to generate transistor–transistor–logic (TTL) signals to time-stamp specific events during EDT (that is, entrance in the zone).

Calcium signal analyses

The signal was first processed using data analysis software from Inscopix (Data Processing Software version 1.2), which applied spatial downsampling (×4), movement artifact correction and smooth correction of the edges. Calcium traces of single cells were represented in terms of units of s.d. through *z*-score normalization.

For the PSTH analysis, overall activity of observer mice was defined by computing the average activity across all neurons. Such average activities were aligned to behavioral outcomes (entrance in the zone), considering a baseline preceding the event ($T = 3$ s) and a baseline following the event ($T = 5$ s). The PSTH quantities were then obtained by subtracting the mean of the baseline activity from the average activity and then dividing by the s.d. of the same. Average plots of PSTH are represented as the mean and s.e.m., putting together all the behavioral outcomes across all the mice. AUCs of the peristimulus curves were computed over an interval of 5 s after the entrance in the zone (at time $T = 0$). Identification of calcium events was performed using custom MATLAB scripts, using the 'findpeaks' function to find the local maxima of neuronal calcium signal. Such maxima were considered calcium events if they overcame thresholds on the minimum event height ('MinHeight', set as the average of the neuronal calcium signal), minimum event prominence ('MinProm', set as 1.5 times the s.d. of the neuronal calcium signal), minimum distance between consecutive events ('MinDist' = 0.5 s) and minimum width of a single event ('MinWidth' = 0.5 s). The calcium event frequency in a given time window was computed by dividing the number of events identified in such a window for the length of the window. Classification of neurons as 'active' or 'inactive' was made by comparing their activity before (3 s) and after (5 s) the behavioral event (entrance in stress or neutral zone). If m and s are, respectively, the average and the s.d. of the activity before the event, neurons were considered active if, after the entrance in the zone, they reached a value of at least $m + 2s$. In an analogous way, neurons were considered inactive if, before the event, they reached at least a value of $M + 2S$, where M and S are the mean and s.d. of the activity after the event. Considering all the neurons on all the entrances in the zone, percentages of entrances followed by neuronal activation or inactivation were computed by dividing the number of entrances overcoming such criteria to the total number of entrances available across all neurons.

In vivo fiber photometry recordings

Calcium signal acquisition

Calcium fluctuations of GCaMP6f-expressing SOM neurons were recorded using a fiber photometry system. A signal processor (RZP5, Tucker Davis Technologies) was used to control two light sources (465-nm LED, CLED_465; 405-nm LED, CLED_405, Doric Lenses), which were modulated at 211 and 539 Hz, respectively. The two wavelengths were combined by a

fluorescence minicube (Doric Lenses) and transmitted through an optical patch cable (Doric Lenses) to the mouse head implant. Emitted fluorescence was collected by the same patch cable, delivered back to the same minicube through a 525-nm filter and sent to a photoreceiver (Femtowatt Silicon Photoreceiver, DC-750 Hz, Newport). Mice were habituated to the patch cable for at least three consecutive days before behavioral testing. Real-time signals were acquired, lowpass-filtered (3 Hz) and demodulated with Synapse Essentials software (Tucker Davis Technologies). The ANY-maze tracking system program (Stoelting) was used to generate TTL signals to time-stamp specific events during EDT (that is, entrance in the zone). Data were extracted from TDT files and analyzed using custom MATLAB scripts.

Calcium signal analyses

First, bleaching was corrected by fitting a double-exponential decay to the fluorescent signal, capturing the exponential decay of the isosbestic (405 nm). Subsequently, the raw signal was divided by the fitted decay and *z*-score normalization was performed to standardize the signal by expressing it in terms of units of s.d.

For the PSTH analysis, the signal was aligned to behavioral outcomes (entrance in the zone), considering a baseline preceding the events ($T = 5$ s) and a baseline following the events ($T = 5$ s). The PSTH quantities were then obtained by subtracting the mean of the baseline activity from the restricted signal and then dividing by the s.d. of the same. Average plots of PSTH were represented as the mean and s.e.m., combining all the behavioral outcomes across all the mice. AUCs of the peristimulus curves were computed over an interval of 5 s after the entrance in the zone (at time $T = 0$).

Histology

At the end of the behavioral procedures, we checked viral expression and the position of the optic fibers and GRIN lenses. Mice were deeply anesthetized (urethane 20%) and transcardially perfused with 4% paraformaldehyde in PBS at pH 7.4. Brains were dissected, fixed overnight and cryoprotected in 30% sucrose in PBS. Coronal sections (40 μm) were cut using a HM450 microtome (Thermo Fisher Scientific). For GFP and SOM immunohistochemical studies, free-floating sections of selected areas were washed in PBS three times for 10 min, then

permeabilized in PBS plus 0.4% Triton X-100 for 30 min and finally blocked by incubation in PBS plus 4% normal goat serum (NGS) and 0.2% Triton X-100 for 30 min (all at room temperature, 20–23 °C). Slices were subsequently incubated with a rabbit anti-GFP polyclonal antibody (1:1,000; Thermo Fisher Scientific, A-11122) or rat anti-SOM monoclonal antibody (1:200, clone-YC7; Millipore, MAB354) diluted in PBS plus 2% NGS and 0.1% Triton X-100 overnight at 4 °C. Incubated slices were washed three times in PBS plus 1% NGS for 10 min at room temperature, incubated for 2 h at room temperature with Alexa Flour 488 goat anti-rabbit IgG (1:1,000; Thermo Fisher Scientific, A11034) or Alexa Flour 488 goat anti-rat IgG (1:500; Thermo Fisher Scientific, A48262) diluted in PBS plus 2% NGS and 0.1% Triton X-100 and subsequently washed three times in PBS for 10 min at room temperature. For mCherry immunohistochemical studies, free-floating sections of selected areas were washed in PBS three times for 10 min and permeabilized in PBS plus 1% Triton X-100 and 10% NGS for 1 h at room temperature. Slices were subsequently incubated with a rabbit anti-dsRED polyclonal antibody (1:1,000; Takara Bio, 632496) diluted in PBS plus 1% NGS and 0.3% Triton X-100 overnight at room temperature. Incubated slices were washed three times in PBS for 10 min, incubated for 2 h at room temperature with a 1:1,000 dilution of Alexa Flour 568 goat anti-rabbit IgG (1:1,000; Thermo Fisher Scientific, A11036) in PBS plus 1% NGS and 0.3% Triton X-100 and subsequently washed three times in PBS for 10 min at room temperature. The sections were mounted on slides and covered with cover slips. All images were acquired on a Nikon 1 confocal laser scanning microscope (Nikon). Digitalized images were analyzed using Fiji (version 2.0.0, National Institutes of Health).

cFos experiments

CRF-cre mice were unilaterally injected into the mPFC with either DIO-EYFP or DIO-eNpH3.0-EYFP and implanted with an optic fiber (Thorlabs, FT200UMT and CFLC230-10). After 7 days of recovery, mice were plugged into the patch cord and left in their cage for 20 min before the test. During this habituation period, a demonstrator mouse underwent restraint stress for 15 min. Then, the stress mouse was introduced, confined under a pencil cup, into the cage of the subject mouse for 5 min. All subject mice were tested with the 532-nm laser on. After this, the stress mouse was removed and the subject mouse was left in the cage without food and water for 45 min. After this period, all subject mice were perfused for immunohistochemistry analysis.

Mice were anesthetized using isoflurane and then perfused with 10 ml of saline. Brains were quickly extracted and incubated in 4% PFA overnight. After 1 h washing in PBS + glycine (0.3 M), 50-µm slices were prepared using a Leica VT1000S vibratome (Leica Biosystems). Slices were incubated overnight at 4 °C with rabbit anti-cFos polyclonal antibody (1:1,000; Abcam, ab190289) diluted in PBS with 0.5% Triton X-100 in PBS. Slices were then washed in PBS and incubated in a secondary antibody (1:500, goat anti-rabbit 647; Thermo Fisher Scientific, A32733) for 2 h at room temperature. After washing in PBS, sections were incubated with Hoechst (1:1,000) for 10 min and then mounted using Fluoromount (Sigma-Aldrich). Cell counting was performed for each brain into three-quarter sections in which YFP^+ cells and the implant scar were visible. Pictures were acquired with Thunder Imager (Leica Microsystem) at a stack of 4.5 optical sections. Total YFP^+ and $cFos^+$ cells were counted to calculate the percentage of overlapping cells for each condition (DIO-EYFP or DIO-eNpH3.0-EYFP).

Statistics

Statistical analyses were performed using GraphPad Prism 10. Results are expressed as the mean ± s.e.m. Data distribution was tested using the D'Agostino and Pearson normality test. For the EDT behavioral analysis, sniffing was reported as the time in seconds and as a percentage to allow direct comparison between different experimental conditions. Specifically, emotion discrimination behavior was divided into three consecutive 2-min epochs, which were analyzed with the multiple *t*-test as previously described9. In the same way, the discrimination index was divided into three consecutive 2-min epochs and analyzed using two-way repeated-measures analysis of variance (RM ANOVA) in the presence of two experimental groups, while three-way RM ANOVA was used in the presence of four experimental groups. Sniffing toward stress demonstrators, grooming behavior and corticosterone levels of observers in different conditions were analyzed using paired or unpaired *t*-tests, depending on the samples. The grooming behavior of demonstrator mice in naive and negative self-experience conditions was analyzed using two-way ANOVA. The total social exploration of observer mice toward stress and neutral demonstrators was analyzed using two-way RM ANOVA in the presence of two experimental groups, while three-way RM ANOVA was used in the presence of four experimental groups. Correlation coefficients were calculated using Pearson correlation. Cumulative sniffing toward two demonstrators was analyzed by comparing two different experimental groups (that is, naive

versus self-experience or light off versus light on) and using three-way RM ANOVA. Comparison of the PSTH and AUC between naive and negative self-experienced observers was assessed by three-way ANOVA. Comparisons of average peaks frequency and amplitude between naive and negative self-experience conditions were analyzed using two-way ANOVA. Comparisons of average peaks frequency and amplitude before and during restraint stress were analyzed using Wilcoxon matched-pair signed-rank tests. Comparisons of DIO-EYFP or DIO-eNpH3.0-EYFP groups for the percentage of $cFos^+$ cells overlapping with YFP^+ cells were analyzed using a nested *t*-test. Bonferroni post hoc correction was used for multiple comparisons.

The accepted value for significance was $P < 0.05$. Numbers of mice are reported in the figure legends. The experiments reported in this work were repeated independently two to four times, using mice from at least three different generations. No statistical methods were used to predetermine sample size for single experiments. The animal numbers were based on estimation from previous studies, including our own published studies[8,9,10]. Mice were excluded post hoc when optic fiber placement or viral expression patterns were not appropriate (for example, outside the target region). For all behavioral tests, littermates were randomly assigned to the different groups. Experimenters were not blinded during data acquisition but all analyses were performed with blinding of the experimental conditions.

Extended data

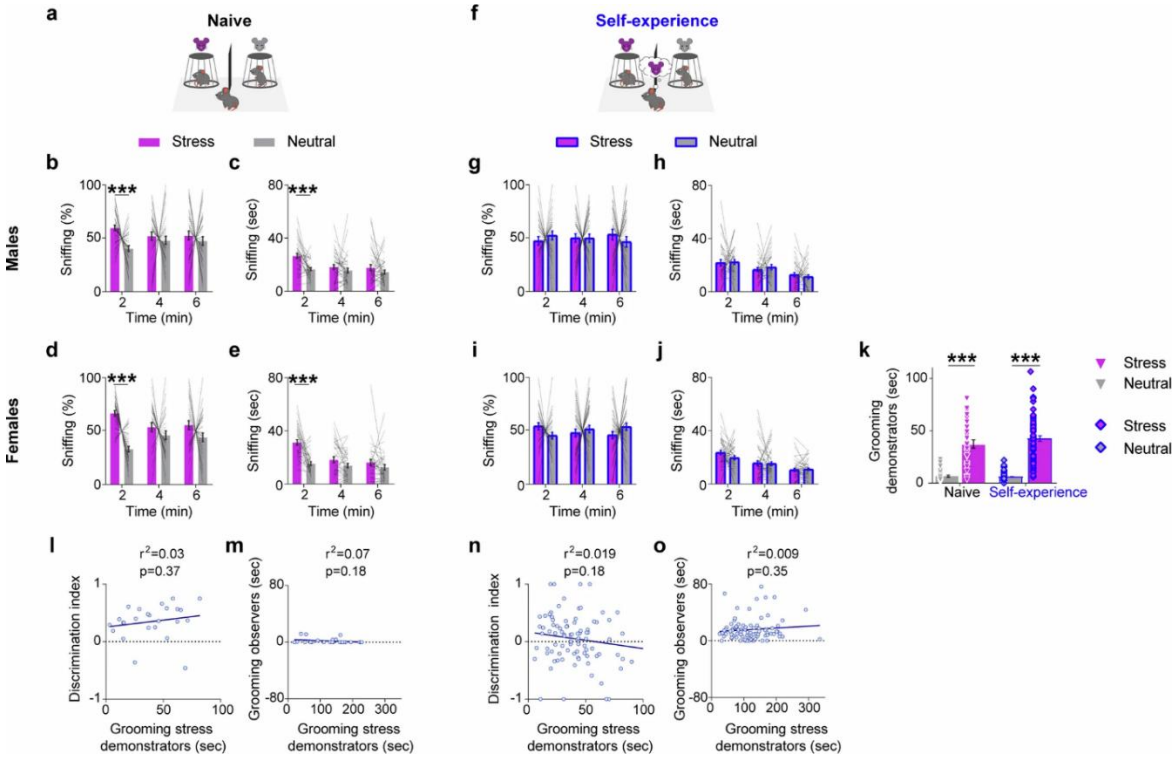

Extended Data Fig. 1 Emotion recognition in naive and restraint stress self-experienced male and female mice.

(a, f) Experimental design of the EDT with one restraint stress (purple) and one neutral (gray) demonstrator in (a) naive and (f) negative self-experience condition. (b, d, g, i) Percentage of time spent sniffing demonstrators in restraint stress (purple bars) or neutral (gray bars) state during the 6-min test, divided into three consecutive 2-min epochs, displayed by (b, g) male and (d, i) female (b, d) naïve and (g, i) self-experience observers (two-tailed multiple t-test, Bonferroni correction. N = 38 Naïve Males and 35 Naïve Females. mice. N = 38 Self-experience Males and 44 Self-experience Females). (c, e, h, j) Time spent sniffing demonstrators in restraint stress (purple bars) or neutral (gray bars) state during the 6-min test, divided into three consecutive 2-min epochs, displayed by (c, h) male and (e, j) female (c, e) naïve and (h, j) self-experienced observers (two-tailed multiple t-test, Bonferroni correction. N = 38 Naïve Males and 35 Naïve Females. N = 38 Self-experience males and 44 Self-experience Females). (k) Time spent grooming during the first 2 min of the test displayed by neutral (gray bars) or restraint stress (purple bars) demonstrators in naïve and restraint stress self-experience condition (two-way ANOVA, Bonferroni correction. N = 32 neutral and N = 32 restraint stress demonstrators). (l, n) No significant correlation was found between observers' discrimination index (in y axis) and restraint stress demonstrators' grooming (in x axis) during the first 2 min of the test in (l) naive and (n) self-experience condition (two-tailed Pearson correlation; N = 25 observers/condition and N = 25 restraint stress demonstrators/condition). (m, o) No correlation was found between observers' grooming behavior (in y axis) and restraint stress demonstrators' grooming (in x axis) during the first 2 min of the test in (m) naïve and (o) restraint stress self-experience condition (two-tailed Pearson correlation; N = 89 observers/condition and N = 89 stress demonstrators/condition). Bar and line graphs show mean ± s.e.m. ***P < 0.0005.

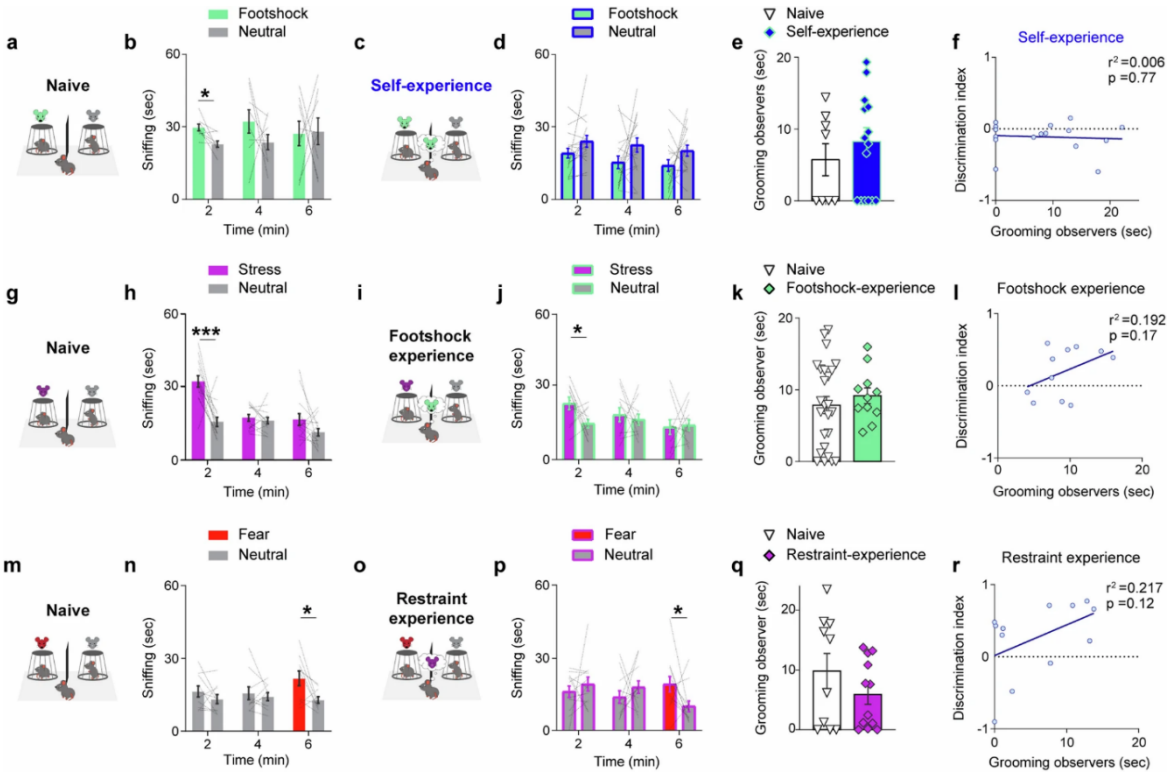

Extended Data Fig. 2 Effects of different stressful experiences on emotion recognition.

(a, c) Experimental design of the EDT with one footshock (green) vs one neutral (gray) demonstrator in (a) naïve and (c) footshock self-experienced observers. (b, d) Time (in seconds) spent sniffing demonstrators in footshock stress (green bars) or neutral (gray bars) state during the 6-min test, divided into three consecutive 2-min epochs, displayed by (b) naïve and (d) footshock self-experienced observer mice (two-tailed multiple t-test, Bonferroni correction. N = 8 naïve and 16 footshock self-experience observers). (e) Mice in naïve (white) and footshock self-experience (blue) condition do not differ based on the amount of time spent grooming across the 6 min test (two-tailed unpaired t-test; N = 8 naïve and N = 16 footshock self-experienced mice). (f) No significant correlation was found between discrimination index (in y axis) and grooming (in x axis) of footshock self-experienced observer (two-tailed Pearson correlation; N = 16 mice). (g, i) Experimental design of the EDT with one restraint stress (purple) vs one neutral (gray) demonstrator in (g) naïve and (i) footshock-experienced mice. (h, j) Time spent sniffing demonstrators in restraint stress (purple bars) or neutral (gray bars) state during the 6-min test, divided into three consecutive 2-min epochs, displayed by (h) naïve and (j) footshock-experienced observer mice (two-tailed multiple t-test, Bonferroni correction. N = 14 naïve and 11 footshock-experience observers). (k) Naïve (white) and footshock-experienced (green) observers did not differ based on the amount of time spent grooming across the 6 min test (two-tailed unpaired t-test; N = 25 naïve and N = 11 footshock-experienced mice). (l) No significant correlation was found between discrimination index (in y axis) and grooming (in x axis) of footshock-experienced observer (two-tailed Pearson correlation; N = 11 mice). (m, o) Experimental design of the EDT with one fear vs one neutral demonstrator in (m) naïve and (o) restraint-experienced mice. (n, p) Time spent sniffing demonstrators in fear (red bars) or neutral (gray bars) state during the 6-min test, divided into three consecutive 2-min epochs, displayed by (n) naïve and (p) restraint-experienced observer mice (two-tailed multiple t-test, Bonferroni correction. N = 10 naïve and

12 restraint-experience observers). (q) Naïve (white) and restraint-experienced observers (purple) did not differ based on the amount of time spent grooming across the 6 min test (two-tailed unpaired t-test; N = 10 naïve and N = 12 restraint-experienced mice). (r) No significant correlation was found between discrimination index (in y axis) and grooming (in x axis) of footshock-experienced observer (two-tailed Pearson correlation; N = 12 mice). Bar and line graphs show mean ± s.e.m. *P < 0.05, ***P < 0.0005.

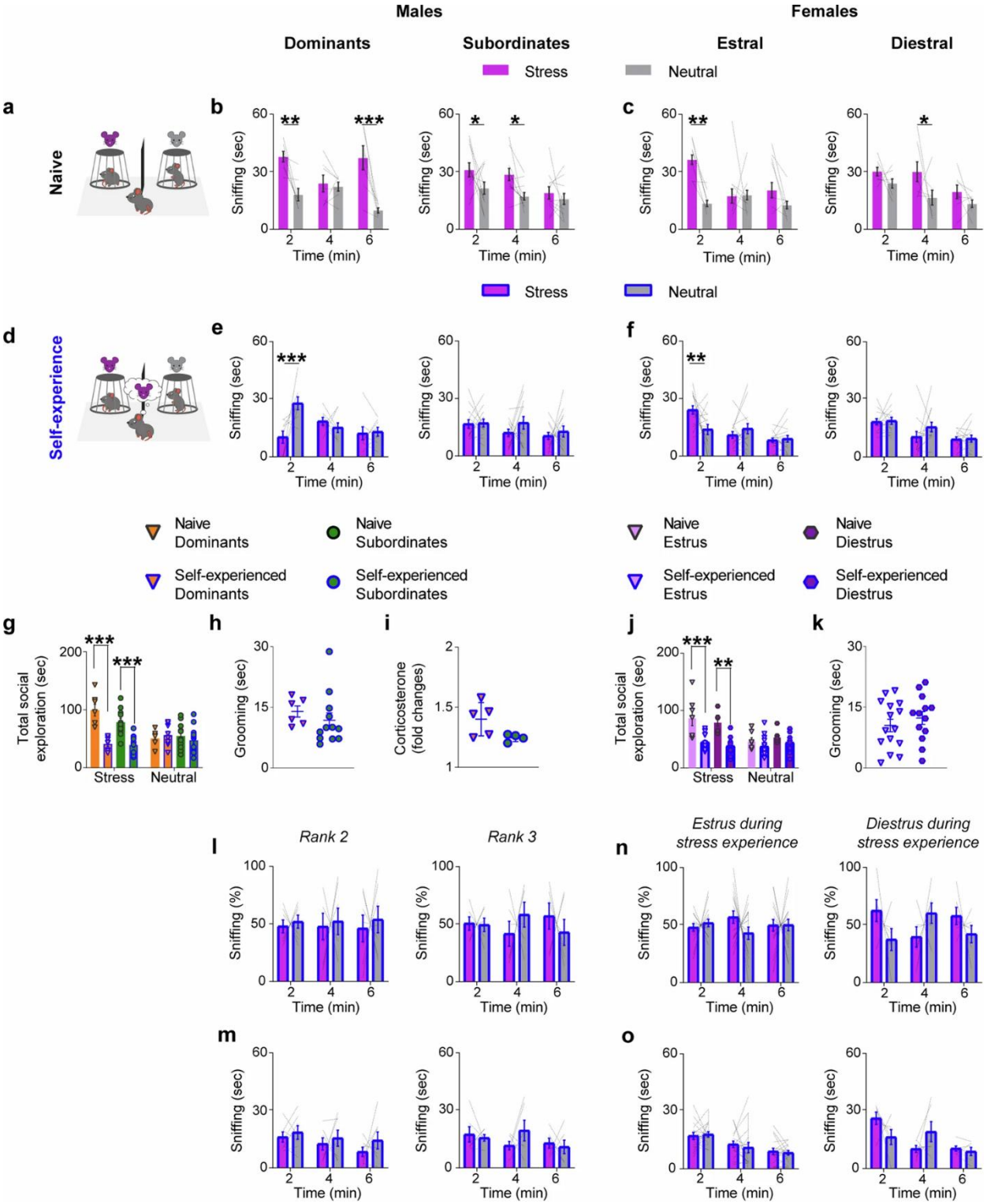

Extended Data Fig. 3 Social hierarchy and estrus cycle in negative self-experience modulation of emotion recognition.

(a, d) Experimental design of the EDT in (a) naïve and (d) self-experience condition. (b, e) Time spent sniffing demonstrators in stress (purple bars) or neutral (gray bars) state during the 6-min test, divided into three consecutive 2-min

epochs, displayed by (left) dominant or (right) subordinate (b) naïve and (e) self-experience males (two-tailed multiple t-test, Bonferroni correction. N = 8 dominant and 13 subordinate observers). (c, f) Time spent sniffing demonstrators in stress (purple bars) or neutral (gray bars) state during the 6-min test, divided into three consecutive 2-min epochs, displayed by (left) estral or (right) diestral (c) naïve and (f) self-experienced females (two-tailed multiple t-test, Bonferroni correction. (N = 7 naïve estral and 7 diestral observers; N = 15 self-experience estral and 13 diestral observers). (g) Both dominant and subordinate self-experienced observers differ from naïve mice in the total social exploration towards stress, but not neutral (Three-way RM ANOVA, Bonferroni correction; N = 7 naïve and 7 self-experienced dominants, N = 11 naïve and 13 self-experienced subordinates). (h) Time spent grooming (two-tailed unpaired t-test; N = 7 dominant and N = 13 subordinate mice) and (i) corticosterone levels (two-tailed unpaired t-test; N = 5 dominant and N = 4 subordinate mice) by self-experience dominant (orange) and subordinate (dark green) observers. (j) Both estral and diestral negative self-experienced observers significantly differ from naïve mice in the total social exploration towards stress, but not neutral, demonstrators (Three-way RM ANOVA, Bonferroni correction; N = 5 naïve and 15 self-experienced estral, N = 7 naïve and 13 negative self-experienced diestral). (k) Estral (light purple) and diestral (purple) self-experienced female mice do not differ in the time spent grooming across the 6 min test (two-tailed unpaired t-test; N = 15 estral and N = 13 diestral observers). (l, m) Time in (l) seconds or (m) percentage of time spent sniffing demonstrators in stress (purple bars) or neutral (gray bars) state during the 6-min test displayed by (left) rank 2 or (right) rank 3 self-experienced subordinate mice (two-tailed multiple t-test, Bonferroni correction. N = 7 rank 2 and 6 rank 3 observers). (n) Time in seconds and (o) percentage of time spent sniffing demonstrators in stress (purple bars) or neutral (gray bars) state during the 6-min test, which occurred 24 hr after self-experience, displayed by observer mice that were in (left) estrus or (right) diestrus when self-experience of stress occurred (two-tailed multiple t-test, Bonferroni correction. (N = 16 in estrus and 6 in diestrus). Bar and line graphs show mean ± s.e.m. *P < 0.05. **P < 0.005. ***P < 0.0005.

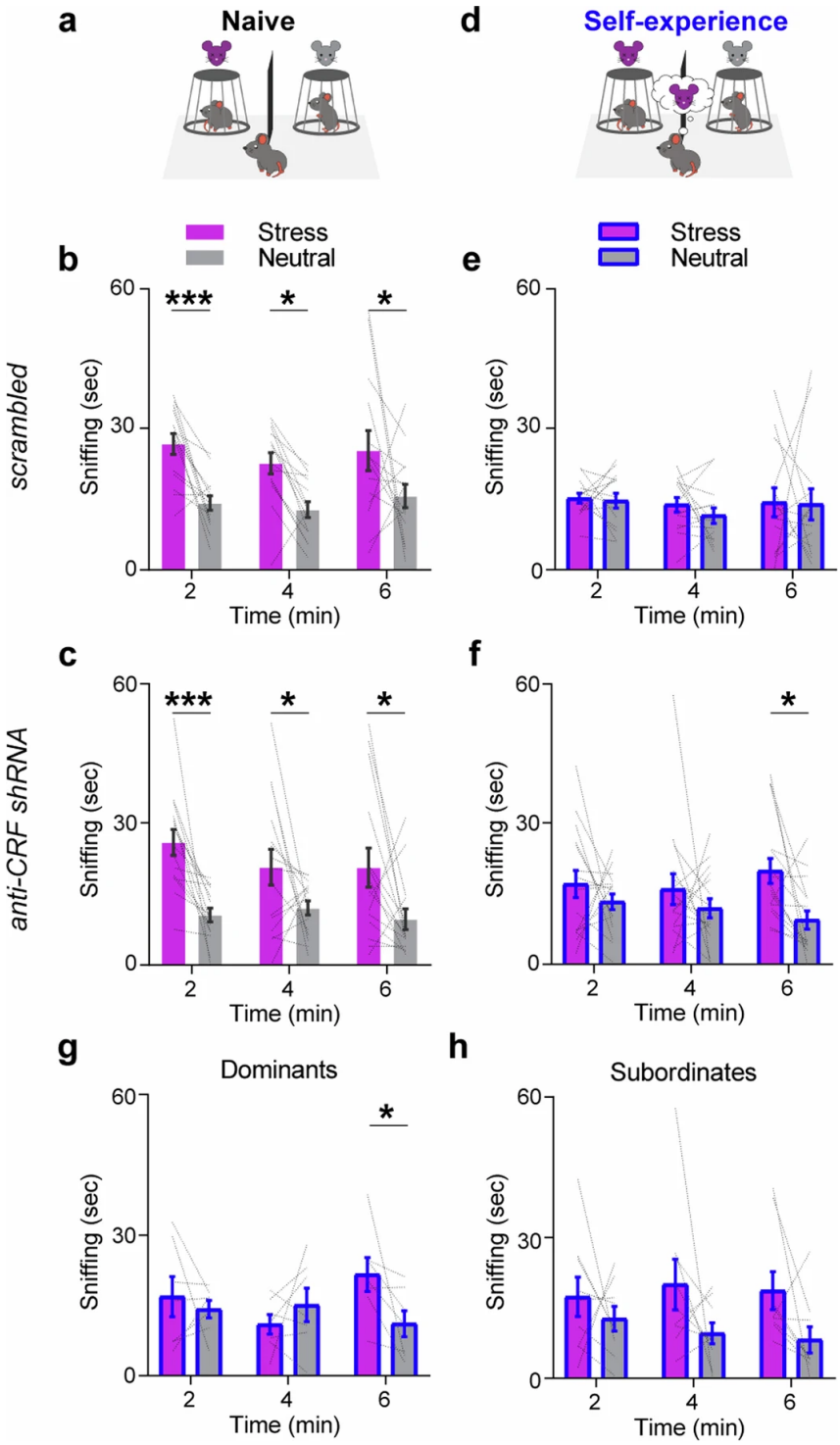

Extended Data Fig. 4 Silencing of CRF in mPFC modulates negative self-experience effect on stress emotion recognition.

(a, d) Experimental design of the EDT in (a) naïve and (d) negative self-experience condition. (b, c) Time spent sniffing demonstrators in stress (purple bars) or neutral (gray bars) state during the 6-min test, divided into three consecutive 2-min epochs, displayed by naïve (b) scrambled and (c) anti-CRF shRNA naïve observers (two-tailed multiple t-test, Bonferroni

correction. (b) SCRAMBLED. 2 min: P = 0.0002, 4 min: P = 0.01, 6 min: P = 0.01, N = 14 observers. (c) anti-CRF shRNA. 2 min: P = 0.0006; 4 min: P = 0.03; 6 min: P = 0.01; N = 15 observers). (e, f) Time spent sniffing demonstrators in stress (purple bars) or neutral (gray bars) state during the 6-min test, divided into three consecutive 2-min epochs, displayed by negative self-experienced (e) scrambled and (f) anti-CRF shRNA observers (two-tailed multiple t-test, Bonferroni correction. (e) SCRAMBLED: no significant differences; N = 14 observers. (f) anti-CRF shRNA. 6 min: P = 0.01; N = 16 observers). (g, h) Time spent sniffing demonstrators in stress (purple bars) or neutral (gray bars) state during the 6-min test, divided into three consecutive 2-min epochs, displayed by anti-CRF shRNA negative self-experienced (g) dominants and (h) subordinates (two-tailed multiple t-test, Bonferroni correction. (g) DOMINANTS. 6 min: P = 0.02; N = 7 mice. (h) SUBORDINATES. 6 min: P = 0.052; N = 9 mice). Bar and line graphs show mean ± s.e.m. *P < 0.05; ***P < 0.0005.

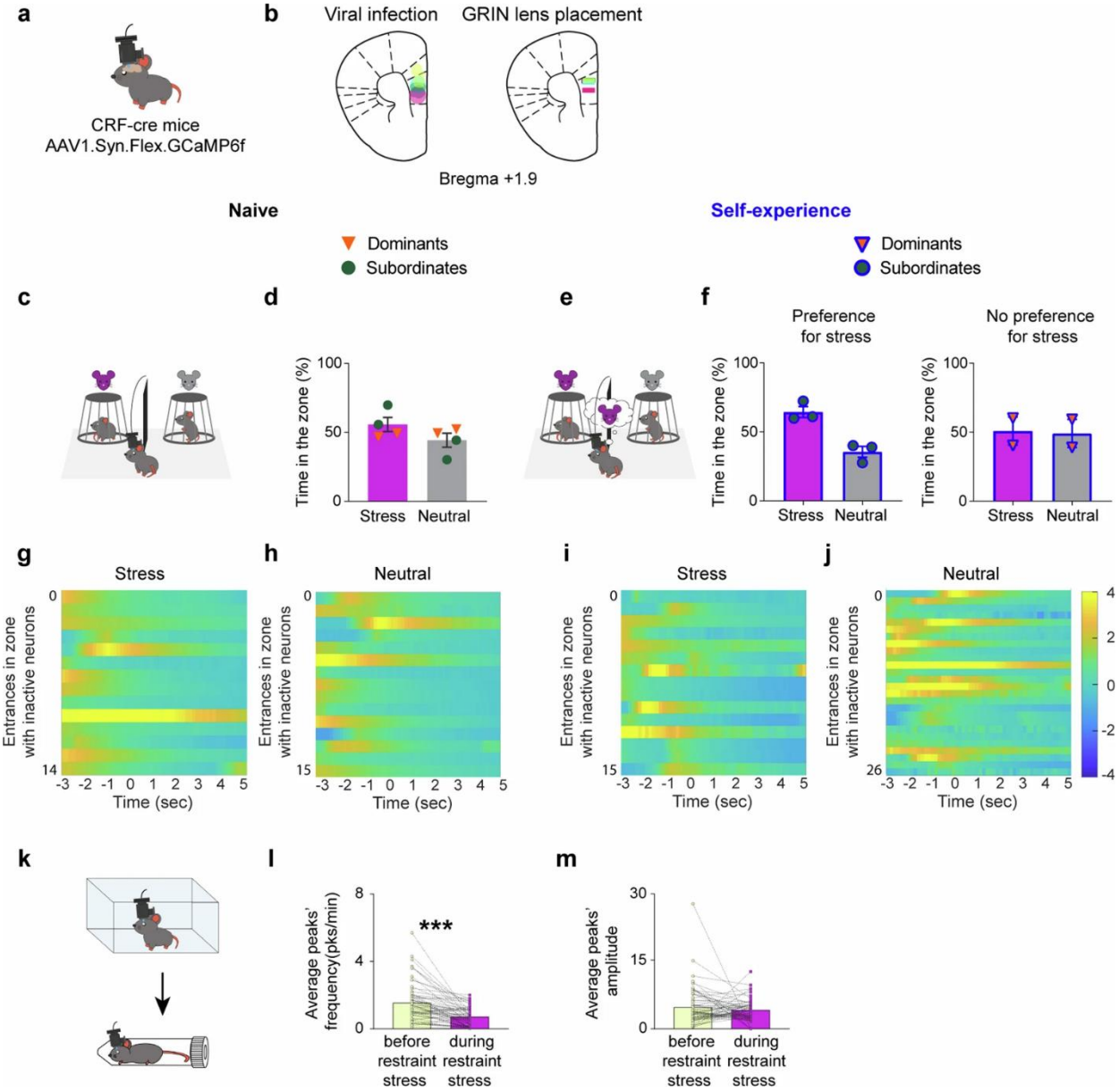

Extended Data Fig. 5 mPFC-CRF neurons activity during EDT and falcon restraint.

(a) CRF-Cre mice were injected into the mPFC with Syn.Flex.GCaMP6f.eYFP and implanted with a GRIN lens (n = 4/5mice). (b) Representative images of viral infection and GRIN lens placement of the five mice tested. (c, e) Experimental design of the EDT in (c) naïve and (e) negative self-experience condition. (d) Averaged percentage of time spent in the zone around a stress (purple bars) or a neutral (gray bars) demonstrator, displayed by naïve observers (two-tailed paired t-test; N = 4 observers). (f) Averaged percentage of time spent in the zone around a stress (purple bars) or a neutral (gray bars) demonstrator, displayed by negative self-experienced observers (left) with or (right) without preference towards stress demonstrators (two-tailed paired t-test. (left) Preference for stress: N = 3 mice. (right) No preference for stress: N = 2 mice. (g-j) Heatmaps of entrances in stress (g, i) or neutral (h, j) zone associated with neuronal inactivation in (g, h) naïve and (i, j) negative self-experience condition. (k) Experimental design: mice were placed for 10 min inside an empty cage (before restraint stress), and subsequently moved inside a 50 ml falcon for 30 min. (l, m) Average peaks' (l) frequency and (m) amplitude before (yellow) and after (purple) restrain stress (two-tailed Wilcoxon matched-pairs signed ranks test. (l) Number of pairs: 62, $p < 0.0001$. (m) Number of pairs: 62, $p = 0.84$). Bar and line graphs show mean ± s.e.m. ***$P < 0.0005$.

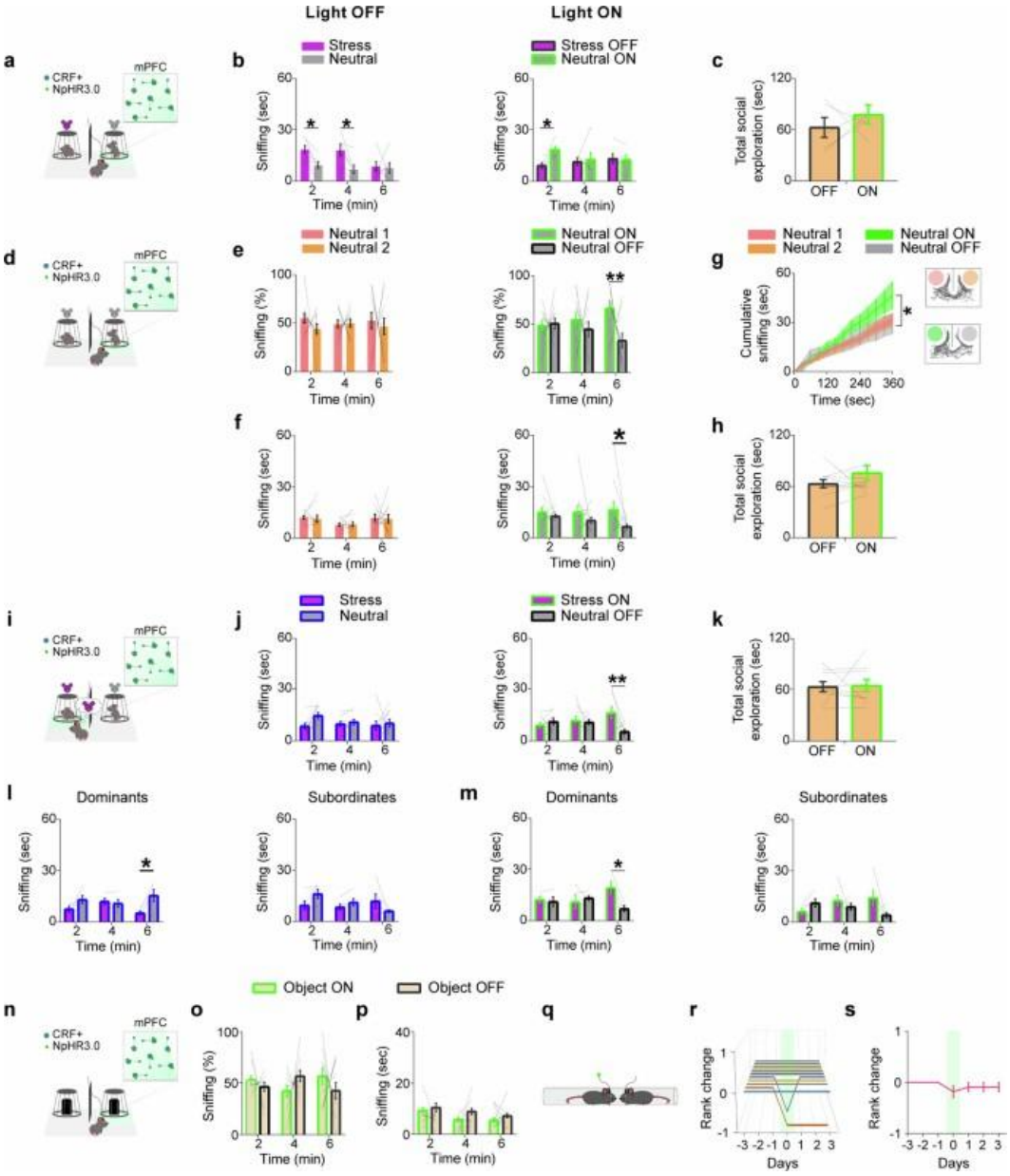

Extended Data Fig. 6 Optogenetic inhibition of mPFC-CRF neurons during Emotion Recognition, Object Discrimination and Tube Test.

(a) Experimental design of the EDT with one stress and one neutral demonstrator in naïve condition. Photoinhibition (λ = 532 nm) was paired to exploration of neutral demonstrator. (b) Time spent sniffing demonstrators in stress (purple bars) or neutral (gray bars) state during the 6-min test, divided into three consecutive 2-min epochs, displayed by naive observers tested in (left) light OFF and (right) light ON condition (two-tailed multiple t-test, Bonferroni correction. N = 5 observers/condition). (c) Total social exploration during the 6-min test, displayed by naive observers tested in light OFF and light ON condition (two-tailed paired t-test; N = 5 observers/condition). (d) Experimental design of the EDT with two neutral demonstrators in naïve condition. Photoinhibition (λ = 532 nm) was paired to the exploration of one demonstrator.

(e, f) Time spent sniffing two neutral demonstrators in (e) percentage or (f) seconds, during the 6-min test divided into three consecutive 2-min epochs, displayed by naïve observers tested in (left) light OFF or (right) light ON condition (two-tailed multiple t-test, Bonferroni correction. N = 11 observers/condition). (g) Left: Cumulative time spent sniffing two neutral demonstrators in light OFF and light ON conditions (three-way RM ANOVA; N = 11 observers). Right: representative tracking plot for light OFF (top) and light ON (bottom) conditions. (h) Total social exploration during the 6-min test, displayed by naïve observers tested in light OFF and light ON condition (two-tailed paired t-test; N = 11 observers/condition). (i) Experimental design of the EDT with one stress and one neutral demonstrator in self-experience condition. Photoinhibition (λ = 532 nm) was paired to exploration of stress demonstrator. (j) Time spent sniffing demonstrators in stress (purple bars) or neutral (gray bars) state during the 6-min test, divided into three consecutive 2-min epochs, displayed by self-experience observers tested in (left) light OFF and (right) light ON condition (two-tailed multiple t-test, Bonferroni correction. N = 9 observers/condition). (k) Total social exploration during the 6-min test, displayed by negative self-experienced observers tested in light OFF and light ON condition (two-tailed paired t-test; N = 9 observers/condition). (l, m) Time spent sniffing demonstrators in stress (purple bars) or neutral (gray bars) state during the 6-min test, divided into three consecutive 2-min epochs, displayed by self-experience (left) dominant or (right) subordinate mice tested in (l) light OFF and (m) light ON condition (two-tailed multiple t-test, Bonferroni correction. N = 4 dominant and 5 subordinate observers). (n) Experimental design of the EDT with two inanimate objects in naïve condition. Photoinhibition (λ = 532 nm) was paired to exploration of one of the two objects. (o, p) Time spent sniffing two objects in (o) percentage or (p) seconds, during the 6-min test divided into three consecutive 2-min epochs, displayed by naïve observers. (two-tailed multiple t-test, Bonferroni correction. N = 10 observers). (q) Experimental design of photoinhibition (λ = 532 nm) during tube test performed on cages of two or three mice. (r) Summary of mPFC-CRF neurons photoinhibition–induced rank change. Each line represents one animal. (s) Mean rank change induced by mPFC-CRF neurons photoinhibition. N = 11 mice. Bar and line graphs show mean ± s.e.m. *P < 0.05. **P < 0.005.

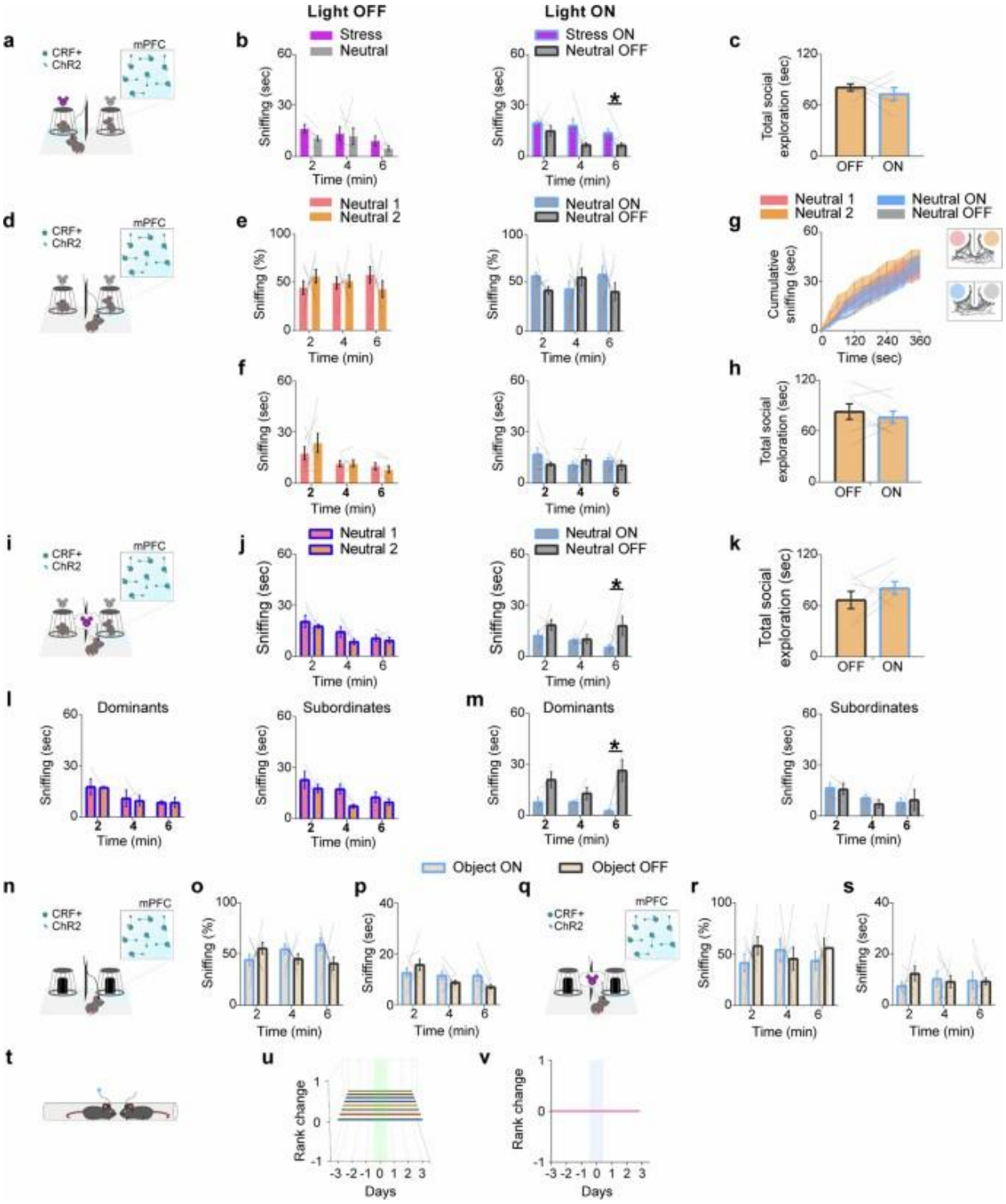

Extended Data Fig. 7 Optogenetic activation of mPFC-CRF neurons during Emotion Recognition, Object Discrimination and Tube Test.

(a) Experimental design of the EDT with one neutral and one stress demonstrator in naive condition. Photostimulation (λ = 473 nm) was paired with one stress demonstrator. (b) Time spent sniffing demonstrators in stress (purple bars) or

neutral (gray bars) state during the 6-min test, divided into three consecutive 2-min epochs, displayed by naïve observers tested in (left) light OFF and (right) light ON condition (two-tailed multiple t-test, Bonferroni correction. N = 6 observers/condition). (c) Total social exploration during the 6-min test, displayed by self-experience observers tested in light OFF and light ON condition (two-tailed paired t-test; N = 6 observers/condition). (d) Experimental design of the EDT with two neutral demonstrators in naive condition. Photostimulation (λ = 473 nm) was paired to exploration of one of the two neutral demonstrators. (e, f) Time spent sniffing two neutral demonstrators in (e) percentage or (f) seconds, during the 6-min test divided into three consecutive 2-min epochs, displayed by naïve observers tested in (left) light OFF and (right) light ON condition (two-tailed multiple t-test, Bonferroni correction. N = 7 observers/condition). (g) Left: Cumulative time spent sniffing two neutral demonstrators in light OFF and light ON conditions (three-way RM ANOVA). Right: representative tracking plot for light OFF (top) and light ON (bottom) conditions. N = 7 observers/condition. (h) Total social exploration during the 6-min test, displayed by naïve observers tested in light OFF and light ON condition (two-tailed paired t-test; N = 7 observers/condition). (i) Experimental design of the EDT with two neutral demonstrators in self-experience condition. Photostimulation (λ = 473 nm) was paired to exploration of one of two neutral demonstrators. (j) Time spent sniffing two neutral demonstrators during the 6-min test, divided into three consecutive 2-min epochs, displayed by self-experienced observers tested in (left) light OFF and (right) light ON condition (two-tailed multiple t-test, Bonferroni correction. N = 5 observers/condition). (k) Total social exploration during the 6-min test, displayed by naive observers tested in light OFF and light ON condition (two-tailed paired t-test; N = 6 observers/condition). (l, m) Time spent sniffing two neutral demonstrators during the 6-min test, divided into three consecutive 2-min epochs, displayed by negative self-experienced (left) dominant and (right) subordinate mice tested in (l) light OFF and (m) light ON condition (two-tailed multiple t-test, Bonferroni correction. N = 3 observers/condition). (n, q) Experimental design of the EDT with two inanimate objects in (n) naïve or (q) self-experience condition. Photostimulation (λ = 473 nm) was paired to exploration of one of the two object. (o, r) Percentage of time spent sniffing two objects during the 6-min test, divided into three consecutive 2-min epochs, displayed by (o) naïve or (r) self-experienced observers (two-tailed multiple t-test, Bonferroni correction. N = 8 naïve and 7 self-experience observers). (p, s) Time spent sniffing two objects during the 6-min test, divided into three consecutive 2-min epochs, displayed by (p) naïve or (s) self-experienced observers (two-tailed multiple t-test, Bonferroni correction. N = 8 naïve and 7 self-experience observers). (t) Experimental design of photostimulation (λ = 473 nm) during tube test performed on cages of two mice. (u) Summary of mPFC-CRF neurons photostimulation–induced rank change. Each line represents one animal. (v) Mean rank change induced by mPFC CRF neurons photostimulation. Bar and line graphs show mean ± s.e.m. *P < 0.05.

Bibliography

1. Adolphs, R. Neural systems for recognizing emotion. Curr. Opin. Neurobiol. 12, 169–177 (2002).

2. Preston, S. D. & de Waal, F. B. Empathy: its ultimate and proximate bases. Behav. Brain Sci. 25, 20–71 (2002).

3. Israelashvili, J., Sauter, D. A. & Fischer, A. H. Different faces of empathy: feelings of similarity disrupt recognition of negative emotions. J. Exp. Soc. Psychol. 87, 103912 (2020).

4. Zaki, J. Empathy: a motivated account. Psychol. Bull. 140, 1608–1647 (2014).

5. Olderbak, S. & Wilhelm, O. Emotion perception and empathy: an individual differences test of relations. Emotion 17, 1092–1106 (2017).

6. Allen-Walker, L. & Beaton, A. A. Empathy and perception of emotion in eyes from the FEEST/Ekman and Friesen faces. Pers. Individ. Dif. 72, 150–154 (2014).

7. Ferretti, V. & Papaleo, F. Understanding others: emotion recognition in humans and other animals. Genes Brain Behav. 18, e12544 (2019).

8. Ferretti, V. et al. Oxytocin signaling in the central amygdala modulates emotion discrimination in mice. Curr. Biol. 29, 1938–1953 (2019).

9. Scheggia, D. et al. Somatostatin interneurons in the prefrontal cortex control affective state discrimination in mice. Nat. Neurosci. 23, 47–60 (2020).

10. Dautan, D. et al. Cortico-cortical transfer of socially derived information gates emotion recognition. Nat. Neurosci. 27, 1318–1332 (2024).

11. Ben-Ami Bartal, I., Decety, J. & Mason, P. Empathy and pro-social behavior in rats. Science 334, 1427–1430 (2011).

12. Burkett, J. P. et al. Oxytocin-dependent consolation behavior in rodents. Science 351, 375–378 (2016).

13. Jeon, D. et al. Observational fear learning involves affective pain system and Cav1.2 Ca2+ channels in ACC. Nat. Neurosci. 13, 482–488 (2010).

14. Langford, D. J. et al. Social modulation of pain as evidence for empathy in mice. Science 312, 1967–1970 (2006).

15. Scheggia, D. et al. Reciprocal cortico-amygdala connections regulate prosocial and selfish choices in mice. Nat. Neurosci. 25, 1505–1518 (2022).

16. Smith, M. L., Asada, N. & Malenka, R. C. Anterior cingulate inputs to nucleus accumbens control the social transfer of pain and analgesia. Science 371, 153–159 (2021).

17. Iarocci, G., Yager, J. & Elfers, T. What gene–environment interactions can tell us about social competence in typical and atypical populations. Brain Cogn. 65, 112–127 (2007).

18. Deussing, J. M. & Chen, A. The corticotropin-releasing factor family: physiology of the stress

response. Physiol. Rev. 98, 2225–2286 (2018).

19. Papaleo, F., Kitchener, P. & Contarino, A. Disruption of the CRF/ CRF1 receptor stress system exacerbates the somatic signs of opiate withdrawal. Neuron 53, 577–589 (2007).

20. Sterley, T. L. et al. Social transmission and buffering of synaptic changes after stress. Nat. Neurosci. 21, 393–403 (2018).

21. Hostetler, C. M. & Ryabinin, A. E. The CRF system and social behavior: a review. Front. Neurosci. 7, 92 (2013).

22. Lim, M. M. et al. CRF receptors in the nucleus accumbens modulate partner preference in prairie voles. Horm. Behav. 51, 508–515 (2007).

23. Cooper, M. A. & Huhman, K. L. Corticotropin-releasing factor type II (CRF-sub-2) receptors in the bed nucleus of the stria terminalis modulate conditioned defeat in Syrian hamsters (Mesocricetus auratus). Behav. Neurosci. 119, 1042–1051 (2005).

24. de Leon Reyes, N. S. et al. Corticotropin-releasing hormone signaling from prefrontal cortex to lateral septum suppresses interaction with familiar mice. Cell 186, 4152–4171 (2023).

25. Kobayashi, T., Kiyokawa, Y., Takeuchi, Y. & Mori, Y. Pretreatment with CP-154526 blocks the modifying effects of alarm pheromone on components of sexual behavior in male, but not in female, rats. Chem. Senses 36, 623–632 (2011).

26. Grimm, S. et al. The interaction of corticotropin-releasing hormone receptor gene and early life stress on emotional empathy. Behav. Brain Res 329, 180–185 (2017).

27. Chen, P. et al. Prefrontal cortex corticotropin-releasing factor neurons control behavioral style selection under challenging situations. Neuron 106, 301–315 (2020).

28. Hiser, J. & Koenigs, M. The multifaceted role of the ventromedial prefrontal cortex in emotion, decision making, social cognition, and psychopathology. Biol. Psychiatry 83, 638–647 (2018).

29. Yuen, E. Y. et al. Acute stress enhances glutamatergic transmission in prefrontal cortex and facilitates working memory. Proc. Natl Acad. Sci. USA 106, 14075–14079 (2009).

30. McKlveen, J. M., Myers, B. & Herman, J. P. The medial prefrontal cortex: coordinator of autonomic, neuroendocrine and behavioural responses to stress. J. Neuroendocrinol. 27, 446–456 (2015).

31. Sanders, J., Mayford, M. & Jeste, D. Empathic fear responses in mice are triggered by recognition of a shared experience. PLoS ONE 8, e74609 (2013).

32. Bos, P. A. et al. Testosterone reduces functional connectivity during the ‘Reading the Mind in the Eyes’ test. Psychoneuroendocrinology 68, 194–201 (2016).

33. Machida, T., Yonezawa, Y. & Noumura, T. Age-associated changes in plasma testosterone levels in male mice and their relation to social dominance or subordinance. Horm. Behav. 15, 238–245 (1981).

34. Jones, C. E. & Monfils, M. H. Dominance status predicts social fear transmission in laboratory rats. Anim. Cogn. 19, 1051–1069 (2016).

35. Fan, Z. et al. Using the tube test to measure social hierarchy in mice. Nat. Protoc. 14, 819–831 (2019).

36. Guapo, V. G. et al. Effects of sex hormonal levels and phases of the menstrual cycle in the processing of emotional faces. Psychoneuroendocrinology 34, 1087–1094 (2009).

37. Mikosz, M., Nowak, A., Werka, T. & Knapska, E. Sex differences in social modulation of learning in rats. Sci. Rep. 5, 18114 (2015).

38. Cora, M. C., Kooistra, L. & Travlos, G. Vaginal cytology of the laboratory rat and mouse: review and criteria for the staging of the estrous cycle using stained vaginal smears. Toxicol. Pathol. 43, 776–793 (2015).

39. McLean, A. C., Valenzuela, N., Fai, S. & Bennett, S. A. Performing vaginal lavage, crystal violet staining, and vaginal cytological evaluation for mouse estrous cycle staging identification. J. Vis. Exp. 15, e4389 (2012).

40. Millan, M. J. & Bales, K. L. Towards improved animal models for evaluating social cognition and its disruption in schizophrenia: the CNTRICS initiative. Neurosci. Biobehav. Rev. 37, 2166–2180 (2013).

41. Locci, A., Yan, Y., Rodriguez, G. & Dong, H. Sex differences in CRF1, CRF, and CRFBP expression in C57BL/6J mouse brain across the lifespan and in response to acute stress. J. Neurochem. 158, 943–959 (2021).

42. Hupalo, S. et al. Corticotropin-releasing factor (CRF) circuit modulation of cognition and motivation. Neurosci. Biobehav. Rev. 103, 50–59 (2019).

43. Berridge, C. W., Martin, A. J., Hupalo, S. & Nicol, S. E. Estrus cycle-dependent working memory effects of prefrontal cortex corticotropin-releasing factor neurotransmission. Neuropsychopharmacology 47, 2016–2023 (2022).

44. Isaacson, J. S. & Scanziani, M. How inhibition shapes cortical activity. Neuron 72, 231–243 (2011).

45. Grynberg, D. & Lopez-Perez, B. Facing others' misfortune: personal distress mediates the association between maladaptive emotion regulation and social avoidance. PLoS ONE 13, e0194248 (2018).

46. Kim, E. J., Kim, E. S., Covey, E. & Kim, J. J. Social transmission of fear in rats: the role of 22-kHz ultrasonic distress vocalization. PLoS ONE 5, e15077 (2010).

47. Atsak, P. et al. Experience modulates vicarious freezing in rats: a model for empathy. PLoS ONE 6, e21855 (2011).

48. Toyoshima, M., Mitsui, K. & Yamada, K. Prior stress experience modulates social preference for stressed conspecifics in male rats. Neurosci. Lett. 765, 136253 (2021).

49. Larrieu, T. et al. Hierarchical status predicts behavioral vulnerability and nucleus accumbens metabolic profile following chronic social defeat stress. Curr. Biol. 27, 2202–2210 (2017).

50. Horii, Y. et al. Hierarchy in the home cage affects behaviour and gene expression in group-housed C57BL/6 male mice. Sci. Rep. 7, 6991 (2017).

51. Osorio, F. L., de Paula Cassis, J. M., Machado de Sousa, J. P., Poli-Neto, O. & Martin-Santos, R. Sex hormones and processing of facial expressions of emotion: a systematic literature review. Front. Psychol. 9, 529

(2018).

52. Mitchell, J. P., Banaji, M. R. & Macrae, C. N. The link between social cognition and self-referential thought in the medial prefrontal cortex. J. Cogn. Neurosci. 17, 1306–1315 (2005).

53. Adolphs, R. The neurobiology of social cognition. Curr. Opin. Neurobiol. 11, 231–239 (2001).

54. Adolphs, R. The social brain: neural basis of social knowledge. Annu. Rev. Psychol. 60, 693–716 (2009).

55. Frith, C. D. & Frith, U. Mechanisms of social cognition. Annu Rev. Psychol. 63, 287–313 (2012).

56. Kensinger, E. A. & Ford, J. H. Guiding the emotion in emotional memories: the role of the dorsomedial prefrontal cortex. Curr. Dir. Psychol. Sci. 30, 111–119 (2021).

57. Kai, Y. et al. A medial prefrontal cortex–nucleus acumens corticotropin-releasing factor circuitry for neuropathic pain-increased susceptibility to opioid reward. Transl. Psychiatry 8, 100 (2018).

58. Hupalo, S., Martin, A. J., Green, R. K., Devilbiss, D. M. & Berridge, C. W. Prefrontal corticotropin-releasing factor (CRF) neurons act locally to modulate frontostriatal cognition and circuit function. J. Neurosci. 39, 2080–2090 (2019).

59. Yizhar, O. et al. Neocortical excitation/inhibition balance in information processing and social dysfunction. Nature 477, 171–178 (2011).

60. Brockhurst, J., Cheleuitte-Nieves, C., Buckmaster, C. L., Schatzberg, A. F. & Lyons, D. M.Stress inoculation modeled in mice. Transl. Psychiatry 5, e537 (2015).

Chapter 4

Somatostatin neurons in the anterior cingulate cortex and the prelimbic cortex have different roles in emotion discrimination in mice

Anna Monai[1,2], Cinzia Molent[1,3], Federica Antonelli[1,2], Giulia Salamanca[4], Cristiano Bombardi[4], Filippo Drago[5], Claudio Bucolo[5], Gian Marco Leggio[5], Francesco Papaleo[1,2*]

[1]*Genetics of Cognition laboratory, Neuroscience area, Istituto Italiano di Tecnologia, Genova, Italy.*
[2]*IRCCS Ospedale Policlinico San Martino, Largo Rosanna Benzi, 10, 16132 Genova, Italy.*
[3]*CSM Area Noncello - Dipartimento di salute mentale e delle dipendenze (DDSM) - Pordenone*
[4] *Normal Veterinary Anatomy Service of the Department of Veterinary Medical Sciences of the University of Bologna, Italy.*
[5]*Department of Biomedical and Biotechnological Sciences, University of Catania, Catania, Italy.*

*Corresponding author: francesco.papaleo@iit.it

Abstract

Recognizing and responding to the emotions of others is critical for adaptive social behavior, yet the circuit mechanisms that support this ability remain poorly understood. Here we show that somatostatin-expressing (SOM) interneurons in the prelimbic cortex (PrL) and in the anterior cingulate cortex (ACC) make distinct contributions to emotion discrimination in mice. Using a validated behavioural paradigm combined with optogenetic manipulations, we found that inhibition of PrL SOM neurons abolished discrimination of affective states, whereas inhibition of ACC SOM neurons left discrimination intact and in some cases enhanced it. By contrast, optogenetic stimulation of SOM neurons in either region disrupted discrimination, suggesting that finely tuned excitatory–inhibitory balance, rather than uniform SOM activity, is essential for such important social ability. Circuit-mapping studies revealed that ACC SOM neurons project to multiple downstream targets, including the medial prefrontal cortex, the dorsal tenia tecta, and the amygdaloid regions, implicating them in a distributed network spanning cognitive and limbic systems. Together, these findings identify region-specific specializations of SOM interneurons within the prefrontal cortex and demonstrate their causal role in shaping emotional behavior. More broadly, they highlight the importance of inhibitory microcircuits in the distributed architecture of the social brain and point to circuit-level mechanisms that may be disrupted in psychiatric disorders characterised by impairments in emotion recognition.

Main

Emotions play a fundamental role in regulating social behavior across species, affecting communication, decision-making, conflict resolution, group cohesion, and collective dynamics ((Adolphs, 2001); (V. Ferretti & F. Papaleo, 2019); (Panksepp & Panksepp, 2013); (Schafer & Schiller, 2018); (van Kleef & Cote, 2022)). Identifying negative emotions in others can trigger a range of responses, from increased vigilance and threat avoidance to prosocial consolatory behavior ((Burkett et al., 2016); (LeDoux, 2000); (Phelps, 2006)). Given their crucial role in survival and social life, the ability to detect and respond to the emotions of others is evolutionarily conserved ((Adolphs, 2001); (Decety, 2011); (V. Ferretti & F. Papaleo, 2019); (Mason & Shan, 2017); (Millan et al., 2012); (Panksepp & Panksepp, 2013); (Raihani, 2021); (Schafer & Schiller, 2018)).

Our previous work has shown that prelimbic (PrL) somatostatin-expressing (SOM) neurons play a crucial role in recognizing emotions (Scheggia et al., 2020). We used a behavioural paradigm that assesses mice's ability to perceive, process, and respond to positive and negative emotional states in other mice ((Ferretti et al., 2019); (V. Ferretti & F. Papaleo, 2019); (Scheggia et al., 2020); (Dautan et al., 2024b); (Maltese et al., 2025)). This paradigm is similar to human emotion recognition tasks and examines social cognitive processes in mice that are distinct from sociability, social memory, and social reward. In the task, an ‘observer’ mouse is presented with two demonstrators, one in an altered emotional state and another in a neutral state, and interacts differently with them based on olfactory and visual cues.

Like the PrL, the anterior cingulate cortex (ACC, Brodmann area 24) is a sub-region of the medial prefrontal cortex and acts as a central hub for detecting and responding to others’ emotions in both rodents and humans ((Antonelli et al., 2025); (Carrillo et al., 2019); (Jeon et al., 2010); (Smith et al., 2021); (Zhang et al., 2024)). However, its role differs from that of the PrL (Keum et al., 2018). This study aims to investigate how these two closely connected regions contribute differently to emotion discrimination ((Utashiro et al., 2024); (Tomioka et al., 2005)), with a focus on optogenetic manipulation and whole brain mapping of SOM neurons in these two brain areas.

Results

Photo-inhibition of SOM+ interneurons in ACC does not affect affective state discrimination

The Anterior Cingulate Cortex (ACC) has been strongly linked to empathy-related behaviors (Apps et al., 2016). Empathy is defined as the capacity to acknowledge and understand another person's feelings, leading the observer to have a responsive reaction ((Post et al., 2014); (Mercer, 2002); (Stevenson, 2010)). The ACC has consistently been involved in these processes in humans (Arioli et al., 2021) and mice (Smith et al., 2021). In line with this, the ACC, particularly somatostatin-positive (SOM+) neurons in the ACC, has been shown to play a role in the social transfer of fear, supporting the ACC's role in emotional contagion (Keum et al., 2018). SOM+ neurons in the medial prefrontal cortex (PFC) have been reported to play a crucial role in emotion discrimination (Scheggia et al., 2020). It remains unclear whether SOM+ neurons in the ACC are also involved in emotion discrimination; thus, we decided to target them.

We began by bilaterally injecting AAV-DIO-eNpHR3.0 into the ACC of SOM-cre mice, and subsequently implanted optogenetic fibers terminating dorsally to this area (Fig. 1A). After handling and habituating both the observers and the demonstrators to the EDT apparatus, we performed for each the relief and the stress protocol (Fig. 1B, 1H). Some mice also underwent the neutral vs neutral, empty vs empty, sociability and social novelty protocols (Extended Fig. 1B, 1F, 1H, 1N). The mice received a continuous green light (530 nm, 5mW) in the whole apparatus during the first two minutes of the test, which is reported to be the most important for assessing emotion recognition ((Ferretti et al., 2019); (Scheggia et al., 2020); (Dautan et al., 2024b)). Without optogenetic manipulation, observer mice discriminated the stress (Fig. 1I, n mice=19), but had issues with the relief demonstrators (Fig. 1C, n mice=23). In contrast to inhibition of mPFC SOM neurons (Scheggia et al., 2020), inhibiting ACC SOM neurons did not alter stress recognition (Fig. 1I, 1L), looking at the total social interaction it transpired that the manipulated group interacted less with the stress demonstrators, however such difference was not significant (Fig. 1M, t=3.210, d.f.=72, p= 0.0119). Regarding the relief protocol, it shows an improvement for the manipulated group (Fig. 1C, $t = 2.834$, d.f. = 88, $P = 0.0342$), however, it is difficult to comment on that since the control did not work (Fig. 1C, t= 0.8440, d.f. =88,

p=0.6890) We tested also with green light activated only when the observer entered the altered-state mouse zone (Fig. 1F, 1N). For the relief, we noticed a slight preference for the altered mouse as the test progressed, although never significant throughout the test (Fig. 1G, min 4-6, p= 0.0776, n mice=7). What we noticed was that with the light on only when entering the altered mouse side, the preference in the control for the neutral was reduced (Fig. 1K). For the stress, no significant differences between the two experimental groups were noted in the first two minutes of the task (n mice=15). However, as the test progressed, the observer tended to spend less time socializing with the altered mouse (Fig. 1O, 1P, 1Q). However, the difference in total social exploration is not statistically significant (Fig. 1Q, p=0.1039). To check if the inhibition was causing social avoidance, we paired the stress protocol with the laser on only on the neutral demonstrator's side (Fig. 1R, n mice=5). We saw no differences in the first two minutes between the two experimental groups, then a preference for the altered mouse in the laser-on situation, counterbalanced by an avoidance of it in the last trial. Looking at the total social interactions, the manipulated group spend less time sniffing the demonstrators; however, this difference is not significant (Fig. 1U, p>0.9999). The inhibition of only one side does not cause side preference (Extended Fig. 1C, 1G) as proven by non-significant differences in the neutral vs neutral and empty vs empty protocols; nor does it disrupt sociability and social novelty (Extended Fig. 1I, 1O). In fact, observers inhibited only on the unfamiliar demonstrator's side, maintained a preference for the unfamiliar throughout the test, compared to the other two experimental groups (Extended Fig. 1P, laser on unfamiliar side, p=0.0100).

The photo-inhibition of ACC SOM does not affect the emotion discrimination ability, as the photo-inhibition of mPFC SOM (Scheggia et al., 2020). However, it seems to have an effect as time passes, especially on the sociability and social novelty (Extended Fig. 1I, 1O).

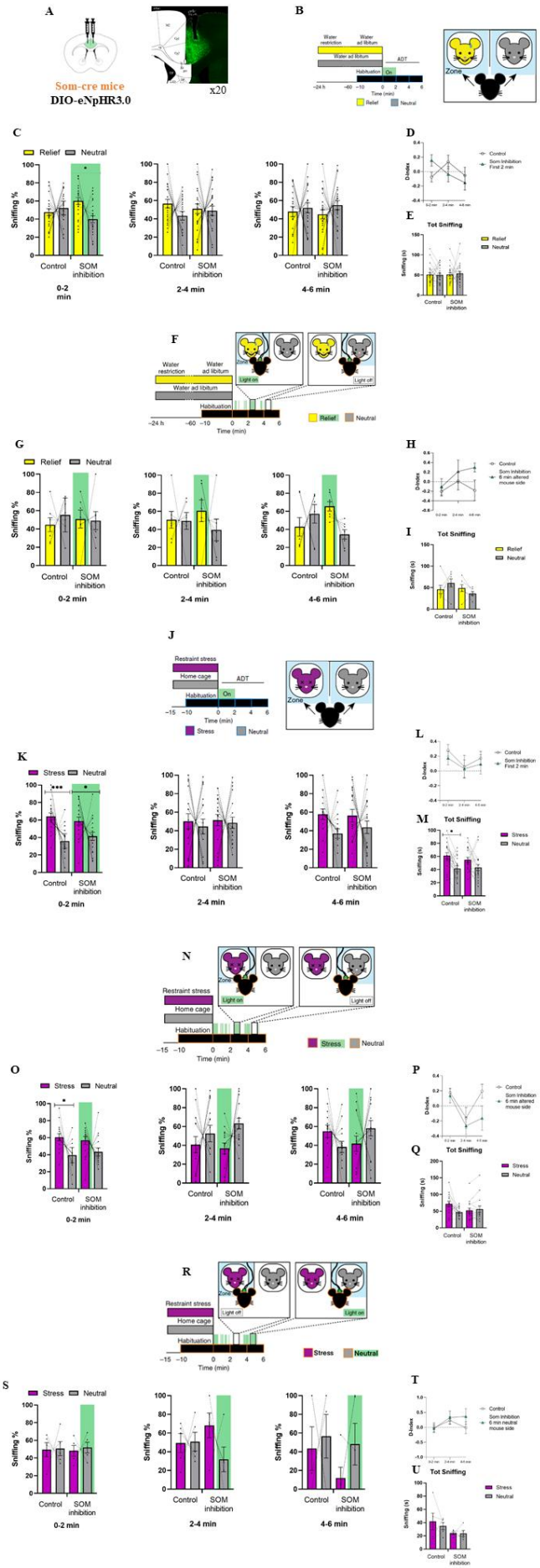
A
Som-cre mice
DIO-eNpHR3.0
x20
B
Water restriction
Water ad libitum
Habituation
ADT
On
Time (min)
Relief
Neutral
Zone
C
Relief
Neutral
Sniffing %
Control
SOM inhibition
0-2 min
2-4 min
4-6 min
D
D-index
Control
Som Inhibition First 2 min
E
Tot Sniffing
Sniffing (s)
F
Light on
Light off
G
H
Som Inhibition 6 min altered mouse side
I
J
Restraint stress
Home cage
Stress
Neutral
K
Stress
L
M
N
O
P
Som Inhibition 6 min altered mouse side
Q
R
Light off
Light on
S
Som Inhibition 6 min neutral mouse side
T
U

Figure 1. Photo-inhibition of SOM+ interneurons in ACC does not affect affective state discrimination

A, Left: SOM-Cre mice were bilaterally injected in the ACC with AAV-EF1a-DIO-eNpHR3.0-eYFP and implanted bilaterally with chronic optic fibers terminating dorsal to the injection area. Right: representative image of coronal ACC section. Findings were replicated in independent experiments with similar results. **B**, Mice were tested in the ADT with one relieved and one neutral demonstrator. Data derived from n = 23 mice. Photo-inhibition was performed for 2 min from the beginning of the test using continuous green light (λ = 532 nm), power 5 mW. **C**, Increased social investigation during optical inhibition of SOM+ cells (two-way repeated-measures ANOVA, affective state × light (off, on), Bonferroni correction, 2 min., F (3, 88) = 2.915, P=0.0387). **D**, **E**, No significant differences in the discrimination index nor in the cumulative sniffing (2-way ANOVA, Bonferroni correction, F (2, 88) = 3.140, P = 0.0992; one-way ANOVA, Bonferroni correction, P >0.9999). **F**, Mice were tested in the ADT with one relieved and one neutral demonstrator. Data derived from n =7 mice. Photo-inhibition with green light was paired to exploration of the relieved demonstrator's side (counterbalanced, left or right, across observers). **G**, No significant differences were noted across the two experimental groups (two-way repeated-measures ANOVA, affective state × light (off, on), Bonferroni correction, F (3, 24) = 0.2539, P=0.8578). **H**, **I**, No significant differences in discrimination indexes nor total social investigation across the two experimental groups (two-way ANOVA, Bonferroni correction, F (2, 24) = 0.9499, P=0.4008; one-way ANOVA, Bonferroni correction, P >0.9999). J, Mice were tested in the ADT with one stressed and one neutral demonstrator, and photoinhibition was performed during the first 2 min. Data derived from n = 19 mice. **K**, Increased exploration of the stressed demonstrator compared to the neutral demonstrator in both experimental groups (two-way repeated-measures ANOVA, affective state × light (off, on), Bonferroni correction, light off t=4.614, d.f. = 72, p=0.0001, light on t=2.848, d.f. =72, p=0.0343). **L**, no significant differences in discrimination index (2-way ANOVA, Bonferroni correction, F (2, 72) = 0.07607, P=0.9268), **M**, decreased social interaction toward altered mouse and increased toward neutral one in light on condition, not significant (one-way ANOVA, Bonferroni correction, P >0.9999), significant differences in total social interaction in light off condition (one-way ANOVA, Bonferroni correction, t=3.210, d.f. =72, p= 0.0119). **N**, Mice were tested in the ADT with one stressed and one neutral demonstrator. Data derived from n =15 mice. Photo-inhibition with green light was paired to exploration of the stressed demonstrator's side (counterbalanced, left or right, across observers). **O**, Increased exploration of the stressed demonstrator compared to the neutral demonstrator in both experimental groups, in light-on condition not significant (two-way repeated-measures ANOVA, affective state × light (off, on), Bonferroni correction, light off t=3.355, d.f. = 56, p=0.0001, light on t=2.848, d.f.=56, p=0.0086). Increased social interaction with neutral demonstrator in light on condition compared to the control group, not significant (two-way repeated-measures ANOVA, Bonferroni correction, p= 0.2126). At min 2-4, both groups show a preference for the neutral demonstrator, not significant (two-way repeated-measures ANOVA, affective state × light (off, on), Bonferroni correction, light off t=1.137, d.f. =56, p>0.9999, light on t=2.558, d.f. =56, p=0.0795. At min 4-6, preference toward neutral in light on condition, not significant (two-way repeated-measures ANOVA, Bonferroni correction, P=0.6884). **P**, **Q**, no statistically significant differences between experimental groups in discrimination index, nor total social exploration. Decreased social interaction in light on group compared to light off, not significant (two-way ANOVA, Bonferroni correction, F (2, 62) = 1.010, P=0.3701; one-way ANOVA, Bonferroni correction, p=0.3835). **R**, Mice were tested in the ADT with one stressed and one neutral demonstrator. Data derived from n =5 mice. Photo-inhibition with green light was paired to exploration of the neutral demonstrator's side (counterbalanced, left or right, across observers). **S**, **T**, **U**, No significant differences in experimental groups regarding social exploration across trials (two-way repeated-measures ANOVA, affective state × light (off, on), Bonferroni correction, light off t=0.1264, d.f. = 16, p=0.9997, light on t=0.3712, d.f. =16, p=0.9995). Light on condition did not statistically altered observers d-index nor total social exploration (two-way ANOVA, Bonferroni correction, F (2, 16) = 0.4701, P=0.6333; one-way ANOVA, Bonferroni correction, p>0.9999).

Photo-stimulation of SOM+ interneurons in ACC affects affective state discrimination

The results from photo-inhibiting ACC SOM were consistent with those reported in the literature (Keum et al., 2018). We did not have references for what their stimulation would do; what we did know, from previous work, was that the photo stimulation of SOM in PrL was creating side preference (Scheggia et al., 2020). To evaluate if this was too the case for ACC, we delivered pulsated blue light (380 nm, 5mW, 30Hz) paired to the entrance of the observer (n mice=3) in one of the two neutral demonstrators' side (counterbalanced left and right) for the entire duration of the test (Extended Fig. 2B). Strikingly, mice did not show a preference for the laser side. In the first two minutes the social exploration was balanced, it went down in the second trial for the laser side's demonstrator, but it picked up again in the last 2 minutes (Extended Fig. 2C). No avoidance was detected when looking at total sniffing (Extended Fig. 2D). We decided to add an emotional valence to the photo-stimulation, starting with delivering the pulsated blue light (380 nm, 5mW, 30Hz) for the first two minutes of the test, in the whole apparatus. In this condition, the observer's discrimination ability was impaired for both the relief (n mice=20) and stress (n mice=16) protocol (Fig. 2C, 2J, with the latter being the most significant affected (Fig. 2C, min 0-2, $F(3, 76) = 5.079$, $P=0.0029$; Fig. 2J, min 0-2, $F(3, 60) = 13.14$, $P<0.0001$). Social exploration was not disrupted in either of the tests (Fig. 2E, Fig. 2M). In the relief protocol, after the turning off of the laser, the mice did not regain the discrimination ability until the last 2 minutes of the test (Fig. 2C, 2D). The same behavior was noted in the stress protocol (Fig. 2K, 2L), but less pronounced than in the relief. To evaluate the limits of the photostimulation, we paired the laser with the entrance of the observer to the altered demonstrators' zones (counterbalanced, left and right, Fig. 2F, n mice=4; Fig. 2N, n mice=10). No significant effects were noted in the relief (Fig. 2F, 2G, 2H). In the stress, the laser slightly reduced the discrimination ability, but it was not disruptive (Fig. 2O, $F(3, 36) = 5.175$, $P=0.6934$; Fig. 2P, 2Q). The photostimulation did not affect their total social exploration. Like we did for the photo-inhibition (Fig. 1R), we checked if the photo-stimulation paired with the neutral demonstrator's zone would affect the behavior (Fig. 2R, n mice=4). While in the photo-inhibition we did not gather any significant effect, the photo-stimulation's data suggest a trend toward the exploration of the neutral demonstrator (Fig. 2S, 2U). No significant difference in index-discrimination was evinced (Fig. 2T, $F(1.729, 10.37) = 3.283$, $P=0.0834$). We performed also the sociability and social novelty tests paired with photo-stimulation in the first 2 minutes of

the test, in the whole apparatus (Extended Fig. 2F, Extended Fig. 2J, n mice=6). In these conditions, the social and social novelty discrimination was abolished already in the first two minutes (Extended Fig. 2G, $F(3, 20) = 8.014$, $P=0.0011$; Extended Fig. 2K, $F(3, 20) = 38.02$, $P<0.0001$). Even after turning off the laser, mice could not discriminate the unfamiliar mouse from the familiar one (Extended Fig. 2K, min 2.4, $F(3, 20) = 5.131$, $P=0.0086$). In both tests, photo-stimulation reduced the interest for the observer toward the novel mouse (Extended Fig. 2H, Extended Fig. 2L, 2M).

This could be explained by the important role the ACC covers in memory ((Bush et al., 2000); (Lenartowicz & McIntosh, 2005)): the photo-stimulation could have created an excitatory/inhibitory imbalance that interfered with the mice's social memory.

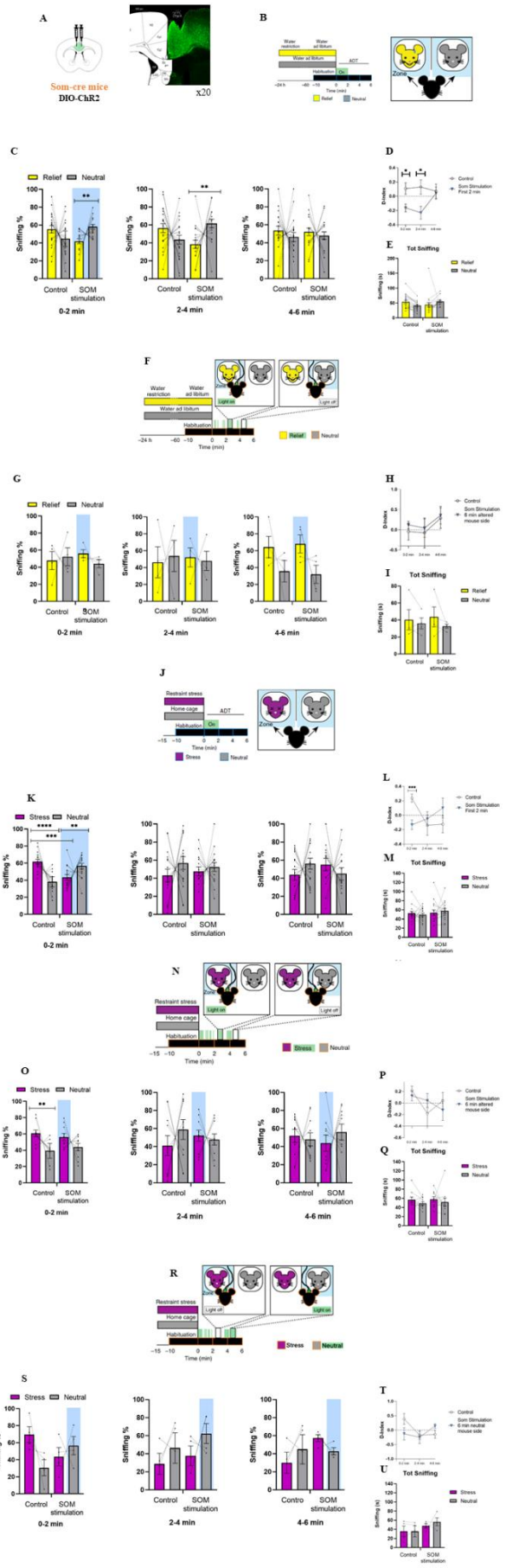
A
Som-cre mice
DIO-ChR2
x20
B
Water restriction
Water ad libitum
Habituation
ADT
On
Time (min)
Relief
Neutral
Zone
C
Relief
Neutral
Sniffing %
Control
SOM stimulation
0-2 min
2-4 min
4-6 min
D
Dindex
Control
Som Stimulation First 2 min
E
Tot Sniffing
Sniffing (s)
F
Light on
Light off
G
H
Som Stimulation 6 min altered mouse side
I
J
Restraint stress
Home cage
Stress
Neutral
K
L
M
N
O
P
Som Stimulation 6 min altered mouse side
Q
R
S
T
Som Stimulation 6 min neutral mouse side
U

Figure 2. Photo-stimulation of SOM+ interneurons in ACC affects affective state discrimination

A, Left: SOM-Cre mice were bilaterally injected in the ACC with AAV-EF1a-DIO-ChR2-eYFP and implanted bilaterally with chronic optic fibers terminating dorsal to the injection area. Right: representative image of coronal ACC section. Findings were replicated in independent experiments with similar results. **B**, Mice were tested in the ADT with one relieved and one neutral demonstrator. Data derived from n = 20 mice. Photo-stimulation was performed for 2 min from the beginning of the test using pulsating blue light (λ = 380 nm) at 30 Hz, power 5 mW. **C**, Increased exploration of the relieved demonstrator compared to the neutral demonstrator during the first 2 min of testing, which was abolished in the light-on condition (two-way repeated-measures ANOVA, affective state × light (off, on), $F(3, 76)=5.079$, $P=0.0029$), immediately after photo-stimulation of SOM+ neurons, the observer mouse kept interacting more with the neutral demonstrator than the relieved one (one-way repeated-measures ANOVA, Bonferroni correction, $P=0.0061$). **D**, the light-on condition impaired the affective state discrimination in the first 2 trials of the test (0-2 min., 2-4 min.) (two-way ANOVA, Bonferroni correction, trial 1 $t= 2.712$, d.f. $=33.32$, $p= 0.0315$; trial 2 $t= 2.653$, d.f. $= 37.56$, $p= 0.0349$). **E**, No difference in total sniffing across the two experimental groups (one-way ANOVA, Bonferroni correction, $p= 0.1481$). **F**, Mice were tested in the ADT with one relieved and one neutral demonstrator. Data derived from n =4 mice. Photo-stimulation with pulsating blue light was paired to exploration of the relieved demonstrator's side (counterbalanced, left or right, across observers). **G**, **H**, **I**, no difference in sniffing divided by trial, total sniffing or discrimination index (two-way repeated-measures ANOVA, affective state × light (off, on), $F(3, 12) = 0.4033$, $P=0.7533$; two-way ANOVA, Bonferroni correction, $F(2, 12) = 0.01781$, $P=0.9824$; one-way ANOVA, Bonferroni correction, $F(3, 12) = 0.2833$, $P=0.8365$). **J**, Mice were tested in the ADT with one stressed and one neutral demonstrator, and photo-stimulation was performed during the first 2 min. Data derived from n mice = 16. **K**, Increased exploration of the stressed demonstrator compared to the neutral demonstrator during the first 2 min of testing, which was abolished in the light-on condition (two-way repeated-measures ANOVA, affective state × light (off, on), Bonferroni correction; light off, $P<0.0001$; light on $P=0.0094$). As the test progressed, no statistical differences were noted across experimental groups. **L**, the light-on condition impaired the affective state discrimination in the first 2 minutes of the test (two-way ANOVA, Bonferroni correction, $t= 4.267$, d.f. $=29.22$, $P= 0.0006$). **M**, no difference in total social exploration (one-way ANOVA, Bonferroni correction, $F(3, 60) = 0.5334$, $P=0.6611$). **N**, Mice were tested in the ADT with one stressed and one neutral demonstrator. Data derived from n =15 mice. Photo-stimulation with pulsating blue light was paired to exploration of the stressed demonstrator's side (counterbalanced, left or right, across observers). **O**, Increased exploration of the stressed demonstrator compared to the neutral demonstrator during the first 2 min of testing, which was abolished in the light-on condition (two-way repeated-measures ANOVA, affective state × light (off, on), Bonferroni correction; light off, $P= 0.0059$; light on $P= 0.1370$). As the test progressed, mice from both experimental groups socialized more with the neutral mouse. **P**, **Q**, no statistical differences were noted in the two groups' discrimination indexes (two-way ANOVA, Bonferroni correction, $P=0.4134$) nor in the total social exploration (one-way ANOVA, Bonferroni correction, $F(3, 36) = 0.4552$, $P=0.7152$). **R**, Mice were tested in the ADT with one stressed and one neutral demonstrator. Data derived from n =4 mice. Photo-stimulation with pulsating blue light was paired to exploration of neutral demonstrator's side (counterbalanced, left or right, across observers). **S**, in the first trial, the control group had increased exploration of the stressed demonstrator compared to the neutral demonstrator; the light-on group had increased exploration of the neutral demonstrator instead. This difference was not statistically significant (two-way repeated-measures ANOVA, affective state × light (off, on), $F(3, 12) = 2.759$, $P=0.0882$). The light-on group increased their exploration toward the stressed demonstrator in the last trial. **T**, **U**, No difference in discrimination index (two-way ANOVA, Bonferroni correction, $P=0.0729$), light-on group had higher total social exploration for both the demonstrators than the control group, but not statistically significant (one-way ANOVA, Bonferroni correction, $F(3, 12) = 1.092$, $P=0.3898$).

Photo-stimulation of SOM+ interneurons in PrL affects affective state discrimination

We determined that photo-stimulation had a different effect on ACC SOM and PrL neurons in a neutral vs neutral setting (Extended Fig. 2C; (Scheggia et al., 2020)). The next question was whether photo-stimulation of PrL SOM neurons could disrupt emotion discrimination as well. We delivered pulsated blue light (380 nm, 5mW, 30Hz) for the first two minutes of the test, in the whole apparatus. We did not see a change in behavior with the relief (Fig. 3B, 3C, n mice=3). Mice that received the stimulation discriminated the affected state mouse throughout the test. In contrast, the control group preferred the neutral demonstrator in the last 2 minutes (Fig. 3C). Looking at the total social exploration, photo-stimulated mice spent less time interacting with the neutral demonstrator, but it was not statistically significant (Fig. 3E, $F(3, 8) = 1.004$, $P=0.4396$).

Next, we tested them in a stress protocol with pulsated blue light for the first two minutes of the test, in the whole apparatus (Fig. 3F, n mice=6). Similar to the photo-stimulation of ACC SOM neurons (Fig. 2K), the discrimination ability was abolished throughout the whole test ($F(3, 20) =11.63$, $P=0.0001$). The photo-stimulation reduced the total social exploration for the stressed mouse (Fig. 3I, $F(3, 20) = 0.8213$, $P=0.4974$) and flattened the discrimination index (Fig. 3H, $F(1.504, 15.04) = 0.7458$, $P=0.4547$). Since we knew that photo-stimulation cause side preference (Scheggia et al., 2020) we tested them in stress protocol with pulsated blue light paired with the stressed demonstrator's side (counterbalanced, left and right) (Fig. 3J, n mice=4). Photo-stimulation caused a reduction in social interaction with the stressed demonstrator in the first two minutes of the test (Fig. 3K, $F(3, 12) = 6.262$, $P=0.0084$), but not significant changes on discrimination index nor on total time spent social exploring (Fig. 3L, $F(1.555, 9.327) = 0.4985$, $P=0.5777$; Fig. 3M, $F(3, 20) = 0.8213$, $P=0.4974$).

The follow-up and last experiment we did was photo-stimulating in a stress vs stress protocol, all apparatus the first 2 minutes (Fig. 3N, n mice=3) and also paired with the entrance to one side (Fig. 3N, n mice=3; counterbalanced, left and right). Neither of the two manipulations caused evident discrepancy in social exploration (Fig. 3P, $F(3, 12) = 0.8348$, $P=0.5003$; Fig. 3Q, $F(1.857, 11.14) = 0.07643$, $P=0.9157$).

Overall, these findings show a different role of ACC SOM in emotion discrimination compared to PrL SOM, with the latter seemingly more sensitive to manipulations.

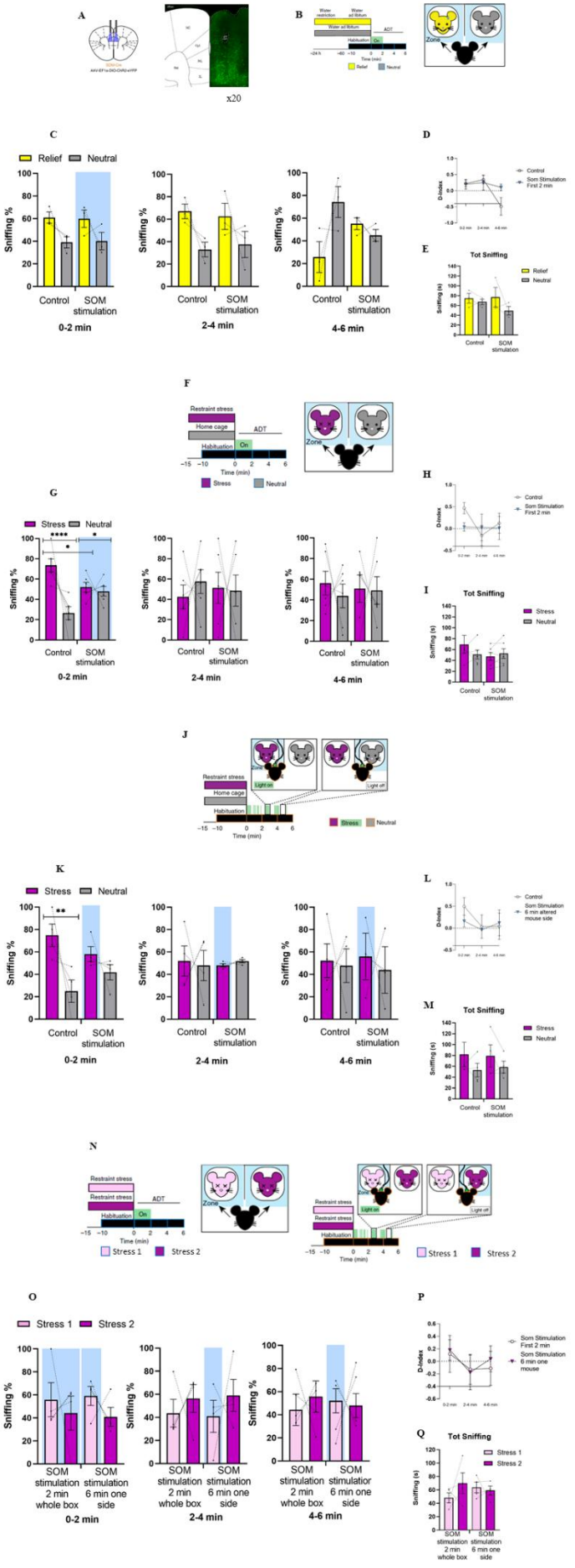
A
x20
B
Habituation
ADT
On
Relief
Neutral
Zone
C
Relief
Neutral
Sniffing %
Control
SOM stimulation
0-2 min
2-4 min
4-6 min
D
D-Index
Control
Som Stimulation First 2 min
E
Tot Sniffing
Sniffing (s)
F
Restraint stress
Home cage
Habituation
ADT
On
Time (min)
Stress
Neutral
G
Stress
Neutral
H
Som Stimulation First 2 min
I
J
Light on
Light off
K
L
Som Stimulation 6 min altered mouse side
M
N
Stress 1
Stress 2
O
SOM stimulation 2 min whole box
SOM stimulation 6 min one side
P
Som Stimulation First 2 min
Som Stimulation 6 min one mouse
Q

Figure 3. Photo-stimulation of SOM+ interneurons in PrL affects affective state discrimination

A, SOM-Cre mice were bilaterally injected in the PrL with AAV-EF1a-DIO-ChR2-eYFP and implanted bilaterally with chronic optic fibers terminating dorsal to the injection area. **B,** Mice were tested in the ADT with one relieved and one neutral demonstrator. Data derived from n = 3 mice. Photo-stimulation was performed for 2 min from the beginning of the test using pulsating blue light (λ = 380 nm) at 30 Hz, power 5 mW. **C,** No statistically significant differences were noted across the two experimental groups (two-way repeated-measures ANOVA, affective state × light (off, on), F (3, 8) = 3.479, P=0.0704). In the last 2 minutes of the test, the control groups increased their sniffing toward the neutral demonstrator. **D, E,** photo-stimulation decreased the social exploration for the neutral demonstrator (two-way ANOVA, Bonferroni correction, F (2, 8) = 2.494, P=0.1440; one-way ANOVA, Bonferroni correction, F (3, 8) = 1.004, P=0.4396). **F**, Mice were tested in the ADT with one stressed and one neutral demonstrator, and photo-stimulation was performed during the first 2 min. Data derived from n mice=6. **G**, photo-stimulation decreased social exploration toward stressed demonstrator and increased toward neutral demonstrator (two-way repeated-measures ANOVA, affective state × light (off, on), Bonferroni correction, light off, t=5.886, d.f. =20, p<0.0001, light on, t= 0.5064, d.f. =20, p= 0.6181; F (3, 20) = 11.63, P=0.0001). After the photo-stimulation, observers showed a slight increase in social exploration toward stressed demonstrators. **H,** photo-stimulation decreased discrimination index, not statistically significant (two-way ANOVA, Bonferroni correction, F (2, 20) = 0.7458, P=0.4871). **I,** photo-stimulation decreased total social exploration of stressed demonstrator, no effect on neutral demonstrator. Not statistically significant (one-way ANOVA, Bonferroni correction, F (3, 20) = 0.8213, P=0.4974). **J**, Mice were tested in the ADT with one stressed and one neutral demonstrator. Data derived from n mice=4. Photo-stimulation with pulsating blue light was paired to exploration of the stressed demonstrator's side (counterbalanced, left or right, across observers). **K**, photo-stimulation reduced social exploration toward stressed demonstrator and increased it toward neutral demonstrator (two-way ANOVA, affective state × light (off, on), light off, t=4.121, d.f. =12, p=0.0085; light on, t= 1.342, d.f. =12, p=0.4682; F (3, 12) = 6.262, P=0.0084). **L, M,** no statistically significant differences across experimental groups regarding discrimination index and total social exploration (two-way ANOVA, Bonferroni correction, F (2, 12) = 0.4985, P=0.6195; one-way ANOVA, Bonferroni correction, F (3, 12) = 0.6935, P=0.5735). **N**, Mice were tested in the ADT with stressed demonstrators. Photo-stimulation was performed for 2 min from the beginning of the test using pulsated blue light, and also paired to exploration of one of the stressed mice's sides (counterbalanced, left or right, across observers). Data derived from n = 4 mice. **O**, photo-stimulation on one side causes a trend in preferring the demonstrator on the stimulated side (two-way ANOVA, affective state × light (on2, on6), F (3, 12) = 0.5428, P=0.6622). **P,** discrimination index was not affect by photo-stimulation of any kind (two-way ANOVA, Bonferroni correction, F (2, 12) = 0.07643, P=0.9269) **Q**, photo-stimulation whole apparatus 2 minutes created a preference for one stressed mouse, not statistically significant. Photo-stimulation on one side did not cause a preference between the two demonstrators (one-way ANOVA, Bonferroni correction. F (3, 16) = 0.05126, P=0.984).

PrL SOM and ACC SOM project to different parts of the brain

Most SOM+ neurons target the apical part of pyramidal cells ((Urban-Ciecko & Barth, 2016); (Huang et al., 2024)), but a subset of them can project to other brain areas through long-range projections and form inhibitory loops ((Katona et al., 2016); (Bertero et al., 2019); (Dautan et al., 2024b)). To explain the different reactions of mPFC and ACC SOM to optogenetic manipulations (Fig, 1, 2, 3; (Scheggia et al., 2020)), we collaborated with the Normal Veterinary Anatomy Service of the Department of Veterinary Medical Sciences of the University of Bologna in collecting whole-brain tracing data. We used AAV-EF1a-DIO- eYFP injected either

in ACC or PrL in 6 Sa-CRE, 3 for each area. Photos were taken at injection and projection sites using an objective 40x (Fig. 4A), the IR% of each area was calculated using ImageJ and normalized on the average of Cingulate 1 and Cingulate 2's IR%. Notably, we discovered that the majority of ACC SOM+ neurons project to the near Infralimbic cortex (IL) with a calculated mean percentage of 64.61 ± 26.72%, followed by the prelimbic cortex (41.36±10.34%), the Dorsal Tenia Tecta (32.315±10.588%) and the Anterior Amygdaloidal Area Ventral (31.163±7.634%) (Fig. 4B). The areas with less IR% were the Ventral Pallidum (7.777±3.055), the Lateral Septal nucleus dorsal part (4.200±4.200%), the Medial Amygdala (3.129±0.280%) and the Lateral Orbital Cortex (0.866±0.866). We did not gather any data regarding the insula, an area of the brain with which the ACC has been confirmed to be very well connected ((Roy et al., 2012);(Keum et al., 2018)). From the literature, the orbitofrontal cortex is another well-connected area (Rolls, 2019); however, regarding the long-range somatostatin neurons, it is one of the least involved ones. This is fitting, since most connectivity research has been done using fMRI, which indirectly measures the areas' general neuronal activity by detecting changes in blood flow and oxygenation (Heeger & Ress, 2002). More refined analyses are needed, but with the data we already have, we could start creating a map of the whole brain for SOM inhibitory neurons.

For the PrL SOM projections we encountered some difficulties with the virus spreading too much and infecting the septum of all the mice we injected. We have started collecting the photos, but we do not have the quantified analysis yet.

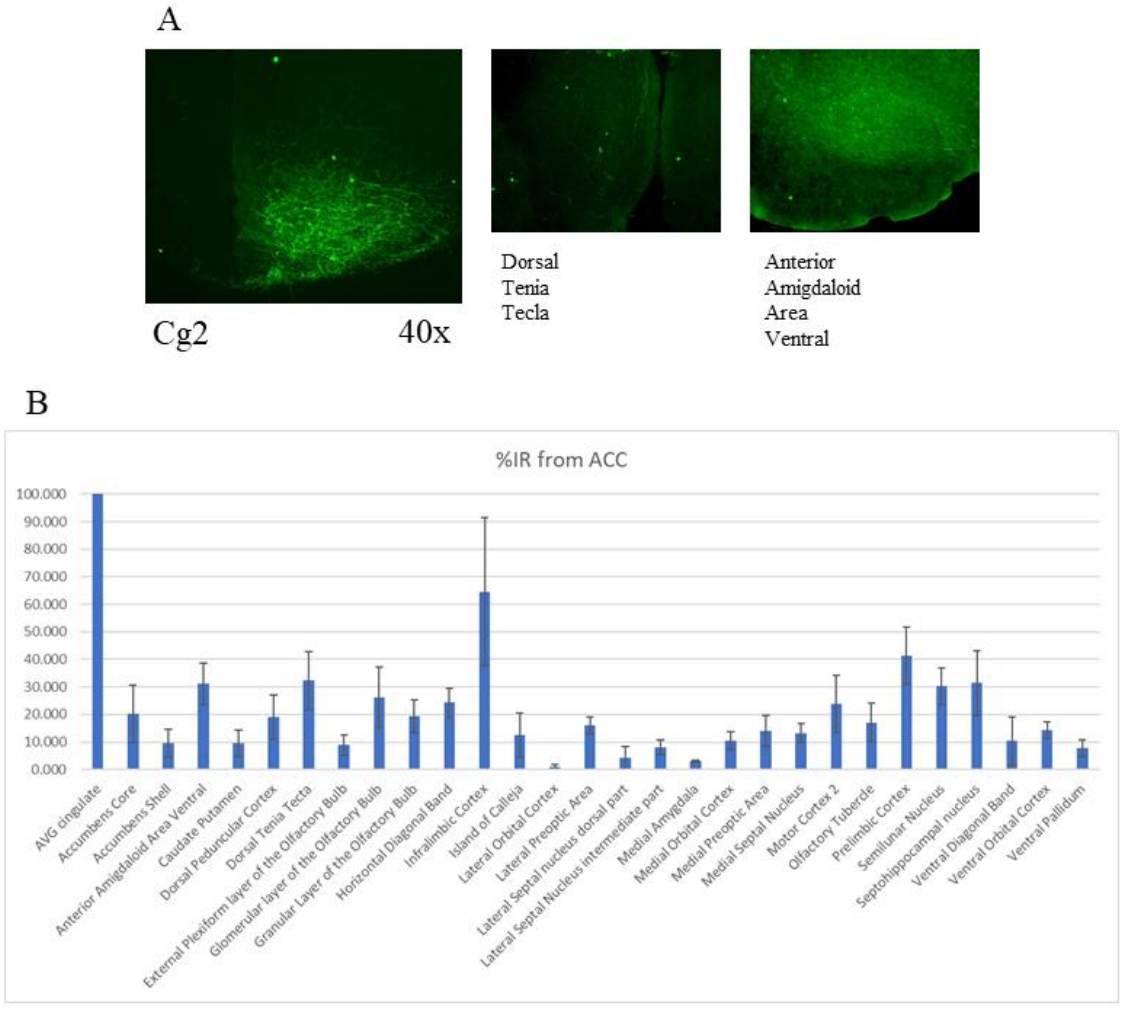

Figure 4. PrL SOM and ACC SOM project to different parts of the brain

A. SOM-Cre mice were bilaterally injected in the PrL and in the ACC with AAV-EF1a-DIO- eYFP. Data derived from n mice=3 for the ACC. N mice=3 for the mPFC. Representative images of photos taken at injection and projection sites. Objective 40x. **B,** the percentage of IR was evaluated quantitatively using ImageJ software and expressed as the percentage mean ± standard deviation. All data collected were normalized by dividing the IR of the single areas by the average IR of Cingulate 1 and Cingulate 2, then multiplying by 100. The majority of ACC SOM+ neurons project to the near infralimbic cortex (f64.61±26.72%) followed by the prelimbic cortex (41.36±10.34%), the Dorsal Tenia Tecta (32.315±10.588%) and the Anterior Amygdaloid Area Ventral (31.163±7.634%). The areas with less IR% were the Ventral Pallidum (7.777±3.055), the Lateral Septal nucleus dorsal part (4.200±4.200%), the Medial Amygdala (3.129±0.280%) and the Lateral Orbital Cortex (0.866±0.866).

Discussion

Emotion recognition and appropriate social responses are essential processes for individual well-being and for the functioning of a cohesive society. In this study, we investigated the role of somatostatin-expressing (SOM) interneurons in two key regions of the social brain—the prelimbic cortex (PrL) and the anterior cingulate cortex (ACC). Both areas are well-established hubs of social cognition ((Adolphs, 2009); (Amodio & Frith, 2006); (Scheggia et al., 2020); (Keum et al., 2018)) and are densely interconnected ((Utashiro et al., 2024); (Tomioka et al., 2005)).

Our findings demonstrate that SOM neurons in the ACC and PrL serve strikingly different roles in emotion discrimination, as revealed by their divergent responses to identical optogenetic manipulations. In line with prior work (Keum et al., 2018), we observed that inhibition of SOM neurons in the ACC did not abolish emotion discrimination, the first step in empathetic processing (de Waal, 2008). On the contrary, in some cases, inhibition appeared to enhance this ability (Fig. 1C). Interestingly, this manipulation did not suppress other social interactions (Extended Data 1), which starkly contrasts with the effects observed in the PrL, where SOM inhibition severely disrupted affective state discrimination (Scheggia et al., 2020)

Conversely, photo-stimulation of SOM neurons in the ACC led to deficits in emotion discrimination, with a pronounced impairment in social memory (Fig. 2, Extended Data 2). This may reflect the ACC's well-documented role in memory encoding and retrieval ((Bush et al., 2000); (Lenartowicz & McIntosh, 2005)), as well as its strong connectivity with the amygdala (Rolls, 2019), a region crucial for consolidating emotionally salient memories (Roozendaal et al., 2009) It is plausible that our manipulation influenced not only local circuitry but also downstream targets, including projections from the ACC to the anterior amygdaloid area and nearby limbic structures (Fig. 4).

It is important to note that SOM interneurons predominantly target the dendrites of pyramidal neurons (Wu et al., 2023). Therefore, optogenetic stimulation likely increased dendritic inhibition, thereby attenuating the pyramidal neurons' output. This heightened inhibition may explain the observed impairments in affective state discrimination. On the other hand, the absence of behavioral disruption during SOM inhibition suggests that while SOM neurons in the

ACC are engaged during social processing, they may not be strictly necessary for emotional information integration.

In the PrL, previous research has shown that pyramidal neurons are generally suppressed during affective state discrimination, and inhibiting local SOM neurons abolishes this ability (Scheggia et al., 2020). Therefore, one might expect that stimulating SOM neurons would mimic natural inhibitory dynamics. Surprisingly, our results demonstrated that photo-stimulation in the PrL also disrupted negative affective state discrimination, indicating a more complex relationship. These findings highlight that examining a single interneuron subtype in isolation may be insufficient to explain behavior: the brain functions via a finely tuned excitatory-inhibitory (E-I) balance ((Yizhar et al., 2011); (Sohal & Rubenstein, 2019)), and disruptions to this balance are often implicated in neuropsychiatric disorders (Lee et al., 2017).

Emotion discrimination is a multifaceted behavior, reliant on a distributed neural network. Though the medial prefrontal cortex (mPFC) plays a central role in social cognition, it does not act in isolation ((Frith & Frith, 2007); (Adolphs, 2009)). To explore this network-level interaction, in collaboration with the Normal Veterinary Anatomy Service at the University of Bologna's Department of Veterinary Medical Sciences, we mapped the downstream targets of SOM+ neurons in the PrL and ACC.

We confirmed that SOM+ projection neurons from the ACC prominently target the medial prefrontal cortex (mPFC), dorsal tenia tecta (dTT), and anterior amygdaloid area ventral (aAAV). The mPFC is widely recognized for its role in modulating social behaviors ((Adolphs, 2009); (Amodio & Frith, 2006); (Friedman & Robbins, 2022); (Kietzman & Gourley, 2023)). The aAAV, as part of the limbic system, contributes to emotional processing (Rolls, 2019), and, along with the ACC and insula, is involved in anxiety-related and affective responses ((Etkin & Wager, 2007); (Craig, 2009); (Thompson et al., 2010); (Bachevalier & Loveland, 2006)). The dTT, sometimes referred to as the anterior hippocampal continuation ((Zaborszky et al., 1986); (McNamara et al., 2004)), has also been implicated in the brain's default mode network and the recognition of emotional facial expressions in humans ((Andrews-Hanna et al., 2010);(Phan et al., 2002); (Hariri et al., 2003); (Fusar-Poli et al., 2009); (Critchley et al., 2000)). Currently, data on the downstream targets of SOM+ neurons in the prelimbic cortex (PrL) remain incomplete. Mapping these projections will be a critical next step, as it will allow us to refine our

understanding of circuit-specific contributions to emotion discrimination and identify which downstream regions are most functionally relevant for this behavior.

Our findings, taken together, show that SOM interneurons in the prefrontal cortex have a region-specific functional specialisation. Although both the ACC and PrL are crucial nodes in the social brain network, their SOM circuits have distinct effects on emotional discrimination and memory processes. This distinction underscores the need to examine inhibitory microcircuits in a regionally nuanced way, rather than assuming they function uniformly across connected areas.

These results emphasise the importance of incorporating local circuit dynamics into the broader framework of distributed brain networks. Social cognition and emotional processing result from the coordination of multiple, hierarchically organized regions, each fulfilling a distinct and context-dependent role. Future research should investigate more thoroughly the functions of various interneuron subtypes—beyond SOM cells—and their interactions with excitatory networks, particularly in the context of disrupted excitation-inhibition (E-I) balance observed in different neuropsychiatric disorders (Lee et al., 2017).

Our optogenetic experiments provide strong evidence that SOM neurons play a causal role in shaping social behavior. However, they might not fully replicate the natural activity patterns of these cells when processing emotional information. It's still unclear whether the effects we observed are due to physiological changes in local circuits or to artificial disruptions of normal network dynamics. In future, we plan to incorporate real-time in vivo recordings, such as calcium imaging or electrophysiology, to see if SOM interneuron activity matches specific behavioural states and to establish a more precise timeline between neural activity and behavior. Although we link our findings to mechanisms underlying psychiatric conditions, we acknowledge that our model doesn't capture the full complexity of these disorders. Instead, our study offers mechanistic insight into a specific behavioural component often disrupted in these conditions. Future research using genetic or environmental models relevant to disease may provide a more direct link to human conditions.

Uncovering the functional structure of inhibitory circuits in key social brain regions may reveal new mechanistic insights and therapeutic targets for conditions characterised by affective and social impairments, including autism spectrum disorders, schizophrenia, and anxiety-related pathologies.

Materials and Methods

1. Animals

All procedures were approved by the Italian Ministry of Health and the local Animal Use Committee and were carried out in accordance with the Guide for the Care and Use of Laboratory Animals of the National Institutes of Health and the European Community Council Directives. Routine veterinary care and animal maintenance are provided by dedicated and trained personnel. Mice on a C57Bl/6J background aged 3-6 months were used as stimuli. Both male and female mice were used, of all ages and sex-matched to the observer mice. Heterozygous somatostatin cre-expressing mice (SOM-cre, Jackson: 013044) and wild-type (WT, Jackson: 000664) mice used for all experiments were bred and housed in our animal facility. Mouse genotypes were determined by Polymerase Chain Reaction (PCR) of ear snip tissue. Mice were weaned at 28 postnatal days, separated by sex and housed 2–4 per cage. Animals were housed in a climate-controlled facility (temperature 22±2°C, humidity 45-65%), with ad libitum access to food and water throughout, and with a 12-hour light/dark cycle (7pm/7am schedule). Experiments were run during the light phase (within 10am-5pm). All mice were handled on alternate days during the week preceding the first behavioural testing.

2. Viral Injection

For somatostatin neurons optogenetic manipulations we used AAV5-Ef1a-DIO eNpHR-3.0-EYFP (Addgene, 26966) for inhibition, AAV5-EF1a-double floxed-hChR2 (H134R)-EYFP-WPRE-HGHpA (Addgene, 20298) for excitation, injected in SOM-cre mice. For tracing studies we used AAV-EF1a-DIO- eYFP (27056–AAV5 addgene), injected in SOM-cre mice.

3. Stereotaxic surgery for viral injection

SOM-cre naïve mice underwent stereotaxic surgeries at 2-3 months old. All mice were anaesthetized with a mix of isoflurane (3%) in oxygen (O_2, 1%) before being positioned on a stereotaxic frame (Kopf Instruments), then maintained at 1-2% isoflurane throughout the operation. Brain coordinates for the ACC were determined using the Mouse Brain Atlas (from (Paxinos, 2001)) as follows (AP/ML/DV, in mm from Bregma and the skull): anterior–posterior (AP), +1.0 mm; medial–lateral (ML), +/-0.3 mm; at two different dorsal–ventral (DV)

coordinates, −1.75 and −1.55 mm. 0.2 µl of virus mixture was infused into each site through a borosilicate micropipette connected to a 10 µl Hamilton syringe filled with mineral oil, using a motorized injector (WPI). The injection rate was set to 0.15 µl/min, and the pipette was kept in position for at least 5 minutes to allow for proper diffusion. Brain coordinates for the PrL were also defined based on the Mouse Brain Atlas (from (Paxinos, 2001)) as follows (AP/ML/DV, in mm from Bregma and the skull): AP, +1.9 mm; ML, ±0.30 mm; with two different DV coordinates: −2.1 and -2.4 mm. The volume of AAV injected was 0.4 µl per hemisphere. Virus was infused through a glass micropipette connected to a 10 µl Hamilton syringe filled with mineral oil, with a motorized injector (WPI). After infusion, the pipette was kept in place for 5 minutes and then slowly withdrawn over 5 minutes.

After viral injection, mice were given between 2 and 3 weeks to recover before the lens or fiber implantation.

4. Stereotaxic surgery for fibers implantation

Optogenetic dual fiber implants (Doric Lenses) recordings were placed at the same AP add ML coordinates as the viral injection. For the ACC at AP: +1.0 mm; ML, +/- 0.3 DV: -1.50 and -1.55. For the PrL at AP, +1.9 mm; ML, ±0.30 mm and DV: -2.00mm All implants were maintained in position using a thin layer of Kwik-Sil (World Precision Instruments), two blunted skull screws, and adhesive dental cement (Sun Medical Super-Bond C&B Kit, Dental Leader). Mice were allowed to recover at least 7 days before starting the handling phase.

5. EDT Apparatus

The EDT apparatus is 3D printed onto a square apparatus (35.5 x 23.5 x 19) containing a two quarter circles (4cm radius) on two opposite sides. Each quarter circle is delimited by metal rods (0.8cm wide) that allow sufficient space for social contact between the demonstrator (freely moving in the apparatus) and the stimuli (freely moving in the quarter-circle). A 3D-printed separator (11 x 19cm) is placed in the middle of the apparatus in between the two quarter-circles to block the reciprocal view of the stimuli animals. Both a top view and an upper-front view of the apparatus were acquired through ANYmaze software (ANYmaze 7.4, Stoelting). For automated scoring, a virtual square (11 x 11 cm) is drawn between each quarter-circle and the separator to define a zone associated with each stimulus. Videos are collected at 15FPS using

the behavioral tracking system (Anymaze 7.4, Stoelting). In optogenetic experiments, live tracking of the mice was used to deliver 5V- TTL through an Anymaze interface (Ami1) to the LEDs and Lasers for optogenetics, based on the zone visited. Following each experiment round, the apparatus was thoroughly cleaned with soap, water and 50% ethanol, wiped, and allowed to air dry. At the end of the experiments and between testing with females or males, an additional cleaning using 70% ethanol was done, and a minimum of 24h air dry was allowed. During habituation and testing, the cages were placed inside a dimly light (6±1 lux) soundproof cubicle (Med Associates).

6. Behavioural Testing

All mice were group-housed and separated based on their experimental role (observer vs demonstrator). All mice were handled once a day for 1 min for at least 3 days before behavioral testing procedures. Additionally, mice assigned to optogenetic manipulations were habituated to wear the opto patch cord for 10 minutes over 3 consecutive days. Observers and demonstrators were individually habituated to the experimental apparatus with the cable attached for three days with daily sessions of 10 minutes, in their respective positions (demonstrators inside their quarter-circle, observers in the free zone). Demonstrator mice were matched by age, sex, and strain to the observers. To avoid confounders due to side preference, neutral-, relief-, and stress-stimulus were counterbalanced in the two sides of the testing arena. Neutral demonstrators were naïve and used for a maximum of 2-to-3 times, with at least 1 week between each experiment. Observers were always exposed to novel demonstrators. No differences were observed in the performance of the observer mice depending on the previous experience of the demonstrator.

On the day of the testing, all mice were brought into the experimental room at least 1h before the experiment began, and kept distant to avoid visual or olfactory contact between observers and demonstrators. Observer mice were gently moved into the arena connected to the patch cord for optogenetics.

To allow optogenetic modulation an 8cm hole was done in the cubicle above the recording box. A high-resolution monochrome camera (Imaging source, DMK 22AUC03) was placed above the cage to collect the mice's behavior during testing.

Observer mice. All observer mice were of the same age and sex of the demonstrator mice. Before the experiments, observer mice were gently moved into the testing apparatus. For optogenetic experiments, observer mice were connected to the patch cord or the electric cord (for LEDs stimulation) during this period. The 6-minute experiment began after placing the demonstrators and/or objects on their compartment. The order of insertion of the two demonstrators was randomly assigned.

Demonstrator mice. Demonstrator mice are matched by age and sex to the observers, were habituated, without the observer, inside the same cage in the quarter-circle 10 min for three consecutive days. Neutral, stress, relief, unfamiliar and familiar demonstrators were counterbalanced in the two sides of the testing apparatus. On the day of test, all demonstrators were brought into the experimental room at least 1h before the experiment began. All demonstrators were group-housed and separated from the cages of each other.

1) Neutral: these mice were habituated to the experimental setting as described above. All demonstrators were test-naïve and used for a maximum of 2-to-3 times, with at least 1 week between each experiment. No differences were observed in the performance of the observer mice depending on the previous experience of the demonstrator.

2) Stress: these mice were habituated to the experimental setting as described above. Then they were subject to restraint in a 50ml falcon tube (with a small hole at the end to let the mouse breathing) for 15 minutes before the beginning of the test, and then were moved immediately to their respective side of the arena.

3) Relief: these mice were habituated to the experimental setting as described above. 23h before the experiment they were water deprived. Ad libitum access to water was given 1h before the test, and mice were transferred to their respective side of the arena for testing. Food was always ad libitum.

4) Familiar: was manipulated as a neutral demonstrator but exposed to the observers for 6 minutes prior to testing.

5) Object: A black 3x3x7cm object was used. These objects were validated to don’t induce any particular aversion/preference in mice.

7. Behavioural Scoring

Acquired videos were used offline by an experimenter blind to the manipulation of both observer and demonstrators for scoring of social contact (sniffing). Time spends in each zone, the number of entries in each zone, or the distance traveled were collected using tracking software (Anymaze). Manual behavioral scorings were performed with videos using custom-made keyboard-scoring software.

8. Optogenetic manipulations

During behavioral testing, the cannula for the optogenetic experiment was connected to a 2x1 rotary joint by a dual-site patch-cord (Doric lenses, DFP_200_0.37_1.0m_GS0.7_2xFC) with the other extremity connected to a blue (380nm Laser CNI Laser or EX-LED, 435–460 nm, average power 5 mW mm−2), a green (OG-LED, 530nm, light power 5 mW mm−2), or a red (560nm LED Doric Lenses, average power 5mW mm-2) light source. Laser and LED stimulations were adjusted to a maximum of 3mW per fiber, under the control of the behavioral tracking software and interface (Anymaze, Ami1). In specific conditions (i.e. time or position of the animals) the Anymaze interface generate a TTL output that was transmitted to the laser or LED used for optogenetic stimulation. Laser and LED stimulations were controlled at 30Hz, with a pulse width of 5ms, with a maximum power of 5mW. Laser inhibitions were controlled as continuous for 2 minutes or the duration of the animal was tracked inside a specific area. The laser beam was modulated through an acousto-optic modulator (AOM, Gooch & Housego, USA).

9. Immunohistochemistry

All animals used for behavioral experiments or tracing were deeply anesthetized following all experiments with an overdose of urethane (>2 g per kg body weight) and then transcardially perfused with ice-cold 0.05 M phosphate buffer saline (PBS) pH 7.4, followed by 4%

paraformaldehyde (PFA) in PBS (0.1 M, pH 7.4). Brains were removed and stored in 4% PFA for 24h post-fixation. Brains were then placed in in 30% sucrose solution (in PBS) for at least 48 h of cryoprotection until sectioning. Brains were mounted on the sectioning chamber and frozen, and 40 µm slices were cut along the coronal axis using a microtome (HM45, Thermo Fisher). Sections were collected in PBS with 0.02% NaN3 until staining. For immunohistochemistry, all sections were first incubated in a blocking solution consisting of 10% normal goat serum (NGS) in PBS containing 1% Triton X-100 for a minimum of 1 h. Following 3–5 washes in PBS solution, primary antibodies were selected based on the target (GFP or mCherry). The primary solution consisted of the primary antibody diluted in 1% NGS, 0.03% Triton X-100 in PBS. Primary incubation occurred at 4 °C for 24–48 h. Following primary incubation, slices were washed 3–5 times in PBS and prepared for the secondary incubation that consists of a solution containing the secondary antibody diluted in 1% NGS, 0.03% Triton X-100 in PBS. Secondary incubation occurred at room temperature (RT) for 4–6 h. Primary antibodies used were: rabbit anti-GFP (1:1,000 dilution; Invitrogen, A11122), chicken anti-GFP (1:1,000 dilution; Abcam, AB290), and rabbit anti-dsRed (1:1,000 dilution; Thermo Fisher, 150128). Secondary antibodies were: Alexa Fluor 488 (goat anti-rabbit, 1:1,000 dilution; A11034, ABclonal), Alexa Fluor 488 (goat anti-chicken, 1:1,000 dilution; A11039, ABclonal) and anti-568 (goat anti-rabbit, 1:1,000 dilution; A11036, ABclonal). Fluorescence images were obtained with a confocal microscope (Nikon, CTR6500) or with an inverted fluorescence microscope (Zeiss Axiozen) using the following filter: 504 nm for Alexa Fluor 488, 560 nm for Alexa Fluor 568, and 650 nm for. Images were collected at ×20 in air or ×10, ×20. All fluorescence images were treated using the software ImageJ and Adobe Illustrator CS6. All primary and secondary antibodies have been previously validated. For tracing data, images were obtained with a 2) Nikon Eclipse Ni microscope equipped with the appropriate filter cubes to differentiate the fluorochrome employed. The images were recorded using a Nikon DS-Qi1Nc digital camera and NIS elements software BR 4.20.01 (Nikon Instruments Europe BV, Amsterdam, Netherlands).

10. Statistics

Results are expressed as mean ± SEM throughout the manuscript. Each observer's behavior toward the two different demonstrator mice was analyzed using a within-groups Repeated-measures ANOVA (RM-ANOVA). The discrimination index with optogenetics was analyzed by Two-Way ANOVAs with opto-stimulation (no light, ChR2, NphR) as between-subjects factors, and time intervals (0-2, 2-4, 4-6min) as repeated-measure within-subject factor. Bonferroni's post hoc test with multiple comparisons corrections was used for making comparisons within groups when the overall ANOVA showed statistically significant differences. All test were two-sided. Specific details on statistics are included in the statistic table added as supplementary. For optogenetic experiments, sniffing time, distance travelled, number of entries in each zone, and time in each zone were then compared across different conditions to the control (no stimulation) experiments. The accepted value for significance was $P \leq 0.05$. The accepted value for significance was $P \leq 0.05$. Statistical analyses were done using GraphPad Prism. The number of mice is reported in the legends and corresponds to similar numbers used in previous publications. Experiments reported in the paper were replicated three to four times for different groups, cages, sexes, or generations. No statistical measures were taken to predetermine the sample size of the experiments. For each animal, only entries to the stimulus area that lasted more than 5 seconds were used for analysis. Mouse exclusion criteria were defined before the beginning of the experiments and include genotyping errors, viral injection and fiber misplacement, and uncompleted experiments due to loss of implants. For all experiments, the side of the allocated stimulus mice and the order of the testing were randomized.

11. Quantification

The percentage of IR was evaluated quantitatively using ImageJ software (version 1.53e, NIH, USA) and expressed as the percentage mean ± standard deviation. For each field, a grayscale thresholding was applied manually using the "Threshold > Default > B&W > Dark background" method to identify IR signal, and the "Analyze > Measure" tool was used to calculate the percentage of immunoreactivity (IR) over total field area selected manually avoiding the inclusion of auto-fluorescence parts, helped by the direct comparison with the original field. Background subtraction was performed uniformly across all images. The mean percentage and standard deviation of the IR signal were calculated for each animal (Bombardi et al., 2025). The

quantification was done by dividing the IR of the single areas by the average IR of Cingulate 1 and Cingulate 2, then multiplying by 100.

Extended Data

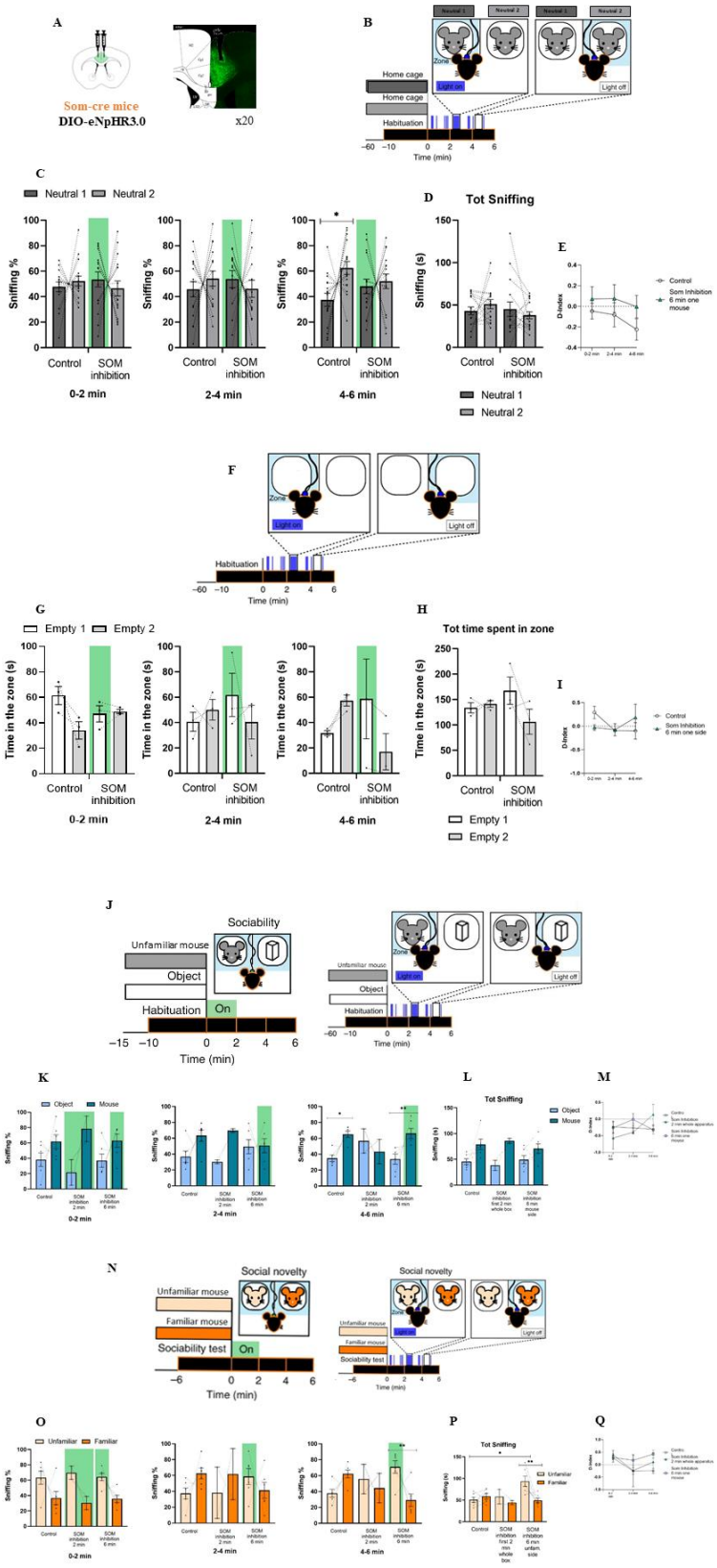

Extended data 1 – Refer to figure 1

A, SOM-Cre mice were bilaterally injected in the ACC with AAV-EF1a-DIO-eNpHR3.0-eYFP and implanted bilaterally with chronic optic fibers terminating dorsal to the injection area. **B**, Mice were tested in the ADT with two naive, non-manipulated neutral demonstrators. Photo-inhibition with green light was paired to exploration of one of the two demonstrators (counterbalanced, left or right, across observers). Data derived from n = 16 mice. **C**, No increased sniffing was noticed in the first 2 min while comparing the two experimental groups (two-way repeated-measures ANOVA, affective state × light (off, on), Bonferroni correction, P >0.9999). A tendency was seen in the third trial, in the control group, for one of the two neutral demonstrators. (2-way ANOVA, Bonferroni correction, p=0.0112). **D**, **E**, no difference was detected in the total social exploration, nor the discrimination index (one-way ANOVA, Bonferroni correction, P=0.4599; two-way ANOVA, Bonferroni correction, F (2, 60) = 0.1165, P=0.0961). **F**, Mice were tested in an empty apparatus. Photo-inhibition with green light was paired to exploration of one of the two sides (counterbalanced, left or right, across observers). Data derived from n = 3 mice. **G**, no significant side preference was detected between experimental groups (two-way repeated-measures ANOVA, affective state × light (off, on), Bonferroni correction, P=0.6640). **H**, There is a preference for the inhibited side across the entire test, but it is not significant (one-way ANOVA, Bonferroni correction, P= 0.5794). **I**, no differences in discrimination index (two-way ANOVA, Bonferroni correction, F (2, 8) = 1.392, P=0.3057). **J**, **N**, data obtained from control n mice=6, light–on 2 min n mice=2, light-on 6 min unfamiliar side n mice=6. **J**, testing mouse sociability, whether they prefer a novel conspecific rather than a novel object. Photo-inhibition was performed for 2 min from the beginning of the test using continuous green light, and also paired to exploration of the novel mouse's side (counterbalanced, left or right, across observers). **K**, in all experimental conditions, the observer preferred the novel mouse compared to the novel object, in the first two minutes. In the protocol of light-on paired with the mouse side, there was an increase of time spent with the object and a decrease of time spent with the mouse. This tendency was restored in the last trial of this condition, with the observers interacting more with the mouse (two-way repeated-measures ANOVA, affective state × light (off, on), Bonferroni correction, condition light off, t= 3.731, d.f. =22, p= 0.0174; light on 6 min. mouse side, t= 3.970, d.f. =22, p=0.0097). **L**, **M**, across the whole test, observers preferred the novel mouse compared to the novel object. No differences were noted in the discrimination index when comparing the three experimental conditions to each other. (two-way ANOVA, Bonferroni correction, F (4, 22) = 1.489, P=0.8331). **N**, testing mice social novelty (preference for a novel mouse compared to a familiar one). Photo-inhibition with green light was performed for 2 min from the beginning of the test using continuous green light, and also paired to exploration of the novel mouse's side (counterbalanced, left or right, across observers). **O**, no difference was noticed across experimental groups. In trial 3, observers paired with light-on in unfamiliar mouse's side spent more time interacting with the unfamiliar mouse (two-way repeated-measures ANOVA, affective state × light (off, on), Bonferroni correction, condition light on 6 min. unfam. mouse side, t= 4.207, d.f.=22, p= 0.0055). **P**, **Q**, experimental group paired with light on 6 min. unfam. mouse side spent more time interacting with unfamiliar side (one-way ANOVA, Bonferroni correction, p=0.0100). No significant difference was noticed from the discrimination index (two-way ANOVA, Bonferroni correction, F (4, 22) = 0.9554, P=0.4513)

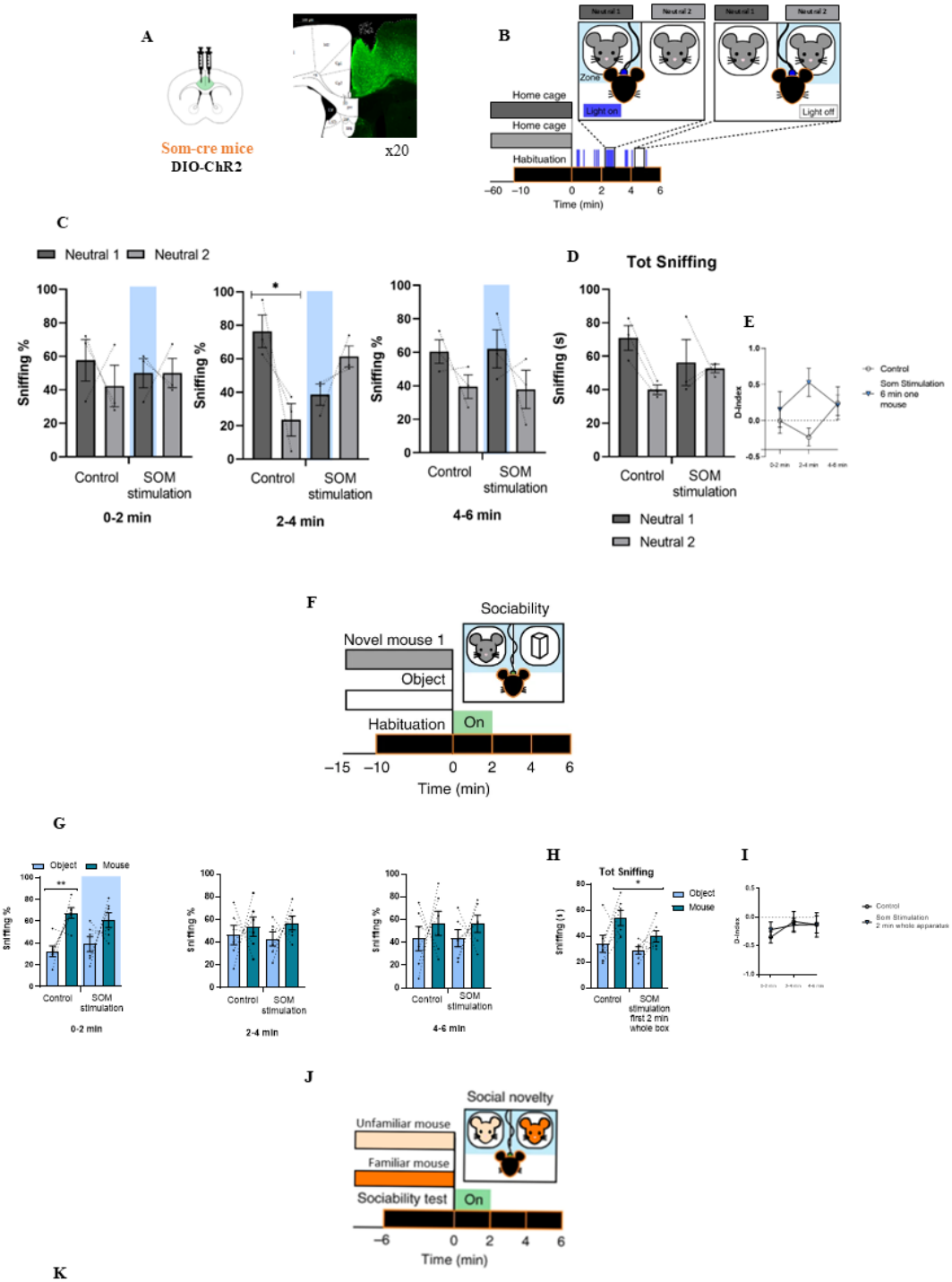
A
Som-cre mice
DIO-ChR2
x20
B
Home cage
Home cage
Habituation
Zone
Light on
Light off
Time (min)
C
Neutral 1
Neutral 2
Sniffing %
Control
SOM stimulation
0-2 min
2-4 min
4-6 min
D
Tot Sniffing
Sniffing (s)
E
D-index
Control
Som Stimulation
6 min one mouse
F
Sociability
Novel mouse 1
Object
Habituation
On
Time (min)
G
Object
Mouse
H
Tot Sniffing
I
J
Social novelty
Unfamiliar mouse
Familiar mouse
Sociability test
On
Time (min)
K
Unfamiliar
Familiar
L
Tot Sniffing
M

Extended data 2 – Refer to figure 2

A, SOM-Cre mice were bilaterally injected in the ACC with AAV-EF1a-DIO-ChR2-eYFP and implanted bilaterally with chronic optic fibers terminating dorsal to the injection area. **B**, Mice were tested in the ADT with two naive, non-manipulated neutral demonstrators. Photo-stimulation with pulsating blue light was paired to exploration of one of the two demonstrators (counterbalanced, left or right, across observers). Data derived from n = 3 mice. **C**, **D**, no difference in total sniffing across groups (one-way ANOVA, Bonferroni correction, $F(3, 8) = 2.517$, $P=0.1319$), control group tended to one neutral mouse in the second trial (two-way repeated measures ANOVA, Bonferroni correction, trial 2 $F(3, 8) = 8.314$, $P=0.0077$). **E**, differences in the discrimination index were not statistically significant (two-way ANOVA, Bonferroni correction, $F(2, 8) = 1.987$, $P=0.1992$). **F**, **J**, data obtained from n mice=6. **F**, testing mouse sociability, whether they prefer a novel conspecific rather than a novel object. Photo-stimulation with pulsating blue light was performed for 2 min from the beginning of the test. **G**, **H**, reduction of social exploration for the novel mouse compared to the object in light-on group (two-way repeated measures ANOVA, Bonferroni correction, trial 1, $t=4.146$, d.f. $=20$, $P= 0.0030$; whole test $F(3, 20) = 4.386$, $P=0.0158$). **I** no difference in discrimination indexes (two-way ANOVA, Bonferroni correction, $F(2, 20) =0.2055$, $P=0.8159$). **K**, Increased exploration of the unfamiliar demonstrator compared to the familiar demonstrator during the first 4 min of testing, which was abolished in the light-on condition (two-way repeated-measures ANOVA, affective state × light (off, on), Bonferroni correction; $F(3, 20)=38.02$, $P<0.0001$). **L**, photo-stimulated group social explored less the unfamiliar mouse (one-way ANOVA, Bonferroni correction, $F(3, 20) = 7.796$, $P=0.0012$). **M**, Statistically significant differences in first trial across experimental groups (two-way ANOVA, Bonferroni correction, $t=6.952$, d.f. $=9.721$, $P= 0.0001$).

Bibliography

1. Adolphs, R. (2001). The neurobiology of social cognition. *Curr Opin Neurobiol*, *11*(2), 231–239. https://doi.org/10.1016/s0959-4388(00)00202-6
2. Adolphs, R. (2009). The social brain: neural basis of social knowledge. *Annu Rev Psychol*, *60*, 693–716. https://doi.org/10.1146/annurev.psych.60.110707.163514
3. Adolphs, R., Sears, L., & Piven, J. (2001). Abnormal processing of social information from faces in autism. *J Cogn Neurosci*, *13*(2), 232–240. https://doi.org/10.1162/089892901564289
4. Amodio, D. M., & Frith, C. D. (2006). Meeting of minds: the medial frontal cortex and social cognition. *Nat Rev Neurosci*, *7*(4), 268–277. https://doi.org/10.1038/nrn1884
5. Andrews-Hanna, J. R., Reidler, J. S., Sepulcre, J., Poulin, R., & Buckner, R. L. (2010). Functional-anatomic fractionation of the brain's default network. *Neuron*, *65*(4), 550–562. https://doi.org/10.1016/j.neuron.2010.02.005
6. Antonelli, F., Bernardi, F., Koul, A., Novembre, G., & Papaleo, F. (2025). Emotions in multi-brain dynamics: A promising research frontier. *Neurosci Biobehav Rev*, *168*, 105965. https://doi.org/10.1016/j.neubiorev.2024.105965
7. Apps, M. A., Rushworth, M. F., & Chang, S. W. (2016). The Anterior Cingulate Gyrus and Social Cognition: Tracking the Motivation of Others. *Neuron*, *90*(4), 692–707. https://doi.org/10.1016/j.neuron.2016.04.018
8. Arioli, M., Cattaneo, Z., Ricciardi, E., & Canessa, N. (2021). Overlapping and specific neural correlates for empathizing, affective mentalizing, and cognitive mentalizing: A coordinate-based meta-analytic study. *Hum Brain Mapp*, *42*(14), 4777–4804. https://doi.org/10.1002/hbm.25570
9. Bachevalier, J., & Loveland, K. A. (2006). The orbitofrontal-amygdala circuit and self-regulation of social-emotional behavior in autism. *Neurosci Biobehav Rev*, *30*(1), 97–117. https://doi.org/10.1016/j.neubiorev.2005.07.002
10. Bertero, A., Feyen, P. L. C., Zurita, H., & Apicella, A. J. (2019). A Non-Canonical Cortico-Amygdala Inhibitory Loop. *J Neurosci*, *39*(43), 8424–8438. https://doi.org/10.1523/JNEUROSCI.1515-19.2019
11. Bombardi, C., Salamanca, G., Tagliavia, C., Grandis, A., Zamith Cunha, R., Gramenzi, A., De Silva, M., Zannoni, A., & Chiocchetti, R. (2025). Cannabinoid Receptors in the Horse Lateral Nucleus of the Amygdala: A Potential Target for Ameliorating Pain Perception, Stress and Anxiety in Horses. *Int J Mol Sci*, *26*(15). https://doi.org/10.3390/ijms26157613
12. Burkett, J. P., Andari, E., Z.V., J., D.C., C., F.B.M., D. W., & L.J., Y. (2016). Oxytocin-dependent consolation behavior in rodents. *Science*, *351*, 375–378. https://doi.org/DOI:10.1126/science.aac4785
13. Bush, G., Luu, P., & Posner, M. I. (2000). Cognitive and emotional influences in anterior cingulate cortex. *Trends Cogn Sci*, *4*(6), 215–222. https://doi.org/10.1016/s1364-6613(00)01483-2

14. Carrillo, M., Han, Y., Migliorati, F., Liu, M., Gazzola, V., & Keysers, C. (2019). Emotional Mirror Neurons in the Rat's Anterior Cingulate Cortex. *Curr Biol*, *29*(8), 1301–1312 e1306. https://doi.org/10.1016/j.cub.2019.03.024
15. Craig, A. D. (2009). How do you feel--now? The anterior insula and human awareness. *Nat Rev Neurosci*, *10*(1), 59–70. https://doi.org/10.1038/nrn2555
16. Critchley, H., Daly, E., Phillips, M., Brammer, M., Bullmore, E., Williams, S., Van Amelsvoort, T., Robertson, D., David, A., & Murphy, D. (2000). Explicit and implicit neural mechanisms for processing of social information from facial expressions: a functional magnetic resonance imaging study. *Hum Brain Mapp*, *9*(2), 93–105. https://doi.org/10.1002/(SICI)1097-0193(200002)9:2<93::AID-HBM4>3.0.CO;2-Z
17. Dautan, D., Monai, A., Maltese, F., Chang, X., Molent, C., Mauro, D., Galbusera, A., Vecchia, D., Antonelli, F., Benedetti, A., Drago, F., Leggio, G. M., Pagani, M., Fellin, T., Gozzi, A., Schumann, G., Manago, F., & Papaleo, F. (2024). Cortico-cortical transfer of socially derived information gates emotion recognition. *Nat Neurosci*, *27*(7), 1318–1332. https://doi.org/10.1038/s41593-024-01647-x
18. de Waal, F. B. (2008). Putting the altruism back into altruism: the evolution of empathy. *Annu Rev Psychol*, *59*, 279–300. https://doi.org/10.1146/annurev.psych.59.103006.093625
19. Decety, J. (2011). The neuroevolution of empathy. *Ann N Y Acad Sci*, *1231*, 35–45. https://doi.org/10.1111/j.1749-6632.2011.06027.x
20. Etkin, A., Egner, T., & Kalisch, R. (2011). Emotional processing in anterior cingulate and medial prefrontal cortex. *Trends Cogn Sci*, *15*(2), 85–93. https://doi.org/10.1016/j.tics.2010.11.004
21. Ferretti, V., & Papaleo, F. (2019). Understanding others: Emotion recognition in humans and other animals. *Genes Brain Behav*, *18*(1), e12544. https://doi.org/10.1111/gbb.12544
22. Ferretti, V., Maltese, F., Contarini, G., Nigro, M., Bonavia, A., Huang, H., Gigliucci, V., Morelli, G., Scheggia, D., Manago, F., Castellani, G., Lefevre, A., Cancedda, L., Chini, B., Grinevich, V., & Papaleo, F. (2019). Oxytocin Signaling in the Central Amygdala Modulates Emotion Discrimination in Mice. *Curr Biol*, *29*(12), 1938–1953 e1936. https://doi.org/10.1016/j.cub.2019.04.070
23. Friedman, N. P., & Robbins, T. W. (2022). The role of prefrontal cortex in cognitive control and executive function. *Neuropsychopharmacology*, *47*(1), 72–89. https://doi.org/10.1038/s41386-021-01132-0
24. Frith, C. D., & Frith, U. (2007). Social cognition in humans. *Curr Biol*, *17*(16), R724–732. https://doi.org/10.1016/j.cub.2007.05.068
25. Fusar-Poli, P., Placentino, A., Carletti, F., Landi, P., Allen, P., Surguladze, S., Benedetti, F., Abbamonte, M., Gasparotti, R., Barale, F., Perez, J., McGuire, P., & Politi, P. (2009). Functional atlas of emotional faces processing: a voxel-based meta-analysis of 105 functional magnetic resonance imaging studies. *J Psychiatry Neurosci*, *34*(6), 418–432.
26. Hariri, A. R., Mattay, V. S., Tessitore, A., Fera, F., & Weinberger, D. R. (2003). Neocortical modulation of the amygdala response to fearful stimuli. *Biol Psychiatry*, *53*(6), 494–501. https://doi.org/10.1016/s0006-3223(02)01786-9

27. Heeger, D. J., & Ress, D. (2002). What does fMRI tell us about neuronal activity? *Nat Rev Neurosci*, *3*(2), 142–151. https://doi.org/10.1038/nrn730
28. https://doi.org/10.1146/annurev-psych-020821-010855
29. Huang, S., Wu, S. J., Sansone, G., Ibrahim, L. A., & Fishell, G. (2024). Layer 1 neocortex: Gating and integrating multidimensional signals. *Neuron*, *112*(2), 184–200. https://doi.org/10.1016/j.neuron.2023.09.041
30. Jeon, D., Kim, S., Chetana, M., Jo, D., Ruley, H. E., Lin, S. Y., Rabah, D., Kinet, J. P., & Shin, H. S. (2010). Observational fear learning involves affective pain system and Cav1.2 Ca2+ channels in ACC. *Nat Neurosci*, *13*(4), 482–488. https://doi.org/10.1038/nn.2504
31. Katona, L., Lapray, D., Viney, T. J., Oulhaj, A., Borhegyi, Z., Micklem, B. R., Klausberger, T., & Somogyi, P. (2016). Sleep and Movement Differentiates Actions of Two Types of Somatostatin-Expressing GABAergic Interneuron in Rat Hippocampus. *Neuron*, *91*(5), 1183. https://doi.org/10.1016/j.neuron.2016.08.023
32. Keum, S., Kim, A., Shin, J. J., Kim, J. H., Park, J., & Shin, H. S. (2018). A Missense Variant at the Nrxn3 Locus Enhances Empathy Fear in the Mouse. *Neuron*, *98*(3), 588–601 e585. https://doi.org/10.1016/j.neuron.2018.03.041
33. Kietzman, H. W., & Gourley, S. L. (2023). How social information impacts action in rodents and humans: the role of the prefrontal cortex and its connections. *Neurosci Biobehav Rev*, *147*, 105075. https://doi.org/10.1016/j.neubiorev.2023.105075
34. LeDoux, J. E. (2000). Emotion circuits in the brain. *Annu Rev Neurosci*, *23*, 155–184. https://doi.org/10.1146/annurev.neuro.23.1.155
35. Lee, E., Lee, J., & Kim, E. (2017). Excitation/Inhibition Imbalance in Animal Models of Autism Spectrum Disorders. *Biol Psychiatry*, *81*(10), 838–847. https://doi.org/10.1016/j.biopsych.2016.05.011
36. Lenartowicz, A., & McIntosh, A. R. (2005). The role of anterior cingulate cortex in working memory is shaped by functional connectivity. *J Cogn Neurosci*, *17*(7), 1026–1042. https://doi.org/10.1162/0898929054475127
37. Maltese, F., Pacinelli, G., Monai, A., Bernardi, F., Capaz, A. M., Niello, M., Walle, R., de Leon, N., Manago, F., Leroy, F., & Papaleo, F. (2025). Self-experience of a negative event alters responses to others in similar states through prefrontal cortex CRF mechanisms. *Nat Neurosci*, *28*(1), 122–136. https://doi.org/10.1038/s41593-024-01816-y
38. Mason, P., & Shan, H. (2017). A valence-free definition of sociality as any violation of inter-individual independence. *Proc Biol Sci*, *284*(1866). https://doi.org/10.1098/rspb.2017.0948
39. McNamara, A. M., Cleland, T. A., & Linster, C. (2004). Characterization of the synaptic properties of olfactory bulb projections. *Chem Senses*, *29*(3), 225–233. https://doi.org/10.1093/chemse/bjh027
40. Mercer, S. W., & Reynolds, W. J. (2002). *Empathy and quality of care* (Vol. 52 (Suppl.)).
41. Millan, M. J., Agid, Y., Brune, M., Bullmore, E. T., Carter, C. S., Clayton, N. S., Connor, R., Davis, S., Deakin, B., DeRubeis, R. J., Dubois, B., Geyer, M. A., Goodwin, G. M., Gorwood, P., Jay, T. M., Joels,

M., Mansuy, I. M., Meyer-Lindenberg, A., Murphy, D.,…Young, L. J. (2012). Cognitive dysfunction in psychiatric disorders: characteristics, causes and the quest for improved therapy. *Nat Rev Drug Discov*, *11*(2), 141–168. https://doi.org/10.1038/nrd3628

42. Panksepp, J., & Panksepp, J. B. (2013). Toward a cross-species understanding of empathy. *Trends Neurosci*, *36*(8), 489–496. https://doi.org/10.1016/j.tins.2013.04.009
43. Phan, K. L., Wager, T., Taylor, S. F., & Liberzon, I. (2002). Functional neuroanatomy of emotion: a meta-analysis of emotion activation studies in PET and fMRI. *Neuroimage*, *16*(2), 331–348. https://doi.org/10.1006/nimg.2002.1087
44. Phelps, E. A. (2006). Emotion and cognition: insights from studies of the human amygdala. *Annu Rev Psychol*, *57*, 27–53. https://doi.org/10.1146/annurev.psych.56.091103.070234
45. Post, S. G., Ng, L. E., Fischel, J. E., Bennett, M., Bily, L., Chandran, L., Joyce, J., Locicero, B., McGovern, K., McKeefrey, R. L., Rodriguez, J. V., & Roess, M. W. (2014). Routine, empathic and compassionate patient care: definitions, development, obstacles, education and beneficiaries. *J Eval Clin Pract*, *20*(6), 872–880. https://doi.org/10.1111/jep.12243
46. Raihani, N. (2021). *The social instinct: how cooperation shaped the world*. St. Martin's Press.
47. Rolls, E. T. (2019). The cingulate cortex and limbic systems for emotion, action, and memory. *Brain Struct Funct*, *224*(9), 3001–3018. https://doi.org/10.1007/s00429-019-01945-2
48. Roozendaal, B., McEwen, B. S., & Chattarji, S. (2009). Stress, memory and the amygdala. *Nat Rev Neurosci*, *10*(6), 423–433. https://doi.org/10.1038/nrn2651
49. Roy, M., Shohamy, D., & Wager, T. D. (2012). Ventromedial prefrontal-subcortical systems and the generation of affective meaning. *Trends Cogn Sci*, *16*(3), 147–156. https://doi.org/10.1016/j.tics.2012.01.005
50. Schafer, M., & Schiller, D. (2018). Navigating Social Space. *Neuron*, *100*(2), 476–489. https://doi.org/10.1016/j.neuron.2018.10.006
51. Scheggia, D., Manago, F., Maltese, F., Bruni, S., Nigro, M., Dautan, D., Latuske, P., Contarini, G., Gomez-Gonzalo, M., Requie, L. M., Ferretti, V., Castellani, G., Mauro, D., Bonavia, A., Carmignoto, G., Yizhar, O., & Papaleo, F. (2020). Somatostatin interneurons in the prefrontal cortex control affective state discrimination in mice. *Nat Neurosci*, *23*(1), 47–60. https://doi.org/10.1038/s41593-019-0551-8
52. Smith, M. L., Asada, N., & Malenka, R. C. (2021). Anterior cingulate inputs to nucleus accumbens control the social transfer of pain and analgesia. *Science*, *371*(6525), 153–159. https://doi.org/10.1126/science.abe3040
53. Sohal, V. S., & Rubenstein, J. L. R. (2019). Excitation-inhibition balance as a framework for investigating mechanisms in neuropsychiatric disorders. *Mol. Psychiatry*, *24*(9), 1248–1257. https://doi.org/10.1038/s41380-019-0426-0
54. Stevenson, A. (2010). *Oxford Dictionary of English (3rd ed.)*.

55. Thompson, L., Thompson, M., & Reid, A. (2010). Neurofeedback outcomes in clients with Asperger's syndrome. *Appl Psychophysiol Biofeedback*, *35*(1), 63–81. https://doi.org/10.1007/s10484-009-9120-3

56. Tomioka, R., Okamoto, K., Furuta, T., Fujiyama, F., Iwasato, T., Yanagawa, Y., Obata, K., Kaneko, T., & Tamamaki, N. (2005). Demonstration of long-range GABAergic connections distributed throughout the mouse neocortex. *Eur J Neurosci*, *21*(6), 1587–1600. https://doi.org/10.1111/j.1460-9568.2005.03989.x
57. Urban-Ciecko, J., & Barth, A. L. (2016). Somatostatin-expressing neurons in cortical networks. *Nat Rev Neurosci*, *17*(7), 401–409. https://doi.org/10.1038/nrn.2016.53
58. Utashiro, N., MacLaren, D. A. A., Liu, Y. C., Yaqubi, K., Wojak, B., & Monyer, H. (2024). Long-range inhibition from prelimbic to cingulate areas of the medial prefrontal cortex enhances network activity and response execution. *Nat Commun*, *15*(1), 5772. https://doi.org/10.1038/s41467-024-50055-z
59. van Kleef, G. A., & Cote, S. (2022). The Social Effects of Emotions. *Annu Rev Psychol*, *73*, 629–658.
60. Wu, S. J., Sevier, E., Dwivedi, D., Saldi, G. A., Hairston, A., Yu, S., Abbott, L., Choi, D. H., Sherer, M., Qiu, Y., Shinde, A., Lenahan, M., Rizzo, D., Xu, Q., Barrera, I., Kumar, V., Marrero, G., Pronneke, A., Huang, S.,…Fishell, G. (2023). Cortical somatostatin interneuron subtypes form cell-type-specific circuits. *Neuron*, *111*(17), 2675–2692 e2679. https://doi.org/10.1016/j.neuron.2023.05.032
61. Yizhar, O., Fenno, L. E., Prigge, M., Schneider, F., Davidson, T. J., O'Shea, D. J., Sohal, V. S., Goshen, I., Finkelstein, J., Paz, J. T., Stehfest, K., Fudim, R., Ramakrishnan, C., Huguenard, J. R., Hegemann, P., & Deisseroth, K. (2011). Neocortical excitation/inhibition balance in information processing and social dysfunction. *Nature*, *477*(7363), 171–178. https://doi.org/10.1038/nature10360
62. Zaborszky, L., Carlsen, J., Brashear, H. R., & Heimer, L. (1986). Cholinergic and GABAergic afferents to the olfactory bulb in the rat with special emphasis on the projection neurons in the nucleus of the horizontal limb of the diagonal band. *J Comp Neurol*, *243*(4), 488–509. https://doi.org/10.1002/cne.902430405
63. Zhang, M., Wu, Y. E., Jiang, M., & Hong, W. (2024). Cortical regulation of helping behaviour towards others in pain. *Nature*, *626*(7997), 136–144. https://doi.org/10.1038/s41586-023-06973-x

Chapter 5

Inter-Brain Dynamics Modulate Emotion Discrimination

Federica Antonelli[1,2], **Anna Monai[1,2]**, Fabrizio Bernardi[1], Atesh Koul[3], Nicola Marie Engel[4], Ilaria Carta[1,2], Francesca Managò[1], Arianna Benedetti[1,2], Anna Maria Borruto[1], Ludovico Spattini[1], Federica Maltese[1,5], Chunzhi Yi[4], Guillaume Dumas[6,7], Stefano Panzeri[4], Giacomo Novembre[3], Francesco Papaleo[1,2*]

[1]*Genetics of Cognition laboratory, Neuroscience area, Istituto Italiano di Tecnologia, Genova, Italy.*
[2]*IRCCS Ospedale Policlinico San Martino, Largo Rosanna Benzi, 10, 16132 Genova, Italy.*
[3]*Neuroscience of Perception and Action Laboratory, Istituto Italiano di Tecnologia, Viale Regina Elena 291, 00161 Roma, Italy.*
[4]*Institute for Neural Information Processing, University Medical Center Hamburg-Eppendorf (UKE), Falkenried 94, 20251 Hamburg, Germany.*
[5]*Institute of Neuroscience, National Research Council, Vedano al Lambro, Italy*
[6]*CHU Sainte-Justine Azrieli Research Centre, Department of Psychiatry and Addictology, University of Montréal, Montréal, Québec, Canada.*
[7]*Mila – Quebec Artificial Intelligence Institute, Montréal, Québec, Canada.*

*Corresponding author: francesco.papaleo@iit.it

In preparation.

Abstract

Perceiving and responding to others' emotions lies at the core of animal social behavior, shaping both individual and societal well-being. Our findings reveal that interacting brains exhibit distinct, cell-type-specific inter-brain dynamics in emotional contexts that guide social choices. Inter-brain correlations among pyramidal neurons in the anterior cingulate cortex (ACC) were disrupted when one of the interacting partners was in a stress state. This was evident in mice, with similar evidence in humans. Conversely, ACC somatostatin (SOM) inhibitory neurons exhibited inter-brain correlation only towards a conspecific in a stress emotional state. Optogenetic manipulations demonstrated the causal role of these inter-brain dynamics in driving socio-emotional choices. Specifically, preventing SOM inter-brain correlation abolished stress emotion discrimination. Conversely, inducing SOM inter-brain correlation biased social preference towards a stress conspecific. In contrast, manipulating inter-brain correlations among pyramidal neurons biased social choices in emotionally neutral contexts. Notably, real-time closed-loop stimulation, using recorded SOM activity from one mouse to drive matching activity in an interacting conspecific, demonstrated that observer-initiated SOM neurons correlation selectively promoted social preference toward a stress partner. These findings establish how inter-brain cortical substrates guide social choices in emotional contexts.

Main

Emotions are key regulators of social behaviors across species, shaping communication, decision-making, conflict resolution, group cohesion, and collective dynamics (Adolphs, 2001; Valentina Ferretti & Francesco Papaleo, 2019; Panksepp & Panksepp, 2013; Schafer & Schiller, 2018; van Kleef & Cote, 2022). Detecting negative emotions in others can elicit a range of responses, from heightened vigilance and threat avoidance to consolatory helping approach (Burkett et al., 2016; LeDoux, 2000; Phelps, 2006). Given their fundamental impact on social life and survival, the ability to detect and respond to others' emotions is evolutionarily conserved (Adolphs, 2001; Decety, 2011; V. Ferretti & F. Papaleo, 2019; Mason & Shan, 2017; Millan et al., 2012; Panksepp & Panksepp, 2013; Raihani, 2021; Schafer & Schiller, 2018). Notably, socio-emotional exchanges depend on a continuous flow of information between interacting partners (Adolphs, 2009; Muller-Pinzler et al., 2017; Schilbach et al., 2008), forming a dynamic, reciprocal feedback loop where actions, reactions, and emotional states are mutually modulated (Butler, 2017; Van Kleef, 2016). Yet, when investigating the neural basis of socio-emotional behaviors, most studies in humans and non-human animals continue to focus on a single "observer" (Adolphs, 2002; Ferretti et al., 2019; Scheggia et al., 2020). This single-brain approach overlooks how interacting brains function as components of an integrated, dynamic system, during socio-emotional contexts.

Pioneering multi-brain studies in humans, followed by mice and bats, discovered that brains of interacting individuals might function jointly, through correlated neural activity (Hasson et al., 2004; Kingsbury et al., 2019; Kohler et al., 2002; Montague et al., 2002; Yeshurun et al., 2021; Zhang & Yartsev, 2019). Such inter-brain correlation has been investigated at the behavioral (Gordon et al., 2020; Keller et al., 2014) and neural system levels (Kingsbury et al., 2019; Rose et al., 2021; Scaglione et al., 2024; Zhang & Yartsev, 2019) and hypothesized to be an organizing principle of how brains interact with, perceive and learn from other social agents in real time (Redcay & Schilbach, 2019). However, whether inter-brain dynamics have a consequential or causative role in social interactions remains actively debated (Hamilton, 2021; Holroyd, 2022; Novembre & Iannetti, 2021). Most notably, the influence of emotions on inter-brain dynamics remains largely anecdotal and poorly understood, with the mechanisms and causal implications in shaping social choices in emotional contexts still unexplored (Antonelli et al., 2025).

The anterior cingulate cortex (ACC, Brodmann area 24) is a major hub orchestrating the detection and reaction to others' emotions in rodents and humans (Antonelli et al., 2025; Carrillo et al., 2019; Jeon et al., 2010; Keum et al., 2018; Smith et al., 2021; Zhang et al., 2024). Moreover, the ACC is often indicated in humans as a critical hub where others' actions and intentions might be codified through an internal mimicking of social partner's neural activity (Antonelli et al., 2025; Bastiaansen et al., 2009). Therefore, we simultaneously recorded neural activity in the ACC of three interacting mice engaged in an emotional state discrimination task (Dautan et al., 2024a; Ferretti et al., 2019; Maltese et al., 2025; Scheggia et al., 2020). In this task, an 'observer' mouse is placed in front of two conspecifics ('demonstrators'), one exhibiting an emotionally altered state and the other a neutral state. With this setup we can access cell-type-specific neural information underlying emotional discriminations that are not apparent in one-on-one interactions (Ferretti et al., 2019; Scheggia et al., 2020), while simultaneously comparing real-time inter-brain dynamics in response to a neutral or emotionally altered conspecific. The task approximates key features of human emotion recognition paradigms (Dautan et al., 2024a; Ferretti et al., 2019; Maltese et al., 2025; Scheggia et al., 2020). Thus, to strengthen the link to analogous processes in humans, we formally investigated inter-brain dynamics during real-time human interactions adding an emotional component, as still scarcely explored (Antonelli et al., 2025). To determine whether inter-brain dynamics causally influence social choices in emotional contexts, we applied several optogenetic manipulations across all three interacting mice to either prevent neural correlations, or induce artificial correlations and anticorrelations. Finally, we implemented a system in which the real-time neural recording of ACC neural subpopulations in one mouse is used to optogenetically drive a similar pattern of activity in another mouse. Our findings uncover cell-type-specific mechanisms through which inter-brain dynamics both respond to and shape socio-emotional reactions, pinpointing somatostatin (SOM) inhibitory neurons in the observer's ACC as critical mediators of neural correlation in emotion-driven social choices.

Results

Mice detect others' stress, but stressed peers break reciprocity

Using three miniscopes implanted in the ACC of one observer and two demonstrator mice (Fig. 1a), we achieved simultaneous single-cell resolution recording of calcium activity from the three brains during the emotional state discrimination task (Dautan et al., 2024a; Ferretti et al., 2019; Maltese et al., 2025; Scheggia et al., 2020).

Observer mice displayed increased sniffing toward restraint stress compared to neutral demonstrators during the first two minutes (Fig. 1b). To assess potential transfer of socio-emotional information throughout time and to provide time-dependent evolution of inter-brain dynamics, we extended the test to 15 minutes finding that also in the middle of the task (i.e. 5-10 min), but not in the last two minutes, the observer mice showed discrimination (Fig. 1b). Similar results for these three time periods were evident considering the time the observers spent in each demonstrator zone (Supplementary Fig. 1). Moreover, as we assume that actions, reactions, and emotional states of each individual are modulated interpersonally and might influence inter-brain dynamics over time, we checked for individual and reciprocal behaviors between all 3 interacting mice. Notably, when comparing epochs of reciprocal sniffing, where both the observer and demonstrators sniffed each other, to epoch in which the observer sniffed the demonstrators' cage while the demonstrator oriented away (non-reciprocated), we found no differences in the duration or number of events between observer-neutral compared to observer-stress pairings (Supplementary Fig. 1). However, when normalized to the observer's total sniffing, reciprocal sniffing was reduced with the stress demonstrator compared to the neutral one in the first two minutes, up to the middle of the task (Fig. 1c), and the duration of reciprocal sniffing was longer in observer-neutral pairings compared to observer-stress pairings in the first two minutes (Fig. 1d). No major signs of transfer of stress or buffering were evident, as the stress demonstrator groomed more and climbed less throughout the task while the observer and neutral mice were showing the same level of low grooming and climbing for the entire 15 minutes (Supplementary Fig. 1). Similarly, the observer exhibited more rearing throughout the task compared to the demonstrators, regardless of whether it was in the stress or neutral mouse zones (Supplementary Fig. 1). These results indicate that observers discriminate and prefer the stress over the neutral

demonstrator. Conversely, the stress demonstrator exhibited reduced social reciprocation, and no evidence of social buffering effects.

Inter-brain correlation of ACC pyramidal neurons is disrupted by stress

Most human inter-brain correlations are based on EEG signal (Antonelli et al., 2025; Yeshurun et al., 2021), which is thought to capture mostly the dendrosomatic dipoles generated at the apical dendrites of glutamatergic pyramidal (PYR) neurons, due to their geometric alignment of their apical dendrites (Le Merre et al., 2021). Thus, we first simultaneous imaged ACC PYR neurons activity across the three interacting mice (Fig. 1e,f Supplementary Fig. 2).

Based on our behavioral findings, and to test whether inter-brain dynamics vary over time, we divided the analysis into three epochs: the first two minutes (capturing initial discrimination and enabling comparison with prior single-brain data (Dautan et al., 2024a; Ferretti et al., 2019; Maltese et al., 2025; Scheggia et al., 2020), the middle 5-10 minutes (when discrimination persists), and the final two minutes. We analyzed a total of 2898 PYR neurons from 6 triads of mice. We first computed the Pearson's correlation coefficient (PCC) between the mean PYR activity of each observer and that of the neutral or stress demonstrator upon entry into their respective zones (Fig. 1f,g). Correlation measures were computed after removing baseline variations in the signals through linear detrending of the traces. ACC PYR neurons displayed increased correlated activity when interacting with the neutral demonstrator and an anticorrelation when interacting with a stress demonstrator, during the last 2 minutes of the task (Fig. 1f,g). These differences were not evident when mice were individually prepared (habituation), when the observer was in the opposite demonstrator zone, or when considering random intervals during the task (Fig. 1f,g). A significant positive correlation was only evident between the observer and the neutral demonstrator in the last two minutes of the task, but also when considering the total time of the test (Fig. 1f,g). To assess whether the peak inter-brain correlation emerged at time lags other than zero, we then measured the cross-correlation (CC) of ACC PYR activity across brains (Fig. 1f,h). This revealed a positive correlation with the neutral demonstrator peaking between -0.3 and 0 sec, and notably an anticorrelation with the stress demonstrator peaking at lag 0.4 sec (Fig. 1f,h). No differences were evident during habituation or when exploring the opposite demonstrator (Fig. 1f,h). These results indicate that inter-brain correlations of ACC PYR neurons are evident only

during close proximity between two equally neutral mice while they are disrupted if one of the two subjects is in a stress state.

We next assessed how inter-brain correlations could be determined at the single neuron level when mice were engaged in reciprocal sniffing (Fig. 1j,k). We confirmed an increased correlation between the observer and the neutral demonstrator with a time-lag of approximately 0 sec which was disrupted toward the stress demonstrator (Fig. 1j,k). This correlation was lower during non-reciprocal observer-only sniffing events (Fig. 1l). When reciprocally sniffing, a lower but significant correlation in ACC PYR activity was also evident for the two demonstrators (Fig. 1k), suggesting some dependence on the similar sniffing movement behavior, as this was not evident during non-reciprocated sniffing (Fig. 1l). No inter-brain correlations were observed when the observer was in the free empty zone of the apparatus, when phase randomized intervals were selected, or when computing correlation between the observer and stress or neutral demonstrators in other cages, but still during reciprocal and non-reciprocated sniffing (Fig. 1k,l). Computing a measure of time asymmetry of the time-lagged cross correlations we also found no asymmetry in PYR inter-brain dynamics (Supplementary Fig. 3), indicating mainly simultaneous coactivation rather than the activity of one animal preceding that of the other. Finally, we found that most of the ACC PYR neurons had a small, but significant inter-brain correlation (Supplementary Fig. 3). Overall, these results illustrate that ACC PYR neurons show inter-brain correlations between equally neutral subjects, which are disrupted if one subject is in a stress state.

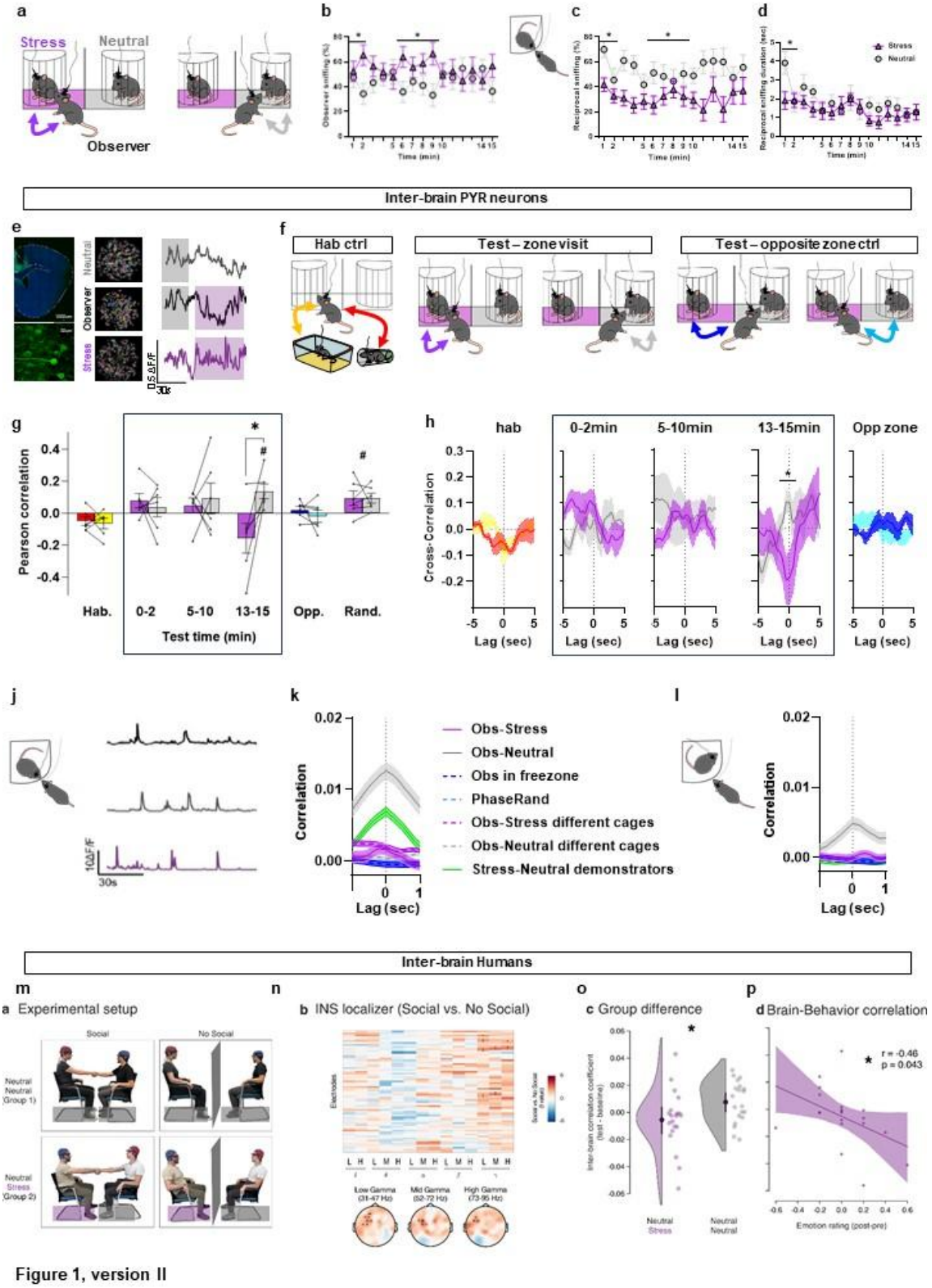

Figure 1, version II

Figure 1. Inter-brain correlation for ACC PYR neurons is disrupted in mice by altered emotion in demonstrator. n = 6 triplets, 2898 neurons.

(a) Experimental design: the 3 mice involved in the EDT were concurrently recorded through microendoscopic calcium imaging. Interbrain correlation measures were computed during observer visits to demonstrators' compartments.

(b) Observers social investigation expressed as percentage of sniffing toward the stressed (purple) and the neutral (grey) demonstrator (two-way ANOVA *, $p < 0.05$).

(c) Reciprocal sniffing between the observer and the stressed and neutral demonstrators expressed as percentage of observer sniffing (two-way ANOVA *, $p < 0.05$).

(d) Reciprocal sniffing duration between the observer and the two demonstrators.

(e) Left: representative GCaMP expression and lens placement in the ACC (top), single pyramidal neuron (bottom). Center: example ROIs for single cell calcium imaging recordings from the 3 mice. Right: example average traces from the 3 mice.

(f) Interbrain correlations were computed during the different phases of the task. Hab ctrl: habituation control, the observer was alone in the testing cages while the stressed demonstrator was under restraint in a falcon tube and the neutral demonstrator was in its home cage. Test – zone visit: interbrain correlation was computed during observer visits to the corresponding demonstrator. Test – opposite zone ctrl: as a control, interbrain correlation was computed during observer visits to the other demonstrator.

(g) Pearson correlation between pyr average activity in the observer and in each demonstrator during the different phases of the test. Hab: habituation. 0-2, 5-10, 13-15 minutes time bins of the test. Opp.: correlation computed between the observer and the non-explored demonstrator. Rand.: interbrain correlations between the observer and each demonstrator irrespectively of observer position in the box.

(h) Cross-correlation between pyr average activity in the observer and in each demonstrator during the different phases of the test defined as for Pearson correlation.

(j) Let: reciprocal sniffing scheme. Right: representative traces from pyramidal single-neurons.

(k) Cross-correlation computed between individual neurons of the observer and each demonstrator during reciprocal sniffing intervals and control conditions.

(l) Cross-correlation computed between individual neurons of the observer and each demonstrator during observer non-reciprocated sniffing intervals and control conditions.

(m) We recorded EEG from 40 human dyads (80 participants) during a social interaction task in which participants faced each other and held their partner's right hand, and a no-social-contact control condition in which an occluder prevented visual and haptic interaction. Each dyad completed both conditions following the viewing of neutral audio-visual stimuli (baseline phase), as well as after exposure to either stress-inducing or additional neutral audio-visual stimuli (test phase), depending on group assignment (Stress–Neutral or Neutral–Neutral).

(n) Inter-brain correlation was computed between homologous electrodes across frequency subbands, based on power envelope time courses. A data-driven localizer analysis identified a cluster of central and frontal electrodes within the

low, mid, and high gamma bands that showed significantly higher inter-brain correlation during social compared to no-social conditions.

(o) We compared inter-brain correlation between dyads composed of one stressed and one neutral participant versus dyads composed of two neutral participants, focusing specifically on the electrode–frequency cluster identified in (N). Correlation coefficients were baseline-corrected by subtracting values obtained in the baseline social interaction block. This analysis revealed that dyads including a stressed individual exhibited significantly reduced inter-brain correlation.

(p) Reductions in inter-brain correlation were associated with the intensity of stress-induced negative affect, as quantified by self-report questionnaires administered before and after the experiment. This suggests that the greater the emotional impact of stress induction, the stronger the reduction in inter-brain correlation within the Stress–Neutral group.

Observer's ACC PYR correlation lacks inter-brain emotional relevance

To examine how inter-brain correlations might relate to single-neuron correlations within individual brains, we analyzed intra-brain correlations in the observer and both demonstrators during interaction epochs, distinguishing between reciprocal and non-reciprocated sniffing. The observer's intra-brain PYR correlations were comparable during reciprocal interactions with either the stress or the neutral demonstrator (Supplementary Fig. 3). However, higher intra-brain correlation was found during unidirectional exploration of the neutral compared to the stress demonstrator (Supplementary Fig. 3), consistent with previous observations (Scheggia et al., 2020). When computing intra-brain dynamics in the demonstrators, we noticed the same levels between the two, however, for the neutral demonstrator, an higher correlation level was evident when receiving a visit from the observer compared to when the observer was in the no interaction zone (Supplementary Fig. 3). These data might suggest that the increased inter-brain correlation between the observer and the neutral mouse could be partially associated with the increased intra-brain correlation in the neutral demonstrator.

Inter-brain correlation disruption by stress extends to humans

To examine whether inter-brain correlation disruption by stress is a general phenomenon that extends beyond mice, we collected EEG data from 20 human dyads in which one participant was in a stress state and another in a neutral state, as well as from 20 dyads in which both participants were in a neutral state (Fig. 1m). Stress and neutral states were induced using validated audio-

visual stimuli (Supplementary Fig. 4a-c)(Siedlecka & Denson, 2019; Uhrig et al., 2016). Immediately following emotional state induction, participants engaged in a social interaction in which they looked at each other while holding their partner's right hand (Fig. 1m), with no verbal or gestural communication allowed (Koul et al., 2023). This was performed to parallel reciprocal sniffing in mice.

We first aimed at identifying EEG electrodes carrying signal that correlated between participants, irrespectively of their emotional state. To achieve this, we computed Pearson's correlation coefficients between electrode- and sub-band-specific EEG power time courses (i.e., envelopes) recorded from the two individuals in each dyad (Koul et al., 2023; Zhang & Yartsev, 2019). Power time courses provide a suitable comparison to the mice results, as they are non-periodic, exhibit similar timescales, and reliably capture inter-brain synchrony (REF). We tested whether inter-brain correlation coefficients were statistically higher during the social interaction condition compared to a no social control condition during which participants were not able to see or touch each other [cluster-based permutation (Maris and Oostenveld, 2007), n = 1000 permutations]. This data-driven localizer analysis revealed that gamma-band envelopes (γ_{env} 31-95 Hz), specifically recorded from frontal scalp electrodes, exhibit inter-brain correlation (Fig. 1n – cluster-corrected $p = 0.025$).

Next, we assessed the effect of emotional manipulation on both participants' self-reported questionaries as well as on their inter-brain correlation, focusing on the previously identified spectral and spatial region of interest. Behavioral (self-report) data indicated that participants who watched the neutral stimuli reduced their negative affect ratings (i.e., they reported feeling less negative emotions) from pre- to post-experiment, while those who viewed the negative stimuli did not (Supplementary Fig. 4e). Similarly, neural data revealed that dyads including a stressed participant exhibited reduced inter-brain correlation compared to dyads composed of two participants in neutral states during the test phase (Fig. 1o). This effect persisted even after thresholding the correlation coefficients using a baseline social condition conducted prior to stress induction (Fig. 1o). Notably, greater decreases in inter-brain correlation were associated with larger changes in participants' stress negative emotional state (Fig. 1p). Like in mice, these results suggest that negative emotions disrupt inter-brain correlation typically observed between individuals in a neutral state. Moreover, inter-brain correlation appears to be specifically driven by the envelopes of EEG gamma oscillations.

Inter-brain correlation of ACC SOM neurons is related to stress

The EEG signal is known to be generated by the activity of the dendrosomatic dipoles of the apical dendrites of PYR neurons (Einevoll et al., 2013). However, both PYR and inhibitory neurons regulate the times and occurrence of the presynaptic spikes that generate these dendrosomatic dipoles, making it impossible to separately identify the contribution of each of these cells subtypes from EEG. Oscillations in a part of gamma band, which we find to be more affected by inter-brain emotional modulation, can be driven by SOM neurons (Veit et al., 2017). Moreover, PFC SOM neurons play a central role in regulating emotion discrimination abilities (Dautan et al., 2024a; Maltese et al., 2025; Scheggia et al., 2020). Thus, we imaged ACC SOM neurons by *in vivo* microendoscopic recordings of calcium activity in all three mice performing the same emotional state discrimination task (Fig. 2a-d).

We analyzed a total of 968 SOM neurons from 9 triads of mice. Lens placement and GCaMP6f expression were confirmed histologically (Fig. 2a and Supplementary Fig. 2). In contrast to PYR cells, ACC SOM overall activity displayed high correlation between the observer and the stress mouse, only during the first 2 minutes of the task, when entering in the respective demonstrator zone (Fig. 2d,e). Cross-correlation analysis showed a peak at 0.0 sec with the stress demonstrator in the first two minutes of the task (Fig. 2d,f). When the observer was interacting with a neutral demonstrator, a tendency towards an anticorrelation in the first two minutes was observed (Fig. 2d,f). No inter-brain correlations were evident during habituation, when mice were individually prepared, when considering the observer and the non-explored opposite demonstrator, or when random intervals were chosen (Fig. 2d,e,f). These results indicate that emotional alteration in one interacting subject enhances inter-brain correlation of ACC SOM cells.

We next assessed whether at the single neuron level inter-brain ACC SOM neurons computed reciprocal or univocal social interactions (Fig. 2g,h). These analyses confirmed a positive correlation between the observer and the stress demonstrator only during reciprocal, but not in non-reciprocated sniffing (Fig. 3g). Notably, this correlation was higher and more asymmetric compared to the correlation between the observer and the neutral demonstrator (Fig. 3g). The inter-brain asymmetry indicated that the observer activity was preceding the activity of the stress demonstrator (Fig. 3g), as further confirmed by time-lagged asymmetry measures showing a negative value only between the observer and the stress demonstrator, only when

reciprocally sniffing (Fig. 3g,h). Most of the ACC SOM neurons had a small, but significant inter-brain correlation (Supplementary Fig. 5). No inter-brain correlations were evident when traces were phase-randomized, when the observer was in the zone without demonstrators, when the observer was interacting with the opposite demonstrator, between the two demonstrators, and between the observer with demonstrators in other cages when reciprocally or non-reciprocally sniffing each other (Fig. 2g,h). These findings indicate that altered emotional states are not only associated with inter-brain correlation in ACC SOM, but also highlight a dynamic, interactive directionality between the two brains involved.

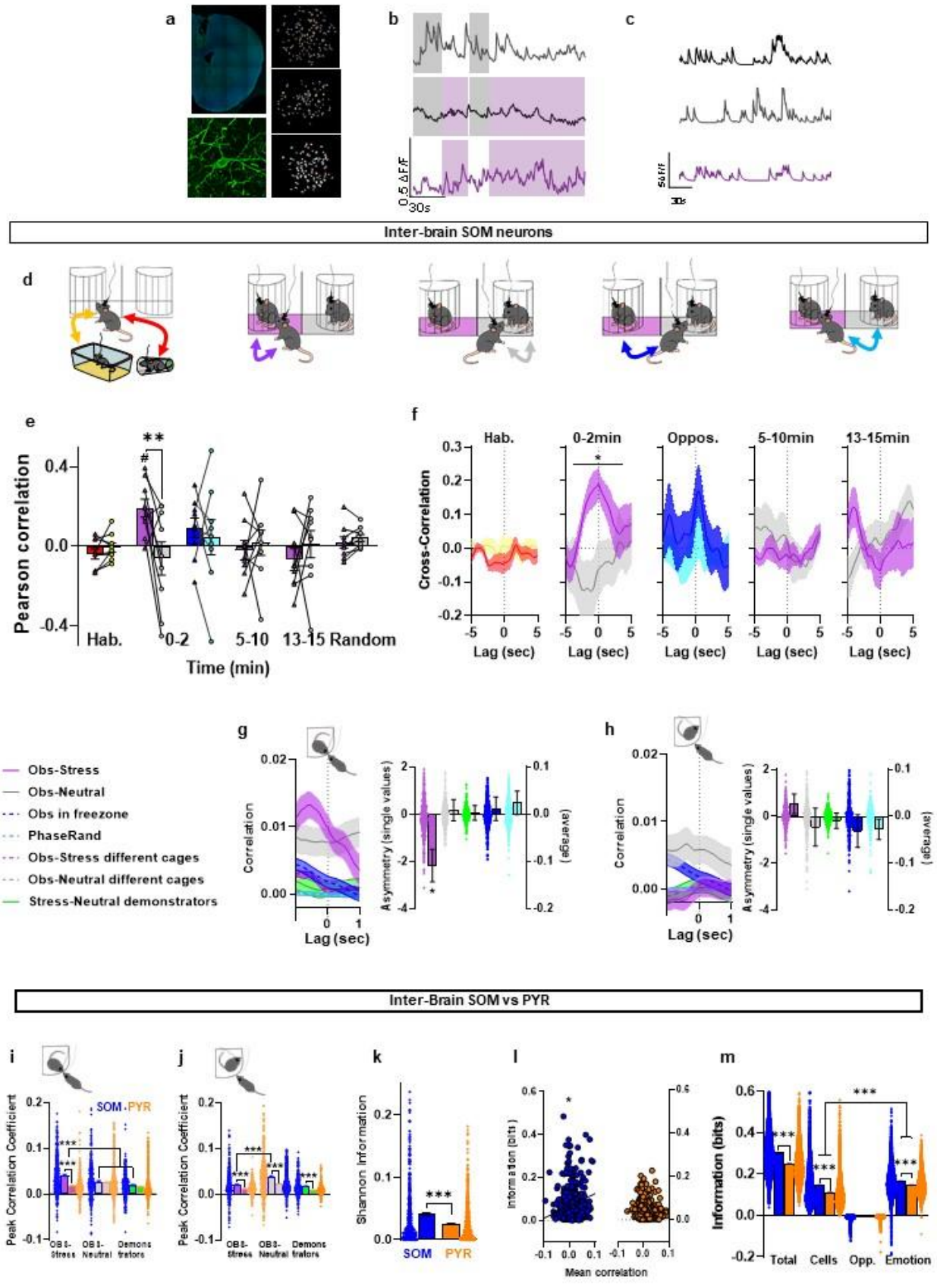
a
b
c
0.5 ΔF/F
30s
Inter-brain SOM neurons
d
e
Pearson correlation
Hab.
0-2
5-10
13-15
Random
Time (min)
f
Hab.
0-2min
Oppos.
5-10min
13-15min
Cross-Correlation
Lag (sec)
Obs-Stress
Obs-Neutral
Obs in freezone
PhaseRand
Obs-Stress different cages
Obs-Neutral different cages
Stress-Neutral demonstrators
g
h
Correlation
Asymmetry (single values)
Asymmetry (average)
Inter-Brain SOM vs PYR
i
j
k
l
m
Peak Correlation Coefficient
SOM
PYR
Shannon Information
Information (bits)
Mean correlation
Total
Cells
Opp.
Emotion

Figure 2

Figure 2. Inter-brain correlation for ACC SOM neurons is evident only with an emotionally altered demonstrator. n = 9 triplets, 968 neurons.

(a) Left: representative GCaMP expression and lens placement in the ACC (top), single pyramidal neuron (bottom). Right: example ROIs for single cell calcium imaging recordings from the 3 mice.

(b) Example average traces from the 3 mice.

(c) Representative traces from SOM single-neurons.

(d) Interbrain correlations were computed during the different phases of the task. Hab ctrl: habituation control, the observer was alone in the testing cages while the stressed demonstrator was under restraint in a falcon tube and the neutral demonstrator was in its home cage. Test – zone visit: interbrain correlation was computed during observer visits to the corresponding demonstrator. Test – opposite zone ctrl: as a control, interbrain correlation was computed during observer visits to the other demonstrator.

(e) Pearson correlation between SOM average activity in the observer and in each demonstrator during the different phases of the test. Hab: habituation. 0-2, 5-10, 13-15 minutes time bins of the test. Opp.: correlation computed between the observer and the non-explored demonstrator. Rand. interbrain correlations between the observer and each demonstrator irrespectively of observer position in the box.

(f) Cross-correlation between SOM average activity in the observer and in each demonstrator during the different phases of the test defined as for Pearson correlation.

(g) Cross-correlation computed between individual neurons of the observer and each demonstrator during reciprocal sniffing intervals and control conditions.

(h) Cross-correlation computed between individual neurons of the observer and each demonstrator during reciprocal sniffing intervals and control conditions.

(i) Interbrain correlation between individual neurons for SOM and PYR during reciprocal sniffing between the observer and the demonstrators. Obs-stress: observer-stress interbrain correlation. Obs-neutral: observer-neutral interbrain correlation. Demonstrator: interbrain correlation between the two demonstrators.

(j) Interbrain correlation between individual neurons for SOM and PYR during non-reciprocated observer sniffing between the observer and the demonstrators. Obs-stress: observer-stress interbrain correlation. Obs-neutral: observer-neutral interbrain correlation. Demonstrator: interbrain correlation between the two demonstrators.

(k) Mutual information analysis for SOM and PYR neurons. Amount of information that observer's neurons carry about the demonstrators' affective state.

(l) Mean correlation

(m) Correlation between the level of interbrain correlation and the information that each neurons carry about demonstrators' affective state

SOM neurons exceed PYR in inter-brain emotional encoding

To compare the relative contributions of each neuronal subpopulation to socio-emotional inter-brain dynamics, we performed a direct comparison of SOM and PYR inter-brain activity under different conditions.

The comparison of Pearson correlation coefficients revealed that the highest values were evident for SOM when the observer and the stress demonstrator were reciprocally interacting compared to equivalent PYR correlations or SOM correlations between observer and stress demonstrator or the two demonstrators (Fig. 2i). However, in non-reciprocated events, the pattern was different with SOM showing always an higher correlation compared to PYR, but this time with SOM correlation between observer and neutral being higher than observer and the stress demonstrator (Fig. 2j). Moreover, mutual information about emotional state of reciprocal interaction partners was higher for SOM compared to PYR ACC neurons (Fig. 2k). Importantly, differences across emotional states in the strength of the inter-brain correlations are not only measurable on average across all time points and interaction windows, but emotional state can be discriminated from inter-brain correlations at the individual time-point and individual reciprocal interaction (Fig. 2l). We computed the information about emotional state carried by the simultaneously recorded activity of triplets of neurons in the observer, in the stress and neutral demonstrators, and found that more than half of the total information carried by neural population activity was contributed by emotion-dependence of the inter-brain correlation strength (Fig. 2l). Thus, emotion-dependent inter-brain correlations carry more information than the firing rates of individual cells. Finally, we found that SOM neurons that are more strongly correlated with the demonstrator's brain also carry more information about the demonstrator's emotional state, while no such correlation was observed for PYR neurons (Fig. 2m). Overall, these results reinforce the evidence that SOM inter-brain dynamics are more tuned and carry more information related to altered emotional states in others.

Intra-brain correlation of ACC SOM relates to emotional state

We next tested ACC SOM intra-brain activity in the observer and two demonstrators computing single-cells correlations during interaction epochs, either reciprocal or unidirectional. When looking at the observer's brain alone, an higher intra-brain ACC SOM correlation was found when interacting with stress compared to the neutral demonstrators (Supplementary Fig. 5), in line with previous findings (Scheggia et al., 2020). Similarly, intra-brain correlations of ACC SOM neurons

was higher in the stress demonstrator when interacting with the observer compared to when no interaction was happening, while this difference was not evident for the neutral demonstrator (Supplementary Fig. 5). These results show that altered emotional states are detected more by intra-brain ACC SOM correlated activity, but in contrast to inter-brain dynamics, this is unrelated to reciprocal interactions between the observer and the demonstrator.

Preventing SOM, but not PYR, inter-brain correlation abolishes emotion discrimination

Whether inter-brain dynamics are a consequence of social interactions or can actively modulate social choices is still an open question (Holroyd, 2022; Novembre & Iannetti, 2021). To address this, we used targeted closed-loop optogenetic manipulations specific to cell type and emotional state.

We first disrupted the observed inter-brain ACC SOM correlation between the observer and the stress demonstrator by optogenetically silencing ACC SOM in the demonstrator whenever the observer visited (Fig. 3a,b). The neutral demonstrator received the same light delivery without any consequence in neuronal activity (Fig. 3a,b). This manipulation abolished the observer's preference towards the stress demonstrator (Fig. 3c,d) which was otherwise present in control experiments where both demonstrators expressed eYFP (Fig 3c,d). This effect was equally present in male and female mice (Supplementary Fig. 6). The optoinhibition did not alter the total duration of social exploration (Supplementary Fig. 6). Moreover, this ACC SOM inhibition did not induce any altered behavior in mice as doing the same manipulation in one of two equally neutral demonstrators did not induce any preference or avoidance in the observer (Supplementary Fig. 6). However, if two equally stress demonstrators were presented, a preference for the non-inhibited mouse appeared (Supplementary Fig. 6), suggesting that the unblocked relative increased correlation with the non-inhibited stress mouse might contribute to drive observer preference. These results demonstrate that blocking inter-brain correlation of ACC SOM neurons between the observer and the stress demonstrator when interacting abolished observer's emotion discrimination.

We next used a similar approach to test if the observed increased inter-brain ACC PYR correlation between the observer and the neutral demonstrator (Fig. 1) is necessary to emotion discrimination. Optogenetically silencing ACC PYR in the neutral demonstrator upon each visit from the observer did not alter emotion discrimination (Fig. 3g,h). Similarly, ACC PYR

optoinhibition had no effect on observer's total duration of social exploration, nor induced any preference if two equally neutral or stress demonstrators were presented (Supplementary Fig. 6). Thus, in contrast to ACC SOM inter-brain correlation, inter-brain correlation of ACC PYR neurons between the observer and the neutral demonstrator is dispensable for emotion discrimination.

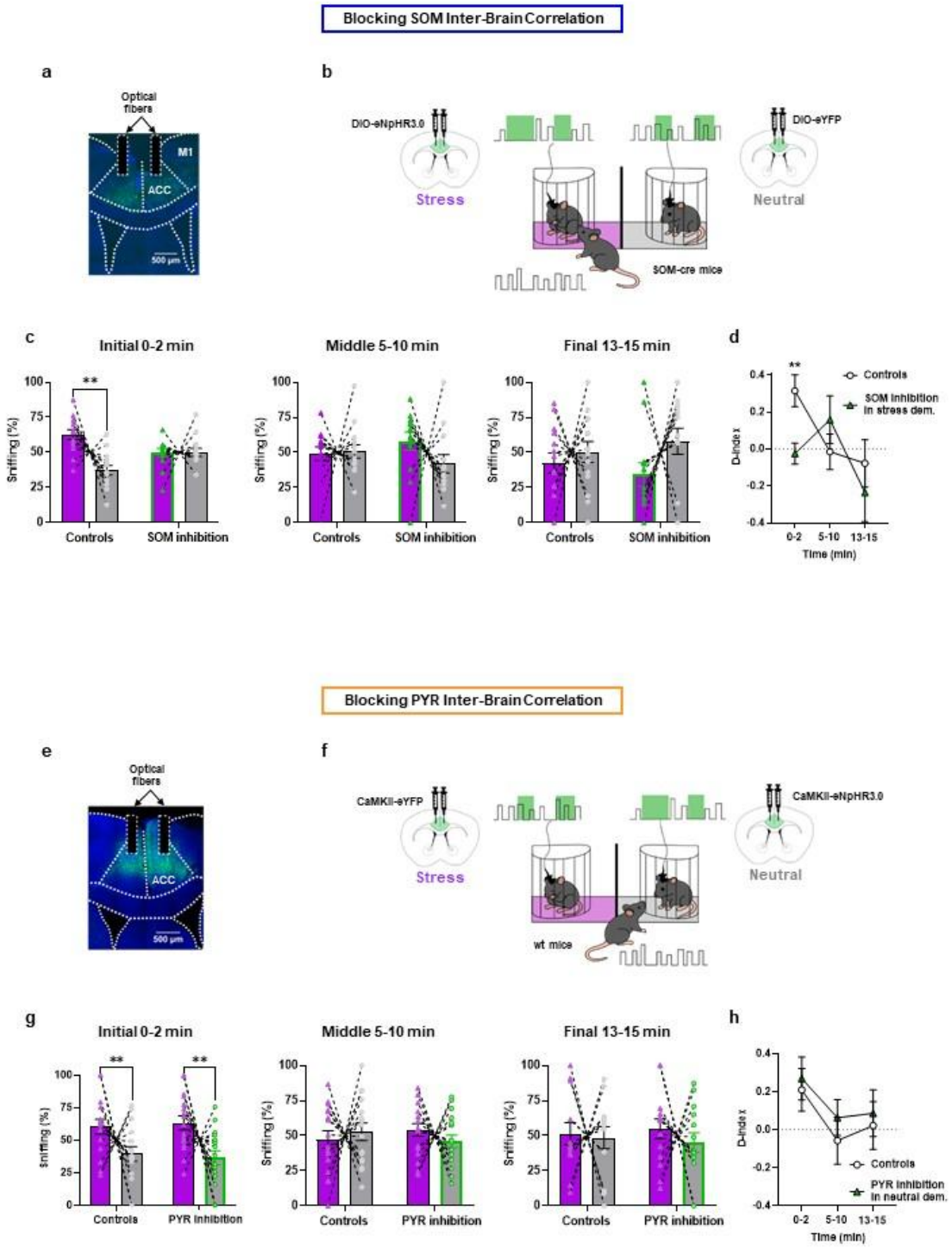

Figure 3

Figure 3. Blocking interneuronal synchrony in mice ACC SOM neurons block emotional preference.

(a) Representative fiber and opsin placement for SOM inhibition experiment.

(b) Stress halorodopsin-expressing mice were paired with neutral fluorophore-expressing mice in the EDT stress paradigm. Both demonstrators received green light in the ACC during observer visits to the respective zone, resulting in SOM inhibition only in the stressed demonstrator, disrupting its physiological interbrain synchronization with the observer.

(c) Observer sniffing percentage for controls and SOM inhibition in stress demonstrator group. Mixed-effect analysis, n controls = 14 n inhibition = 13 (Optogenetic treatment x Affective state ***p=0.0009; multiple-comparison: control stress vs control neutral ****p<0.0001).

(d) Discrimination index (sniffing time stress – sniffing time neutral / total sniffing time) for controls and SOM inhibition in stress demonstrator group. Two-tailed parametric t-test (**p=0.0034).

(e) Representative fiber and opsin placement for pyramidal neurons inhibition experiment.

(f) Experimental design: neutral halorodopsin-expressing mice were paired with stress fluorophore-expressing mice in the EDT stress paradigm. Both demonstrators received green light in the ACC during observer visits to the respective zone, resulting in pyramidal inhibition only in the neutral demonstrator, disrupting its physiological interbrain synchronization with the observer.

(g) Observer sniffing percentage for controls and pyramidal inhibition in neutral demonstrator group. Mixed-effect analysis, n controls = 16 n inhibition = 17 (optogenetic treatment x affective state p=0.5793, affective state ***p=0.0007. Multiple comparison: control stress vs neutral *p=0.0119, inhibition stress vs neutral **=0.0013).

(h) Discrimination index for controls and pyramidal inhibition in neutral demonstrator group.

Inducing inter-brain correlation in ACC SOM neurons drives emotional preference

To further prove the possible causal implication of inter-brain correlations in shaping socio-emotional behaviors, we next artificially mimicked correlation in emotional or non-emotional contexts based on our imaging data (Fig. 1, 2).

We exposed observer mice to two emotionally equal demonstrators (neutral or stress), correlating their ACC SOM activity only when interacting with one of the two demonstrators (Fig. 4a). Observer mice were equally stimulated when exploring both demonstrators. This manipulation did not induce discrimination towards two neutral demonstrators (Fig. 4b,d), similarly to no-stimulation conditions (Supplementary Fig. 7). In contrast, the same manipulation induced a preference for the synchronized stress demonstrator over the non-synchronized one in

the first two minutes (Fig. 4c,d). This timing preference is similar to mice's spontaneous preference for stress versus neutral demonstrators (Fig 1,2 and (Dautan et al., 2024a; Maltese et al., 2025; Scheggia et al., 2020). However, a preference for the non-synchronized stress demonstrator, but not different to the neutral-neutral condition, emerged during the middle of the task (Fig 4c,d). This latter effect may reflect a non-physiological artifact resulting from prolonged synchronization during a period when such interbrain correlation is not observed (Fig. 2). No sex-dependent effects or effects on the total amount of social explorations were evident (Supplementary Fig. 7). Moreover, stimulating only one of the two stress demonstrators without stimulating the observer did not induce any discrimination (Supplementary Fig. 7). This data strengthens the conclusion that SOM inter-brain correlation is important to drive observer's social preference only in a stress emotional context.

Inducing inter-brain correlation in ACC PYR reduces preference in neutral conditions

We then used the same optogenetic approach to test possible causal implication of ACC PYR inter-brain correlations.

Equally stimulating PYR ACC cells in both the observer and one of two neutral demonstrators during their social interactions induced an avoidance (Fig. 4e,g), in agreement with increased inter-brain ACC PYR correlation between the observer and the less preferred neutral demonstrator (Fig. 1). In contrast, the same optostimulation, but with two equally stress demonstrators, had no effects (Fig. 4f,g). No sex-dependent effects or effects on total sniffing were evident (Supplementary Fig. 7). No discriminatory behavior was evident if the ACC PYR of the observer were not stimulated, and only one of two equally neutral demonstrators was stimulated (Supplementary Fig. 8). These data indicate that ACC PYR inter-brain correlation contributes to reducing social preference for a neutral demonstrator.

Inter-brain ACC SOM anticorrelation drives aversion in neutral conditions

Our imaging experiments identified not only inter-brain correlations, but also patterns of anticorrelation (Fig. 1,2), which mathematically derived from moments in which one subject has some calcium neuronal activity while the other did not (Supplementary Fig. 9). Thus, here we checked if these patterns might also be causative of socio-emotional reactions.

We first activated ACC SOM neurons of the observer mice every time they entered the zone of two equally neutral or stress demonstrators (Fig. 4h). Simultaneously, only one of the two demonstrators received the inhibition of ACC SOM neurons every time the observer entered their zone (Fig. 4h). The other demonstrator received light, but no neural inhibition, when receiving the observer's visit. When presenting two equally neutral demonstrators, an avoidance for the anticorrelated demonstrator was induced (Fig. 4i,k). In contrast, with two equally stress demonstrators, this same optomanipulation did not induce any discriminatory behavior (Fig. 4j,k). These results corroborate our recording findings (Fig. 2), indicating that anticorrelated ACC SOM activity with the neutral demonstrator contribute in reducing preference for that mouse.

Reversing the stimulation/inhibition protocol, with ACC SOM neurons inhibited in observers upon entering the zone of one of two equally neutral or stressed demonstrators and activated in only that demonstrator, produced no effect under either condition (Supplementary Fig. 9).

Overall, these data indicate that inter-brain ACC SOM anticorrelation is meaningful in reducing preference, only in an emotionally-neutral situation, with the observer brain driving it.

Inducing inter-brain anticorrelation in ACC PYR neurons induces social preference

We then checked if the observed patterns of ACC PYR inter-brain anticorrelation (Fig. 1) might be as well causative for socio-emotional choices.

Activating ACC PYR neurons of observer mice each time they entered the zone of two equally neutral or stress demonstrators, and simultaneously inhibiting the ACC PYR neurons of only one of the two demonstrators upon the observer's visit (Fig. 4h), induced a preference for the anticorrelated demonstrator in both neutral and stress conditions (Fig. 4l-n). These results are in line with the imaging data (Fig. 1), indicating that ACC PYR inter-brain activity shows an anticorrelation with the most preferred mouse, even if the timing of the induced social preference differed depending on the emotional context. In contrast, inhibiting ACC PYR of observer mice every time they entered the zone of two equally neutral or stress demonstrators, while simultaneously activating ACC PYR of only one demonstrator had no effects (Supplementary Fig. 9).

These data indicate that inter-brain anticorrelation of ACC PYR is meaningful in inducing a preference independently of emotional contexts, and again driven by the observer.

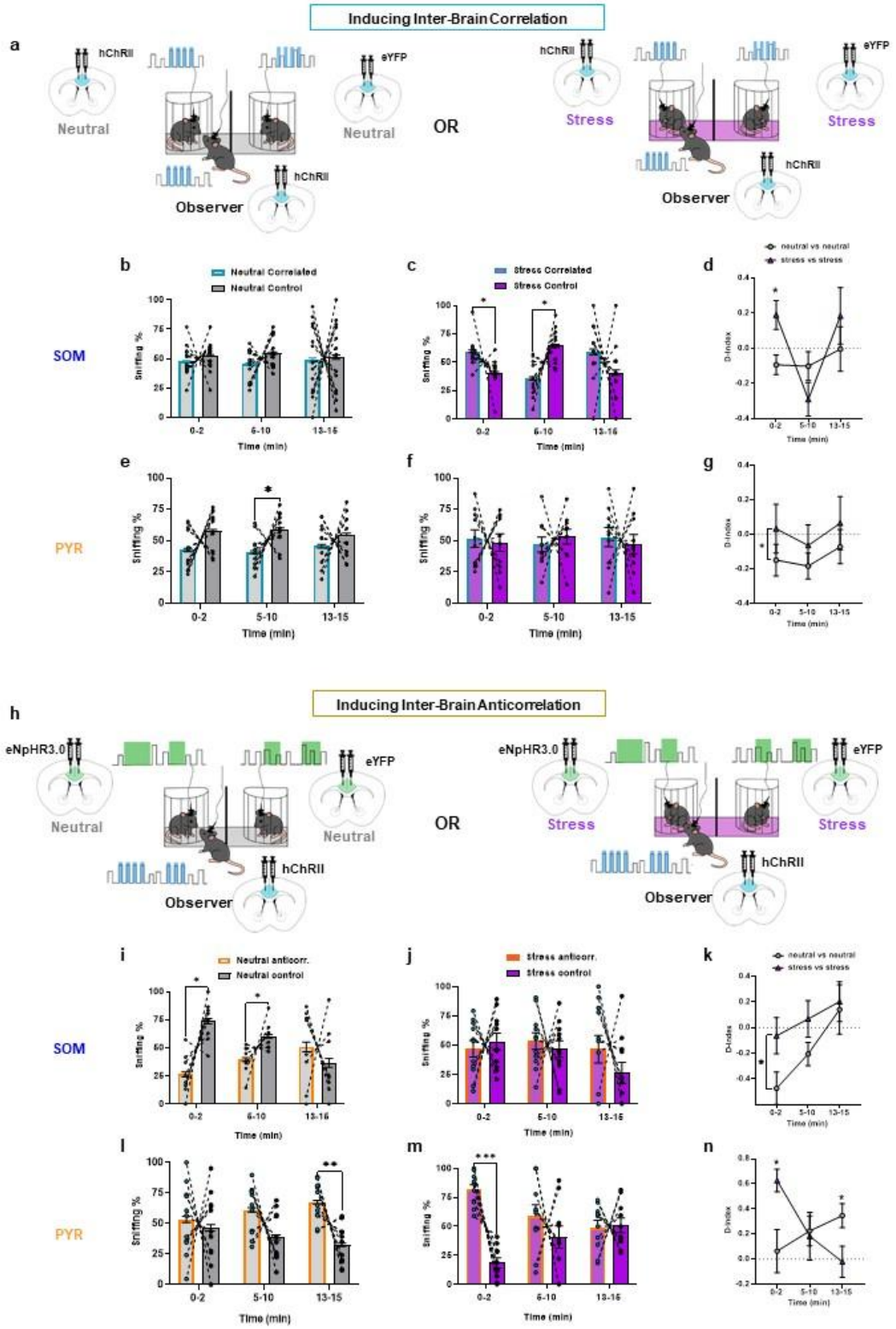

Figure 4

Figure 4. Inducing interneuronal synchrony in mice ACC SOM and PYR neurons drives emotional preference.

(a) Experimental design: concurrent optogenetic stimulation of ACC neurons in the observer and in one of two emotionally-equivalent mice.
(b) Observer sniffing toward neutral synchronized and neutral control demonstrators.
(c) Increased observer sniffing and significant discrimination index induced by optogenetic synchronization of SOM neurons in the observer and in one of two stressed demonstrators.
(d) Discrimination index for SOM synchronization in neutral-neutral and stress-stress configurations.
(e) Decreased observer sniffing induced by optogenetic synchronization of pyramidal neurons in the observer and in one of two neutral demonstrators.
(f) Observer sniffing toward synchronized and control stressed demonstrators.
(g) Discrimination index for PYR synchronization in neutral-neutral and stress-stress configurations.
(h) Experimental design: concurrent optogenetic stimulation of ACC neurons in the observer and inhibition in one of two emotionally-equivalent mice.
(i) Decreased observer sniffing and discrimination index during optogenetic desynchronization of SOM neurons in the observer and in one of two neutral demonstrators.
(j) Observer sniffing toward stress SOM desynchronized and stress control demonstrators. Right: discrimination index. n=11.
(k) Discrimination index for SOM desynchronization in neutral-neutral and stress-stress configurations.
(l) Increased observer sniffing toward the desynchronized demonstrator in the neutral vs neutral configuration.
(m) Increased observer sniffing toward the desynchronized demonstrator in the stress vs stress configuration.
(n) Discrimination index for PYR desynchronization in neutral-neutral and stress-stress configurations

Real-time close-loop induction of inter-brain correlation in ACC SOM drives emotional preference

The inter-brain optogenetic manipulations employed so far were artificially imposed and may not fully recapitulate the natural dynamical pattern of physiological brain activity. Thus, we set up a paradigm in which the recorded neuronal activity of one mouse (either the observer or one demonstrator) could optogenetically drive a similar pattern in another mouse, in stress or neutral conditions (Fig. 5a, Supplementary Fig. 10).

When the observer mouse's ACC SOM activity drove optogenetic stimulation of ACC SOM in one of two equally neutral demonstrators (Fig. 5b,d), no effects were evident. In contrast, a preference towards the synchronized demonstrator appeared during the first two minutes of the task when the observer was facing two equally stress demonstrators (Fig. 5c,d). When inverting the role (i.e. recording from the demonstrator drove stimulation to the observer), no effects were

evident (Fig. 5e-g). When using the same approach to drive PYR inter-brain synchronization no effects were evident in both the observer-to-demonstrator and demonstrator-to-observer configuration and in both neutral-neutral and stress-stress configuration (Fig. 5h-m). However, combining the two configurations together, a less preference for the ACC PYR neutral correlated demonstrator appears while the ACC SOM-driven preference for the stress correlated demonstrator got less significant (Fig. 5n). These further analyses reveal that while ACC SOM inter-brain coupling is clearly driven by observer activity targeting the stress demonstrator, ACC PYR inter-brain correlations during the neutral state are equally supported by both the observer and the demonstrator.

Overall, these results further strengthen the findings that ACC SOM inter-brain correlation initiated by the observer mouse drive emotion discrimination.

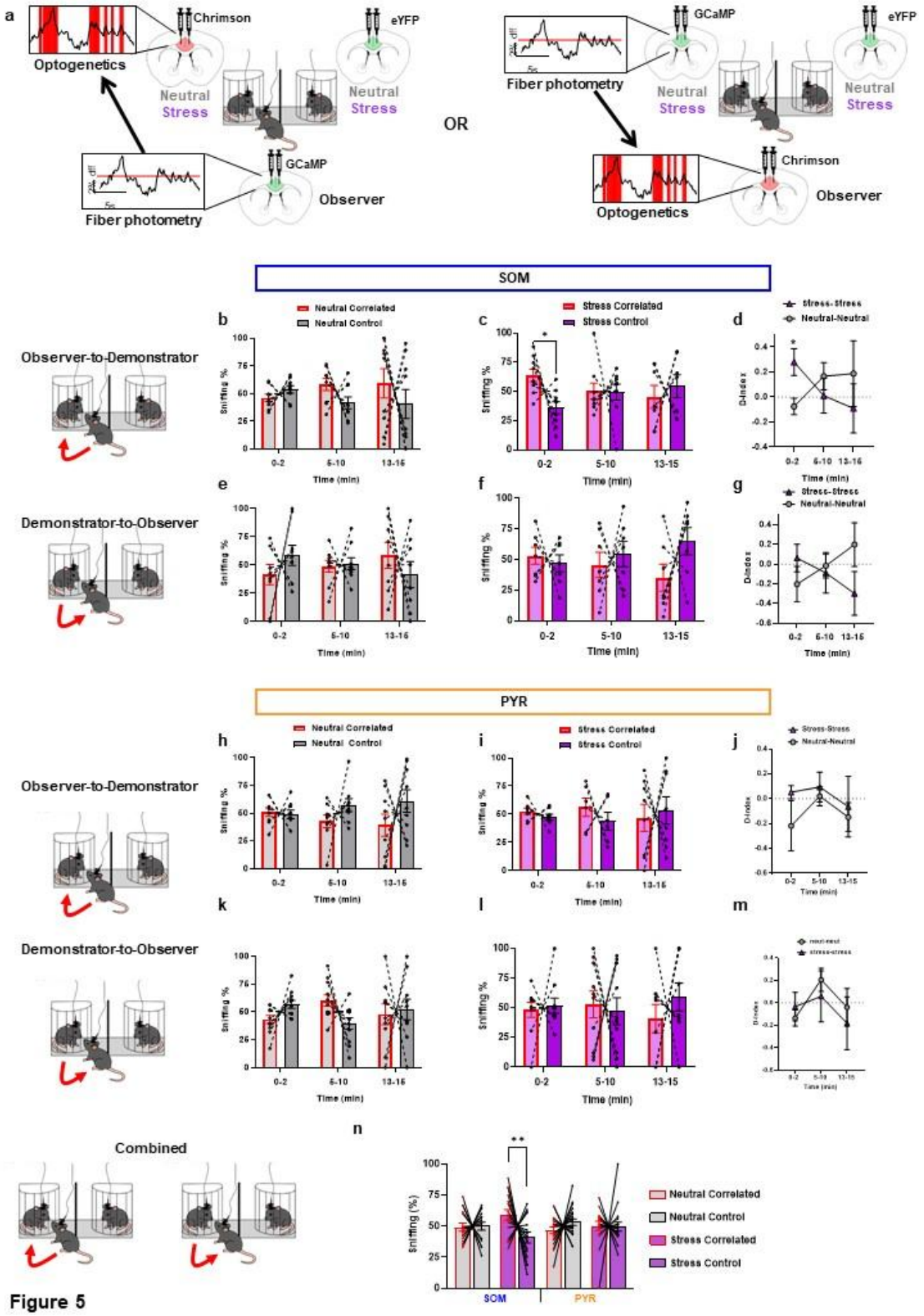
a
Chrimson
eYFP
Optogenetics
Neutral
Stress
Neutral
Stress
GCaMP
Observer
Fiber photometry
OR
GCaMP
eYFP
Fiber photometry
Neutral
Stress
Neutral
Stress
Chrimson
Observer
Optogenetics
SOM
Observer-to-Demonstrator
Demonstrator-to-Observer
b
Neutral Correlated
Neutral Control
c
Stress Correlated
Stress Control
d
Stress-Stress
Neutral-Neutral
e
f
g
PYR
h
i
j
k
l
m
Sniffing %
D-Index
Time (min)
0-2
5-10
13-15
Combined
n
Sniffing (%)
Neutral Correlated
Neutral Control
Stress Correlated
Stress Control
SOM
PYR

Figure 5

Figure 5. Close loop exp. Observer SOM activation drives synchronization and social preference only towards emotionally altered mice.

(a) Experimental design. Left: observer SOM activity was recorded and used to control optogenetic stimulation to one of two emotionally-equivalent demonstrators when the signal exceed a threshold. Right: one demonstrator activity was recorded and used to deliver an optogenetic stimulation to the observer when the normalized signal exceeds a threshold.

(b) Observer sniffing during observer-driven SOM interbrain synchronization toward one of two neutral demonstrators.

(c) Observer sniffing during observer-driven interbrain synchronization toward one of two stressed demonstrators.

(d) Discrimination index for SOM closed-loop synchronization driven by the observer in neutral-neutral and stress-stress configurations

(e) Demonstrator sniffing during demonstrator-driven SOM interbrain synchronization toward one of two neutral demonstrators.

(f) Observer sniffing during demonstrator -driven interbrain synchronization toward one of two stressed demonstrators.

(g) Discrimination index for SOM closed-loop synchronization driven by the demonstrator in neutral-neutral and stress-stress configurations

(h) Observer sniffing during observer-driven PYR interbrain synchronization toward one of two neutral demonstrators.

(i) Observer sniffing during observer-driven PYR interbrain synchronization toward one of two stressed demonstrators.

(j) Discrimination index for PYR closed-loop synchronization driven by the observer in neutral-neutral and stress-stress configurations

(k) Demonstrator sniffing during demonstrator-driven PYR interbrain synchronization toward one of two neutral demonstrators.

(l) Observer sniffing during demonstrator-driven PYR interbrain synchronization toward one of two stressed demonstrators.

(m) Discrimination index for PYR closed-loop synchronization driven by the demonstrator in neutral-neutral and stress-stress configurations

(n) Observer sniffing during the first 2 minutes of all conditions.

Discussion

We discovered that emotions modulate inter-brain dynamics in a neuron-type-specific manner. Inter-brain ACC SOM inhibitory neurons correlations and PYR anticorrelations are recruited when one partner is in a stress state. Conversely, inter-brain ACC PYR correlations and SOM anticorrelations arise when two subjects are in a neutral state. Importantly, we demonstrate that these substrate-specific-dynamics causally influence social preference, with SOM neurons playing a central role in socio-emotional contexts.

We found that an altered emotional state changes inter-brain dynamics. This expands previous literature showing inter-brain correlation between dyads of monkeys, bats and mice in basal neutral states (Kingsbury et al., 2019; Lee et al., 2024; Rose et al., 2021; Scaglione et al., 2024; Tseng et al., 2018; Zhang & Yartsev, 2019). Our initial comparative study with humans suggests that the same organizing principles of emotion-dependent inter-brain dynamics operate across species, pointing to conserved neural mechanisms. Specifically, reciprocal information exchange in the presence of stress in one partner disrupted overall inter-brain cortical correlations, evident in reduced EEG correlation in humans and PYR in mice. These findings mirror prior human studies reporting enhanced inter-brain correlation during positive emotional interactions (Anders et al., 2020; Liu et al., 2023; Santamaria et al., 2020). Overall, our findings open to cross-species, cell-type-specific and time-dependent inter-brain dynamics influenced by emotions.

We reveal that inter-brain dynamics rely on distinct neural substrates depending on the socio-emotional context. Stress initially links interacting brains, with ACC SOM activity correlating and PYR anticorrelating across individuals inducing emotion discrimination. In contrast, during neutral interactions, inter-brain ACC PYR correlation and SOM anticorrelation developed over time. Notably, these correlations did not always paralleled the preference for one of the two demonstrators, indicating that more than the quantity of the interaction, inter-brain correlations change based on the quality of the interaction. This is a step forward compared to most humans' and other animals' studies finding a positive association between inter-brain correlation and the quantity of social interactions, still without considering the effect of individual emotions (Antonelli et al., 2025). Furthermore, our current findings strengthen previous single-brain evidence reporting a special role of cortical SOM neurons in emotion discrimination (Dautan et al., 2024a; Scheggia et al., 2020), but now in an inter-brain perspective. Intriguingly, recent

work implicates GABAergic neurons in shared-space inter-brain dynamics in mouse dyads in neutral states (Zhang et al., 2025). Given that our data show marginal SOM neurons involvement in neutral-neutral interactions, and that this prior study did not distinguish among GABAergic subtypes, our findings raise the possibility that PV neurons may underline inter-brain correlations during non-emotional social interactions. This would be in line with single brain evidence reporting PV as mainly involved in basic sociability with no emotions (Scheggia et al., 2020). Thus, our findings reveal that inter-brain correlated activity arises from distinct, molecularly defined neural substrates, shaped by the emotional states of the interacting individuals.

We proved that inter-brain dynamics actively modulate social decisions in emotional contexts. This finding represents an initial step toward resolving whether inter-brain correlations are simply byproducts of social interaction or play a causal role as modulators (Hamilton, 2021; Holroyd, 2022). We first demonstrated that preventing inter-brain correlation by silencing SOM neurons, but not PYR, in the stress demonstrator impaired emotion discrimination. Furthermore, in line with our imaging experiments, optogenetic manipulations artificially inducing inter-brain correlations demonstrated differential effects of SOM and PYR inter-brain dynamics depending on the socio-emotional relationships of the interacting subjects. All this strengthens the idea that the neuronal activity of one subject not only influences their own behavior, but is interconnected with that of others influencing multi-brain responses. In contrast to a previous study (Yang et al., 2021), optogenetic induction of an artificial inter-brain PYR correlations in our setup led to avoidance rather than preference. This earlier study involved free interaction of only two mice, lacking real-time control over a non-correlated mouse, and targeted the PrL region of the PFC. Thus, together with our findings, this could indicate that PYR inter-brain correlations during two-choice social discrimination may have a different role than during free, reciprocal interactions. Alternatively, the discrepancy could reflect distinct contributions of PFC subregions (i.e. ACCs or PrL) to inter-brain dynamics. Notably, implementing a new and more ethologic-naturalistic approach where one mouse brain closed-loop drove a similar pattern of activity in another brain, revealed further that ACC SOM activity of the observer drove the preference towards a stress demonstrator, while PYR inter-brain correlation induce avoidance only in neutral state conditions. This setting avoids artifacts of artificial stimulations and strengths our conclusions that different neural substrates drives social choices in different socio-emotional contexts.

We demonstrated that not only correlations, but also inter-brain anticorrelations have a meaningful implication in socio-emotional choices. Specifically, ACC PYR show inter-brain anticorrelation with the preferred stress demonstrator, and in agreement, optogenetic induction of PYR anticorrelation in only one of two equally stress demonstrators caused social preference. Conversely, SOM activity tend to be anticorrelated between the observer and the less preferred neutral demonstrator, and optogenetic induction of SOM anticorrelation induced avoidance towards one of two equally neutral, but not two stress, demonstrators. Notably, in both PYR and SOM anticorrelation manipulations, the discriminatory effects appeared only when stimulating the observer, but not the demonstrators. The importance of alternating correlated and anticorrelated brain and behavioral patterns in supporting social goals has been theorized (Mayo & Gordon, 2020). Here, we demonstrate the previously unexplored causal role of anticorrelated inter-brain activity during socio-emotional choices.

In summary, we provide initial evidence that inter-brain dynamics originate from distinct neuronal substrates in emotional compared to neutral states social contexts. Notably, cell-specific correlated and anticorrelated inter-brain dynamics are both causative in determining social choices towards others' emotions. This constitutes a new vision in socio-emotional responses, with fundamental impact on all animals' lives.

Methods

Mouse Subjects

All procedures were approved by the Italian Ministry of Health and the local Animal Use Committee and were conducted in accordance with the Guide for the Care and Use of Laboratory Animals of the National Institutes of Health and the European Community Council Directives. Routine veterinary care and animal maintenance are provided by dedicated and trained personnel. Adult mice between 3-6 months old with C57Bl/6J background were used. For the miniscopes recording experiments only males were used because better able to support the weight of the devices. For all other experiments, both male and female mice were used. Heterozygous somatostatin cre-expressing mice (SOM-cre, Jackson: 013044) and Wild-Type (WT, Jackson: 000664) used for all experiments were bred in our animal facility. Mouse genotypes were determined by Polymerase Chain Reaction (PCR) of ear snip tissue. Animals were housed in cages with 2-to-4 cagemates in a climate-controlled facility (22°c) with *ad libitum* access to food and water and a 12hr light-dark cycle (07:00-19:00 light, 19.00-7.00 dark). All experiments were run during the light phase.

Viral vectors

For large-scale calcium imaging AAV1.Syn.Flex.GCaMP6f.WPRE.SV40 (Addgene, 100833-AAV1) was injected in SOM-cre heterozygous mice and pENN.AAV1.CamKII.GCaMP6f.WPRE.SV40 (Addgene, 100834-AAV1) was injected in WT mice. Both viral vectors were diluted 1:6 in saline before the injection. For somatostatin neurons optogenetic manipulations we used AAV5-Ef1a-DIO eNpHR-3.0-EYFP (Addgene, 26966) for inhibition, AAV5-EF1a-double floxed-hChR2(H134R)-EYFP-WPRE-HGHpA (Addgene, 20298) for excitation, or AAV5-Ef1a-fDIO-EYFP (University of Pennsylvania, CS0378) for controls, all injected in SOM-cre mice. For pyramidal neurons we used AAV1-CaMKIIa-eNpHR 3.0-eYFP.WRGE.hGH (University of Pennsylvania, V4188MI-R) for inhibition, AAV1-CaMKIIa-hChR2(H134R)-eYFP.WRGE.hGH (University of Pennsylvania, CS0717-3CS) for excitation, or AAV1-CaMKII0.4-eGFP.WRGE.rGH (University of Pennsylvania, CS0934) for controls, injected in wt mice. For fiber photometry and closed-loop optogenetic stimulation we

injected a 1:6 mix of either AAV1.Syn.Flex.GCaMP6f.WPRE.SV40 (Addgene, 100833-AAV1) and AAV5-Syn-FLEX-rc[ChrimsonR-tdTomato] (Addgene, 62723-AAV5) or a 1:6 mix of pENN.AAV1.CamKII.GCaMP6f.WPRE.SV40 (Addgene, 100834-AAV1) and AAV5-CamKIIa-ChrimsonR-mScarlet-KV2.1 (Addgene, 124651-AAV9) in SOM-cre or wt mice respectively.

Stereotaxic surgeries

C57Bl/6J and SOM-cre naïve mice were subjected to stereotaxic surgeries at 2-3 months old. All mice were anesthetized with a mix of isoflurane (3%) in Oxygen (O_2, 1%) before being mounted on a stereotaxic frame (Kopf Instruments), then kept at 1-2% isoflurane throughout the surgery. Brain coordinates for the ACC were defined based on the Mouse brain Atlas (from Paxinos and Franklin's) as follows (AP/ML/DV, in mm from Bregma and the skull): AP, +1.0 mm and ML, +0.3 mm; at two different DV coordinates, −1.75 and −1.55. 0.2 µl of virus mix were infused in each site through a borosilicate micropipette connected to a 10µl Hamilton syringe filled with mineral oil, with a motorized injector (WPI). The injection rate was set to 0.15µl /min and the pipette was maintained in position for at least 5 min to allow for proper diffusion. After viral injection mice were given between 2 and 3 weeks to recover before the lens or fiber implantation. Mice underwent a second surgery for the implantation of a 0.5 mm outer diameter gradient-index (GRIN) lens (ProView lenses, Inscopix) at the same coordinates as the virus injections, 10–14 d following virus injections. Before lowering the GRIN lens, a pre-track was performed using a blunted needle (25 gauge) to reduce tissue damage and minimize brain pressure. GRIN lens insertion was monitored and positioned at the focal point presenting the highest Ca^{2+} signal. Optogenetic dual fiber implants (Doric Lenses) and optic fibers (RWD) for fiber photometry recordings were placed at the same AP and ML coordinates as the viral injection, and at DV: -1.50 and - 1.55 respectively. All implants were maintained in position using a thin layer of Kwik-Sil (World Precision Instruments), two blunted skull screws, and adhesive dental cement (Sun Medical Super-Bond C&B Kit, Dental Leader). Mice were allowed to recover at least 7 days before starting the handling phase.

Apparatus

To allow neuronal recording and manipulation, the testing cage is placed inside a custom-made canopy structure where the cables and two high-resolution monochrome cameras (Imaging source, DMK 22AUC03) were accommodated during testing. The EDT apparatus is 3D printed onto a square apparatus (35.5 x 23.5 x 19) containing a two quarter circles (4cm radius) on two opposite sides. Each quarter circle is delimited by metal rods (0.8cm wide) that allow sufficient space for social contact between the demonstrator (freely moving in the apparatus) and the stimuli (freely moving in the quarter-circle). A 3D-printed separator (11 x 19cm) is placed in the middle of the apparatus between the two quarter-circles to block the reciprocal view of the stimuli animals. Both a top view and an upper-front view of the apparatus were acquired through ANYmaze software (Anymaze 7.4, Stoelting). For automated scoring, a virtual square (11 x 11 cm) is drawn between each quarter-circle and the separator to define a zone associated with each stimulus. Videos are collected at 15FPS using the behavioral tracking system (Anymaze 7.4, Stoelting). In optogenetic experiments, live tracking of the mice was used to deliver 5V- TTL through an Anymaze interface (Ami1) to the acquisition hardware (DAQs) calcium data or LEDs and Lasers for optogenetics, based on the zone visited.

Behavioral procedure

All mice were group-housed and separated based on their experimental role (observer vs demonstrator). All mice were handled once a day for 1 min for at least 3 days before behavioral testing procedures. Additionally, mice assigned to miniscope recordings were habituated to wear the miniscope for 15 minutes over 3 consecutive days in their home cage. Observers and demonstrators were individually habituated to the experimental apparatus with the cable attached for three days with daily sessions of 15 minutes, in their respective positions (demonstrators inside their quarter-circle, observers in the free zone). Demonstrator mice were matched by age, sex, and strain to the observers. To avoid confounders due to side preference, neutral-, stress-, manipulated-, and controls- stimulus were counterbalanced in the two sides of the testing arena. Neutral demonstrators were naïve and used for a maximum of 2-to-3 times, with at least 1 week between each experiment. Observers were always exposed to novel demonstrators. No differences were

observed in the performance of the observer mice depending on the previous experience of the demonstrator.

On the day of the testing, all mice were brought into the experimental room at least 1h before the experiment began, and kept distant to avoid visual or olfactory contact between observers and demonstrators. Observer mice were gently moved into the arena connected to the patch cord for optogenetics/fiber photometry, or the electric cord for miniscope recordings. The neutral demonstrator stayed in its home-cage while the stress demonstrator was subjected to a 15-minutes restraint inside a 50mL falcon tube with a hole in the tip for air exchange and a long and narrow opening on top for the cable. The demonstrators were then moved immediately to their respective side of the arena, and the observer was allowed to explore the two demonstrators for 15 min. Following each experiment, the apparatus is thoroughly cleaned with 50% ethanol, wiped, and allowed to air dry.

Miniscope acquisition setting

To concurrently image the GCaMP6 calcium indicator from 3 mice we took advantage of three miniature fluorescent microscopes (nVoke 3.0, Inscopix) with an integrated blue LED (EX-LED, 435–460 nm, average power 1 mW mm^{-2}) and red LED (OG-LED, 590–650 nm, light power 0–5 mW mm^{-2}). On the first day of mice habituation to the cables the miniature microscope was positioned on the head of the animals and the focal plane was adjusted through the Acquisition Software (version 1.2.0, Inscopix). Optimum laser power, imaging gain, and focal distance were selected for each animal and conserved across all experiments. On the experiment day Ca^{2+} signals were collected at 20 Hz during the habituation of the observer, the stress phase for the stressed demonstrator, while the neutral demonstrator was in its home-cage, and during the entire 15 min period of the EDT. In order to synchronize the 3 miniscopes and the behavioral video, calcium recording was controlled by the tracking software and interface (Anymaze, Ami1) through a TTL concurrently delivered to the miniscopes at the start of the habituation and the test.

Calcium signal analyses

Before proceeding to behavior-based segmentation of calcium activity and inter-brain correlation analysis, the signal was processed using data analysis software (Inscopix Data Processing

Software version 1.2, Inscopix). Both signals recorded during the EDT and their respective habituation period were merged in a time series and analyzed together to track the same neurons before and after exposure to the demonstrators. Dropped frames were corrected by a smooth correction of the edges. Data were pre-processed through the following steps: spatial and temporal downsampling, using x2 scale factors of space and time; spatial filtering of the image to remove low and high frequencies with a bandpass filtering; motion correction between different frames of the videos; pixel normalization over the mean value of the movie. The selection of neurons was done using manual regions of interest (ROIs), for which a selection tool was used to delimitate the borders of putative GCaMP-expressing neurons. After neurons selection, an OASIS algorithm was applied to deconvolve the traces. At the end of these steps, the final data available consist of a list of every neuron detected, and the corresponding ΔF/F value for each frame. To make Ca^{2+} signals traces comparable with each other, individual neuron traces were normalized by their standard deviation.

Spearman correlation of neuronal activity across brains:

To test inter-brain correlations during emotion discrimination, we first averaged the Ca^{2+} activity of all recorded cells (except those active only during habituation) for each animal and applied a detrending function to exclude the effect of photo bleaching on correlations. We then computed the Spearman correlation coefficient to consider possible non-linear correlations across brains.

Cross-correlation

In order to gain more insight into the timescale at which inter-brain correlations occur, we performed a cross-correlation analysis using the neural activity from interacting animals in the EDT. The cross-correlation curve between the two activities is expressed over different values of the reciprocal lag between the two. A peak in the cross-correlation curve expresses a state of synchronization of the two signals, one being shifted in time from the other by the corresponding lag value. As a consequence, once computing the cross-correlation curve between two time-dependent activities, one can identify its maximum value and retrieve the corresponding value of the lag, estimating the true delay between the signals. We calculated the correlation between ΔF/F activity traces during intervals in which mice were close (observer in demonstrator's zone) with different time shifts, ranging from -5 seconds to +5 seconds, and plotted the correlation as a function of time lag (Fig 4.2).

Single-neurons correlation analysis

For each observer neuron i, we computed the time shifted Pearson correlation between the activity of i and the activity of another neuron j (either in the observer brain for the within brain condition, or in the demonstrator brain for the across brain condition), and then we averaged over j to obtain a within-brain and an across brain time-lagged coupling function for each neuron i in the observer brain. To emphasize the short-scale correlations, we regressed out the slow variations of rates across behavioral interaction windows by computing partial Pearson correlations, where we partialled out the mean activity of both signals within each interaction window. We regressed out the slow variations of rates across behavioral interaction windows to emphasize better the short-scale correlations (compare regressed vs non-regressed to appreciate the importance).

Asymmetry measure, Directionality Index

We first computed the mean Pearson correlation for a neurons i across all neurons j for different time shifts (Δt), obtaining a curve resulting in a correlation curve across time shifts. Negative time shifts indicate that the activity of neuron i precedes that of the other neurons j (observer is preceding the demonstrator's activity), while positive shifts indicate that neuron i follows the activity of neurons j (demonstrator is preceding the observer's activity). Correlation values with negative time shift indicate that the observer is preceding the demonstrator's activity. Conversely, correlation values with positive time shift indicate that the demonstrator is preceding the observer's activity. To compute the time-asymmetry directionality index we take the integral of the correlations with a positive time shift and subtract the integral of the correlations with a negative time shift. This results in an overall measure that captures the balance of directional influences: if the asymmetric measure is positive, it indicates that the demonstrator drives the observer (stronger correlations in the positive time-shift region); if negative, it indicates that the observer drives the demonstrator (stronger correlations in the negative time-shift region).

Mutual information analysis

We quantified how much information the neural activity of the observer (R) carries about the affective state of the demonstrators (T) using mutual information, I(R:T). This information-theoretic measure captures the reduction in uncertainty about the target affective state given the

observer's neural responses. For each neuron we computed mutual information carried by R as follows:

[Equation]

To quantify the amount of information about demonstrator's emotional states codified by observer's neurons, we computed the mutual information, I(S;R), between position in the linear track, stimulus (S), and the calcium event trace, response (R), as follows:

$$I(S;R) = \sum_{s\in S, r\in R} p(r)p(r|s)\ log_2 \frac{p(r|s)}{p(s)},$$

With R and T representing the sets of all possible discrete values of neural responses and affective states. [Equation] is the joint probability of response r and target state t, [Equation] and [Equation] the marginal probabilities of response and state.

S and R representing the arrays of all possible discrete values of stimulus or response, p(s) the probability of the stimulus s, p(r) the probability of the response r across all trials to any stimulus, and p(r|s) the conditional probability of the responses r given presentation of stimulus s.

Information breakdown for triplets of neurons

To assess the extent to which across-brain correlations encode information about which is the affective state of the demonstrator that is interacting with the observer, we proceeded as follows. We first computed the Shannon information about affective state carried by the simultaneously recorded activity of triplets of neurons each located in the observer, in the stressed demonstrator and neutral demonstrator brain using Shannon formula and similarly to what we did to compute single-neuron affective state information (Methods section XX). We then used the Information breakdown (Cite) to decompose this Shannon information into components I_lin (the sum of the information separately conveyed by each of the single cells), I_(sig-sim) (contribution of the similarity across neurons of trial-averaged responses to different affective states), I_(cor-ind) (contribution of the interplay between the signs of similarity of affective state tuning and of across-brain correlations), and of I_(cor-dep) (quantifying information added by the modulation of across-brain correlation strength by the affective state).

Optogenetic manipulations

All optogenetic manipulations involved bilateral AAV injection in the ACC and subsequent implantation with dual fiber optic implants terminating dorsally to the injection area (Doric Lenses, DFC_200/245-0.37_2mm_GS0.7_FLT). During behavioral experiments, implants were connected to splitter branching patchcord (Doric Lenses, SBP(2)_200/230/900-0.37_1m_FCM-GS0.7), which were in turn connected to blue (480 nm) or green light (530 nm) LEDs (Prizmatix Laser) using a 1 × 1 fiberoptic rotary joint (Prizmatix) located above the cubicle containing the testing arena. Laser power was adjusted such that the light at the tip of the fiberoptic cable was approximately 3 mW. Behaviorally-controlled light delivery was achieved through TTL signals from the behavioral tracking software and interface (Anymaze, Ami1) to the LEDs. In all experiments, opsin-expressing and fluorophore demonstrators were paired and both received light, to concurrently exclude possible effects of the light on observer preference and control for non-specific effects of LED light delivery in the demonstrator. Both observers and demonstrators were tested up to 3/4 times, always keeping their original roles. Demonstrators always started being tested as neutral, 1/2 times, and then became stressed demonstrators 2 more times.

Preventing interbrain correlation

For optogenetic inhibition experiments we used AAV carrying: (1) for SOM, a Cre-dependent halorhodopsin (AAV5-EF1a-DIO-eNpHR3.0- eYFP, Addgene, 26966) or a cre-dependent eYFP (AAV5-Ef1a-fDIO-EYFP, University of Pennsylvania, CS0378); (2) for PYR, a CaMKIIa-dependent halorhodopsin (AAV1-CaMKIIa-eNpHR 3.0-eYFP.WRGE.hGH, University of Pennsylvania, V4188MI-R) or a CaMKII-dependent eYFP (AAV1-CaMKII0.4-eGFP.WRGE.rGH, University of Pennsylvania, CS0934) into the ACC of SOM- or C57BL/6J mice (Fig. 3a). During behavioral experiments we delivered a continuous green light to each demonstrator only during observer visits to their compartment. For SOM experiments, demonstrators were pseudo-randomly paired as the stress demonstrators expressed halorhodopsin while the neutral demonstrator eYFP. For PYR experiments, demonstrators were pseudo-randomly paired as the neutral demonstrators expressed halorhodopsin while the stress demonstrator eYFP. In control experiments both demonstrators expressed eYFP and received light during observer's visits.

Inducing inter-brain correlation

For optogenetic excitation experiments we injected AAV expressing: (1) for SOM, a Cre-dependent channelrhodopsin (AAV5-EF1a-DIO-hChR2(H134R)-EYFP-WPRE-HGHpA, Addgene, 20298) or a cre-dependent eYFP; (2) for PYR, a CaMKIIa-dependent channelrhodopsin (AAV1-CaMKIIa-hChR2(H134R)-eYFP.WRGE.hGH, University of Pennsylvania, CS0717-3CS) or a CaMKII-dependent eYFP into the ACC of SOM- or C57BL/6J mice. Photo-stimulation protocol involved 5 ms pulses of blue light delivered at 5Hz controlled by observer position in the arena. All observers expressed ChRII and received optogenetic stimulation during the visits to both demonstrators. Synchronized demonstrators (ChRII-expressing) were paired with YFP-expressing demonstrators and both received light when the observer was exploring their specific compartment. Overall, resulting in synchronous observer-demonstrator stimulation in the synchronized demonstrator side and observer-only stimulation in the control demonstrator side.

Inducing inter-brain anti-correlation

We injected AAV carrying: (1) for SOM, a Cre-dependent ChRII or a cre-dependent halorhodopsin or a cre-dependent eYFP; (2) for PYR, a CaMKIIa-dependent ChRII or a CaMKIIa-dependent halorhodopsin or a CaMKII-dependent eYFP into the ACC of SOM- or C57BL/6J mice. Two experimental designs were used to achieve anti-correlation:

- Observer photo-stimulation and concurrent demonstrator photo-inhibition: in this configuration observers expressed ChRII and received pulsed blue light in both demonstrators' compartments. Anti-correlated demonstrators (Halorhodopsin-expressing) were paired with YFP-expressing demonstrators and both received continuous green light when the observer was exploring their specific compartment.
- Observer photo-inhibition and concurrent demonstrator photo-stimulation: halorhodopsin expressing observers received continuous green light in both demonstrators' compartments. Anti-correlated demonstrators (hChRII-expressing) were paired with YFP-expressing demonstrators and both received pulsed blue light when the observer was exploring their specific compartment.

Fiber photometry and closed-loop optogenetic setting

Optic-fiber implants connected to metal or zirconia ferrules were cleaned and connected to a low-auto fluorescence patch cord (2.5 m long, 0.5 NA, Doric Lenses). A second dummy patch cord

was attached and connected to the dummy ferrule to reduce oscillations and thus prevent artifacts. Calcium signals were acquired through an integrated fiber photometry system (Aquineuro, Fiber Photometry recording System), delivering alternated light at 470nm for GCaMP excitation and at 410nm for isosbestic control.

For closed loop stimulation, activity dependent optogenetic stimulation was delivered. During the experiment, the recording software computed real-time data normalization from the signal acquired from the mouse chosen to drive the stimulation and a 2% variation of fluorescence was set as threshold to deliver optogenetic stimulation to the mouse chosen to receive stimulation, through a TTL from the fiber photometry system and the 635nm Laser (Aquineuro, Intelligent Optogenetics System).

The estimated delay from when the recorded signal crosses the 2% threshold and the stimulation is sent is around 200 ms.

Behavioral analyses

All behaviours were manually scored by three expert scorers, blinded to the treatments, through the software BORIS, allowing frame-by-frame videos inspection. Observer sniffing was defined as observer approaching and nose-touching demonstrator's cages. Reciprocal sniffing was defined as closeness between mice noses displaying interest for each other. Grooming, rearing and climbing were scored one at a time for each video. Data collected were then extracted as start/stop time for each event and analysed in Matlab, graphs and statistics were done using Graphpad Prism software.

Immunohistochemistry

All animals used for behavioural experiments or tracing were deeply anesthetized following all experiments with an overdose of urethane (>2 g per kg body weight) and then transcardially perfused with ice-cold 0.05 M phosphate buffer saline (PBS) pH 7.4, followed by 4% paraformaldehyde (PFA) in PBS (0.1 M, pH 7.4). Brains were removed and stored in 4% PFA for 24h post-fixation. Brains were then placed in in 30% sucrose solution (in PBS) for at least 48 h of

cryoprotection until sectioning. Brains were mounted on the sectioning chamber and frozen, and 40 µm slices were cut along the coronal axis using a microtome (HM45, Thermo Fisher). Sections were collected in PBS with 0.02% NaN3 until staining. For immunohistochemistry, all sections were first incubated in a blocking solution consisting of 10% normal goat serum (NGS) in PBS containing 1% Triton X-100 for a minimum of 1 h. Following 3–5 washes in PBS solution, primary antibodies were selected based on the target (GFP or mCherry). The primary solution consisted of the primary antibody diluted in 1% NGS, 0.03% Triton X-100 in PBS. Primary incubation occurred at 4 °C for 24–48 h. Following primary incubation, slices were washed 3–5 times in PBS and prepared for the secondary incubation that consists of a solution containing the secondary antibody diluted in 1% NGS, 0.03% Triton X-100 in PBS. Secondary incubation occurred at room temperature (RT) for 4–6 h. Primary antibodies used were: rabbit anti-GFP (1:1,000 dilution; Invitrogen, A11122), chicken anti-GFP (1:1,000 dilution; Abcam, AB290), and rabbit anti-dsRed (1:1,000 dilution; Thermo Fisher, 150128). Secondary antibodies were: Alexa Fluor 488 (goat anti-rabbit, 1:1,000 dilution; A11034, ABclonal), Alexa Fluor 488 (goat anti-chicken, 1:1,000 dilution; A11039, ABclonal) and anti-568 (goat anti-rabbit, 1:1,000 dilution; A11036, ABclonal). Fluorescence images were obtained with a confocal microscope (Nikon, CTR6500) or with an inverted fluorescence microscope (Zeiss Axiozen) using the following filter: 504 nm for Alexa Fluor 488, 560 nm for Alexa Fluor 568, and 650 nm for. Images were collected at ×20 in air or ×10, ×20. All fluorescence images were treated using the software ImageJ and Adobe Illustrator CS6. All primary and secondary antibodies have been previously validated.

ELISA corticosterone assay

The corticosterone concentration was analysed from plasma. Thirty minutes after exposure to the laser stimulation, each mouse was killed by decapitation. The blood was quickly collected in tubes coated with 0.5 M EDTA and centrifuged at 664 rcf for 10 min; the supernatant obtained was immediately processed. The corticosterone concentration was detected by a commercially available Detect X corticosterone ELISA kit (Arbor Assays, K014-H1) following the manufacturer's protocol. Original samples were diluted 1:100 in assay buffer. Each standard and sample was loaded in duplicate and plates were read using a 450 nm wavelength into a) multi-plate reader (Tecan). Measures of absorbance were converted in concentration expressed as

mg/ml using a Four Parameter Logistic (4PL) Regression fit, and normalized to the blank (negative control). The level of corticosterone was expressed as fold changes compared to the control group average.

Statistics

Results are expressed as the mean ± s.e.m. throughout the paper. Each observer's behaviour toward the two different demonstrator mice was analysed using a within-groups RM-ANOVA. The discrimination index with optogenetics stimulation was analysed by two-way ANOVAs with optostimulation (no light, ChR2, NphR) as between-subjects factors, and time intervals (0–2 min, 5-10 min and 13-15 min) as RM within-subjects factors. Bonferroni's post hoc test with multiple-comparison corrections was used for making comparisons within groups when the overall ANOVA showed statistically significant differences. All tests were two sided. Spearman correlation coefficients were compared using a two-tailed paired or unpaired *t*-test. For optogenetic experiments, sniffing time, distance travelled, number of entries in each zone and time in each zone was then compared across different conditions to the control (no stimulation) experiments. The accepted value for significance was $P \leq 0.05$. Statistical analyses were done using GraphPad Prism. The number of mice is reported in the legends and corresponds to similar numbers used in previous publications. Experiments reported in the paper were replicated three to four times for a different group, cage, sex or generation. No statistical measures were taken to predetermine the sample size of the experiments. For each animal, only entries to the stimulus area that lasted more than 5 s were used for analyses. Mouse exclusion criteria were defined before the beginning of the experiments and include genotyping errors, viral injection and fiber misplacement, and uncompleted experiments due to loss of implants. For all experiments, the side of the allocated stimulus mice and the order of the testing were randomized.

Human experiment

Participants

Eighty participants (mean age = 27.64 years, range = 18-49 years) were recruited and randomly assigned to two groups. To maintain experimental consistency with the mice studies, the sample was restricted to male participants, and all dyad members were unfamiliar with each other. All participants had normal or corrected to normal vision and reported no history of psychological or neurological disorders. Written informed consent was obtained from all participants, who were compensated with 25 Euros for their participation. All experimental procedures were approved by the local ethical committee and were carried out in accordance with the principles of the revised Helsinki Declaration (World Medical Association General Assembly, 2008). The sample size was determined a priori based on previous studies investigating interpersonal neural synchronization (Dumas et al., 2010; Goldstein et al., 2018; Hirsch et al., 2017; Noah et al., 2020).

Experimental stimuli selection

The experimental stimuli comprised 3 stress-inducing and 3 neutral audio-video clips (Supplementary Figure 4a). Audio-video clips, i.e. images paired with background music, were chosen as stimuli because such a combination is known to effectively evoke negative affect in humans (Uhrig et al., 2016). To ensure the effectiveness of the stress-inducing stimuli, the images were pre-selected through an online survey (Anwyl-Irvine et al., 2020). For this, we first compiled an initial set of 120 negative affect images obtained from both previously validated image databases and web sources. Specifically, we included 23 images from the Nencki Affective Picture System (Marchewka et al., 2014), 21 images from the Open Affective Standardized Image Set (Kurdi et al., 2017), 10 images from the Geneva Affective Picture Database (Dan-Glauser & Scherer, 2011), and 66 additional images from the web. The web-sourced images were selected to highlight negative affect concerning contemporary themes such as climate change, natural disasters, and war-related destruction.

Participants taking part to the online survey were located in Italy at the time of the experiment and were recruited via the Prolific platform (www.prolific.com). They were compensated at a rate of £8 per hour. During the survey, participants observed the images on a computer screen and rated

their valence i.e., how negative they perceived each image to be (see Supplementary Figure 4b). To ensure participants were paying attention to the task, we included six control images. For these images, participants were instructed to enter a specific valence rating (e.g., "Please enter a value of 3 for valence"). Each image was displayed for 5 seconds, and participants had a maximum of 6 seconds to respond.

All participants demonstrated high accuracy on the control task, with the exception of one individual who achieved only 33% accuracy and was consequently excluded from further analysis. The final sample comprised 21 participants (11 males; mean age = 26.57 years; mean accuracy = 99.20%). We then averaged the valence ratings across participants and selected the 30 images with the highest average valence (see Supplementary Figure 4c). We also confirmed that the selected images were rated as significantly more negative than the non-selected images (Welch Two Sample t-test $t(117.67) = 14.46$, $p < 0.001$; Supplementary Figure 4c).

Next, we selected the three audio clips with the highest negative valence ratings from the validated Database for Emotional Analysis in Music (DEAM) (Aljanaki et al., 2017). The three audio clips were combined with the 30 previously selected visual images. The images were divided into three groups of ten, with each group paired with one of the audio clips. Within each audio-visual stimulus, each image was presented for 4 seconds, followed by a 2-second blank screen.

Finally, three neutral audio-video clips were created using 30 images previously rated as neutral in the validated datasets described above. Specifically, the neutral set consisted of 13 images from NAPS, 12 from OASIS, and 5 from GAPED. These images were combined with neutral audio clips—identified as such in the DEAM database—following the same procedure used for the stress-inducing stimuli.

Experimental design and procedure

The study employed a between-subjects design comprising a stress group (Stress–Neutral) and a control group (Neutral–Neutral) (Fig. 1m). Emotional content was manipulated only in the Stress–Neutral group, where one participant in each dyad (counterbalanced across participants) viewed stress-inducing audio-video stimuli, while the partner viewed neutral stimuli. In contrast, participants in the Neutral–Neutral group viewed only neutral stimuli. The experiment comprised

three different procedures: emotion induction, social interaction, and no social interaction (Supplementary Fig. 4d). During the emotion induction, participants viewed experimental stimuli on a monitor (placed at a distance of approximately 1 m) with no visual contact permitted between partners. Immediately following the emotion induction, participants engaged in the social interaction condition, during which they were asked to look towards their partner and hold each other's right hand. Finally, in the no social condition, participants' view of one another was obstructed by an occluder placed between them, preventing any visual or haptic social contact.

Experimental procedures were structured into repeated trials, each lasting one minute, and implemented in the following sequence: (1) no social interaction, (2) emotion induction (neutral-neutral for all groups), (3) social interaction (baseline), (4) no social interaction, (5) emotion induction (neutral-neutral or stress-neutral, depending on group assignment), (6) social interaction (test), and (7) a final no social interaction phase (see Supplementary Fig. 4d). Each no social interaction condition was composed of three consecutive trials. Similarly, the emotion induction followed by social interaction block was repeated three times. To prevent stimulus-driven synchrony and maintain independence of perceptual experience, stimulus order was randomized across dyad members, such that the two participants viewed different stimuli at any given time. In the second social interaction block (test phase), participants in the Stress-Neutral group were exposed to asymmetric emotional stimulation: one participant viewed stress-inducing stimuli while the other viewed neutral stimuli. In the Neutral-Neutral group, both participants were presented with neutral stimuli.

Behavioral and neural recordings

Behavioral data: We assessed participants' current affect using the Italian version of the short-form Positive and Negative Affect Schedule (PANAS-SF; Thompson, 2007). PANAS-SF is a self-report questionnaire with 10-items assessing positive and negative affect. Participants were asked to rate their current affective state i.e., how intensively they felt each emotion in that particular moment. This measure has proven to be a reliable and valid self-report tool (Terracciano et al., 2003). We collected these reports both at the start and at the end of the experiment.

Neural recordings: We recorded neural activity, simultaneously from both participants, using dual electroencephalography (EEG). EEG was recorded from 64 Ag/AgCl active electrodes placed on the scalp according to the extended international 10–10 system (Biosemi ActiveTwo system). EEG signal was locally amplified and digitized using a sampling rate of 1024 Hz.

Data analysis

Behavioral data: To assess the effectiveness of the emotion induction, we analysed participants' subjective ratings from the questionnaire administered before and after the experiment. We averaged participants' responses to the negative items on the questionnaire and computed the difference in ratings (post-experiment minus pre-experiment) for each individual. To evaluate whether these ratings changed significantly from pre- to post-experiment within each group, we conducted a one-sample test against a reference value of zero, indicating no change. As the data did not meet the assumptions of normality (Shapiro-Wilk test, $p < 0.05$), we employed non-parametric Wilcoxon signed-rank tests for the analysis.

Neural data analysis: EEG data preprocessing was performed using a fully data-driven pipeline that was previously developed for denoising EEG data in humans and awake monkeys (Bianco et al., 2024; Bigand et al., 2025). This pipeline combines algorithms from Fieldtrip and EEGLAB toolboxes (Delorme & Makeig, 2004; Oostenveld et al., 2011). Specifically, the recorded EEG data were band-pass filtered (cutoff frequencies: 0.3 Hz and 95 Hz, Butterworth, filter-order: 3). A notch filter (47–53 Hz) was also used to remove electrical noise. We used an automated pipeline to remove noisy electrodes [defined as flat-lined, uncorrelated channels (correlation with other channels < 0.8) or channels carrying amplitude values that deviated more than 2.75 standard deviations from the mean of all channels]. We used Artifact Subspace Reconstruction (ASR) (Kothe & Makeig, 2013) to remove transient and large-amplitude movement artifacts (Kothe and Makeig, 2013; Plechawska-Wojcik et al., 2019). Artifact Subspace Reconstruction (ASR) is an adaptive algorithm that uses principal component analysis (PCA) to automatically identify clean segments of data, which are then used to establish variance thresholds. Based on these thresholds, the algorithm rejects components exhibiting abnormally high variance. Based on the comparative results from (Chang et al., 2018), we used a threshold value of 10. We then re-referenced the data using Common Average Reference. Next, we submitted the data to ICLabel (Pion-Tonachini et

al., 2019), which uses independent component analysis to automatically remove eye blinks or eye movements artifacts. Finally, previously removed channels were reconstructed through interpolation, using the mean voltage of adjacent electrodes with denoised signals.

The resulting pre-processed data were then analyzed as in (REF). EEG timeseries were time frequency transformed using a sliding window Fourier analysis with a tapering function. To reduce spectral leakage and control the frequency smoothing, we used a Hanning-tapered window with a frequency dependent time window that linearly decreased from 500 ms (1 Hz) to 100 ms (95 Hz) (using the 'ft_freqanalysis' function with 'mtmconvol' method as implemented in FieldTrip)(Novembre et al., 2019). We computed power estimates for all frequencies between 1 and 95 Hz in steps of 1 Hz and a time resolution of 100 ms (10 Hz). To avoid overrepresentation of certain bands embracing a disproportionate amount of frequency bins (in particular, gamma band spanning from 31–95 Hz), we defined sub-bands (c.f. REF) for further analyses as illustrated in Table XX.

Table XX. Frequency bands and sub-bands definitions:

Band	**Sub-band**	**Frequency**
Delta (d)	Low	1-2 Hz
	High	2-3 Hz
Theta (q)	Low	3-4 Hz
	Mid	5-6 Hz
	High	7-8 Hz
Alpha (a)	Low	8-9 Hz
	Mid	10-11 Hz
	High	11-12 Hz
Beta (b)	Low	13-18 Hz
	Mid	19-25 Hz

	High	26-31 Hz
Gamma (g)	Low	31-47 Hz
	Mid	52-72 Hz
	High	73-95 Hz

Next, we computed inter-brain correlation by calculating Pearson's correlation coefficients between electrode- and frequency bin-specific normalized EEG power time courses (i.e., power envelopes) recorded from the two individuals within each dyad (Koul et al., 2023; Liu et al., 2021; Rose et al., 2021; Zamm et al., 2018; Zhang & Yartsev, 2019). We normalized the power time series as below:

$$normalized\ data_c = \frac{data_c - mean(data_c)}{data_c + mean(data_c)}$$

Where $data_c$ is the (channel- and frequency bin- specific) power time course data for the entire duration of a single trial (0–60 s) and mean ($data_c$) is the average (over time) of this data.

The inter-brain correlation measure was both channel- and frequency bin-specific and was only computed among homologous channels and bins. We averaged the correlation coefficients across trials belonging to the same condition and Fisher z-transformed (inverse hyperbolic tangent function) them to obtain averaged normalized correlation coefficients for each channel and each frequency bin (across conditions within each dyad). Next, we averaged the coefficients according to frequency sub-bands.

Finally, we conducted a data-driven localizer analysis to identify regions exhibiting greater inter-brain correlation during the social condition compared to the no social condition. The localizer was defined using a cluster-based non-parametric permutation test (Maris & Oostenveld, 2007). This procedure controls for false-alarm rate by using a cluster statistic that is evaluated under a single permutation distribution. More specifically, this algorithm compares power estimates between conditions, separately for each channel and frequency sub-band, using two-sided independent-samples t-tests, yielding one t-value for each channel and frequency sub-band. The algorithm then forms clusters of (at least two) neighboring channels whose t-values exceed the

significance criterion (here $p < .05$) and computes a cluster-level statistic value (sum of t-values within the cluster). Next, cluster-level statistics from 1000 random partitions of the data are used to build a distribution upon which the significance probability (here $p < .05$) of the experimental cluster can be estimated.

To assess whether inter-brain correlation during the social conditions varied as a function of emotion induction, we computed the difference in inter-brain correlation between the two social interaction blocks (social test – social baseline). This difference was extracted specifically from the inter-brain correlation localizer cluster and compared between the Stress-Neutral and Neutral-Neutral groups using an independent-samples t-test.

Extended Data

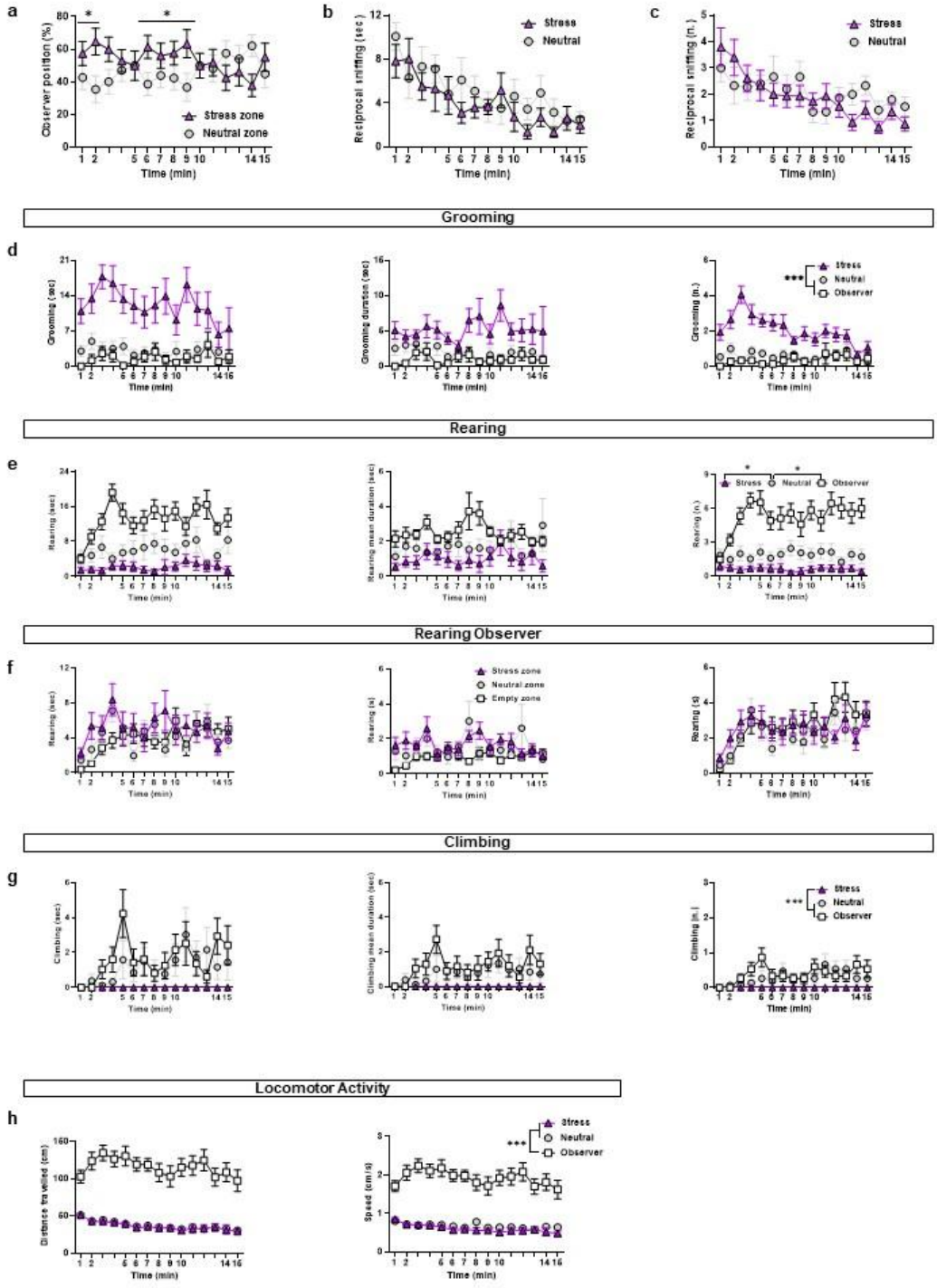

Supplementary Figure 1. Related to Figure 1.

Supplementary figure 1

a. Time in the zone spent by the observer in perentage

(b) Reciprocal sniffing time between the observer and the two demonstrators.

(c) Number of reciprocal sniffing events between the observer and the two demonstrators.

(d) Grooming behavior for the three mice. Left: time in seconds; center: mean duration of each event; right: number of events.

(e) Rearing behavior for the three mice. Left: time in seconds; center: mean duration of each event; right: number of events.

(f) Rearing behavior for the three mice. Left: time in seconds; center: mean duration of each event; right: number of events.

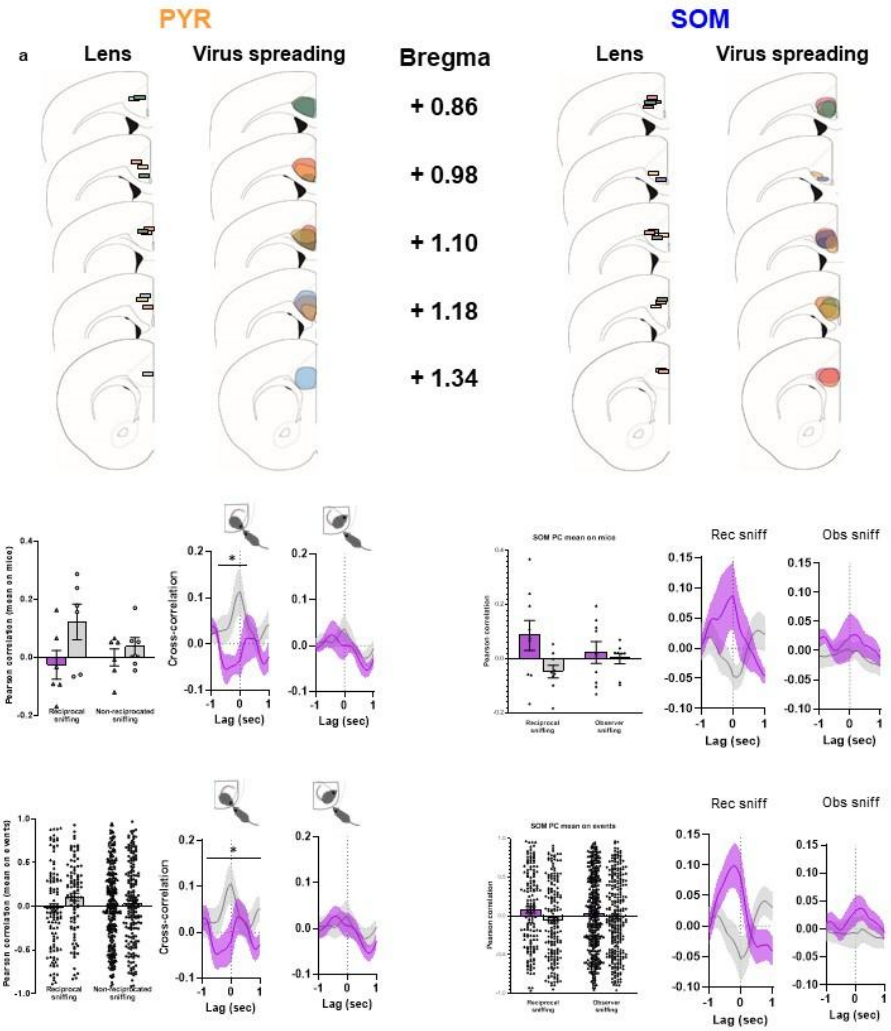

Supplementary Figure 2. Related to Figure 1 and 2.

Supplementary figure 2

Representative lens and virus placements for PYR and SOM calcium imaging recordings.

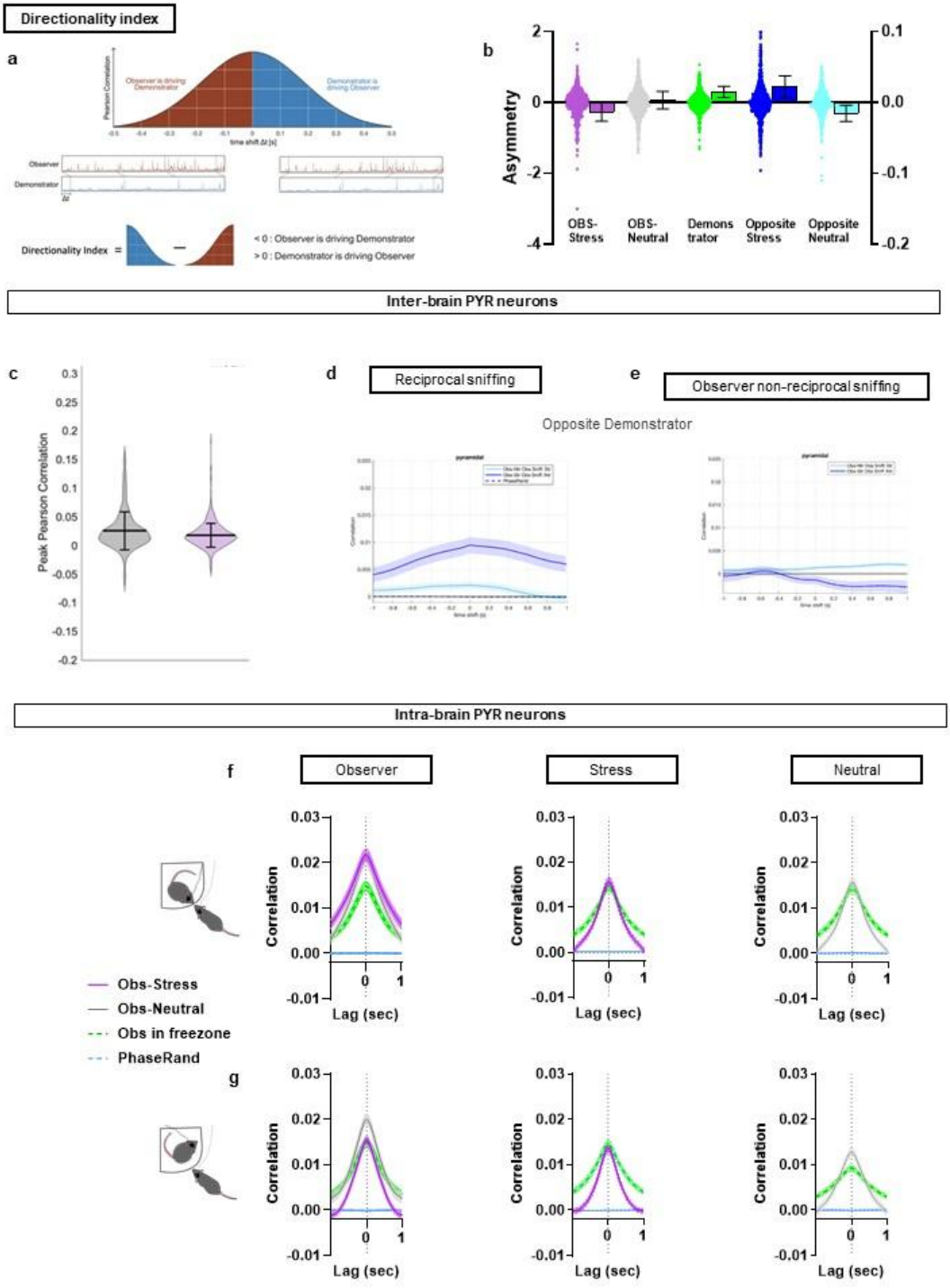

Supplementary Figure 3. Related to Figure 1.

Supplementary figure 3

(a) Directionality index computation

(b) Directionality index for PYR inter-brain correlations

(c) Distribution of single neurons inter-brain peak correlation during reciprocal sniffing.

(d) Inter-brain PYR correlations between the observer and the non-explored demonstrator during reciprocal sniffing intervals.

(e) Inter-brain PYR correlations between the observer and the non-explored demonstrator during observer non-reciprocated sniffing intervals.

(f) Intra-brain PYR correlation in the observer (left), the stress demonstrator (center) and the neutral demonstrator (right) during reciprocal sniffing intervals.

(g) Intra-brain PYR correlation in the observer (left), the stress demonstrator (center) and the neutral demonstrator (right) during observer non-reciprocated sniffing intervals.

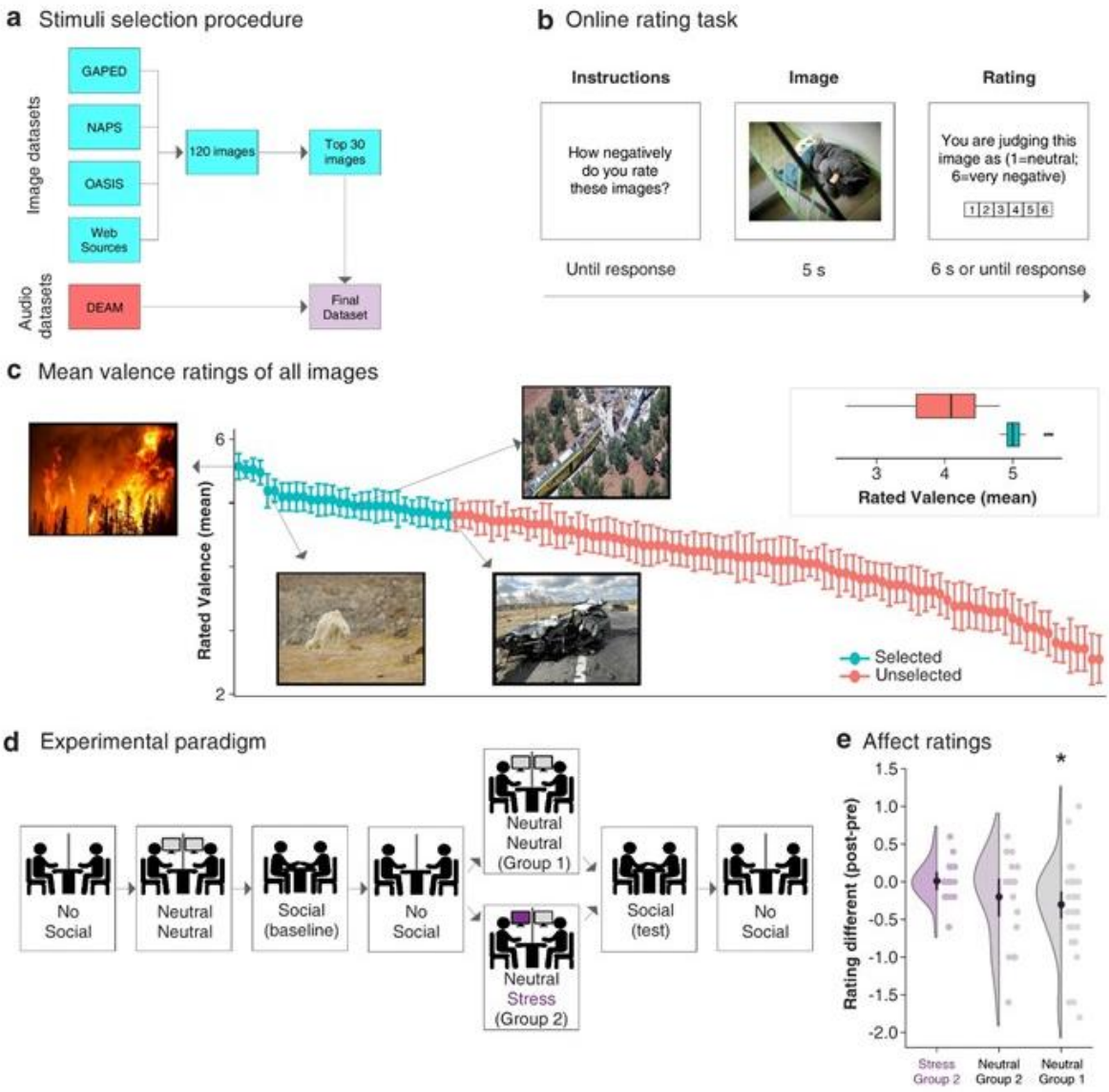

Supplementary Figure 4. Related to Figure 1.

Supplementary figure 4

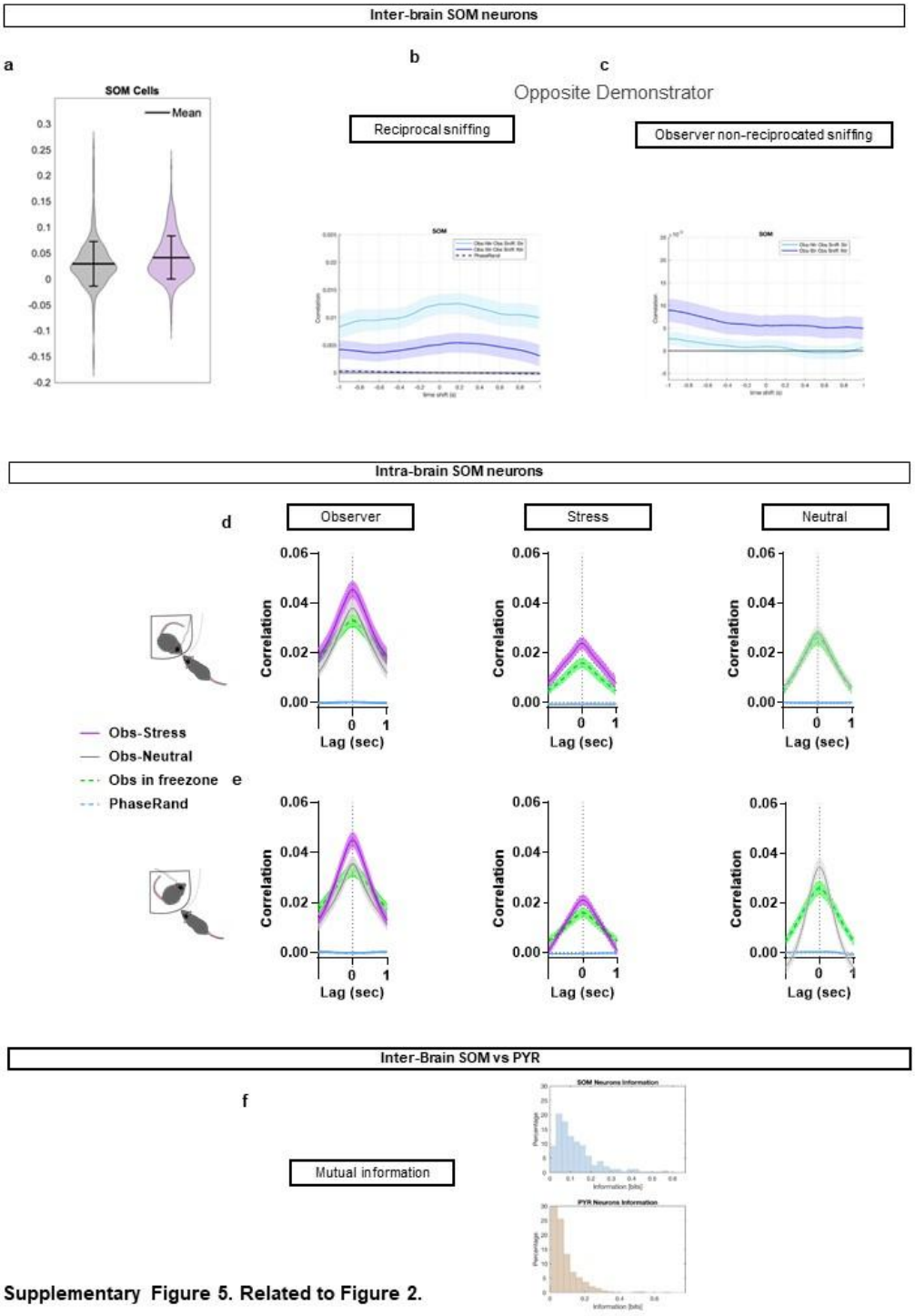

Supplementary Figure 5. Related to Figure 2.

Supplementary figure 5

(a) Distribution of single neurons inter-brain SOM peak correlation during reciprocal sniffing.

(b) Inter-brain SOM correlations between the observer and the non-explored demonstrator during reciprocal sniffing intervals.

(c) Inter-brain SOM correlations between the observer and the non-explored demonstrator during observer non-reciprocated sniffing intervals.

(d) Intra-brain SOM correlation in the observer (left), the stress demonstrator (center) and the neutral demonstrator (right) during reciprocal sniffing intervals.

(e) Intra-brain SOM correlation in the observer (left), the stress demonstrator (center) and the neutral demonstrator (right) during observer non-reciprocated sniffing intervals.

(f) Distribution of information carried by observer neurons about demonstrator's affective state. Top: SOM neurons, bottom: PYR neurons.

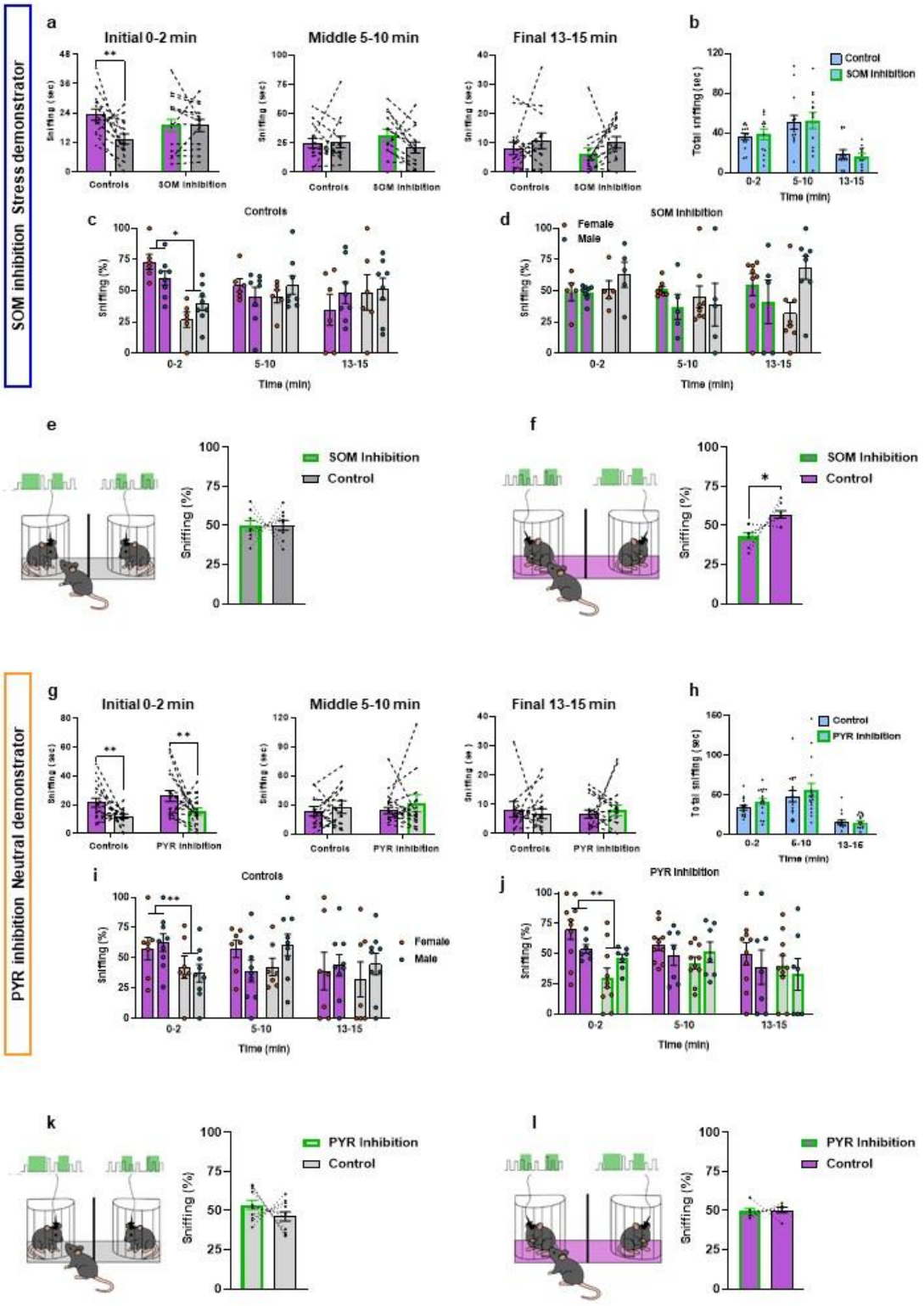

Supplementary Figure 6. Related to Figure 3.

Supplementary figure 6

(a) Observer sniffing time for controls and SOM inhibition in stress demonstrator group.

(b) No differences in the total sniffing time (stress + neutral) between controls and SOM inhibition group.

(**c)- (d)** No sex differences in control **(c.)** and SOM inhibition group **(d.)**.

(**e)** Observer sniffing during SOM inhibition in one of two equally neutral mice.

(**f)** Observer sniffing during SOM inhibition in one of two equally stressed mice.

(g) Observer sniffing time for controls and pyramidal inhibition in neutral demonstrator group.

(h) No differences in the total sniffing time (stress + neutral) between controls and PYR inhibition group.

(**i)-(j)** No sex differences in control **(i)** and PYR inhibition group **(j)**.

(**k)** Observer sniffing during PYR inhibition in one of two equally neutral mice.

(**l)** Observer sniffing during PYR inhibition in one of two equally stressed mice.

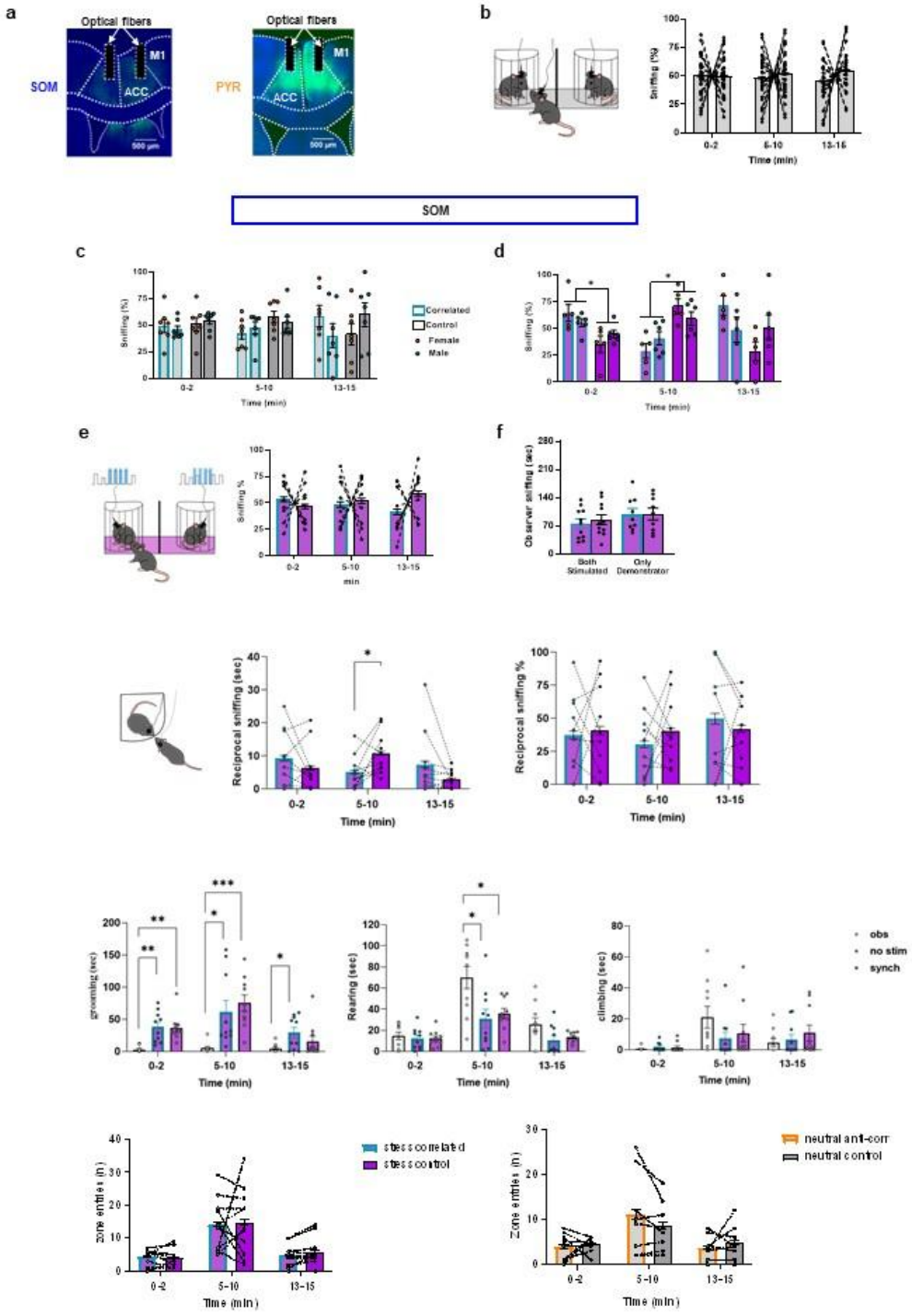

Supplementary Figure 7. Related to Figure 4.

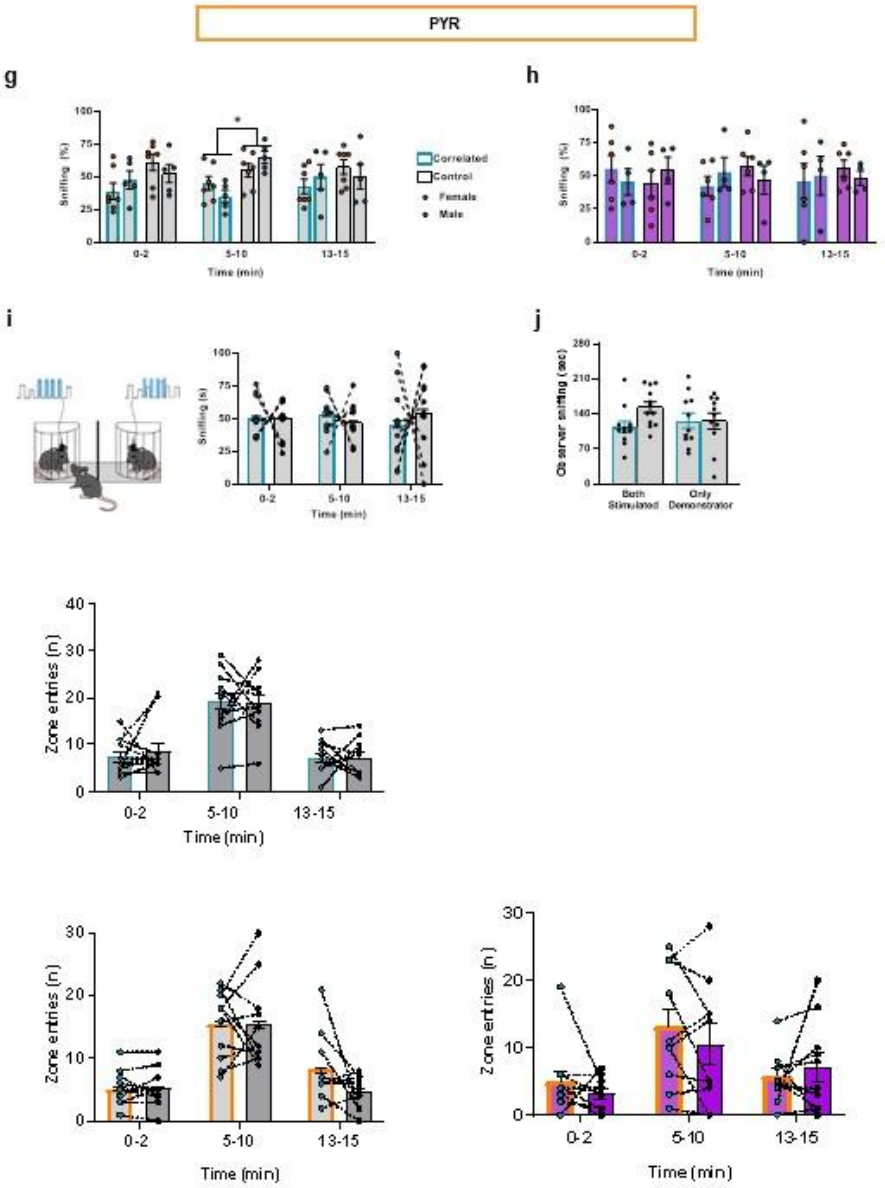

Supplementary Figure 7. Related to Figure 4.

Supplementary figure 7

(a) Representative fiber and opsin placement for SOM+ neurons stimulation and pyramidal neurons inhibition experiment.

(b) Observer sniffing in neutral-neutral protocol.

(**c)- (d)** Observer sniffing during SOM correlation neutral-neutral **(c.)** and stress-stress configuration **(d.)** divided by sex.

(**e)** Observer total sniffing (SOM synch + control) in neutral-neutral and stress-stress configuration.

(**f)** Observer sniffing during SOM excitation in one of two equally neutral mice.

(**g)** Observer sniffing during SOM excitation in one of two equally stressed mice.

(**h)- (i)** Observer sniffing during PYR correlation neutral-neutral **(h)** and stress-stress configuration **(i)** divided by sex.

(**j)** Observer total sniffing (PYR synch + control) in neutral-neutral and stress-stress configuration.

(k**)** Observer sniffing during PYR excitation in one of two equally neutral mice.

(**l)** Observer sniffing during PYR excitation in one of two equally stressed mice.

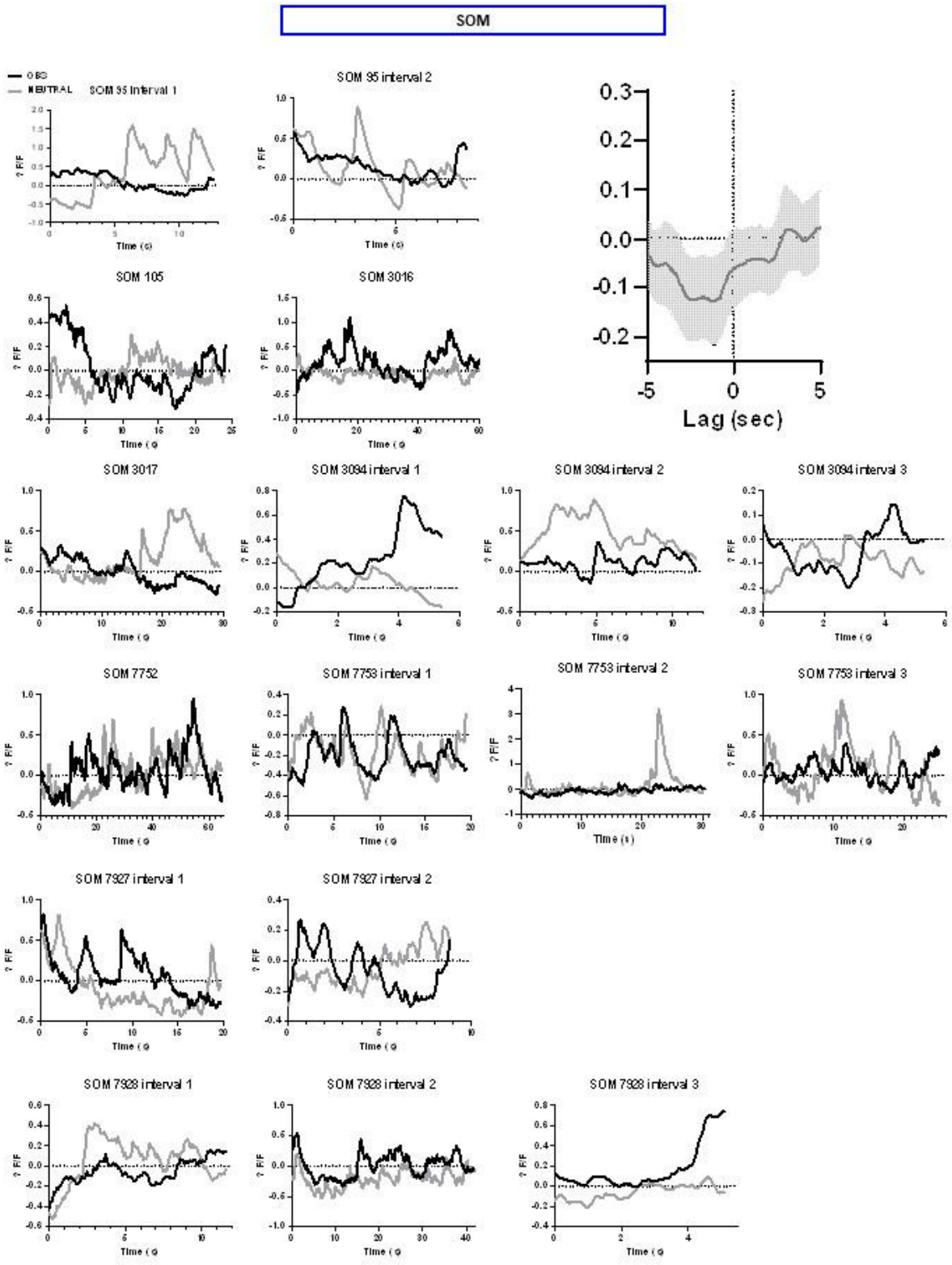

Supplementary Figure 8. Related to Figure 4.

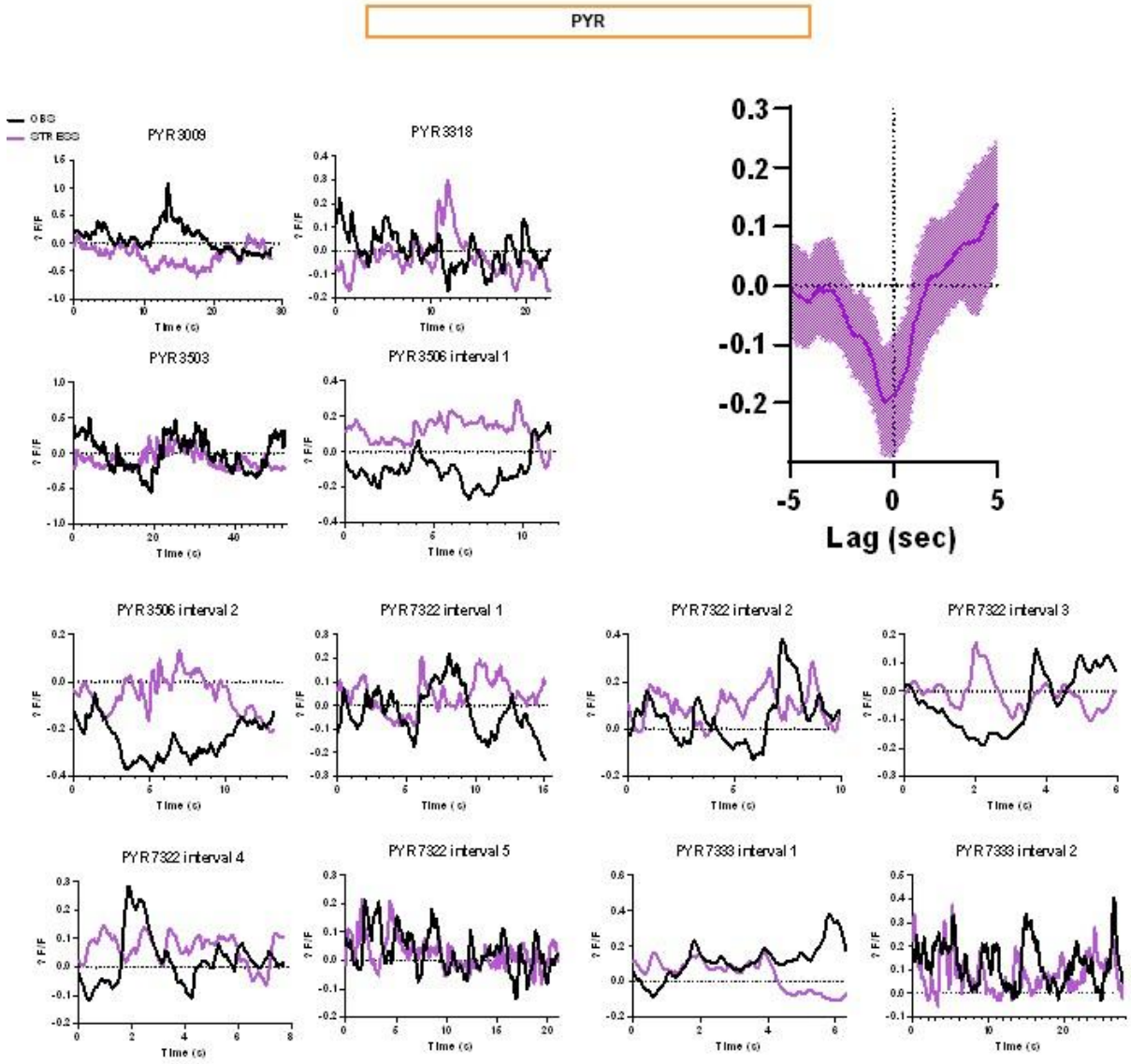

Supplementary Figure 8. Related to Figure 4.

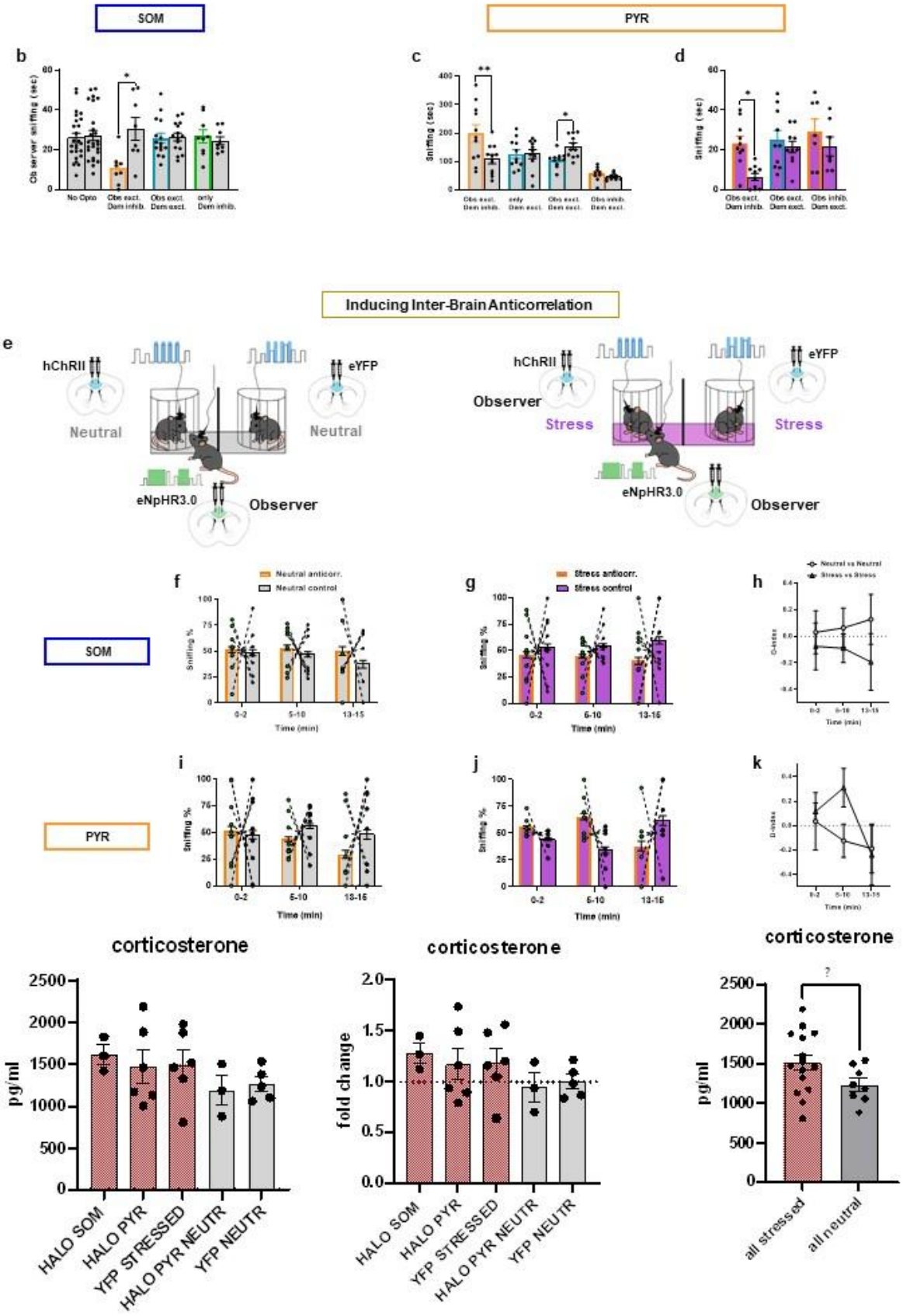

Supplementary Figure 8. Related to Figure 4.

Supplementary figure 8

(a) Representative virus and fibers placement for SOM corr/anti-corr experiments.

(b) Representative SOM traces

(**c)** Representative interbrain SOM anticorrelation between the observer and the neutral demonstrator.

(d) Representative virus and fibers placement for PYR corr/anti-corr experiments.

(e) Representative PYR traces

(**f)** Representative interbrain PYR anticorrelation between the observer and the neutral demonstrator.

(**h)** Experimental design for artificially induced anti-correlation inhibiting the observer and stimulating one of two neutral (left) or two stressed (right) demonstrators.

(**i)** Observer sniffing toward SOM anti-correlated and control demonstrator in neutral-neutral setting.

(**j)** Observer sniffing toward SOM anti-correlated and control demonstrator in stress-stress setting.

(**k)** Discrimination index for SOM anti-correlation in neutral-neutral and stress-stress configuration

(**l)** Observer sniffing toward PYR anti-correlated and control demonstrator in neutral-neutral setting.

(**m)** Observer sniffing toward PYR anti-correlated and control demonstrator in stress-stress setting.

(**n)** Discrimination index for PYR anti-correlation in neutral-neutral and stress-stress configuration.

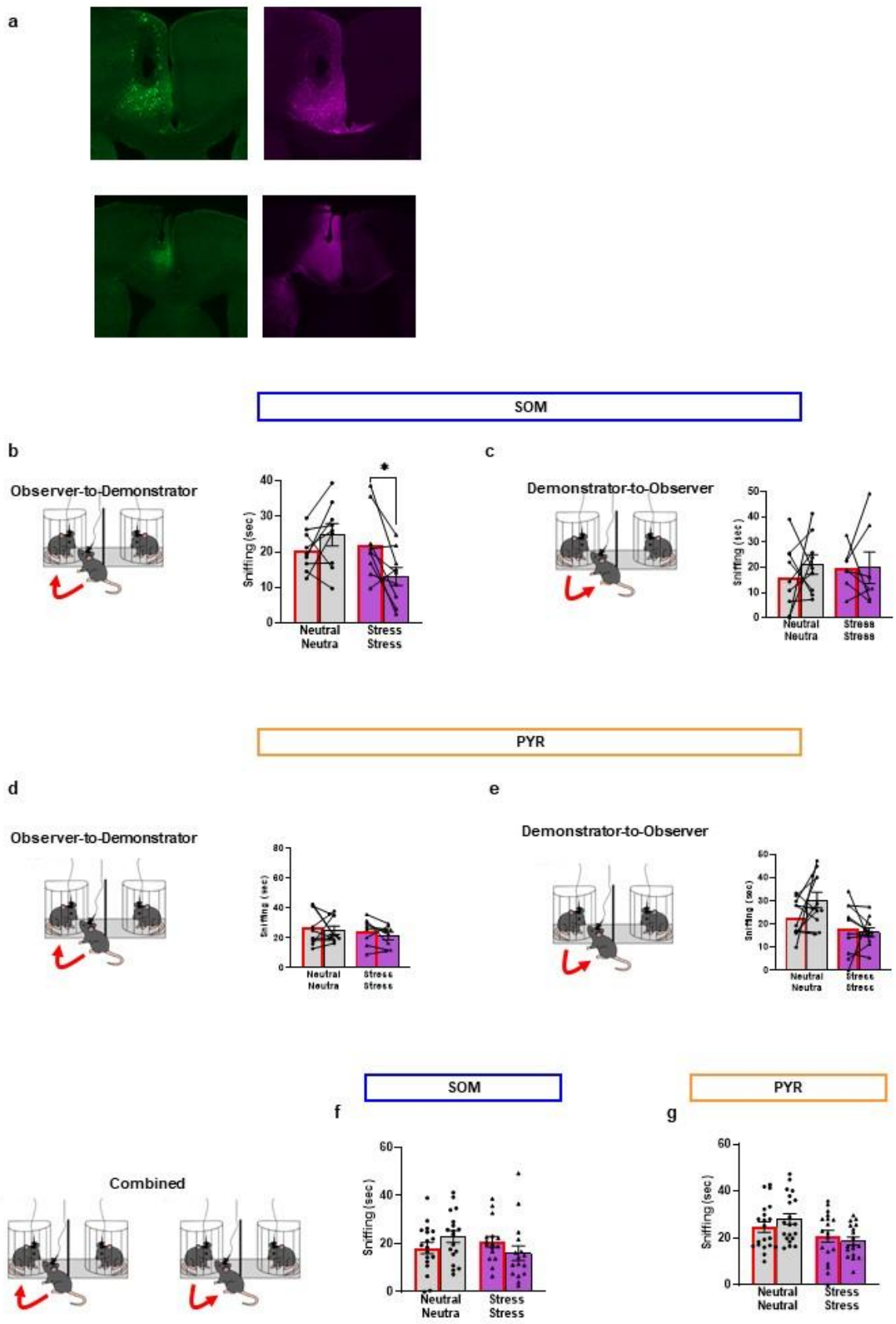

Supplementary Figure 9. Related to Figure 5.

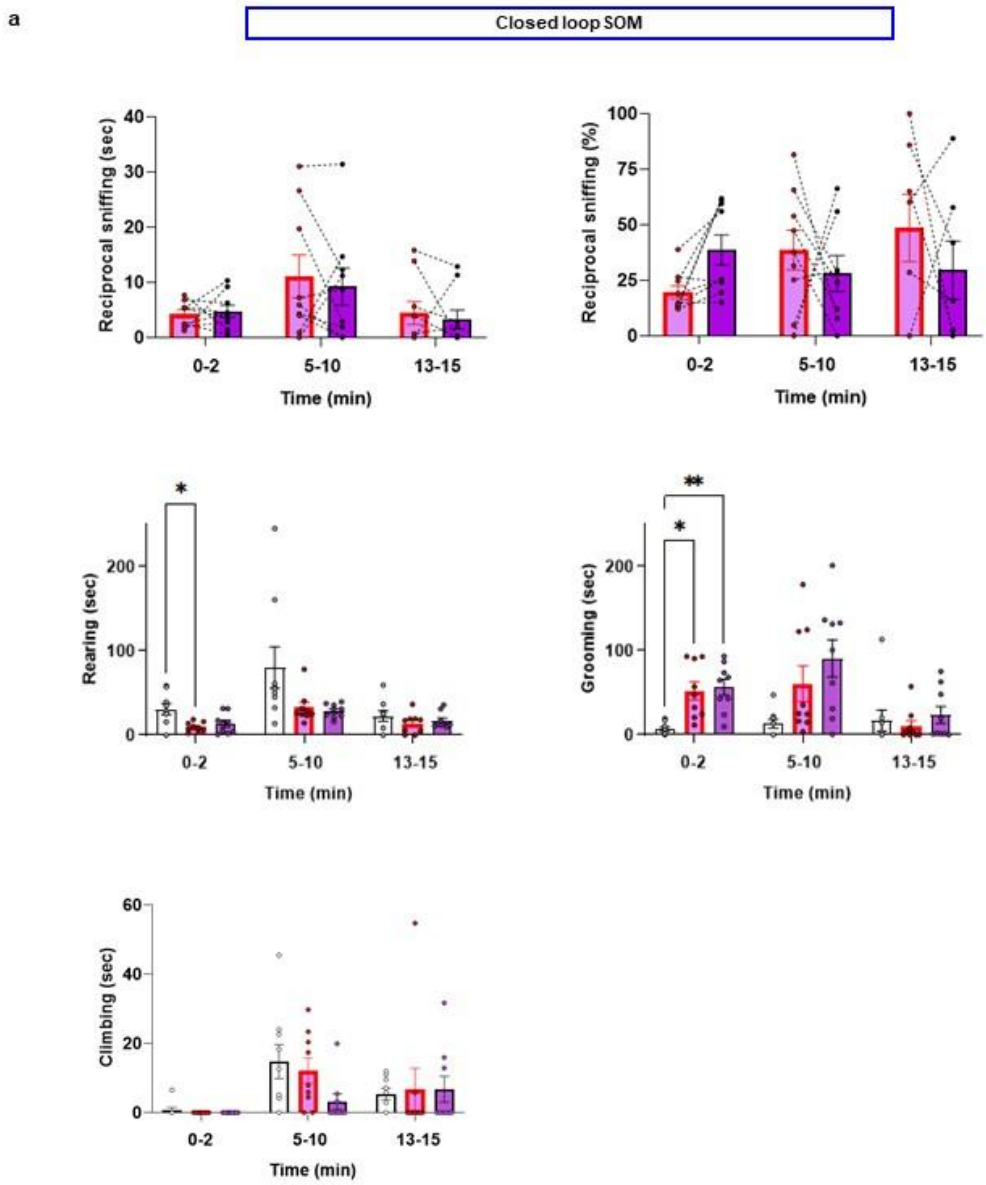

Supplementary figure 9

(a) Representative virus and fibers placement for SOM close-loop experiment.

Bibliography

1. Adolphs, R. (2001). The neurobiology of social cognition. *Curr Opin Neurobiol*, *11*(2), 231–239. https://doi.org/10.1016/s0959-4388(00)00202-6
2. Adolphs, R. (2002). Neural systems for recognizing emotion. *Curr Opin Neurobiol*, *12*(2), 169–177.
3. Adolphs, R. (2009). The social brain: neural basis of social knowledge. *Annu Rev Psychol*, *60*, 693–716. https://doi.org/10.1146/annurev.psych.60.110707.163514
4. Adolphs, R., Sears, L., & Piven, J. (2001). Abnormal processing of social information from faces in autism. *J Cogn Neurosci*, *13*(2), 232–240. https://doi.org/10.1162/089892901564289
5. Aljanaki, A., Yang, Y. H., & Soleymani, M. (2017). Developing a benchmark for emotional analysis of music. *PLoS One*, *12*(3), e0173392. https://doi.org/10.1371/journal.pone.0173392
6. Almasi, Z., David, C., Witte, M., & Staiger, J. F. (2019). Distribution Patterns of Three Molecularly Defined Classes of GABAergic Neurons Across Columnar Compartments in Mouse Barrel Cortex. *Front Neuroanat*, *13*, 45. https://doi.org/10.3389/fnana.2019.00045
7. Amodio, D. M., & Frith, C. D. (2006). Meeting of minds: the medial frontal cortex and social cognition. *Nat Rev Neurosci*, *7*(4), 268–277. https://doi.org/10.1038/nrn1884
8. Anastasiades, P. G., Collins, D. P., & Carter, A. G. (2021). Mediodorsal and Ventromedial Thalamus Engage Distinct L1 Circuits in the Prefrontal Cortex. *Neuron*, *109*(2), 314–330 e314. https://doi.org/10.1016/j.neuron.2020.10.031
9. Anders, S., Verrel, J., Haynes, J. D., & Ethofer, T. (2020). Pseudo-hyperscanning shows common neural activity during face-to-face communication of affect to be associated with shared affective feelings but not with mere emotion recognition. *Cortex*, *131*, 210–220. https://doi.org/10.1016/j.cortex.2020.06.015
10. Anderson, S. W., Barrash, J., Bechara, A., & Tranel, D. (2006). Impairments of emotion and real-world complex behavior following childhood- or adult-onset damage to ventromedial prefrontal cortex. *J Int Neuropsychol Soc*, *12*(2), 224–235. https://doi.org/10.1017/S1355617706060346
11. Andreasen, N. C., Paradiso, S., & O'Leary, D. S. (1998). "Cognitive dysmetria" as an integrative theory of schizophrenia: a dysfunction in cortical-subcortical-cerebellar circuitry? *Schizophr Bull*, *24*(2), 203–218. https://doi.org/10.1093/oxfordjournals.schbul.a033321
12. Andrews-Hanna, J. R., Reidler, J. S., Sepulcre, J., Poulin, R., & Buckner, R. L. (2010). Functional-anatomic fractionation of the brain's default network. *Neuron*, *65*(4), 550–562. https://doi.org/10.1016/j.neuron.2010.02.005
13. Antonelli, F., Bernardi, F., Koul, A., Novembre, G., & Papaleo, F. (2025). Emotions in multi-brain dynamics: A promising research frontier. *Neurosci Biobehav Rev*, *168*, 105965. https://doi.org/10.1016/j.neubiorev.2024.105965
14. Antonelli F., M. A., Bernardi F., Koul A., Engel N.M., Carta I., Managò F., Benedetti A., Borruto A.M., Spattini L., Maltese F., Yi C., Dumas G., Panzeri S., Novembre G., Papaleo F. . (2025). *Inter-Brain Dynamics Modulate Emotion Discrimination*.
15. Anwyl-Irvine, A. L., Massonnie, J., Flitton, A., Kirkham, N., & Evershed, J. K. (2020). Gorilla in our midst: An online behavioral experiment builder. *Behav Res Methods*, *52*(1), 388–407. https://doi.org/10.3758/s13428-019-01237-x
16. Apps, M. A., Rushworth, M. F., & Chang, S. W. (2016). The Anterior Cingulate Gyrus and Social Cognition: Tracking the Motivation of Others. *Neuron*, *90*(4), 692–707. https://doi.org/10.1016/j.neuron.2016.04.018
17. Arioli, M., Cattaneo, Z., Ricciardi, E., & Canessa, N. (2021). Overlapping and specific neural correlates for empathizing, affective mentalizing, and cognitive mentalizing: A coordinate-based meta-analytic study. *Hum Brain Mapp*, *42*(14), 4777–4804. https://doi.org/10.1002/hbm.25570

18. Bachevalier, J., & Loveland, K. A. (2006). The orbitofrontal-amygdala circuit and self-regulation of social-emotional behavior in autism. *Neurosci Biobehav Rev*, *30*(1), 97–117. https://doi.org/10.1016/j.neubiorev.2005.07.002
19. Bak, L. K., Schousboe, A., & Waagepetersen, H. S. (2006). The glutamate/GABA-glutamine cycle: aspects of transport, neurotransmitter homeostasis and ammonia transfer. *J Neurochem*, *98*(3), 641–653. https://doi.org/10.1111/j.1471-4159.2006.03913.x
20. Barbas, H. (2010). *Prefrontal Cortex: Structure and Anatomy*.
21. Bardeen, J. R., Kumpula, M. J., & Orcutt, H. K. (2013). Emotion regulation difficulties as a prospective predictor of posttraumatic stress symptoms following a mass shooting. *J Anxiety Disord*, *27*(2), 188–196. https://doi.org/10.1016/j.janxdis.2013.01.003
22. Barrash, J., Tranel, D., & Anderson, S. W. (2000). Acquired personality disturbances associated with bilateral damage to the ventromedial prefrontal region. *Dev Neuropsychol*, *18*(3), 355–381. https://doi.org/10.1207/S1532694205Barrash
23. Bastiaansen, J. A., Thioux, M., & Keysers, C. (2009). Evidence for mirror systems in emotions. *Philos Trans R Soc Lond B Biol Sci*, *364*(1528), 2391–2404. https://doi.org/10.1098/rstb.2009.0058
24. Bechara A, D. A. (2005). The somatic marker hypothesis: A neural theory of economic decision *Games and Economic Behavior*, *52*, 336–372. https://doi.org/https://doi.org/10.1016/j.geb.2004.06.010
25. Bechara, A., Damasio, A. R., Damasio, H., & Anderson, S. W. (1994). Insensitivity to future consequences following damage to human prefrontal cortex. *Cognition*, *50*(1-3), 7–15. https://doi.org/10.1016/0010-0277(94)90018-3
26. Bechara, A., Damasio, H., & Damasio, A. R. (2000). Emotion, decision making and the orbitofrontal cortex. *Cereb Cortex*, *10*(3), 295–307. https://doi.org/10.1093/cercor/10.3.295
27. Beckmann, M., Johansen-Berg, H., & Rushworth, M. F. (2009). Connectivity-based parcellation of human cingulate cortex and its relation to functional specialization. *J Neurosci*, *29*(4), 1175–1190. https://doi.org/10.1523/JNEUROSCI.3328-08.2009
28. Beierlein, M., Gibson, J. R., & Connors, B. W. (2000). A network of electrically coupled interneurons drives synchronized inhibition in neocortex. *Nat Neurosci*, *3*(9), 904–910. https://doi.org/10.1038/78809
29. Beierlein, M., Gibson, J. R., & Connors, B. W. (2003). Two dynamically distinct inhibitory networks in layer 4 of the neocortex. *J Neurophysiol*, *90*(5), 2987–3000. https://doi.org/10.1152/jn.00283.2003
30. Ben-Ami Bartal, I., Decety, J., & Mason, P. (2011). Empathy and pro-social behavior in rats. *Science*, *334*(6061), 1427–1430. https://doi.org/10.1126/science.1210789
31. Benarroch, E. E. (2012). GABAB receptors: structure, functions, and clinical implications. *Neurology*, *78*(8), 578–584. https://doi.org/10.1212/WNL.0b013e318247cd03
32. Benes, F. M., Davidson, J., & Bird, E. D. (1986). Quantitative cytoarchitectural studies of the cerebral cortex of schizophrenics. *Arch Gen Psychiatry*, *43*(1), 31–35. https://doi.org/10.1001/archpsyc.1986.01800010033004
33. Benes, F. M., Kwok, E. W., Vincent, S. L., & Todtenkopf, M. S. (1998). A reduction of nonpyramidal cells in sector CA2 of schizophrenics and manic depressives. *Biol Psychiatry*, *44*(2), 88–97. https://doi.org/10.1016/s0006-3223(98)00138-3
34. Berlin, H. A., Rolls, E. T., & Kischka, U. (2004). Impulsivity, time perception, emotion and reinforcement sensitivity in patients with orbitofrontal cortex lesions. *Brain*, *127*(Pt 5), 1108–1126. https://doi.org/10.1093/brain/awh135
35. Bertero, A., Feyen, P. L. C., Zurita, H., & Apicella, A. J. (2019). A Non-Canonical Cortico-Amygdala Inhibitory Loop. *J Neurosci*, *39*(43), 8424–8438. https://doi.org/10.1523/JNEUROSCI.1515-19.2019

36. Bianco, R., Zuk, N. J., Bigand, F., Quarta, E., Grasso, S., Arnese, F., Ravignani, A., Battaglia-Mayer, A., & Novembre, G. (2024). Neural encoding of musical expectations in a non-human primate. *Curr Biol*, *34*(2), 444–450 e445. https://doi.org/10.1016/j.cub.2023.12.019
37. Bigand, F., Bianco, R., Abalde, S. F., Nguyen, T., & Novembre, G. (2025). EEG of the Dancing Brain: Decoding Sensory, Motor, and Social Processes during Dyadic Dance. *J Neurosci*, *45*(21). https://doi.org/10.1523/JNEUROSCI.2372-24.2025
38. Biria, M., Banca, P., Healy, M. P., Keser, E., Sawiak, S. J., Rodgers, C. T., Rua, C., de Souza, A., Marzuki, A. A., Sule, A., Ersche, K. D., & Robbins, T. W. (2023). Cortical glutamate and GABA are related to compulsive behaviour in individuals with obsessive compulsive disorder and healthy controls. *Nat Commun*, *14*(1), 3324. https://doi.org/10.1038/s41467-023-38695-z
39. Bloem, B., Schoppink, L., Rotaru, D. C., Faiz, A., Hendriks, P., Mansvelder, H. D., van de Berg, W. D., & Wouterlood, F. G. (2014). Topographic mapping between basal forebrain cholinergic neurons and the medial prefrontal cortex in mice. *J Neurosci*, *34*(49), 16234–16246. https://doi.org/10.1523/JNEUROSCI.3011-14.2014
40. Bloom, F. E., & Iversen, L. L. (1971). Localizing 3H-GABA in nerve terminals of rat cerebral cortex by electron microscopic autoradiography. *Nature*, *229*(5287), 628–630. https://doi.org/10.1038/229628a0
41. Bombardi, C., Salamanca, G., Tagliavia, C., Grandis, A., Zamith Cunha, R., Gramenzi, A., De Silva, M., Zannoni, A., & Chiocchetti, R. (2025). Cannabinoid Receptors in the Horse Lateral Nucleus of the Amygdala: A Potential Target for Ameliorating Pain Perception, Stress and Anxiety in Horses. *Int J Mol Sci*, *26*(15). https://doi.org/10.3390/ijms26157613
42. Borg, C., Bedoin, N., Bogey, S., Michael, G. A., Poujois, A., Laurent, B., & Thomas-Anterion, C. (2012). Implicit and explicit emotional processing in Parkinson's disease. *J Clin Exp Neuropsychol*, *34*(3), 289–296. https://doi.org/10.1080/13803395.2011.639296
43. Bormann, J. (2000). The 'ABC' of GABA receptors. *Trends Pharmacol Sci*, *21*(1), 16–19. https://doi.org/10.1016/s0165-6147(99)01413-3
44. Bowery, N. G., & Brown, D. A. (1997). The cloning of GABA(B) receptors. *Nature*, *386*(6622), 223–224. https://doi.org/10.1038/386223a0
45. Bowery, N. G., Brown, D. A., White, R. D., & Yamini, G. (1979). [3H]gamma-Aminobutyric acid uptake into neuroglial cells of rat superior cervical sympathetic ganglia. *J Physiol*, *293*, 51–74. https://doi.org/10.1113/jphysiol.1979.sp012878
46. Bowery, N. G., Hill, D. R., & Hudson, A. L. (1985). [3H](-)Baclofen: an improved ligand for GABAB sites. *Neuropharmacology*, *24*(3), 207–210. https://doi.org/10.1016/0028-3908(85)90075-9
47. Bremner, J. D., Randall, P., Vermetten, E., Staib, L., Bronen, R. A., Mazure, C., Capelli, S., McCarthy, G., Innis, R. B., & Charney, D. S. (1997). Magnetic resonance imaging-based measurement of hippocampal volume in posttraumatic stress disorder related to childhood physical and sexual abuse--a preliminary report. *Biol Psychiatry*, *41*(1), 23–32. https://doi.org/10.1016/s0006-3223(96)00162-x
48. Brothers, L. (2002). *The Social Brain: A Project for Integrating Primate Behavior and Neurophysiology in a New Domain*. https://doi.org/10.7551/mitpress/3077.003.0029
49. Buchanan, K. A., Blackman, A. V., Moreau, A. W., Elgar, D., Costa, R. P., Lalanne, T., Tudor Jones, A. A., Oyrer, J., & Sjostrom, P. J. (2012). Target-specific expression of presynaptic NMDA receptors in neocortical microcircuits. *Neuron*, *75*(3), 451–466. https://doi.org/10.1016/j.neuron.2012.06.017
50. Buckner, R. L., Andrews-Hanna, J. R., & Schacter, D. L. (2008). The brain's default network: anatomy, function, and relevance to disease. *Ann N Y Acad Sci*, *1124*, 1–38. https://doi.org/10.1196/annals.1440.011
51. Burkett, J. P., Andari, E., Z.V., J., D.C., C., F.B.M., D. W., & L.J., Y. (2016). Oxytocin-dependent consolation behavior in rodents. *Science*, *351*, 375–378. https://doi.org/DOI:10.1126/science.aac4785

52. Bush, G., Luu, P., & Posner, M. I. (2000). Cognitive and emotional influences in anterior cingulate cortex. *Trends Cogn Sci*, *4*(6), 215–222. https://doi.org/10.1016/s1364-6613(00)01483-2
53. Butler, E. A. (2017). Emotions are temporal interpersonal systems. *Curr Opin Psychol*, *17*, 129–134. https://doi.org/10.1016/j.copsyc.2017.07.005
54. Cardin, J. A. (2018). Inhibitory Interneurons Regulate Temporal Precision and Correlations in Cortical Circuits. *Trends Neurosci*, *41*(10), 689–700. https://doi.org/10.1016/j.tins.2018.07.015
55. Carrillo, M., Han, Y., Migliorati, F., Liu, M., Gazzola, V., & Keysers, C. (2019). Emotional Mirror Neurons in the Rat's Anterior Cingulate Cortex. *Curr Biol*, *29*(8), 1301–1312 e1306. https://doi.org/10.1016/j.cub.2019.03.024
56. Castro-Vale, I., Severo, M., & Carvalho, D. (2020). Lifetime PTSD is associated with impaired emotion recognition in veterans and their offspring. *Psychiatry Res*, *284*, 112666. https://doi.org/10.1016/j.psychres.2019.112666
57. Cauda, F., Geda, E., Sacco, K., D'Agata, F., Duca, S., Geminiani, G., & Keller, R. (2011). Grey matter abnormality in autism spectrum disorder: an activation likelihood estimation meta-analysis study. *J Neurol Neurosurg Psychiatry*, *82*(12), 1304–1313. https://doi.org/10.1136/jnnp.2010.239111
58. Cecilione, J. L., Rappaport, L. M., Verhulst, B., Carney, D. M., Blair, R. J. R., Brotman, M. A., Leibenluft, E., Pine, D. S., Roberson-Nay, R., & Hettema, J. M. (2017). Test-retest reliability of the facial expression labeling task. *Psychol Assess*, *29*(12), 1537–1542. https://doi.org/10.1037/pas0000439
59. Chan, A. S., Cheung, M. C., Sze, S. L., Leung, W. W., & Shi, D. (2011). An herbal nasal drop enhanced frontal and anterior cingulate cortex activity. *Evid Based Complement Alternat Med*, *2011*, 543648. https://doi.org/10.1093/ecam/nep198
60. Chang, C. Y., Hsu, S. H., Pion-Tonachini, L., & Jung, T. P. (2018). Evaluation of Artifact Subspace Reconstruction for Automatic EEG Artifact Removal. *Annu Int Conf IEEE Eng Med Biol Soc*, *2018*, 1242–1245. https://doi.org/10.1109/EMBC.2018.8512547
61. Chen, P., Lou, S., Huang, Z. H., Wang, Z., Shan, Q. H., Wang, Y., Yang, Y., Li, X., Gong, H., Jin, Y., Zhang, Z., & Zhou, J. N. (2020). Prefrontal Cortex Corticotropin-Releasing Factor Neurons Control Behavioral Style Selection under Challenging Situations. *Neuron*, *106*(2), 301–315 e307. https://doi.org/10.1016/j.neuron.2020.01.033
62. Chiu, C. Q., Lur, G., Morse, T. M., Carnevale, N. T., Ellis-Davies, G. C., & Higley, M. J. (2013). Compartmentalization of GABAergic inhibition by dendritic spines. *Science*, *340*(6133), 759–762. https://doi.org/10.1126/science.1234274
63. Chronwall, B. M., Davis, T. D., Severidt, M. W., Wolfe, S. E., McCarson, K. E., Beatty, D. M., Low, M. J., Morris, S. J., & Enna, S. J. (2001). Constitutive expression of functional GABA(B) receptors in mIL-tsA58 cells requires both GABA(B(1)) and GABA(B(2)) genes. *J Neurochem*, *77*(5), 1237–1247. https://doi.org/10.1046/j.1471-4159.2001.00323.x
64. Collins, D. P., Anastasiades, P. G., Marlin, J. J., & Carter, A. G. (2018). Reciprocal Circuits Linking the Prefrontal Cortex with Dorsal and Ventral Thalamic Nuclei. *Neuron*, *98*(2), 366–379 e364. https://doi.org/10.1016/j.neuron.2018.03.024
65. Corbett, B. A., Carmean, V., Ravizza, S., Wendelken, C., Henry, M. L., Carter, C., & Rivera, S. M. (2009). A functional and structural study of emotion and face processing in children with autism. *Psychiatry Res*, *173*(3), 196–205. https://doi.org/10.1016/j.pscychresns.2008.08.005
66. Corcoran, K. A., & Quirk, G. J. (2007). Activity in prelimbic cortex is necessary for the expression of learned, but not innate, fears. *J Neurosci*, *27*(4), 840–844. https://doi.org/10.1523/JNEUROSCI.5327-06.2007
67. Craig, A. D. (2009). How do you feel--now? The anterior insula and human awareness. *Nat Rev Neurosci*, *10*(1), 59–70. https://doi.org/10.1038/nrn2555
68. Critchley, H., Daly, E., Phillips, M., Brammer, M., Bullmore, E., Williams, S., Van Amelsvoort, T., Robertson, D., David, A., & Murphy, D. (2000). Explicit and implicit neural mechanisms for

processing of social information from facial expressions: a functional magnetic resonance imaging study. *Hum Brain Mapp*, *9*(2), 93–105. https://doi.org/10.1002/(SICI)1097-0193(200002)9:2<93::AID-HBM4>3.0.CO;2-Z
69. Critchley, H. D., Mathias, C. J., Josephs, O., O'Doherty, J., Zanini, S., Dewar, B. K., Cipolotti, L., Shallice, T., & Dolan, R. J. (2003). Human cingulate cortex and autonomic control: converging neuroimaging and clinical evidence. *Brain*, *126*(Pt 10), 2139–2152. https://doi.org/10.1093/brain/awg216
70. Dal Monte, O., Krueger, F., Solomon, J. M., Schintu, S., Knutson, K. M., Strenziok, M., Pardini, M., Leopold, A., Raymont, V., & Grafman, J. (2013). A voxel-based lesion study on facial emotion recognition after penetrating brain injury. *Soc Cogn Affect Neurosci*, *8*(6), 632–639. https://doi.org/10.1093/scan/nss041
71. Dan-Glauser, E. S., & Scherer, K. R. (2011). The Geneva affective picture database (GAPED): a new 730-picture database focusing on valence and normative significance. *Behav Res Methods*, *43*(2), 468–477. https://doi.org/10.3758/s13428-011-0064-1
72. Dautan, D., Monai, A., Maltese, F., Chang, X., Molent, C., Mauro, D., Galbusera, A., Vecchia, D., Antonelli, F., Benedetti, A., Drago, F., Leggio, G. M., Pagani, M., Fellin, T., Gozzi, A., Schumann, G., Manago, F., & Papaleo, F. (2024a). Cortico-cortical transfer of socially derived information gates emotion recognition. *Nat Neurosci*. https://doi.org/10.1038/s41593-024-01647-x
73. Dautan, D., Monai, A., Maltese, F., Chang, X., Molent, C., Mauro, D., Galbusera, A., Vecchia, D., Antonelli, F., Benedetti, A., Drago, F., Leggio, G. M., Pagani, M., Fellin, T., Gozzi, A., Schumann, G., Manago, F., & Papaleo, F. (2024b). Cortico-cortical transfer of socially derived information gates emotion recognition. *Nat Neurosci*, *27*(7), 1318–1332. https://doi.org/10.1038/s41593-024-01647-x
74. Davidson, R. J., Pizzagalli, D., Nitschke, J. B., & Putnam, K. (2002). Depression: perspectives from affective neuroscience. *Annu Rev Psychol*, *53*, 545–574. https://doi.org/10.1146/annurev.psych.53.100901.135148
75. Davies, S., Bishop, D., Manstead, A. S., & Tantam, D. (1994). Face perception in children with autism and Asperger's syndrome. *J Child Psychol Psychiatry*, *35*(6), 1033–1057. https://doi.org/10.1111/j.1469-7610.1994.tb01808.x
76. de Leon Reyes, N. S., Sierra Diaz, P., Nogueira, R., Ruiz-Pino, A., Nomura, Y., de Solis, C. A., Schulkin, J., Asok, A., & Leroy, F. (2023). Corticotropin-releasing hormone signaling from prefrontal cortex to lateral septum suppresses interaction with familiar mice. *Cell*, *186*(19), 4152–4171 e4131. https://doi.org/10.1016/j.cell.2023.08.010
77. de Lima, A. D., & Morrison, J. H. (1989). Ultrastructural analysis of somatostatin-immunoreactive neurons and synapses in the temporal and occipital cortex of the macaque monkey. *J Comp Neurol*, *283*(2), 212–227. https://doi.org/10.1002/cne.902830205
78. de Waal, F. B. (2008). Putting the altruism back into altruism: the evolution of empathy. *Annu Rev Psychol*, *59*, 279–300. https://doi.org/10.1146/annurev.psych.59.103006.093625
79. Decety, J. (2011). The neuroevolution of empathy. *Ann N Y Acad Sci*, *1231*, 35–45. https://doi.org/10.1111/j.1749-6632.2011.06027.x
80. Delorme, A., & Makeig, S. (2004). EEGLAB: an open source toolbox for analysis of single-trial EEG dynamics including independent component analysis. *J Neurosci Methods*, *134*(1), 9–21. https://doi.org/10.1016/j.jneumeth.2003.10.009
81. Dennison-Cavanagh, M. E., Papadopoulos, G., & Parnavelas, J. G. (1993). The emergence of the cortical GABAergic neuron: with particular reference to some peptidergic subpopulations. *J Neurocytol*, *22*(9), 805–814. https://doi.org/10.1007/BF01181325
82. Devinsky, O., Morrell, M. J., & Vogt, B. A. (1995). Contributions of anterior cingulate cortex to behaviour. *Brain*, *118 (Pt 1)*, 279–306. https://doi.org/10.1093/brain/118.1.279

83. Dienel, S. J., Wade, K. L., Fish, K. N., & Lewis, D. A. (2025). Alterations in Prefrontal Cortical Somatostatin Neurons in Schizophrenia: Evidence for Weaker Inhibition of Pyramidal Neuron Dendrites. *Biol Psychiatry*, *98*(2), 156–166. https://doi.org/10.1016/j.biopsych.2025.01.010
84. Dionisio, L., Jose De Rosa, M., Bouzat, C., & Esandi Mdel, C. (2011). An intrinsic GABAergic system in human lymphocytes. *Neuropharmacology*, *60*(2-3), 513–519. https://doi.org/10.1016/j.neuropharm.2010.11.007
85. Diorio, D., Viau, V., & Meaney, M. J. (1993). The role of the medial prefrontal cortex (cingulate gyrus) in the regulation of hypothalamic-pituitary-adrenal responses to stress. *J Neurosci*, *13*(9), 3839–3847. https://doi.org/10.1523/JNEUROSCI.13-09-03839.1993
86. Drossman, D. A. (2005). Brain imaging and its implications for studying centrally targeted treatments in irritable bowel syndrome: a primer for gastroenterologists. *Gut*, *54*(5), 569–573. https://doi.org/10.1136/gut.2004.058446
87. Dumas, G., Nadel, J., Soussignan, R., Martinerie, J., & Garnero, L. (2010). Inter-brain synchronization during social interaction. *PLoS One*, *5*(8), e12166. https://doi.org/10.1371/journal.pone.0012166
88. Dunbar, R. I. (2009). The social brain hypothesis and its implications for social evolution. *Ann Hum Biol*, *36*(5), 562–572. https://doi.org/10.1080/03014460902960289
89. Dyck, M., Loughead, J., Gur, R. C., Schneider, F., & Mathiak, K. (2014). Hyperactivation balances sensory processing deficits during mood induction in schizophrenia. *Soc Cogn Affect Neurosci*, *9*(2), 167–175. https://doi.org/10.1093/scan/nss120
90. Ehring, T., & Quack, D. (2010). Emotion regulation difficulties in trauma survivors: the role of trauma type and PTSD symptom severity. *Behav Ther*, *41*(4), 587–598. https://doi.org/10.1016/j.beth.2010.04.004
91. Einevoll, G. T., Kayser, C., Logothetis, N. K., & Panzeri, S. (2013). Modelling and analysis of local field potentials for studying the function of cortical circuits. *Nat Rev Neurosci*, *14*(11), 770–785. https://doi.org/10.1038/nrn3599
92. Eisenberger, N. I., & Lieberman, M. D. (2004). Why rejection hurts: a common neural alarm system for physical and social pain. *Trends Cogn Sci*, *8*(7), 294–300. https://doi.org/10.1016/j.tics.2004.05.010
93. Ekman, P. (1992). **An argument for basic emotions**. *Cognition and Emotion 6*(3-4), 169–200.
94. Elston, T. W., & Bilkey, D. K. (2017). Anterior Cingulate Cortex Modulation of the Ventral Tegmental Area in an Effort Task. *Cell Rep*, *19*(11), 2220–2230. https://doi.org/10.1016/j.celrep.2017.05.062
95. Etkin, A., Egner, T., & Kalisch, R. (2011). Emotional processing in anterior cingulate and medial prefrontal cortex. *Trends Cogn Sci*, *15*(2), 85–93. https://doi.org/10.1016/j.tics.2010.11.004
96. Etkin, A., & Wager, T. D. (2007). Functional neuroimaging of anxiety: a meta-analysis of emotional processing in PTSD, social anxiety disorder, and specific phobia. *Am J Psychiatry*, *164*(10), 1476–1488. https://doi.org/10.1176/appi.ajp.2007.07030504
97. Fanselow, E. E., Richardson, K. A., & Connors, B. W. (2008). Selective, state-dependent activation of somatostatin-expressing inhibitory interneurons in mouse neocortex. *J Neurophysiol*, *100*(5), 2640–2652. https://doi.org/10.1152/jn.90691.2008
98. Fellows, L. K. (2007). Advances in understanding ventromedial prefrontal function: the accountant joins the executive. *Neurology*, *68*(13), 991–995. https://doi.org/10.1212/01.wnl.0000257835.46290.57
99. Ferretti, V., Maltese, F., Contarini, G., Nigro, M., Bonavia, A., Huang, H., Gigliucci, V., Morelli, G., Scheggia, D., Manago, F., Castellani, G., Lefevre, A., Cancedda, L., Chini, B., Grinevich, V., & Papaleo, F. (2019). Oxytocin Signaling in the Central Amygdala Modulates Emotion Discrimination in Mice. *Curr Biol*, *29*(12), 1938–1953 e1936. https://doi.org/10.1016/j.cub.2019.04.070
100. Ferretti, V., & Papaleo, F. (2019). Understanding others: Emotion recognition in humans and other animals. *Genes Brain Behav*, *18*(1), e12544. https://doi.org/10.1111/gbb.12544

101. Ferretti, V., & Papaleo, F. (2019). Understanding others: Emotion recognition in humans and other animals. *Genes, Brain and Behavior*, *18*(1). https://doi.org/10.1111/gbb.12544
102. Fett, A. K., Viechtbauer, W., Dominguez, M. D., Penn, D. L., van Os, J., & Krabbendam, L. (2011). The relationship between neurocognition and social cognition with functional outcomes in schizophrenia: a meta-analysis. *Neurosci Biobehav Rev*, *35*(3), 573–588. https://doi.org/10.1016/j.neubiorev.2010.07.001
103. Fino, E., & Yuste, R. (2011). Dense inhibitory connectivity in neocortex. *Neuron*, *69*(6), 1188–1203. https://doi.org/10.1016/j.neuron.2011.02.025
104. Fornito, A., Yucel, M., Dean, B., Wood, S. J., & Pantelis, C. (2009). Anatomical abnormalities of the anterior cingulate cortex in schizophrenia: bridging the gap between neuroimaging and neuropathology. *Schizophr Bull*, *35*(5), 973–993. https://doi.org/10.1093/schbul/sbn025
105. Francis-Oliveira, J., Leitzel, O., & Niwa, M. (2022). Are the Anterior and Mid-Cingulate Cortices Distinct in Rodents? *Front Neuroanat*, *16*, 914359. https://doi.org/10.3389/fnana.2022.914359
106. Frewen, P., Thornley, E., Rabellino, D., & Lanius, R. (2017). Neuroimaging the traumatized self: fMRI reveals altered response in cortical midline structures and occipital cortex during visual and verbal self- and other-referential processing in women with PTSD. *Eur J Psychotraumatol*, *8*(1), 1314164. https://doi.org/10.1080/20008198.2017.1314164
107. Friedman, N. P., & Robbins, T. W. (2022). The role of prefrontal cortex in cognitive control and executive function. *Neuropsychopharmacology*, *47*(1), 72–89. https://doi.org/10.1038/s41386-021-01132-0
108. Frith, C. D. (2008). Social cognition. *Philos Trans R Soc Lond B Biol Sci*, *363*(1499), 2033–2039. https://doi.org/10.1098/rstb.2008.0005
109. Frith, C. D., & Frith, U. (2007). Social cognition in humans. *Curr Biol*, *17*(16), R724–732. https://doi.org/10.1016/j.cub.2007.05.068
110. Fujiwara, H., Hirao, K., Namiki, C., Yamada, M., Shimizu, M., Fukuyama, H., Hayashi, T., & Murai, T. (2007). Anterior cingulate pathology and social cognition in schizophrenia: a study of gray matter, white matter and sulcal morphometry. *Neuroimage*, *36*(4), 1236–1245. https://doi.org/10.1016/j.neuroimage.2007.03.068
111. Fusar-Poli, P., Placentino, A., Carletti, F., Landi, P., Allen, P., Surguladze, S., Benedetti, F., Abbamonte, M., Gasparotti, R., Barale, F., Perez, J., McGuire, P., & Politi, P. (2009). Functional atlas of emotional faces processing: a voxel-based meta-analysis of 105 functional magnetic resonance imaging studies. *J Psychiatry Neurosci*, *34*(6), 418–432.
112. Garcia-Leon, M. A., Fuentes-Claramonte, P., Valiente-Gomez, A., Natividad, C., Salgado-Pineda, P., Gomar, J. J., Guerrero-Pedraza, A., Portillo, F., Ortiz-Gil, J., Alonso-Lana, S., Maristany, T., Radua, J., Salvador, R., Sarro, S., & Pomarol-Clotet, E. (2021). Altered brain responses to specific negative emotions in schizophrenia. *Neuroimage Clin*, *32*, 102894. https://doi.org/10.1016/j.nicl.2021.102894
113. Gilbertson, M. W., Shenton, M. E., Ciszewski, A., Kasai, K., Lasko, N. B., Orr, S. P., & Pitman, R. K. (2002). Smaller hippocampal volume predicts pathologic vulnerability to psychological trauma. *Nat Neurosci*, *5*(11), 1242–1247. https://doi.org/10.1038/nn958
114. Girgenti, M. J., Wohleb, E. S., Mehta, S., Ghosal, S., Fogaca, M. V., & Duman, R. S. (2019). Prefrontal cortex interneurons display dynamic sex-specific stress-induced transcriptomes. *Transl Psychiatry*, *9*(1), 292. https://doi.org/10.1038/s41398-019-0642-z
115. Goldberg, E. M., & Coulter, D. A. (2013). Mechanisms of epileptogenesis: a convergence on neural circuit dysfunction. *Nat Rev Neurosci*, *14*(5), 337–349. https://doi.org/10.1038/nrn3482
116. Goldstein, P., Weissman-Fogel, I., Dumas, G., & Shamay-Tsoory, S. G. (2018). Brain-to-brain coupling during handholding is associated with pain reduction. *Proc Natl Acad Sci U S A*, *115*(11), E2528–E2537. https://doi.org/10.1073/pnas.1703643115

117. Gonzalez-Burgos, G., Hashimoto, T., & Lewis, D. A. (2010). Alterations of cortical GABA neurons and network oscillations in schizophrenia. *Curr Psychiatry Rep*, *12*(4), 335–344. https://doi.org/10.1007/s11920-010-0124-8
118. Gordon, I., Gilboa, A., Cohen, S., Milstein, N., Haimovich, N., Pinhasi, S., & Siegman, S. (2020). Physiological and Behavioral Synchrony Predict Group Cohesion and Performance. *Sci Rep*, *10*(1), 8484. https://doi.org/10.1038/s41598-020-65670-1
119. Govindpani, K., Calvo-Flores Guzman, B., Vinnakota, C., Waldvogel, H. J., Faull, R. L., & Kwakowsky, A. (2017). Towards a Better Understanding of GABAergic Remodeling in Alzheimer's Disease. *Int J Mol Sci*, *18*(8). https://doi.org/10.3390/ijms18081813
120. Gray, H. M., & Tickle-Degnen, L. (2010). A meta-analysis of performance on emotion recognition tasks in Parkinson's disease. *Neuropsychology*, *24*(2), 176–191. https://doi.org/10.1037/a0018104
121. Green, M. F., Horan, W. P., & Lee, J. (2015). Social cognition in schizophrenia. *Nat Rev Neurosci*, *16*(10), 620–631. https://doi.org/10.1038/nrn4005
122. Green, M. F., Penn, D. L., Bentall, R., Carpenter, W. T., Gaebel, W., Gur, R. C., Kring, A. M., Park, S., Silverstein, S. M., & Heinssen, R. (2008). Social cognition in schizophrenia: an NIMH workshop on definitions, assessment, and research opportunities. *Schizophr Bull*, *34*(6), 1211–1220. https://doi.org/10.1093/schbul/sbm145
123. Grimaldi, D. A., Patane, A., Cattarinussi, G., & Sambataro, F. (2025). Functional connectivity of the striatum in psychosis: Meta-analysis of functional magnetic resonance imaging studies and replication on an independent sample. *Neurosci Biobehav Rev*, *174*, 106179. https://doi.org/10.1016/j.neubiorev.2025.106179
124. Gur, R. C., Sara, R., Hagendoorn, M., Marom, O., Hughett, P., Macy, L., Turner, T., Bajcsy, R., Posner, A., & Gur, R. E. (2002). A method for obtaining 3-dimensional facial expressions and its standardization for use in neurocognitive studies. *J Neurosci Methods*, *115*(2), 137–143. https://doi.org/10.1016/s0165-0270(02)00006-7
125. Hamilton, A. F. C. (2021). Hyperscanning: Beyond the Hype. *Neuron*, *109*(3), 404–407. https://doi.org/10.1016/j.neuron.2020.11.008
126. Hamilton, J. P., Glover, G. H., Hsu, J. J., Johnson, R. F., & Gotlib, I. H. (2011). Modulation of subgenual anterior cingulate cortex activity with real-time neurofeedback. *Hum Brain Mapp*, *32*(1), 22–31. https://doi.org/10.1002/hbm.20997
127. Hariri, A. R., Mattay, V. S., Tessitore, A., Fera, F., & Weinberger, D. R. (2003). Neocortical modulation of the amygdala response to fearful stimuli. *Biol Psychiatry*, *53*(6), 494–501. https://doi.org/10.1016/s0006-3223(02)01786-9
128. Harms, M. B., Martin, A., & Wallace, G. L. (2010). Facial emotion recognition in autism spectrum disorders: a review of behavioral and neuroimaging studies. *Neuropsychol Rev*, *20*(3), 290–322. https://doi.org/10.1007/s11065-010-9138-6
129. Harris, K. D., & Shepherd, G. M. (2015). The neocortical circuit: themes and variations. *Nat Neurosci*, *18*(2), 170–181. https://doi.org/10.1038/nn.3917
130. Hasson, U., Nir, Y., Levy, I., Fuhrmann, G., & Malach, R. (2004). Intersubject synchronization of cortical activity during natural vision. *Science*, *303*(5664), 1634–1640. https://doi.org/10.1126/science.1089506
131. Heeger, D. J., & Ress, D. (2002). What does fMRI tell us about neuronal activity? *Nat Rev Neurosci*, *3*(2), 142–151. https://doi.org/10.1038/nrn730
132. Heller, J., Mirzazade, S., Romanzetti, S., Habel, U., Derntl, B., Freitag, N. M., Schulz, J. B., Dogan, I., & Reetz, K. (2018). Impact of gender and genetics on emotion processing in Parkinson's disease - A multimodal study. *Neuroimage Clin*, *18*, 305–314. https://doi.org/10.1016/j.nicl.2018.01.034
133. Henry, J. D., von Hippel, W., Molenberghs, P., Lee, T., & Sachdev, P. S. (2016). Clinical assessment of social cognitive function in neurological disorders. *Nat Rev Neurol*, *12*(1), 28–39. https://doi.org/10.1038/nrneurol.2015.229

134. Hilz, M. J., Devinsky, O., Szczepanska, H., Borod, J. C., Marthol, H., & Tutaj, M. (2006). Right ventromedial prefrontal lesions result in paradoxical cardiovascular activation with emotional stimuli. *Brain*, *129*(Pt 12), 3343–3355. https://doi.org/10.1093/brain/awl299
135. Hirsch, J., Zhang, X., Noah, J. A., & Ono, Y. (2017). Frontal temporal and parietal systems synchronize within and across brains during live eye-to-eye contact. *Neuroimage*, *157*, 314–330. https://doi.org/10.1016/j.neuroimage.2017.06.018
136. Hiser, J., & Koenigs, M. (2018). The Multifaceted Role of the Ventromedial Prefrontal Cortex in Emotion, Decision Making, Social Cognition, and Psychopathology. *Biol Psychiatry*, *83*(8), 638–647. https://doi.org/10.1016/j.biopsych.2017.10.030
137. Holroyd, C. B. (2022). Interbrain synchrony: on wavy ground. *Trends Neurosci*, *45*(5), 346–357. https://doi.org/10.1016/j.tins.2022.02.002
138. Huang, S., Wu, S. J., Sansone, G., Ibrahim, L. A., & Fishell, G. (2024). Layer 1 neocortex: Gating and integrating multidimensional signals. *Neuron*, *112*(2), 184–200. https://doi.org/10.1016/j.neuron.2023.09.041
139. Hupalo, S., Martin, A. J., Green, R. K., Devilbiss, D. M., & Berridge, C. W. (2019). Prefrontal Corticotropin-Releasing Factor (CRF) Neurons Act Locally to Modulate Frontostriatal Cognition and Circuit Function. *J Neurosci*, *39*(11), 2080–2090. https://doi.org/10.1523/JNEUROSCI.2701-18.2019
140. Israelashvili, J., Sauter, D. A., & Fischer, A. H. (2020). Different faces of empathy: Feelings of similarity disrupt recognition of negative emotions. *J Exp Soc Psychol*, *87*, 103912. https://doi.org/10.1016/j.jesp.2019.103912
141. Jacobs, D. H., Shuren, J., Bowers, D., & Heilman, K. M. (1995). Emotional facial imagery, perception, and expression in Parkinson's disease. *Neurology*, *45*(9), 1696–1702. https://doi.org/10.1212/wnl.45.9.1696
142. Janer, K. W., & Pardo, J. V. (1991). Deficits in selective attention following bilateral anterior cingulotomy. *J Cogn Neurosci*, *3*(3), 231–241. https://doi.org/10.1162/jocn.1991.3.3.231
143. Jeon, D., Kim, S., Chetana, M., Jo, D., Ruley, H. E., Lin, S. Y., Rabah, D., Kinet, J. P., & Shin, H. S. (2010). Observational fear learning involves affective pain system and Cav1.2 Ca2+ channels in ACC. *Nat Neurosci*, *13*(4), 482–488. https://doi.org/10.1038/nn.2504
144. Johansen, J. P., & Fields, H. L. (2004). Glutamatergic activation of anterior cingulate cortex produces an aversive teaching signal. *Nat Neurosci*, *7*(4), 398–403. https://doi.org/10.1038/nn1207
145. Jones, E. G. (1993). GABAergic neurons and their role in cortical plasticity in primates. *Cereb Cortex*, *3*(5), 361–372. https://doi.org/10.1093/cercor/3.5.361-a
146. Jumah, F. R., & Dossani, R. H. (2025). Neuroanatomy, Cingulate Cortex. In *StatPearls*.
147. Kai, Y., Li, Y., Sun, T., Yin, W., Mao, Y., Li, J., Xie, W., Chen, S., Wang, L., Li, J., Zhang, Z., & Tao, W. (2018). A medial prefrontal cortex-nucleus acumens corticotropin-releasing factor circuitry for neuropathic pain-increased susceptibility to opioid reward. *Transl Psychiatry*, *8*(1), 100. https://doi.org/10.1038/s41398-018-0152-4
148. Kan, Y., Kawamura, M., Hasegawa, Y., Mochizuki, S., & Nakamura, K. (2002). Recognition of emotion from facial, prosodic and written verbal stimuli in Parkinson's disease. *Cortex*, *38*(4), 623–630. https://doi.org/10.1016/s0010-9452(08)70026-1
149. Kapfer, C., Glickfeld, L. L., Atallah, B. V., & Scanziani, M. (2007). Supralinear increase of recurrent inhibition during sparse activity in the somatosensory cortex. *Nat Neurosci*, *10*(6), 743–753. https://doi.org/10.1038/nn1909
150. Katona, L., Lapray, D., Viney, T. J., Oulhaj, A., Borhegyi, Z., Micklem, B. R., Klausberger, T., & Somogyi, P. (2016). Sleep and Movement Differentiates Actions of Two Types of Somatostatin-Expressing GABAergic Interneuron in Rat Hippocampus. *Neuron*, *91*(5), 1183. https://doi.org/10.1016/j.neuron.2016.08.023
151. Kaupmann, K., Malitschek, B., Schuler, V., Heid, J., Froestl, W., Beck, P., Mosbacher, J., Bischoff, S., Kulik, A., Shigemoto, R., Karschin, A., & Bettler, B. (1998). GABA(B)-receptor

subtypes assemble into functional heteromeric complexes. *Nature*, *396*(6712), 683–687. https://doi.org/10.1038/25360
152. Kawaguchi, Y. (1997). Neostriatal cell subtypes and their functional roles. *Neurosci Res*, *27*(1), 1–8. https://doi.org/10.1016/s0168-0102(96)01134-0
153. Kawaguchi, Y., & Kubota, Y. (1996). Physiological and morphological identification of somatostatin- or vasoactive intestinal polypeptide-containing cells among GABAergic cell subtypes in rat frontal cortex. *J Neurosci*, *16*(8), 2701–2715. https://doi.org/10.1523/JNEUROSCI.16-08-02701.1996
154. Kawaguchi, Y., & Kubota, Y. (1997). GABAergic cell subtypes and their synaptic connections in rat frontal cortex. *Cereb Cortex*, *7*(6), 476–486. https://doi.org/10.1093/cercor/7.6.476
155. Kawaguchi, Y., & Shindou, T. (1998). Noradrenergic excitation and inhibition of GABAergic cell types in rat frontal cortex. *J Neurosci*, *18*(17), 6963–6976. https://doi.org/10.1523/JNEUROSCI.18-17-06963.1998
156. Keller, P. E., Novembre, G., & Hove, M. J. (2014). Rhythm in joint action: psychological and neurophysiological mechanisms for real-time interpersonal coordination. *Philos Trans R Soc Lond B Biol Sci*, *369*(1658), 20130394. https://doi.org/10.1098/rstb.2013.0394
157. Kennedy, D. P., & Adolphs, R. (2012). The social brain in psychiatric and neurological disorders. *Trends Cogn Sci*, *16*(11), 559–572. https://doi.org/10.1016/j.tics.2012.09.006
158. Kepecs, A., & Fishell, G. (2014). Interneuron cell types are fit to function. *Nature*, *505*(7483), 318–326. https://doi.org/10.1038/nature12983
159. Keum, S., Kim, A., Shin, J. J., Kim, J. H., Park, J., & Shin, H. S. (2018). A Missense Variant at the Nrxn3 Locus Enhances Empathy Fear in the Mouse. *Neuron*, *98*(3), 588–601 e585. https://doi.org/10.1016/j.neuron.2018.03.041
160. Kietzman, H. W., & Gourley, S. L. (2023). How social information impacts action in rodents and humans: the role of the prefrontal cortex and its connections. *Neurosci Biobehav Rev*, *147*, 105075. https://doi.org/10.1016/j.neubiorev.2023.105075
161. Kim, H., Ahrlund-Richter, S., Wang, X., Deisseroth, K., & Carlen, M. (2016). Prefrontal Parvalbumin Neurons in Control of Attention. *Cell*, *164*(1-2), 208–218. https://doi.org/10.1016/j.cell.2015.11.038
162. Kim, Y., Yang, G. R., Pradhan, K., Venkataraju, K. U., Bota, M., Garcia Del Molino, L. C., Fitzgerald, G., Ram, K., He, M., Levine, J. M., Mitra, P., Huang, Z. J., Wang, X. J., & Osten, P. (2017). Brain-wide Maps Reveal Stereotyped Cell-Type-Based Cortical Architecture and Subcortical Sexual Dimorphism. *Cell*, *171*(2), 456–469 e422. https://doi.org/10.1016/j.cell.2017.09.020
163. Kingsbury, L., Huang, S., Wang, J., Gu, K., Golshani, P., Wu, Y. E., & Hong, W. (2019). Correlated Neural Activity and Encoding of Behavior across Brains of Socially Interacting Animals. *Cell*, *178*(2), 429–446 e416. https://doi.org/10.1016/j.cell.2019.05.022
164. Kitayama, N., Quinn, S., & Bremner, J. D. (2006). Smaller volume of anterior cingulate cortex in abuse-related posttraumatic stress disorder. *J Affect Disord*, *90*(2-3), 171–174. https://doi.org/10.1016/j.jad.2005.11.006
165. Kohler, C. G., Turner, T. H., Bilker, W. B., Brensinger, C. M., Siegel, S. J., Kanes, S. J., Gur, R. E., & Gur, R. C. (2003). Facial emotion recognition in schizophrenia: intensity effects and error pattern. *Am J Psychiatry*, *160*(10), 1768–1774. https://doi.org/10.1176/appi.ajp.160.10.1768
166. Kohler, C. G., Walker, J. B., Martin, E. A., Healey, K. M., & Moberg, P. J. (2010). Facial emotion perception in schizophrenia: a meta-analytic review. *Schizophr Bull*, *36*(5), 1009–1019. https://doi.org/10.1093/schbul/sbn192

167. Kohler, E., Keysers, C., Umilta, M. A., Fogassi, L., Gallese, V., & Rizzolatti, G. (2002). Hearing sounds, understanding actions: action representation in mirror neurons. *Science*, *297*(5582), 846–848. https://doi.org/10.1126/science.1070311
168. Kothe, C. A., & Makeig, S. (2013). BCILAB: a platform for brain-computer interface development. *J Neural Eng*, *10*(5), 056014. https://doi.org/10.1088/1741-2560/10/5/056014
169. Koul, A., Ahmar, D., Iannetti, G. D., & Novembre, G. (2023). Spontaneous dyadic behavior predicts the emergence of interpersonal neural synchrony. *Neuroimage*, *277*, 120233. https://doi.org/10.1016/j.neuroimage.2023.120233
170. Kubota, Y. (2014). Untangling GABAergic wiring in the cortical microcircuit. *Curr Opin Neurobiol*, *26*, 7–14. https://doi.org/10.1016/j.conb.2013.10.003
171. Kumfor, F., Sapey-Triomphe, L. A., Leyton, C. E., Burrell, J. R., Hodges, J. R., & Piguet, O. (2014). Degradation of emotion processing ability in corticobasal syndrome and Alzheimer's disease. *Brain*, *137*(Pt 11), 3061–3072. https://doi.org/10.1093/brain/awu246
172. Kurdi, B., Lozano, S., & Banaji, M. R. (2017). Introducing the Open Affective Standardized Image Set (OASIS). *Behav Res Methods*, *49*(2), 457–470. https://doi.org/10.3758/s13428-016-0715-3
173. Lai, M. C., Lombardo, M. V., & Baron-Cohen, S. (2014). Autism. *Lancet*, *383*(9920), 896–910. https://doi.org/10.1016/S0140-6736(13)61539-1
174. Lawrence, A. D., Goerendt, I. K., & Brooks, D. J. (2007). Impaired recognition of facial expressions of anger in Parkinson's disease patients acutely withdrawn from dopamine replacement therapy. *Neuropsychologia*, *45*(1), 65–74. https://doi.org/10.1016/j.neuropsychologia.2006.04.016
175. Le Merre, P., Ahrlund-Richter, S., & Carlen, M. (2021). The mouse prefrontal cortex: Unity in diversity. *Neuron*, *109*(12), 1925–1944. https://doi.org/10.1016/j.neuron.2021.03.035
176. Le Merre, P., Esmaeili, V., Charriere, E., Galan, K., Salin, P. A., Petersen, C. C. H., & Crochet, S. (2018). Reward-Based Learning Drives Rapid Sensory Signals in Medial Prefrontal Cortex and Dorsal Hippocampus Necessary for Goal-Directed Behavior. *Neuron*, *97*(1), 83–91 e85. https://doi.org/10.1016/j.neuron.2017.11.031
177. LeDoux, J. E. (2000). Emotion circuits in the brain. *Annu Rev Neurosci*, *23*, 155–184. https://doi.org/10.1146/annurev.neuro.23.1.155
178. Lee, A. T., Vogt, D., Rubenstein, J. L., & Sohal, V. S. (2014). A class of GABAergic neurons in the prefrontal cortex sends long-range projections to the nucleus accumbens and elicits acute avoidance behavior. *J Neurosci*, *34*(35), 11519–11525. https://doi.org/10.1523/JNEUROSCI.1157-14.2014
179. Lee, E., Lee, J., & Kim, E. (2017). Excitation/Inhibition Imbalance in Animal Models of Autism Spectrum Disorders. *Biol Psychiatry*, *81*(10), 838–847. https://doi.org/10.1016/j.biopsych.2016.05.011
180. Lee, J., Kwak, D., Lee, G. U., Kim, C. Y., Kim, J., Park, S. H., Choi, J. H., Lee, S. Q., & Choe, H. K. (2024). Social context modulates multibrain broadband dynamics and functional brain-to-brain coupling in the group of mice. *Sci Rep*, *14*(1), 11439. https://doi.org/10.1038/s41598-024-62070-7
181. Lenartowicz, A., & McIntosh, A. R. (2005). The role of anterior cingulate cortex in working memory is shaped by functional connectivity. *J Cogn Neurosci*, *17*(7), 1026–1042. https://doi.org/10.1162/0898929054475127
182. Lewis, D. A. (2014). Inhibitory neurons in human cortical circuits: substrate for cognitive dysfunction in schizophrenia. *Curr Opin Neurobiol*, *26*, 22–26. https://doi.org/10.1016/j.conb.2013.11.003
183. Li, P., & Jeong, H. (2020). The social brain of language: grounding second language learning in social interaction. *NPJ Sci Learn*, *5*, 8. https://doi.org/10.1038/s41539-020-0068-7
184. Li, Y. D., Luo, Y. J., Su, W. K., Ge, J., Crowther, A., Chen, Z. K., Wang, L., Lazarus, M., Liu, Z. L., Qu, W. M., & Huang, Z. L. (2024). Anterior cingulate cortex projections to the

dorsal medial striatum underlie insomnia associated with chronic pain. *Neuron*, *112*(8), 1328–1341 e1324. https://doi.org/10.1016/j.neuron.2024.01.014
185. Liu, H., Zhao, C., Wang, F., & Zhang, D. (2021). Inter-brain amplitude correlation differentiates cooperation from competition in a motion-sensing sports game. *Soc Cogn Affect Neurosci*, *16*(6), 552–564. https://doi.org/10.1093/scan/nsab031
186. Liu, X., Dimidschstein, J., Fishell, G., & Carter, A. G. (2020). Hippocampal inputs engage CCK+ interneurons to mediate endocannabinoid-modulated feed-forward inhibition in the prefrontal cortex. *Elife*, *9*. https://doi.org/10.7554/eLife.55267
187. Liu, Z., Lu, K., Hao, N., & Wang, Y. (2023). Cognitive Reappraisal and Expressive Suppression Evoke Distinct Neural Connections during Interpersonal Emotion Regulation. *J Neurosci*, *43*(49), 8456–8471. https://doi.org/10.1523/JNEUROSCI.0954-23.2023
188. Lu, R., Sun, W., Liang, Y., Kerlin, A., Bierfeld, J., Seelig, J. D., Wilson, D. E., Scholl, B., Mohar, B., Tanimoto, M., Koyama, M., Fitzpatrick, D., Orger, M. B., & Ji, N. (2017). Video-rate volumetric functional imaging of the brain at synaptic resolution. *Nat Neurosci*, *20*(4), 620–628. https://doi.org/10.1038/nn.4516
189. Ma, Y., Hu, H., Berrebi, A. S., Mathers, P. H., & Agmon, A. (2006). Distinct subtypes of somatostatin-containing neocortical interneurons revealed in transgenic mice. *J Neurosci*, *26*(19), 5069–5082. https://doi.org/10.1523/JNEUROSCI.0661-06.2006
190. Maier, S. F., Amat, J., Baratta, M. V., Paul, E., & Watkins, L. R. (2006). Behavioral control, the medial prefrontal cortex, and resilience. *Dialogues Clin Neurosci*, *8*(4), 397–406. https://doi.org/10.31887/DCNS.2006.8.4/smaier
191. Maltese, F., Pacinelli, G., Monai, A., Bernardi, F., Capaz, A. M., Niello, M., Walle, R., de Leon, N., Manago, F., Leroy, F., & Papaleo, F. (2025). Self-experience of a negative event alters responses to others in similar states through prefrontal cortex CRF mechanisms. *Nat Neurosci*, *28*(1), 122–136. https://doi.org/10.1038/s41593-024-01816-y
192. Mandal, M. K., Pandey, R., & Prasad, A. B. (1998). Facial expressions of emotions and schizophrenia: a review. *Schizophr Bull*, *24*(3), 399–412. https://doi.org/10.1093/oxfordjournals.schbul.a033335
193. Marchewka, A., Zurawski, L., Jednorog, K., & Grabowska, A. (2014). The Nencki Affective Picture System (NAPS): introduction to a novel, standardized, wide-range, high-quality, realistic picture database. *Behav Res Methods*, *46*(2), 596–610. https://doi.org/10.3758/s13428-013-0379-1
194. Marin, O. (2024). Parvalbumin interneuron deficits in schizophrenia. *Eur Neuropsychopharmacol*, *82*, 44–52. https://doi.org/10.1016/j.euroneuro.2024.02.010
195. Maris, E., & Oostenveld, R. (2007). Nonparametric statistical testing of EEG- and MEG-data. *J Neurosci Methods*, *164*(1), 177–190. https://doi.org/10.1016/j.jneumeth.2007.03.024
196. Markram, H., Toledo-Rodriguez, M., Wang, Y., Gupta, A., Silberberg, G., & Wu, C. (2004). Interneurons of the neocortical inhibitory system. *Nat Rev Neurosci*, *5*(10), 793–807. https://doi.org/10.1038/nrn1519
197. Mason, P., & Shan, H. (2017). A valence-free definition of sociality as any violation of inter-individual independence. *Proc Biol Sci*, *284*(1866). https://doi.org/10.1098/rspb.2017.0948
198. Mattavelli, G., Barvas, E., Longo, C., Zappini, F., Ottaviani, D., Malaguti, M. C., Pellegrini, M., & Papagno, C. (2021). Facial expressions recognition and discrimination in Parkinson's disease. *J Neuropsychol*, *15*(1), 46–68. https://doi.org/10.1111/jnp.12209
199. Mayo, O., & Gordon, I. (2020). In and out of synchrony-Behavioral and physiological dynamics of dyadic interpersonal coordination. *Psychophysiology*, *57*(6), e13574. https://doi.org/10.1111/psyp.13574
200. McGarry, L. M., & Carter, A. G. (2016). Inhibitory Gating of Basolateral Amygdala Inputs to the Prefrontal Cortex. *J Neurosci*, *36*(36), 9391–9406. https://doi.org/10.1523/JNEUROSCI.0874-16.2016

201. McNamara, A. M., Cleland, T. A., & Linster, C. (2004). Characterization of the synaptic properties of olfactory bulb projections. *Chem Senses*, *29*(3), 225–233. https://doi.org/10.1093/chemse/bjh027
202. Medford, N., & Critchley, H. D. (2010). Conjoint activity of anterior insular and anterior cingulate cortex: awareness and response. *Brain Struct Funct*, *214*(5-6), 535–549. https://doi.org/10.1007/s00429-010-0265-x
203. Melzer, S., Michael, M., Caputi, A., Eliava, M., Fuchs, E. C., Whittington, M. A., & Monyer, H. (2012). Long-range-projecting GABAergic neurons modulate inhibition in hippocampus and entorhinal cortex. *Science*, *335*(6075), 1506–1510. https://doi.org/10.1126/science.1217139
204. Menon, V., & Uddin, L. Q. (2010). Saliency, switching, attention and control: a network model of insula function. *Brain Struct Funct*, *214*(5-6), 655–667. https://doi.org/10.1007/s00429-010-0262-0
205. Mercer, S. W., & Reynolds, W. J. . (2002). *Empathy and quality of care* (Vol. 52 Suppl(Suppl)).
206. Miles, S. R., Menefee, D. S., Wanner, J., Teten Tharp, A., & Kent, T. A. (2016). The Relationship Between Emotion Dysregulation and Impulsive Aggression in Veterans With Posttraumatic Stress Disorder Symptoms. *J Interpers Violence*, *31*(10), 1795–1816. https://doi.org/10.1177/0886260515570746
207. Millan, M. J., Agid, Y., Brune, M., Bullmore, E. T., Carter, C. S., Clayton, N. S., Connor, R., Davis, S., Deakin, B., DeRubeis, R. J., Dubois, B., Geyer, M. A., Goodwin, G. M., Gorwood, P., Jay, T. M., Joels, M., Mansuy, I. M., Meyer-Lindenberg, A., Murphy, D.,…Young, L. J. (2012). Cognitive dysfunction in psychiatric disorders: characteristics, causes and the quest for improved therapy. *Nat Rev Drug Discov*, *11*(2), 141–168. https://doi.org/10.1038/nrd3628
208. Miller, E. K. (2000). The prefrontal cortex and cognitive control. *Nat Rev Neurosci*, *1*(1), 59–65. https://doi.org/10.1038/35036228
209. Miller, E. K., & Cohen, J. D. (2001). An integrative theory of prefrontal cortex function. *Annu Rev Neurosci*, *24*, 167–202. https://doi.org/10.1146/annurev.neuro.24.1.167
210. Miller, L. A., Hsieh, S., Lah, S., Savage, S., Hodges, J. R., & Piguet, O. (2012). One size does not fit all: face emotion processing impairments in semantic dementia, behavioural-variant frontotemporal dementia and Alzheimer's disease are mediated by distinct cognitive deficits. *Behav Neurol*, *25*(1), 53–60. https://doi.org/10.3233/BEN-2012-0349
211. Montague, P. R., Berns, G. S., Cohen, J. D., McClure, S. M., Pagnoni, G., Dhamala, M., Wiest, M. C., Karpov, I., King, R. D., Apple, N., & Fisher, R. E. (2002). Hyperscanning: simultaneous fMRI during linked social interactions. *Neuroimage*, *16*(4), 1159–1164. https://doi.org/10.1006/nimg.2002.1150
212. Morey, R. A., Gold, A. L., LaBar, K. S., Beall, S. K., Brown, V. M., Haswell, C. C., Nasser, J. D., Wagner, H. R., McCarthy, G., & Mid-Atlantic, M. W. (2012). Amygdala volume changes in posttraumatic stress disorder in a large case-controlled veterans group. *Arch Gen Psychiatry*, *69*(11), 1169–1178. https://doi.org/10.1001/archgenpsychiatry.2012.50
213. Moyer, C. E., Erickson, S. L., Fish, K. N., Thiels, E., Penzes, P., & Sweet, R. A. (2016). Developmental Trajectories of Auditory Cortex Synaptic Structures and Gap-Prepulse Inhibition of Acoustic Startle Between Early Adolescence and Young Adulthood in Mice. *Cereb Cortex*, *26*(5), 2115–2126. https://doi.org/10.1093/cercor/bhv040
214. Muller-Pinzler, L., Krach, S., Kramer, U. M., & Paulus, F. M. (2017). The Social Neuroscience of Interpersonal Emotions. *Curr Top Behav Neurosci*, *30*, 241–256. https://doi.org/10.1007/7854_2016_437
215. Munoz, W., & Rudy, B. (2014). Spatiotemporal specificity in cholinergic control of neocortical function. *Curr Opin Neurobiol*, *26*, 149–160. https://doi.org/10.1016/j.conb.2014.02.015

216. Munoz, W., Tremblay, R., Levenstein, D., & Rudy, B. (2017). Layer-specific modulation of neocortical dendritic inhibition during active wakefulness. *Science*, *355*(6328), 954–959. https://doi.org/10.1126/science.aag2599
217. Nakao, T. O., Hideki & Northoff, Georg. (2010). Decision making and the medial prefrontal cortex function in social context. *Japanese Journal of Physiological Psychology and Psychophysiology*, *28*, 45–55.
218. Noah, J. A., Zhang, X., Dravida, S., Ono, Y., Naples, A., McPartland, J. C., & Hirsch, J. (2020). Real-Time Eye-to-Eye Contact Is Associated With Cross-Brain Neural Coupling in Angular Gyrus. *Front Hum Neurosci*, *14*, 19. https://doi.org/10.3389/fnhum.2020.00019
219. Novembre, G., & Iannetti, G. D. (2021). Hyperscanning Alone Cannot Prove Causality. Multibrain Stimulation Can. *Trends Cogn Sci*, *25*(2), 96–99. https://doi.org/10.1016/j.tics.2020.11.003
220. Novembre, G., Pawar, V. M., Kilintari, M., Bufacchi, R. J., Guo, Y., Rothwell, J. C., & Iannetti, G. D. (2019). The effect of salient stimuli on neural oscillations, isometric force, and their coupling. *Neuroimage*, *198*, 221–230. https://doi.org/10.1016/j.neuroimage.2019.05.032
221. Ongur, D., & Price, J. L. (2000). The organization of networks within the orbital and medial prefrontal cortex of rats, monkeys and humans. *Cereb Cortex*, *10*(3), 206–219. https://doi.org/10.1093/cercor/10.3.206
222. Oostenveld, R., Fries, P., Maris, E., & Schoffelen, J. M. (2011). FieldTrip: Open source software for advanced analysis of MEG, EEG, and invasive electrophysiological data. *Comput Intell Neurosci*, *2011*, 156869. https://doi.org/10.1155/2011/156869
223. Panksepp, J., & Panksepp, J. B. (2013). Toward a cross-species understanding of empathy. *Trends Neurosci*, *36*(8), 489–496. https://doi.org/10.1016/j.tins.2013.04.009
224. Paxinos, G., & Franklin, K. B. J. . (2001). *The mouse brain in stereotaxic coordinates (2nd ed.)*.
225. Penn, D. L., Corrigan, P. W., Bentall, R. P., Racenstein, J. M., & Newman, L. (1997). Social cognition in schizophrenia. *Psychol Bull*, *121*(1), 114–132. https://doi.org/10.1037/0033-2909.121.1.114
226. Phan, K. L., Wager, T., Taylor, S. F., & Liberzon, I. (2002). Functional neuroanatomy of emotion: a meta-analysis of emotion activation studies in PET and fMRI. *Neuroimage*, *16*(2), 331–348. https://doi.org/10.1006/nimg.2002.1087
227. Phelps, E. A. (2006). Emotion and cognition: insights from studies of the human amygdala. *Annu Rev Psychol*, *57*, 27–53. https://doi.org/10.1146/annurev.psych.56.091103.070234
228. Pickup, G. J., & Frith, C. D. (2001). Theory of mind impairments in schizophrenia: symptomatology, severity and specificity. *Psychol Med*, *31*(2), 207–220. https://doi.org/10.1017/s0033291701003385
229. Pion-Tonachini, L., Kreutz-Delgado, K., & Makeig, S. (2019). ICLabel: An automated electroencephalographic independent component classifier, dataset, and website. *Neuroimage*, *198*, 181–197. https://doi.org/10.1016/j.neuroimage.2019.05.026
230. Poljac, E., Montagne, B., & de Haan, E. H. (2011). Reduced recognition of fear and sadness in post-traumatic stress disorder. *Cortex*, *47*(8), 974–980. https://doi.org/10.1016/j.cortex.2010.10.002
231. Popova, E. (2014). Ionotropic GABA Receptors and Distal Retinal ON and OFF Responses. *Scientifica (Cairo)*, *2014*, 149187. https://doi.org/10.1155/2014/149187
232. Posner, M. I., & DiGirolamo, G. J. (1998). Executive attention: conflict, target detection, and cognitive control. *The Attentive Brain*.
233. Post, S. G., Ng, L. E., Fischel, J. E., Bennett, M., Bily, L., Chandran, L., Joyce, J., Locicero, B., McGovern, K., McKeefrey, R. L., Rodriguez, J. V., & Roess, M. W. (2014). Routine, empathic and compassionate patient care: definitions, development, obstacles, education and beneficiaries. *J Eval Clin Pract*, *20*(6), 872–880. https://doi.org/10.1111/jep.12243

234. Pouille, F., & Scanziani, M. (2004). Routing of spike series by dynamic circuits in the hippocampus. *Nature*, *429*(6993), 717–723. https://doi.org/10.1038/nature02615
235. Preston, S. D., & de Waal, F. B. (2002). Empathy: Its ultimate and proximate bases. *Behav Brain Sci*, *25*(1), 1–20; discussion 20–71. https://doi.org/10.1017/s0140525x02000018
236. Qi, C., Sima, W., Mao, H., Hu, E., Ge, J., Deng, M., Chen, A., Ye, W., Xue, Q., Wang, W., Chen, Q., & Wu, S. (2025). Anterior cingulate cortex parvalbumin and somatostatin interneurons shape social behavior in male mice. *Nat Commun*, *16*(1), 4156. https://doi.org/10.1038/s41467-025-59473-z
237. Raihani, N. (2021). *The social instinct : how cooperation shaped the world*. St. Martin's Press.
238. Ramachandran, S., Krogh, N., Jorgensen, T. E., Johansen, S. D., Nielsen, H., & Babiak, I. (2020). The shift from early to late types of ribosomes in zebrafish development involves changes at a subset of rRNA 2'-O-Me sites. *RNA*, *26*(12), 1919–1934. https://doi.org/10.1261/rna.076760.120
239. Rauch, S. L., Shin, L. M., Segal, E., Pitman, R. K., Carson, M. A., McMullin, K., Whalen, P. J., & Makris, N. (2003). Selectively reduced regional cortical volumes in post-traumatic stress disorder. *Neuroreport*, *14*(7), 913–916. https://doi.org/10.1097/01.wnr.0000071767.24455.10
240. Redcay, E., & Schilbach, L. (2019). Using second-person neuroscience to elucidate the mechanisms of social interaction. *Nat Rev Neurosci*, *20*(8), 495–505. https://doi.org/10.1038/s41583-019-0179-4
241. Reyes, A., Lujan, R., Rozov, A., Burnashev, N., Somogyi, P., & Sakmann, B. (1998). Target-cell-specific facilitation and depression in neocortical circuits. *Nat Neurosci*, *1*(4), 279–285. https://doi.org/10.1038/1092
242. Rolls, E. T. (2019). The cingulate cortex and limbic systems for emotion, action, and memory. *Brain Struct Funct*, *224*(9), 3001–3018. https://doi.org/10.1007/s00429-019-01945-2
243. Roozendaal, B., McEwen, B. S., & Chattarji, S. (2009). Stress, memory and the amygdala. *Nat Rev Neurosci*, *10*(6), 423–433. https://doi.org/10.1038/nrn2651
244. Rose, M. C., Styr, B., Schmid, T. A., Elie, J. E., & Yartsev, M. M. (2021). Cortical representation of group social communication in bats. *Science*, *374*(6566), eaba9584. https://doi.org/10.1126/science.aba9584
245. Rossi, A. F., Pessoa, L., Desimone, R., & Ungerleider, L. G. (2009). The prefrontal cortex and the executive control of attention. *Exp Brain Res*, *192*(3), 489–497. https://doi.org/10.1007/s00221-008-1642-z
246. Roux, L., & Buzsaki, G. (2015). Tasks for inhibitory interneurons in intact brain circuits. *Neuropharmacology*, *88*, 10–23. https://doi.org/10.1016/j.neuropharm.2014.09.011
247. Roy, M., Shohamy, D., & Wager, T. D. (2012). Ventromedial prefrontal-subcortical systems and the generation of affective meaning. *Trends Cogn Sci*, *16*(3), 147–156. https://doi.org/10.1016/j.tics.2012.01.005
248. Rudy, B., Fishell, G., Lee, S., & Hjerling-Leffler, J. (2011). Three groups of interneurons account for nearly 100% of neocortical GABAergic neurons. *Dev Neurobiol*, *71*(1), 45–61. https://doi.org/10.1002/dneu.20853
249. Rushworth, M. F., & Behrens, T. E. (2008). Choice, uncertainty and value in prefrontal and cingulate cortex. *Nat Neurosci*, *11*(4), 389–397. https://doi.org/10.1038/nn2066
250. Rushworth, M. F., Noonan, M. P., Boorman, E. D., Walton, M. E., & Behrens, T. E. (2011). Frontal cortex and reward-guided learning and decision-making. *Neuron*, *70*(6), 1054–1069. https://doi.org/10.1016/j.neuron.2011.05.014
251. Santamaria, L., Noreika, V., Georgieva, S., Clackson, K., Wass, S., & Leong, V. (2020). Emotional valence modulates the topology of the parent-infant inter-brain network. *Neuroimage*, *207*, 116341. https://doi.org/10.1016/j.neuroimage.2019.116341

252. Scaglione, A., Lucchesi, J., Mascaro, A. L. A., & Pavone, F. S. (2024). https://doi.org/10.1101/2024.05.21.593536
253. Scanziani, M., Gahwiler, B. H., & Charpak, S. (1998). Target cell-specific modulation of transmitter release at terminals from a single axon. *Proc Natl Acad Sci U S A*, *95*(20), 12004–12009. https://doi.org/10.1073/pnas.95.20.12004
254. Scarpina, F., & Tagini, S. (2017). The Stroop Color and Word Test. *Front Psychol*, *8*, 557. https://doi.org/10.3389/fpsyg.2017.00557
255. Schafer, M., & Schiller, D. (2018). Navigating Social Space. *Neuron*, *100*(2), 476–489. https://doi.org/10.1016/j.neuron.2018.10.006
256. Scheggia, D., La Greca, F., Maltese, F., Chiacchierini, G., Italia, M., Molent, C., Bernardi, F., Coccia, G., Carrano, N., Zianni, E., Gardoni, F., Di Luca, M., & Papaleo, F. (2022). Reciprocal cortico-amygdala connections regulate prosocial and selfish choices in mice. *Nat Neurosci*, *25*(11), 1505–1518. https://doi.org/10.1038/s41593-022-01179-2
257. Scheggia, D., Manago, F., Maltese, F., Bruni, S., Nigro, M., Dautan, D., Latuske, P., Contarini, G., Gomez-Gonzalo, M., Requie, L. M., Ferretti, V., Castellani, G., Mauro, D., Bonavia, A., Carmignoto, G., Yizhar, O., & Papaleo, F. (2020). Somatostatin interneurons in the prefrontal cortex control affective state discrimination in mice. *Nat Neurosci*, *23*(1), 47–60. https://doi.org/10.1038/s41593-019-0551-8
258. Schilbach, L., Eickhoff, S. B., Mojzisch, A., & Vogeley, K. (2008). What's in a smile? Neural correlates of facial embodiment during social interaction. *Soc Neurosci*, *3*(1), 37–50. https://doi.org/10.1080/17470910701563228
259. Schmaal, L., Hibar, D. P., Samann, P. G., Hall, G. B., Baune, B. T., Jahanshad, N., Cheung, J. W., van Erp, T. G. M., Bos, D., Ikram, M. A., Vernooij, M. W., Niessen, W. J., Tiemeier, H., Hofman, A., Wittfeld, K., Grabe, H. J., Janowitz, D., Bulow, R., Selonke, M.,…Veltman, D. J. (2017). Cortical abnormalities in adults and adolescents with major depression based on brain scans from 20 cohorts worldwide in the ENIGMA Major Depressive Disorder Working Group. *Mol Psychiatry*, *22*(6), 900–909. https://doi.org/10.1038/mp.2016.60
260. Schneider, K. N., Sciarillo, X. A., Nudelman, J. L., Cheer, J. F., & Roesch, M. R. (2020). Anterior Cingulate Cortex Signals Attention in a Social Paradigm that Manipulates Reward and Shock. *Curr Biol*, *30*(19), 3724–3735 e3722. https://doi.org/10.1016/j.cub.2020.07.039
261. Senju, A. (2012). Spontaneous theory of mind and its absence in autism spectrum disorders. *Neuroscientist*, *18*(2), 108–113. https://doi.org/10.1177/1073858410397208
262. Silberberg, G., & Markram, H. (2007). Disynaptic inhibition between neocortical pyramidal cells mediated by Martinotti cells. *Neuron*, *53*(5), 735–746. https://doi.org/10.1016/j.neuron.2007.02.012
263. Singer, T., Seymour, B., O'Doherty, J., Kaube, H., Dolan, R. J., & Frith, C. D. (2004). Empathy for pain involves the affective but not sensory components of pain. *Science*, *303*(5661), 1157–1162. https://doi.org/10.1126/science.1093535
264. Smith, M. L., Asada, N., & Malenka, R. C. (2021). Anterior cingulate inputs to nucleus accumbens control the social transfer of pain and analgesia. *Science*, *371*(6525), 153–159. https://doi.org/10.1126/science.abe3040
265. Sohal, V. S., & Rubenstein, J. L. R. (2019). Excitation-inhibition balance as a framework for investigating mechanisms in neuropsychiatric disorders. *Mol Psychiatry*, *24*(9), 1248–1257. https://doi.org/10.1038/s41380-019-0426-0
266. Somogyi, P., Tamas, G., Lujan, R., & Buhl, E. H. (1998). Salient features of synaptic organisation in the cerebral cortex. *Brain Res Brain Res Rev*, *26*(2-3), 113–135. https://doi.org/10.1016/s0165-0173(97)00061-1
267. Spilka, M. J., Arnold, A. E., & Goghari, V. M. (2015). Functional activation abnormalities during facial emotion perception in schizophrenia patients and nonpsychotic relatives. *Schizophr Res*, *168*(1-2), 330–337. https://doi.org/10.1016/j.schres.2015.07.012

268. Stevens, F. L., Hurley, R. A., & Taber, K. H. (2011). Anterior cingulate cortex: unique role in cognition and emotion. *J Neuropsychiatry Clin Neurosci*, *23*(2), 121–125. https://doi.org/10.1176/jnp.23.2.jnp121
269. Stevenson, A. (2010). *Oxford Dictionary of English (3rd ed.)*.
270. Strick, P. L., Dum, R. P., & Picard, N. (1998). Motor areas on the medial wall of the hemisphere. *Novartis Found Symp*, *218*, 64–75; discussion 75–80, 104–108. https://doi.org/10.1002/9780470515563.ch5
271. Sullivan, R. M., & Gratton, A. (1999). Lateralized effects of medial prefrontal cortex lesions on neuroendocrine and autonomic stress responses in rats. *J Neurosci*, *19*(7), 2834–2840. https://doi.org/10.1523/JNEUROSCI.19-07-02834.1999
272. Takahashi, H., Koeda, M., Oda, K., Matsuda, T., Matsushima, E., Matsuura, M., Asai, K., & Okubo, Y. (2004). An fMRI study of differential neural response to affective pictures in schizophrenia. *Neuroimage*, *22*(3), 1247–1254. https://doi.org/10.1016/j.neuroimage.2004.03.028
273. Takashima, A., Petersson, K. M., Rutters, F., Tendolkar, I., Jensen, O., Zwarts, M. J., McNaughton, B. L., & Fernandez, G. (2006). Declarative memory consolidation in humans: a prospective functional magnetic resonance imaging study. *Proc Natl Acad Sci U S A*, *103*(3), 756–761. https://doi.org/10.1073/pnas.0507774103
274. Tamamaki, N., & Tomioka, R. (2010). Long-Range GABAergic Connections Distributed throughout the Neocortex and their Possible Function. *Front Neurosci*, *4*, 202. https://doi.org/10.3389/fnins.2010.00202
275. Tasic, B., Menon, V., Nguyen, T. N., Kim, T. K., Jarsky, T., Yao, Z., Levi, B., Gray, L. T., Sorensen, S. A., Dolbeare, T., Bertagnolli, D., Goldy, J., Shapovalova, N., Parry, S., Lee, C., Smith, K., Bernard, A., Madisen, L., Sunkin, S. M.,…Zeng, H. (2016). Adult mouse cortical cell taxonomy revealed by single cell transcriptomics. *Nat Neurosci*, *19*(2), 335–346. https://doi.org/10.1038/nn.4216
276. Taylor, S. F., Kang, J., Brege, I. S., Tso, I. F., Hosanagar, A., & Johnson, T. D. (2012). Meta-analysis of functional neuroimaging studies of emotion perception and experience in schizophrenia. *Biol Psychiatry*, *71*(2), 136–145. https://doi.org/10.1016/j.biopsych.2011.09.007
277. Terracciano, A., McCrae, R. R., & Costa, P. T., Jr. (2003). Factorial and construct validity of the Italian Positive and Negative Affect Schedule (PANAS). *Eur J Psychol Assess*, *19*(2), 131–141. https://doi.org/10.1027//1015-5759.19.2.131
278. Thompson, L., Thompson, M., & Reid, A. (2010). Neurofeedback outcomes in clients with Asperger's syndrome. *Appl Psychophysiol Biofeedback*, *35*(1), 63–81. https://doi.org/10.1007/s10484-009-9120-3
279. Thomson, A. M. (2003). Presynaptic frequency- and pattern-dependent filtering. *J Comput Neurosci*, *15*(2), 159–202. https://doi.org/10.1023/a:1025812808362
280. Todtenkopf, M. S., Vincent, S. L., & Benes, F. M. (2005). A cross-study meta-analysis and three-dimensional comparison of cell counting in the anterior cingulate cortex of schizophrenic and bipolar brain. *Schizophr Res*, *73*(1), 79–89. https://doi.org/10.1016/j.schres.2004.08.018
281. Tomioka, R., Okamoto, K., Furuta, T., Fujiyama, F., Iwasato, T., Yanagawa, Y., Obata, K., Kaneko, T., & Tamamaki, N. (2005). Demonstration of long-range GABAergic connections distributed throughout the mouse neocortex. *Eur J Neurosci*, *21*(6), 1587–1600. https://doi.org/10.1111/j.1460-9568.2005.03989.x
282. Tremblay, R., Lee, S., & Rudy, B. (2016). GABAergic Interneurons in the Neocortex: From Cellular Properties to Circuits. *Neuron*, *91*(2), 260–292. https://doi.org/10.1016/j.neuron.2016.06.033
283. Tseng, P. H., Rajangam, S., Lehew, G., Lebedev, M. A., & Nicolelis, M. A. L. (2018). Interbrain cortical synchronization encodes multiple aspects of social interactions in monkey pairs. *Sci Rep*, *8*(1), 4699. https://doi.org/10.1038/s41598-018-22679-x

284. Uhrig, M. K., Trautmann, N., Baumgartner, U., Treede, R. D., Henrich, F., Hiller, W., & Marschall, S. (2016). Emotion Elicitation: A Comparison of Pictures and Films. *Front Psychol*, *7*, 180. https://doi.org/10.3389/fpsyg.2016.00180
285. Urban-Ciecko, J., & Barth, A. L. (2016). Somatostatin-expressing neurons in cortical networks. *Nat Rev Neurosci*, *17*(7), 401–409. https://doi.org/10.1038/nrn.2016.53
286. Utashiro, N., MacLaren, D. A. A., Liu, Y. C., Yaqubi, K., Wojak, B., & Monyer, H. (2024). Long-range inhibition from prelimbic to cingulate areas of the medial prefrontal cortex enhances network activity and response execution. *Nat Commun*, *15*(1), 5772. https://doi.org/10.1038/s41467-024-50055-z
287. van Heukelum, S., Mars, R. B., Guthrie, M., Buitelaar, J. K., Beckmann, C. F., Tiesinga, P. H. E., Vogt, B. A., Glennon, J. C., & Havenith, M. N. (2020). Where is Cingulate Cortex? A Cross-Species View. *Trends Neurosci*, *43*(5), 285–299. https://doi.org/10.1016/j.tins.2020.03.007
288. Van Kleef, G. A. (2016). *The interpersonal dynamics of emotion*. Cambridge University Press.
289. van Kleef, G. A., & Cote, S. (2022). The Social Effects of Emotions. *Annu Rev Psychol*, *73*, 629–658. https://doi.org/10.1146/annurev-psych-020821-010855
290. Vargas, R. A. (2018). The GABAergic System: An overview of physiology, physiopathology and therapeutics. *International Journal of Clinical Pharmacology & Pharmacotherapy*, *3*. https://doi.org/https://doi.org/10.15344/2456-3501/2018/142
291. Veit, J., Hakim, R., Jadi, M. P., Sejnowski, T. J., & Adesnik, H. (2017). Cortical gamma band synchronization through somatostatin interneurons. *Nat Neurosci*, *20*(7), 951–959. https://doi.org/10.1038/nn.4562
292. Villarreal, G., Hamilton, D. A., Petropoulos, H., Driscoll, I., Rowland, L. M., Griego, J. A., Kodituwakku, P. W., Hart, B. L., Escalona, R., & Brooks, W. M. (2002). Reduced hippocampal volume and total white matter volume in posttraumatic stress disorder. *Biol Psychiatry*, *52*(2), 119–125. https://doi.org/10.1016/s0006-3223(02)01359-8
293. Vogt, B. A. (2016). Midcingulate cortex: Structure, connections, homologies, functions and diseases. *J Chem Neuroanat*, *74*, 28–46. https://doi.org/10.1016/j.jchemneu.2016.01.010
294. Wang, J., Rao, H., Wetmore, G. S., Furlan, P. M., Korczykowski, M., Dinges, D. F., & Detre, J. A. (2005). Perfusion functional MRI reveals cerebral blood flow pattern under psychological stress. *Proc Natl Acad Sci U S A*, *102*(49), 17804–17809. https://doi.org/10.1073/pnas.0503082102
295. Wang, Y., Toledo-Rodriguez, M., Gupta, A., Wu, C., Silberberg, G., Luo, J., & Markram, H. (2004). Anatomical, physiological and molecular properties of Martinotti cells in the somatosensory cortex of the juvenile rat. *J Physiol*, *561*(Pt 1), 65–90. https://doi.org/10.1113/jphysiol.2004.073353
296. Whissell, P. D., Cajanding, J. D., Fogel, N., & Kim, J. C. (2015). Comparative density of CCK- and PV-GABA cells within the cortex and hippocampus. *Front Neuroanat*, *9*, 124. https://doi.org/10.3389/fnana.2015.00124
297. Woodward, S. H., Kaloupek, D. G., Streeter, C. C., Martinez, C., Schaer, M., & Eliez, S. (2006). Decreased anterior cingulate volume in combat-related PTSD. *Biol Psychiatry*, *59*(7), 582–587. https://doi.org/10.1016/j.biopsych.2005.07.033
298. Wu, S. J., Sevier, E., Dwivedi, D., Saldi, G. A., Hairston, A., Yu, S., Abbott, L., Choi, D. H., Sherer, M., Qiu, Y., Shinde, A., Lenahan, M., Rizzo, D., Xu, Q., Barrera, I., Kumar, V., Marrero, G., Pronneke, A., Huang, S.,…Fishell, G. (2023). Cortical somatostatin interneuron subtypes form cell-type-specific circuits. *Neuron*, *111*(17), 2675–2692 e2679. https://doi.org/10.1016/j.neuron.2023.05.032
299. Xu, H., Jeong, H. Y., Tremblay, R., & Rudy, B. (2013). Neocortical somatostatin-expressing GABAergic interneurons disinhibit the thalamorecipient layer 4. *Neuron*, *77*(1), 155–167. https://doi.org/10.1016/j.neuron.2012.11.004

300. Yamawaki, N., Li, X., Lambot, L., Ren, L. Y., Radulovic, J., & Shepherd, G. M. G. (2019). Long-range inhibitory intersection of a retrosplenial thalamocortical circuit by apical tuft-targeting CA1 neurons. *Nat Neurosci*, *22*(4), 618–626. https://doi.org/10.1038/s41593-019-0355-x
301. Yang, Y., Wu, M., Vazquez-Guardado, A., Wegener, A. J., Grajales-Reyes, J. G., Deng, Y., Wang, T., Avila, R., Moreno, J. A., Minkowicz, S., Dumrongprechachan, V., Lee, J., Zhang, S., Legaria, A. A., Ma, Y., Mehta, S., Franklin, D., Hartman, L., Bai, W.,…Rogers, J. A. (2021). Wireless multilateral devices for optogenetic studies of individual and social behaviors. *Nat Neurosci*, *24*(7), 1035–1045. https://doi.org/10.1038/s41593-021-00849-x
302. Yeshurun, Y., Nguyen, M., & Hasson, U. (2021). The default mode network: where the idiosyncratic self meets the shared social world. *Nat Rev Neurosci*, *22*(3), 181–192. https://doi.org/10.1038/s41583-020-00420-w
303. Yeung, M. K. (2022). A systematic review and meta-analysis of facial emotion recognition in autism spectrum disorder: The specificity of deficits and the role of task characteristics. *Neurosci Biobehav Rev*, *133*, 104518. https://doi.org/10.1016/j.neubiorev.2021.104518
304. Yizhar, O., Fenno, L. E., Prigge, M., Schneider, F., Davidson, T. J., O'Shea, D. J., Sohal, V. S., Goshen, I., Finkelstein, J., Paz, J. T., Stehfest, K., Fudim, R., Ramakrishnan, C., Huguenard, J. R., Hegemann, P., & Deisseroth, K. (2011). Neocortical excitation/inhibition balance in information processing and social dysfunction. *Nature*, *477*(7363), 171–178. https://doi.org/10.1038/nature10360
305. Young, D. A., Chao, L., Neylan, T. C., O'Donovan, A., Metzler, T. J., & Inslicht, S. S. (2018). Association among anterior cingulate cortex volume, psychophysiological response, and PTSD diagnosis in a Veteran sample. *Neurobiol Learn Mem*, *155*, 189–196. https://doi.org/10.1016/j.nlm.2018.08.006
306. Zaborszky, L., Carlsen, J., Brashear, H. R., & Heimer, L. (1986). Cholinergic and GABAergic afferents to the olfactory bulb in the rat with special emphasis on the projection neurons in the nucleus of the horizontal limb of the diagonal band. *J Comp Neurol*, *243*(4), 488–509. https://doi.org/10.1002/cne.902430405
307. Zaki, J. (2014). Empathy: a motivated account. *Psychol Bull*, *140*(6), 1608–1647. https://doi.org/10.1037/a0037679
308. Zamm, A., Debener, S., Bauer, A. R., Bleichner, M. G., Demos, A. P., & Palmer, C. (2018). Amplitude envelope correlations measure synchronous cortical oscillations in performing musicians. *Ann N Y Acad Sci*. https://doi.org/10.1111/nyas.13738
309. Zeidan, F., Martucci, K. T., Kraft, R. A., McHaffie, J. G., & Coghill, R. C. (2014). Neural correlates of mindfulness meditation-related anxiety relief. *Soc Cogn Affect Neurosci*, *9*(6), 751–759. https://doi.org/10.1093/scan/nst041
310. Zhang, M., Wu, Y. E., Jiang, M., & Hong, W. (2024). Cortical regulation of helping behaviour towards others in pain. *Nature*, *626*(7997), 136–144. https://doi.org/10.1038/s41586-023-06973-x
311. Zhang, W., & Yartsev, M. M. (2019). Correlated Neural Activity across the Brains of Socially Interacting Bats. *Cell*, *178*(2), 413–428 e422. https://doi.org/10.1016/j.cell.2019.05.023
312. Zhang, X., Phi, N., Li, Q., Gorzek, R., Zwingenberger, N., Huang, S., Zhou, J. L., Kingsbury, L., Raam, T., Wu, Y. E., Wei, D., Kao, J. C., & Hong, W. (2025). Inter-brain neural dynamics in biological and artificial intelligence systems. *Nature*. https://doi.org/10.1038/s41586-025-09196-4
313. Zhang, Z., Fan, Q., Zhu, Y., Tan, L., Chen, Y., Gao, R., Zhang, H., Li, Y., & Xiao, Z. (2017). Intrinsic functional connectivity alteration of dorsal and rostral anterior cingulate cortex in obsessive-compulsive disorder: A resting fMRI study. *Neurosci Lett*, *654*, 86–92. https://doi.org/10.1016/j.neulet.2017.06.026

Chapter 6

General Discussion

Recognizing emotions and responding suitably in social situations are essential for an individual's well-being and the overall cohesion of society. These skills depend on interconnected neural networks that balance stimulation and inhibition, with the medial prefrontal cortex (mPFC) playing a vital role in social cognition ((Adolphs, 2009); (Amodio & Frith, 2006); (Frith & Frith, 2007)). Within this network, the prelimbic cortex (PrL) and the anterior cingulate cortex (ACC) are well-established hubs ((Adolphs, 2009); (Amodio & Frith, 2006); (Scheggia et al., 2020); (Keum et al., 2018)), and their dense connections suggest they may work together but have distinct functions ((Tomioka et al., 2005); (Tamamaki & Tomioka, 2010); (Utashiro et al., 2024)). This thesis examined the role of somatostatin-expressing (SOM) interneurons in emotion recognition within these regions, as well as their long-range connections, inter-brain dynamics, and modulation by personal self-experience.

A first key insight was uncovering a cortico-cortical inhibitory–excitatory loop between the mPFC and retrosplenial cortex (RSC) that directly supports emotion recognition. Fiber photometry and optogenetics showed that emotion recognition was associated with reduced activity of mPFC-to-RSC SOM projections, alongside increased activity of RSC-to-mPFC pyramidal projections, a pattern mirrored by inverse mPFC–RSC coupling in human fMRI data. Manipulations confirmed a causal role: reducing inhibitory drive from mPFC SOM neurons to RSC rescued recognition deficits, while stimulating these terminals impaired recognition. These results extend evidence for long-range inhibitory projections ((Melzer et al., 2012); (Lee et al., 2014); (Bertero et al., 2019); (Yamawaki et al., 2019)) by identifying a previously uncharacterized mPFC-to-RSC SOM pathway crucial for emotion recognition. Significantly, this pathway's function differed from the overall mPFC SOM population (Scheggia et al., 2020), illustrating the heterogeneity of cortical SOM neurons ((Munoz et al., 2017); (Urban-Ciecko & Barth, 2016)).

While these experiments define the cellular and circuit-level mechanisms underlying emotion recognition, social interactions are rarely context-free. We demonstrated that prior self-

experience influences responses to others' emotions in a sex- and hierarchy-dependent manner, mediated by corticotropin-releasing factor (CRF) neurons in the mPFC. Self-experienced stress triggered different behavioural strategies, ranging from approach to avoidance, mirroring human findings that prior experience can lead to empathic concern or personal distress ((Preston & de Waal, 2002); (Zaki, 2014); (Israelashvili et al., 2020)). In rodents, similar effects have been reported in prosocial contexts ((Ben-Ami Bartal et al., 2011);(Burkett et al., 2016); (Scheggia et al., 2022)). Here, we demonstrated that mPFC CRF neurons are selectively activated after self-experience, store stress memories, and later bias responses to stressed conspecifics. This expands their known involvement in stress, reward, and social familiarity ((Kai et al., 2018); (Chen et al., 2020); (Hupalo et al., 2019); (de Leon Reyes et al., 2023)) to empathy-related behaviors.

The contribution of inhibitory interneurons to emotion recognition is region-specific. In the ACC, SOM inhibition did not abolish discrimination—the first step in empathetic processing (de Waal, 2008)—and sometimes enhanced it, consistent with prior work ((Keum et al., 2018)). In contrast, stimulation impaired discrimination and social memory, in line with the ACC's role in memory encoding and retrieval ((Bush et al., 2000); (Lenartowicz & McIntosh, 2005)) and its connectivity with the amygdala, critical for emotionally salient memories ((Rolls, 2019); (Roozendaal et al., 2009)). Because SOM interneurons primarily target pyramidal dendrites (Wu et al., 2023), stimulation likely increased dendritic inhibition, reducing pyramidal output. By contrast, PrL SOM neurons were indispensable for negative affective state discrimination: both inhibition and stimulation disrupted behavior (Scheggia et al., 2020), highlighting the need for precise excitatory–inhibitory balance ((Yizhar et al., 2011); (Sohal & Rubenstein, 2019)). Mapping ACC SOM projections revealed targets in the mPFC, dorsal tenia tecta (dTT), and anterior amygdaloid area ventral (aAAV), all key nodes in social and affective processing ((Adolphs, 2009); (Amodio & Frith, 2006); (Friedman & Robbins, 2022);(Kietzman & Gourley, 2023); (Rolls, 2019); (Etkin & Wager, 2007); (Craig, 2009)). Notably, the dTT has been linked to the default mode network and human emotion recognition ((Zaborszky et al., 1986); (Phan et al., 2002); (Hariri et al., 2003); (Andrews-Hanna et al., 2010)). Together, these findings reveal a regionally specialized functional architecture of SOM circuits in the prefrontal cortex.

Finally, our results highlight that emotion recognition is not only a single-brain computation but also a distributed, multi-brain process. We found that inter-brain dynamics in the ACC depended on both neuronal subtype and emotional context: stress increased inter-brain SOM correlations and pyramidal anti-correlations, whereas neutral interactions induced the reverse. Crucially, manipulations showed that these inter-brain dynamics causally influenced social preference. This extends prior reports of inter-brain coupling in monkeys, bats, and rodents during neutral states ((Kingsbury et al., 2019); (Zhang & Yartsev, 2019); (Rose et al., 2021); (Scaglione et al., 2024); (Lee et al., 2024); (Tseng et al., 2018)) by demonstrating emotion-dependent, cell-type-specific mechanisms. Moreover, our data identified causal roles for both correlated and anti-correlated activity in social decisions, addressing the open question of whether inter-brain synchrony is epiphenomenal or mechanistic ((Hamilton, 2021); (Holroyd, 2022)).

Together, these findings reveal a multi-layered inhibitory architecture of emotion recognition. At the local level, SOM neurons in the ACC and PrL play distinct roles; at the circuit level, mPFC-to-RSC SOM projections regulate cortico-cortical communication; at the network level, inter-brain dynamics guide socio-emotional choices; and at the individual level, CRF neurons integrate self-experience with social perception. This framework provides mechanistic insight into how inhibitory circuits shape socio-emotional processes, and suggests translational targets for psychiatric disorders characterized by social and emotional deficits, including autism, schizophrenia, and anxiety ((Green et al., 2015); (Hiser & Koenigs, 2018); (Dienel et al., 2025); (Yeung, 2022)).

Bibliography

1. Adolphs, R. (2009). The social brain: neural basis of social knowledge. *Annu Rev Psychol*, *60*, 693–716. https://doi.org/10.1146/annurev.psych.60.110707.163514
2. Amodio, D. M., & Frith, C. D. (2006). Meeting of minds: the medial frontal cortex and social cognition. *Nat Rev Neurosci*, *7*(4), 268–277. https://doi.org/10.1038/nrn1884
3. Andrews-Hanna, J. R., Reidler, J. S., Sepulcre, J., Poulin, R., & Buckner, R. L. (2010). Functional-anatomic fractionation of the brain's default network. *Neuron*, *65*(4), 550–562. https://doi.org/10.1016/j.neuron.2010.02.005
4. Ben-Ami Bartal, I., Decety, J., & Mason, P. (2011). Empathy and pro-social behavior in rats. *Science*, *334*(6061), 1427–1430. https://doi.org/10.1126/science.1210789
5. Bertero, A., Feyen, P. L. C., Zurita, H., & Apicella, A. J. (2019). A Non-Canonical Cortico-Amygdala Inhibitory Loop. *J Neurosci*, *39*(43), 8424–8438. https://doi.org/10.1523/JNEUROSCI.1515-19.2019
6. Burkett, J. P., Andari, E., Z.V., J., D.C., C., F.B.M., D. W., & L.J., Y. (2016). Oxytocin-dependent consolation behavior in rodents. *Science*, *351*, 375–378. https://doi.org/DOI:10.1126/science.aac4785
7. Bush, G., Luu, P., & Posner, M. I. (2000). Cognitive and emotional influences in anterior cingulate cortex. *Trends Cogn Sci*, *4*(6), 215–222. https://doi.org/10.1016/s1364-6613(00)01483-2
8. Chen, P., Lou, S., Huang, Z. H., Wang, Z., Shan, Q. H., Wang, Y., Yang, Y., Li, X., Gong, H., Jin, Y., Zhang, Z., & Zhou, J. N. (2020). Prefrontal Cortex Corticotropin-Releasing Factor Neurons Control Behavioral Style Selection under Challenging Situations. *Neuron*, *106*(2), 301–315 e307. https://doi.org/10.1016/j.neuron.2020.01.033
9. Craig, A. D. (2009). How do you feel--now? The anterior insula and human awareness. *Nat Rev Neurosci*, *10*(1), 59–70. https://doi.org/10.1038/nrn2555
10. de Leon Reyes, N. S., Sierra Diaz, P., Nogueira, R., Ruiz-Pino, A., Nomura, Y., de Solis, C. A., Schulkin, J., Asok, A., & Leroy, F. (2023). Corticotropin-releasing hormone signaling from prefrontal cortex to lateral septum suppresses interaction with familiar mice. *Cell*, *186*(19), 4152–4171 e4131. https://doi.org/10.1016/j.cell.2023.08.010
11. de Waal, F. B. (2008). Putting the altruism back into altruism: the evolution of empathy. *Annu Rev Psychol*, *59*, 279–300. https://doi.org/10.1146/annurev.psych.59.103006.093625
12. Dienel, S. J., Wade, K. L., Fish, K. N., & Lewis, D. A. (2025). Alterations in Prefrontal Cortical Somatostatin Neurons in Schizophrenia: Evidence for Weaker Inhibition of Pyramidal Neuron Dendrites. *Biol Psychiatry*, *98*(2), 156–166. https://doi.org/10.1016/j.biopsych.2025.01.010
13. Etkin, A., Egner, T., & Kalisch, R. (2011). Emotional processing in anterior cingulate and medial prefrontal cortex. *Trends Cogn Sci*, *15*(2), 85–93. https://doi.org/10.1016/j.tics.2010.11.004
14. Friedman, N. P., & Robbins, T. W. (2022). The role of prefrontal cortex in cognitive control and executive function. *Neuropsychopharmacology*, *47*(1), 72–89. https://doi.org/10.1038/s41386-021-01132-0

15. Frith, C. D., & Frith, U. (2007). Social cognition in humans. *Curr Biol*, *17*(16), R724–732. https://doi.org/10.1016/j.cub.2007.05.068
16. Green, M. F., Horan, W. P., & Lee, J. (2015). Social cognition in schizophrenia. Nature reviews. Neuroscience, 16(10), 620–631. https://doi.org/10.1038/nrn4005
17. Hamilton, J. P., Glover, G. H., Hsu, J. J., Johnson, R. F., & Gotlib, I. H. (2011). Modulation of subgenual anterior cingulate cortex activity with real-time neurofeedback. *Hum Brain Mapp*, *32*(1), 22–31. https://doi.org/10.1002/hbm.20997
18. Hariri, A. R., Mattay, V. S., Tessitore, A., Fera, F., & Weinberger, D. R. (2003). Neocortical modulation of the amygdala response to fearful stimuli. *Biol Psychiatry*, *53*(6), 494–501. https://doi.org/10.1016/s0006-3223(02)01786-9
19. Hiser, J., & Koenigs, M. (2018). The Multifaceted Role of the Ventromedial Prefrontal Cortex in Emotion, Decision Making, Social Cognition, and Psychopathology. *Biol Psychiatry*, *83*(8), 638–647. https://doi.org/10.1016/j.biopsych.2017.10.030
20. Holroyd, C. B. (2022). Interbrain synchrony: on wavy ground. *Trends Neurosci*, *45*(5), 346–357. https://doi.org/10.1016/j.tins.2022.02.002
21. Hupalo, S., Martin, A. J., Green, R. K., Devilbiss, D. M., & Berridge, C. W. (2019). Prefrontal Corticotropin-Releasing Factor (CRF) Neurons Act Locally to Modulate Frontostriatal Cognition and Circuit Function. *J Neurosci*, *39*(11), 2080–2090. https://doi.org/10.1523/JNEUROSCI.2701-18.2019
22. Israelashvili, J., Sauter, D. A., & Fischer, A. H. (2020). Different faces of empathy: Feelings of similarity disrupt recognition of negative emotions. *J Exp Soc Psychol*, *87*, 103912. https://doi.org/10.1016/j.jesp.2019.103912
23. Kai, Y., Li, Y., Sun, T., Yin, W., Mao, Y., Li, J., Xie, W., Chen, S., Wang, L., Li, J., Zhang, Z., & Tao, W. (2018). A medial prefrontal cortex-nucleus acumens corticotropin-releasing factor circuitry for neuropathic pain-increased susceptibility to opioid reward. *Transl Psychiatry*, *8*(1), 100. https://doi.org/10.1038/s41398-018-0152-4
24. Keum, S., Kim, A., Shin, J. J., Kim, J. H., Park, J., & Shin, H. S. (2018). A Missense Variant at the Nrxn3 Locus Enhances Empathy Fear in the Mouse. *Neuron*, *98*(3), 588–601 e585. https://doi.org/10.1016/j.neuron.2018.03.041
25. Kietzman, H. W., & Gourley, S. L. (2023). How social information impacts action in rodents and humans: the role of the prefrontal cortex and its connections. *Neurosci Biobehav Rev*, *147*, 105075. https://doi.org/10.1016/j.neubiorev.2023.105075
26. Kingsbury, L., Huang, S., Wang, J., Gu, K., Golshani, P., Wu, Y. E., & Hong, W. (2019). Correlated Neural Activity and Encoding of Behavior across Brains of Socially Interacting Animals. *Cell*, *178*(2), 429–446 e416. https://doi.org/10.1016/j.cell.2019.05.022
27. Lee, A. T., Vogt, D., Rubenstein, J. L., & Sohal, V. S. (2014). A class of GABAergic neurons in the prefrontal cortex sends long-range projections to the nucleus accumbens and elicits acute avoidance behavior. *J Neurosci*, *34*(35), 11519–11525. https://doi.org/10.1523/JNEUROSCI.1157-14.2014

28. Lee, J., Kwak, D., Lee, G. U., Kim, C. Y., Kim, J., Park, S. H., Choi, J. H., Lee, S. Q., & Choe, H. K. (2024). Social context modulates multibrain broadband dynamics and functional brain-to-brain coupling in the group of mice. *Sci Rep*, *14*(1), 11439. https://doi.org/10.1038/s41598-024-62070-7
29. Lenartowicz, A., & McIntosh, A. R. (2005). The role of anterior cingulate cortex in working memory is shaped by functional connectivity. *J Cogn Neurosci*, *17*(7), 1026–1042. https://doi.org/10.1162/0898929054475127
30. Melzer, S., Michael, M., Caputi, A., Eliava, M., Fuchs, E. C., Whittington, M. A., & Monyer, H. (2012). Long-range-projecting GABAergic neurons modulate inhibition in hippocampus and entorhinal cortex. Science (New York, N.Y.), 335(6075), 1506–1510. https://doi.org/10.1126/science.1217139
31. Munoz, W., Tremblay, R., Levenstein, D., & Rudy, B. (2017). Layer-specific modulation of neocortical dendritic inhibition during active wakefulness. *Science*, *355*(6328), 954–959. https://doi.org/10.1126/science.aag2599
32. Phan, K. L., Wager, T., Taylor, S. F., & Liberzon, I. (2002). Functional neuroanatomy of emotion: a meta-analysis of emotion activation studies in PET and fMRI. *Neuroimage*, *16*(2), 331–348. https://doi.org/10.1006/nimg.2002.1087
33. Preston, S. D., & de Waal, F. B. (2002). Empathy: Its ultimate and proximate bases. *Behav Brain Sci*, *25*(1), 1–20; discussion 20–71. https://doi.org/10.1017/s0140525x02000018
34. Rolls, E. T. (2019). The cingulate cortex and limbic systems for emotion, action, and memory. *Brain Struct Funct*, *224*(9), 3001–3018. https://doi.org/10.1007/s00429-019-01945-2
35. Roozendaal, B., McEwen, B. S., & Chattarji, S. (2009). Stress, memory and the amygdala. *Nat Rev Neurosci*, *10*(6), 423–433. https://doi.org/10.1038/nrn2651
36. Rose, M. C., Styr, B., Schmid, T. A., Elie, J. E., & Yartsev, M. M. (2021). Cortical representation of group social communication in bats. *Science*, *374*(6566), eaba9584. https://doi.org/10.1126/science.aba9584
37. Scaglione, A., Lucchesi, J., Mascaro, A. L. A., & Pavone, F. S. (2024). https://doi.org/10.1101/2024.05.21.593536
38. Scheggia, D., La Greca, F., Maltese, F., Chiacchierini, G., Italia, M., Molent, C., Bernardi, F., Coccia, G., Carrano, N., Zianni, E., Gardoni, F., Di Luca, M., & Papaleo, F. (2022). Reciprocal cortico-amygdala connections regulate prosocial and selfish choices in mice. Nature neuroscience, 25(11), 1505–1518. https://doi.org/10.1038/s41593-022-01179-2
39. Scheggia, D., Manago, F., Maltese, F., Bruni, S., Nigro, M., Dautan, D., Latuske, P., Contarini, G., Gomez-Gonzalo, M., Requie, L. M., Ferretti, V., Castellani, G., Mauro, D., Bonavia, A., Carmignoto, G., Yizhar, O., & Papaleo, F. (2020). Somatostatin interneurons in the prefrontal cortex control affective state discrimination in mice. *Nat Neurosci*, *23*(1), 47–60. https://doi.org/10.1038/s41593-019-0551-8
40. Sohal, V. S., & Rubenstein, J. L. R. (2019). Excitation-inhibition balance as a framework for investigating mechanisms in neuropsychiatric disorders. *Mol Psychiatry*, *24*(9), 1248–1257. https://doi.org/10.1038/s41380-019-0426-0

41. Tamamaki, N., & Tomioka, R. (2010). Long-Range GABAergic Connections Distributed throughout the Neocortex and their Possible Function. *Front Neurosci*, *4*, 202. https://doi.org/10.3389/fnins.2010.00202
42. Tomioka, R., Okamoto, K., Furuta, T., Fujiyama, F., Iwasato, T., Yanagawa, Y., Obata, K., Kaneko, T., & Tamamaki, N. (2005). Demonstration of long-range GABAergic connections distributed throughout the mouse neocortex. *Eur J Neurosci*, *21*(6), 1587–1600. https://doi.org/10.1111/j.1460-9568.2005.03989.x
43. Tseng, P. H., Rajangam, S., Lehew, G., Lebedev, M. A., & Nicolelis, M. A. L. (2018). Interbrain cortical synchronization encodes multiple aspects of social interactions in monkey pairs. *Sci Rep*, *8*(1), 4699. https://doi.org/10.1038/s41598-018-22679-x
44. Urban-Ciecko, J., & Barth, A. L. (2016). Somatostatin-expressing neurons in cortical networks. *Nat Rev Neurosci*, *17*(7), 401–409. https://doi.org/10.1038/nrn.2016.53
45. Utashiro, N., MacLaren, D. A. A., Liu, Y. C., Yaqubi, K., Wojak, B., & Monyer, H. (2024). Long-range inhibition from prelimbic to cingulate areas of the medial prefrontal cortex enhances network activity and response execution. *Nat Commun*, *15*(1), 5772. https://doi.org/10.1038/s41467-024-50055-z
46. van Kleef, G. A., & Cote, S. (2022). The Social Effects of Emotions. *Annu Rev Psychol*, *73*, 629–658.
47. Wu, S. J., Sevier, E., Dwivedi, D., Saldi, G. A., Hairston, A., Yu, S., Abbott, L., Choi, D. H., Sherer, M., Qiu, Y., Shinde, A., Lenahan, M., Rizzo, D., Xu, Q., Barrera, I., Kumar, V., Marrero, G., Pronneke, A., Huang, S.,…Fishell, G. (2023). Cortical somatostatin interneuron subtypes form cell-type-specific circuits. *Neuron*, *111*(17), 2675–2692 e2679. https://doi.org/10.1016/j.neuron.2023.05.032
48. Yamawaki, N., Li, X., Lambot, L., Ren, L. Y., Radulovic, J., & Shepherd, G. M. G. (2019). Long-range inhibitory intersection of a retrosplenial thalamocortical circuit by apical tuft-targeting CA1 neurons. *Nat Neurosci*, *22*(4), 618–626. https://doi.org/10.1038/s41593-019-0355-x
49. Yeung, M. K. (2022). A systematic review and meta-analysis of facial emotion recognition in autism spectrum disorder: The specificity of deficits and the role of task characteristics. *Neurosci Biobehav Rev*, *133*, 104518. https://doi.org/10.1016/j.neubiorev.2021.104518
50. Yizhar, O., Fenno, L. E., Prigge, M., Schneider, F., Davidson, T. J., O'Shea, D. J., Sohal, V. S., Goshen, I., Finkelstein, J., Paz, J. T., Stehfest, K., Fudim, R., Ramakrishnan, C., Huguenard, J. R., Hegemann, P., & Deisseroth, K. (2011). Neocortical excitation/inhibition balance in information processing and social dysfunction. *Nature*, *477*(7363), 171–178. https://doi.org/10.1038/nature10360
51. Zaborszky, L., Carlsen, J., Brashear, H. R., & Heimer, L. (1986). Cholinergic and GABAergic afferents to the olfactory bulb in the rat with special emphasis on the projection neurons in the nucleus of the horizontal limb of the diagonal band. *J Comp Neurol*, *243*(4), 488–509. https://doi.org/10.1002/cne.902430405
52. Zaki, J. (2014). Empathy: a motivated account. *Psychol Bull*, *140*(6), 1608–1647. https://doi.org/10.1037/a0037679
53. Zhang, W., & Yartsev, M. M. (2019). Correlated Neural Activity across the Brains of Socially Interacting Bats. *Cell*, *178*(2), 413–428 e422. https://doi.org/10.1016/j.cell.2019.05.023

Glossary

1. Acetylcholine: Ach
2. Adenovirus: AAV
3. Anterior cingulate: ACC
4. Basolateral amygdala: BLA
5. Calretinin: CR
6. Channelrhodopsin: ChR2
7. Cholecystokinin: CCK
8. Cholera toxin subunit B: CTb
9. Cingulate Gyrus: CG
10. Claustrum: CLA
11. Cortico-thalamic: CT
12. Default Mode Network: DMN
13. Dorsal Anterior Cingulate Cortex: dACC
14. Dorsal Anterior Cingulate Cortex: dACC
15. Dorsal medial prefrontal cortex: dmPFC
16. Emotion discrimination task: EDT
17. Excitatory post synaptic current: EPSP
18. Figure: Fig.
19. GABA transaminase: GABA-T
20. Glutamate decarboxylase: GAD
21. Green fluorescent calcium sensor: GCamP
22. Halorhodopsin: NPHR
23. Immunostaining: IHC
24. Infralimbic cortex: IL
25. Interneurons: INs
26. Intra-telencephalic: IT
27. Lateral Prefrontal Cortex: LPFC
28. Medial agranular cortex: mAG
29. Medial Cingulate Cortex: MCC
30. Medial prefrontal cortex: mPFC
31. medial thalamic nucleus: mTh
32. Nitric-oxide synthase: NOS
33. Normal Donkey Serum: NDS
34. Orbitofrontal Cortex : OFC
35. Orbitofrontal Cortex: OFC
36. Parvalbumin: PV

37. Parvalbumin: PV
38. Periaqueductal gray: PAG
39. Phencyclidine: PCP
40. Phosphate buffered saline: PBS
41. Polymerase chain reaction: PCR
42. Posterior superior temporal sulcus: pSTS
43. Prefrontal cortex: PFC
44. Prelimbic: PrL
45. Primary motor cortex: M1
46. Principal cells: PCs
47. Pyramidal tracts: PT
48. Retrograde adenovirus: AAVrg
49. Retrosplenial cortex: RSC
50. Rostral-ventral anterior cingulate cortex: rACC
51. Rostral-ventral anterior cingulate cortex: rACC
52. Serotonin: 5-HT
53. Signal ratio noise: SNR
54. Somatostatin interneurons: SST INs or SOM INs
55. Somatostatin: SST or SOM
56. Striatum: STR
57. Succinate semialdehyde dehydrogenase: SSADH
58. Superior temporal sulcus: STS
59. Supplementary motor area: SMA, or MII
60. Thalamus: THAL
61. Transistor-transistor logic: TTL
62. Tucker Davis Technology: TDT
63. Ventral hippocampus: vHPC
64. Ventral medial prefrontal cortex: vmPFC
65. Ventral tegmental area: VTA
66. vertical band of Broca: VBB